



UNIVERSITÀ
DEGLI STUDI
FIRENZE

DOTTORATO DI RICERCA IN
Scienze della terra

CICLO XXVII

COORDINATORE Prof. Lorenzo Rook

*Optimization of ground based radar
techniques for early warning systems*

Settore Scientifico Disciplinare GEO/05

Dottorando

Dott. Bardi Federica

Tutore

Prof. Casagli Nicola

Coordinatore

Prof. Rook Lorenzo

Anni 2012/2014

Abstract

From a geologic standpoint, natural slopes are only temporary topographic features: sooner or later they suffer the effect of deterioration provided by different factors, related to natural and artificial causes.

Landslide phenomena represent one of the main modes of the process of deterioration. Therefore, landslides, defined as downslope movements of rock, soil, or related debris, have to be considered "normal" events in areas that present a certain kind of slope.

In this regard, learning to live with landslides is the only option for people living in those areas affected by this type of event.

Among the strategies available for living with these phenomena is the implementation of mitigation measures, specifically in terms of Early Warning Systems (EWS), and can be considered the best solution.

The three-year PhD research programme, discussed in this manuscript, has the main objective of improving this type of risk mitigation strategy, by exploiting advanced technologies, such as landslide monitoring systems, based on the physical principle of radar interferometry. In particular, Ground Based Interferometric Synthetic Aperture Radar (GB-InSAR) systems have been used and optimized to integrate existent Early Warning Systems, in order to reduce landslide risk.

The optimization mainly consisted in hardware and software modifications of GB-InSAR prototypal instruments, to implement their versatility and transportability and their flexibility, especially in terms of acquisition parameters.

Considering the effect of decorrelation due to the interaction between radar signal and atmosphere, a new algorithm finalized to the reduction of this decorrelation on SAR images has been created.

Moreover, a procedure to integrate data obtained by GB-InSAR systems with data obtained by satellite InSAR systems has been developed, both in qualitative and in semi-quantitative terms. The integration procedure, especially in quasi-quantitative terms, was made possible also thanks to the availability of new-generation satellite data, characterized by acquisition times that are more comparable with the GB-InSAR ones. The integration implied a projection of the data obtained from the different platforms towards a common direction, allowing us to partially overcome one of the main limitations of these techniques - that it can only detect displacements only along the line of sight of the sensor (LOS).

By applying these optimization measures, an EWS, completely based on InSAR data, has been proposed.

The introduced methodologies have been tested on four case studies, selected to be as representative as possible of the proposed theoretical approaches: the Capriglio landslide (Parma Province, Emilia Romagna Region, Northern Italy), a section of the A16 highway (Naples-Bari highway, Southern Italy), the San Fratello landslide (Messina Province, Southern Italy), and the Norwegian rockslide of Åknes, located on the western coast of Norway.

Riassunto

Dal punto di vista geologico, un pendio può essere definito tale solo “temporaneamente”, in quanto soggetto a normale deterioramento, ad opera di fattori naturali e/o antropici. Tra i vari attori del deterioramento, un ruolo centrale è rappresentato dai fenomeni franosi, i quali agiscono in modo più o meno naturale su tutte quelle aree interessate da una certa pendenza. In questo senso, imparare a convivere con gli eventi franosi rappresenta, per l’uomo, l’unica scelta possibile. “Convivere” con fenomeni di questo tipo vuol dire, innanzitutto, ridurre gli effetti, in termini di mitigazione dei rischi connessi.

In questo contesto si è sviluppato il presente progetto di ricerca, sostanzialmente finalizzato all’ottimizzazione di tecniche interferometriche radar da terra (*Ground Based Interferometric Synthetic Aperture Radar* (GB-InSAR)), con l’obiettivo di implementarne l’uso in sistemi di allerta rapida (*Early Warning Systems* (EWS)), per la mitigazione del rischio di frana.

L’ottimizzazione è consistita essenzialmente nell’implementazione, dal punto di vista *hardware* e *software*, di un sistema GB-InSAR prototipale. Le modifiche apportate hanno avuto come obiettivo principale l’incremento di versatilità, trasportabilità e flessibilità del sistema, in modo tale da favorirne l’utilizzo in condizioni di emergenza. Inoltre, è stato proposto un nuovo algoritmo per la correzione atmosferica, che ha permesso, in contesti specifici, la realizzazione di immagini radar a rumorosità ridotta, caratterizzate da bassa decorrelazione atmosferica.

E’ stata inoltre proposta, in via sperimentale, una metodologia finalizzata all’integrazione qualitativa e semi-quantitativa dei dati GB-InSAR con dati radar interferometrici, ottenuti da piattaforme satellitari di nuova generazione, ossia caratterizzate da tempi di rivisitazione relativamente ridotti e quindi da acquisizioni maggiormente comparabili a quelle di sistemi GB-InSAR.

Le misure di ottimizzazione introdotte sono state sfruttate al fine di proporre un sistema di *early warning* completamente basato su dati radar interferometrici.

Le metodologie proposte sono state testate su quattro casi di studio, scelti come i più rappresentativi possibile. La frana di Capriglio, nel comune di Tizzano Val Parma (PM), ha rappresentato il *test site* ideale, per il monitoraggio tramite il sistema GB-InSAR, implementato dal punto di vista *hardware*. Lo stesso sistema GB-InSAR è stato testato lungo una tratta dell’autostrada A16 (Napoli-Bari), interessata da fenomeni franosi; i dati GB-InSAR ottenuti sono stati elaborati utilizzando il nuovo algoritmo di correzione atmosferica e successivamente utilizzati in un sistema integrato di *early warning*. La frana di San Fratello (ME) ha rappresentato un caso di studio utile per testare la metodologia di integrazione tra dati GB-InSAR e dati InSAR satellitari, grazie alla disponibilità di entrambi i *dataset*, relativi agli stessi intervalli temporali. La stessa procedura di integrazione è stata testata anche presso la frana di Åknes, che interessa uno dei fiordi più famosi della Norvegia occidentale; in questo caso, la disponibilità di dati di letteratura relativi alle percentuali di spostamento reali della frana, osservabili tramite GB-InSAR e tramite i satelliti TerraSAR-X e Tandem-X, ha permesso di testare la procedura proposta, anche dal punto di vista quantitativo.

Table of contents

Introduction.....	1
1. State of the art	5
1.1 Space borne InSAR.....	15
1.2 Ground based InSAR.....	21
1.3 Landslide InSAR monitoring	28
2. Ground based InSAR optimization	31
2.1 Hardware features	32
2.2 Software features.....	36
2.3 Integration with satellite InSAR data.....	40
2.3.1 The use of satellite InSAR data in near-real time landslide monitoring	40
2.3.2 Integration methodology	44
3. Landslide Early Warning System	51
3.1 Landslide risk and mitigation.....	52
3.2 EWS definition	56
3.3 Proposal of an EWS based on InSAR data	62
3.3.1 Design activity.....	62
3.3.2 Monitoring phase	67
3.3.3 Forecasting phase.....	69
3.3.4 Public education phase.....	74
4. Applications and case studies	77
4.1 The Capriglio test site (Parma Province, Italy)	79
4.1.1 Geological framework	80
4.1.2 The landslide.....	81
4.1.3 GB-InSAR monitoring activities	84
4.2 Highways monitoring project (A16 – Naples-Bari Highway, Southern Italy)	90
4.2.1 The test site	91
4.2.2 GB-InSAR monitoring.....	95
4.2.3 Data transmission	102
4.2.4 Early Warning System.....	102
4.3 San Fratello test site (Messina Province, Southern Italy)	105

4.3.1	Geological and geomorphological framework.....	105
4.3.2	Landslide occurrence.....	107
4.3.3	The 2010 landslide	109
4.3.4	Activities	112
4.4	Åknes (Tafjord-Norway).....	121
4.4.1	Geological framework	122
4.4.2	InSAR monitoring activities	123
4.4.3	Satellite- and GB-InSAR data comparison	134
5.	Discussion and results.....	136
6.	Conclusions.....	143
7.	References	145
8.	Publications.....	161
	Annexes.....	162

Introduction

Landslides are defined as movements of mass of rock, debris or earth materials down a slope, including a wide range of motions through which falling, sliding and flowing under the influence of gravity (Cruden, 1991; IPCC, 2012).

On the basis of recent evaluations, landslides represent the most frequent geo-hazard and they cause much damage and many deaths every year. Landslides not only pose a serious threat to human lives, but also determine socio-economic losses, countable in billions of Euros and expressed in terms of damage to property and infrastructures and environmental degradation.

For many decades, the global impact of slope failures on population, structures, infrastructures, economy and environment, remained largely undetermined. To represent areas prone to landslide risk on a global or continental scale is often a challenge.

A few attempts have been made to assess landslide susceptibility, hazard or risk, being aware that obtained results have to be considered as a general pattern of the potential distribution of landslides. An estimation of the Global Landslide Hazard Distribution was provided in 2005, as the outcome of the collaboration between the Center for Hazards and Risk Research (CHRR), the Norwegian Geotechnical Institute (NGI) and Columbia University Center for International Earth Science and Information Network (CIESIN) (Columbia University, 2000). As expected, the areas along the circum-pacific belt on the Pacific Coast in central and South America and in the Japan-Philippines regions, the Alpine Orogenic Belt from Pyrenees to the Himalayas Ranges (India, Nepal) and South-East Asia passing through the Alps, the Balkan regions, and the Middle East (Turkey, Georgia, Azerbaijan, Iran) are those characterized by the highest landslide hazard. The total area prone to landslide is estimated at 2% of the world land area.

In Europe, the total area prone to landslide is estimated at 4% (including Turkey). The countries characterized by the highest total area prone to landslide are Albania (~40%), Slovenia (~25%), Bosnia & Herzegovina (~22%), Turkey (~19%), Greece (~15%), Italy (~13%), Austria (~10%), Serbia & Montenegro (~9%) (Columbia University, 2000).

Regarding Italy, more detailed records of landslide exist. The IFFI (Inventory of Landslide Phenomena in Italy, *Inventario dei Fenomeni Franosi in Italia*) and PAI (hydrogeological setting plan, *Piano di Assetto Idrogeologico*) are projects carried out to supply a detailed picture of the distribution of landslide phenomena on a national level. Moreover, in the last decades, more detailed landslide inventory maps have been constructed, at a regional level (e.g., Guzzetti & Cardinali, 1989), on a basin level (e.g., Righini et al., 2012; Ardizzone et al., 2012) and on even more local scales (e.g., Galli et al., 2008).

A first attempt to describe the socioeconomic significance of landslides was carried out by Schuster & Fleming, 1986, who estimated an annual cost of 10 billion dollars worldwide in terms of property damage from landslides. In Italy, the estimated landslide losses range from 1 to 2 billion of dollars annually, corresponding to about 0.15% of the national domestic product

(Canuti et al., 2004). Also the impact of landslides (in terms of casualties and fatalities) in Italy has been statistically analysed by Guzzetti, 2000 and Salvati et al., 2010, exploiting catalogues of the data on historical landslides collected in recent years by the National Research Council (CNR): in the 58-year period between 1950 and 2008, 2204 landslide events caused 4077 deaths, 26 missing persons and at least 2019 injured people and 177.376 evacuees and homeless people (Salvati et al., 2010).

Moreover, landslide disasters show a documented increasing trend mainly related to an increased susceptibility of the soils, owing to the over exploitation of natural resources, poor land-use planning and growing urbanization, which determines an increase in the population exposed to the landslide risk (Nadim et al., 2006). In those countries characterized by a young geological and tectonically active territory, the susceptibility to instability phenomena is further increased. It is the case, for example, of the Italian Peninsula, where about 70% of the territory can be considered exposed to landslide risk (<http://www.protezionecivile.gov.it/>).

Unfortunately, the population is more and more at the mercy of nature through increasing demands for resources, urbanization and environmental changes, and landslides, triggered by both natural processes and human activities, happen and will continue to happen.

Among the triggering factors, the most important is represented by precipitation events, which are becoming more and more frequent and intense, increasing, as a consequence, the landslide occurrence. In this sense, some studies exist which investigate the existence of a possible correlation between landslide occurrences and climate changes (Jakob & Lambert, 2009; Borgatti & Soldati, 2010).

The situation is complex and society has the only option of learning to live with landslide risk.

In this sense, the effort of the research community to determine every possible measure of risk mitigation must be encouraged and supported.

Despite, as proved, the fact that landslides represent a serious threat to human life and is widespread all over the world, the related risk perception is very low.

For all the above mentioned reasons, exhaustive knowledge of the spatial distribution of landslides (location, extent and typology) and temporal evolution (style, state of activity and kinematics) has become mandatory, especially in those areas where property, infrastructures and human lives are at risk. Knowledge of a phenomenon is the first step towards its understanding and preventing disaster and to ensure an adequate level of safety to people living in the affected areas. Also citizens, the ultimate beneficiary of the geo-hazard-related strategies, can take advantage of information on where, when and to what extent the ground may become unstable. Moreover, other important duties of the scientific community and authorities in charge of landslide risk mitigation is to make the population aware of the existing risk, to establish simple but firm rules on how to minimize impact from landslides and to educate citizens to adopt correct procedures in the case of events, by conducting awareness and vigilance campaigns. The successful achievement of these objectives could improve the effectiveness of the community as a whole to deal with calamities, survive them and restore normal life conditions.

During the last decade, different monitoring and remote sensing techniques devoted to landslide analysis have undergone rapid development. Among them, Interferometric Synthetic Aperture Radar (InSAR) techniques have seen an increasingly greater diffusion.

InSAR techniques belong to the family of active remote sensing techniques and, thanks to their intrinsic characteristics, they present a lot of advantages in the field of landslide monitoring and management as compared to the use of traditional techniques.

Among the several advantages that could be counted, the possibility to produce near-real time displacement maps of areas over several square kilometres, without physical access to the observed area, can be considered the crucial benefit of these techniques. Moreover, they are able to observe the investigated scenario 24 hours per day and in all-weather conditions.

Firstly conceived and developed for data acquired from space borne platforms, these methods were later applied also on ground based platforms (GB-InSAR). Especially as regards monitoring landslides and unstable slopes, GB-InSAR systems have become more and more popular over the last few years ([Luzi, 2010](#)).

This thesis represents the main outcome of a three-year-long activity at the Earth Sciences Department of the University of Firenze and at the Norwegian Geotechnical Institute of Oslo.

The main objective of this PhD programme was to optimize existent GB-InSAR instruments and their output data, in order to make them as useful as possible in the field of landslide risk mitigation.

Considering that risk mitigation is more and more conceived as a combination of actions which involve prevention and prevision of the landslide event, it is no longer sufficient that landslide management be applied only in emergency situations, and after the occurrence of event. The most complete method of reducing landslide risk can be found in the Early Warning Systems (EWSs). Therefore, the GB-InSAR optimizations were finalized to implement better-structured EWSs, following the guidelines proposed by the European Project [SafeLand \(2011\)](#) and then by [Intrieri et al. \(2013\)](#).

Optimization has been achieved by following two principal steps:

- Proposing hardware and software modifications to a prototypal GB-InSAR instrument, to implement some of its benefits, in order to increase its utility in EWS activities;
- Proposing a procedure finalized to the integration of InSAR data obtained from ground based and space borne platforms, also finalized to exploiting the results in an EWS.

The proposed optimizations and the resulting EWS have been tested on some case studies, selected during the three year PhD activity with the main idea to consider the most adequate and representative situations to apply and practically exploit the methodology previously presented from the theoretical point of view.

In addition to the *Introduction*, this thesis includes a total of eight chapters, structured as follows:

- *Chapter 1* describes the basic principles of InSAR techniques applied both on space borne and ground based platforms, and their applications for landslides investigations.
- *Chapter 2* describes the optimization measures performed on GB-InSAR systems, applied both on hardware and software components; it also includes a brief overview on the utility of new-generation satellite InSAR data in EWSs and the procedure implemented to integrate these data with the GB-InSAR data.
- *Chapter 3* contains an introduction on EWSs, their definition and their crucial importance in landslide risk mitigation, and the proposal of the implemented EWS, completely based on InSAR data.
- *Chapter 4* describes the application of the methodology proposed in the previous chapters to selected case studies.
- *Chapter 5* mainly deals with discussions regarding applicability, limitations and uncertainties of the GB-InSAR proposed optimizations and data integration.
- *Chapter 6* summarizes the main findings of this thesis.
- *Chapter 7* contains the main references of this work, listed in alphabetical order.
- *Chapter 8* consists in a list of the articles and papers written during the three year PhD course. The already published papers are attached as Annexes.

1. State of the art

The microwave portion of the electromagnetic spectrum finds wide applications in the field of remote sensing. The use of microwaves allows us to obtain information about targets located far away from the sensor, in all weather conditions and 24 hours per day. Indeed, these techniques are an example of active remote sensing: the sensors emit microwave in order to scan or analyse a specific target, and the characteristics of the microwave (frequency and wavelength) allow us to penetrate clouds and to lightly interact with the atmosphere, because the related absorption bands are very restricted. Therefore, darkness and weather conditions, like rain or snow covers, do not affect the microwave signal. Specifically, the microwave radiation regards the portion of the electromagnetic spectrum ranging between 1 m and 3 mm of wavelength (frequency range: 100 GHz- 300 MHz) (Figure 1).

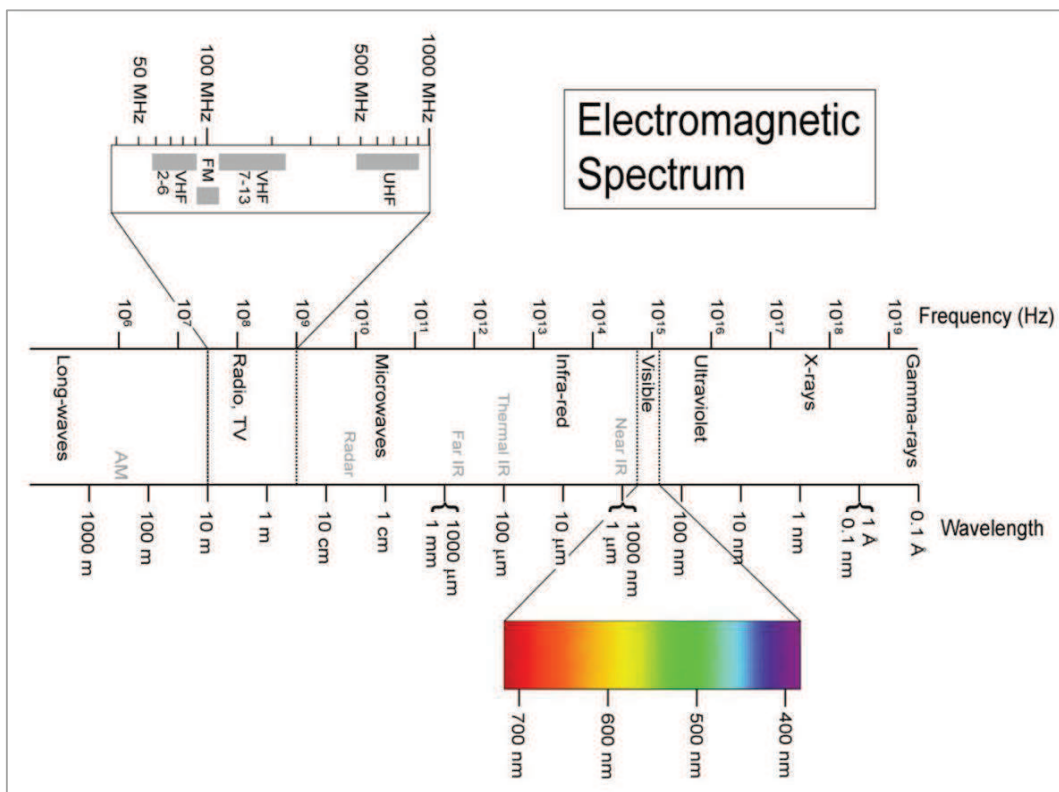


Figure 1. Electromagnetic spectrum (from: <http://www.nasa.gov/>).

The microwave range is divided into "sub-bands" that are defined by the Radio Society of Great Britain as indicated in Table 1.

The family of the active techniques that exploit microwaves to obtain information on a target placed far away from the sensor is defined with the term RADAR, that is the acronym of *RADio Detection And Ranging*. Radar sensors can be installed on satellite, aerial and ground based platforms.

Sub-Band definition	Frequency range (GHz)
P	0.3 - 1
L	1 - 2
S	2 - 4
C	4 - 8
X	8 - 12
Ku	12 - 18
K	18 - 26
Ka	26 - 40
Q	30 - 50
U	40 - 60
V	50 - 75
E	60 - 90
W	75 - 110
F	90 - 140
D	110 - 170

Table 1. Microwave sub-bands definition (from: <http://rsgb.org/>).

A radar sensor is generally equipped with a microwave transmitter and receiver, energized by an electrical supply. The observed scenario is irradiated by a microwave beam, that is reflected by the intercepted objects; the backscattered waves are detected by the receiving antenna. Therefore, the sensor measures the time necessary for the signals to travel from the antenna to the observed scenario and back; these measurements are generally converted into a distance. The result is an array, where each value is a complex number which includes the information related to the phase component and the amplitude of the received waves. The reflection intensity mainly depends on some characteristics related to the acquisition mode, the features of the signal, the target geometry and its dielectric and electromagnetic properties.

First of all, the penetration depth of the signal depends on the frequency: it tends to be deeper with longer wavelengths. For example, considering a forest, the radiation will only penetrate the first leaves on the top of the trees using the X-band radiation (8-12 GHz, ~ 3.1 cm wavelength); on the other hand, using L-band radiation (1-2 GHz ~ 23 cm wavelength), the signal will be able to penetrate leaves and small branches, and so on (Figure 2).

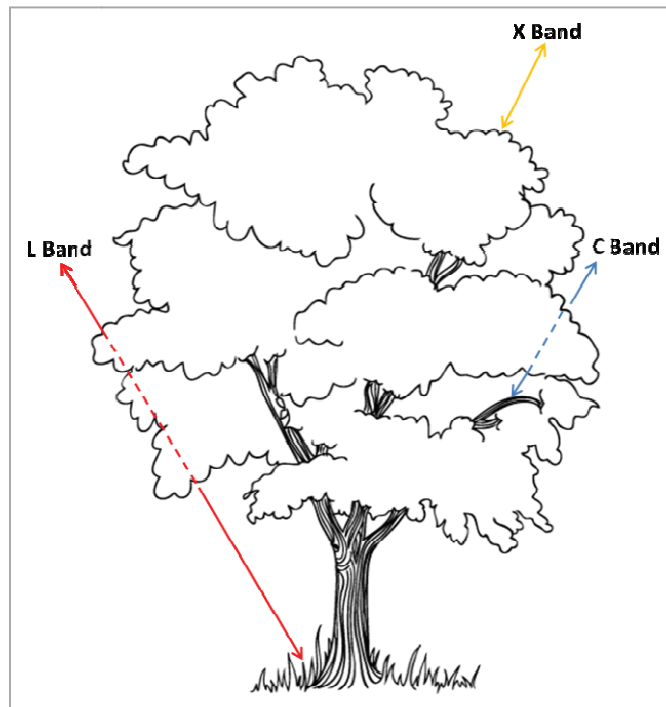


Figure 2. Examples of radar signal penetration (modified from: <http://eijournal.com>).

It is also true that the penetration capability is related to the moisture of the target: microwaves do not penetrate water more than a few millimetres. The moisture content of a considered material is related to its dielectric constant, that is a complex value that contains information about the electric properties of a material, like permittivity and conductivity. These properties also influence the radar backscatter: the increase of the dielectric constant value produces an increase of the reflection intensity. Indeed, wet materials are generally characterized by high radar reflectivity.

Another feature of the signal that can influence the radar response is the polarization; this depends on the orientation of the electric field component of the electromagnetic wave. It is possible to produce radar images with different polarization configurations that depend on the combinations between the polarization of the emitted and reflected radiation. In this way the polarization configurations can have the same type of polarization for both the waves (HH and VV polarization, where H is Horizontal and V is Vertical), or different polarization respectively for the two different waves (HV, VH) (Figure 3). The polarization can influence the penetration depth of the radar wave and, in specific cases, can provide information on the different layers on a target. Information about the shape and the orientation of the small scattering elements composing the observed scenario can be provided by polarization.

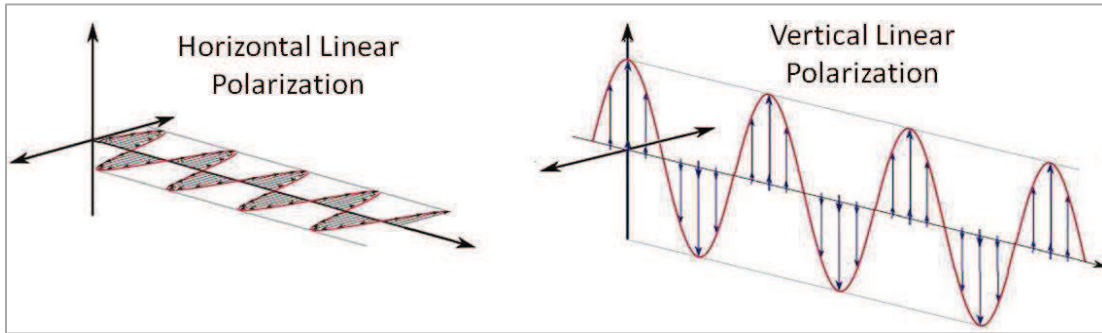


Figure 3. Example of possible polarization of an electromagnetic wave.

As regards the target characteristics, the radar reflectivity mostly depends on the surface roughness of the observed object. This is a relative feature, that depends upon wavelength and incidence angle and that can be evaluated in different ways, for instance considering the standard deviation of the height of the discontinuities. A smooth surface, such as a still water surface, produces a specular reflection, that is directed away from the sensor, giving slight backscatter as a result. On the contrary, land surfaces generally present high roughness, permitting a high intensity of backscatter.

The target orientation, with respect to the sensor position, influences the backscatter intensity too, because it conditions the possibility to generate a reflected signal that can return to the radar antenna.

Potentially, bare slopes and rocks without vegetation represent optimal radar targets, because of their reflectance parameters, that produce strong radar responses. Therefore, instability phenomena are widely analysed by using these techniques; specifically, according to [Atzeni et al., 2001](#), the C and the Ku bands of the microwaves are the most utilized for these applications.

The output of a radar acquisition is a two-dimensional map, visualized as an image, where each pixel value represents the reflection intensity of the respective ground area. The pixel dimensions are defined by the resolution of the technique.

Range resolution is the capacity of a radar system to distinguish between two or more targets at different ranges, in the direction of its line of sight; it mainly depends on the width of the transmitted pulse (t). Therefore the theoretical range resolution (R_{range}) for a radar system is given by ([Lillesand & Kiefer, 1979](#)):

$$R_{range} = ct/2 \quad (1)$$

where c is the light speed.

R_{range} projection on the ground is given by:

$$R_{GroundRange} = ct/2\sin\alpha \quad (2)$$

where α is the incidence angle value.

The azimuth (or cross range) resolution defines the resolution in the sensor movement direction; it depends on the width of the radar beam (b), which is related to the employed wavelength (λ) and to the physical (i.e., real) aperture (A) of the transmitting antenna (Lillesand & Kiefer, 1979):

$$b = \lambda/A \quad (3)$$

The azimuth resolution ($R_{azimuth}$) for a real aperture radar system is given by:

$$R_{azimuth} = r*b \quad (4)$$

where r is the distance between the sensor and the target.

Real aperture radar sensors, hosted by satellite platforms do not provide suitable resolution. For instance, given a beam width of 10 milliradians, at a distance of 800 kilometres, the azimuth resolution is 8 km.

For such systems, azimuth resolution can be improved by increasing the length of the physical antenna used to illuminate the target scene or by using a shorter wavelength. Decrease of the wavelength leads to a higher cloud and atmosphere impact on the capability of imaging radars. On the other hand, to obtain a finer resolution (in the order of few meters), a physical antenna some kilometres long would be needed. A satisfactory azimuth resolution requires big antennas: to overcome this problem the synthetic aperture radar (SAR) technique was created.

SAR imaging consists of irradiating the targets with a moving antenna (a few meters long) transmitting a stream of pulses. Indeed, from different positions, the antennas repeatedly illuminate a specific target to synthesize an aperture bigger than the real one: as the antenna moves, it provides repeated observations of each spot of the scenario. SAR can be obtained by exploiting the motion of the satellite and aerial platforms hosting the radar sensors or exploiting the movement of the antennas mounted on a mechanical linear rail in the case of ground based radar. The technique takes advantage of frequency variations in the returned signals due to the Doppler effect; the SAR azimuth resolution (R_{azim_SAR}) is dependent on the length of the synthetic aperture (Lillesand & Kiefer, 1979):

$$R_{azim_SAR} = r\lambda/2D \quad (5)$$

where r is the sensor-target distance, and D is the length of the synthetic aperture.

The basic physics of a SAR system are schematically shown in Figure 4.

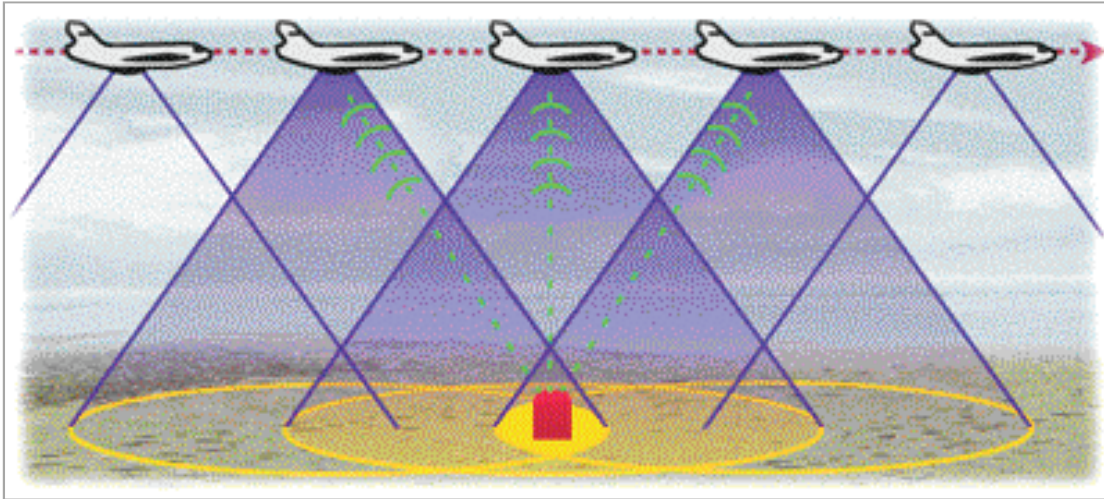


Figure 4. Basic principle of a SAR system; the example refers to an airborne platform (from: <http://www.nrcan.gc.ca/>).

Since a single SAR image is of limited practical use, a suitable approach to exploit SAR data consists in the comparison of the phase matrixes of two SAR images, acquired at different times from the same point or from different points at the same time; this is the main principle of the interferometry SAR (InSAR) technique. Satellite SAR imagery can be obtained either from SAR systems equipped with two separate receiving antennas hosted by the same platform (single-pass interferometry), or collecting data over the same test site on separate occasions, using one antenna onboard a platform that moves slightly between two acquisitions (repeat-pass interferometry). Comparing images (called "master" and "slave"), acquired in different times from the same point, it is possible to estimate the eventual displacement of the observed area, analysing the related phase displacement of the reflected waves, following the principle of interference between two coherent waves. This principle is related to the overlapping of the waves in the medium: the intensity result varies between a maximum value that is the sum of the intensity of the two waves (constructive interference- Figure 5A), and a minimum characterized by null intensity (destructive interference - Figure 5B).

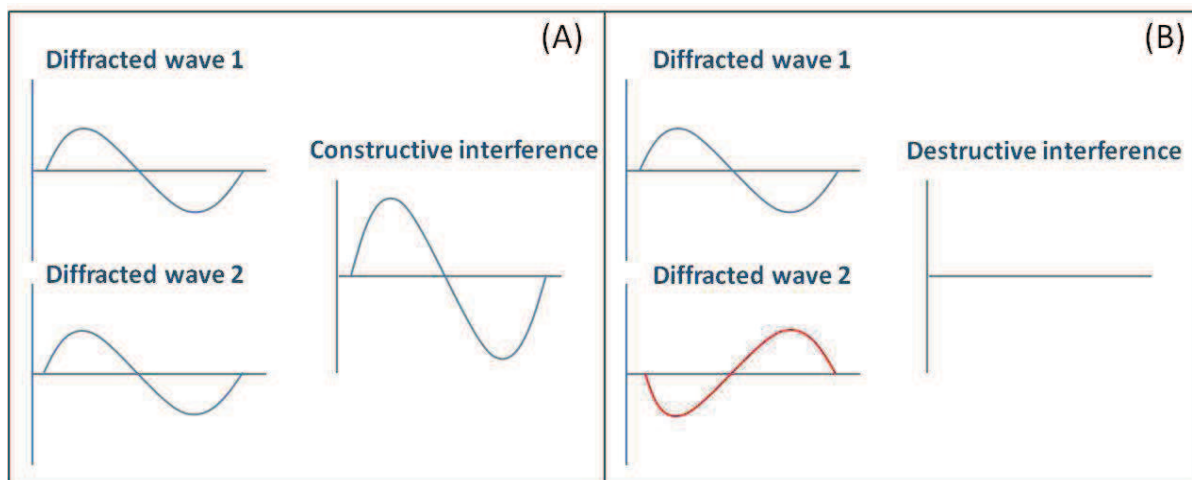


Figure 5. Schematic representation of the interference principle. (A) Constructive interference; (B) destructive interference (modified from: <http://www.ntns.it/>).

The result is an image called "interferogram", that represents the phase displacement occurred in the time span between the two acquisitions.

Using the principles of wave mechanics, an undulatory function can be used to define a wave:

$$y = h \sin (kx - \omega t) = h \sin (2\pi x / \lambda - \omega t) \quad (6)$$

The " $2\pi x / \lambda$ " represents the phase component of the wave related to the distance variation. It is an angular value, so that it can range between 0 and 2π or $-\pi$ and $+\pi$. Therefore it is possible to obtain information about the phase displacement related only to the last round of the wave.

The phase displacement, occurring during two subsequent acquisitions, can be translated into displacement values, over a range between 0 and $\lambda/2$ (or $-\lambda/4$ and $+\lambda/4$); so that the maximum displacement that can be detected without ambiguity is 0.5λ .

In addition to the eventual displacement, the phase value depends on the boundary conditions, such as atmospheric interactions with the microwaves (φ_{ATM}), random noise (φ_{NOISE}) and the topographic characteristics ($\Delta\varphi_{TOP}$) of the observed scenario.

If these boundary conditions remain the same in the two SAR images, the only contribution to the phase variation ($\Delta\varphi$) is related to the eventual target displacement, and in fact the other terms of the equation are negligible:

$$\Delta\varphi = \cancel{\Delta\varphi_{TOP}} + \Delta\varphi_{DISP} + \cancel{\Delta\varphi_{ATM}} + \cancel{\Delta\varphi_{NOISE}} = \Delta\varphi_{DISP} \quad (7)$$

The interferometry applied to SAR instruments is exploited to produce aerial maps of the observed scenario, where every phase displacement value is visualized with a specific colour.

More specifically, the interferometry is the result of a comparison between two SAR images (S_1 and S_2), mathematically defined as follow:

$$S_1 = A_1 \exp(\varphi_{i1}) \quad (8)$$

$$S_2 = A_2 \exp(\varphi_{i2}) \quad (9)$$

Multiplying S_1 with the S_2 complex conjugate (S_2^*) the result is:

$$S_1 \cdot S_2^* = A_1 \cdot A_2 \cdot \exp[i \cdot (\varphi_1 - \varphi_2)] \quad (10)$$

$$\text{Because } \Delta\varphi = \varphi(S_1 \cdot S_2^*) = (4\pi/\lambda) \cdot \Delta r \quad (11)$$

and

$$\Delta r = (\lambda/4\pi) \cdot \Delta\varphi \quad (12)$$

the displacement value can be defined using only the phase displacement contribution.

The phase difference is measured along the line of sight (LOS) of the sensor with respect to the reference (or master) SAR image; LOS is defined as the line from the antenna to the imaged element on the ground (Figure 6).

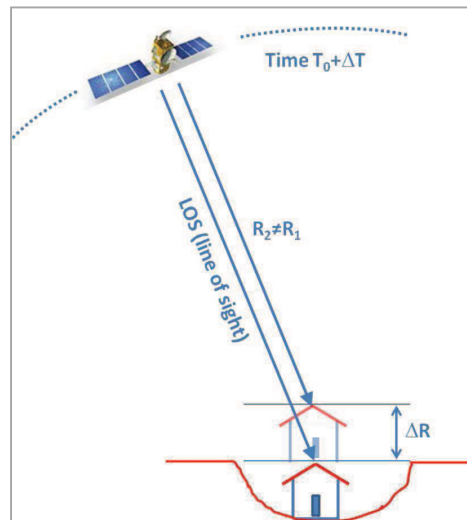


Figure 6. Schematic representation of the interferometry principle (modified from: <http://treuropa.com/>).

The scale that is generally used to represent the interferogram is a colour scale and it corresponds to a variation from $-\lambda/4$ to $+\lambda/4$.

A phase difference larger than 2π cannot be detected: when this problem occurs, the phase is defined as wrapped, and has to be unwrapped by using specific algorithms. This problem is recognized as "phase ambiguity" and it determines that, when the displacements exceed the maximum detectable, they are represented on the map with the colour correspondent to $N \lambda/2$ displacements. The effects of phase ambiguity appear as a series of coloured bands, called interferometric fringes (Figure 7).

Specifically, the technique applied to achieve the retrieval of the ground displacement that occurred between the two different acquisitions is called Differential InSAR (DInSAR) (Zebker & Goldstein, 1986; Gabriel et al., 1989; Massonnet and Rabaute, 1993; Goldstein et al., 1988; Massonnet & Feigl, 1998; Rosen et al., 2000; Tarchi et al., 2003).

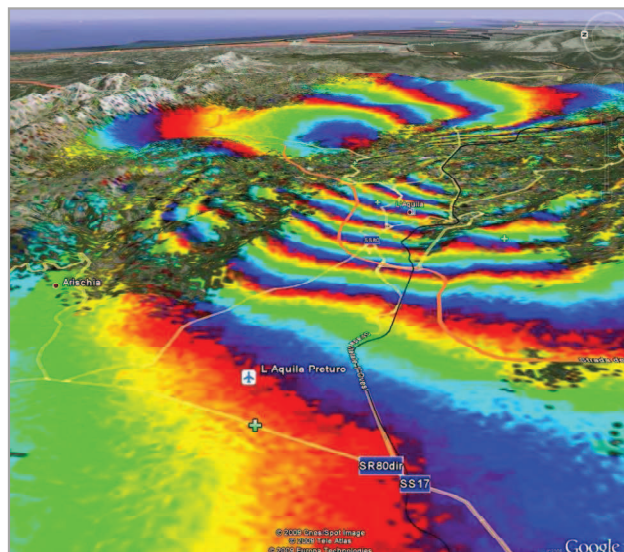


Figure 7. Example of interferometric fringes, related to the SAR acquisitions of the Envisat satellite before and after L'Aquila Earthquake (6th April 2006) (from: Nitti et al., 2009).

A *sine qua non* condition applying to the InSAR techniques is related to phase and amplitude stability of the signal during the entire period of acquisitions. Amplitude data of backscattered signals are analysed to identify those targets that maintain a high amplitude stability. Signal analysis of these radar targets, exhibiting high phase stability over the entire observation time period, allows us to estimate the displacements. Eventual variations, together with a change in the target reflection features, can invalidate the interferometric results. A quantification of the stability of these parameters is given by the coherence value, that ranges between 0 (minimum coherence value) and 1 (maximum coherence value). A coherence matrix expresses the coherence value of each cell of observation and it can be represented on a two-dimensional map. Therefore, it is possible to neglect the pixels that present coherence values lower than a specific threshold value.

Some factors contribute to a reduction of coherence (Zebker and Villasenor, 1992):

- the long term temporal decorrelation: a variation of the electromagnetic properties of the target in the span between the first and the last observation. In land observations, this is related to vegetation changes, like seasonal variations or growth phases etc.;
- the short term temporal decorrelation: this happens during the acquisition of a single image and is related to rapid changes of the observed scene, for example rapid movements of the scenario, related to a rapid flow of material (*i.e.* lava flows, very fast earth/debris flows, vegetation movements related to wind energy etc.);
- spatial decorrelation: this happens when the same scene is acquired in different times from slightly different viewpoints (different geometrical baseline);
- thermal decorrelation: this depends on the thermal effects on the instrument that can determine a loss of coherence in the transmitted radar signal.

Besides the reduction of coherence, other problems can reduce technique applicability:

- the speckle effect: this is related to the random noise, and affects more or less every radar image. It is related to different echoes in the same cell of the image, so that some pixels will be strongly reflective because of the constructive interference between the different echoes; others will be less reflective in relation to the destructive interference phenomenon. Averaging data obtained from different acquisitions makes it possible to reduce this effect.
- Geometrical distortions: these problems are related to the radar sensors ability to detect displacements only in the LOS direction and depend on the sensor-target's relative positions. Geometrical distortions in radar images are frequent, especially when sensors illuminate target surfaces such as mountain slopes with high relief (*i.e.*, surfaces with different angles). Most common effects in radar images are *foreshortening*, *layover* and *shadowing* (Figure 8) that are generally stronger in aerial and satellite sensors, where the acquisition mode is characterized by a side-looking view.

Foreshortening occurs when the radar beam reaches the base of a tall feature tilted towards the radar (*e.g.* a mountain) before it reaches the top. Because the radar measures distance in slant-range, the slope will appear compressed (shortened) and the length of the slope will be

represented incorrectly in the image. Shortened slopes appear bright-toned in the radar image. In case of *layover* the radar beam reaches the top of a tall feature before it reaches the base; the return signal from the top of the feature will be received before the signal from the bottom. As a result, the top of the feature is displaced towards the radar from its true position on the ground. On the contrary, topographic surfaces on the opposite side of incoming beams generally aren't illuminated and they suffer from *shadowing* (dark-toned). The effect is more pronounced for sensors that use steeper *incidence angles* (angle defined by the incident radar beam and the normal to the illuminated surface) and for steeper slopes (Colesanti & Wasowsky, 2006).

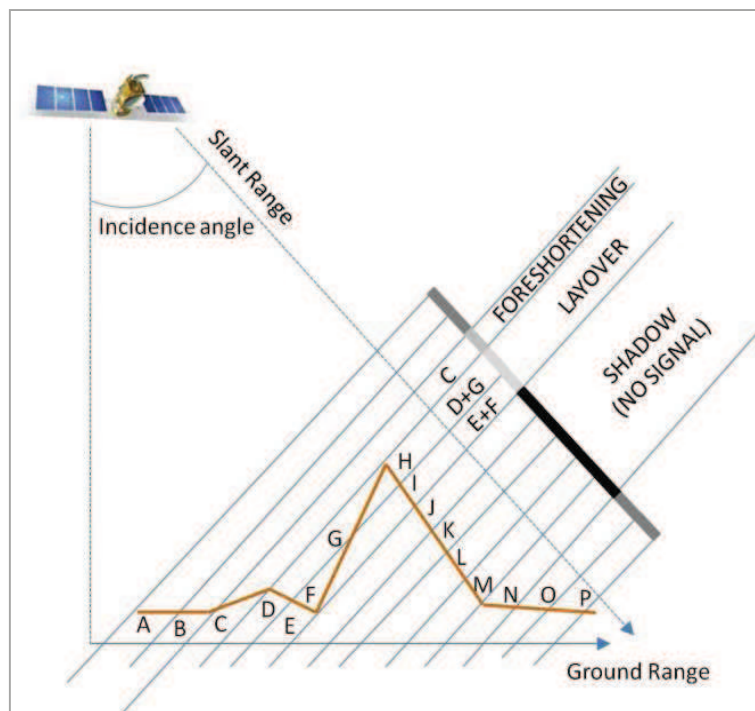


Figure 8. Foreshortening, shadowing and layover effects (modified from Colesanti & Wasowsky, 2006).

More detailed information about the radar techniques and their applications in the field of geology and engineering geology are discussed in the next sub-paragraphs, where space borne and ground based techniques are described separately.

1.1 Space borne InSAR

In the large family of the InSAR techniques, the satellite images cover a very important role: a high number of satellites host SAR instruments for acquiring data from the Earth's surface. In 1978, the SEASAT, the first satellite with an imaging SAR, was launched; it was used as a scientific sensor and it opened the road to the following missions: ERS, Radarsat, ENVISAT, JERS, TerraSARX and Cosmo-SkyMED among others (Luzi, 2010).

Since then, many different SAR satellites have been or are still in orbit, providing large coverage of the planet. This large amount of data can be used for InSAR applications.

The satellites orbit the Earth following sun-synchronous, near-polar paths, with an altitude ranging between 500 and 800 km above the surface. The LOS (sensor to target direction) is inclined at an angle respect to the vertical; this angle is called *off-nadir* angle (or *look angle*) and it varies according to the satellite employed. Combining the Earth's rotation movement with their orbits, satellites are able to gather information about the same target with two opposite acquisition geometries: ascending (from the South Pole to the North Pole) and descending (from the North Pole towards the South Pole). SAR systems are side-looking: the radar antenna transmits and receives microwaves only on one side of the satellite (typically the right side). These radar signals are transmitted in pulses by a microwave beam, illuminating a *swath*. Each backscattered pulse is recorded by a receiving antenna and then it is processed to produce a spatial image from raw SAR signals.

Space borne SAR instruments usually can operate at X, C and L-band of the microwave portion of the electromagnetic spectrum.

The specific satellite acquisition mode defines the investigable area extension and the maximum velocity of movement that a satellite is able to detect, which depends on the employed wavelength and on the satellite *revisiting time* (the span taken by the satellite to re-scan the same area). Generally, satellite SAR frames cover areas up to 100 square kilometres, with a resolution of a few meters.

There are basically three operating modes of SAR system: *Stripmap*, *ScanSAR* and *SpotLight* (Franceschetti and Lanari, 1999). The most popular is the *Stripmap* mode, since this was the acquisition type of early space borne systems (ERS1/2, ERS-2, and JERS-1). In this case the radar look angle is fixed. The antenna points along a fixed direction to one side of the flight platform path (cross-track direction). As the platform moves, the antenna footprint covers a relatively narrow strip (70 and 100 km wide swath for JERS1 and ERS1/2, respectively).

A new operating family of SAR satellite platforms (Radarsat1/2, Envisat ASAR and ALOS Palsar) was designed to acquire images in both *Stripmap* and *ScanSAR* mode. Space borne radar application exploiting *ScanSAR* images are ideally suited for mapping large areas and for monitoring wide area deformations. *ScanSAR* mode can achieve a wide swath coverage periodically sweeping the antenna look angle. As the platform moves, the antenna is capable of illuminating several sub-swaths (in the cross-track direction), increasing the width of the image swath up to 400–500 km. Moreover, *ScanSAR* can acquire images for a given target area more

frequently than the *Stripmap* mode, significantly improving the temporal resolution of deformation mapping, but, according to [Monti Guarnieri & Rocca 1999](#), lower resolution images are obtained by operating in the *ScanSAR* mode, since the increased coverage led to a loss in the azimuth resolution. Typical swath widths of Radarsat 1/2, Envisat ASAR and ALOS Palsar images are 500, 400 and 350 km, respectively. Up to now, *ScanSAR* is the established mode in SAR for wide-swath imaging. Nevertheless, the mode has several drawbacks caused by the focusing of the same target from different portions of the antenna ([Meta et al., 2010](#)). A more detailed description of benefits and disadvantages in *ScanSAR* mode are included in [Monti Guarnieri & Prati, 1996](#), [Moreira et al., 1996](#) and [Holzner & Bamler, 2002](#).

The *Spotlight* SAR version of imaging radar can produce imagery with high spatial resolution. Higher resolution is obtained by pointing the radar look angle to keep the target area within the illumination beam for a longer time. Thanks to a longer synthetic aperture, *Spotlight* SAR improves significantly the capability of SAR sensor of acquiring high-resolution imagery, albeit at the expense of spatial coverage.

The newest X-band satellite generation (TerraSAR-X and COSMO-SkyMed) is capable of acquiring images in *Stripmap*, *ScanSAR* and *SpotLight* mode, achieving in the last case an image pixel resolution of up to 1m.

Table 2 shows an overview of previously in-orbit satellites, currently available sensors and future missions, linked according to their relative operative wavelength band and their revisiting time.

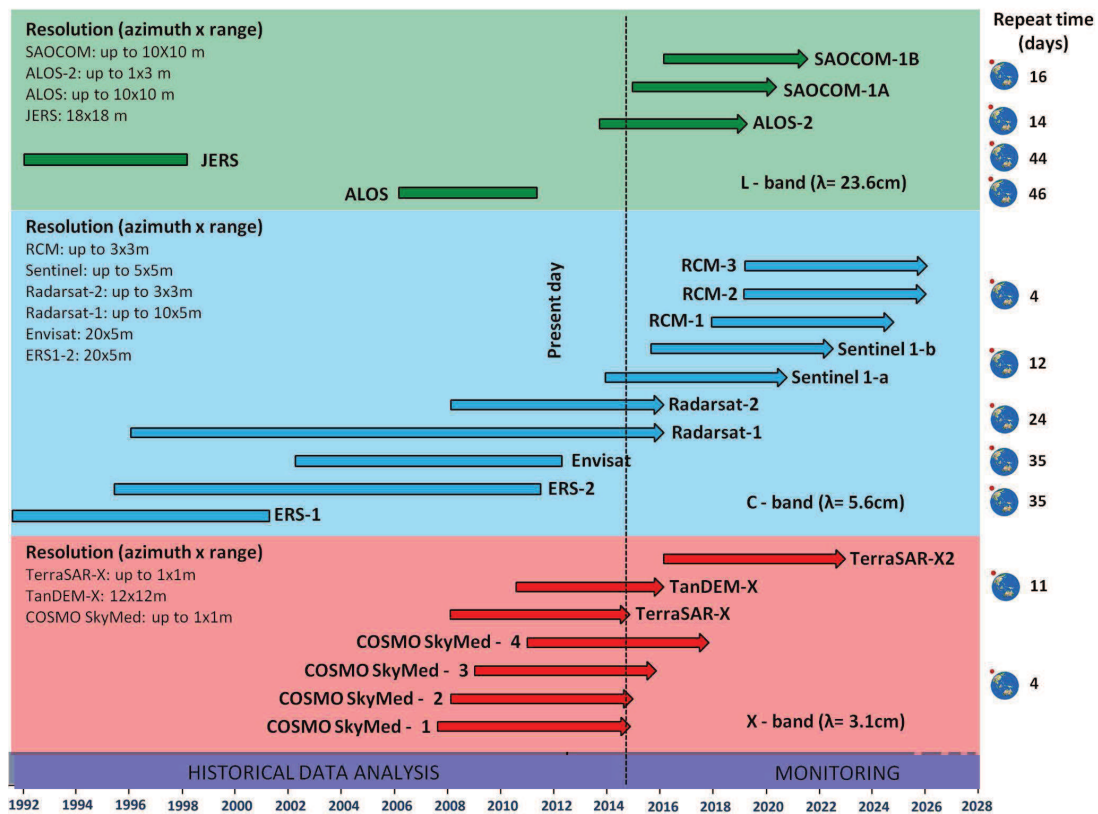


Table 2. Satellite missions for interferometric applications (modified from: Raspini, 2012).

In the field of the space borne InSAR techniques, limits related to the conventional DInSAR method were overcome by the development of multi-temporal interferometric approaches, that allow a reduction of the atmospheric impact on the estimated displacement values, by using a long temporal series of SAR images. Indeed, the principal limitation of the classical DInSAR techniques is due to atmospheric noises (Massonnet & Feigl, 1995, Colesanti et al., 2003a) than can be removed or, at least, reduced using this new approach.

PS-InSAR (Permanent Scatterer InSAR) (Ferretti et al., 2000, 2001) was the first technique, developed by TRE (TeleRilevamento Europa), specifically implemented for the processing of several (at least 15 or more) co-registered, multi-temporal space borne SAR images of the same target area (Figure 9); this multi-interferogram approach allows us to obtain more precise ground deformation maps on sparse grid of phase stable radar targets, the so-called Persistent Scatterers (PS). A PS corresponds to resolution elements containing a single dominant scatterer characterized by high electromagnetic reflectivity. Therefore, a PS has a stable radar signature with high coherence values and stable scattering behaviour and it is only slightly affected by decorrelation phenomena. PS targets mainly correspond to man-made (buildings, roads, monuments, metallic structures) objects or natural (such as rock outcrops) features. Analysing the backscattered signal from the observed scene, the so-called *amplitude stability index* (Ferretti et al., 2001) is identified; for a specific pixel of the SAR image, the index is defined by the ratio between the average amplitude of the return signal and its standard deviation. Values over a defined threshold of the index allow us to identify the PS network. The high phase stability of these targets, during the entire observation period, allows us to distinguish the phase component related to the displacement, from the other contributions. On the other hand, the topographic and noise elements can easily be neglected. Spurious atmospheric effects are strongly correlated in space (within the same SAR scene) but highly decorrelated in time (*i.e.*, among different acquisitions). The atmospheric term is estimated and removed through a statistical analysis of the signals and applying specific algorithms.

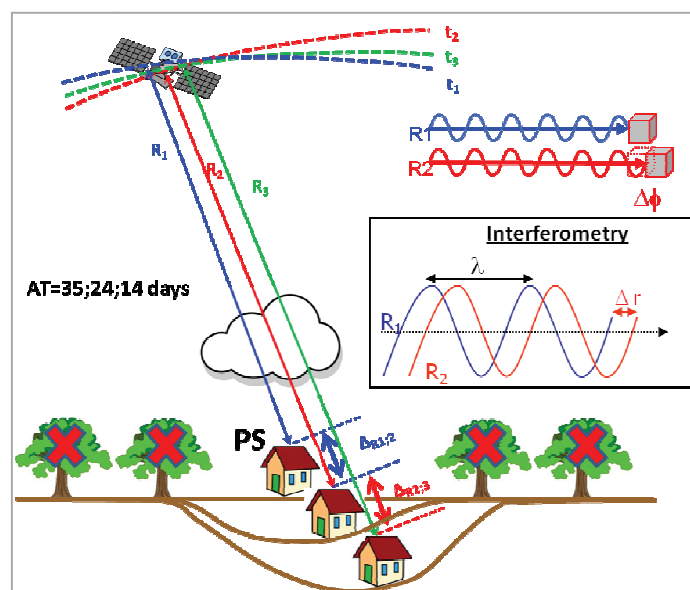


Figure 9. Schematic description of the PSI technique (modified from: <http://treuropa.com/>).

Generally, urbanized areas are characterized by a dense PS network, because of the presence of several man-made structures, such as buildings, roads, bridges, monuments, pylons etc. In these areas the PS density can reach up to several hundred per square kilometre, and the PS-InSAR technique application allows us to obtain LOS velocity values with millimetric precision (fraction of the operating wavelength), sometimes even better than 1 mm/year. The same precision can be reached in presence of natural reflectors, such as rock outcrops, non-vegetated slopes, like instable scarps and so on.

The PS-InSAR technique also allows us to obtain PS displacement time series, retrieved step by step acquisition by acquisition, with accuracy on single measurements generally ranging from 1 to 3 mm (Colesanti et al., 2003a). The PS positioning precision varies in relation with the used satellite: for C-band ERS1/2, it is about ± 7 m in the East direction, ± 2 in the North and ± 1.5 on the vertical direction; for X band sensors, like TerraSAR-X constellation, it is ± 4 m in the East direction, ± 1 m in the North and in the vertical direction (Colesanti et al., 2003b).

The main limitation of the PS-InSAR technique is related to the absence or low density of the reflectors (PSs), as happens within vegetated, rural and forested areas, in less urbanized and agricultural environments: in these areas PS-InSAR partially fails due to complete decorrelation of the great majority of scatterers. Two different approaches have been developed to extend the ability of PS-InSAR to natural terrains: the SqueeSAR and StaMPS technique.

The SqueeSAR method, developed by T.R.E. (Telerilevamento Europa), represents the natural evolution of the PS-InSAR technique (Ferretti 2001, 2011). This new approach uses, to apply the multi-temporal interferometry, both the Persistent Scatterers and the so-called Distributed Scatterers (DS), which correspond to homogeneous areas spread over a group of pixels in a SAR image (rangeland, pasture, shrubs, bare soils) (Figure 10). The application of this new algorithm provides a significant increase in the density of ground deformation points, especially over non-urban areas, allowing us to apply the technique to maps and monitoring and analyse ground motion in natural terrains (Ferretti et al., 2011; Raspini et al., 2013; Meisina et al., 2013; Bardi et al., 2014; Bellotti et al., 2014) and thus improving the knowledge and the overall understanding of surface displacement occurring in an area of interest.

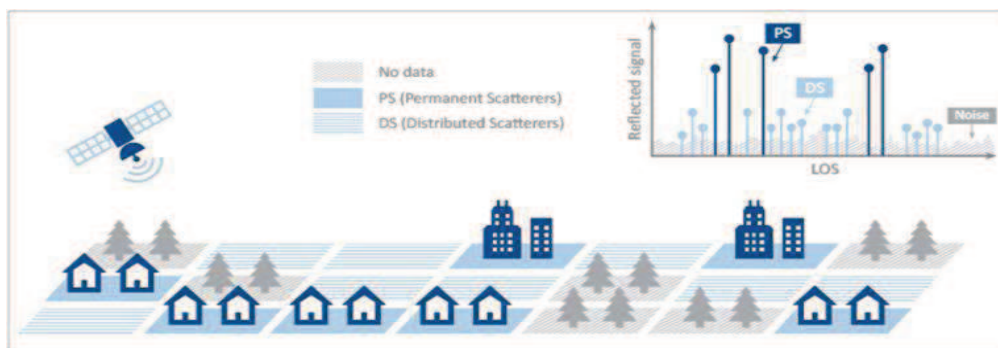


Figure 10. Comparing between PS-InSAR and SqueeSAR techniques (from: <http://treuropa.com/>).

The StaMPS (Stanford Method for Persistent Scatterers) was proposed by Hooper et al., 2004 and is based on the analysis of the spatial correlation of the interferometric phase, so it is applicable to low-amplitude natural targets (Sousa et al., 2010, 2011).

Several other approaches have been proposed for the processing of multi-interferometric long series of SAR images; most of them have been satisfactorily compared by [Raucoules et al., 2009](#).

The intrinsic features of the satellite InSAR techniques make them especially useful for analysing natural phenomena which induce terrain deformation, such as volcanic activity, earthquakes, land subsidence, instability phenomena ([Massonnet and Feigl, 1998](#)). The first application of these techniques to the study of natural events was developed in the '70s ([Graham, 1974](#)).

Focusing the attention on the InSAR analysis of the slope instability, the launch of the ERS-1 satellite in 1991 significantly promoted the development of these applications. In [Mantovani et al., 1996](#) and then in [Metternich et al., 2005](#) and in [Guzzetti et al., 2012](#) comprehensive reviews on the application of remote sensing techniques for landslide studies can be found.

Space borne InSAR techniques have been proved to be very useful and effective in landslide mapping and monitoring, permitting high precision measurements over wide areas, also thanks to the presence of data archives that cover long periods and date back to the early nineties. The analysis can be applied at different spatial scales, to detect single or multiple landslides and covering small to very large areas.

As regards landslide analysis, the homogenization of the radar datasets with the ancillary data (such as topographical and geological maps, optical images etc.) managed in GIS (Geographical Information System) environment allows us to easily produce inventory maps and monitoring reports, following the methodology illustrated in Figure 11.

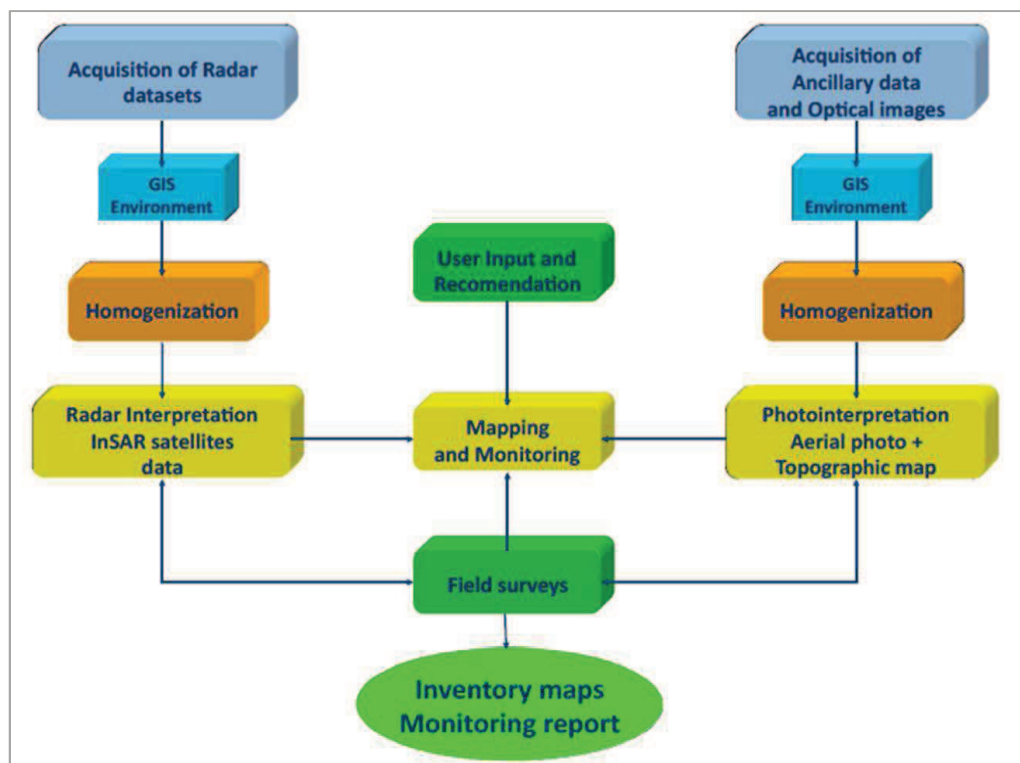


Figure 11. Schematic representation of the InSAR data analysis to produce landslide inventory maps and monitoring reports.

The following table (Table 3) schematizes the main advantages and the principal drawbacks of the PS-InSAR techniques (<http://treuropa.com/>).

ADVANTAGES	LIMITATIONS
<ul style="list-style-type: none"> - Regular updates over large areas; - Cost-effective; - High PS density (up to 1000 PS/km²); - Fast data processing/low user interaction; - High accuracy; - Data easily imported in GIS; - Availability of historical archives; - Possibility to exploit historical archive (mainly provided by European Space Agency and Canadian Space Agency) 	<ul style="list-style-type: none"> - Vegetated and forested areas prevent any PS-InSAR data processing; - Low-reflectivity areas (e.g. smooth surfaces and certain materials); - Temporal sampling limited by satellite repeat-cycles; - Only "slow" deformation can be measured (<10 cm/y in LOS); - Geometrical distortions; - Limitation of time measurements in relation with the satellites' orbiting intervals.

Table 3. Principal advantages and main limitations of the PS-InSAR technique (<http://treuropa.com/>).

1.2 Ground based InSAR

The physical principles of the InSAR techniques can also be applied to data acquired by ground based platforms. The possibility of applying this technology to ground based instruments (defined GB-InSAR) provides big advantages: first of all, the possibility to generate high-resolution images, especially for local scale phenomena, like the study of buildings, small urban areas, single hillsides etc. (Luzi, 2010). Monitoring a limited area, ground based InSAR systems have some important advantages with respect to satellite based ones: they offer measurements of much shorter time intervals (minutes rather than several days) and a better spatial resolution without being affected by satellite geometry (Casagli et al., 2010). Acquiring from a fixed position, GB-InSAR systems usually have zero geometrical baselines. These systems can operate within a distance interval ranging from a few meters up to several kilometres from the target area; to obtain good spatial resolutions, the maximum acquisition distance depends on the power of the transmitted signal (Antonello et al., 2004).

These and other features were the cause of the big development of these techniques in the last fifteen years, specifically in the field of stability assessment for buildings and structures and in landslide monitoring.

The first scientific report on the application of this technique to the monitoring of buildings or structures can be found in Tarchi et al., 1997.

In these instruments, the synthetic aperture is obtained through the motion of the transmitter and the receiver along linear rails, which are mounted beside each other in a quasimonostatic configuration; the system is computer controlled and is capable of synthesizing a linear aperture along the azimuth direction. Generally, GB-InSAR systems are continuous wave step frequency (cw-sf) radar, in contrast with the satellite SAR systems that are generally based on standard pulse radar.

The first prototype of a GB-InSAR instrument, named LiSA (acronym of Linear SAR), was developed by the Joint Research Center (JRC) of the European Commission (Figure 12).

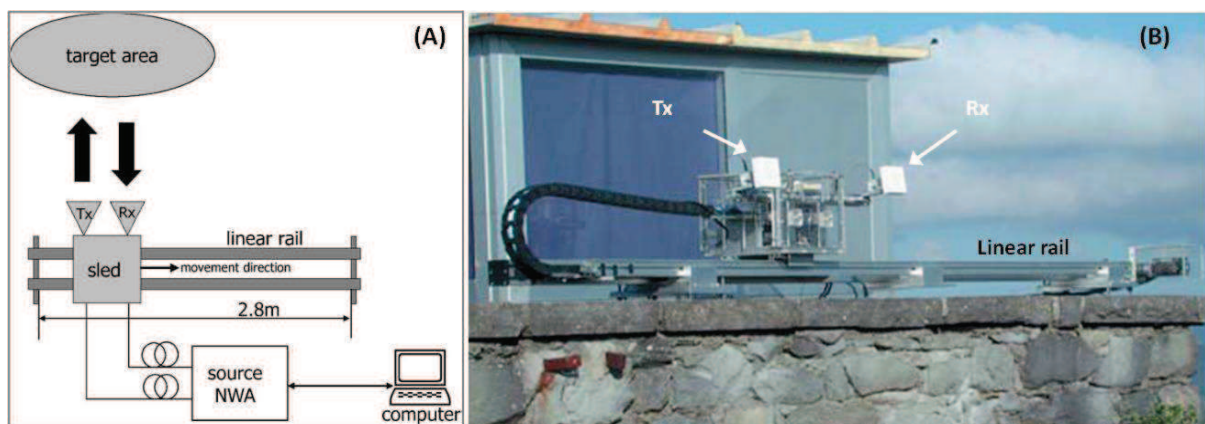


Figure 12. Principal components of a GB-InSAR instrument. Network Analyser (NWA); transmitting antenna (Tx); receiving antenna (Rx) (from: Tarchi et al., 2002).

The sensor was based on a Vector Network Analyser (VNA) for generating the microwave signal, a coherent transmitting and receiving antenna, a mechanical guide and a PC devoted to data acquisition and a control unit (Tarchi et al., 1997, 1999, 2002).

On June 2003, the Ellegi-LiSALab company, a spin-off of the JRC, obtained an exclusive license to commercially exploit this technology; nowadays the company holds an Italian, a European and a US patent on this technology (www.lisalab.com).

Usually, the radar systems can operate in Ku, C and L microwave band, covering an interval ranging between 14.5 and 18 GHz; the used polarization is generally "VV".

When the decorrelation among different acquisitions is low, the interferometric algorithms can be applied, and eventual target movements can be detected. In relation with the deformation rate of the observed phenomena, the time of a single acquisition (*i.e.*, the time to perform the synthetic aperture along the rail) is chosen; the minimum technical time is around a few minutes. Usually, a GB-InSAR is able to detect sub-millimetric displacements for an aerial scenario up to few hectares wide. The instrument is capable of automatic acquisition over long periods; the acquisitions are obtained step by step, during the antenna motion on the linear rail. The step number is defined previously, in relation to the velocity to detect. The rail length generally ranges between 1 and 4 m; the minimum vertex aperture of the observed cone varies between 30° and 60°. The system needs an electric supply, so that the instruments are usually equipped with a *UPS* (uninterruptible power supply) to cover eventual power cuts.

Interferograms and deformation maps are elaborated and visualized by specific software.

In one of the most common LiSA configurations, the range resolution is about 1.5 m and the azimuth resolution, which mainly depends on the target distance and on the rail length, ranges between 3 m (at a distance of 900 m) and 11 m (at a distance of 3300 m), considering a linear rail 3 m long (Figure 13).

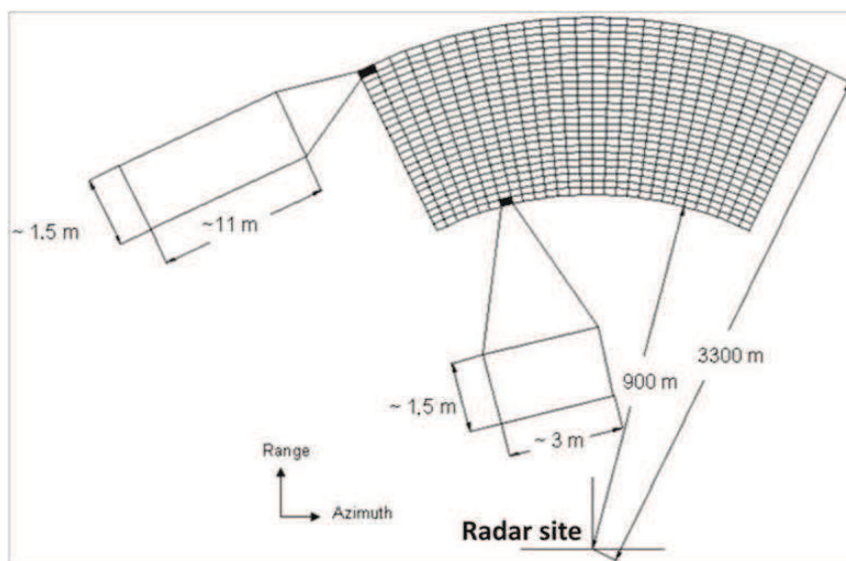


Figure 13. Resolutions of a GB-InSAR in a typical configuration. Specifically, the shown resolution grid is related to the GB-InSAR instrument installed to monitor the San Fratello landslide, occurred in Messina Province on February 2010 (Bardi et al., 2014).

Considering the problem of the phase ambiguity, GB-InSAR systems are able to detect a specific range of displacements. In addition, the repeat time (ranging between 4 and 15 minutes for ground based instruments) influences the maximum velocity value that can be detected. As regards the landslide analysis, taking into account the [Cruden & Varnes \(1996\)](#) classification, the GB-InSAR ordinary applicability usually includes movements characterized by a maximum velocity of about 1.6 m/year (Figure 14).

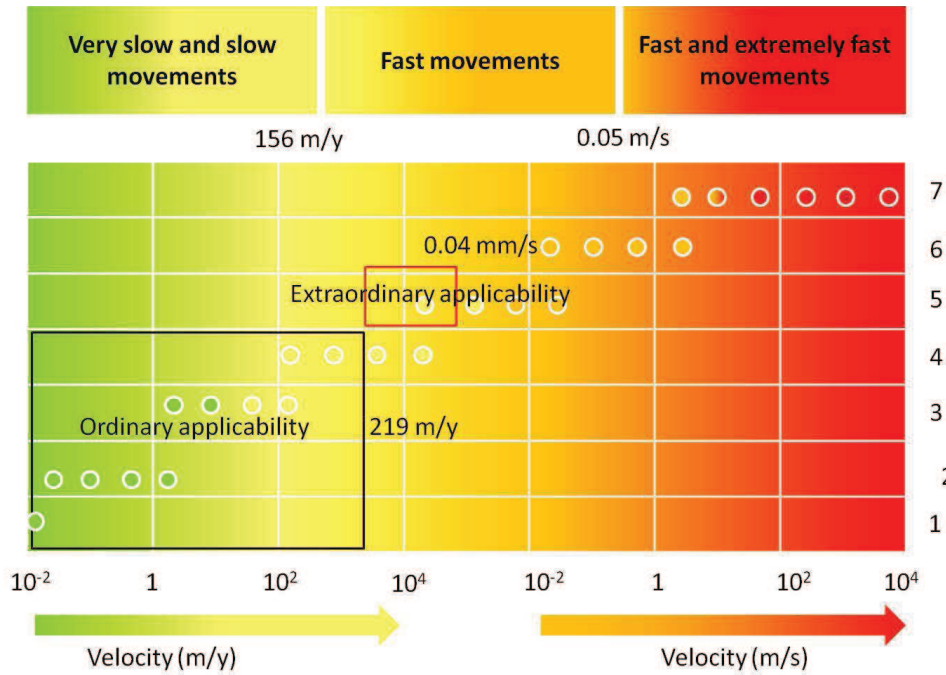


Figure 14. Landslide velocity ranges and related applicability of GB-InSAR monitoring systems (modified from www.lisalab.com). Numbers on the vertical axis correspond to the classes of landslide velocities proposed by [Cruden & Varnes \(1996\)](#).

A synthesis of the main advantages and the principal drawbacks of the GB-InSAR systems in the field of landslide monitoring can be found in Table 4.

ADVANTAGES	LIMITATIONS
<ul style="list-style-type: none"> - High operative flexibility; - High versatility and transportability; - Near-real time measurements (every few minutes) without the need to access the monitored area; - Very high precision of measurements (0.3 – 0.7 mm); - Fast acquisition time: between 5-15 minutes; - Long working distance: up to 3-4 km from the installation site; - Map displacement production. 	<ul style="list-style-type: none"> - Reduced applicability in vegetated areas; - Possibility to detect only the LOS component of the displacement; - Possibility to detect a limited range of velocity values; - Visible area extension: few km²; - Distortions related to atmospheric interactions; - Power supply: the system cannot operate without batteries, generators or solar panels.

Table 4. Synthesis of the principal advantages and limitations of a GB-InSAR system, to monitor landslide phenomena.

In recent years, the increase of microwave technologies has led to the implementation of other different instruments, besides the LiSA; other versions of Linear SAR set-up have been developed (Noferini et al., 2005).

An exhaustive record of the available systems based on radar technique also non-strictly based on SAR principle can be found in Monserrat et al., 2014. Nowadays, besides the LiSA systems, the most employed instruments in the field of slope monitoring are the products of IDS Company (Ingegneria dei Sistemi) (www.idscorporation.com/) and GAMMA Remote Sensing Company (www.gamma-rs.ch/).

The Italian Company IDS (Ingegneria dei Sistemi) started to work on the implementation of GB-InSAR systems in the late 90's, in the field of a research project realized in collaboration with, among the others, the Electronic Engineering Department of the University of Florence. After almost seven years of research, IDS released a commercial, user-friendly interferometric radar in two configurations: IBIS-S for structural applications and IBIS-L, mainly for landslide monitoring (Farina et al., 2011).

Focusing on the IBIS-L configuration (example in Figure 15), the instrument is able to generate microwave signals at definite increasing frequencies sweeping a radiofrequency band. The big difference, compared to the LiSA system, regards the mechanism for generating microwaves: in this case the signal is produced by a prototype of an industrialized method, developed by the Department of Electronics of the University of Florence; the possibility to replace the VNA strongly reduces the weight, increasing the transportability of the system that becomes very useful in emergency conditions. Indeed, later, a new version of LiSA no longer based on VNA was developed, making the instrument faster and lighter (SafeLand, 2011).

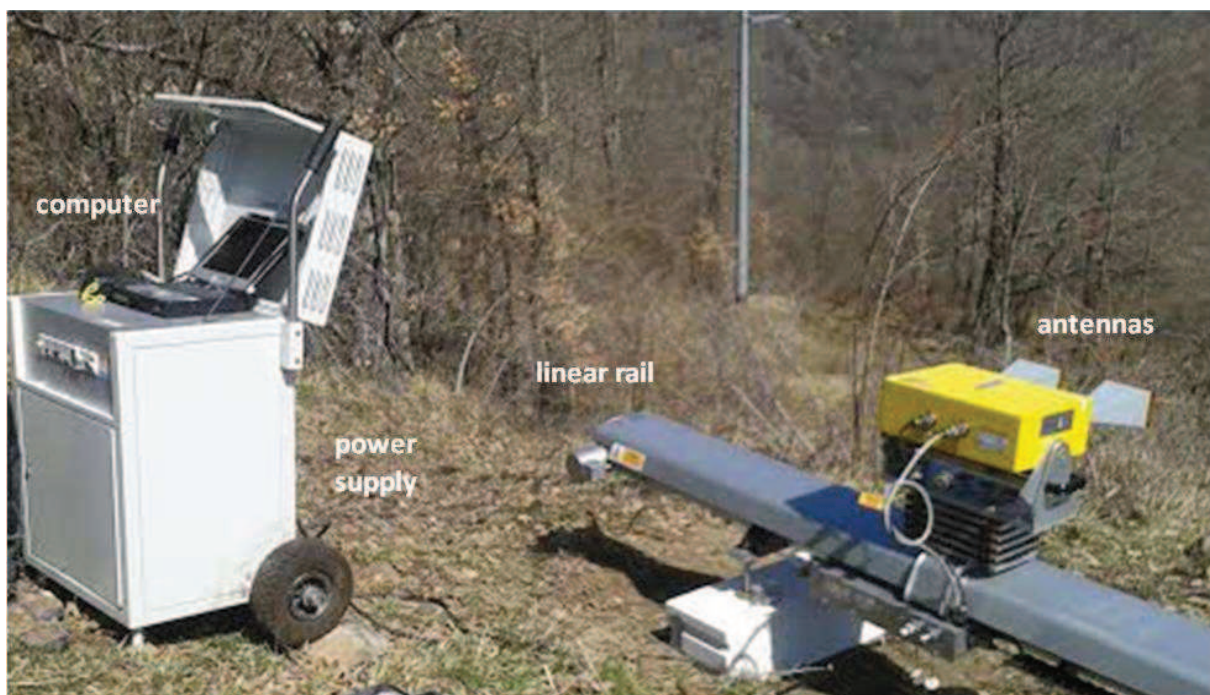


Figure 15. IBIS-L system and its principal components.

A grid representing the typical resolution values of an IBIS-L system in ordinary configuration is shown in Figure 16, together with the characteristic extension of the target area.

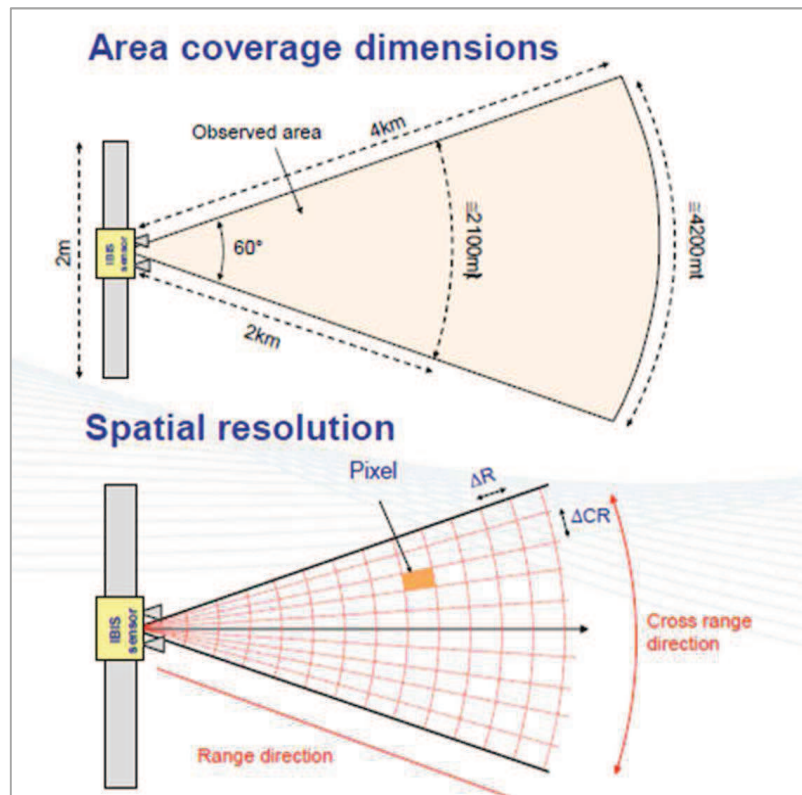


Figure 16. Resolution grid of an IBIS-L system in a typical configuration (from: www.idscorporation.com/).

The ground based system produced by GAMMA Remote Sensing Company (www.gamma-rs.ch; Werner et al., 2008) is a new system which exploits real aperture antennas, one transmitter and two receivers. In this sense it cannot be considered an InSAR system, but it is more precisely defined as an InRAR (Interferometric Real Aperture Radar) system. Other instruments based on RAR principle exist, especially employed in the monitoring of stability of open pit mines (Noon & Harries, 2007; Monserrat et al., 2014). In the case of the GAMMA system, the three antennas are mounted parallel to one another on a rigid 1 m high tower, mounted on a precision rotational scanner. The rotating of antennas on the vertical axis allows us to obtain radar imagery, characterized by high azimuth resolution. The vertical separation between the two receiving antennas permits the formation of a spatial interferometer, that is useful for measuring height information (Werner et al., 2008; Strozzi et al., 2012): phase differences between simultaneous acquisitions by these antennas are used to calculate the precise look angle relative to the baseline, permitting derivation of the surface topography; expected statistical noise in the height measurements is on the order of 1 meter. Phase differences between successive images acquired from the same location are used to determine line of sight displacements. The instrument works using a 17.2 GHz frequency and has measurement sensitivity better than 1 mm. Moreover, the antennas can be tilted vertically to illuminate the

region of interest. In elevation, the antennas have a beam width of approximately 45° . Other components of the instrument are the scanners, a digital chirp generator, an analogue to digital converter, a computer and a microwave assembly, that contains the transmitter and the receivers. This technique uses continuous wave step frequency (cw-sf) approach, that is well suited for near-range imaging. A scheme of GAMMA's portable radar interferometer and its components is shown in together with a photo of the instrument (Figure 17).

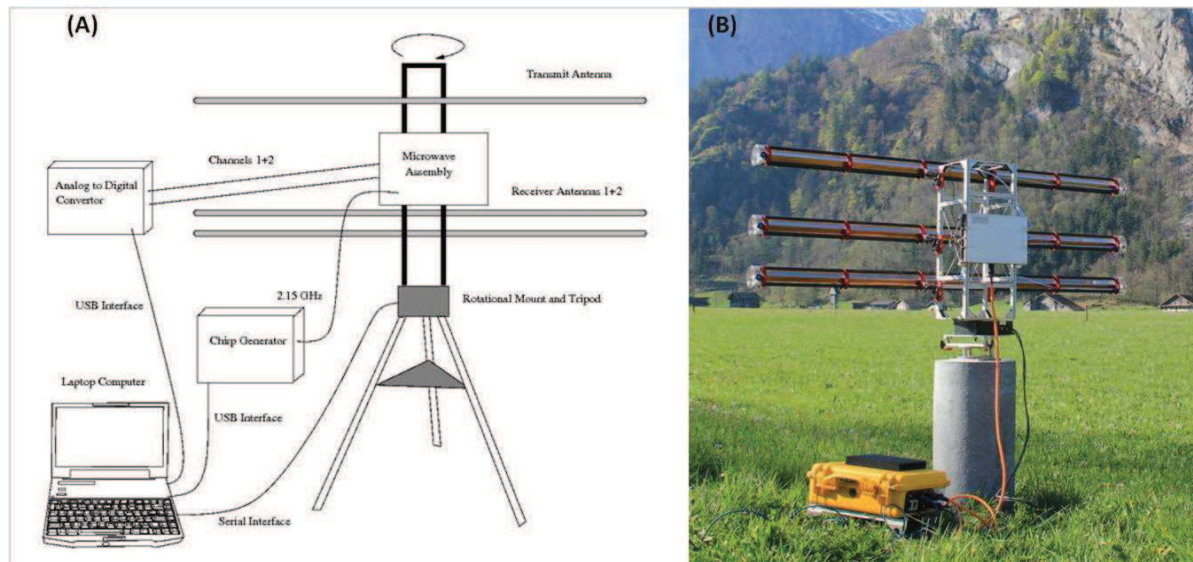


Figure 17. (A) Schematic representation of the components of the GAMMA interferometer (from: Werner et al., 2008. (B) Photo of the instrument.

For further information, another new generation instrument must be introduced. It is the Multiple-input and Multiple-output (MIMO) radar. This technique, implemented by JRC, is based on the principle that independent signals are transmitted through different antennas, and that these signals, after propagating through the environment, are received by multiple antennas (Bliss et al., 2006). This system produces a temporal resolution improvement, in fact MIMO system has larger number of degrees of freedom, because it can work with multiple simultaneous waveforms at multiple receivers (Wang et al., 2008). Specifically, MIMO SAR uses M orthogonal waveforms, each transmitted from different phase centres, and N received phase centres (Sammartino et al., 2010; Tarchi et al., 2012). This is the substantial difference in respect to current SAR, because this one uses closely spaced antenna arrays, instead in new MIMO system at each of the receive phase centres, the received signals are match filtered for each of the transmitted waveforms forming $M \times N$ channels (Wang, 2011). Picture (Figure 18) below shows a diagram of the MIMO SAR acquisition system and a photo of the new JRC radar system, based on the MIMO technique, named MELISSA that is the acronym of MIMO-Enhanced Linear Short SAR (Tarchi et al., 2012; Sammartino et al., 2014).

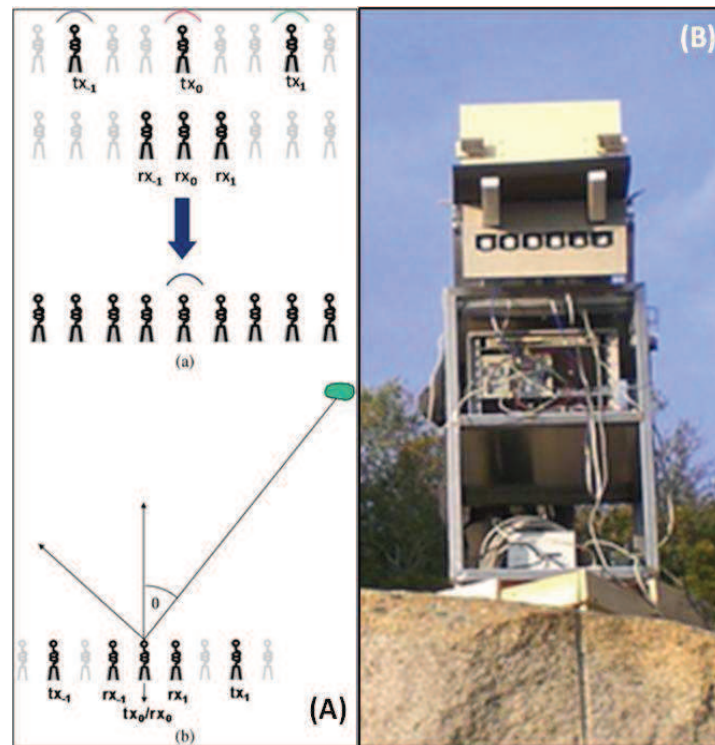


Figure 18.(A) Sketches of MIMO configurations. (a) MIMO transmit array (top), receive array (middle) and equivalent Nyquist-spaced array with one element only transmitting (bottom); (b) MIMO geometry for deriving equations (Tarchi et al., 2012). (B) A photo of the MIMO technology MELISSA, applied in the Costa Concordia Emergency.

MIMO has not yet been tested on instability phenomena. Nowadays, its first and only application regards the monitoring of the movements of the Costa Concordia ship, which wrecked on the Giglio Island Coasts on January 2012 (Sammartino et al., 2014).

1.3 Landslide InSAR monitoring

According to the Cruden (1991) definition, the term “*landslide*” refers to “*the movement of a mass of rock, debris or earth down a slope*”; hence, it is a generic term which includes a wide range of mass movements (e.g. deep failures, slides, shallow mudslides, debris and earth flows, rock falls and so on).

Landslides represent one of the natural hazards that most frequently occur worldwide; they are the main geomorphologic process by which landscape evolves, encompassing a wide range of surface deformation and displacements. The occurrence of landslides is more widely distributed than earthquakes and volcanic activity (IGOS, 2004) and it represents one of the main causes of fatalities by natural hazards in the world (Figure 19).

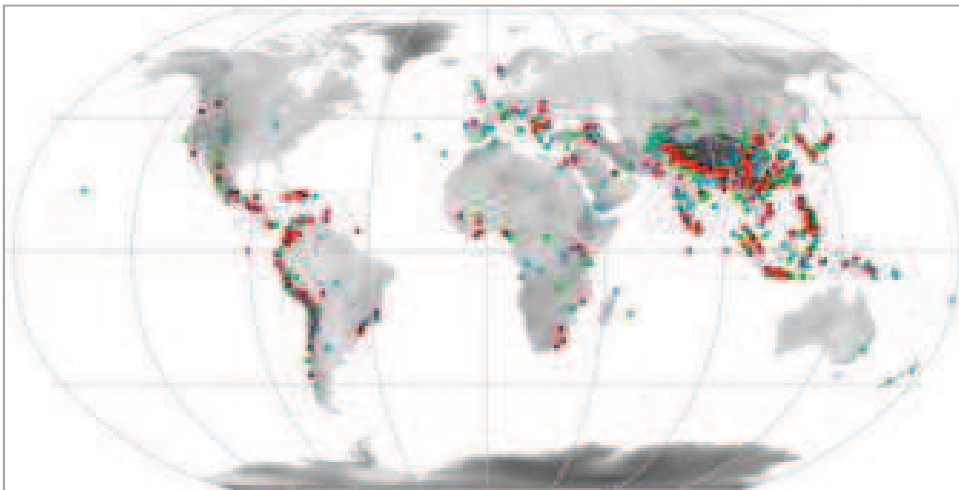


Figure 19. Worldwide distribution of fatal landslides in 2008 (red dots), in 2007 (blue dots) and in 2006 (green dots) (AGU, 2010).

All the landslide typologies are characterized by the displacement of solid material driven by gravitational forces, resulting in actions at different depths and with different velocities and involving a great range of volume of material. The action of gravity and the reduction of the shear strength of material are of course the primary forces for the occurrence of a mass movement, but landslide phenomena are the result of a complex interaction of a large number of interrelated factors. First of all, it is necessary to take into account the predisposing factors, which are specific surface conditions that make the slope susceptible to failure, such as soil and rock geo-mechanical properties, geomorphic and geometrical features of the slope (gradient and aspect), soil lithological properties, land coverage characteristics. In fact, a landslide often requires a triggering or dynamic factor before being released. The most typical trigger is intense or prolonged rainfall; besides this, a rapid snowmelt, volcanic eruptions, earthquakes, undercutting of toe slope by rivers or sea waves, wildfire and permafrost thawing in response to the increase of global temperature can be responsible for landslide activation. Human activities, like deforestation, land use changes, heavy load imposition, slope excavation, rapid

reservoir drawdown, blasting vibrations, and water leakage from utilities can induce the landslide trigger.

Scientific attention to the problem and the related studies conducted over recent years has revealed that the knowledge of the phenomenon is the first step toward its understanding and prevention of disasters.

In 1991, Brabb wrote: *"Thousands of people may be killed by landslides each year and property damage may be in the tens of billions of dollars, but the techniques for recognizing and coping with landslide are well developed. Landslides are generally more manageable and predictable than earthquakes, volcanic eruptions, and some storms, but only a few countries have taken advantage of this knowledge to reduce landslide hazards."*; the sentence emphasizes the importance of landslide monitoring systems since the early '90s.

In fact, the results of monitoring represent an important tool for landslide risk assessment and mitigation, which is one of the main goals of the scientific community.

This monitoring can be managed in *"real time"* or in *"deferred time"*; during *"real time"* (measurable in hours or less, days or months) the performed emergency activities include urgent, immediate actions such as event now-casting, containment of effects, assessments of evolving hazards, countermeasures for risk mitigation, residual risk assessment and restoration of previous living conditions.

On the other hand, research, forecasts and prediction aimed at guaranteeing permanent safeguard of human lives and property over the long term are carried out in *"deferred time"* (measurable in months, years or decades).

The use of conventional methods for landslide mapping and monitoring takes a big advantage of remote sensing techniques both in real and in deferred time; these advanced techniques allow systematic and easily updatable acquisitions of data over small and wide areas. With respect to the conventional, ground-based techniques, remote sensing methods are more cost effective and, thanks to the generation of synoptic views of the investigated area, allow us to optimize and prioritize field work.

Among the many new technologies used in landslide investigations, InSAR interferometry is one of the most established remote sensing methods. It is widely exploited by geomorphologists primarily to measure, at specific points, ground deformation, and to construct time series of displacement. The so-called *"radar interpretation"* (Farina et al., 2003, 2006; Casagli et al., 2008; Herrera et al., 2009) consists in the assignment of a geomorphological meaning to the results of the interferometric analysis.

On one hand, the availability of archives for satellite InSAR data (such as those provided by ESA satellites ERS and Envisat) allowed geologists and geomorphologists to map and monitor slow ground movements and to reconstruct the extent and the magnitude of ground motion over a target area. The *"hotspot mapping"* approach was introduced: it consists in coupling and integrating PS-InSAR and optical data for the detection of extremely slow to very slow moving mass movements (according to the classification provided by Cruden & Varnes, 1996), to

identify the “hotspots” that are the sites characterized by high hydrogeological hazard/risk (Bianchini et al., 2012; Raspini et al., 2013). Indeed, the intrinsic characteristics of space-borne interferometry provide high precision measurements over wide data. SAR-based information can be exploited at different scales, to detect single or multiple landslides, from large (1:5.000) to very small (1:500.000) scale, and covering small to very large areas (*i.e.*, extension ranging from 1 to thousands of km²).

On the other hand, the versatility and very high transportability of ground based interferometers allow an increase in the detail of the landslide monitoring. In general, dealing with landslide monitoring, the most critical issue is the time needed to refresh a single image of the target area (*i.e.*, the time to acquire/generate an updated image of the area under investigation). Ground-based interferometers are able to acquire data every few minutes, becoming the crucial method for obtaining precise, accurate and comparable results (Tarchi et al., 2003; Leva et al., 2003). Thanks to these performances and to these acquisition capabilities, it is possible to perform near-real time monitoring. The technique can provide multi-temporal deformation maps, with a spatial resolution of a few meters and an accuracy in the displacement assessment within millimetres along the LOS system. It is very effective on unstable areas with a spatial extension of several square kilometres (0.1-5 km²) and it can be exploited to monitor mass movements characterized by different failure mechanisms, materials involved, kinematics, water content and deformation rate. Compared to other geotechnical instrumentations, the spatially distributed information and the remote sensing data can be used to improve the understanding of the deformation field of the observed phenomenon, as well as augmenting the frequency of data acquisition in areas not normally accessible. Thanks to the possibility of obtaining information of the entire observed scenario, the system can be employed as a support to traditional monitoring networks, both in the design phase of monitoring systems (*e.g.*, for the optimization of the sensors arrangement) and to obtain information from inaccessible or fast-moving areas. Moreover, the instruments can be installed in significant positions and can be employed for long duration campaigns of measurements, as a permanent monitoring system, in the so-called "continuous" configuration mode. It is also possible to install and dismount the system at each campaign ("discontinuous" configuration mode (D-GBSAR), Crosetto et al., 2014), increasing the chances of monitoring slow deformation phenomena; indeed, this last configuration allows us to revisit a given site periodically, *e.g.* monthly, yearly, etc. depending on the kinematics of the deformation phenomenon at hand and the monitoring requirements (Noferini et al., 2008; Luzzi et al., 2010; Crosetto et al., 2014).

The short time needed to install the instrumentation and the flexibility in terms of the acquisition parameters make the system robust for landslide monitoring during emergencies (Antonello et al., 2004).

In literature, many articles can be found regarding the application of GB-InSAR systems in landslide emergency conditions; some examples can be found in Luzzi et al., 2004; Casagli et al., 2009, 2010; Gigli et al., 2011; Intrieri et al., 2012; Di Traglia et al., 2012, 2013.

2. Ground based InSAR optimization

Part of the PhD programme regarded the attempt to improve the applicability of the InSAR techniques in the field of early warning for landslides, through the optimization of ground based InSAR techniques. How this purpose was achieved, the relative results obtained and some applications are described in this chapter.

Considering as a starting point the main limitations and the principal advantages of the technique (Table 4), the objectives were to partially overcome the drawbacks and try to increase the benefits and improve performance.

Optimization was performed in three steps:

1. the improvement of the hardware features of the typical GB-InSAR instruments, exploiting and testing a prototypal system implemented by the LiSALab Society (the LiSA-Mobile system);
2. the optimization of the features of the GB-InSAR software, with the elaboration of new algorithms;
3. the integration between ground based and satellite InSAR data aimed at landslide early warning, taking into account the use of new generation satellite data for near-real time monitoring activities.

In the next sub-chapters these three steps are described separately.

2.1 Hardware features

One of the most important advantages of ground based InSAR systems is related to their high operative flexibility and their versatility and transportability. Indeed, when a landslide occurs, generally the short time available to manage the situation needs monitoring systems of rapid installation and characterized by the possibility to adapt *in situ* their acquisition parameters to the observed scenario. GB-InSAR instruments well answer to these requirements, becoming particularly useful both in emergency situations and in long term monitoring activities. In order to increase these advantageous characteristics, an attempt to improve the hardware features of an existing GB-InSAR system was made. The prototype is a specific instrument produced by the LiSALab Society and named LiSA-Mobile, in relation to its specific characteristic of transportability.

Normally a GB-InSAR system consists of specific components:

- a **linear rail** along which two antennas move with millimetric steps, to define a synthetic aperture;
- the microwave **transmitter**, that produces, step by step, continuous waves around a centre frequency; it moves along the rail, observing a portion of the scenario determined by the field of view of the real antenna;
- the **receiver**, that records the amplitude and the phase of the microwave signal backscattered by the target;
- the antenna support;
- the **power base**, containing a *UPS (Uninterruptible Power Supply)* to guarantee constant electric supply, and boards to increase memory.

The planned system maintains the characteristics of precision and accuracy of a classical GB-InSAR, with some new features that allow easier and faster instrument installation.

First of all, the “new” system is conceived in a modular configuration: the main components are separately arranged in order to reduce their weights and dimensions. Each hardware component of this implemented system is described below, emphasizing the changes that contribute to the achievement of the defined goals.

The **linear rail** is 210 cm long, allowing a synthetic aperture of maximum 180 cm. It is easily transported by a normal motorized vehicle but its length is enough to obtain high resolution images, also at a distance from the scenario that can reach more than 1 km. The linear rail can also be replaced with another characterized by different lengths, answering to the specific needs of the observed scenario: for example, when the logistics require installation far from the landslide phenomena, the system can be implemented with a longer rail, to increase the azimuth resolution also for the farthest targets. In order to have an idea of the variation of the azimuth resolution values in relation to the linear length, we can consider that, by using the frequency value of 17.2 GHz, at a distance of 2 km far from the instrument location, it is

possible to obtain a resolution of 17 meters with a rail 2 meters long; this resolution reaches the value of 11 meters, by using a rail 1 meter longer (in total 3 meters). At a distance of 3 km from the installation point, the azimuth resolution is 25 meters using a linear rail 2 meters long, and 17 meters, with a rail 2 meters long, maintaining the frequency term constant (17.2 GHz).

The **transmitter and the receiver**, that move on the rail on a specific support, have been optimized in order to allow for changes in the vertical aperture: it is possible to reach a vertical aperture angle of about 60° (with respect to the 40° of the previous version). Moreover, the sensor can be tilted along the antenna axis to direct the antenna beam to the object under observation. This "mobility" allows for monitoring areas located at a lower and/or bigger elevation than the installation point. It is also useful in those situations where the scenario is represented by quasi-vertical slopes; in these cases, a GB-InSAR capable of horizontal light is not suitable for observing eventual displacements, having a LOS perpendicular to the supposed movement; by rotating the antennas, it is possible to change the LOS direction by some degrees, allowing the monitoring of vertical slopes too. As regards the lateral view, an antenna along a linear guide has a view that theoretically could be 180°, but in practice is about 90°, given that a physical antenna has a beam that cannot cover 180°. Therefore, being able to change and tilt the antennas represents a valid tool to change the irradiated area in relation with the monitored scenario.

The **power base** represents the control centre of the system; it contains a personal computer that manages the definition of input parameters used in the acquisition phase and a *UPS (Uninterruptible Power Supply)* to guarantee constant electric supply; it also works on data elaboration and as a storage data platform, in fact it is equipped with two boards increasing the memory to 1.8 TiB.

Therefore this component has mainly three roles:

- input features management, allowing the operator to choose the most useful parameters, in relation to the observed scenario;
- the guarantee of a constant power supply;
- data elaboration and storage.

As regards the input features management we must note the fact that the instrument is conceived to be flexible also in terms of acquisition parameters, rendering it useful in various scenarios. It is possible to define the **radiofrequency bandwidth** that influences the resolution; this parameter is generally fixed on the Ku band of the microwaves, because it represents the best compromise between the availability of allowed frequencies and the possibility to obtain good results for measuring target displacement by using this type of instrument. This centre frequency determines the interferometric sensitivity, *i.e.* the minimum measurable displacement, usually smaller than the correspondent wavelength: when the transceiver operates at Ku microwave band, a sub-millimetric sensitivity can be gained. It is also possible to define the **frequency steps** and the **number of the mechanical steps on the rail**, influencing the maximum detectable velocity values and, once again, the output data resolution. Therefore, the minimum and maximum **range distance** (distance between the interferometer and the

monitoring targets) can be selected; it generally varies from 10 meters up to 4.5 kilometres and, in specific cases it is possible to choose between different range options: from 10 meters up to 500 meters; from 10 meters up to 1500 meters; from 10 meters up to 2500 meters and from 10 meters up to more than 2500 meters.

Another important advantage of the technical improvement is given by the possibility to choose the **synthetic aperture length**. In relation to the observed scenario and the velocity of the analysed displacement, a bigger or shorter aperture could be useful to analyse faster velocities than those typically detected by these instruments. Indeed, the use of a shorter aperture allows more acquisitions in shorter times and, consequently, more interferograms in reduced spans. Obviously, a shorter synthetic aperture corresponds to a reduction of the azimuth resolution that could be compensated for by installing the instrument as near as possible to the observed scenario. This “fast acquisition” method was first tested to monitor the landslide of Tizzano Val Parma: in April 2013, the Tizzano Val Parma village, located in the Emilia Romagna Region (northern Italy), was affected by a large landslide that started as a rotational slide and evolved in an earth flow. In the emergency phase, in May 2013, a LiSA-Mobile system was installed. Thanks to the possibility of being able to choose the synthetic aperture length, in the early period, when the landslide moved very fast (about 70 meters per day), two acquisition modes were predisposed: one to detect the higher velocities of the landslide body, with a synthetic aperture only 1 meter long; another to detect the slower movements affecting the areas contiguous to the landslide, involving two villages (Capriglio and Pianestolla) and some cultivated areas. More information about this landslide and the monitoring system, still active in Tizzano Val Parma, can be found in the paragraph 4.1 of this thesis. Thus, the possibility of acquiring two configurations and to detect displacement values bigger than the defined limit of 0.04 mm/s (Figure 14) represents an important step ahead in the development of the technique.

As regards the power supply, generally the classical GB-InSAR systems require 220/110 VAC and 50/60 Hz and an absorption power of electric supply ranging between 0.15 and 0.82 kW (LiSALab, 2010). As regards the LiSA-Mobile, it needs 820 W, 230 VAC and 50 Hz. The integrated UPS guarantees the continuity of the electric supply in case of necessity, for a period of maximum 12 hours after the power cut.

In the specific case of short time monitoring, a portable power generator can be enough; using a power unit of 5 litre capacity, we have continuous monitoring for about 5 hours, as tested during the first trials of the instrument.

Another important step in the direction of improving the transportability of the instrument is represented by its supports: the new system is designed to be installed on two high transportable tripods, very easy to move, but at the same time capable of supporting the instrument's weight.

The total weight of the instrument is 95 kg, equally distributed over the different components. It allows easy transportation and installation: tests proved that two operators are able to complete the setting up in a maximum of 30 minutes; no tools are required for the installation.

The main hardware components of the system are shown in Figure 20.

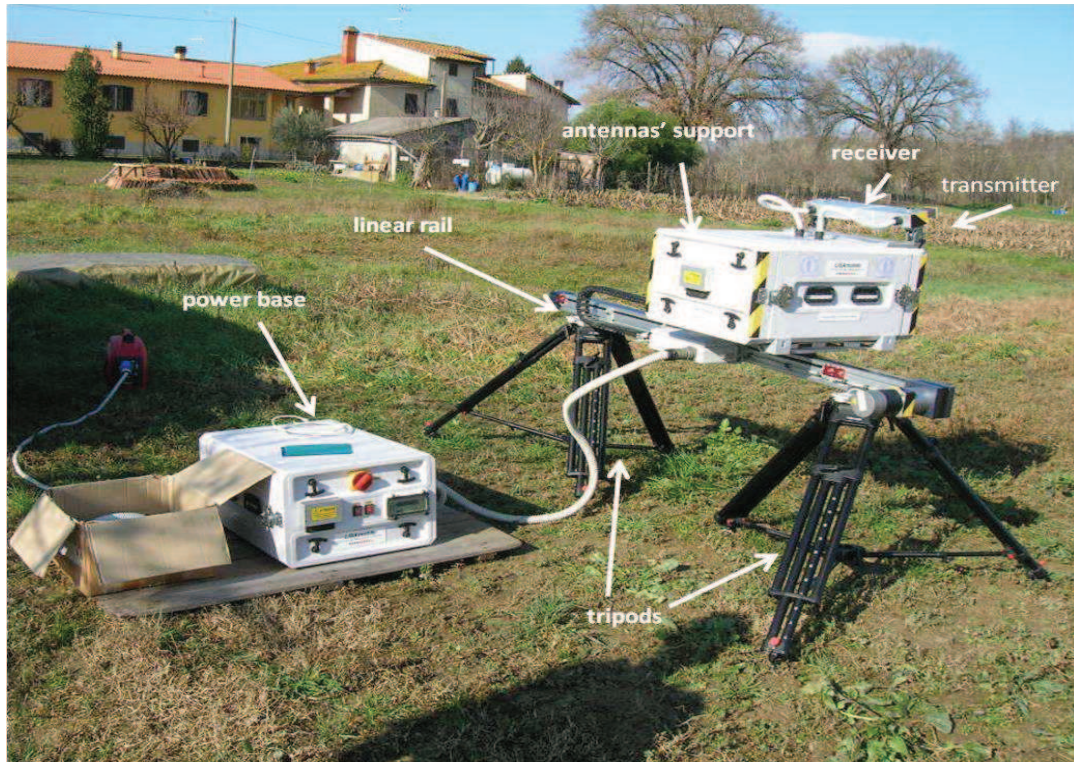


Figure 20. Components of the LiSA-Mobile system.

Below, a synthesis of the most used technical features of the instrument is listed:

- *Range* distance from the scenario: from 10 m to 4500 m, choosing between four different options (from 10 m to 500 m; from 10 m to 1150 m; from 10 m to 2500 m; from 10 m up to more than 2500 m);
- *Band frequency*: from 17.1 GHz to 17.3 GHz (Ku band);
- *Range resolution*: between 0.38 m and 0.75 m;
- *Azimuth resolution* (500 m far from the installation point): 2.18 m.

In conclusion, the improved system is more transportable, thanks to the modularization of the components and the reduced weight of its components; it is characterized by more versatility in terms of acquisition parameters and it is capable of functioning in different configurations, detecting displacements characterized by different velocity values.

2.2 Software features

As regards the improvement in the software features, attention has been focalized on one of the main limitations of the applicability of the technique: the atmospheric effects (Luzi et al., 2004). Separating these contributions from the others is not easy, but it is necessary in order to retrieve the displacement information from the interferometric equation. Indeed, InSAR measurements are often significantly affected by this type of problem, as the radar signals propagate through the atmosphere whose state varies both in space and in time; independently from the presence or absence of rainfall, eventual variations of air temperature and humidity values contribute to produce a phase shift in the reflected wave.

In the used frequency band, the atmospheric delay is independent of frequency and is a function of changes in the refractive index, Δn . In turn, this index is related to temperature, humidity and pressure differences. Microwaves are most sensitive to humidity changes. By applying the relation proposed by Zebker et al. (1997), at a distance of 1 km, with a temperature of 20°C, under atmospheric pressure, the atmospheric effect induced by a humidity change of 1% along the propagation path is about $\pi/4$.

Considering the importance of the atmospheric effects on the wave phase, one of the main steps of the InSAR data processing consists in the atmospheric correction. There are at least two approaches to obtain this correction:

- the use of meteorological observations (temperature, humidity and pressure) by evaluating the shift (an example can be found in Iannini and Guarnieri (2011))
- the determination of the atmospheric delay by its estimation at stable targets (ground control points) also applying spatial interpolation algorithms or filters (an example can be found in Luzi et al., 2010).

The relation between path delay and atmospheric parameters can be determined only under the assumption of a uniform atmosphere (constant atmospheric parameters). Obviously, the larger the distance between weather station and target, the larger the errors induced by this assumption. This limitation is reduced if the atmospheric delay is estimated for each time step using phase observations of ground control points (*i.e.* targets with null displacement values). In correspondence of the stable targets, the phase only depends on the atmospheric component and the random noise. This approach, thanks to its easy applicability, is the most widespread; it considers the atmospheric signal composed of the spatial low frequency component. The principal drawback of this method, and in general of all methods using the GB-InSAR data themselves to determine the atmospheric contribution, is that they rely on stable targets being correctly identified. If the selected points are not stable, the low frequency component of the displacement signal will be regarded as atmosphere and neglected.

Moreover, this method allows us to define the atmospheric variations only in the range direction and by assuming a linear relation between the effect of the atmosphere and the distance instrument-target. Effectively, the longer this distance, the greater the effect of the atmospheric interaction will be; but it is not true that this relation is always linear. Actually, this

approximation is not always acceptable because the relation is intrinsically connected to the characteristics of the observed scenario.

Therefore, on the one hand, the atmospheric variations in cross-range can be estimated by applying two-dimensional interpolation methods or filters, on the other hand, the approximation related to the linear relation between distance and atmospheric delay has to be overcome. An attempt in this direction has been proposed by [Iglesias et al., 2013](#): the authors presented a method which is an extension of already existing techniques, but now taking into account the effect of steep topography in the atmospheric phase screen compensation process.

During the here described activity, an attempt to produce a new algorithm finalized to overcoming this drawback was also implemented, in order to optimize the software features of the existing GB-InSAR systems. The main purpose was to obtain a more flexible algorithm, capable of adapting itself to the variability of the possible situations that depend on the monitoring site features, on the logistic emergency conditions, and so on.

As described above, the usual algorithms define the atmospheric contribution calibrating it in correspondence to several stable targets or a considered stable region on the observed area, and assuming a linear proportionality between the distance and the intensity of atmospheric distortion.

The implemented algorithm is based on the opposite logic: calibration is performed taking into account the entire scenario, discarding the areas considered unstable or potentially unstable, or characterized by low values of coherence or amplitude of the radar signal. Therefore, this algorithm takes into account the variation of the atmospheric contribution over the whole area under observation, assuming great importance in the situations where the scenario is wide and the radar system is far from the targets. Generated in *MatLab* environment, the algorithm is named *REACT*, that is the acronym of *Region-removal Atmospheric Corrective Transformation*. The use of a wide region to calibrate the correction algorithm allows a significant statistical analysis on the relation between the atmospheric phase shift and the target-sensor distance, permitting the definition of a regression function of this relation that is not necessarily characterized by a linear trend. For example, the algorithm application allows for the recognition of cases such as areas where the altitude varies widely where the height differences contribute to the atmospheric effects following a square law.

With the perspective of the application in emergency conditions, the reduction of noise becomes a crucial point; in this sense *REACT* represents a valid step ahead in increasing the data reliability, in near-real time measurements, too.

The main limitation of the implemented algorithm is related to the need of an "*a priori*" knowledge of the observed scenario, in order to correctly distinguish stable from unstable areas. Especially in emergency conditions, where the scenario is generally unknown, and the phases of installation, acquisition and imagery elaboration have to be as fast as possible, opportunities of acquiring "pre-monitoring" information becomes difficult.

However, the new algorithm has been applied on some test sites (Chapter 4), giving good results; an example is shown in Figure 21, where an interferogram acquired on the test site of

A16 highway (see paragraph 4.2) was corrected using both the traditional method (A) and *REACT* (B).

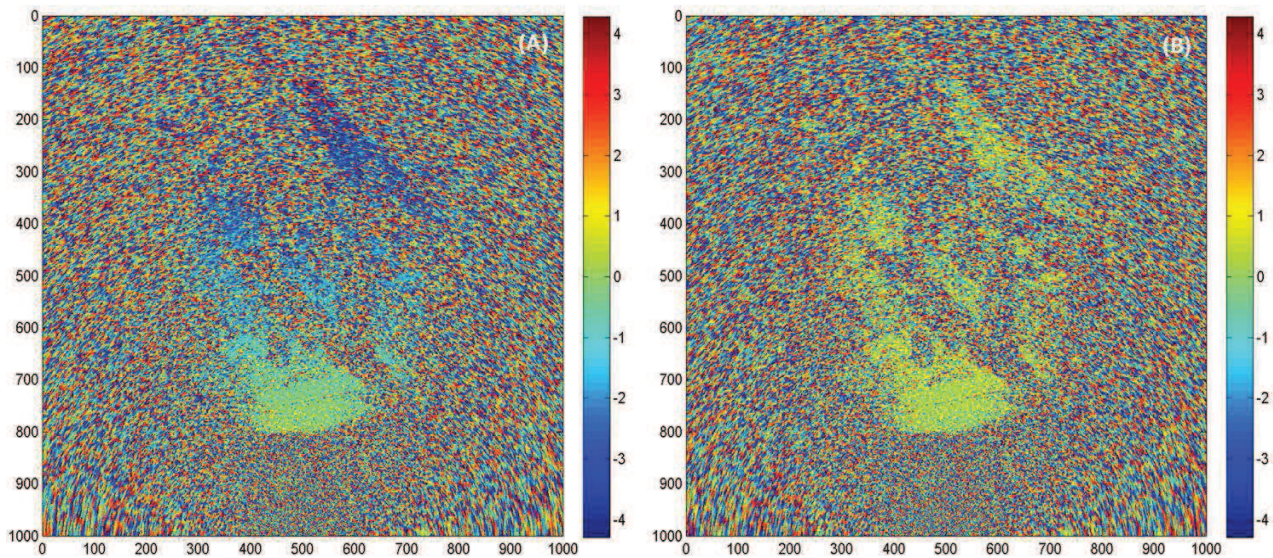


Figure 21. An interferogram created during the monitoring campaign on the A16 test site (see paragraph 4.2) (A) Imagery corrected using traditional algorithms; (B) imagery corrected using *REACT*.

In order to reduce data noise, another improvement on the procedure of data elaboration was developed: as data are traditionally averaged only after interferogram procedure, this improvement consists in the possibility of applying the average to every single image. Thus, the number of pixels characterized by unstable phase values is reduced and the maximum information possible is obtained, also in areas where the coherence has lower values.

In Figure 22 the comparison between an interferogram obtained from averaged data and another produced from raw (not averaged) data is shown; they also refer to the A16 test site.

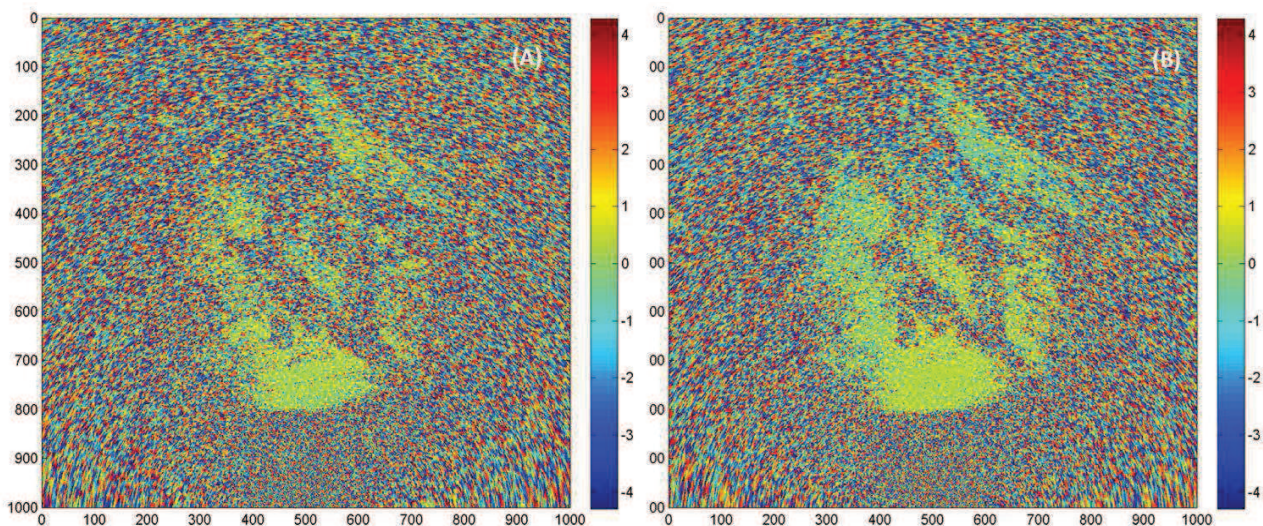


Figure 22. Interferogram related to the A16 test site, obtained from not averaged images (A), and averaged images (B).

In emergency conditions, another point of central attention is characterized by the data transmission, that has to answer to two objectives: it has to reduce the “*in situ*” space where

data are stocked and it has to be as fast as possible so as not to overload the transmission network. In order to absolve these requirements, the data elaboration is generally performed "*in situ*", in order to transmit only elaborated, useful data. When the conditions require the fastest transmission time, the software is transmitted to another PC that works as a control centre for the displacement time series of selected points on the interferogram. From these data, we can characterize the movement and eventually define threshold values and warning levels; in this way, by using the minimum space on the transmission network, a lot of information is obtained. Finally, cutting the interferograms down to the precise region of interest it is possible to transmit them, too, reducing data transfer to the minimum.

In order to answer to these requests, the GB-InSAR systems are equipped with bigger and bigger PCs in terms of memory. For example, the previous mentioned LiSA-Mobile (paragraph 2.1) is provided with a computer containing two more boards than the traditional type, one board for data storage and the other one for *in situ* data elaboration.

More information about the application of the implemented algorithm and the optimized software can be found in the section of this thesis regarding the case studies; specifically in paragraph 4.2.

In conclusion, the new implemented algorithm represents an important step ahead in the field of the GB-InSAR techniques, and it gives satisfactory results when applied on the selected test sites (paragraph 4.2). At the same time, some points have to be enhanced to make an additional step forward in the improvement of the technique applicability. The main goal to be overcome is the limited applicability of the algorithm in unknown conditions, defining a more general method for the assessment of atmospheric contribution on the wave phase.

2.3 Integration with satellite InSAR data

The intrinsic features of ground based and satellite InSAR techniques, specifically considering their advantages and limitations (Table 3 Table 4), make them particularly suitable to be applied together in the field of landslide mapping, monitoring and risk management. Indeed, as widely discussed in the Chapter 1, these techniques are in a way complementary. On one hand, satellite InSAR techniques are useful for monitoring unstable areas only under specific conditions: the main limitations related to its applicability regard the sensor revisiting time, the slope exposure with respect to the satellite LOS, and the velocity of the investigated movements. Nevertheless, the satellite InSAR technique ability of measuring very slow and smooth ground displacements (up to few millimetres per year) represents a valuable support to landslide hazard prevention activities over wide areas, giving the opportunity to detect extremely slow movements that usually occur several weeks or months before the catastrophic failure, preceding major landslide disasters. On the other hand, GB-InSAR allows a continuous monitoring of the displacements from a few millimetres per day up to 1 or more meters per day on a more local scale. Furthermore, the instrument versatility enables the investigation of very steep unstable slopes not visible from the satellite, and it allows us to choose the best LOS. These characteristics make this technique particularly useful for emergency phases.

Because of the above-mentioned characteristics and differences, the integration of these techniques enables us to obtain useful information on ground displacement measurements, with high precision and improved spatial and temporal resolution. In particular, the use of satellite InSAR techniques allows us to perform a preliminary study on ground displacements at basin scale, over a specific area affected by landslides, providing hotspot mapping, which can be useful prior to planning a GB-InSAR system installation for a monitoring campaign.

In this paragraph, an attempt to define a procedure to integrate ground based and satellite InSAR datasets is described, in order to use the results of both the techniques, in those areas where both the data are available. Before starting to describe the integration procedure, an *excursus* on the properties of new generation satellites and their discovered utility also in near-real time landslide monitoring is presented.

2.3.1 The use of satellite InSAR data in near-real time landslide monitoring

As anticipated in the previous chapter, satellite InSAR techniques play a key role in the field of landslide monitoring. Moreover, in recent years, the main limitations of these techniques were partially overcome, making a step forward in the reduction of the problems related to the landslide effects, starting from the increase of the knowledge of the involved scenario, up to the possibility of using also satellite data in near-real time monitoring activities.

To explain this concept, we can start by taking into account one of the main limitations of satellite InSAR techniques: the effects of the satellite repeat-cycles on the obtainable data. The revisited times of the most common satellites notably influence the range of detectable deformation, reducing the technique applicability only to “slow” movements (Cruden & Varnes,

1996). Low frequent temporal sampling also implies an increase of the eventual effect of temporal decorrelation.

The problem was partially solved by launching new constellations of satellites actually characterized by shorter revisited times. These constellations work using the X-band of the microwaves ($\approx 8-12$ GHz), and they were firstly launched in 2008 (Table 2), with COSMO-SkyMed constellation that in a sense opened the way for a "new frontier" in the satellite remote sensing.

These new satellites are able to acquire at least every 16 days, splitting about in half the repeat times of the C-band ($\approx 4-8$ GHz) satellites (ERS, ENVISAT, RADARSAT). The use of X-band microwaves also allows us to obtain an improvement in spatial resolution with respect to the satellites that acquire in C-band. For example, in *Stripmap* configuration, COSMO-SkyMed is able to spotlight an area 40 km x 40 km wide, with 1 m of pixel resolution. By applying PS-InSAR approach to X-band SAR data, the number of detectable PSs notably increases, obtaining considerably wider information besides that obtained from C-band sensors.

As, on one hand, new generation satellites acquire with shorter revisiting times, on the other hand C-band satellite data can be mixed together to reduce their temporal sampling. This method, applied on the PS-InSAR data, consists in a reprocessing of the datasets of two different satellites, recalibrating them in order to obtain maps (cross-interferograms) and time series containing the information acquired by both of the sensors (Colesanti et al., 2003b). The main goal of this method was to stitch coherently the ENVISAT measurements to ERS displacement time series relative to individual PS. To this end, the interferometric phase of point-wise targets was modelled taking into account the different ERS and ENVISAT carrier frequencies. Then, the main constraints to be met at individual PS were identified in order to guarantee the feasibility of coherent stitching.

Very long time series were produced, specifically for the test site of San Fratello, a village located in southern Italy, involved in a landslide event on February 2010 (paragraph 4.3). Stitched data provided time series covering a period from 1992 to 2010. Indeed, this method proves to be very useful in increasing the historical information of each persistent scatterer; moreover, reduced temporal sampling can be provided for those periods in which data were contemporarily acquired by both of the stitched satellites.

This last objective becomes crucial if the considered data are acquired by new constellation satellites, as COSMO-SkyMed, TerraSAR-X, TanDEM-X and so on. In this case, considering that every sensor is still characterized by a short revisiting time (about few days), the stitching of these new sensors could strongly reduce the temporal sampling, considerably increasing the maximum detectable velocity.

Following specific requests of Civil Protection authorities, these new satellites could be acquired every day, providing very useful results for emergency conditions. Certainly, this proposal is relevant only in those areas where more than one sensor acquires continuously.

Actually, COSMO-SkyMed constellation is partially able to acquire every day. In other words, COSMO-SkyMed (that is the acronym for *CONstellation of small Satellites for Mediterranean*

basin Observation) was conceived to work in three different operative system modes, in terms of time performances:

- ROUTINE: the requests of the users pertaining image acquisitions are planned and sent to the constellation **once a day**;
- CRISIS: the request operations are done **twice a day**;
- VERY URGENT: this mode is asynchronous, allowing the servicing of an image acquisition request with **the minimum possible latency**.

The system is capable of satisfying a User Request (that is the ability to deliver the image product required by an End User in a timely manner) within 72 hours for routine mode, 36 hours for crisis mode and 18 hours for very urgent mode. Changing System Modes must be requested to the Government Authorities. Indeed, COSMO-SkyMed mission is commissioned and funded by the Italian Space Agency (ASI) and Italian Ministry of Defence for civilian and defence ends.

The system consists in a constellation of four Low Earth Orbit satellites, each equipped with a multi-mode high resolution X-band SAR, fitted with particularly flexible and innovative data acquisition and transmission equipment. The challenges of the mission are finalized to provide information and services to a number of activities and applications, such as risk management, cartography and planning applications, agriculture, forest, hydrology, geology etc.

In nominal conditions, the four satellites are equiphased in the same orbital plane (Figure 23).

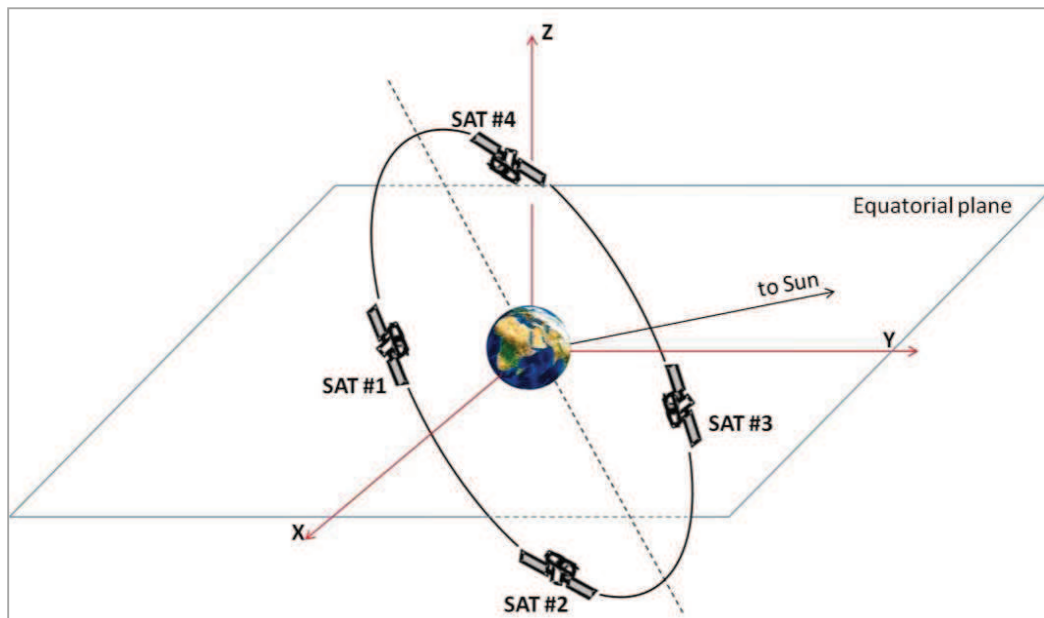


Figure 23. COSMO constellation nominal configuration (modified from <http://www.cosmo-skymed.it/>).

The nominal configuration allows us to provide a global Earth access of a few hours, with the possibility of access to the same target site at least two times in a day, but with different incidence angles (different observing conditions). Beside this, the interferometric orbiting configuration exists: it was conceived to produce three dimensional SAR images and is named

Tandem; in this case two sensors fly in close proximity, achieving the interferometric acquisitions.

The characteristic of this constellation allows, at least for the Italian territory, a notable reduction of the time required to obtain interferometric available data, whose importance is vital in emergency conditions. On one hand, the mission provides a historical archive of non interferometric images, that could be elaborated using InSAR algorithms by mixing them with new acquired *on demand* images of a defined area; on the other hand, *Tandem* acquisitions provide interferometric data in near-real time.

Once the InSAR data become available, the processing phase must start. This is another step that requires time, the reduction of which could represent a big challenge in the field of real time monitoring; in this direction, the employment of user-friendly software could be of great help. An example is represented by NEST (Next ESA Toolbox) that, thanks to its characteristics, not least its open source nature, allows us to strongly reduce the times of data processing. It is produced by the European Space Agency (ESA) under contract by Array Systems. The software is used for reading, post-processing, analysing and visualizing SAR data from ESA missions that include ERS 1-2, ENVISAT, SAR data from JERS, ALOS, TerraSAR-X, Radarsat 1 and 2 and COSMO-SkyMed. It works by using the BEAM platform that is an open source toolbox and a development platform for the viewing, analysing and processing of remote sensing raster data. Originally, BEAM was conceived to facilitate the use of image data from ENVISAT's optical instruments; later it was implemented in order to support a growing number of other raster data formats, among them other Earth Observation (EO) sensors.

NEST includes a function named "*Graph Builder*" that allows the user to sequentially process a stack of SAR images, setting the parameters only once for all the available scenes. The function allows us to automatically set a list of available commands and connect operator nodes which represent the chain of operators necessary to produce the interferograms. Every command is intrinsically related to the previous one, by a cause-effect relationship. In Figure 24 an example of the NEST interface, related to the Graph Builder activity, is shown.

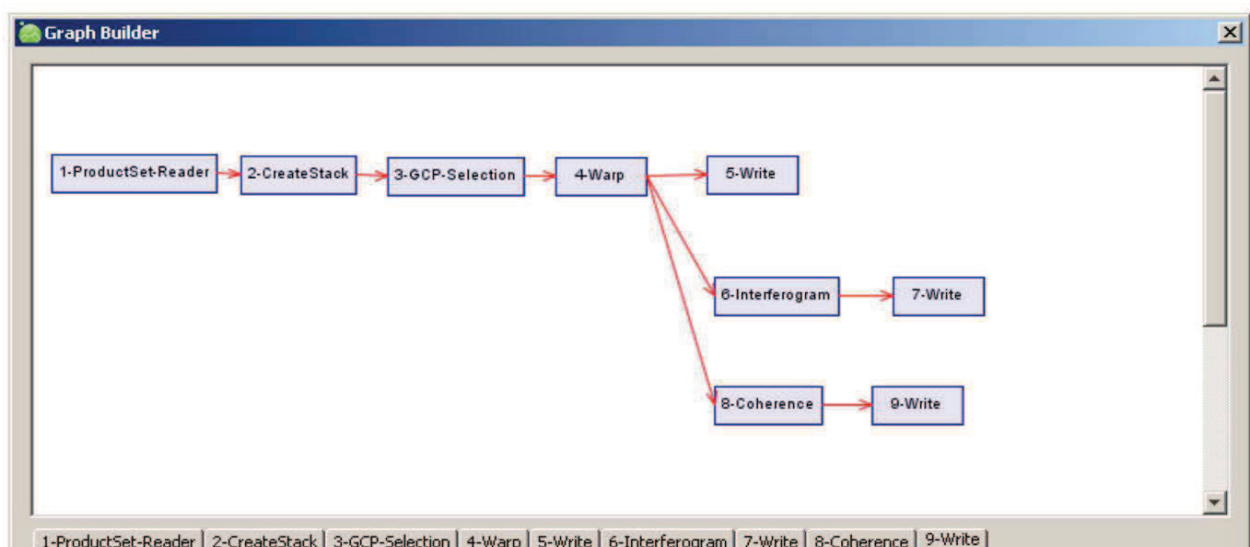


Figure 24. Example of the Graph Builder function of the NEST software.

In the example, the steps for the creation of a series of interferograms performing batch processing by using NEST are shown, starting from the creation of the stack using the available images, and finishing with the generation of the interferogram and coherence maps.

Potentials and effectiveness of the NEST software in terms of processing capability, for the generation of interferograms in a short time, represent an important tool in the application of satellite InSAR data in near-real time monitoring activities.

2.3.2 Integration methodology

In relation with the above mentioned technique features, the integration between satellite and ground based InSAR datasets, in post-processing phase, could represent a valid tool in the field of landslide monitoring, mapping and risk management. In some cases, data integration allows the observation of different aspects of the same event, for example two different displacement patterns, having different geometries; in other cases, such as the test site of San Fratello (Messina Province) or the Åknes rockslide, affecting a Norwegian fjord, data integration is useful to observe the same characteristics of a specific event but from different points of view, allowing us to complete the knowledge of the event, partially overcoming the problems related to the possibility of detecting only the displacement occurring along the LOS (paragraphs 4.3 and 4.4).

Firstly, integration can be achieved with a qualitative and/or a semi-quantitative approach.

The **qualitative approach** is preparatory, allowing us to collect more information regarding the displacement directions and the eventual presence of shadow areas, that are not visible by using only one of the techniques, but that could become detectable by using both of the techniques.

A preliminary phase is characterized by data collection, including the acquisition of ancillary data (*i.e.* orthophotos of the study area, existing landslide inventory maps, the results of geological and geomorphological field surveys etc.) and the available SAR data, acquired both from space borne and ground based platforms.

Data are distinguished, on the basis of the acquisition time, in pre- sin- and post-event datasets and they are compared with each other considering the span time to which they refer. Generally, SAR satellite data cover longer periods than the GB-InSAR ones, thanks to the existence of historical archives resulting from the spatial missions carried out over recent years, starting from 1992 with the launch of ERS-1 satellite. On the other hand, ground based systems generally provide post-, or at least sin-event data, because they are usually installed in emergency phases, when the landslide has already triggered. By using GIS (Geographical Information System) platforms, InSAR data can be easily observed in a two-dimensional geo-referred space. Integrated satellite and ground-based displacement maps can be made to distinguish the areas characterized by displacements from the ones without evidence of movements, following a binary approach (stable/unstable). The combined use of the satellite and the ground-based SAR data can provide ground displacement measurements with high

spatial and temporal accuracy, allowing us to better and more accurately trace the landslide boundaries, as in the case of the San Fratello test site (paragraph 4.3). Therefore, in order to compare the results of both of the techniques, we can study the same area from different points of view and in different temporal intervals.

In order to validate the integration methodology, the results can be qualitatively compared with the available ancillary data, or with the results of scheduled field surveys.

Moving on to the **semi-quantitative approach**, as a first step, it is necessary to take into account that the compared data are characterized by different resolutions, in terms of time and space. So, firstly data have to be homogenized. The level of homogenization that is possible to obtain, considering the features of the available data, defines the integration accuracy.

Generally, datasets with better resolution are re-sampled, reducing their resolution to values comparable with the ones of the other datasets. For example, with respect to the satellites (in the best conditions, new generation sensors are able to acquire every day), ground based systems have a better resolution, indeed they are able to acquire several times per day; however, ground based datasets are rescaled to become comparable with the data acquired by space borne sensors. The same happens for the spatial resolution, where the data are re-sampled referring to the pixel size of the data with coarser resolution (normally the satellite data).

Another important limitation of the quantitative integration is related to the intrinsic feature of the technique to be capable of acquiring only the LOS component of the displacements. Overcoming this problem also allows us, in some occasions, to obtain real displacement values.

In the best conditions, satellite data are available from two different acquisition geometries: ascending and descending. Combining the information obtained by these different geometries, it is possible to extract the vertical and horizontal (in the east-west direction) components of the movement and, consequently, the real vector of displacement (Figure 25).

Once the real displacement is identified, satellite data are compared with ground based datasets, in order to calculate the displacement percentage also detected by GB-InSAR systems. Generally, because of the different acquisition geometries, space borne sensors are able to estimate a small component of the 3D real motions, on the contrary ground based platforms, whose LOS is normally as parallel as possible to the displacement direction, are able to detect a big part of the real vector of displacement.

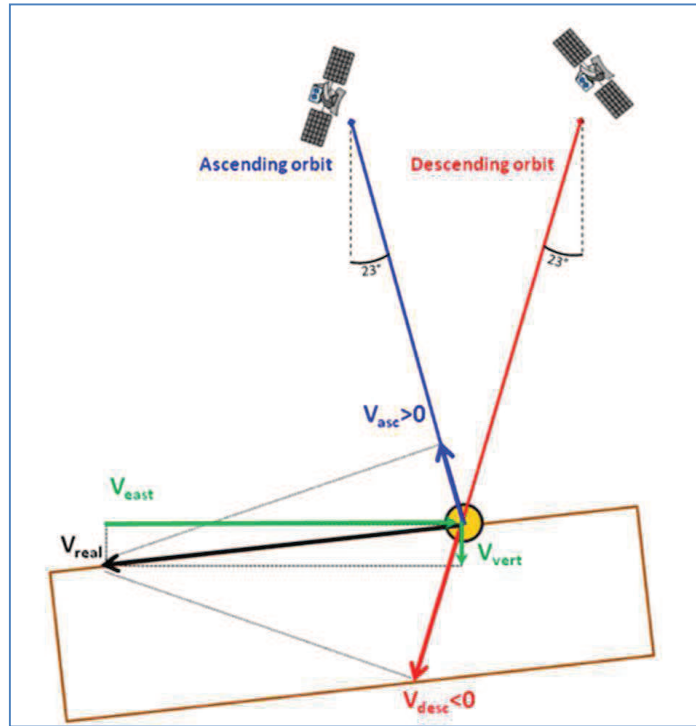


Figure 25. Reconstruction of the real vector of displacement for a landslide phenomena.

Usually, satellite datasets are often available in only one of the possible configurations (ascending or descending). In these very frequent cases, satellite and ground based data are projected on a common direction, considered as the most probable direction along which the real displacement develops. Generally, this direction is approximately considered the downslope direction; it is almost true if the investigated phenomena has a surface rupture as parallel as possible to the topography, that is typical of translational slides. The methodology used for the projection is described in [Colesanti & Wasowki \(2006\)](#) and later in [Cascini et al. \(2010\)](#), [Herrera et al. \(2013\)](#) and [Bardi et al. \(2014\)](#). The input data give the angular values of *Aspect* and *Slope* (derivable from the Digital Terrain Model) of the area affected by the investigated landslide phenomena and the *Azimuth* angle and the *Incidence* angle of the LOS, both from the satellite and the GB-InSAR.

After calculating the direction cosines of LOS and Slope (respectively functions of *Azimuth* and *Incidence* angles and *Aspect* and *Slope* angles) in the directions of Zenith (Z_{los} , Z_{slope}), North (N_{los} , N_{slope}) and East (E_{los} , E_{slope}), the coefficient C is defined as follow:

$$C = Z_{los} \times Z_{slope} + N_{los} \times N_{slope} + E_{los} \times E_{slope} \quad (13)$$

C represents the percentage of real displacement detected by space borne/ground based sensors.

The real displacement (D_{real}) is defined as the ratio between the displacement recorded along the LOS (D_{los}) and the C value:

$$D_{real} = D_{los}/C \quad (14)$$

By using *MatLab* interface, an automation of the projection procedure is obtained (Figure 26).

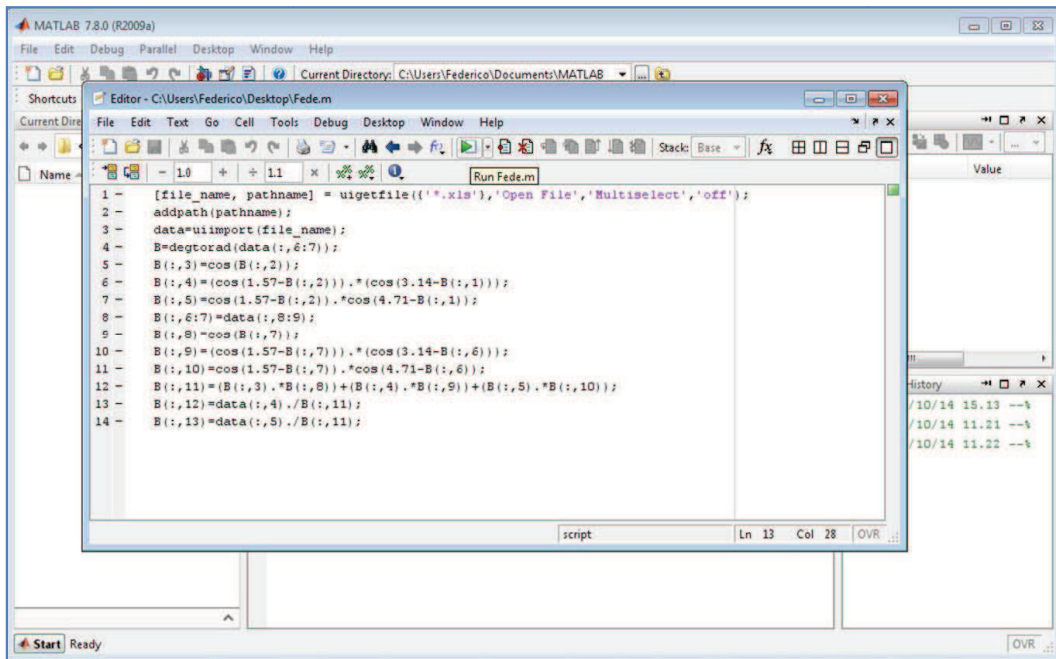


Figure 26. Example of *MatLab* interface related to the automation of the downslope projection algorithm.

In some cases, the projection algorithm could be applied to a set of angular conditions in which the LOS and the downslope angle directions are nearly perpendicular: in these situations the projection could lead to large estimate errors, especially when small movements in the LOS are processed. These particular values, for simplicity called "outliers", can be highlighted by applying a filter on the *MatLab* script, allowing us to obtain output maps differentiating pixels having a movement for which projection is possible from pixels having a movement for which projection is not possible because falling in the outlier angle range (Figure 27). This problem generally appears in satellite datasets, where the LOS is likely to be very different from the downslope direction; it is less common in the case of ground based projected data, because of the similarity between the GB-InSAR LOS and the downslope direction of the investigated slope.

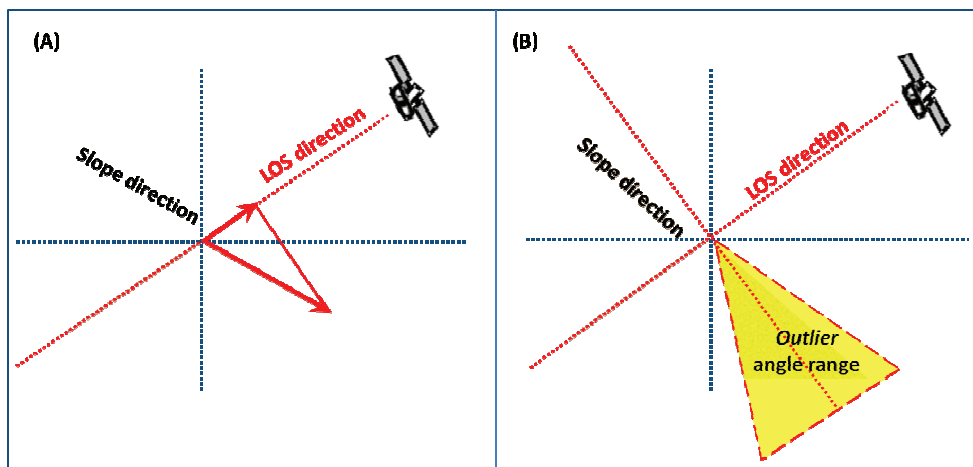


Figure 27. Projection geometry of LOS movement on slope direction (A) and definition of outlier angle range (B).

On some occasions, the problem of the *outliers* could manifest in relation with local features of the scenario (*i.e.* counterslopes, small valleys etc.) where *Aspect* and *Slope* angular values have strong spatial variation. In these situations, a sub sampling of those angles could overcome the problem. Indeed, these angular data are generally extracted from a Digital Terrain Model (DTM) of the interested area; it has been found through tests that using a very high resolution DTM (for instance those obtained by LiDAR campaigns) could increase the number of *outlier* pixels, because an excessive precision in these input parameters could measure *Aspect* and *Slope* angles in areas where the presence of buildings or artefacts or topographic features are discordant with the dominant geometry of the scenario which represents the interested direction.

The possible consequence of projecting satellite data by using *Aspect* angular values from a high precise DTM is shown in Figure 28, where a detail of this projection in correspondence with a building roof is shown. The projected data are displayed by coloured arrows (the colour corresponds to the velocity class which the arrows belongs to), rotated according to the *Aspect* direction. It is possible to observe how the data have been wrongly projected by following the direction of the roof, instead of the downslope direction, that is oriented toward south-west and that corresponds to the effective landslide direction.

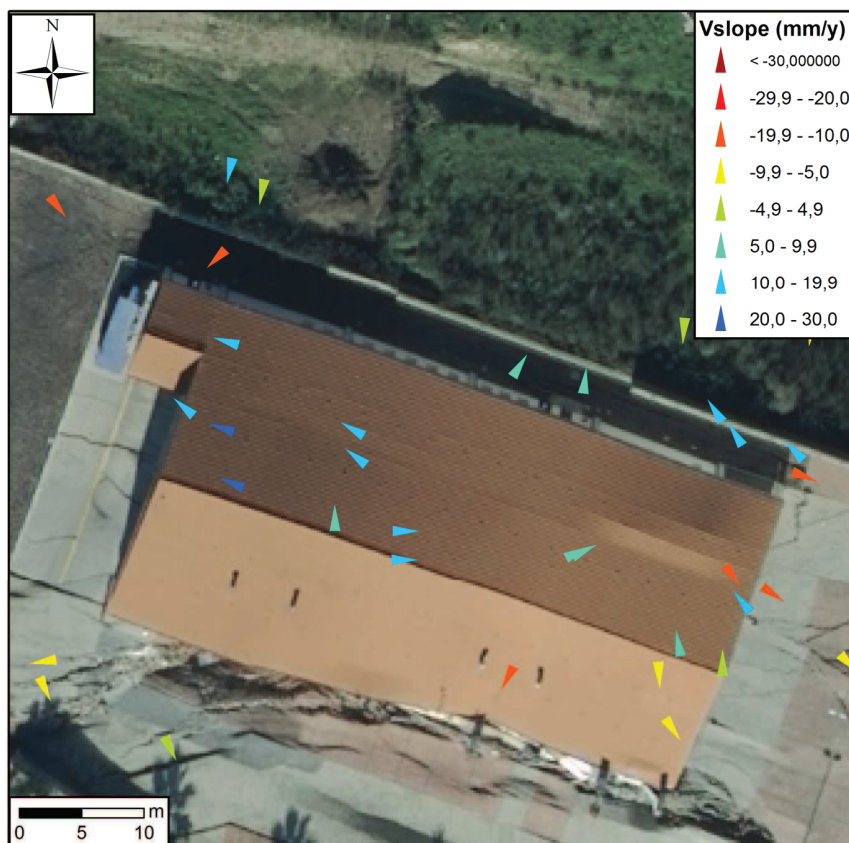


Figure 28. Example of the “local DTM effects” on downslope data projection.

Another example related to the error generated by the use of a very high precision DTM to project InSAR data on downslope direction can be found in paragraph 4.3 of this thesis, where the San Fratello case study is described.

In any case, the result of the data integration by using a semi-quantitative approach consists in the production of ground deformation maps or ground velocity maps in relation with the projected input data (displacement or velocity values). These maps, containing the information related to both satellite and ground based InSAR data, can also be superimposed on ancillary data.

An additional step in the quantitative approach to the integration methodology is represented by the time series analysis; comparing displacement/velocity time series of selected points on the ground deformation/velocity maps allows us to increase the quantitative information deriving from projected data.

The selected points are generally chosen in areas where the radar signal is characterized by high stability, high signal/noise ratio, high power and coherence parameters.

In correspondence with these "stable" points, both the satellite and ground based time series can be analysed, discriminating their main components (Figure 29).

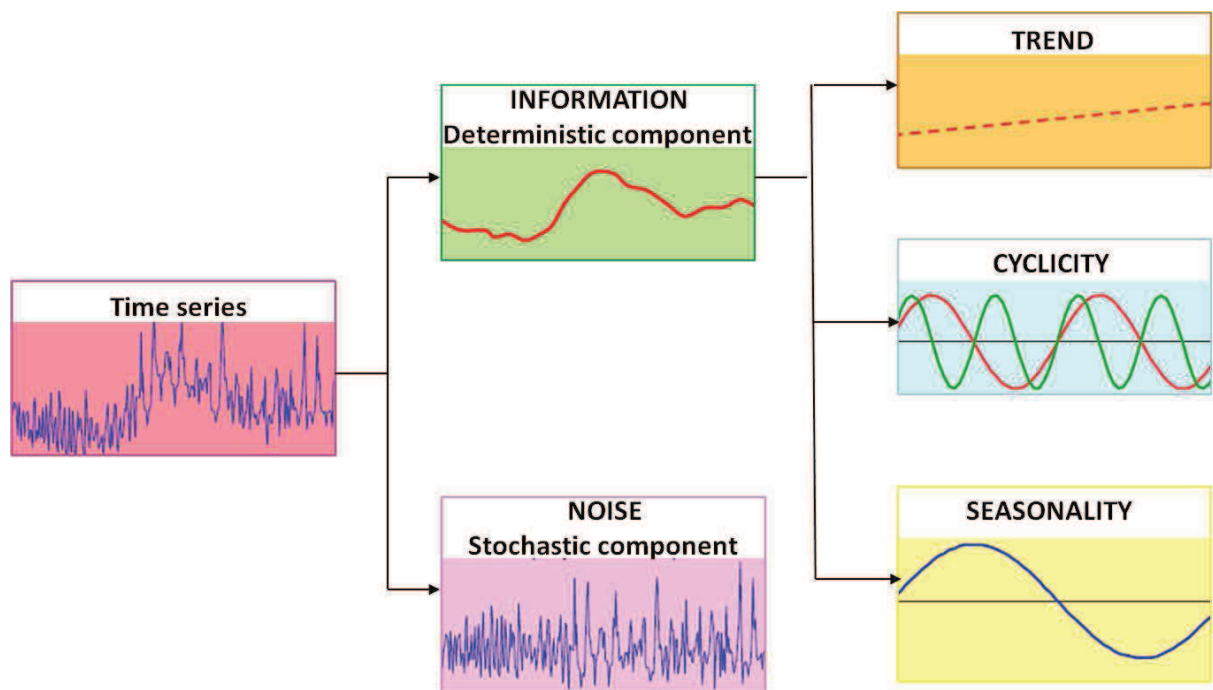


Figure 29. The scheme shows the main factors that are responsible to bring about changes in a time series, also called the components of time series. These factors can be distinguished in stochastic or irregular components and deterministic components, which can contain a trend, a cyclic and a seasonal component.

Firstly, the stochastic component has to be isolated, in order to highlight the attention to the deterministic component, which can contain a trend, a cyclic component and a seasonal component. In the perspective of data integration, the exclusion of the stochastic component

represents a central step in data comparison analysis. The noise definition could be obtained by applying the spectral analysis, in order to distinguish the high frequency component of the signal, usually represented by the stochastic component. Moreover, the de-noising could be effected also by applying smoothing spline models, at that point comparable with the results of spectral analysis. These studies have been done by using the open source statistical software “R” and “Past” (<http://www.r-project.org/>; <http://nhm2.uio.no/norlex/past/download.html>).

After the isolation of the stochastic component, the time series acquired both from space borne and ground based platforms can be compared in order to evaluate the eventual presence of common trends, or cyclic/seasonal components etc. The average displacement values can be compared in a more quantitative sense, not forgetting to take into account the range of error related to the high sampling times and the periods of lacking data.

A schematic description of the applied integration methodology is shown in Figure 30.

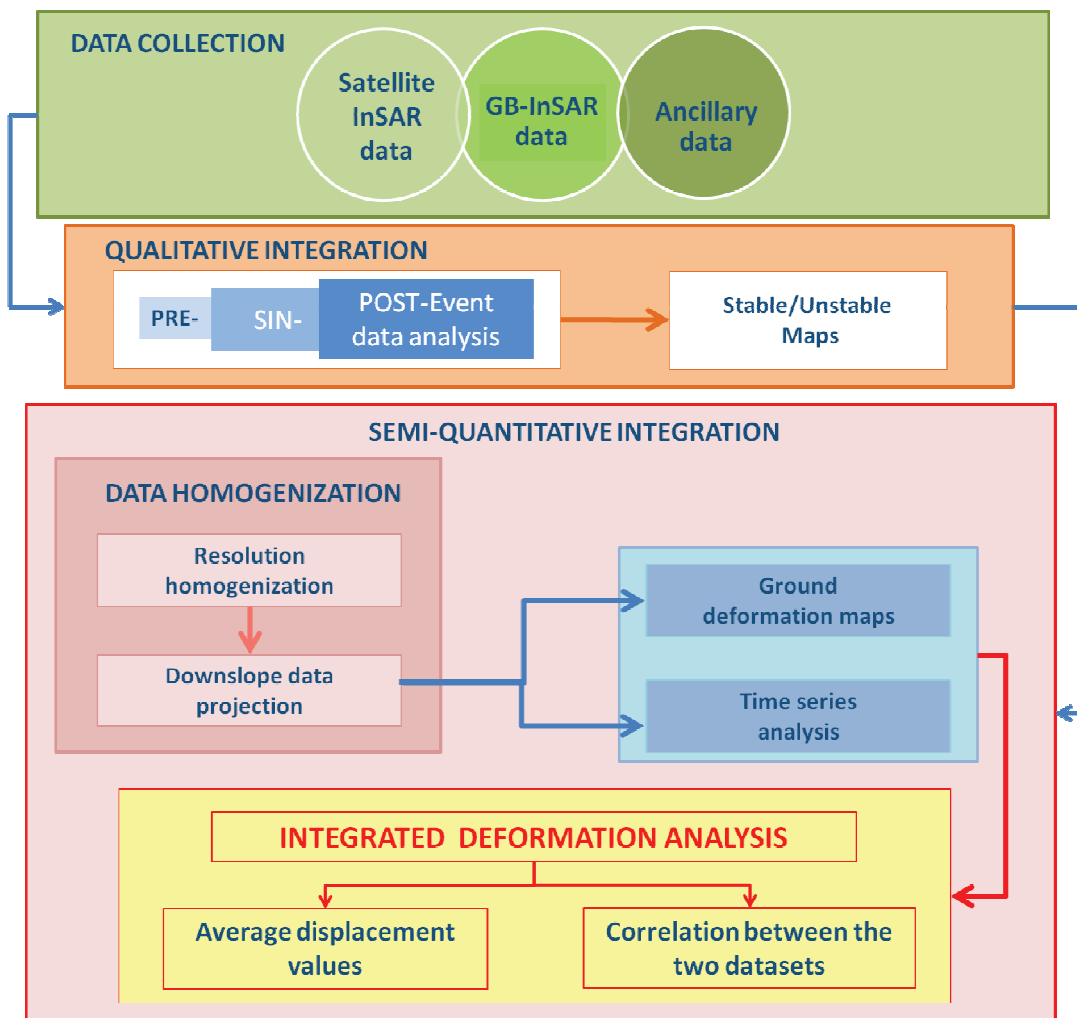


Figure 30. Schematic representation of the applied integration methodology.

3. Landslide Early Warning System

In the disaster databases, much of the damage and fatalities caused by natural hazards are attributed to earthquakes and tropical cyclones. In effect, the landslides triggered by these dangers are the real cause of death and losses, and in these terms they represent the most frequent geo-hazard.

By considering the importance of the landslide problem, in this chapter, the main challenge is to apply the results illustrated in the previous section to the field of landslide risk mitigation, specifically by means of early warning system procedures.

In this sense the chapter is organized as follow:

- firstly, a paragraph containing an overview of the definition of landslide risk and its mitigation is presented (3.1);
- secondly, the Early Warning System (EWS) is defined, together with the steps to generate a valid EWS (3.2);
- finally, a proposal, devoted to the integration of InSAR data (also those acquired by satellite platforms) within the existent EWSs, is described. The proposal also takes into account the improvement in the data processing developed during this PhD project (paragraph 3.3).

3.1 Landslide risk and mitigation

In order to introduce the widespread problem of landslide risk and mitigation, it could be useful to define some of the most used terms.

Indeed, in 2009, The United Nations Office for Disaster Risk Reduction ([UNISDR, 2009](http://www.unisdr.org/we/inform/terminology)) developed a collection of basic definitions on disaster risk reduction usable by public, authorities and practitioners, in order to increase the common understanding on this topic. These "Terminology documents" have been translated into a lot of languages and they are available at the following address: <http://www.unisdr.org/we/inform/terminology>.

Previously, the International Society of Soil Mechanics and Geotechnical Engineering ([ISSMGE, 2004](#)) Technical Committee on Risk Assessment and Management developed a Glossary of Terms for Risk Assessment.

Taking into account the introduced Glossaries as starting points, it could be useful to define what "landslide risk" means.

The "landslide risk (R)" is defined as "the expected number of lives lost, person injured, damage to property, or disruption of economic activity due to a landslide". In other terms, it can be expressed by the following equation:

$$R = H \times E \times V \quad (15)$$

Where:

H stays for "natural Hazard" and it represents "the probability of occurrence within a specified period of time and within a given area of a potentially damaging landslide phenomenon";

E are the "Elements at risk" or "the population, properties, economic activities, including public services etc. at risk in a given area";

V is the "Vulnerability" and it means "the degree of loss to a given element or set of elements at risk resulting from the occurrence of a landslide of a given magnitude".

In a more general meaning, "Risk" can be defined as "effect of uncertainty on objectives" ([ISO Guideline, 2009](#)), considering that "an effect is a deviation from the expected-positive and/or negative" and that "objectives can have different aspects (such as health, safety, and environmental goals) and can apply at different levels (such as strategic, organization-wide, project, and process)". Also in this case, the risk is often characterized by reference to potential events and consequences, or as a combination of the consequences of an event (including changes in circumstances) and the associated likelihood of occurrence, completely according to the meaning of the risk equation (15).

The activities finalized to risk reduction consist in a reduction of the components of the 15 equation (H, E, V) that are respectively subordinate to their specific knowledge.

Therefore, this knowledge represents an essential step in the *"risk assessment"*, defined as *"the process of making a decision recommendation on whether existing risks are tolerable and present risk control measures are adequate, and if not, whether alternative risk control measures are justified or will be implemented."* The risk assessment incorporates *"risk analysis"* (*"the use of available information to estimate the risk to individuals or populations, property or the environment, from hazards"*) and *"risk evaluation"* (*"the stage at which values and judgment enter the decision process, explicitly or implicitly, by including consideration of the importance of the estimated risks and the associated social, environmental, and economic consequences, in order to identify a range of alternatives for managing the risks"*).

In brief, the *"risk assessment"* passes from the knowledge of the components of the risk equation, which permits to define the *"risk scenarios"* (*"where potential losses are estimated within a pre-defined hazard and vulnerability scenarios"*), in order to identify how to mitigate the damage.

The risk management is the result of the risk analysis activities, the risk assessment measures and the mitigation actions, following the scheme proposed by [Fell et al. \(2008\)](#) and shown in Figure 31.

Risk analysis includes hazard and consequences analysis, with *"consequence"* being the result of the product between vulnerability and the elements at risk, in the risk equation (15).

As regards hazard analysis, it involves the characterization of the landslide, in terms of size, velocity, mechanics, travel angle and so on, and its annual probability of occurrence ([Fell et al., 2008](#)). To quantitatively compute the Hazard, several methods exist, based on heuristic, statistical or probabilistic approaches ([Gorsevski et al., 2006](#), [Pardeshi et al., 2013](#)). Indeed, the wide spectrum of landslide phenomena and the complexity and variability of their interactions with external factors, both natural and human, cause difficulties not only for the quantitative definition of landslide hazard, but also for its qualitative assessment; each type of slope movement poses different threats and may require a separate assessment ([Guzzetti, 2006](#)).

As regards consequence analysis, this includes the identification and quantification of elements at risk, taking into account the temporal and spatial probability involved in a specific type of damage, and their vulnerability. As for the Hazard, Consequence can be expressed qualitatively, by using descriptive ratings (*i.e.* from very low to very high) and quantitatively, for example by using a range from 0 to 1 (from null to total loss or damage to a specific element at risk). This problem has been widely discussed in literature, together with the problem of landslide risk. A good review can be found in [Guzzetti, 2006](#).

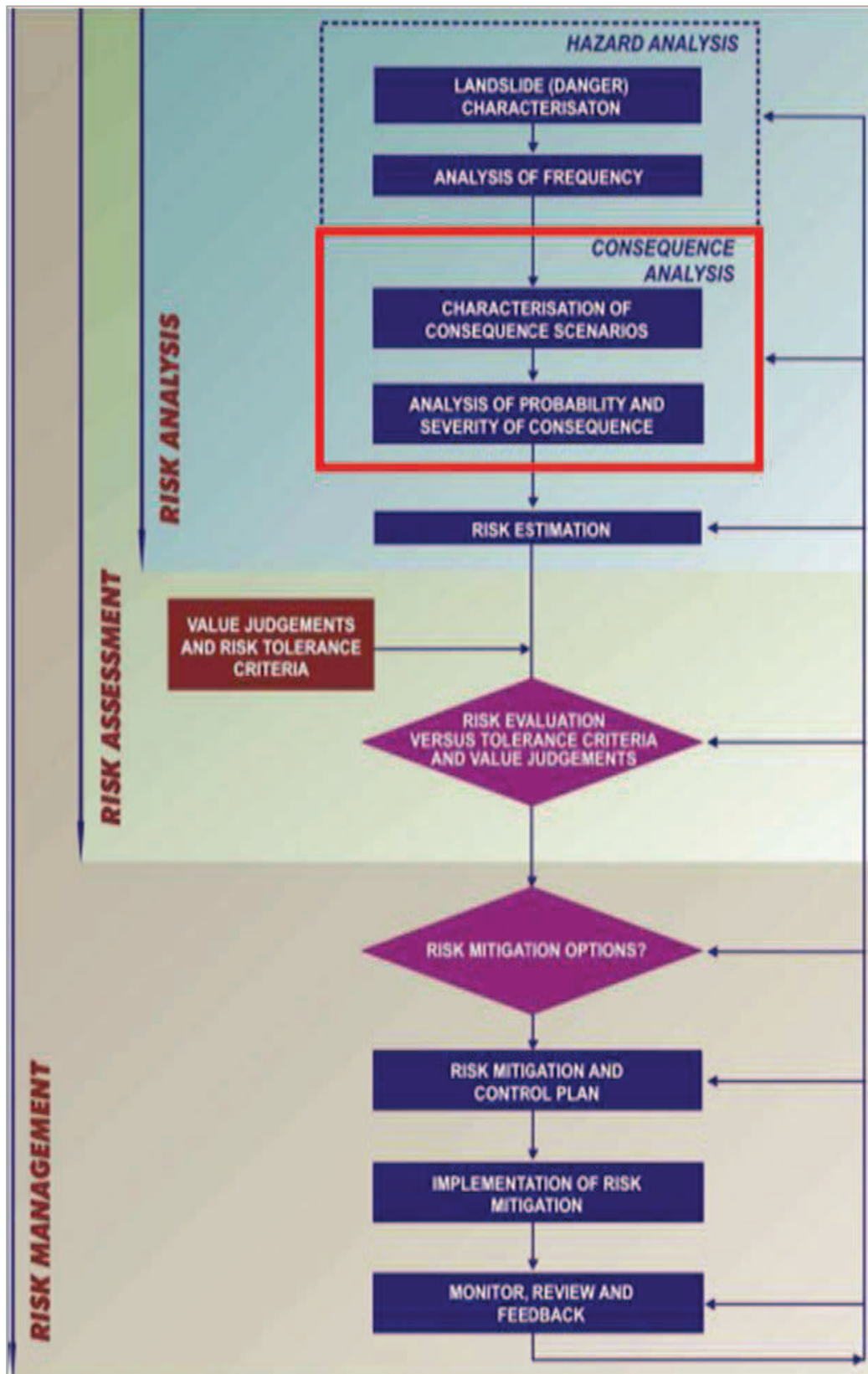


Figure 31. Flow chart for landslide risk management (from Fell et al., 2008).

During the risk assessment phase the results of the hazards and consequences evaluation must be considered, in accordance with the definition of values of risk tolerability, defining as “tolerable” a “risk within a range that society can live with so as to secure certain net benefits”.

The evaluation of tolerable risk is also difficult and it is generally connected to the expected number of fatalities. It is a social problem, related to the population perception of risk; generally, a single event with many fatalities is considered less acceptable than several accidents with few fatalities (Geotechnical Engineering Office 1998, Bell et al., 2005). The "objective risk" is often different from the "perceived risk", as shown in the diagram in Figure 32.

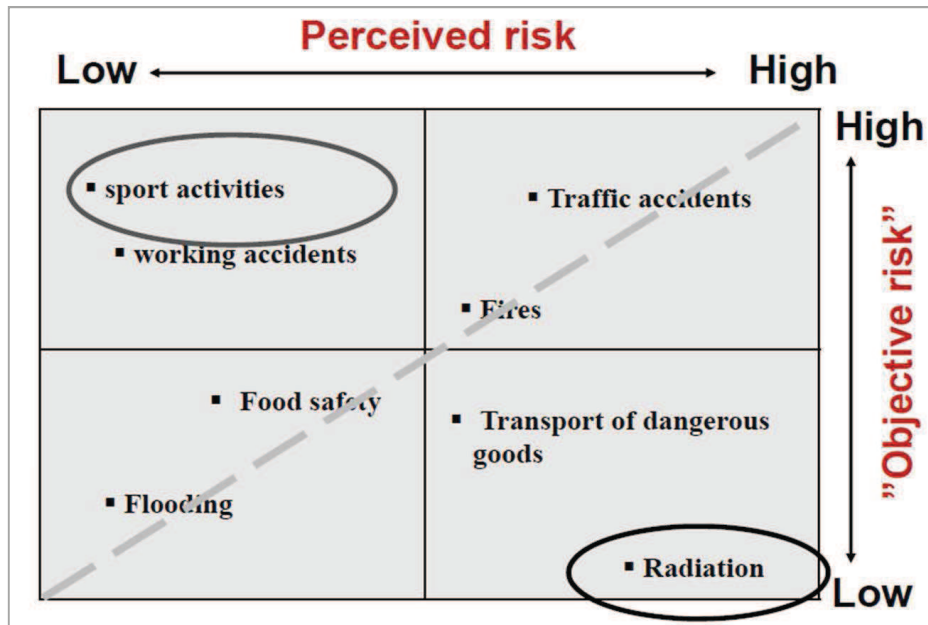


Figure 32. Risk perception by society vs. "objective risk" diagram (from: Max Geldens Stichting, 2002).

In the scheme of risk management, the definition of risk tolerability is a criteria for establishing the need of mitigation measures that becomes essential when the risk value is considered unacceptable.

In the family of "mitigation measures" it is possible to distinguish structural from non-structural activities. Actions including engineering works to reduce the Hazard or to physically reinforce, protect or isolate the elements at risk, consequently increasing the control of Vulnerability, are defined as "structural measures". Everything that is finalized to an increase of awareness and acceptance of risk or those actions devoted to a permanent or temporary reduction of the exposure of the elements at risk are considered as "non-structural measures".

The field of non-structural measures includes land-use planning and/or relocation of existing facilities, public preparedness and last, but not least, early warning systems.

The efficiency of the mitigation measures are evaluated in terms of risk reduction. In this sense a well-structured early warning system (EWS) should result in an effective decrease of the risk values.

3.2 EWS definition

Di Biagio & Kjekstad (2007), disserting about early warning, instrumentation and monitoring landslides, introduced the problem by considering that on the geological time scale, natural slopes are only temporary topographic features. The action of natural processes, such as weathering, erosion, earthquakes, gravity and so on represents a fundamental force in the geological cycle, which acts by deteriorating older mountains and creating new depositions of geological material to allow the subsequent formation of new mountains. Therefore, Di Biagio & Kjekstad wrote: *“Our only recourse is to learn to live with landslides. To do this we must be able to understand and predict landslide behaviour”*.

In this sense, the early warning systems, considered as a component of a risk management system for detecting and dealing with an anticipated natural or man-made hazard, acquire crucial importance.

The most recent definition of EWS was proposed by UNISDR (2009) and is defined as: *“the set of capacities needed to generate and disseminate timely and meaningful warning information to enable individuals, communities and organizations threatened by a hazard to prepare and to act appropriately and in sufficient time to reduce the possibility of harm or loss”*.

Similar definitions were previously proposed by UNISDR (2006a), Medina-Cetina & Nadim (2008), Lacasse & Nadim (2009).

Every listed definition expresses the importance of obtaining “people-centred” EWSs, focusing the attention on the audience, represented by citizens and governments, who must be informed on a seamless timescale spanning from minutes, for immediate threats requiring urgent evacuation, to weeks, for more advanced preparedness.

Therefore, an EWS is a multidisciplinary problem: it at least involves both scientific-technological areas and social-organizational fields. The phenomena analysis, the risk scenario definition, the instrument installation, the monitoring phases, the data transmission and elaboration, the definition of the threshold values are typical scientific matters; beside these, the public education, the problem of decision making, the communication of alerts and so on are activities that mainly involve organizational and social aspects.

In order to create a valid people-centred early warning system, some steps have to be taken into account: it is necessary to increase the knowledge of and the means of forecasting the danger faced, to enhance the information from technical monitoring and visual observations, to define response plans, to disseminate meaningful warnings to the population exposed to risk and increase public awareness and preparedness to respond to warnings.

An answer to these needs was furnished by UNISDR who, in 2006b, defined four key elements (A, B, C, D) that an EWS has to necessarily include:

- A. The knowledge of the risk: consisting in the systematic collection of data and performing risk assessment by answering the following questions:
 1. Are the hazards and the vulnerabilities well known?
 2. What are the patterns and trends in these factors?
 3. Are risk maps and data widely available?
- B. Monitoring, analysis and forecasting of the hazards: development of hazard monitoring and early warning services.
 1. Are the right parameters being monitored?
 2. Is there a sound scientific basis for making forecasts?
 3. Can accurate and timely warnings be generated?
- C. Dissemination and communication: communicate risk information and early warnings.
 1. Do warnings reach all of those at risk?
 2. Are the risks and the warnings understood?
 3. Is the warning information clear and useable?
- D. Response capability: build national and community response capabilities.
 1. Are response plans up to date and tested?
 2. Are local capacities and knowledge made use of?
 3. Are people prepared and ready to react to warnings?

Almost completely in accordance with the proposed guidelines, Di Biagio & Kjelstad (2007) proposed a list of the four main components of an EWS, defined as (i) Monitoring, (ii) Data Analysis and Forecasting, (iii) Dissemination of Understandable warnings, (iv) Response of People.

A block diagram including the UNISDR guidelines and the defined four components proposed by Di Biagio & Kjelstad is shown in Figure 33.

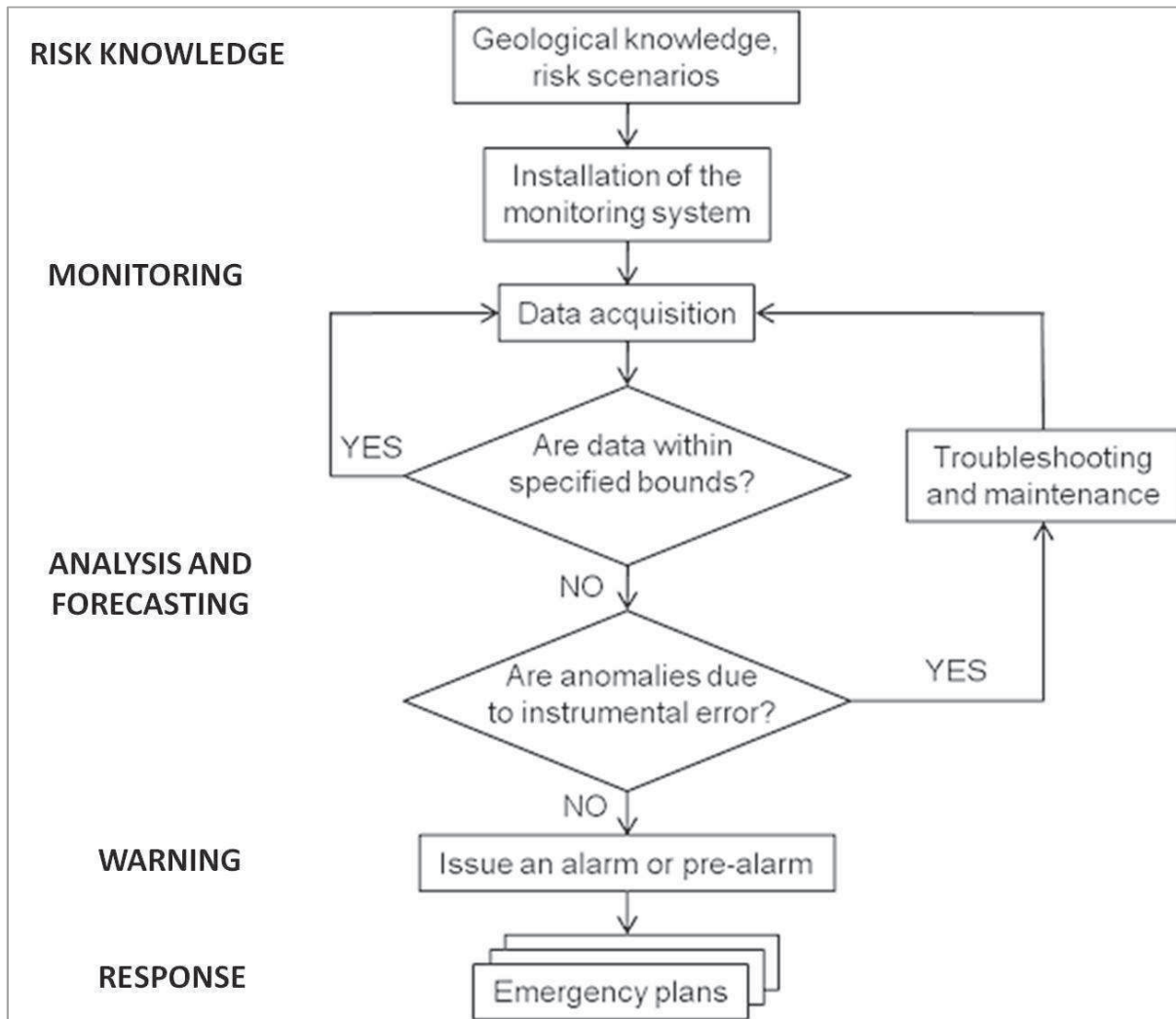


Figure 33. Block diagram of the main components of a typical early warning system (schematization proposed by Di Biagio & Kjelstad (2007) and modified by Intrieri et al., 2012).

The problem of defining a link between the components of warning systems started in the early 90's, when Mileti and Sorenson (1990) presented the first model of integrated warning systems, analysing the different components of the system. Later, the UN's People Centred Model of UNISDR (2005) was proposed and later analysed by Basher (2006). Every proposal funnelled in the exposed guidelines of UNISDR (2006a).

The most recent definition of the steps of a complete EWS can be found in Intrieri et al., 2013, where an elaboration of the definitions provided by UNISDR (2006b) and Di Biagio and Kjekstad (2007) is proposed to describe the EWS as the result of a balanced combination between four main activities: design, monitoring, forecasting and education, the specific features of which are schematized in Figure 34.

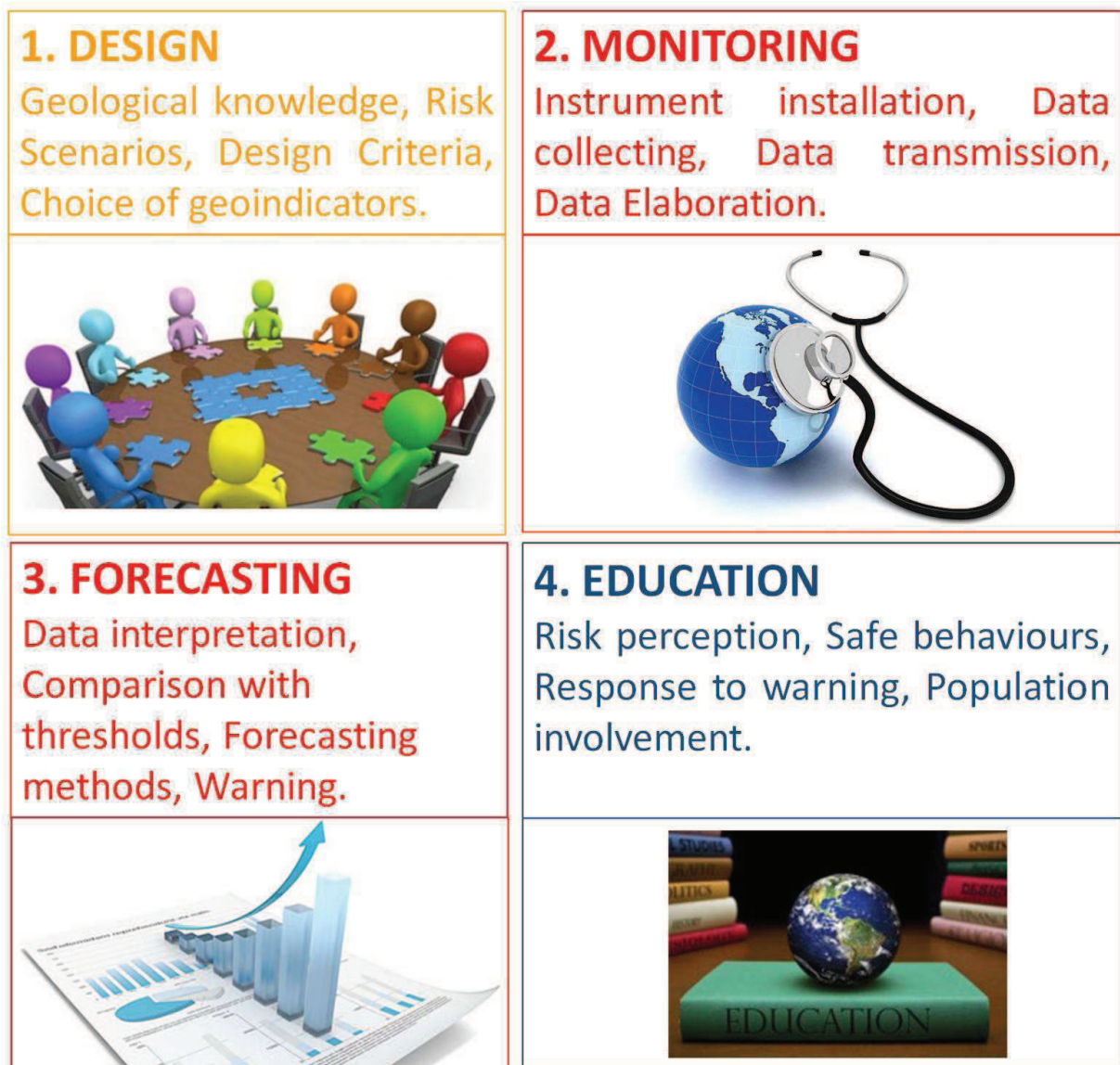


Figure 34. Typical components of an EWS according to Intrieri et al. 2013.

According to [Intrieri et al. \(2013\)](#), the design phase comprises the determination of the needs and vulnerabilities of the population at risk, the identifications of eventual impediments to the population taking action in case of warnings, the characterization of geological and meteorological conditions (geo-indicators) that could lead to a landslide trigger.

In the monitoring step, the installation of the instruments (chosen in the design phase) takes place, together with the start of data communication and analysis. Part of the monitoring activities start in the design phase, in support of the research step, which includes the landslide occurrence and behaviour. After the definition of all the criteria to develop the early warning, the monitoring activities become an effective part of the so-called “monitoring phase”.

The forecasting phase comprises some crucial steps, *i.e.* the definition of thresholds that vary in relation with the specific case and the definition of models and activities that lead to a warning. It is a delicate step, because it is necessary to construct a compromise between the intrinsic

uncertainties related to the evolution prediction of natural events and the need to define the threshold values as precisely as possible. Indeed, an EWS is organized in attention levels, the switch to a higher level is defined by the overcoming of these threshold values: a well-functioning EWS mainly depends on the choice of these values. A proper threshold value guarantees avoiding false alarms and missed events. An excessively high threshold value means that the lead time for the emergency plans will be short or that some events will be completely missed. On the other hand, a threshold value that is too conservative may lead to false alarms, reducing the reliability of the system for the citizens and authorities involved. It is very important to reduce these problems because the consequences are often serious (Nadim & Intrieri, 2011). It is, however, very difficult to completely avoid the false alarms, therefore the public also has to be educated for this eventuality.

In fact, the last step concerns education: the population has to be instructed to the risk perception and to the correct behaviour to prevent damage and losses, besides being instructed in the correct reaction to false alarms. It is a step that should not be underestimated, because the reaction-mode of the stakeholders determines the effective validity of the whole early warning structure.

Other authors have proposed EWS models, especially following the tsunami of Sumatra (26th December 2004), which determined an increase in the attention of authorities towards the reduction of impacts of natural hazards on human lives and physical environment by means of early warning systems (UNISDR, 2006a). Some of these models can be found in Villagran et al. (2006), Leonard et al. (2008), Bell et al. (2009).

The most recent and complete overview of EWSs was developed in 2011, in the framework of the European project, named "SafeLand". In one of the key areas of the project, a toolbox that can help the end-users to create a landslide EWS for every need was proposed (SafeLand, 2011). The suggested toolbox also takes into account the differences in the EWS structures, related to the scale of the analysed phenomena: a single slope scale system, operating on a specific landslide (examples can be found in Froese et al., 2006, Blikra, 2008, Durville et al., 2011, Intrieri et al., 2012) is obviously organized in a different way respect to a regional scale EWS (examples can be found in Kunlong et al. 2007, Baum & Godt 2009, Lagomarsino et al., 2012). Differences also exist regarding the duration of the EWS, that can be temporary or permanent; a temporary solution is considered appropriate if a short-term risk reduction is required (Rose & Hungr, 2007); a permanent solution is applied when there are no immediate remedial available actions and the cost/benefit ratio is advantageous to a construction of a long term system to risk reduction.

The guidelines suggest organizing the warning levels as simple as possible; generally at least three attention levels are defined:

- an ordinary level, where the displacements are considered characterized by normal activity, including seasonal variations, daily data observation and monthly communication through bulletins and similar;

- an attention level, where the increase in phenomena activity requires an increase in the observation frequency, daily communications and 24h operator surveillance;
- an alarm level, which corresponds to an accelerating trend of the displacements, associated with a very high frequency of data observation and two or more communications (through bulletins or similar) per day.

A low number of levels allows the reduction of the number of thresholds that represents the most delicate step in the EWS definition, this is the reason why three levels EWS are generally suggested; obviously EWS characterized by more levels exist, in relation to the specific needs of the analysed phenomena/area/site.

3.3 Proposal of an EWS based on InSAR data

The main goal of the presented thesis was to apply the results of the optimization of InSAR data, described in Chapter 2, to contribute to the mitigation of landslide risk. In this sense, the introduced optimizations have been used to integrate existent EWSs. By taking into account the guidelines proposed by the [SafeLand project \(2011\)](#) and the four main EWS components proposed by [Intrieri et al. \(2013\)](#), the next sub-chapters will suggest an EWS scheme based on InSAR data.

As defined in the previous paragraph, an EWS has a complex structure and involves several different fields: the structure of an EWS depends on several variables, such as the scale of the analysed phenomena (local or regional), the time validity (temporary or permanent), the specific characteristics of the case study (landslide type, risk scenarios, available resources etc.); these factors imply that it is impossible to develop a single EWS valid for any situation.

As regards the proposal of an InSAR-based EWS, the aim is to consider the possibility in which these datasets can be useful in warning activities, and how they can be applied and elaborated to obtain a valid support for every step of a well-structured EWS.

3.3.1 Design activity

The Design phase represents a fundamental step in the EWS organization. Careful planning activities are suggested, taking into account the knowledge of the analysed area, including the scale of intervention, the available economical budget, the validity over time for which the system is designed and so on.

Considering the needs of a well-organized EWS, an InSAR based EWS could potentially benefit from some aspects intrinsically related to the InSAR techniques.

Indeed, on one hand, satellite InSAR techniques are capable of scanning wide areas, by performing regular and financially acceptable measurements with high accuracy; the fast data processing, together with the simplicity of exporting data into the GIS environment lead to fast and easy data elaboration; moreover, the availability of historical archives allows us to analyse data over periods that go a long way back in the past. However, satellites' orbiting intervals limit the time measurements allowing us to detect only slow or extremely slow deformation values ([Cruden & Varnes, 1996](#)).

On the other hand, GB-InSAR systems are characterized by high operative flexibility, high versatility and transportability, high measurement precision, associated with the possibility of detecting a wider range of velocity values than the satellites (from extremely slow to fast landslides according to the [Cruden & Varnes \(1996\)](#) classification).

The integration between satellite and GB-InSAR techniques proposed in Chapter 2 of this thesis allows us to exploit the advantages of both the techniques, also within the EWS definition context.

In the design phase, the main developing criteria on which the EWS will be structured must be defined.

In this sub-paragraph, it has been decided to better emphasize those aspects of the design phase in which the technicians are more involved. Also the expert operators must consider the guidelines (SafeLand, 2011) for the elaboration of a well-structured EWS. Therefore, for sake of clarity and completeness, the main criteria that an EWS must respect are listed below, following the scheme of Intrieri et al. (2013) and taking into account the involvement of all the EWS stakeholders:

1. Communication: it must be carried out at all levels, among stakeholders and towards the population and in every moment (every level of the EWS, from ordinary to alarm). Eventual failure in the communication could compromise the whole system. Communication includes public education, notifications among stakeholders, alarm spreading etc.
2. Earliness: data must be collected and elaborated as quickly as possible; in case of emergency, it must be known in advance what actions must be taken. Necessary time must be granted for eventual evacuation measures. Monitoring activities must be as close as possible to real-time.
3. Simplicity: the EWS scheme must be clear and it must not generate confusion or loss of time (that could result in a new kind of emergency). The planning actions to be taken at every level must be clear and fast, eventual human errors are not tolerable. Messages destined to population must be as simple and as clear as possible.
4. Reliability: this gives an idea of how capable the system is of catching real events and avoiding false alarms and it also depends on how deep and continuative is the knowledge of what is happening on the site during every step of the EWS. High reliability is the result of a precise, accurate and robust system, that is able to work round-the-clock in all weather conditions.

Taking into account these general criteria, the here proposed EWS has been structured in two main steps: a first step definable as a sort of "pre-EWS", based only on satellite InSAR data and designed for expert operators, and a successive step represented by the effective EWS, based on InSAR integrated data.

In the "pre-EWS" activity, a regional scale study of the slope instability, based on satellite InSAR data analysis, is proposed. It is conceived as a sort of EWS addressed to expert people, organized to exist permanently and produced on limited budgets.

The satellite InSAR data well answer the exposed design criteria and they could provide a sort of preliminary warning, resulting from a continuous and long-term monitoring of areas affected by extremely slow and slow landslides; accelerations of these phenomena can be detected from satellite platforms, specifically from new-generation satellite systems, characterized by faster acquisition times (shorter revisiting times) and higher resolutions.

In Italy, the intent finds the support of the generated archive of COSMO-SkyMed data, created in the context of the so-defined “Map Italy” mission. It consists in the mapping of the entire Italian Peninsula through COSMO-SkyMed acquisitions in interferometric, *Stripmap* configuration, by using all the four satellites that constitute the COSMO-constellation. The satellites acquire in ascending and descending passages, every 16 days.

The result is an archive of interferometric satellite data that can be analysed for EWS purposes; the use of existent data contributes to reduce the costs of this “pre-EWS” phase.

On the basis of these archives of data, processed by using PS-InSAR and SqueeSAR techniques, an improvement in the landslide mapping of extremely slow and slow phenomena can be achieved. By analysing the PS-InSAR displacement time series, it is possible to define threshold values of displacements. This “pre-EWS” can be structured on three levels, such as the simplest existent EWSs: an ordinary level, an attention level and a pre-alarm level; the passage from one level to another is defined by how much it exceeds the thresholds. The passage from ordinary to attention level will determine an increase in the frequency of data observation, in those areas where the threshold values are exceeded. The exceeding of the second threshold value, consisting in the passage to the “pre-alarm” level, also represents the entrance to the effective EWS. In fact, the passage from one level to another must be checked by expert operators, also taking into account the level of risk in the affected area. A high displacement value in an area characterized by very low risk values will not correspond to a level switch.

Therefore, in this “pre-EWS” phase, expert operators analyse existent InSAR databases, defining two threshold values, by studying the displacement time series, and finally qualitatively by comparing the exceeding of thresholds with the landslide risk in the same area (considering all the components of the risk equation). Only if the risk is considered high enough to affect the population and compromise economic activities, the exceeding of the last threshold value will correspond to an increasing in the attention on the area, thus entering the real EWS phase. These actions imply a good knowledge of the investigated territory, of the techniques applied and of the analysed phenomena, and of the risk assessment strategies over wide areas. However, this “pre-EWS” is based on specific planning criteria: restrained budget, regional scale, permanent duration, analysis of extremely slow to slow landslide phenomena (that could accelerate, as in the case of the third phase of the creep landslides (Crosta & Agliardi, 2003)), addressed to expert operators. This “pre-EWS” is not conceived to involve the population.

The exceeding of the second threshold value and the entrance in the “pre-alarm” phase also represents the starting phase of the effective EWS.

The “pre-alarm” phase will be related to a localized area, affected by an increase in the activity of the observed phenomena which represents a threat for population or economic activities. In this sense the EWS structure will be based on different criteria than the above defined “pre-EWS”; the EWS will be carried out on a local scale, with a duration that will depend on the landslide activity evolution. The increasing risk will also determine the involvement of local authorities and population at risk in the EWS structure. An effective structure of early warning will become necessary and in relation to the risk intensity, the allocated budget will increase.

Therefore, in this phase, the satellite measures have to be integrated by observations acquired by a GB-InSAR instrument. The increase in the costs, mainly related to the purchase of the GB-InSAR system, will be balanced by an increase in the precision of the measurements, in an improvement in the flexibility of the instrument in the acquisition phase, and in the possibility to detect a bigger range of velocity values.

Actually, a local scale system allows us to analyse in higher detail the observed phenomena, to better define the threshold values and the probable evolution of displacements, especially by using the InSAR data integration analysis, as proposed in the sub-paragraph 2.3.2 of this thesis.

The following diagrams (Figure 35, Figure 36 and Figure 37) represent the operative protocol on which this EWS proposal is organized. Also in this case, the proposal structure contemplates three warning levels: an ordinary level (default level, normal activity including seasonal variations, daily data observations, monthly communications in the form of bulletins), an attention level (increase in the activity, increase in the observation frequency, daily bulletins, operator surveillance 24h), an alarm level (accelerating trend, very high frequency of data observation: two or more bulletins per day), separated by two pre-defined threshold values. It is important to choose these threshold values higher than the ones defined in the "pre-EWS".

The diagrams only regard the involvement of expert operators.

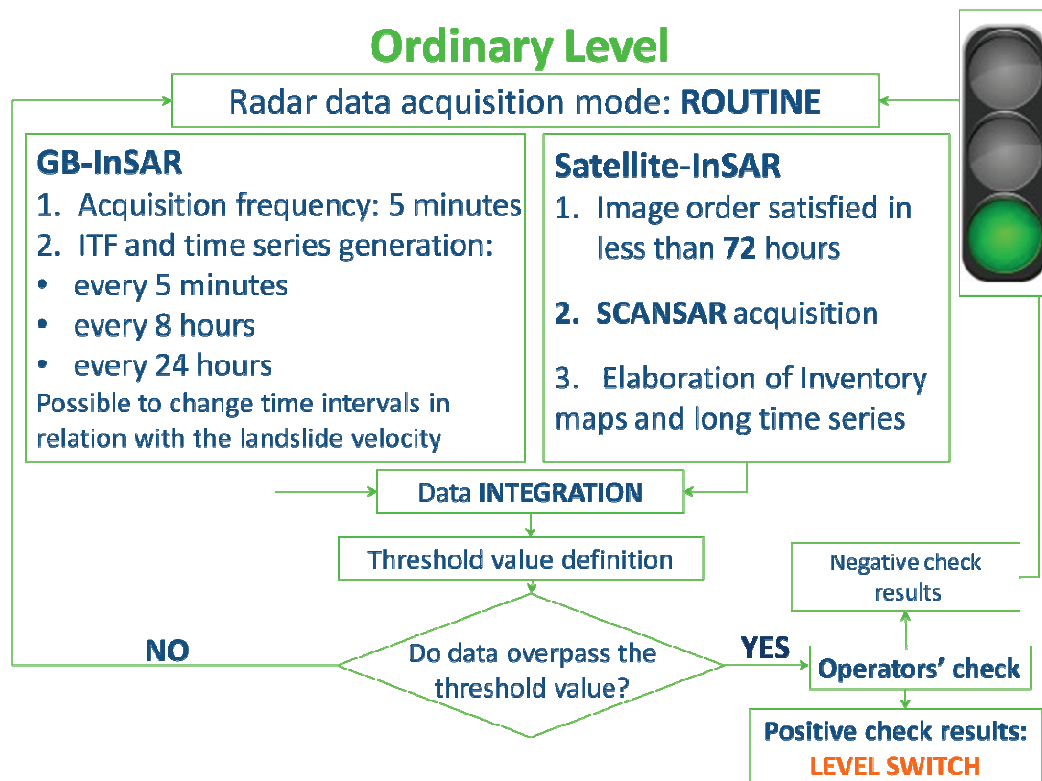


Figure 35. Operative scheme to adopt in the ordinary level of the proposed EWS.

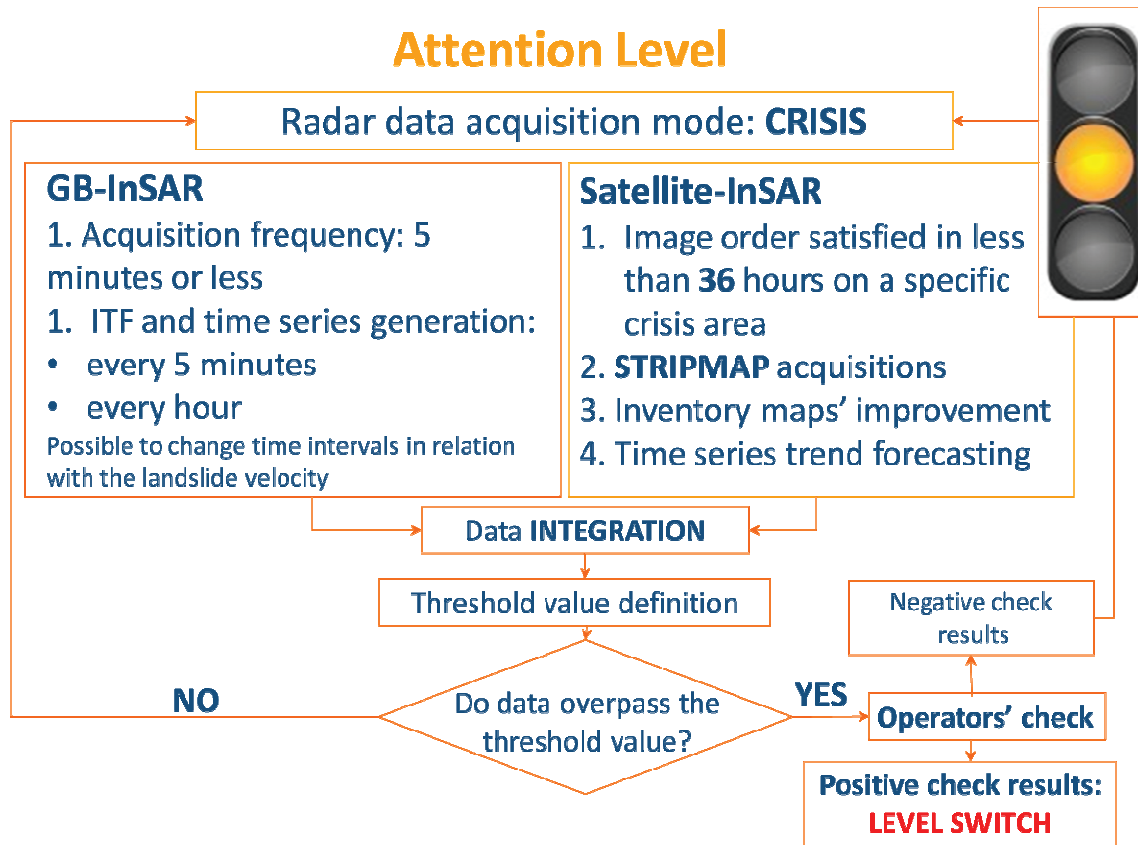


Figure 36. Operative scheme to adopt in the attention level of the proposed EWS.

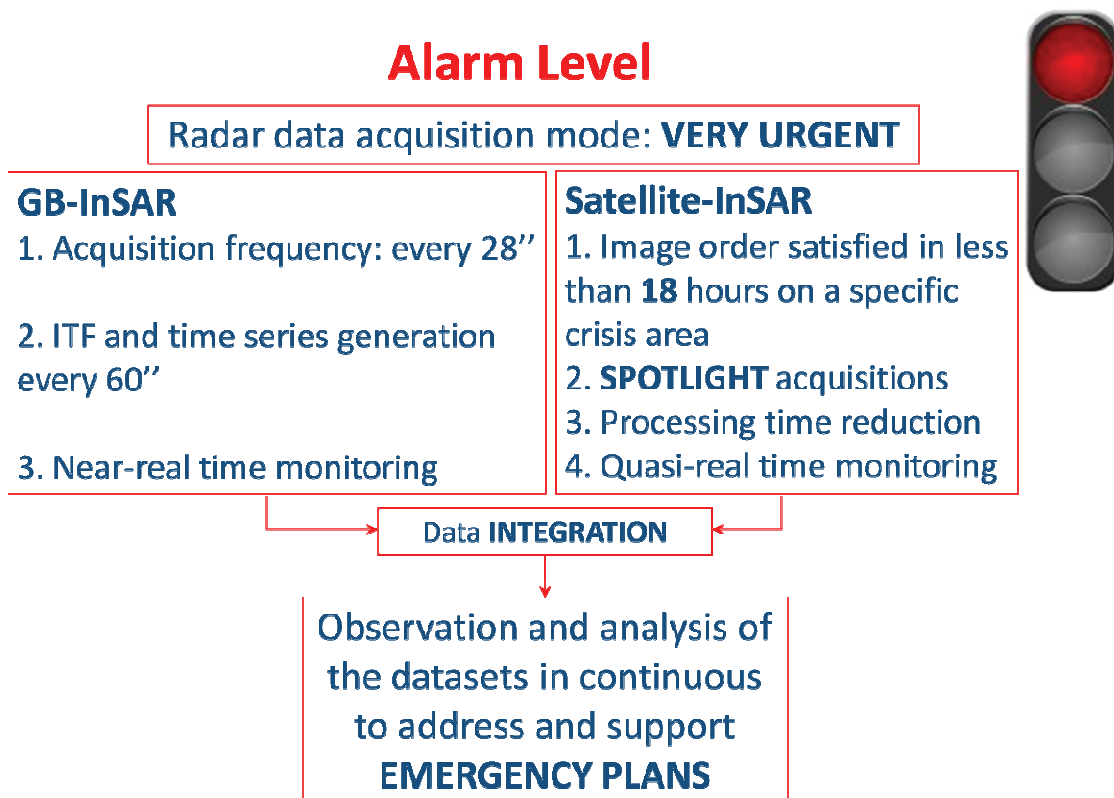


Figure 37. Operative scheme to adopt in the alarm level of the proposed EWS.

The proposed diagrams must be considered as examples of possible adoptable procedures for the different levels of the EWS; the increase in the frequency of data acquisitions, data observations and communications, passing from a lower level to a higher, is clearly emphasized in the diagrams.

A well-structured EWS passes from a well-defined planning, which must be carried out in the design phase taking into account all the presented guidelines.

3.3.2 Monitoring phase

The monitoring phase represents a crucial activity in the creation of an early warning system; it must be performed to be active throughout the whole life of the EWS, starting from the design phase to characterize the phenomenon and to define the thresholds, continuing during the ordinary phase, intensifying in pre-alarm and alarm periods; sometimes the monitoring activities continue after the emergency phase, in order to assess the real end of the emergency and to assess the residual risk.

The monitoring activity can be defined as *"measuring through time the surface displacement fields induced by the landslide event"* (Mantovani et al., 1996; Metternicht et al., 2005). It requires operators with a very good knowledge of the monitoring instruments and of the observed scenario; the operators' attention is required in every phase of the EWS life, in order to eventually change the monitoring parameters, which must be adapted to the specific needs of the phenomenon, evolving continuously; moreover, instruments could be affected by occasional interruptions or malfunctions that must be solved as soon as possible by the experts, carrying out a continuous maintenance.

In the early warning activities, monitoring instruments represent the means by which stakeholders are clearly informed about the conditions of instability phenomena; for this reason, the efficacy of a monitoring system is increased by the possibility to monitor continuously and to obtain measures in near-real time. These needs are widely satisfied by some features of the InSAR techniques, such as the capability to collect data in almost every meteorological condition and the ability to work round-the-clock; the possibility to acquire data during precipitation events represents an important advantage, considering that precipitations are one of the most frequent triggering factor for slope instability.

The proposal of an EWS based on InSAR techniques determines some consequences in the monitoring activities, mainly related to the remote sensing nature of the used techniques. First of all, monitoring in remote mode allows us to observe the phenomenon without access to the instability area, increasing the safety of the operators and also permitting to monitor non-accessible areas. Moreover, remote sensing instruments do not risk damage from the landslide itself, or to be destroyed after the failure, permitting to continue monitoring activities and evaluate the residual risk after the collapse, as required in the construction of a highly performing EWS. On the other hand, the "action at a distance" requires some kind of validation that, in the best cases can be performed by field surveys. In the case of impossibility to access

to the affected area, the validation can be carried out by integrating other activities, such as aero-photogrammetric surveys, LiDAR acquisitions and so on (Dvigalo & Melekestsev, 2009; Ardizzone et al., 2007; NOAA, 2012). The validation procedure plays a key role and it must be included in the monitoring activities.

However, InSAR techniques provide two different types of product: displacement maps, which allow us to analyse two-dimensional movements, and time series of displacement. In the case of satellite platforms, the maps regard wide areas (up to 100 km²) and long term series are generally available, thanks to the existence of historical archives of satellite InSAR datasets; the historical archives also make it possible to exploit existent interferometric products in the form of maps. Historical data can be analysed together with the near-real time data, that can be acquired by new generation satellites up to twice a day in the emergency periods (very urgent mode - Figure 37).

On the other hand, GB-InSAR instruments provide near-real time, automatically acquired, monitoring data. The GB-InSAR optimization, implemented during the here presented PhD research period, allows us to make this type of instrument even more transportable, versatile and flexible than it was before (Chapter 2). These improvements, also including the high acquisition frequency and the rapidity of installation, make this type of instrument a promising tool for managing local emergencies. Moreover, the systems are generally characterized by a robustness that implies only occasional interruptions, mainly due to problems in power supply.

Sequences of deformation maps provided by a GB-InSAR can allow us to study the landslide's temporal evolution, even when the acceleration changes are very small, and to evaluate the volume of the material involved in the mass movement. Thanks to the displacement maps provided by the GB-InSAR, it is possible to delimitate the area affected by movement and to identify temporal phases, characterized by different activity levels. The usefulness of the GB-InSAR system is not only limited to its capability of fully characterizing the landslide in spatial terms; it also permits the operators to follow, during the whole campaign, the evolution of the mass movement and to study its kinematic behaviour, which is fundamental in assessing the risk scenarios' temporal evolution.

The results of monitoring activities can be used to perform products in real (and near-real) time and in deferred time. During real time (measurable in months, days, hours or less) the monitoring activities resulting in performed emergency activities include urgent, immediate actions such as event now-casting, containment of effects, assessment of evolving hazards, countermeasures for risk mitigation, residual risk assessment and restoration of previous living conditions.

On the other hand, study, forecast and prediction, aimed at guaranteeing the permanent safeguard of human lives and property over the long term, are carried out in "deferred time" (measurable in years or decades).

Therefore, as previously emphasized, monitoring activities assume a central role in the EWS structure and they take part in all the defined phases of the system, not only in the here described monitoring phase: in the design phase they are crucial in the phenomenon

characterization and threshold values definition, in the forecasting phase (described in the next sub-chapter), monitoring plays a key role in the providing of data necessary for the application of the algorithms and methods useful for predicting the landslide evolution.

3.3.3 Forecasting phase

The forecasting phase represents another important step in the creation of a valid EWS. The capacity to quantitatively analyse monitoring data in order to predict the displacement evolution of a specific phenomena (local scale activity) increases the utility of these data exponentially. The main goal of the forecasting analysis is to determine how and especially when a landslide will collapse. The evolution prediction will be compared with threshold values defined in the design phase and then it will be translated into eventual warnings, always taking into account a range of uncertainty, intrinsically related to the interpretative nature of forecasting analysis.

Indeed, the forecasting phase probably consists in the most important and difficult part of an EWS; it is usually carried out through forecasting models applied under the supervision of expert operators. Predicting the collapse of a landslide is a very difficult matter, in relation to the intrinsic complexity of the studied phenomena: landslides are indeed related to a large number of variables, which contribute to their evolution. Many indicators can be linked with the landslide collapse (such as the rainfall, the pore water pressure, the seismicity and so on), but the approach for forecasting the time of failure is generally based on the analysis of the displacement (or velocity) values.

Displacement series analysis is not easy: the geometrical complexity of the landslides and, particularly, the non linearity relation between displacement and time variables, the eventual seasonal component in the displacement time series, the inducing landslide factors (such as seismicity and precipitation) are only examples of features that influence the trend of the displacement-time curve, making it very difficult to prevent its evolution (Crosta & Agliardi, 2002, 2003; Rose & Hungr, 2007).

The proposed EWS can exploit time series resulting from the integration between satellite and GB-InSAR datasets; indeed, among the results of data integration, time series can be satisfactorily exploited in the forecasting activities.

Firstly, the time series are statistically analysed: the application of the spectral analysis to distinguish the main components of the series, the use of filters to isolate the noise components, the employment of "run tests" to evaluate the presence of eventual trends are carried forward in order to define the general behaviour of the analysed time series. Obviously, the analysis will be carried out on check points representative of the displacement of the whole area; indeed the results must be applicable to the entire mass involved in the movement.

This preliminary analysis of the displacement series is generally followed by the application of models, defined in literature, which provide simplified time-displacement curves of typical unstable slopes. The most frequently used models are based on the fact that, if viewed over a

long period of time, measured slope displacements may take the form of a standard creep curve, wherein accelerating slope displacements are taken as a warning of imminent failure (Crosta & Agliardi, 2002; Eberhardt, 2008). “Slope creep” is a time-dependent deformation, occurring without a stress change, characterized by a plastic behaviour (after an initial elastic recoverable strain, the remaining deformation is not recoverable). In the creep model, materials, after laboratory tests, show a typical evolution of the strain pattern characterized by three phases: a primary creep (also called “decelerating” or “transient”), characterized by a logarithmic decreasing of the strain rate; a secondary creep (also defined as “steady-state creep”), showing a constant strain rate; a third (or accelerating) creep, in which a continuous strain acceleration leads the material to failure (Figure 38).

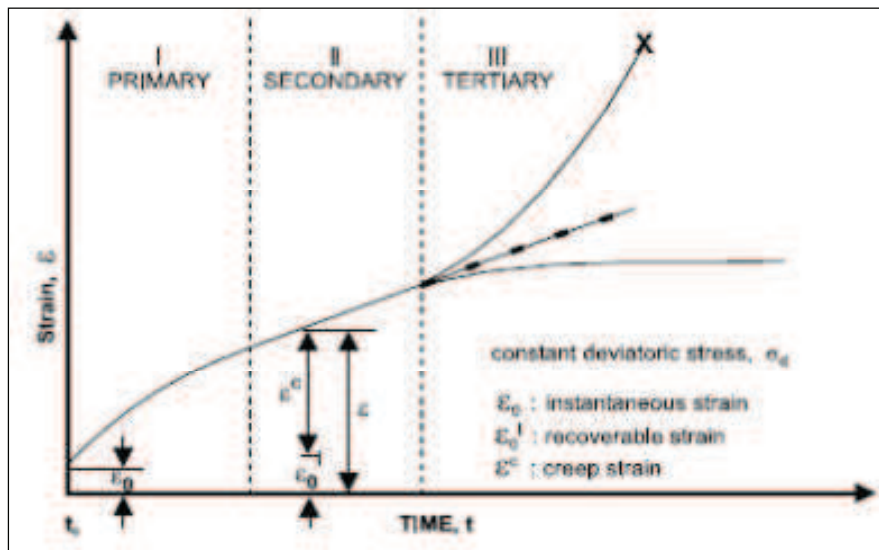


Figure 38. Theoretical creep behaviour for continuous materials and cohesive soils analysed in laboratory; X indicates the instant of failure (from: Crosta & Agliardi, 2002).

Three main approaches can be considered in the landslide study, taking into account the creep behaviour:

- a “micromechanical” approach, which studies the stress-strain relations on a molecular scale (Mitchell et al., 1968);
- a “rheological-mechanical” approach, which is founded on ideal models that are able to mathematically explain the processes (Dieterich, 1978, 1979; Cornelius & Scott, 1993);
- an “empirical” approach, in which displacement time series are used to describe evolution and behaviour of the unstable material, by applying empirical or semi-empirical relations (Saito, 1965, 1969; Fukuzono, 1985a; Voight, 1988, 1989a, 1989b).

The empirical methods are generally the most commonly used, because they fit better with the variability of experimental data: these methods are in fact based on the observation of real displacement data for predicting future behaviour.

The first complete dissertation on a method for forecasting the remaining time to slope failure from the secondary creep curve was proposed by Saito, in 1965; the same author also developed a forecasting method based on the analysis of the tertiary creep curve (Saito, 1969).

straight line passing through A_1' and N' with a straight line passing through M' and parallel to the time axis. The justification of this procedure is done through a geometrical process.

As [Saito \(1969\)](#) wrote, the effectiveness of the predictions is strongly related to the temporal span of the monitoring: it is important to start the measurements of the displacements as early as possible, in order to obtain better forecasts.

The simplest graphical method for finding the time of failure was later proposed by [Fukuzono \(1985a, 1985b, 1990\)](#). When a landslide is at equilibrium, its safety factor is exactly 1, defining the safety factor as the ratio between stabilizing and destabilizing forces. It happens in the secondary creep conditions (limit equilibrium); instead in the third creep phase, the landslide approaches the failure at the time t_0 , and is affected by an acceleration. The possible evolutions at this step can be two:

- the velocity can increase asymptotically, until it reaches the collapse at the time t_f , which theoretically corresponds to a velocity that approaches infinity;
- after an initial acceleration, the velocity decreases, reaching a new equilibrium phase, without collapsing.

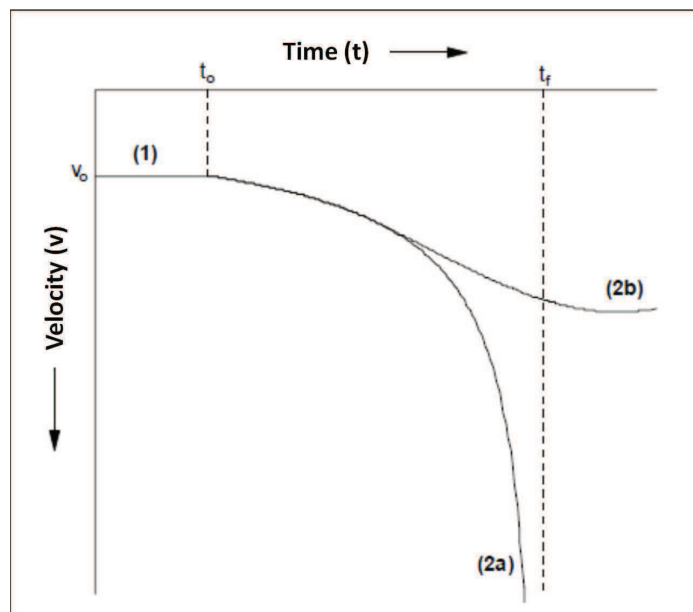


Figure 40. Possible kinematic evolution of a landslide phenomena. After a period of equilibrium limit characterized by constant velocity v_0 (1), the landslide can accelerate until it collapses, or it can accelerate and then reach a new equilibrium (2b) (from: Casagli et al., 2010).

The [Fukuzono \(1985a\)](#) approach was based on the next equation, which expresses the value of inverse velocity:

$$\Lambda \equiv 1/v = [A (\alpha - 1)]^{1/(\alpha-1)} \cdot (t_f - t)^{1/(\alpha-1)} \quad (18)$$

Where A and α are two constants empirically found.

Plotting the inverse of velocity ($1/v$ or Λ) versus time, it is very easy to graphically obtain the time of failure: while the landslide is at equilibrium, the graph is represented by a line parallel

to the time axis, but when the velocity asymptotically increases, the plot displays a line with negative angular coefficient that intersects the time axis when the velocity approaches infinity ($1/v$ is 0).

Therefore, from displacement data, the inverse velocity is calculated and then, the inverse velocity curve is extrapolated until it reaches the time axis at the point that corresponds to the rupture time (t_r): the extrapolation is graphically obtained through the intersection between the abscissa axis and the tangent or the regression line of the measure points (Figure 41).

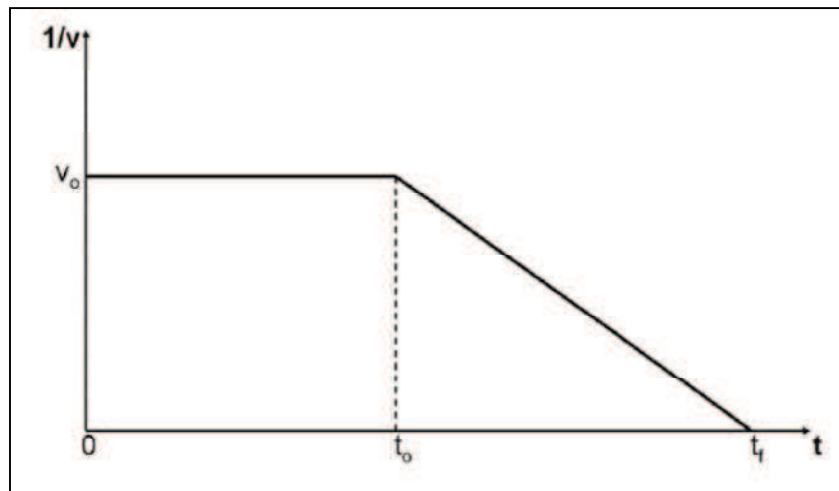


Figure 41. Plot of the inverse velocity versus time of a landslide approaching collapse.

The simplicity of the method makes it particularly useful and a lot of applications can be found, nevertheless it is important to take serious account of the uncertainties of all the approaches in order to estimate the failure time, partly related to the uncertainties in extrapolating the creep curves that could be highly irregular, partly because external or internal conditions of various origin could stochastically influence the results.

A generalization of the Fukuzono method, also applied to volcanic environments was proposed by Voight (1988, 1989a, 1989b). It is a more physically based method with respect to the ones proposed by Fukuzono and Saito; it estimates a threshold value considering the slope geometry and materials and groundwater conditions. An application of this method to determine threshold values for large rockslides was proposed by Crosta & Agliardi (2002).

Other authors proposed approaches to estimate the failure time of unstable slopes, such as Azimi et al. (1988) and Mufundirwa et al. (2010). However, the graphical method proposed by Fukuzono, thanks to its simplicity, remains the most used in the analysis of InSAR data for forecasting purposes.

Unfortunately, in literature only a few cases of successful predictions can be found (Kennedy & Niermeyer, 1970; Zvelebill, 1984; Suwa, 1991; Feltus, 1993; Hungr & Kent, 1995; Zvelebill & Moser, 2001; Rose & Hungr, 2007; Eberhardt, 2008; Casagli et al., 2009; Gigli et al., 2011); it is mainly related to the intrinsic difficulty of the forecasting evaluation.

Therefore, the forecasting phase represents a still open field in the research world.

3.3.4 Public education phase

The proposed EWS, based on the acquisition of InSAR data, must be organized in order to be “people-centred”, as suggested by the most recent guidelines on this matter; in other words, EWSs must consider supporting and empowering people at risk to protect themselves as its primary purpose. This objective can be reached by giving space in the EWS structure to the activities finalized to the public education.

First of all, the stakeholders of an EWS must be identified, together with their principal roles in the structured system. For simplicity, they have been divided into three main groups: the scientific stakeholders, the operational stakeholders and the citizens; their components and their activities in the EWS are listed below.

The “Scientific stakeholders” group includes universities, geosciences research departments, environmental agencies, national geological surveys and, generally, those institutes dealing with ground motions and working on the prediction, monitoring and supervision of the various types of geo-hazard processes. Their main goal is the collection and exploitation of data (in the specific case of InSAR data), through validation by *in situ* measurements and incorporation into models providing reliable services and useful information to the ultimate recipients (included within the EWS chain).

Scientific stakeholders deal with long-term monitoring of geo-hazards, collection of data and information related to natural hazards. The scientific community carries out prediction and prevention research activities, and collaborates at both functional and operative levels with the authorities to develop monitoring and surveillance for hydrogeological risks, mainly in the deferred time and, partially, in near-real time.

Scientific activities include education, capacity building actions, technical-scientific training and assistance for the civil protection agencies and local authorities, in the framework of simulated events, as well as the development of methodologies for the identification of ground displacement triggers, forecasting models, assessment of hydrological thresholds and the dangerousness of landslide processes, the definition of operative procedures and protocols for the identification of risk scenarios, in agreement with national and/or local authorities. This group of users is of crucial importance for the success of the EWS, especially during a geo-hazard-related emergency, when it represents the primary provider of information supporting decision makers, Civil Protection authorities, providing them with direct suggestions and recommendations and straddling both scientific and operational roles.

The “Operational stakeholders” group includes Civil Protection Authorities and policy makers and planners. These stakeholders need easily accessible, final, derived products, rather than the raw data on which they are based.

Civil Protection Authorities include all the structures and activities put into place by governments to safeguard the integrity of life, goods, buildings, cultural heritage and the environment from any damage arising from natural disasters, catastrophes and any other hazardous event. In joint collaboration with the scientific community, the civil protection

agencies coordinate the forecast of risk scenarios, manage monitoring and the whole early warning system, lead prevention activities aimed at minimizing damages, relief operations (rescuing people, ensuring early assistance to the population affected by disasters), as well as training activities to ensure citizen preparedness. Civil protection emergency management and support have demanding needs; resources (*e.g.* computing, data, services, knowledge and expertise) need to be shared in a coordinated, effective and timely fashion (simple and clear procedures); information including rapid identification of affected areas needs to be frequently updated.

In many situations this group represents the contact point between the scientific community and local authorities, and provides them with direct suggestions and recommendations during emergencies.

Policy makers and planners include a wide range of elected government officials at the national, regional or local level, politicians, administrators, land use planners and all those authorities taking part in the selection of the best actions to be performed among several alternative scenarios.

Decision makers are interested in simple long-term effective information on geo-hazards, to support their role in hazard mitigation (*e.g.* through stabilization and remediation works) and risk management (*e.g.* implementation of land use planning strategies, regulation and controls driven by clear and firm laws). Their information needs include identification, mapping and classification of areas with present or past ground instability, *e.g.* location, aerial extent, volume of displaced material, kinematical behaviour and evolution of the phenomenon in space and time. During and after emergencies, real-time information mainly includes monitoring activities (a continuous stream of information to remote control stations and alert systems), residual risk mapping (identification of affected areas and residual risk zonation) and analysis of stability of surrounding areas (selection of safe areas where the affected population can be relocated).

The "Operational stakeholders" group also includes a wide range of stakeholders from all sectors (*e.g.* environment, economic and transport), such as insurance, engineering and construction companies, infrastructure operators, land owners and pressure groups potentially affected by the planning activities in general. The different stakeholders have widely varying views, interests and needs, but, generally, they all require a true participation in early warning activities.

The citizens represent the ultimate beneficiaries of early warning activities and services, as they are those who are affected by risk and can benefit from proper strategies of risk mitigation, or suffer the consequences of inappropriate policies and actions. They need to be informed on where, when and to which extent ground instabilities will take place, in the short term.

Correct and thorough knowledge of a phenomenon is the first step in understanding and dealing with it properly preventing possible dangers. Regarding slope instability, one of the most important duties of the scientific community and responsible authorities is to make the population aware of the proper behaviour to adopt if a landslide occurs, by setting up

awareness and preparedness campaigns (increasing the ability to be prepared during unpredictable events), and establishing simple rules on how to prevent or minimize the damage induced by landslide phenomena.

Summarizing, the communication between all the stakeholders represents a crucial step in a well-organized EWS; this exchange of information includes the activities of public education and awareness addressed to citizens and operational users that effectively make the EWS “people-centred”.

The achievement of these objectives require systematic approach and activities involving all the components of the system and are described below, as proposed by [Basher \(2006\)](#):

1. Identification of the target population at risk, directly interacting with the people to determine needs and capacities;
2. Organization of meetings involving the population, finalized at exploiting and mapping their risks and planning their responses;
3. Promotion of the development by the communities of monitoring and warning systems for local risk;
4. Generation of public information customized to target groups and projects for the innovative use of the media and education systems;
5. Creation of formal mechanisms to publicly display monitoring activities and the warning system design;
6. Use of surveys to test the public awareness and satisfaction;
7. Increment of public memory by the organization of public events, creating monuments, publications and similar;
8. Organization of training on social factors addressed by technical experts, authorities and communicators who operate the warning system;
9. Organization of simulations and exercises to enable people to experience and practice warning interpretation and responses, including the possibility of dealing with false alarms.

In the complex picture of the public education phase, the role of the technician is fundamental for spreading the knowledge; in the specific case of landslide EWS it is essential to convey some basic notions of geology, in order that the potential risk, the causes behind the warnings, the reasons for the decisions taken by the authorities, etc. can be fully understand; in this sense the geologist represents a central figure who covers the role of the transmitter of the safety message, and the promoter of most of the activities listed above.

4. Applications and case studies

The approaches and methodologies presented in the previous chapters have been applied to specific case studies, analysed during this PhD research period.

The case studies regard landslide phenomena occurred over recent years. In some cases these phenomena are still active.

In order to provide a synoptic view of all four analysed phenomena, they have been schematized, following the geotechnical classification of landslide phenomena, proposed by [Sassa in 1989](#). It consists in the classification of the landslide events by taking into account: i) the failure mechanism, subdivided in fall, slide, slow or liquefaction and creep; ii) the material involved, that can be rock, granular material or cohesive material and iii) the post-failure mechanism of movement, such as the possible evolution of the landslide after the collapse, including fall or topple, slide or flow. A new class has been added to the classification, including the risk scenario, or better the most relevant elements at risk actually and/or potentially involved in the landslide event (Table 5).

CASE STUDIES		CAPRIGLIO	A16 HIGHWAY	SAN FRATELLO	ÅKNES (NORWAY-STORFIORD)	
CLASSIFICATION	FAILURE MECHANISM	FALL				
		SLIDE	X	X	X	
		FLOW/LIQUEFACTION			X	
		CREEP			X	
	MATERIAL	ROCK				X
		GRANULAR		X		
		COHESIVE	X		X	
	POST-FAILURE MOVEMENT	FALL/TOPPLE				
		SLIDE			X	X
		FLOW	X	X	X	
RISK SCENARIO		VILLAGES	HIGHWAY	VILLAGE	FJORD TSUNAMI	

Table 5. Case studies geotechnical classification (modified from Sassa, 1989).

The presented case studies have been selected (among existent landslide events), during the three year PhD activity, with the main aim being to cover a range variability that is as wide as possible, in terms of both failure mechanism, involved mechanism and post failure movement. Hence, the selected landslides have been considered the most proper and representative situations to practically apply and exploit the methodology theoretically presented in the previous chapters of this thesis.

The Capriglio landslide affected the Tizzano Val Parma municipality (Parma Province), in Northern Italy. A big slide, evolved in a flow and involving mainly cohesive materials, activated in the first week of April 2013, after a period of intense and prolonged rainfall events. A GB-InSAR was installed in the area during the previous days of emergency and is still active.

As regards the landslides involving the A16 highway (a major route connecting Naples to Bari, in Southern Italy), the study conducted during this PhD is part of a bigger project sponsored by the Italian Ministry of Education, Universities and Research (MIUR). It was aimed at the creation of an integrated system for monitoring and mitigating hydrogeological risk events and to the implementation of early warning measures along major Italian transport routes.

During the whole period of the PhD research, a long term InSAR monitoring was carried out, both from satellite and ground based platforms, in the San Fratello village (Messina Province); the area was involved in a translational slide evolved in a flow, at the beginning of February 2010. The phenomenon has been considered particularly interesting for the testing of some of the approaches proposed in this thesis.

The last case study that will be presented regards the Åknes rockslide, involving one of the most famous fjords of the Western Norwegian coast. This case study was part of my project during a research period conducted at the Norwegian Geotechnical Institute of Oslo (Norway), where I spent four months of my three year PhD course. A lot of literature exists and a number of studies have been done concerning rockslides, which were very useful for validating some of the methodologies and elaborations proposed in this thesis.

An overview of the location of the presented case studies is shown in Figure 42. The next subparagraphs will describe each case in detail.



Figure 42. Location of the presented case studies. The black star corresponds to the Norwegian case study (Åknes landslide); the red star is referred to the Italian case studies (1: Capriglio, Parma Province, Emilia Romagna Region; 2: San Fratello, Messina Province, Sicily Region; 3: A16 Highway, on the boundary between Campania and Puglia Regions).

4.1 The Capriglio test site (Parma Province, Italy)

In the spring of 2013, the Parma Province (Emilia-Romagna Region, Northern Italy) was affected by a large number of landslides, as a result of heavy and persistent rainfall (and snowfall melt), that occurred between January and April. This resulted in the triggering of about 1400 mapped landslides distributed in over 100 municipalities, causing more than 60 evacuees and severe damages to urbanized areas, infrastructures, cultivated and pasture lands.

In particular on 6th April 2013, a large landslide activated in the Tizzano Val Parma municipality. The upper crown destroyed a sector of the provincial roadway S.P. 101, putting at risk the villages of Capriglio and Pianestolla (Figure 43 and Figure 44).

Following these catastrophic events, the Earth Sciences Department of the Florence University (DST-UNIFI), on behalf of the Emilia-Romagna Region Civil Protection Department (DPC-RER), started a GB-InSAR monitoring campaign, in order to measure the possible ground deformation in correspondence with the above-mentioned villages, to detect the landslide kinematics and to support the local authorities in the emergency management. The installed GB-InSAR system is the prototype implemented and tested during the presented PhD research project (Chapter 2). In the framework of these activities, on 5th May 2013, aerial thermal and photographic surveys were also conducted, in order to map the area covered by the landslide in high detail. Field and GPS surveys were also conducted, with the aim of supporting and integrating the landslide mapping and monitoring activities.

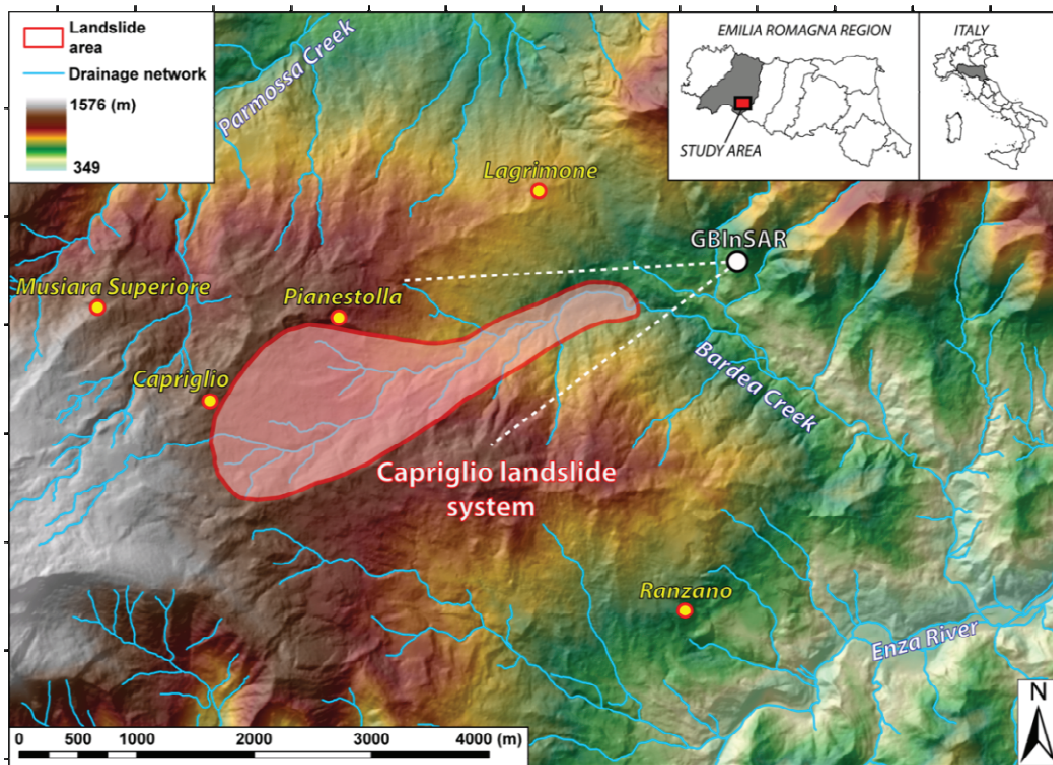


Figure 43. Location map of the Capriglio landslide and GB-InSAR system installation point.

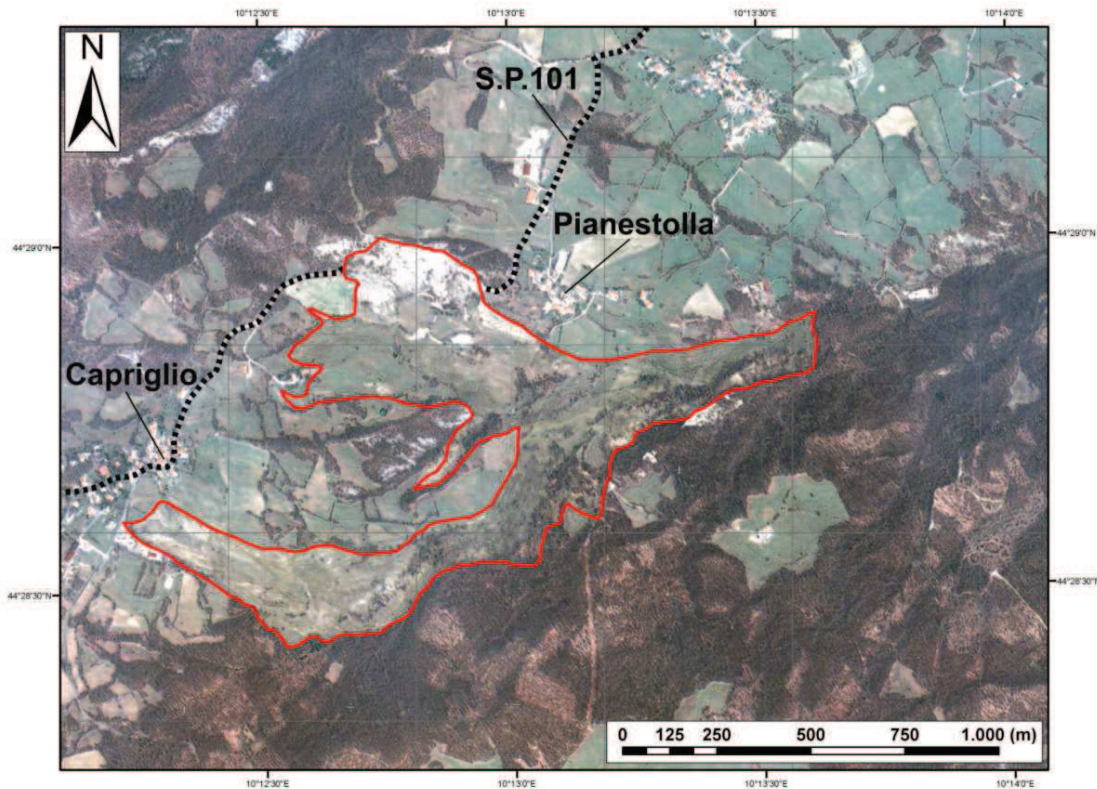


Figure 44. Satellite orthophoto of the Capriglio landslide, acquired after the event, on 16th April 2013 by Ikonos-2 satellite (courtesy of Emilia-Romagna Region Civil Protection Department). In red the preliminary landslide boundary assessment.

4.1.1 Geological framework

The Capriglio landslide is located on the Northern Apennines, specifically on the upper part of the Enza River basin, about 35 km SSW of the city of Parma, in the Emilia Romagna Region (Northern Italy). In particular the landslide area affects the left bank of the Bardea Creek, which is a tributary of the Enza River. It involves a middle-low mountain area where weak rock masses, constituted by an Upper Cretaceous turbiditic deposit extensively outcrops in the form of Monte Caio Flysch (Figure 45). This layer, which is part of the Monte Cassio Flysch Unit (Upper Campanian, Maastrichtian), in turn part of the Ligurian Units, is formed by thick bedded limestone and marlstones alternating with dark grey coloured claystone sequences (Bertolini & Pellegrini, 2001).

In the study area, the Flysch strata dip towards the SE sectors with low to middle angles (about 10-30°).

Besides the bedrock, the Capriglio landslide also involved the quaternary cover, represented in the area by various types of smaller pre-existing active and inactive landslides (Figure 45).

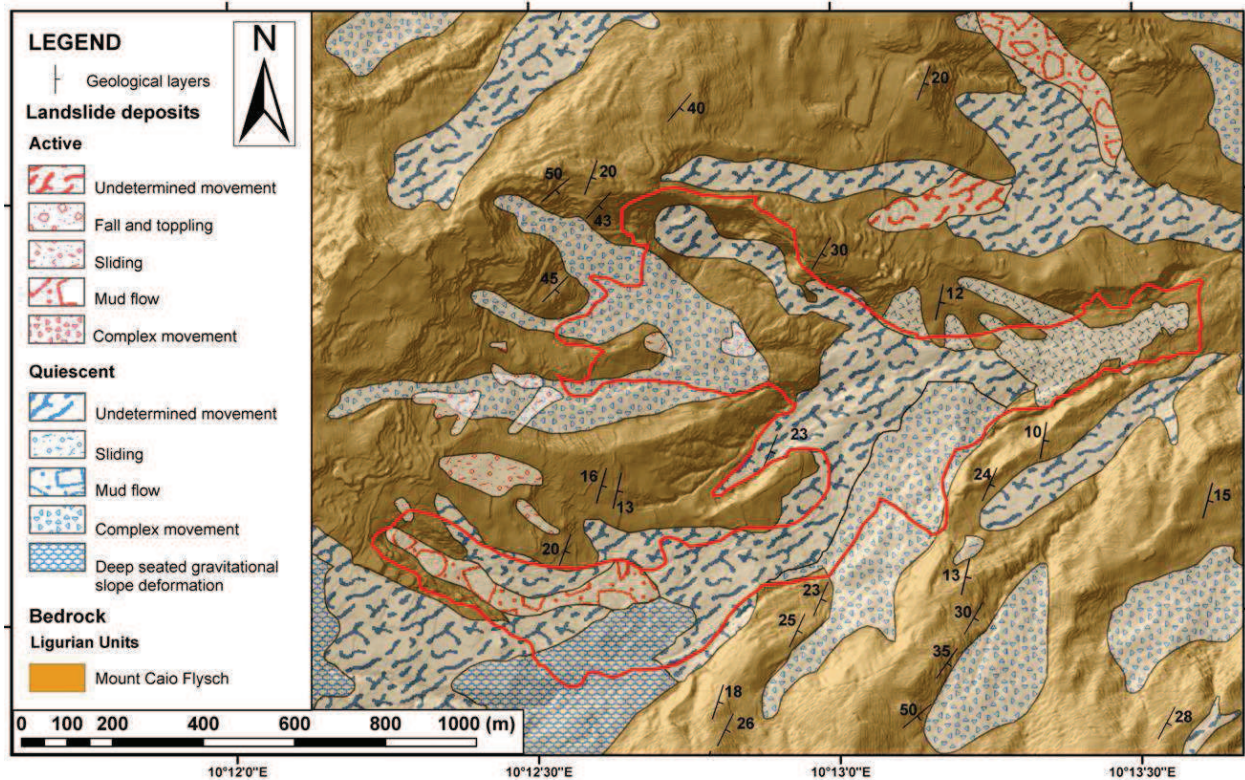


Figure 45. Geological map of the landslide area (in red the preliminary landslide boundary assessment).

The structural and lithological nature of the area, especially the abundance of weak clayey Units, generally located on the top of the successions, and the wide extension of detritus covers, represent the main predisposing factors of the high landslide susceptibility of the area. Moreover, the Monte Caio Flysch homoclinal dip also influences the slope's instability (Bertolini et al., 2005).

The hydrogeological setting of the area reflects the geology: the alternation between detritus covers, with variable permeability, and clayey layers, characterized by very low permeability values, determines the water accumulation in the covers, making them highly prone to landslide phenomena.

4.1.2 The landslide

The Capriglio landslide stretches from an altitude of 980 m to about 630 m a.s.l., covering an area of approximately 0.92 km² with a length of about 3.6 km, with a travel angle of about 6°. It can be considered as a composite system of two complex mass movements: a right bank landslide whose crown develops downstream the village of Capriglio; whereas the larger left bank one threatens the village of Pianestolla (Figure 46 A, B, C, D). Both are constituted in their upper sector by roto-translational earth slides evolved into earth flows which channel into the Bardea Creek bed, uniting and forming a large scale earth flow.

In the landslide, some sectors can be identified:

- the area in correspondence of the Capriglio village, where the landslide also involved the bedrock layer of the Monte Caio Flysch;
- the area upstream of Pianestolla, where most of the damage was registered: two buildings were evacuated and two others were destroyed, together with the destruction and interruption of the provincial roadway S.P. 101. In correspondence with the road, the landslide mainly involved the marly litofacies of the Monte Caio Flysch (bedrock);
- the landslide body, downstream of Pianestolla and along the Bardea Creek valley, where the landslide induced the major morphological changes and nowadays continues to modify the topography;
- the landslide toe, which develops in correspondence with a restriction in the Bardea valley; this morphological restriction implied a reduction in the landslide velocity and an increase in its thickness: these factors also caused instability on the flank slopes. Fortunately the landslide stopped at a distance of about 70 meters from a bridge on the Bardea Creek, on the Provincial Road S.P. 665R. Nevertheless, it is not possible to exclude eventual reactivations that could represent strong threats for the bridge and the Provincial Road.

In spite of the geological evidence, which suggest that the phenomena could be a reactivation of a previous one, no historical data exist to support this theory.

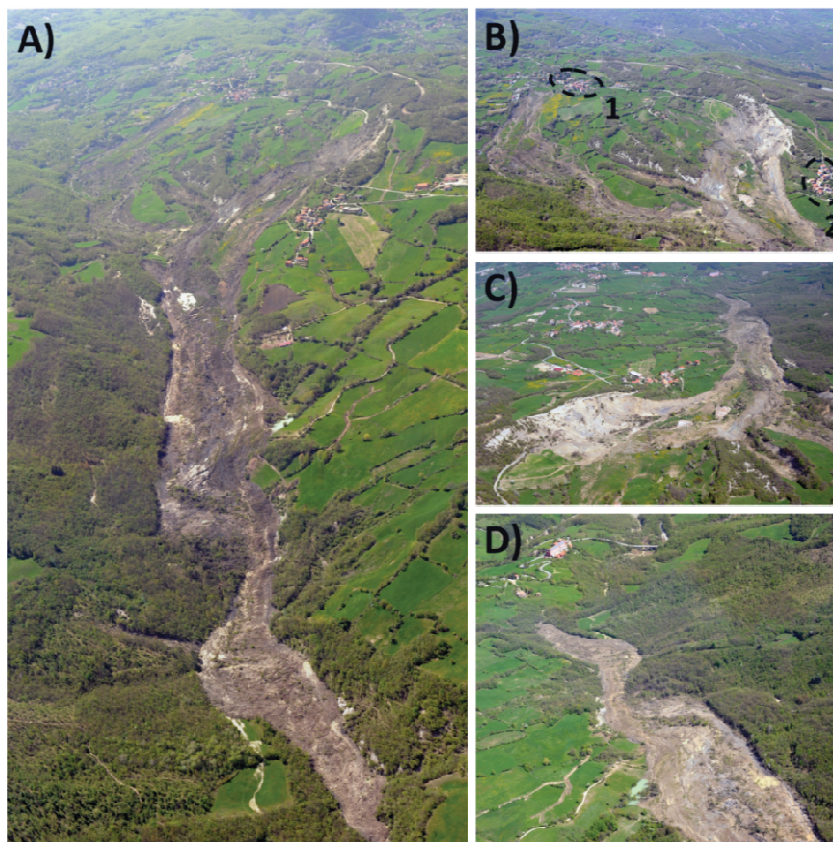


Figure 46. Aerial photographs of the landslide, acquired on 5th May 2013: A) landslide body overview; B) landslide upper sector; dashed ovals highlight the villages of Capriglio (1) and Pianestolla (2); C) the left bank crown; D) landslide lower sector and toe.

Thanks to an aerial thermal and photographic survey carried out on 5th May 2013, high resolution images of the landslide are available. The survey was carried out by mounting a thermal and an optical camera on-board an ultra-light aircraft (property of DST-UNIFI). In order to avoid image geometrical distortions, the cameras were placed in the aircraft hatch in order to obtain a line of sight as much as possible in a perpendicular direction with respect to the topographic surface. The line of flight was aligned along the landslide's longitudinal axis at an average altitude of 300 meters above ground level, leading to a geometric resolution of about 20 cm for both optical and thermo-graphic images. The latter were sequentially extracted from an infrared movie sequence (30 frames/sec) acquired by means of FLIR Research IR software. Non geo-referenced aerial images were also acquired from different lines of sight in order to provide a synoptic picture of the landslide. Overlapping images allowed a manual mosaicing and geo-referencing in a GIS environment using a previously acquired DEM and aerial optical image of the Emilia Romagna Region as base reference maps (Figure 47).

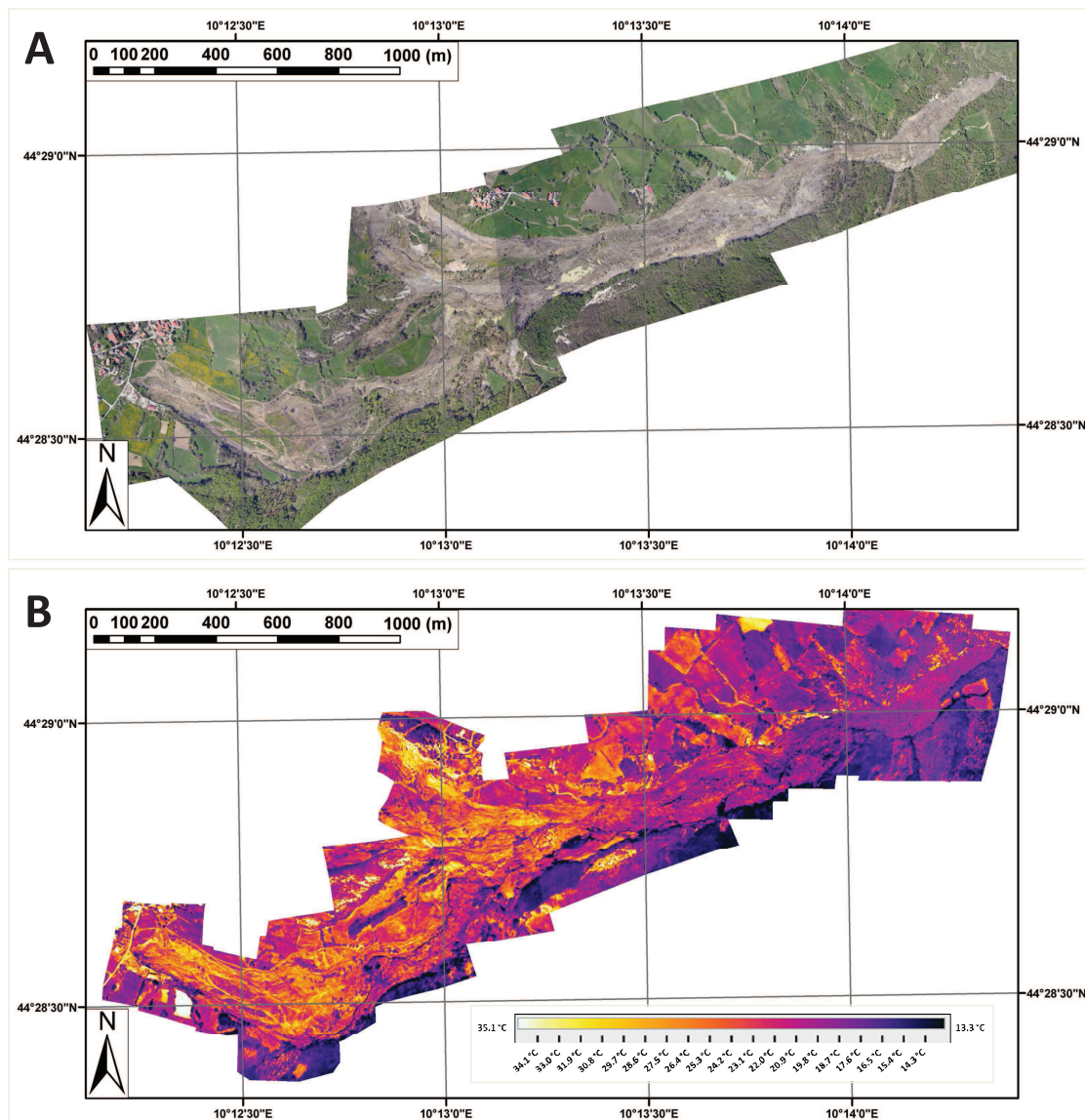


Figure 47. Aerial optical (A) and thermographic (B) images mosaics of the landslide.

The starting field surveys and GPS campaigns and the acquisitions of the aerial photos allowed monitoring of the landslide toe evolution and velocity with respect to the boundary initially assessed through the satellite image provided on 16th April 2013 by the DPC-RER (Figure 44).

This led to the estimation of the very fast evolution velocity (from about 80 to 10 meters/day) of the landslide toe, in the first two weeks of post-failure phase.

4.1.3 GB-InSAR monitoring activities

On 23th May 2013 a GB-InSAR system was installed in Lagrimone, a village located on the opposite slope of the Capriglio landslide, in the Tizzano Val Parma municipality. It was installed to monitor the displacements of the Capriglio landslide, as well as eventual millimetric movements affecting the villages of Capriglio and Pianestolla.

The system employed is a portable SAR device known as LiSA-Mobile, produced by the Ellegi Society; it is a new generation system performed in accordance with the proposed optimizations widely discussed in the second Chapter of this thesis.

The instrument was installed in order to develop long term monitoring that is in fact still active.

From 24th May 2013 up to today the system is continuously acquiring deformation maps and displacement time series of the landslide and of the villages of Capriglio and Pianestolla. In Figure 48, a picture of the employed system (A) and its view of the scenario are shown (B).

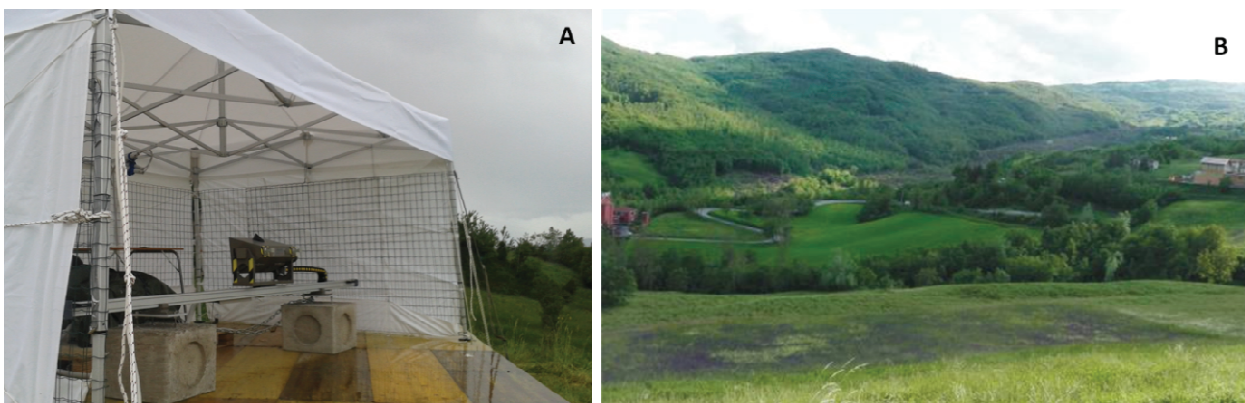


Figure 48. Picture of the employed GB-InSAR system (A) and view of the scenario from the instrument installation point (B).

In the initial phases of the monitoring activity, the landslide velocity was very high (about 10 meters per day). In this preliminary phase the use of the optimized interferometer was fundamental: thanks to the implemented possibility of obtaining very fast acquisitions, the detectable velocity highly increases. In other words, fast acquisitions were achieved, by using only a 1-meter aperture rail, obtained in less than 1 minute, by using the Ku microwave frequency, equal to 17.2 GHz. This configuration mode, defined as “very fast mode” allowed us to obtain acquisitions every 28 seconds, at the start of the monitoring activities. These parameters permit detecting velocity values up to 7 m/day (Figure 50Figure 49 A), corresponding to those landslides classified as “very fast” according to the Cruden & Varnes

(1996) classification. The reduced aperture of the rail implies an increase of the temporal resolution. At the same time this leads to the detriment of the spatial resolution; therefore the "fast configuration" allowed detection of only the fast displacements of the landslide body, but it didn't allow the monitoring of the Capriglio and Pianestolla villages, located very far from the installation point, at a distance of about 4.5 km and 2.8 km, respectively.

By exploiting the incremented flexibility of the instrument, in the initial phase, an alternation between "fast acquisitions" and "slow acquisitions" was performed. The "slow" configuration mode was based on the exploitation of the maximum available rail aperture (*i.e.*, 3 meters), by acquiring images every 8 minutes, with the same microwave frequency used in the fast modality (17.2 GHz).

The "slow" configuration allowed detection over a wider area, also including the villages, where the registered displacement values were centimetric (between May and August 2013).

Data were collected, stored, and processed on laptop computers installed directly on the field.

In Figure 49, the detectable areas in fast (red) and slow (yellow) configurations are displayed, emphasizing the GB-InSAR location, with respect to the Capriglio and Pianestolla villages and the landslide body.

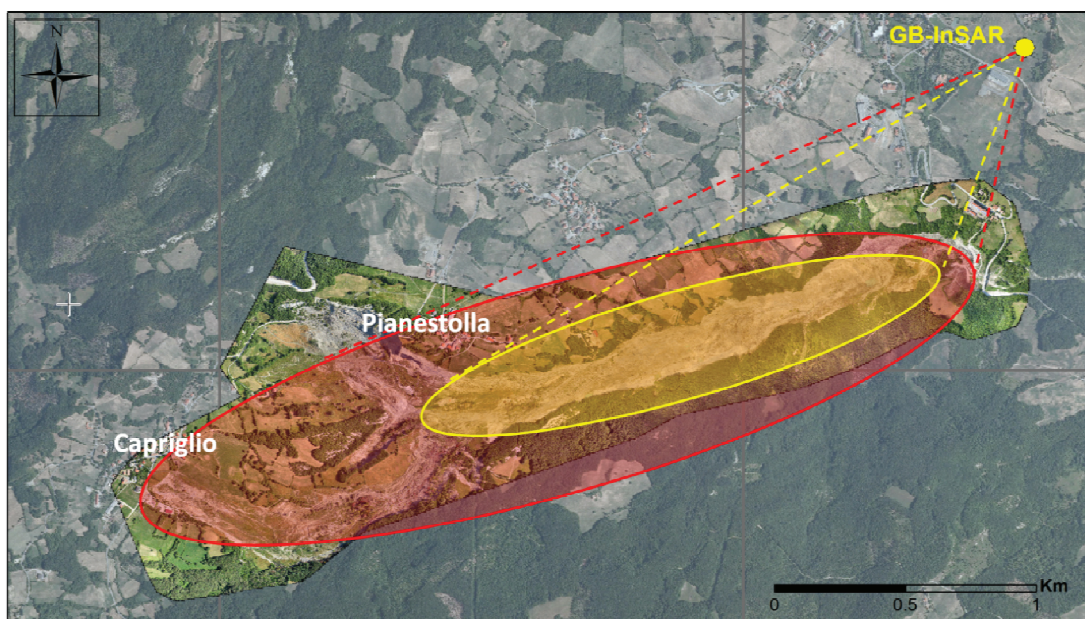


Figure 49. Detectable area in fast (yellow) and slow (red) acquisition modes.

It is important to take into account that the azimuth resolution reduced with the increasing of the distance from the installation point, therefore in correspondence with Pianestolla and especially Capriglio the azimuth resolution has low values. However, these resolution values are high enough to detect building clusters displacements.

Examples of interferograms acquired in "fast mode" are shown in Figure 50.

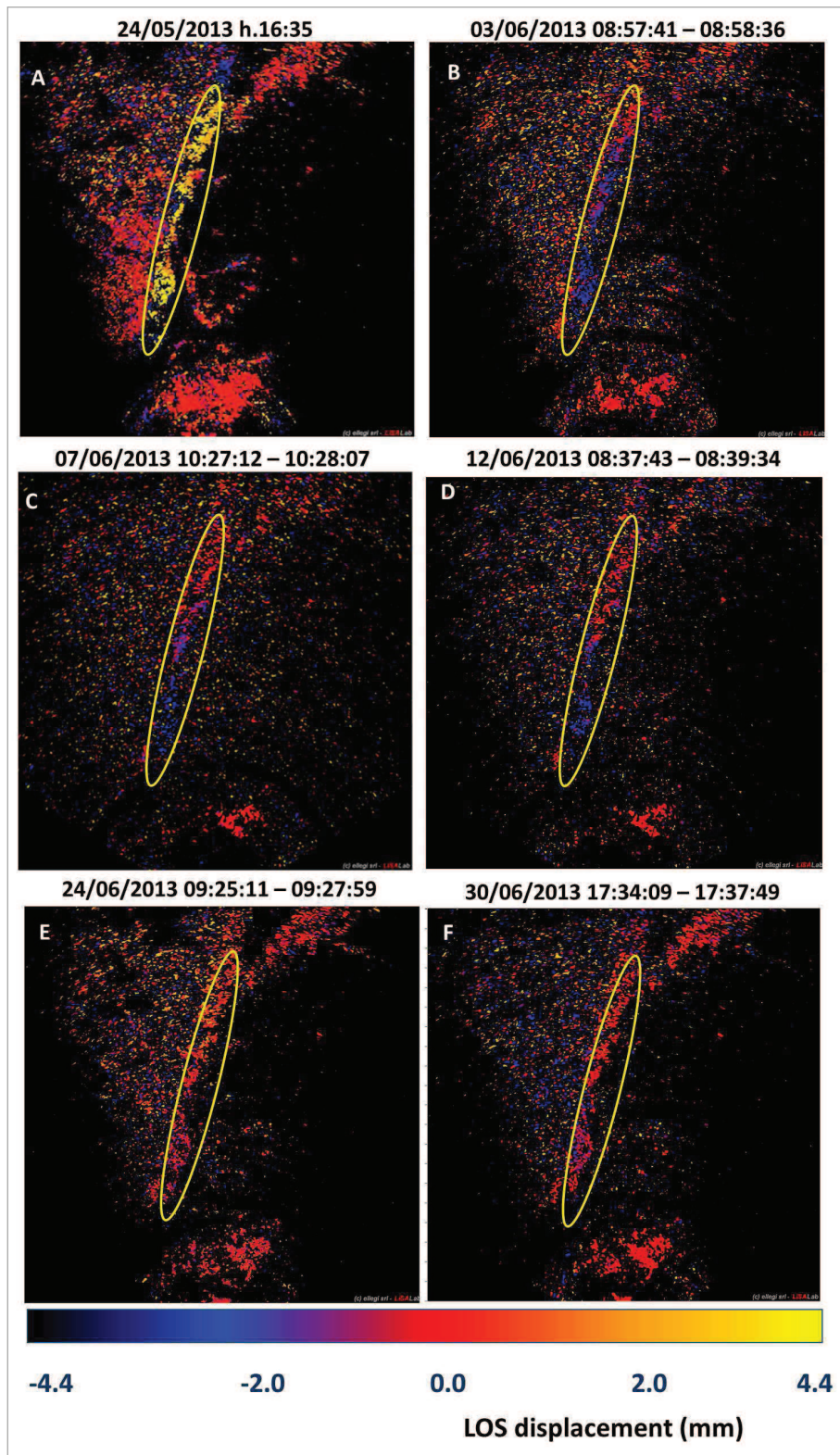


Figure 50. Interferograms (ITF) acquired in “fast modality”. Yellow dash represents the landslide body area. **A**: 28 seconds ITF – about 6.5 m/day; **B**: 55 seconds ITF – about 4 m/day; **C**: 55 seconds ITF – about 3 m/day; **D**: 1 minute and 52 seconds ITF – about 1.5 m/day; **E**: 2 minutes and 48 seconds ITF – about 0.3 m/day; **F**: 3 minutes and 40 seconds ITF – about 0.5 m/day.

Interferograms in Figure 50 clearly show the rapid decrease of the landslide velocity from the beginning of the monitoring, on 24th May 2014 (about 6.5 meters of displacement per day), up to the end of June 2013, when the velocity reached values less than 1 meter per day.

During the same period, "slow mode" acquisitions, every 8 minutes, were obtained; by using these interferograms a cumulated displacement map was produced (Figure 51), emphasizing the centimetric displacements which affected the Pianestolla and Capriglio villages in the period between 28th May and 28th August 2013.

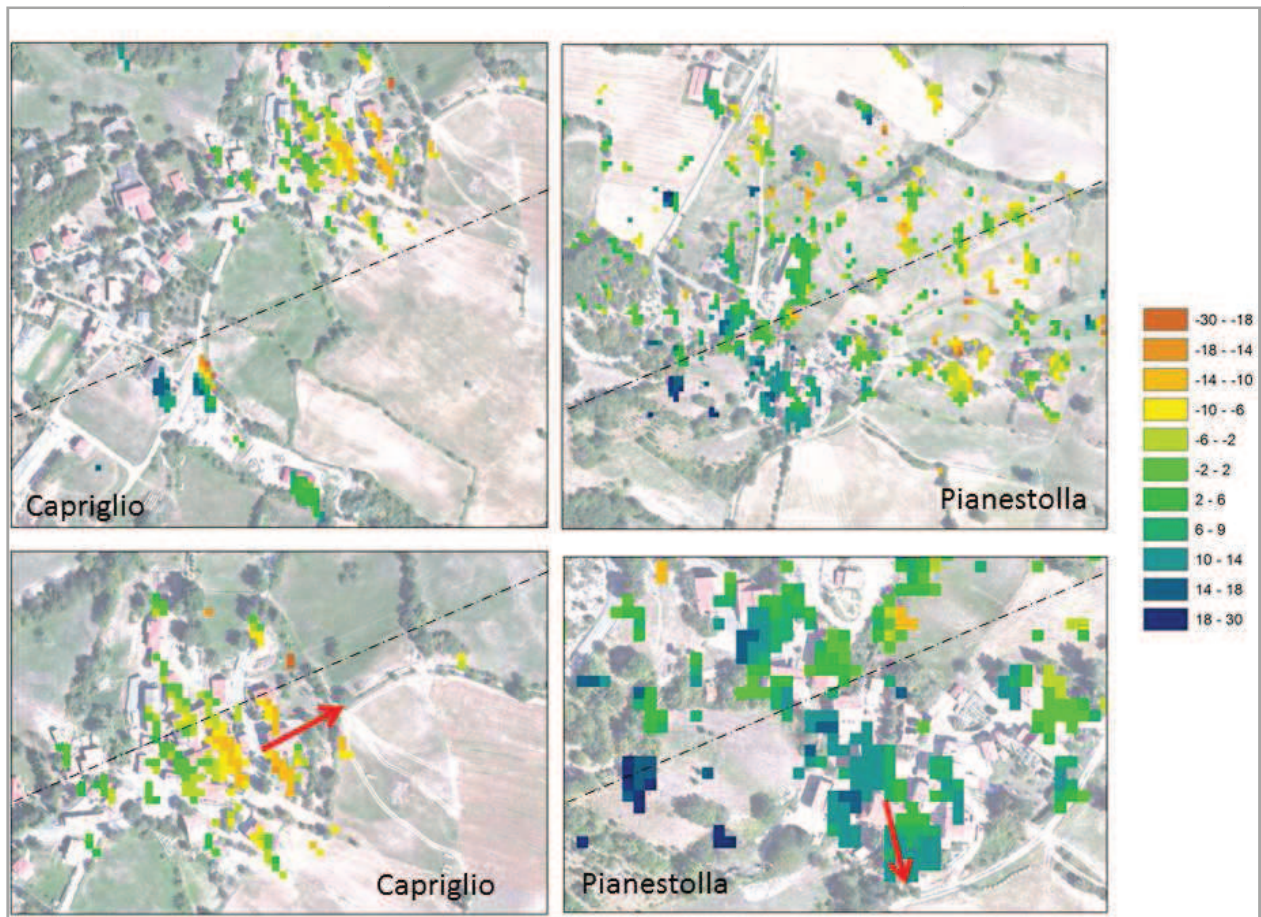


Figure 51. Cumulated displacements (cm) registered along the GB-InSAR LOS from 28th May to 28th August 2013 in Capriglio and Pianestolla. Red arrows represent the downslope direction, the dashed line is the LOS direction.

After the middle of July 2013, fast mode acquisitions were interrupted because the landslide velocity reached very low values (a few millimetres per day).

Slow acquisitions became ordinary and nowadays the instrument is acquiring in this modality, every 8 minutes. From these acquisitions, interferograms averaged on a period of 24 hours were generated and used to detect the velocity of the landslide and the villages. "Slow mode" interferograms are shown in Figure 52. They display the landslide body (A), Pianestolla (B) and Capriglio (C). During the monitoring activity, new sectors affected by deformation were identified; these areas are indicated by letters D and E in Figure 52– 3 and 4.

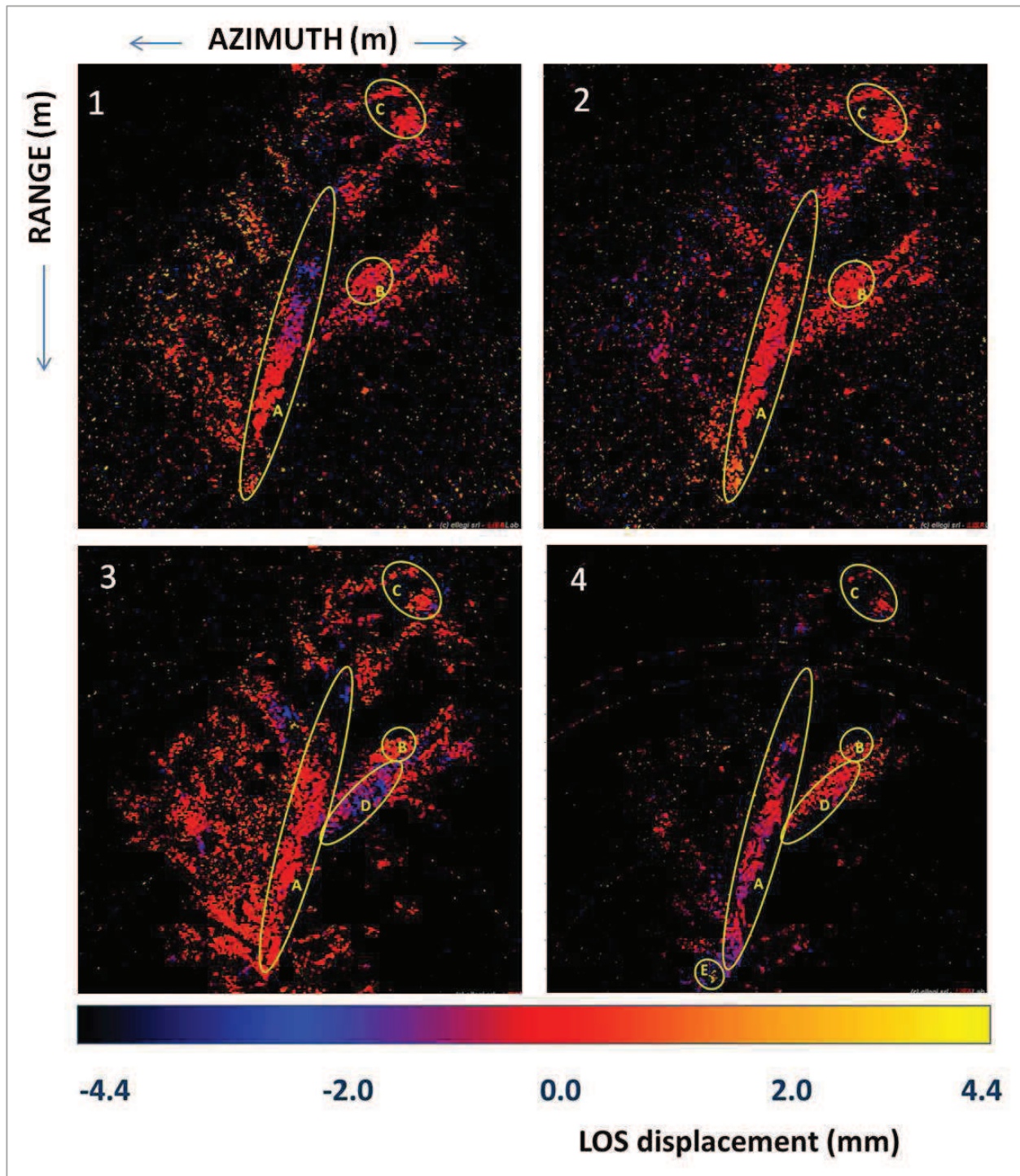


Figure 52. Interferograms acquired in “slow mode” and referred to a period of 24 hours. 1: 15th- 16th July 2013 – sector A = 2 mm/day, sectors B and C = less than 1 mm/day; 2: 16th- 17th July 2013 – sector A = 1 mm/day, sectors B and C = less than 1 mm/day; 3: 19th- 20th January 2014 – sector A = 1 mm/day, sectors B and C = less than 1 mm/day, sector D = 2 mm/day; 4: 18th- 19th February 2014 – sector A = 1 mm/day, sectors B, C and D = less than 1 mm/day, sector E = 5 mm/day.

The interferograms in Figure 52 show the substantial stability of the landslide body (A) and the villages (B and C); the two other identified sectors respectively correspond to a field near Pianestolla, affected by millimetric displacements since January 2014 (D) and an area covering the right flank of the landslide, in correspondence with the landslide toe (E), whose movement started on February 2014. Field surveys have been carried out in these sectors, to validate the

InSAR data; strong evidence of movements have been observed, especially in correspondence with the E sector. Fortunately, the activation of these sectors stopped in few weeks.

Data from check points located on the landslide toe were plotted on a graph, together with the displacement values estimated during the initial field surveys and GPS campaigns, and by the aerial and satellite photos. An example of these time series is shown in Figure 53.

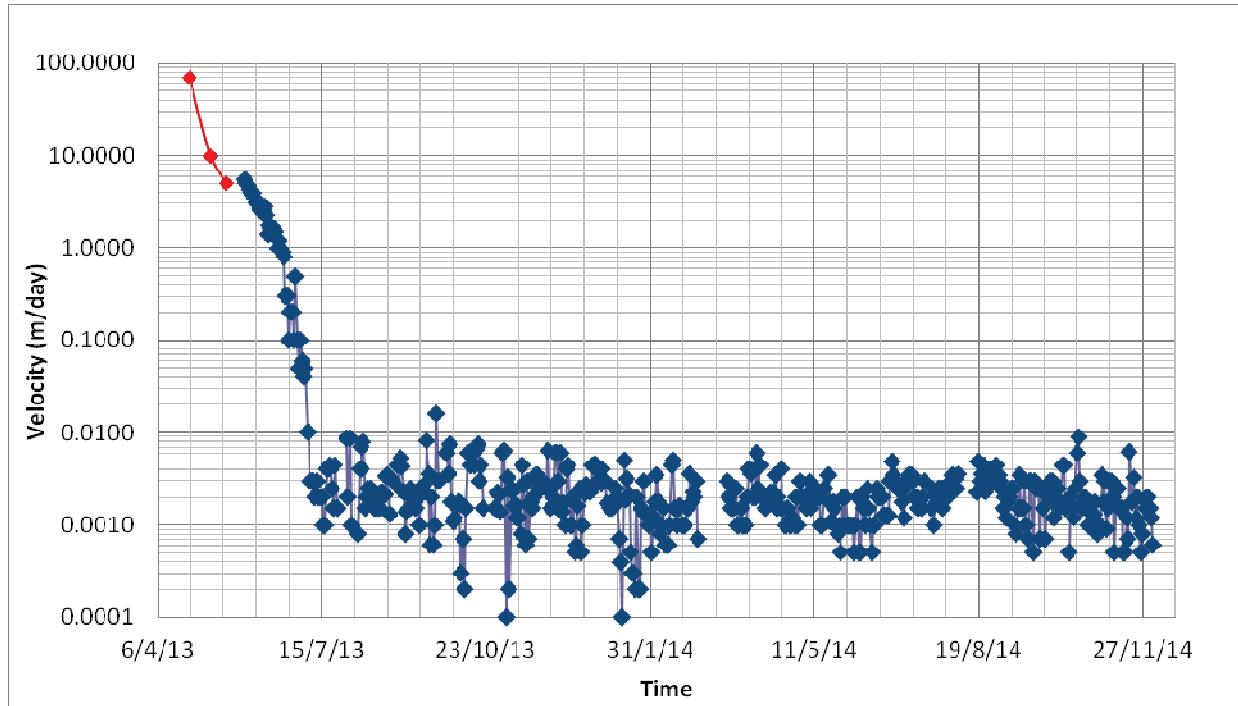


Figure 53. Time series of a control point selected in correspondence of the landslide toe. In red are shown displacement values estimated from aerophotogrammetric methods, field surveys and GPS campaign.

After the initial period, characterized by a rapid decrease in the displacement values, the landslide seemed to have a stable evolution, with displacement oscillations varying in the range of the technique precision. This pattern still persists today.

By projecting the data on a downslope direction, following the methodology proposed in the second Chapter of this thesis (sub-paragraph 2.3.2), projected data were analysed obtaining minimal differences respect to the non-projected data, except for the Pianestolla village; in this case displacements could be underestimated if the real movement direction effectively corresponds to the downslope one, which is, in this sector, almost perpendicular to the LOS (Figure 51).

4.2 Highways monitoring project (A16 – Naples-Bari Highway, Southern Italy)

The research presented in this thesis is partially included in a big Italian project, in turn part of a National Operational Programme (NOP), founded by the Italian Ministry of Education, University and Research and managed by the Department of Earth Sciences of the University of Florence (DST-Unifi), in collaboration with the Engineering Department of the Calabria University (UNICAL). The project, entitled “Integrated systems for monitoring, early warning and hydrogeological risk mitigation, along major transport routes”, aims to reduce landslide risk along Italian highways, by developing an integrated monitoring system, finalized to the implementation of early warning activities.

In this context, the DST-Unifi proposed to implement and validate a procedure to rapidly evaluate the landslide criticality level in correspondence with sections of those major Italian transport routes, selected as test sites. To this end, an *ad-hoc* GB-InSAR system, produced by taking into account the hardware and software optimizations proposed in Chapter 2, was implemented and tested on one of the test sites of the project. The system was performed in order to optimize existent instruments and overcome their major criticalities. Great attention was given to the data transmission, in order to create a network in which interferometric data can be channelled into an integrated system, that also includes data provided by other instruments, installed and managed by the other partners of the project.

The chosen test site is represented by a section of the A16 highway, which is located in Southern Italy and connects Naples to Bari; it represents a major conjunction between the Campania and Puglia Regions, and is located between the junctions of Lacedonia (Avellino Province, Campania Region) and Candela (Foggia Province, Puglia Region), on the East flank of the road.

Exactly in correspondence with the regional borders, the implemented GB-InSAR system was installed, in order to monitor a selected landslide phenomena, already mapped in local inventories. The selected area was chosen also taking into account the defined Geomorphological Sub-Units (SUG); these areas have been defined, in the context of the NOP project, in correspondence with the most critical zones along the highway. They have been inventoried and the selected test site is included in the SUG number 2 as shown in Figure 54.

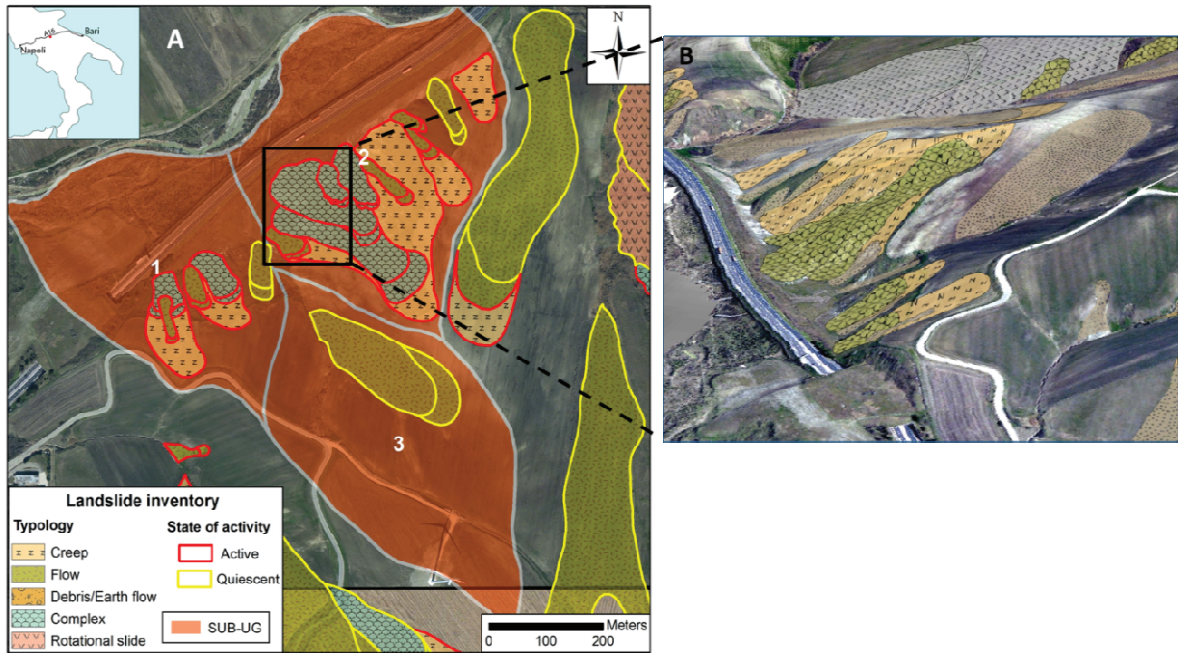


Figure 54. Test site location, corresponding to a section of the A16 highway (A). Monitored area (B).

4.2.1 The test site

The section along the A16, selected as the test site, develops in SW-NE direction in the Southern Italian Apennine, in correspondence with the valley of the Calaggio Creek (Figure 55).

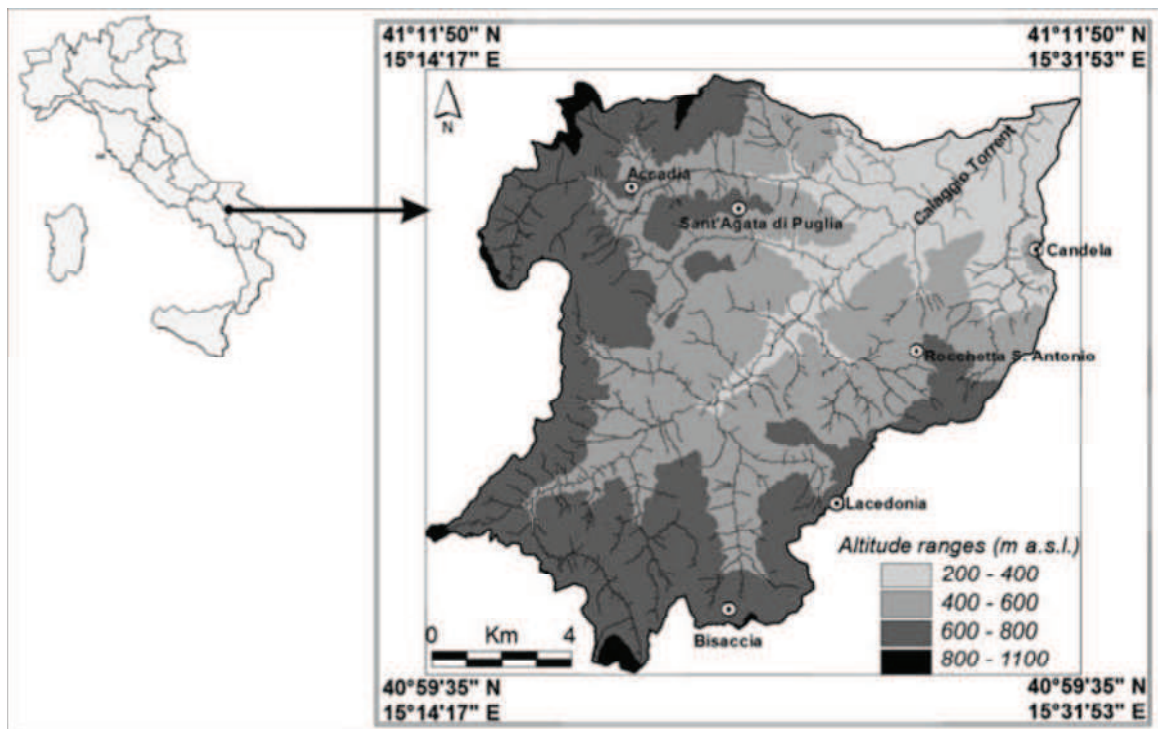


Figure 55. Digital terrain model of Calaggio Creek basin (from: Magliulo et al., 2008).

The highway runs on the right flank of the Creek at an altitude between 300 and 400 m a.s.l.. The area is characterized by sweet hills, with low relief energy. This morphology is related to the large presence of highly erosive materials, made up of loose gravel and clayey layers.

The area is tectonically active, but the lithological control strongly prevails over the tectonic one.

The unstable slopes are characterized by widespread landslides and areas affected by soil creep and solifluction. In particular, in the area of interest, the sandy and clayey superficial layers are frequently involved in slope instability.

The first step of the project activities was finalized to the selection of the specific test site, within the SUG defined in the context of the NOP project. In order to achieve this objective, some field surveys were carried out.

To be selected, a phenomena must answer to specific characteristics and needs, finalized to selecting the best to be monitored by a GB-InSAR system. At the same time, the risk intensity insisting on the highway has to be taken into account. Ideal areas have been searched, in order to test instruments and early warning procedures.

The features that make a test site ideal for the project finalities are listed below:

- Deformation typology: the ability of a GB-InSAR system to obtain deformation maps and eventually forecast the landslide evolution, by using approaches to prevent the time of failure gives its best results if the observed phenomena follows the rules of the "creep" deformation (Figure 38).
- Vegetation cover: using the Ku band of the microwaves, which is generally employed in the implemented GB-InSAR systems, it is not possible to penetrate the vegetation cover; moreover its seasonal variations and the continuous movements make it a source of decorrelation in the radar images. Therefore, the best scenario to perform a GB-InSAR campaign must be characterized by poorly vegetated cover.
- Velocity: the implemented GB-InSAR system is able to detect only a specific range of landslide deformation; it generally varies between very slow (not extremely slow, detectable only in long term monitoring campaigns) and very fast landslides, following the [Cruden and Varnes \(1996\)](#) classification. Creep deformation in pre-collapse phases generally respects these limits.
- Logistics: this element must not be underestimated because adequate resources are required to perform GB-InSAR monitoring; a power supply is necessary, a portable generator can also be used for short periods of monitoring activities. Moreover, data transmission is fundamental to the early warning purposes of the project, therefore a functioning transmission network is required.

It is very difficult to satisfy all the listed features together, therefore a compromise is always required.

In the specific case of the study area a phenomenon, that can be considered a good compromise between the listed characteristics, was selected in correspondence with the

boundary between Campania and Puglia Regions, in correspondence to the 112th kilometre of the highway, on the East carriageway.

A geological detailed map of the area was produced in the framework of the NOP project and is shown in Figure 56. The map shows the widespread presence of clayey lithologies, widely affected by instability phenomena, categorized as active by the regional landslide inventory, not far from the carriageway. The unstable areas were classified as soil creep and complex movements, widely affected by fractures in correspondence with the landslide crowns. The fractures can reach lateral persistence ranging between 5 and 10 meters and apertures up to 20 centimetres. Landslide scarps can also be observed, characterized by an average height between 2 and 5 meters.

Diffused and concentrated erosion phenomena can be also observed.

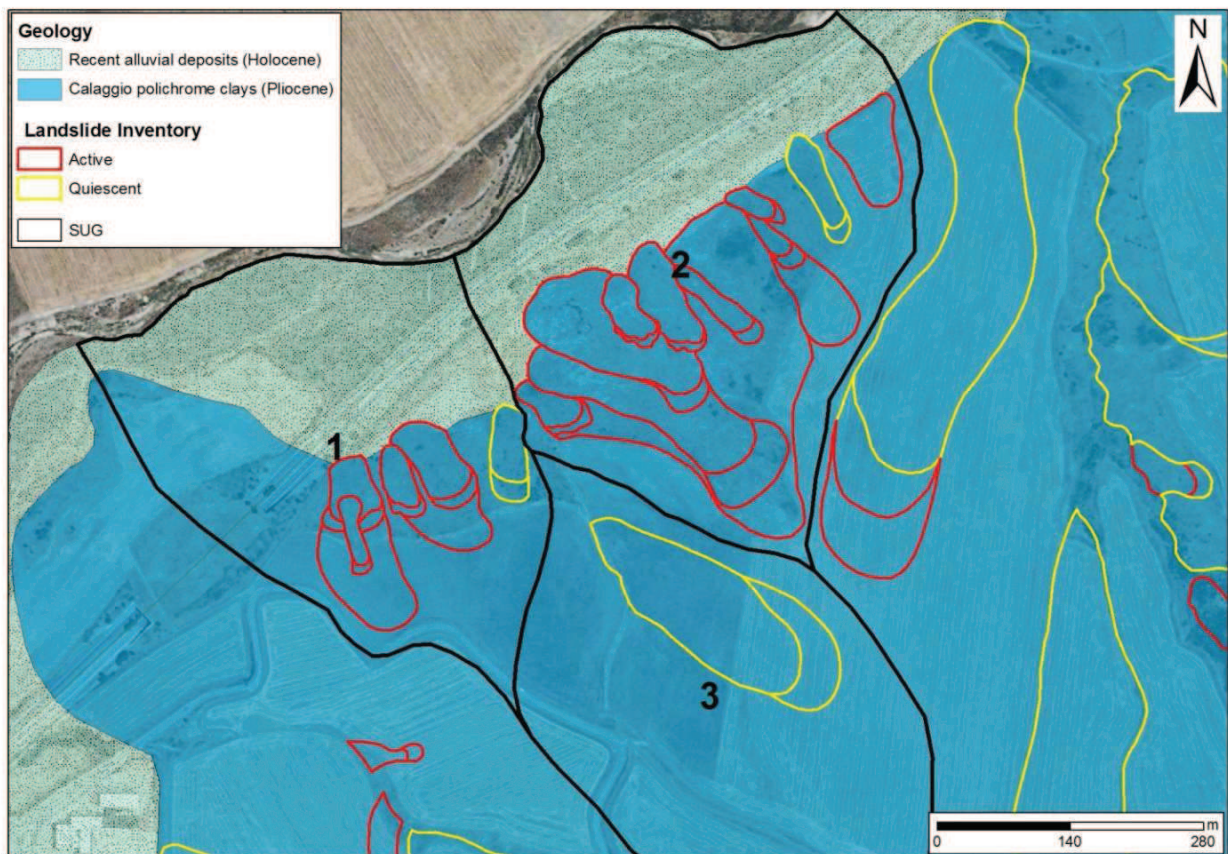


Figure 56. Detailed geological map of the study area, produced in the framework of the NOP project.

The chosen area is also affected by a reduced vegetation cover, in accordance with one of the required features for a proper selection. Two photos of the area, taken during the preliminary field surveys, are shown in Figure 57 and in Figure 58.



Figure 57. Panoramic view of the test site. It is possible to observe some of the instability phenomena, mapped by the regional landslide inventory.



Figure 58. Detail of a quiescent, vegetated landslide body.

4.2.2 GB-InSAR monitoring

The implemented GB-InSAR system was installed on the test site on 1st July 2014. The installation point was chosen taking into account the view of the scenario, the distance from the power supply network and from the highway.

A covered structure was built in order to protect the instrument from atmospheric agents and eventual acts of vandalism, in the perspective of a long term monitoring.

The transmission network was provided by a GSM modem, exploiting the 3G network. In addition to the PC integrated in the radar power base, a further external PC was exclusively employed for data transmission.

In Figure 59 the installation phases are shown.



Figure 59. Phases of GB-InSAR installation.

The system started its acquisitions on 1st July 2014 and today it is still acquiring. It is designed to produce radar images every 5 minutes and to elaborate these acquisitions *in situ*, producing interferograms every 5 minutes, and, by using averaged images, every 8 and every 24 hours.

The installation point allows us to observe an area, in the *range* direction, between 40 and 400 meters away from the instrument position, and about 360 m wide in the azimuth direction.

These dimensions, together with the 40° vertical aperture of the antennas, allow us to detect an area whose extension is about 360 m x 360 m. Nevertheless, the presence of a counterslope in the observed scenario determines a shadow area which partially reduces the extension of observable area, separating the scenario into two distinct sub-areas (Figure 60).



Figure 60. Aerial view of the GB-InSAR monitored area.

The observed scenario is characterized by poor vegetation. The landslide crowns are clearly observable; these latter, representing good reflectors for microwaves, are easily detectable on the interferograms. In Figure 61, a microwave power map is shown, together with the location of the major reflectors on the observed scenario.

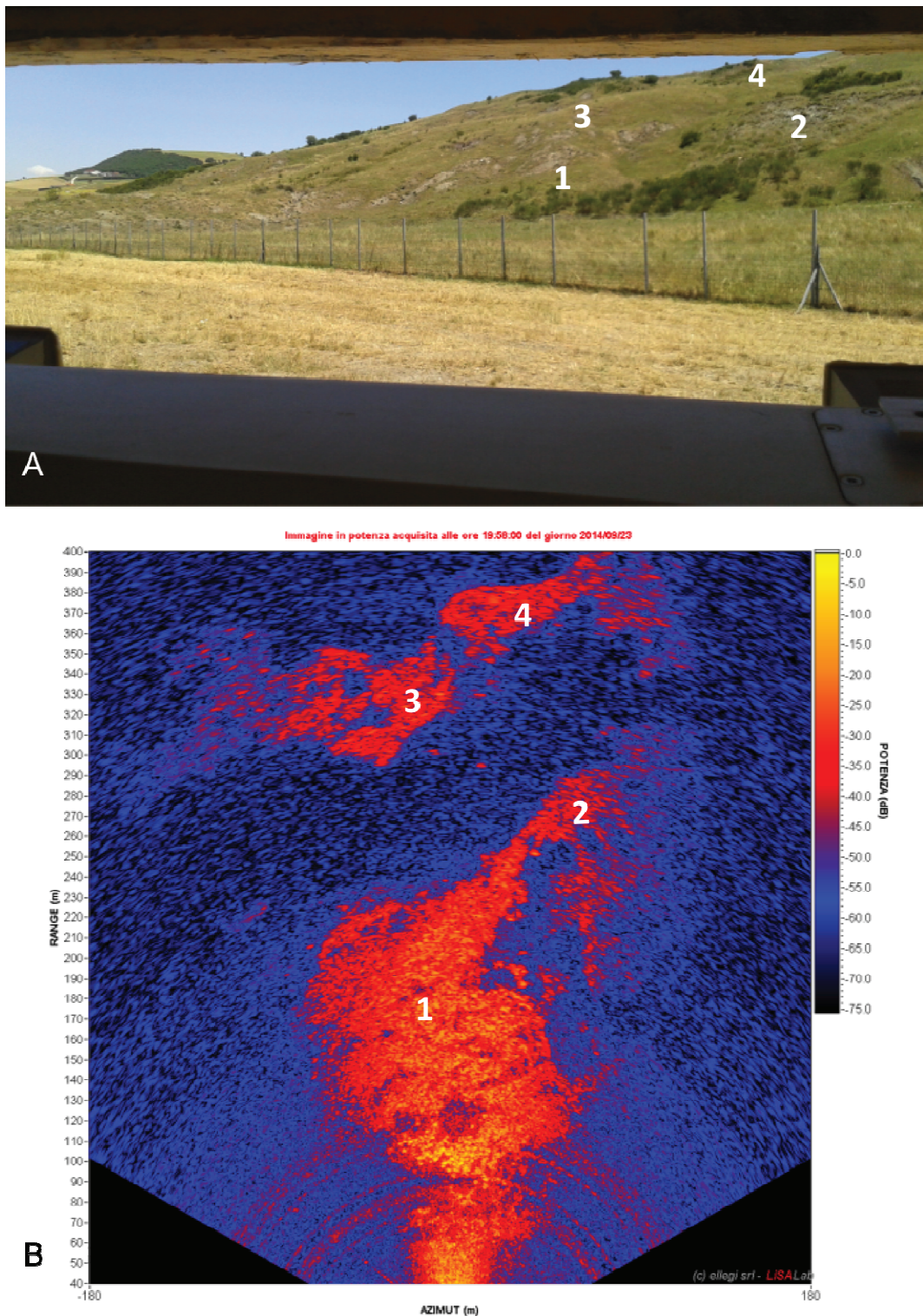


Figure 61. Observed scenario from the GB-InSAR installation point (A). Power map of the investigated area (B). The numbers represent the principal microwave reflectors on the photo and their equivalent positions on the power map.

The slope is mainly characterised by good reflectance to the microwave signal, allowing good quality interferograms, in spite of the presence of a metallic net, delimiting the highway

property, which interferes with the radar signal, determining noise in the lower part of the observed scenario.

Moreover, decorrelation effects have been verified in correspondence with the vegetated portions of the slope.

The monitoring campaign, still in course, allowed us to produce interferograms and time series of the observed area, which seems to be affected by a substantial stability.

Examples of interferograms, related to different span times, are shown in Figure 62.

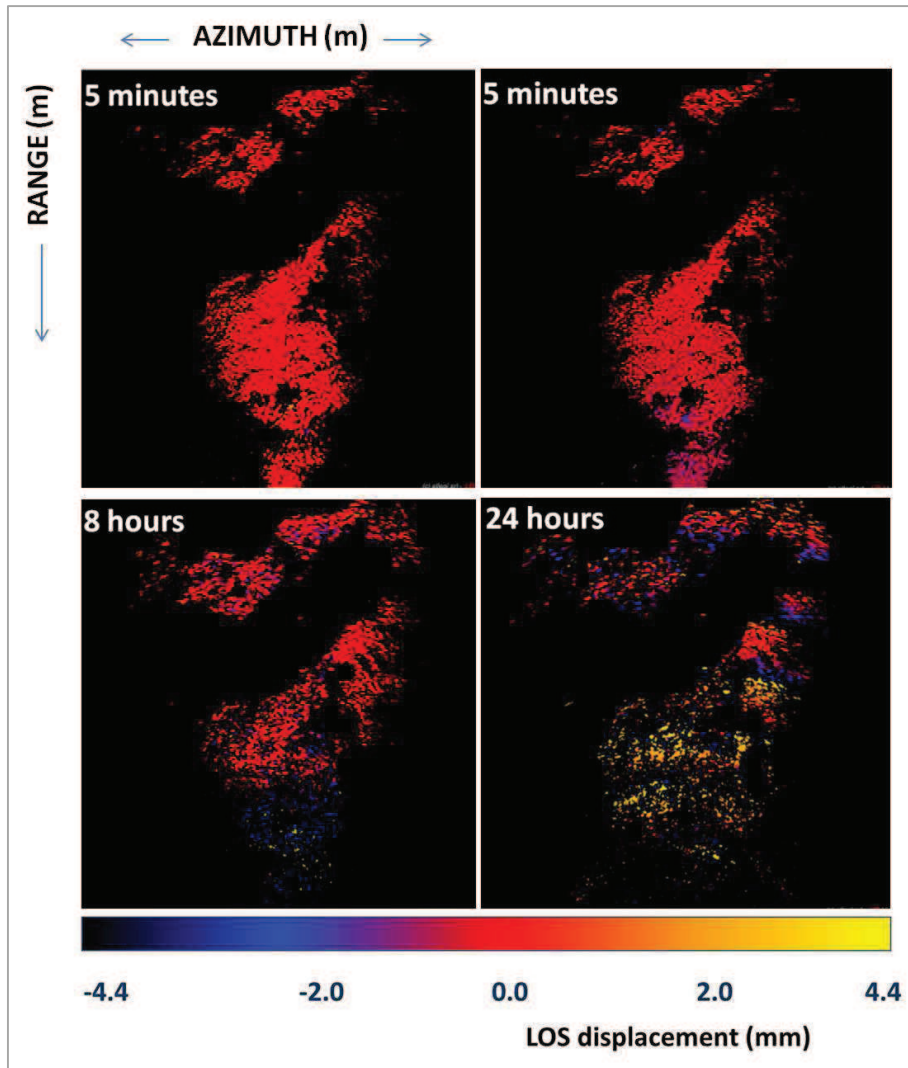


Figure 62. Examples of acquired interferograms related to different span times.

The lower portion of the interferograms is generally affected, with different intensity, by the decorrelation related to the metallic net; instead, the temporal decorrelation related to the vegetation cover grows with the increasing time interval covered by the interferograms: it is null on 5 minute interferograms, medium on 8 hour interferograms and it could become highly intense on 24 hour interferograms (Figure 62).

The application of the implemented algorithm, REACT (paragraph 2.2), to isolate the atmospheric component from the microwave phase, shows its utility, in fact the corrected interferograms don't show disturbance related to the atmospheric interactions.

In order to obtain more detailed information from GB-InSAR data, they were projected on a downslope direction, following the methodology proposed in the sub-paragraph 2.3.2 of this thesis.

The results consist in the production of a map representing the percentage of the real displacement that the GB-InSAR is able to observe from its position, by considering as "real" the movement which follows the downslope direction (Figure 63). Moreover, maps representing the downslope deformation values have also been produced (Figure 64).

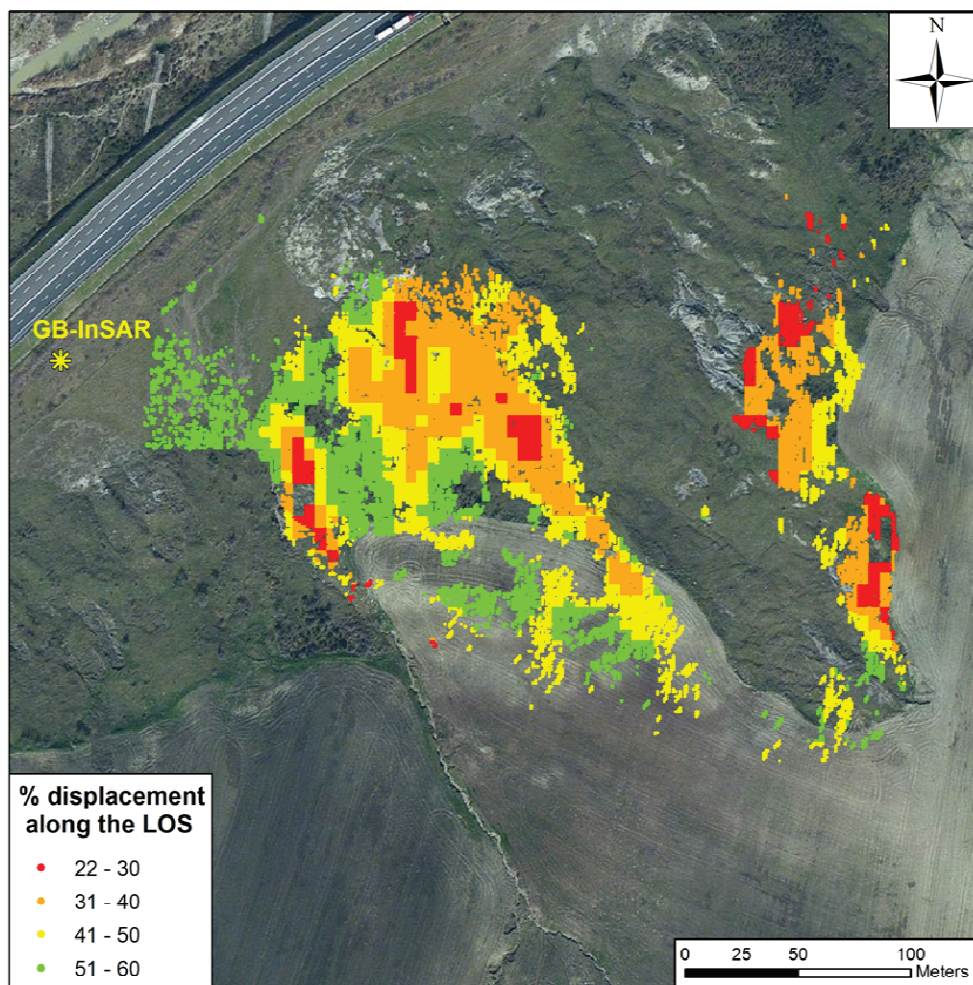


Figure 63. Percentage of real displacement (downslope projected) detected by the GB-InSAR system.

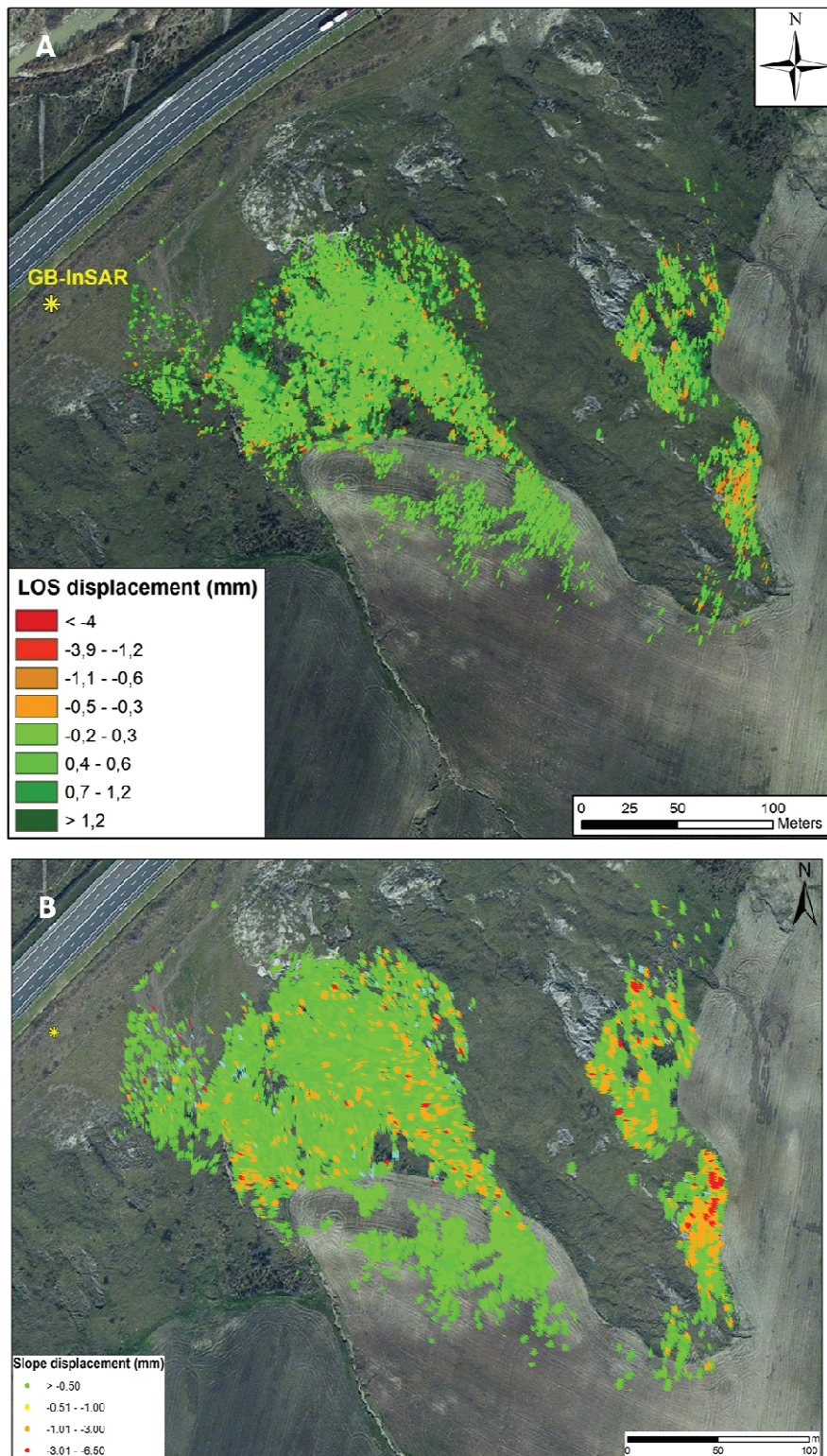


Figure 64. Cumulated displacement maps referred to a period between 1st July 2014 and 1st November 2014. A: displacement values registered on the GB-InSAR LOS direction; B: displacement values on downslope direction.

Assuming that the observed landslide actually moves along the downslope direction, the percentage of real displacement, detectable by the GB-InSAR, ranges between 22 and 60 % (Figure 63).

The general stability of the area is confirmed by the displacement values observable on the interferogram in Figure 64 A, that represents a cumulated displacement map related to a period from 1st July 2014 to 1st November 2014. The comparison between the LOS displacement (Figure 64 A) and downslope displacements (Figure 64 B) doesn't show big differences between the two maps, determining a further confirmation of the substantial stability of the area. Only the eastern portion results are affected by maximum displacements of about 4 mm in 4 months; these values can be still considered in the range of stability.

The monitoring system is also programmed to create a displacement time series of check points selected on the interferograms. The points have been chosen in correspondence with the interferogram portions characterized by the best signal to noise ratios.

The three most significant time series are shown in Figure 65.



Figure 65. Representative displacement time series of the test site.

Time series were statistically analysed in order to discard or reduce the noise component and to individuate eventual trends.

Simple mobile averages were applied to reduce the noise component, and Z score values evaluation was carried out to define the presence of trends.

The substantial stability of the area was also confirmed by these statistical analyses that did not emphasize the presence of any trend.

4.2.3 Data transmission

Great attention was given to data transmission which represents a crucial step in creating a network finalized to early warning activities.

The system was designed in order to allow data storage on the PC integrated with the instrument (part of the power base). This PC is connected, by LAN cable, to the external PC and they communicate with one another by exploiting the GSM-3G network. A *MatLab* script, working on the external PC, recovers useful data from the “inner” PC, converts them into ASCII format and stocks them. GB-InSAR images in ASCII format are represented by matrixes constituted by 1001x1001 complex values; every image dimension is about 8 MiB and two of them are required to produce an interferogram. It has been programmed that the PC extracts and stocks interferograms related to specific intervals (in the specific case of the A16 test site, these intervals correspond to 5 minutes, 8 hours and 24 hours) and the related displacement time series.

In the context of the NOP project, these data must be transmitted to a control centre, together with the data provided by other monitoring systems that must be installed to monitor the same test site. This finality strongly increases the importance of reducing the weight of transmitted data: the decision to transmit data related to specific time intervals and their conversion in ASCII formats have been defined in order to reduce to the minimum the load on transmission network and, later, on the operative centre, where data provided by all the monitoring systems are physically collected.

4.2.4 Early Warning System

The main finality of the NOP project is to create an integrated network of monitoring systems, finalized to perform early warning activities capable of mitigating the landslide risk; in the end, an operative protocol on the management of landslide risk in correspondence of the major routes must be created.

As regards the part of the project included in this PhD programme, GB-InSAR data have been used to perform the monitoring and forecasting phases of an early warning system, following the guidelines and the proposals widely discussed in Chapter 3 of this thesis.

Monitoring activities have been organized in order to continuously acquire data, every 5 minutes, and to transmit and stock them in the form of interferograms and time series related to 5 minutes, 8 hours and 24 hours time intervals.

The system was also implemented to automatically evaluate the eventual instability on slope portions. This evaluation can be carried out in four steps:

1. Continuous automatic data acquisition, thanks to the high acquisition frequency of the employed GB-InSAR (every 5 minutes) and the availability of a software able to automatically elaborate the data;

2. Rapid data transmission thanks to the optimization of transmission operations, finalized to a remote data control;
3. Automatic evaluation of the eventual exceeding of pre-defined threshold values, followed by real-time communication to operators of the excess, to permit manual validation;
4. When possible, automatic evaluation in advance of failure time, followed by real-time communication to expert operators for manual evaluation.

After the definition of transmission data procedures and adequate data stream that can be supported by the network, also in emergency conditions when the transmission must be as fast as possible, threshold values must be assessed, in order to determine different warning levels.

The number of warning levels is set at four, according to the NOP project requirements. Different levels are indicated by a number from 0 to 3 and correspond to an increase in the detected displacements.

In a preliminary phase, threshold values were defined on the basis of literature data: observing the geological and geomorphological evidence of movement, it is possible to pre-determine the most probable velocities of the landslide, referring to the classes proposed by [Cruden & Varnes \(1996\)](#), as shown in Table 6 and in Table 7.

Class	Description	Typical velocity values
I	Extremely slow	6 mm/year
II	Very slow	16 mm/year
III	Slow	1.6 m/year
IV	Moderate	13 m/month
V	Fast	1.8 m/h
VI	Very fast	3 m/min
VII	Extremely fast	5 m/s

Table 6. Landslide classification, based on velocity values (Cruden & Varnes, 1996).

Typology	Fall	Slide				Flow			
		Rock		Debris	Earth		Rock	Debris	Earth
Activity		N	R		N	R			
Velocity	VI-VII	V-VI	I-V	I-VI	V-VI	I-V	I-II	I-VII	I-IV

Table 7. Landslide typical velocity (referred to Table 6) in relation with type of movement, material and activity state (N: Neoformation; R: Reactivation) of the phenomena (from: Canuti & Casagli, 1996).

Table 7 has been used to define indicative threshold values which, in the next phase, will be calibrated on the basis of the results of the monitoring activities.

In level 0 (no variation respect to the ordinary), data images are acquired every 5 minutes and interferograms are generated on time intervals proportioned with the registered velocities (generally these intervals correspond to the mentioned 5 minutes, 8 hours and 24 hours).

The switch to the next level (Level 1) is related to the exceeding of the first threshold, which usually corresponds to the instrument precision: indeed a displacement variation over the theoretical precision could determine a significant variation in the landslide activity. However, the level switch is subordinated to an exceeding of the threshold in areas where the registered value is defined compatible with an effective displacement, considering also the stochastic noise component, eventual external factors and so on; therefore, the switch must be validated by an expert operator, who also must have a good knowledge of the interested area and of the employed instrument.

The procedure that corresponds to the switch to the other levels (Levels 2 and 3) is substantially the same.

The evaluation of the Z score value of displacement time series has been used to define these thresholds in the A16 test site: the threshold values, determining respectively the switch from level 1 to 2 and from level 2 to 3, were defined as 0.5 and 1 standard deviations of the average of the displacement distributions.

When displacements exceed the defined thresholds, emails are automatically sent to expert operators. The automation is obtained in *MatLab* environment and it allows the operators to manually validate the effectiveness of the exceeding.

When the Level 2 (medium intensity variation of the landslide activity) is passed, the operators start to apply tests to evaluate and forecast the time of an eventual failure, using the Fukuzono method (sub-paragraph 3.3.3).

The monitoring activities are still operating; until today, the displacements never exceed the defined thresholds, so only ordinary activities have been tested and carried on.

4.3 San Fratello test site (Messina Province, Southern Italy)

The village of San Fratello is located in north-eastern Sicily, Italy (Messina Province), on the north-western hillside of the Nebrodi Mountains (Figure 66), a 70-km-long ridge with an ENE-WSW direction, within the southern Apennine chain.

The northern part of Sicily has been historically affected by landslides (Goswami et al., 2011; Mondini et al., 2011; Del Ventisette et al., 2012b; Bianchini et al., 2014). In particular, the Messina province is prone to landslide hazard, mainly due to the steep topography, the nature of the lithotypes, mainly consisting of flysch units with tectonized silt-clay levels, and the occurrence of intense and seasonally high rainfall events. The main landslide types can be prevalently classified as debris flows, complex slides (Varnes, 1978) and shallow and deep-seated landslides.

Between the end of 2009 and the beginning of 2010, the Nebrodi Mountains were highly affected by several landslide events, causing intense damages and casualties. Some of these landslides are still active at present day. Intense and exceptional rainfall events (about 900 mm in the period between October 2009 and January 2010) were the main factor that, combined with the strong topographical relief, triggered several slope movements. One of the most important mass movements has been recorded in February 2010 in the San Fratello village, a place chronically affected by landslides.

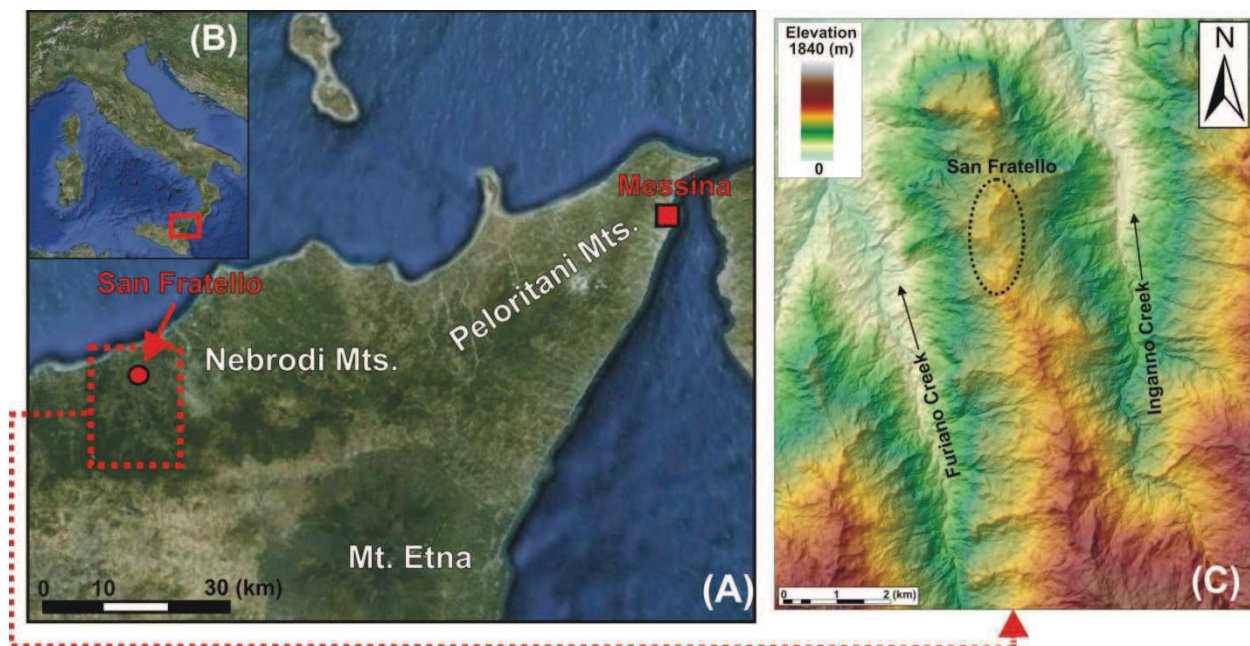


Figure 66. Location map of the San Fratello village. In (A) and (B) geographic framework, in (C) digital elevation model of the area of interesting.

4.3.1 Geological and geomorphological framework

From a geological point of view, the study area is part of the collisional system, developed since the Late Cretaceous, as the result of the convergence between the European and African-

Adriatic plates (Corrado et al., 2009). The study area is characterized by the presence of two main structural domains: the Kabilian-Peloritan-Calabrian units at northeast, overthrust on the Apenninic-Maghrebian domain to the southwest (Lentini et al., 2000; Lavecchia et al., 2007). The Kabilian-Peloritan-Calabrian units are made of imbricate sheets of Paleozoic metamorphic and igneous rocks and the related Mesozoic sedimentary cover (Somma et al., 2005). These units, cropping out within the Peloritani mountains, are covered by Upper Oligocene-Lower Burdigalian deposits (Lentini et al., 2000). The Apenninic-Maghrebian domain crops out in the Nebrodi Mountains and is made of imbricate sheets of Mesozoic-Tertiary sedimentary rocks. The boundary between the two domains, corresponds to the limit between the Peloritani and Nebrodi mountain chains; this boundary is represented by an active frontal thrust marked by the Longi-Taormina lineament (Catalano et al., 2006; Billi et al., 2007). San Fratello is located in proximity to this fault (Figure 67).

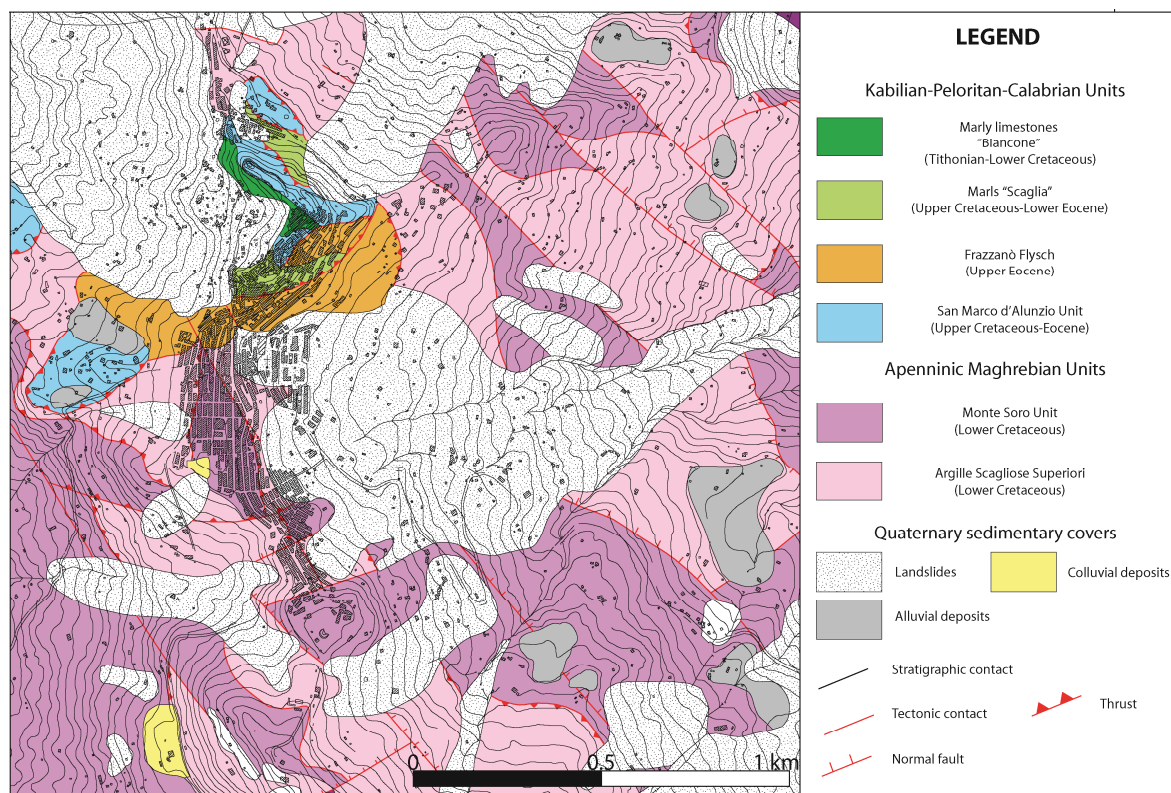


Figure 67. Schematic geological map of the village of San Fratello (courtesy of DRPC, Regional Department of Civil Protection).

The rock outcrops within the San Fratello area consist of a Cretaceous-Oligocene terrigenous-flyschoid to calcareous sedimentary sequence. In particular, the western and southern part of the study area is mostly characterized by terrigenous terrains, represented by the Apenninic-Maghrebid Units (clays alternating with sandstones and clayey-marly formations). In the northern portion of the area, the uppermost units (Kabilo-Calabride Units) crop out, occurring as Liassic carbonate platform sequences overlapped by a terrigenous Late Eocene-Oligocene Flysch. Cretaceous pelagic dolostones and limestones (San Marco D'Alunzio Unit) crop out in the N-NE sector of San Fratello (Giunta et al., 2000; Lavecchia et al., 2007). The poor geotechnical properties of the clay-silt and flyschoid lithotypes are one of the predisposing

factors of the landsliding phenomena, combined with the steep topography, with the occurrence of intense rainfall events acting as trigger.

From a geomorphological point of view San Fratello is located at about 650 m a.s.l. along a N–S oriented divide, on which both the west and east facing slopes are characterized by a steep gradient and creek erosion at their toe. The geomorphology of the study area shows the typical features of the Sicilian Tyrrhenian coastline: steep slopes, rising abruptly from the coastal plain, are deeply cut by N-NW–directed creek valleys (called *fiumare*). The test site is strongly influenced by the geo-structural conditions and by the recent tectonic activity. The landscape is typical of recently uplifted areas: steep slopes, narrow valleys, high topographical gradient and remarkable relief energy are the most impressive geomorphological features of the study area. Moreover, all the geological units are highly tectonized, being these clays highly fissured and the stone-like lithotypes extensively fractured.

In this context, the village of San Fratello is located about 5 km south of the seaside, on a divide separating the Furiano Creek valley to the west from the Inganno Creek valley to the east (Figure 66 C).

4.3.2 Landslide occurrence

San Fratello is an old village, characterized by several sites of cultural-artistic interest that have been affected by the long-lasting catastrophic natural phenomena. Beside the most recent landslide occurred on 14th February 2010 (which affected the eastern sector of the village, causing several damages to buildings and infrastructures), other landslides affected the village of San Fratello across last centuries. The oldest documented one occurred in 1754, destroying the north-eastern part of the village, of medieval age. On 8th January 1922 another large landslide seriously damaged the north-western quarters, causing the village delocalization (Figure 68).

The remains of the very first inhabited territory of San Fratello, dating back to the III century B.C., are located uphill on the Old Mountain (718 m a.s.l.), northward of the present village, where the ancient Norman Sanctuary of the three Saints, built up in the XII century, is also located (Figure 68, point 1). Since the Norman age, San Fratello village expanded near the rocky massif called Roccaforte (Figure 68, points 3 and 11) and developed until the Middle Age, when many churches and religious sites were built across time.

After the Middle Age the richest and most powerful families of Sicily Region started building and embellishing the churches of the village: some examples are the St. Crocifisso Church (Figure 68, point 7), the St. Maria delle Grazie Church dating back to the XVIII century (Fig. 2, point 2), the St. Benedetto il Moro Church (Figure 68, point 9) and the St. Antonio Abate Church (Figure 68, point 4).

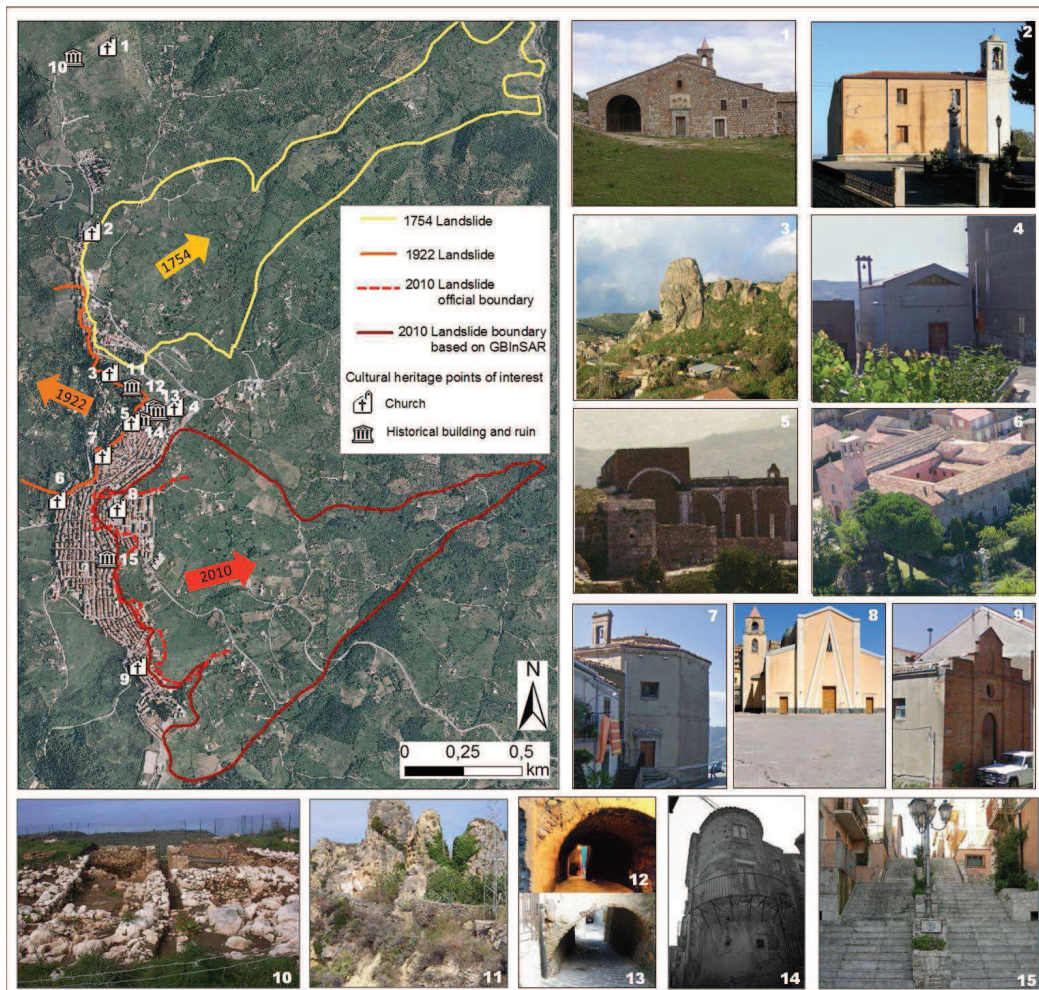


Figure 68. Boundaries and main directions of the three most important and recorded landslides in San Fratello, occurring in 1754, 1922, 2010. Location and photos of the main cultural sites of interest: 1 sanctuary of the three Saints Alfio, Filadelfio and Cirino on the Old Mountain; 2 Maria St. delle Grazie Church; 3 rocky massif Roccaforte; 4 St. Antonio Abate Church; 5 St. Nicolò Old Cathedral; 6 complex of St. Maria Assunta, former convent of S.S. Maria di Gesù` and library; 7 St. Crocifisso Church; 8 St. Nicolò New Cathedral (now demolished); 9 St. Benedetto Il Moro Church; 10 Apollonia Archeological site; 11 ruins of St. Filadelfio Castle; 12 St. Nicolò Arcway 13 Stesicorea Arcway; 14 Historical Mammana palace; 15 Historical Stairway of Vittorio Veneto knights.

Many cultural sites of San Fratello have been destroyed by landslides and re-built again across time. The landslide that occurred on 8th January 1922 destroyed most of the village (about two-thirds of San Fratello village). The Maria St. Assunta mother-church, built in the XIII century in the western portion of San Fratello, was completely destroyed by the phenomenon. The newly built Maria St. Assunta church, together with the former convent of Santissima Maria di Gesù and the library (Figure 68, point 6), can be regarded today as the centre of religion, culture and art of San Fratello. The Old St. Nicolò Cathedral (Figure 68, point 5), dating back to the XVI century, has been severely damaged by the 1922 landslide. In the 50s a new St. Nicolò Cathedral was built in the modern Stazzone district (Figure 68, point 8). Unfortunately also this church has been affected by the 14th February 2010 landslide and has recently been demolished, in February 2013, due to the irreversible and non-repairable damages. The majority of the historical old houses of San Fratello, the oldest ones dating back to the Norman settlement, have remained uninjured after the natural disasters up to nowadays (Figure 68, points 12–15).

4.3.3 The 2010 landslide

As previously mentioned, in the last three centuries, the village of San Fratello was affected by three large landslides, developed in different periods. The oldest one occurred in 1754 and almost completely destroyed the village. On 8th January 1922, a landslide occurred in the northwestern sector of San Fratello, causing hundreds of deaths; about ten thousand people were evacuated and another village (called Acquedolci) was built along the coast, as ordered by a Royal Decree (Faranda, 2010). In Figure 69, the landslide inventory map (PAI, Hydrogeological Setting Plan databases) of the area is shown; it was performed before the 2010 collapse and confirmed the existence of a large, dormant, complex, landslide phenomena as well as several other smaller, active, shallow-seated mass movements.

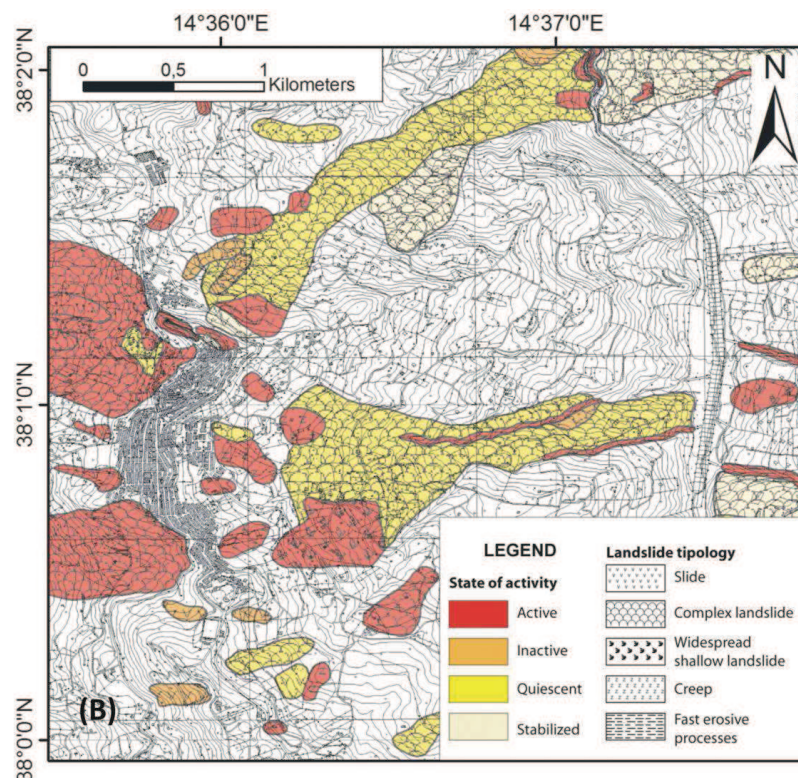


Figure 69. Inventory landslide map of the San Fratello area (PAI, 2010).

Nevertheless, San Fratello was re-populated again across time and, more recently, on 14th February 2010, another huge landslide, developed on the southern–eastern slope, causing huge damages to the roads and structures and forcing the evacuation of 200 people. This landslide affected the eastern urban districts (*i.e.*, the Stazzone, Riana, Porcaro, and San Benedetto districts). About 2000 inhabitants were initially evacuated, approximately 300 houses were slightly damaged and 50 needed to be demolished (D.R.P.C. 2010). In detail, the 2010 landslide, affecting an area of about 1 km², developed from the eastern sector of the village area toward the Inganno Creek valley for a length of about 1.8 km (Figure 70). This landslide, mainly involving the silty-clayey overlay, is a complex rotational mass movement that intensively modified the topographic slope surface, producing multiple failures, traction cracks, and counterslopes (Figure 70). On this geomorphological map, some kinematic indicators are represented, emphasizing the direction of the flow toward the valley of the Inganno Creek; the

areas characterized by ground and building lacerations were also pointed out, together with the damaged drain pipelines and the hydrographic network that was intensely modified, producing concentrated runoff and several small landslide lakes. The landslide, in its lower sector, evolved in an earth flow, channelizing into a stream bed corresponding to a tributary of the Inganno Creek.

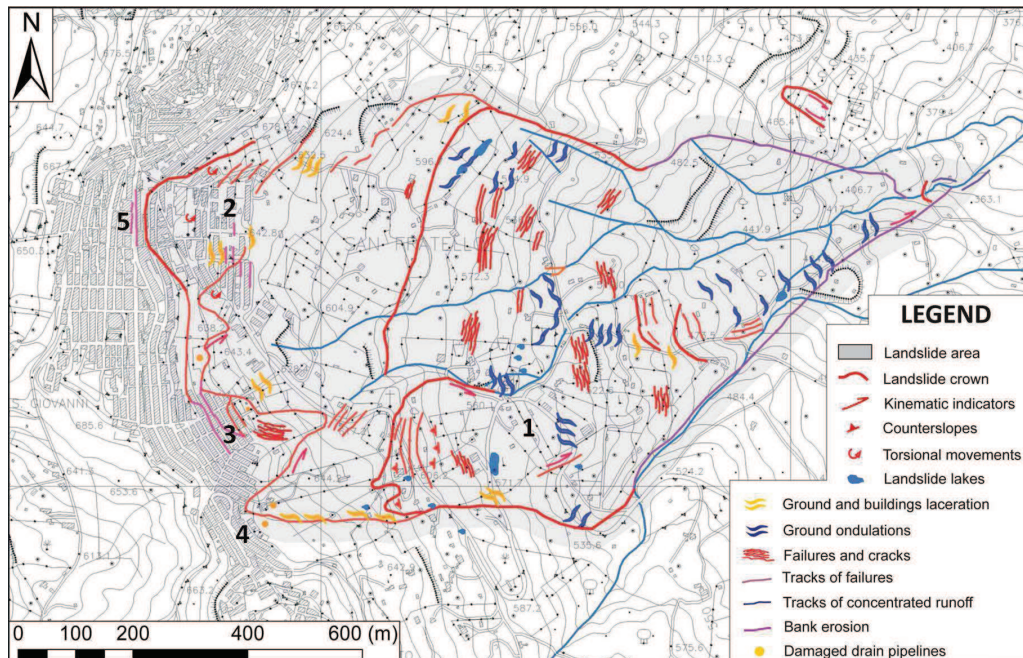


Figure 70. Geomorphological map of the 2010 landslide (Pino et al., 2010). San Fratello Quarters: 1, Porcaro; 2, Stazzone; 3 Riana; 4 S. Benedetto; 5 Latteri Street.

In particular, the landslide main scarps, characterized by heights between 5 and 10 m, are located in the middle and upper part of the slope about 500 m east of the village centre (sector 1, Porcaro quarter, in Figure 70). In this latter sector, where the ground surface planar translation reached 50 m, severe damages to some isolated buildings and local roads occurred. In the eastern village sector, characterized by a high building density, translational sliding phenomena determined sub-parallel fracture systems and scarps in the Riana quarter (sector 3 in Figure 70), while in correspondence of the Stazzone quarter (sector 2 in Figure 70), rotational phenomena induced several extensional and compressive fractures. In both quarters, several buildings were intensively damaged (*e.g.*, the church and the primary school in the Stazzone quarter in particular) or completely destroyed together with the sewer system. The southern village sector (San Benedetto quarter, sector 4 in Figure 70) was affected by translational and rotational phenomena, which induced intense ground laceration and formed scarps up to 5 m high, destroying several buildings, water pipes and roads. The upper part of the village, in correspondence with the divide (sector 5 in Figure 70), was also affected by intense ground deformation phenomena.

An accurate field survey in November 2012 led to the damage assessment map presented in Figure 71, covering the whole village area of San Fratello. A total amount of 738 buildings were mapped on the basis of the damages observable on their walls and facades. Buildings interior damages were evaluated by interviewing the local inhabitants. The degree of damages for each

building was evaluated using a modified version of ranking scheme of building damage categories of Cooper (2006) (Table 8).

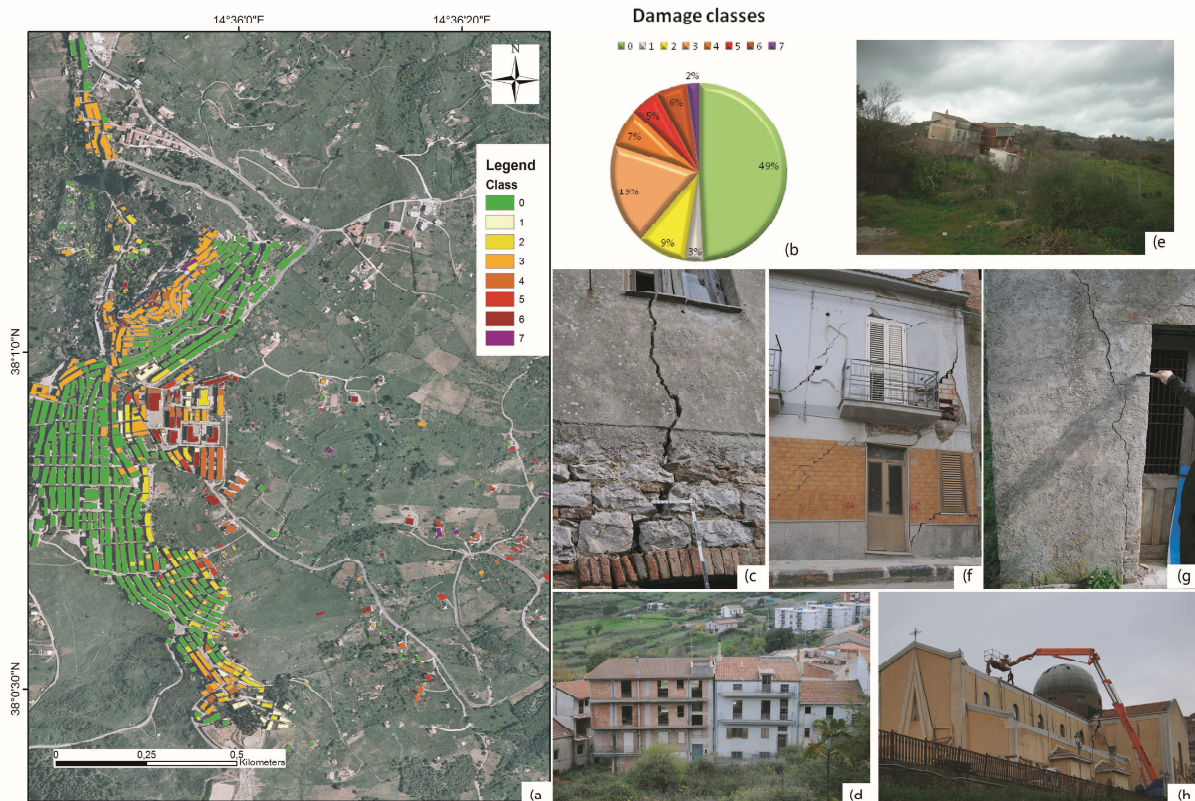


Figure 71. Damage assessment map of San Fratello according to the degree of damages of Table 8 (a); and the related frequency of buildings considering the degree of damages (b). Some examples of the damages of San Fratello (c) class 3; (d) class 6; (e) class 7; (f) class 5; (g) class 2; (h) class 5 (from: Ciampalini et al., 2014).

Class	Description
0	No damages.
1	Hairline cracking not visible from outside. Fine cracks, generally restricted to internal wall finishes: rarely visible in external brickwork. Typical crack widths up to 1 mm. Generally not visible from outside.
2	Cracks not necessarily visible externally, some external repointing may be required. Doors and windows may stick slightly. Typical crack widths up to 5 mm. Difficult to record from outside.
3	Cracks that can be patched by a builder. Repointing of external brickwork and possibly a small amount of brickwork to be replaced. Doors and windows sticking, slight tilt to walls, service pipes may fracture. Typical crack widths are 5–15 mm, or several of say 3 mm. Visible from outside.
4	Extensive damage that requires breaking-out and replacing sections of walls, especially over doors and windows. Windows and door frames distorted, floors sloping noticeably; some loss of bearing in beams, distortion of structure. Service pipes disrupted. Typical crack widths are 15–25 mm, but also depends on number of cracks. Noticeable from outside.
5	Structural damage, which requires a major repair job, involving partial or complete rebuilding. Beams lose bearing capacity, walls lean badly and require shoring. Windows broken with distortion. Danger of instability. Typical crack widths are >25 mm, but depend on the number of cracks. Very obvious from outside.
6	Partial collapse. Very obvious from outside.
7	Total collapse. Very obvious from outside.

Table 8. Ranking scheme of building damage categories (modified after Cooper, 2006).

The map shows that more than half of San Fratello buildings are affected by damages caused by slope instability; amongst them 20% of buildings are strongly damaged (more than class 4). The most affected areas are located on the village eastern slope, within the Stazzone quarter and East of the city centre (Figure 71). In these areas, also some of the most recent buildings collapsed or were damaged to the point that they required to be demolished. Intense damages can be also observed in the Riana and San Benedetto quarters, along the 2010 landslide crown. The field surveys also revealed the presence of several damaged buildings located in the northwestern part of the village, corresponding to the 1922 landslide crown area.

The triggering factors of the 2010 landslide may have been the intense rainfall that has increased the static water table within the shallow aquifer, determining soil saturation processes in the clays and causing mass movements.

The phenomenon has been caused by predisposing variables that deal with soil and rock geomechanical properties, and with the geostructural and hydrogeological setting of the area. The geological framework determines the overlapping of geological formations, with marked differences in geotechnical properties, deeply influencing the study area landscape and slope instability phenomena: hilltops, made of hard-brittle lithologies, are undermined by the weathering and erosional processes, taking place in the underlying soft clayey formations. In the San Fratello area, on the top of the bedrock, a silty-clayey cover lies with an average thickness of about 10 m; the 2010 landslide affected this layer, involving all the thickness or the biggest part of it, with a surface rupture 8-10 m deep (Pino et al., 2010). The low quality of the geotechnical properties of this layer probably played an important role in the landslide trigger, together with the steep slope angle (more than 30°) and the intense precipitation events of the period. Throughout the inhabited area, an aquifer is also present, at a depth of between 0.5 and 2.5 m from the surface ground level.

The February 2010 landslide is still active nowadays and ground movements are kept under control as the instability scenario is still very critical in San Fratello area.

4.3.4 Activities

In the post-event phase, in order to monitor the San Fratello 2010 landslide and to assess its residual risk, a GB-InSAR system was set up on the left flank of the Inganno Creek valley, in the Sanguinera village area, opposite to the San Fratello village (Figure 72). The instrument was installed on 8th March 2010 and it started to acquire two days later. The employed system is a ground based SAR, designed and implemented by the Joint Research Centre (JRC) of the European Commission and its spin-off company Ellegi-LiSALab s.r.l. (Tarchi et al., 2003; Antonello et al., 2004; Casagli et al., 2009, 2010; Gigli et al., 2011; Del Ventisette et al., 2011, 2012a; Tapete et al., 2012; Di Traglia et al., 2013; Intrieri et al., 2013). The radar system was installed at an average distance of 2100 m with respect to the landslide (Figure 72). The area covered by a GB-InSAR system depends on this distance, which is usually limited to a few hundreds of meters up to a few kilometres, corresponding to a patch-landscape scale. In the

specific case of San Fratello, the covered area is about 1 km², like the landslide extension. The accurate displacement maps can be produced only for the upper part of the landslide, because the lower vegetated part is not visible by the GB-InSAR.

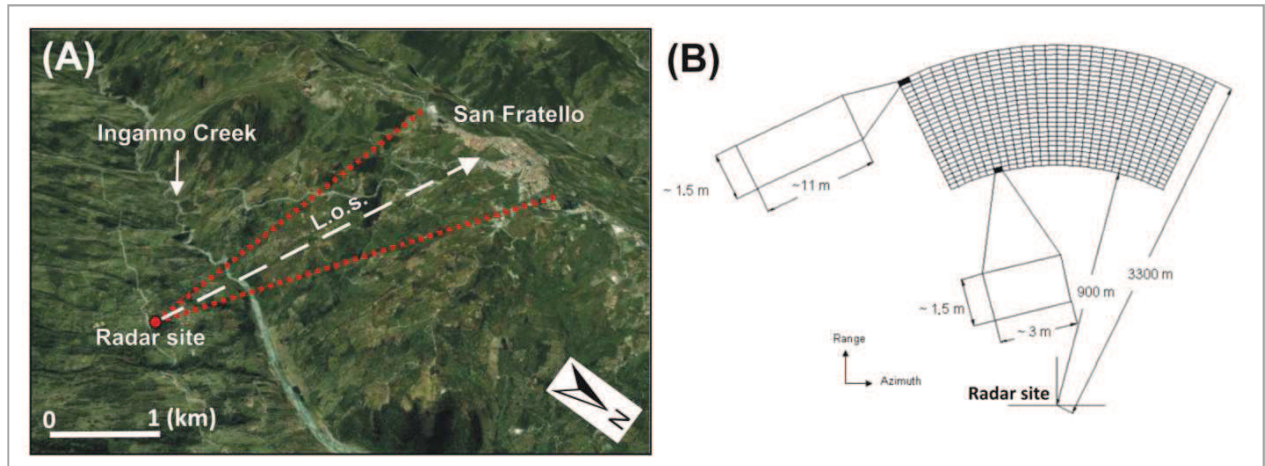


Figure 72. Location of the San Fratello GB-InSAR system installation (A) and resolution grid size and parameters used during the monitoring campaign (B).

The radar parameters used during the measurement campaign are summarized in Table 9. As regards the aliasing effect, it reduces to 4.4 mm the maximum displacement that can be recognized without ambiguity, using the system installed on the test site. GB-InSAR measures were acquired every 14 minutes: during the monitoring period the displacements never exceeded the threshold of 4.4 mm in 14 minutes, so the aliasing effect was avoided.

Central frequency	Bandwidth	Synthetic aperture length	Min. distance	Max. distance	ΔR_r	ΔR_{raz} (at 900 m distance)	ΔR_{raz} (at 3300 m distance)	Scanning time
17.1 GHz	200 MHz	3.00 m	900 m	3300 m	1.5 m	3 m	11m	14 min

Table 9. GB-InSAR system parameters used to monitor the San Fratello landslide.

Beside the GB-InSAR instrument, five different satellite sensors (for a total of eight datasets) were used to monitor the buildings of San Fratello: ERS1/2, ENVISAT, RADARSAT-1, COSMO-SkyMed (CSK) and TerraSAR-X (TSX) covering a very long interval of time, spanning from 1992 up to 2012 (Table 10). Satellite SAR datasets were processed by T.R.E. (Tele Rilevamento Europa) with both PS-InSAR and SqueeSAR approaches.

Sensor	Geometry	Time interval	No. of scenes	Density (PS/km ²)
ERS 1/2	Ascending	11/09/92–05/06/00	34	6.55
ERS 1/2	Descending	01/05/92–08/01/01	70	46.45
ENVISAT	Ascending	22/01/03–22/09/10	65	64.74
ENVISAT	Descending	07/07/03–13/09/10	49	20.41
RADARSAT	Ascending	30/012/05–26/01/10	47	85.86
RADARSAT	Descending	31/01/06–03/02/10	47	85.86
COSMOSky-Med	Descending	16/05/11–02/05/12	32	400.62
TERRASar-X	Descending	28/10/11–22/09/12	30	813

Table 10. Used PSI datasets.

Regarding the 2010 landslide, the displacements were studied during the pre- and post-event by the integration between space-borne and ground based InSAR techniques. The integration methodology follows the scheme proposed in the sub-paragraph 2.3.2 of this thesis.

During the data collection phase, geological and geomorphological field surveys were realized together with the acquisition of ancillary data (*i.e.*, an orthophoto of the study area, landslide inventory map from 2010 PAI databases, damage assessment map). Then satellite and ground-based SAR datasets were collected, covering both pre- (ERS 1/2, ENVISAT, RADARSAT-1) and post-event (COSMO-SkyMed and GB-InSAR) periods. During the second step, the SAR data post-processing was performed in order to increase the comparability of the different datasets: at the beginning, only satellite datasets were projected along the slope direction, which is quite similar to the GB-InSAR LOS. The downslope projected velocity was called V_{slope} . Ground deformation velocity (V_{slope}) maps were obtained and superimposed on the orthophoto (characterized by a 1-m geometric resolution) and compared with the available landslide delimitation, performed a few days after the event, on the basis of the field evidences (geomorphological surveys and building damage assessment; Figure 70 and Figure 71).

To classify the PS-InSAR data, a stability V_{los} threshold value of ± 2 mm/y for C-band data was considered. This threshold is based on several published PS-InSAR analyses on landslide studies (*e.g.*, [Righini et al., 2012](#); [Herrera et al., 2013](#)).

In the study area, the velocity ranges of PS-InSAR datasets measured by the different satellite systems are comparable for all the PS populations: all the maximum (positive) and minimum (negative) velocity values range within a few tens of millimetres per year. The C-band data show a standard deviation of the velocity of about 2.0 mm/y. The X-band PS-InSAR data have a slightly higher standard deviation (3.7 mm/y) than C-band. This feature mainly depends on the number and distribution of SAR scenes used for the processing over the temporal acquisition period. Nevertheless, in our case, X-band COSMO-SkyMed dataset includes a sufficient number of images (*i.e.*, 32 images), homogeneously distributed over one year acquisition. Considering this characteristic, the same stability threshold value (± 2 mm/y) has been used for C-band and for X-band data in order to make all the used PS-InSAR datasets, acquired by different satellite sensors, as comparable as possible. Moreover, this value is acceptable as it does not exceed the precision of the PSI technique.

To classify V_{slope} data, the same statistical considerations were taken into account, considering the negative skewness of the V_{slope} PS population. So the V_{slope} positive data that represent outliers in the distribution are negligible, and therefore the V_{slope} stability value is chosen between 0 and -2 mm/y.

At the same time, GB-InSAR data were analysed to obtain displacement maps and time series of 10 control points, chosen in areas where the radar signal is characterized by high stability, high signal/noise ratio, high power and coherence parameters.

Finally, data integration has been produced, starting from a qualitative integration between satellite V_{slope} maps and ground-based displacement maps; the integration was based on a binary approach to separate the areas characterized by displacements to the ones without

evidence of movement, during the pre- and post-event period. The purpose was to update the landslide boundary and to perform a more precise landslide map. The combined use of the satellite and the ground-based SAR data provided displacement measurements with high spatial and temporal accuracy, allowing us to improve the delimitation of the 2010 landslide, in terms of accuracy and precision. Furthermore, the integration of PS- and GB-InSAR approaches allows overcoming their physical limitations. Therefore, in order to compare the results of both the techniques, it is possible to study the same area from different points of view and in different temporal intervals.

In Figure 73, the GB-InSAR cumulative displacement map (from March 2010 to March 2013) is shown together with the COSMO-SkyMed V_{slope} , whose acquisition period partially corresponds to the GB-InSAR period (May 2011- May 2012). On the map (Figure 73), it is also possible to observe the proposed new landslide boundary.

The extension of the landslide boundaries is confirmed by the spatial distribution of the damages of buildings and infrastructures. In particular, in Figure 73 it is possible to observe how the main scarps delineate areas affected by major displacements, also recognized by the SAR data. The new boundary determines a new estimation of the landslide area, from 1 to 1.2 km².

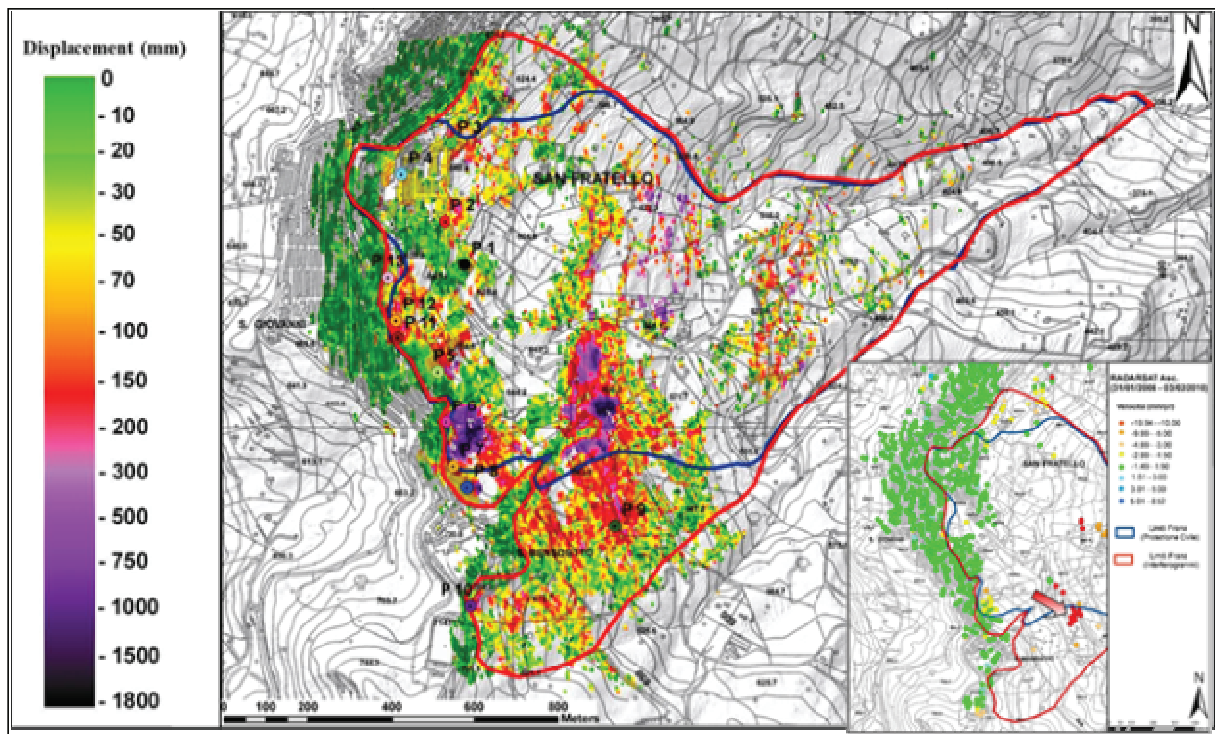


Figure 73. Propose of a new contouring of the landslide (in red), outlined by the results of GB-InSAR and PS-InSAR campaigns.

Continuing to follow the procedure proposed in the sub-paragraph 2.3.2 of this thesis, a semi-quantitative integration between GB-InSAR and PS-InSAR data has been developed.

In this step, data comparison is focalized on datasets which refer to the same temporal interval, which corresponds to a one year of acquisitions, between May 2011 and May 2012 (*i.e.*, post-event datasets).

Data homogenization required downslope projection also of GB-InSAR data; the values of the C coefficient, which expresses the percentage of real displacements detectable from the GB-InSAR position, have been mapped as shown in Figure 74.

The main assumption behind the downslope data projection is based on the fact that the most probable displacement direction accords with the fall line. The translational nature of the San Fratello 2010 landslide makes this assumption acceptable; moreover the GB-InSAR location implies that its LOS is more or less parallel to the downslope direction, determining very high values of the C coefficient. A wide portion of landslide area is well observable from the GB-InSAR position, allowing to detect more than 90% of the real displacements; only in limited areas, such as in the southern part of the San Fratello village, or in correspondence of local areas probably affected by local flattening, the C value lightly reduces, reaching values less than 85 % (Figure 74).

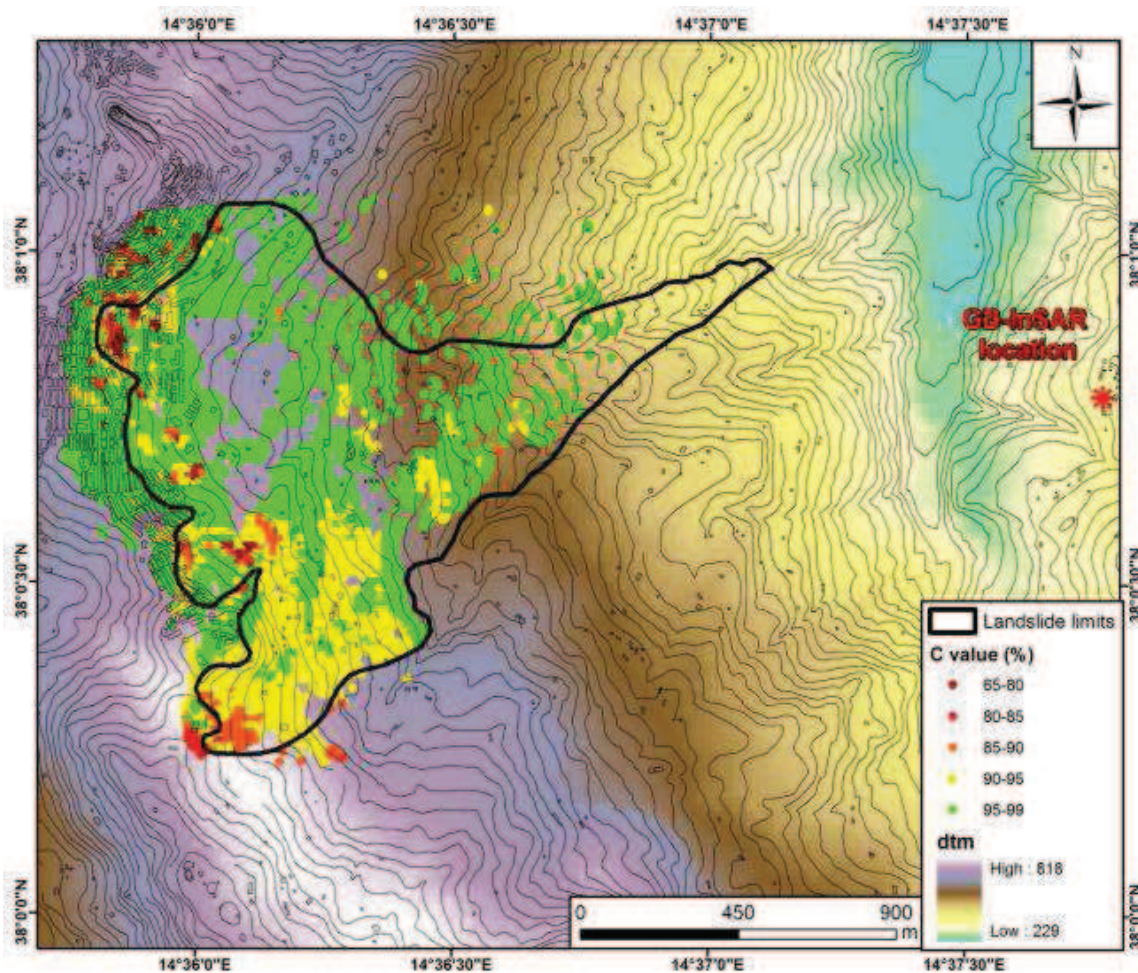


Figure 74. Percentages of real displacement values detectable along GB-InSAR LOS.

In light of the above, no big differences exist between LOS displacement and downslope displacement maps (Figure 75). The maps referred to cumulated displacement values acquired by the GB-InSAR in the period between May 2011 and May 2012; maximum displacements are concentrated in a localized area in the upper part of the landslide, where the slope moved about 1.2 m in a year; this value increases of about 10% if data are projected downslope.

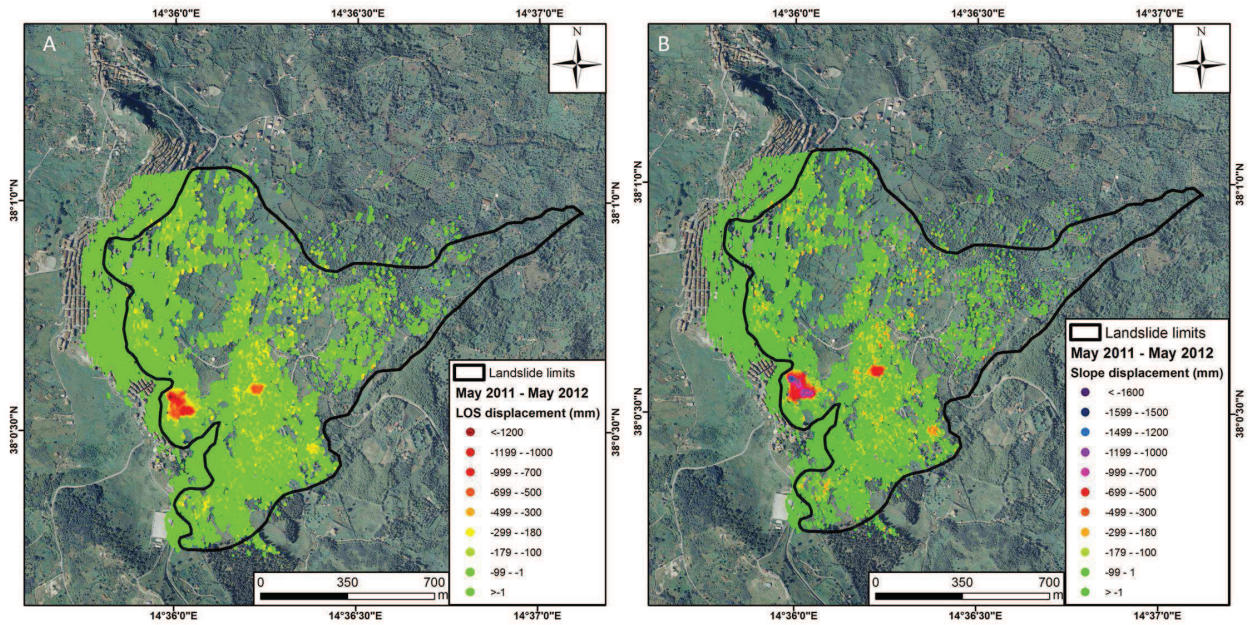


Figure 75. LOS displacement (A) and slope displacement (B) cumulated maps acquired by GB-InSAR in a period between May 2011 to May 2012.

As regards the data projection, the situation is a bit different in the case of satellite data. In the post event period, specifically between May 2011 and May 2012, COSMO-SkyMed data, acquired in descending orbit, are available. These datasets have been projected downslope, following the same procedure applied to GB-InSAR data. The resulting displacement map shows high differences respect to the LOS registered displacement, related to the not-parallelism between COSMO-SkyMed LOS and slope directions (Figure 76).

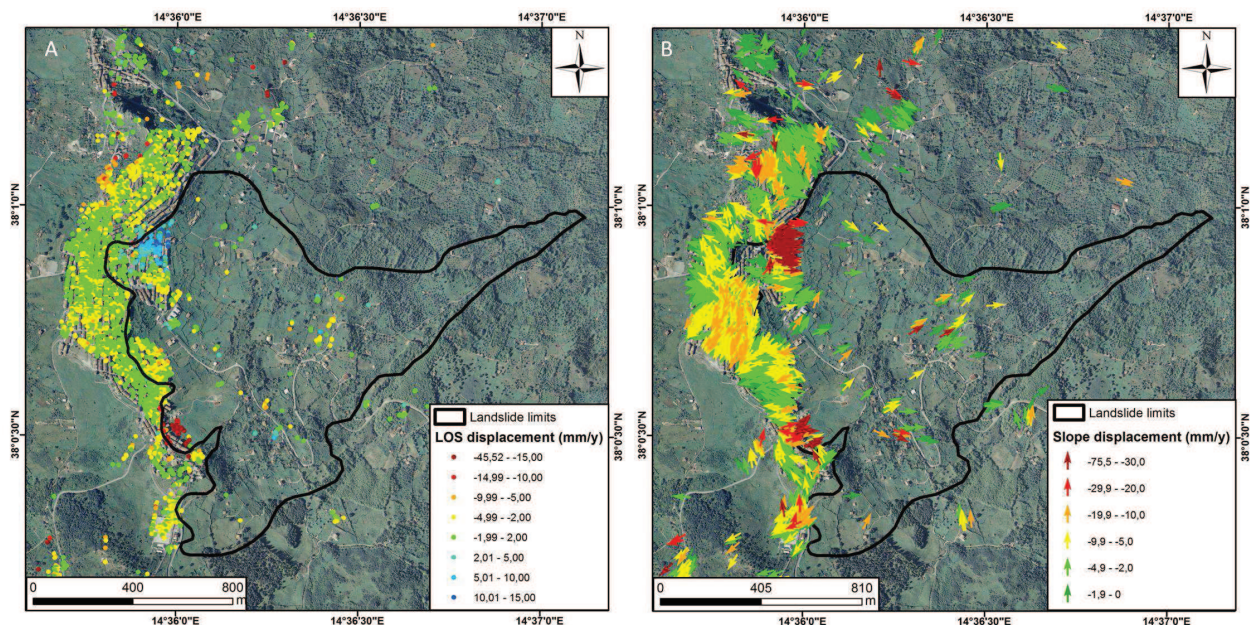


Figure 76. LOS (A) and slope (B) deformation velocity maps acquired by COSMO-SkyMed between May 2011 and May 2012.

In contrast with the GB-InSAR, COSMO-SkyMed LOS is often almost perpendicular to the downslope direction, determining underestimation of the real displacement values; moreover

it also implies problems in the downslope projection, producing a high number of outliers values (see Figure 27).

These problems, especially the presence of outliers, in correspondence of which the data can't be projected and maintain their original values, determine a shift in the displacement values registered by the different techniques; in particular COSMO-SkyMed detects values about 20% lower than the ones registered by the GB-InSAR instrument.

In this context, only a semi-quantitative integration can be produced, also on displacement time series datasets.

To compare displacement time series, the GB-InSAR ones have been extracted in correspondence of 13 control points identified on the displacement map. Displacement values have been temporally re-sampled, according to the acquisitions of COSMO-SkyMed, which are not regular, but have a frequency value more or less of 4 days.

The integration has been obtained between Permanent Scatterers and GB-Control Points having similar location (Figure 77), in order to also compare landslide portion with the same downslope direction. PSs respecting this condition are available only for 6 of the 13 GB-InSAR control points; integrated time series are shown in Figure 78.



Figure 77. GB-InSAR control points location.

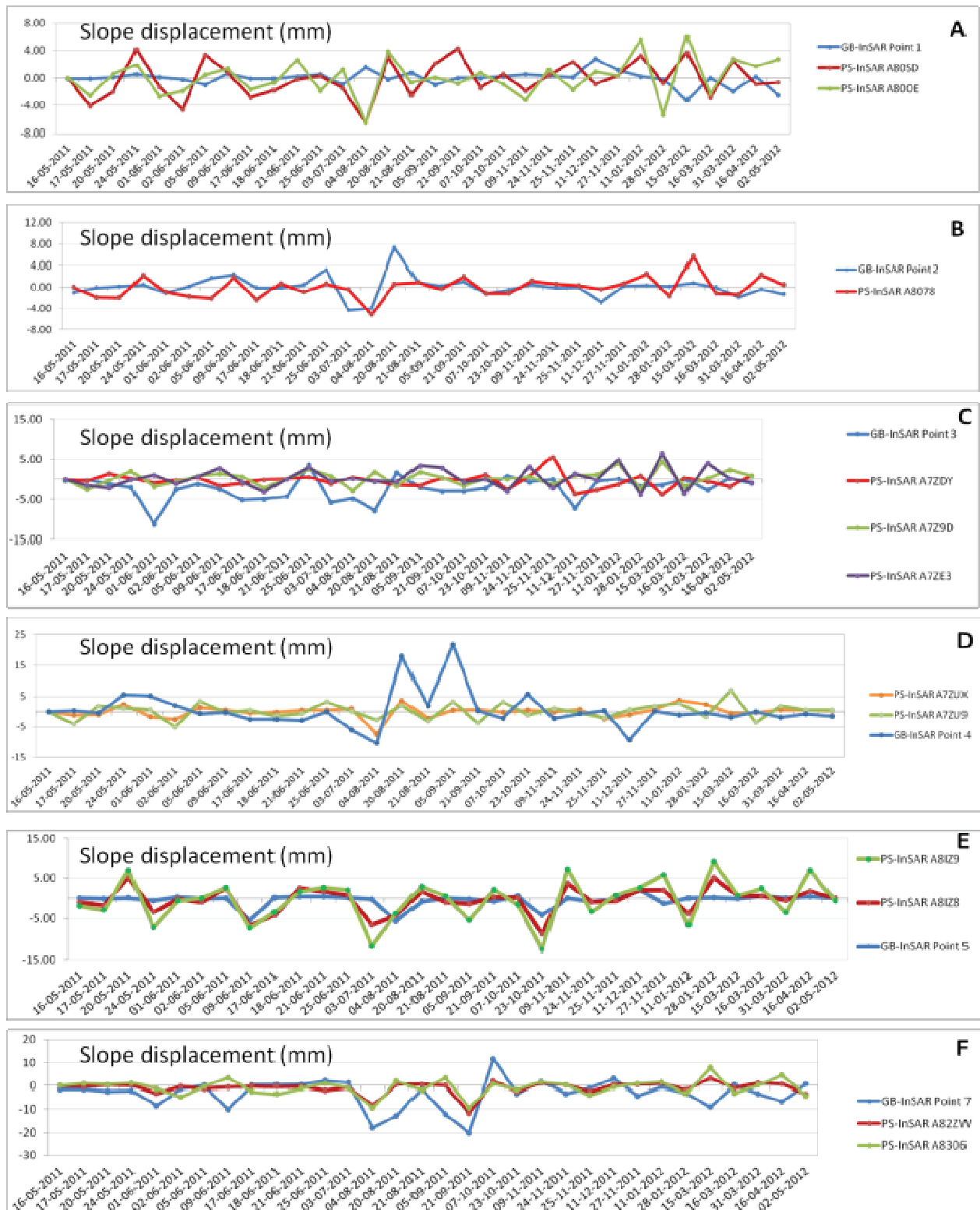


Figure 78. Slope displacement time series of COSMO-SkyMed PSs and GB-Control Points. In the same diagram PSs and GB-Control Points having the same location are displayed. GB-Control Points, which locations are shown in Figure 77, are A) Point 1; B) Point 2; C) Point 3; D) Point 4; E) Point 5; F) Point 7; their time series are blue; the other colours represent the PSs displacement series.

Time series show values, projected on downslope direction, of the differential displacements registered by the sensors (both satellite and ground based) in the span time between two subsequent satellite acquisitions (Figure 78). Partial displacement values have been plotted in order to verify the correlation, acquisition by acquisition, between the two datasets: this partially masks the increasing trend of the displacements, but allows us to assess the goodness of the integration.

As above discussed, COSMO-SkyMed LOS is more or less perpendicular to the downslope direction in a wide portion of the landslide, determining the impossibility to project data in this direction. It is, for example, the case of the time series shown in Figure 78 A and C, where the PS-InSAR partial displacements are related to the displacements detected on the LOS direction. It makes very difficult to evaluate the correlation between these datasets and the projected GB-InSAR displacement values.

Moreover, the landslide velocity seems to maintain high values of displacement velocities, also in the period which data integration is referred. In this case, aliasing effect could affect PSs values, determining an underestimation of the real displacement values. This problem could also explain the differences in the displacement values, observable on the maps (Figure 75 and Figure 76).

4.4 Åknes (Tafjord-Norway)

Åknes is a large rockslide, affecting the north-western side of Sunnlyvsfjorden, a branch of the Storfjorden (Figure 79), in the western Norwegian coast. Åknes landslide is considered one of the most hazardous rockslide areas in Norway (Ganerød et al., 2008). Its estimated volume is 35-40 million m³ (Derron et al., 2005) and it is interested by continuous creep; the instability of the rock mass and the location of the landslide body, situated above the fjord and in the vicinity of several communities, make the surrounding area exposed to a high level of risk, especially in relation to the possible tsunami induced by the eventual fall of the mass rock in the fjord. Moreover, the area is one of the Norway's most visited tourist attractions, in relation with the natural beauty of the mentioned fjord (the near Geirangerfjord is listed on the UNESCO's World heritage list). These characteristics make Åknes the most investigated rockslide in the world.

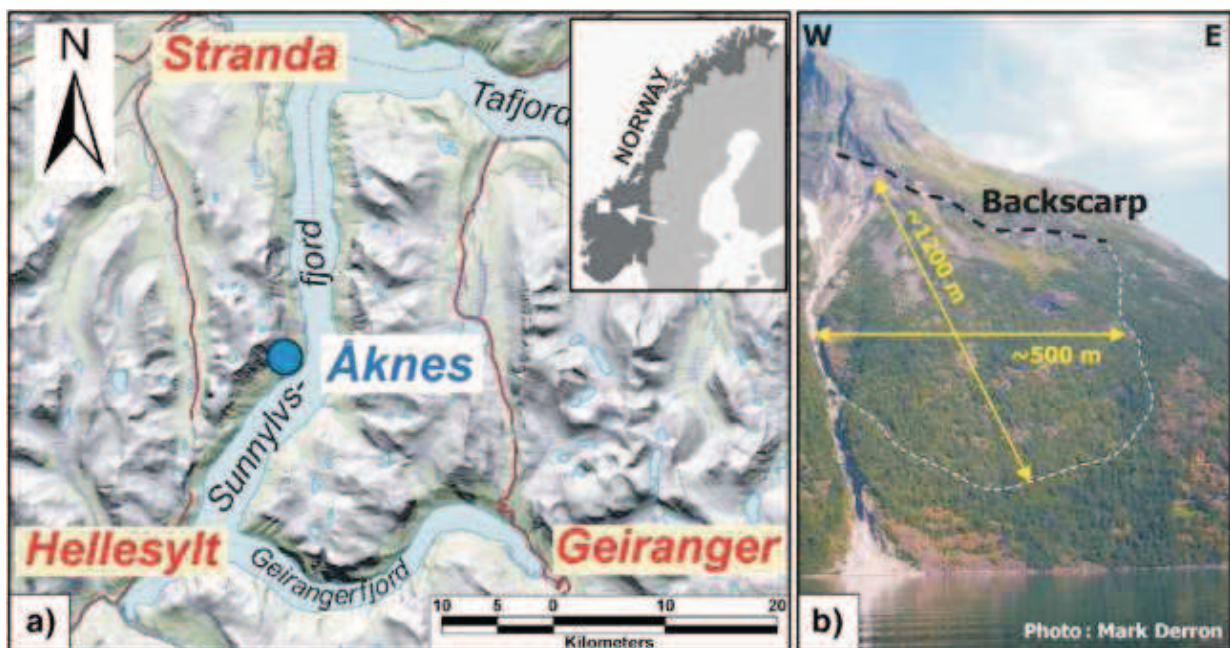


Figure 79. Location of the rockslide site of Åknes, in western Norway (from: Kveldsvik et al., 2006).

Large rockslides represent one of the most serious hazards in Norway, therefore in the 90's a systematic study on this landslide typology has been developed by the Geological Survey of Norway. Numerous rockslide deposits have been inventoried, some of which represent a threat to population, buildings and infrastructure (Blikra et al., 2004, 2005; Braathen et al., 2004).

Historical data recorded some examples of disasters generated by this type of phenomena, as in 1934, when a rock mass of about 3 million m³ dropped into Tafjord (the same on which the Åknes rockslide stands), generating a tsunami wave that reached 62 m and destroying several villages (Jørstad, F. 1968).

As regards the Åknes rock slope, three historical rock slides are known, approximating dated 1859-1900, 1940 and 1960 (Kveldvisik et al., 2006).

The Åknes slope is dipping towards SSE with angles of 35-40° that reach about 20° just below sea level. It is defined by a back scarp, a basal shear zone at 50 m depth and a toe zone where

the basal sliding surface reaches the ground level. Several open cracks interest the slope; the upper western flank is separated from the back wall by about 20-30 m. The width of the cracks decreases going towards the east of the upper western flank, reaching values around 1 m.

By photogrammetric studies, displacement rates in the upper part of the slope have been detected since 1960, with values around 5-6 cm/year (Kveldvisik et al., 2006).

The area has been classified as “high susceptibility zone”, taking mainly into account the spatial distribution and the temporal pattern of the events (Longva et al., 2009).

A programme of extensive investigations, research and monitoring activities has been launched in 2004, also including tsunami modelling (Eidsvig and Harbitz, 2005).

Modelling activities also include investigations by employing InSAR techniques, exploiting both ground based and space borne sensors.

4.4.1 Geological framework

From a geological point of view, the Åknes rockslide is located in the Western Gneiss Region of Norway. Gneisses of Proterozoic age represent the dominant lithology in the bedrock of the area and they exhibit the effect of alteration and reshuffle suffered during the Caledonian orogeny (Tveten et al., 1988).

The geological setting of the area, especially the gneisses lithologies, is characterized by intense foliation, contributing to determine the instability of the slope; indeed the main cracks are developed along the foliation plans.

It is possible to distinguish various sub-domains (four in the distinction made by Ganerød et al., 2008, as shown in Figure 80) in the rockslide; firstly the upper part is mainly interested by extension forces, in contrast with the lower part, which is characterized by generalized compression. The upper zone of the rockslide is delimited by a back scarp that is controlled by the pre-existing foliation planes, which develop parallel to the scarp. In those zones where the foliation is not oriented according to the extensional trend, the back scarp follows a set of pre-existing fractures.

The basal sliding surface seems in turn to be controlled by foliation; it dips 30-35° to S-SSE and runs sub-parallel to the topographic slope.

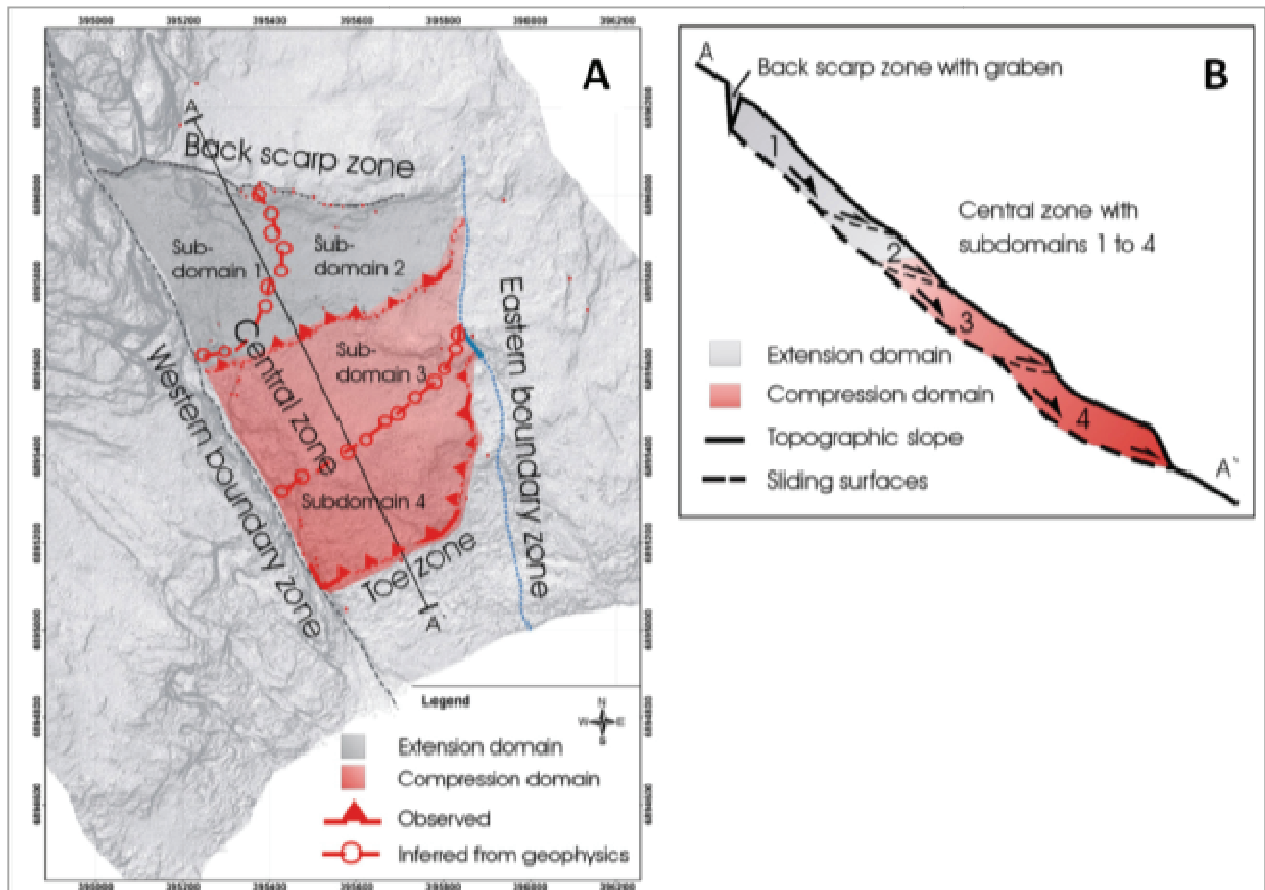


Figure 80. A: Map that locates domains and sub-domains (1, 2, 3 and 4) and key structures which determine the rockslide morphology. B: Schematic profile with domains, sub-domains and key structures (from: Ganerød et al., 2008).

As regards the persistence of the fractures, the upper boundary tension crack is approximate 800 m long; the western boundary is defined by a steeply dipping, NNW-SSE striking strike slip fault, while the eastern boundary is signed by the presence of a gently NW dipping, NNE-SSW trending fault (Ganerød et al., 2008).

The toe is not clear, but it can be approximately located at 75-100 m a.s.l. (Frei et al., 2008).

More information about the geological setting of the rock slope can be found in Nordvik and Nyrnes 2009; in this paper the results of an extensive field work in the area, obtained in the summers of 2004-2007 and including detailed geological mapping and geophysical investigations, are summarized.

4.4.2 InSAR monitoring activities

As above mentioned, Åknes is probably the most studied rockslide in the world.

It takes advantage of one of the best organized early warning systems (Blikra, 2008), which in turn can exploit a really complete monitoring network.

This network consists in: nine GPS antennas, two lasers, three extensometers, a robotic total station that measures 28 prisms, a micro seismic network and a meteorological station to continuously monitor values of temperature, precipitation, snow depth and wind speed. Three boreholes have also been drilled and equipped with DMS columns, 100 and 120 m deep, to penetrate the basal sliding surface, measuring the columns inclination on every meter of their length.

Moreover, starting from 2006, GB-InSAR campaigns have also been realized, in the context of the Åknes/Tafjord project (<http://www.aknes.no/>). The instrument was provided by the Italian Society Ellegi LiSALab s.r.l. and it is not so different from the one described in the second Chapter of this thesis. Five GB-InSAR campaigns have been realized, specifically in the spring-summer seasons of 2006, 2008, 2009, 2010 and 2012.

The system was installed on the opposite side of the fjord respect to the rockslide, in a location named Oaldsbygda, equipped with internet network and power supply. Very strong atmospheric effects interested the images acquired from this location, because of the sudden and very fast changes of local atmospheric conditions on the fjord, which must be intersect by radar signal during the acquisitions. For this reason, in 2012, another GB-InSAR instrument, very similar to the other one, was installed at Fjellvåken, a site located on the same slope of the rockslide, immediately outside the unstable area, near to the western limit of the landslide. This further instrument was focused on the upper and most active part of the rockslide, for a four weeks campaign finalized to implement the existent early warning system with InSAR data. Indeed, data acquired from the other GB-InSAR were considered less reliable in quantitative terms, to be used in the EWS.

The technical features of the two GB-InSAR systems are listed in Table 11.

	Oaldsbygda	Fjellvåken
Rail length	3 m	3 m
Central frequency	17.2 GHz	17.2 GHz
Bandwidth	60 MHz	300 MHz
Number of frequencies	2501	2501
Steps along the rail	601	751
Image acquisition time	8 minutes	9 minutes
Processed image range	1800-4200 m	150-750 m
Processed image azimuth	±1200 m	±300 m

Table 11. Parameters of the employed radar systems (from: Kristensen et al., 2013).

The restricted observed area, the proximity of the installation point to the scenario, the increased bandwidth, make the range resolution of the GB-InSAR located at Fjellvåken higher than the one installed at Oaldsbygda.

Nevertheless, the availability of several campaigns make the Oaldsbygda data more useful to analyse the evolution of the deformation pattern of the rockslide.

Kristenses et al. (2013) give a satisfactory list of the problems which affect radar images, provided during these multiple campaigns:

1. The lower part of the rockslide is widely vegetated, determining loss in coherence in the SAR images;
2. The need, by the microwave, to cross the fjord, in its travel from the instrument to the rockslide and return, determines strong atmospheric interactions and the related decorrelation effects;
3. The sea in the fjord operates as a mirror on the microwaves, producing multi-path effects; moreover the tide effects determine further decorrelation in the yet noisy lower part of the landslide, covered by vegetation.

Filters, mainly dedicate to atmospheric correction, have been applied, leading to acceptable results.

Data about the campaign from Oaldsbygda have been analysed in this thesis, by courtesy of the Åknes/Tafjord Early Warning Centre, according with LiSALab s.r.l., which software has been used to process all the images, including the application of the filters for the atmospheric correction.

Daily cumulated maps have been produced in order to reduce the problem of phase wrapping that could manifest looking longer time intervals; then data have been analysed in GIS environment, upon the application of georeferencing transformations on the images.

Thanks to the availability of different monitoring systems and, specifically, comparing GB-InSAR data with the data acquired by GPS, Kristensen et al. (2013) have been estimated the percentage of real displacement detected by the radar system, overpassing, in this way, the LOS drawback. Indeed, fortunately, at Åknes, an overlapping interval of measurements obtained from the two different techniques is available. Measurements of GPS antennas, referred to a total station, provide displacement vectors in three coordinates, by comparing these values with the values obtained along the LOS direction, it was possible to estimate the percentage of displacement detected by the GB-InSAR along its LOS.

Comparison results show that, from Oaldsbygda, the central part of the rockslide is highly visible by the GB-InSAR that is able to detect about 70% of the real displacement. The upper sector of the landslide is mainly interested by vertical movements; in this area the instrument of Oaldsbygda is able to observe only 30% of the displacement.

Instead, the radar installed in Fjellvåken is able to detect about 42% of the true displacement, in correspondence of the most active part of the landslide (Figure 81).

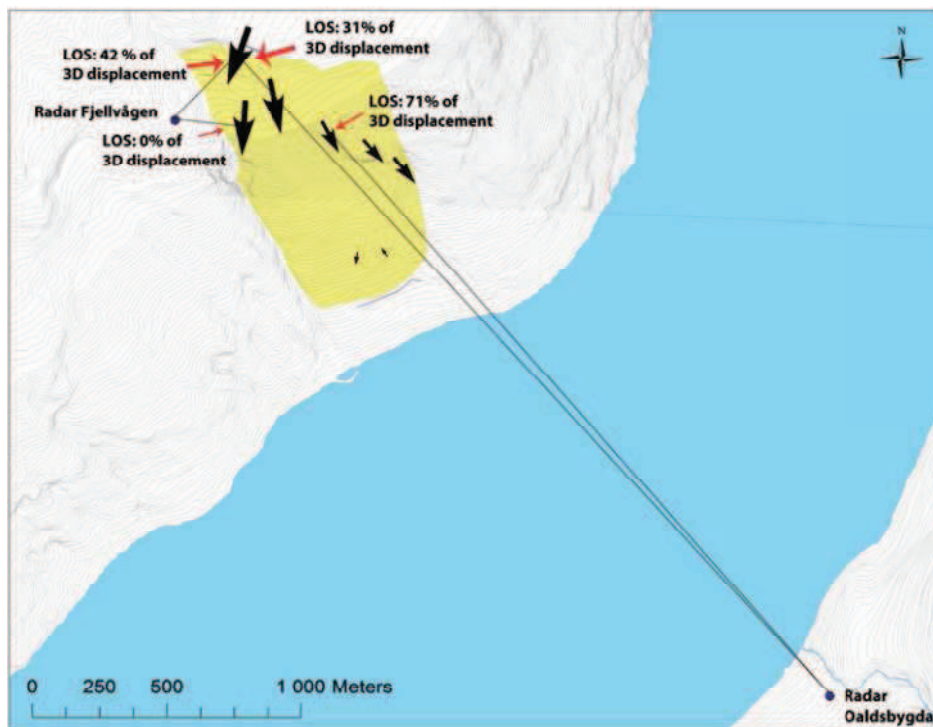


Figure 81. Location of GB-InSAR instruments and relative % of displacement detectable along the respective LOSs. Black arrows show size and direction of displacement registered by *in situ* instruments (from: Kirstensen et al., 2013).

As previously mentioned, data that have been provided by the Åknes/Tafjord Early Warning Centre regard the acquisition campaigns obtained from Oaldsbygda (Figure 82). All campaigns started in July and stopped in October; their duration differs only for few days. In Figure 83, cumulated displacement maps related to the total period of every acquisition campaign are displayed (2006, 2008, 2009, 2010). Moreover, in Figure 84, the displacement cumulated map registered from Oaldsbygda in the period between July and October 2012 (Figure 84 A) and the displacement cumulated map of the 2012 acquisition campaign from Fjellvåken (shown in Kristensen et al., 2013) are displayed.

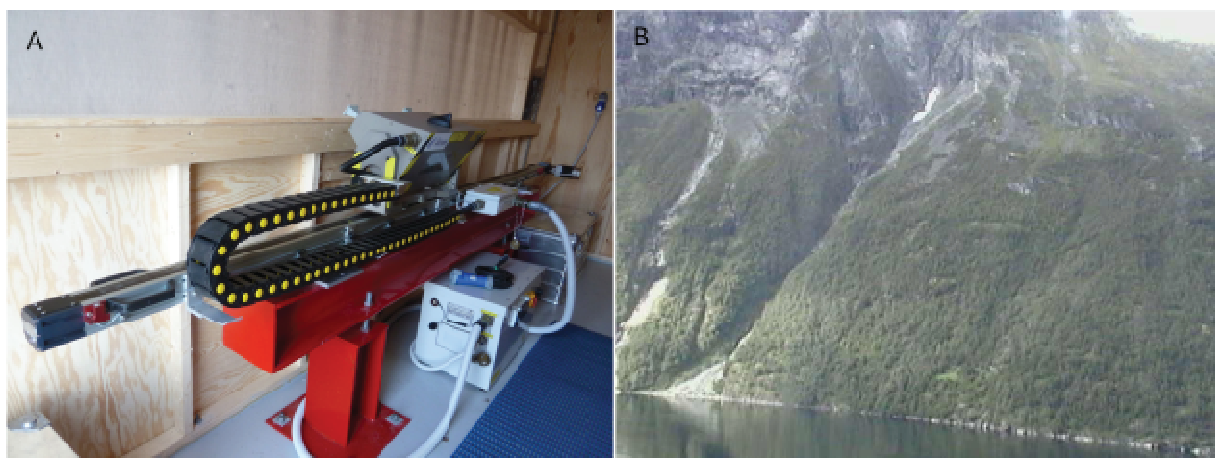


Figure 82. GB-InSAR system employed at Oaldsbygda (A) and its view of the Åknes slope (B).

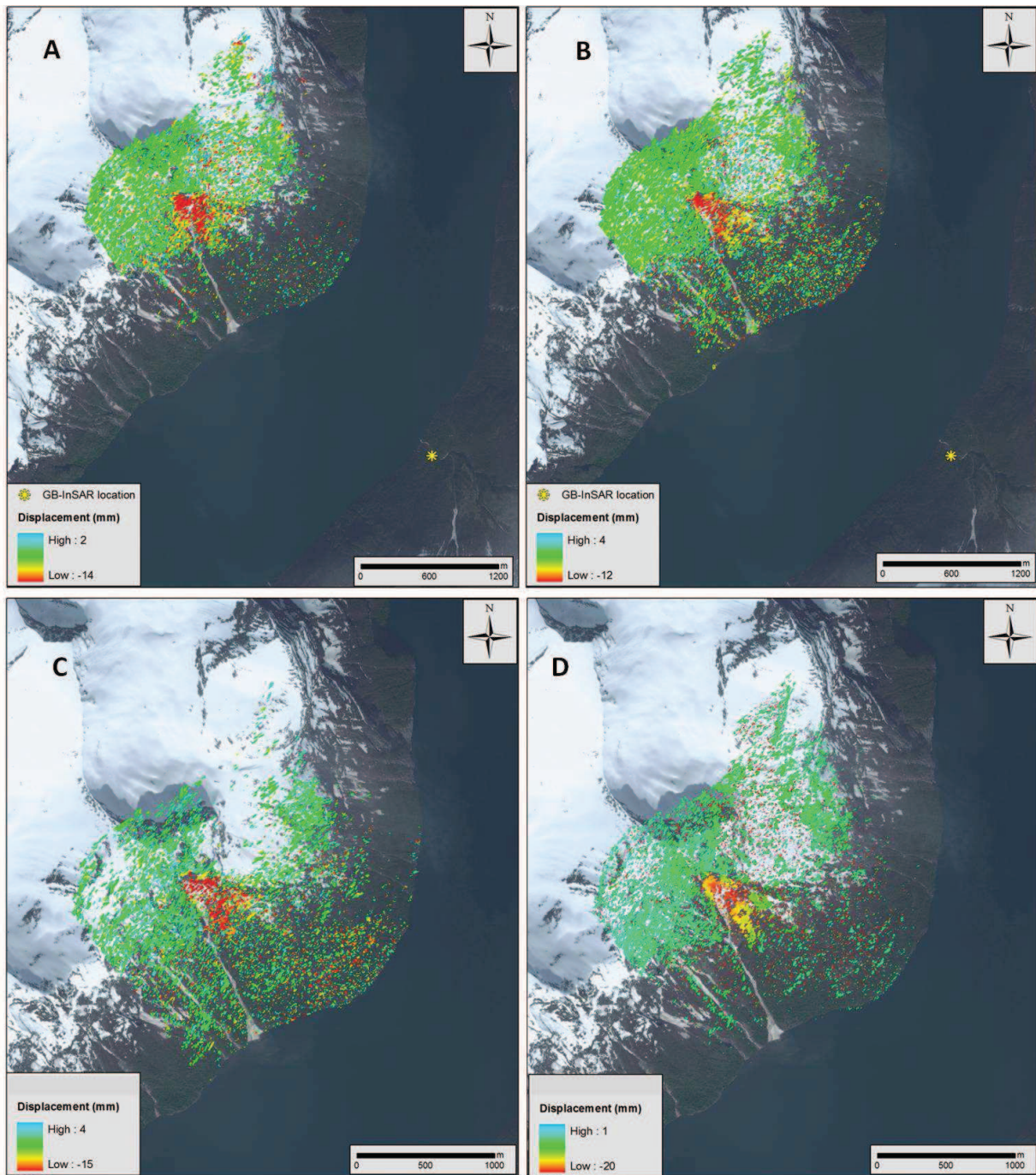


Figure 83. Cumulated displacement maps of GB-InSAR campaigns from Oaldsbygda. A: time interval of 95 days, between July and October 2006; B: time interval of 88 days between July and October 2008; C: time interval of 108 days, between July and October 2009; D: time interval of 114 days, between July and October 2010. Negative displacements represent movements approaching to the sensor.

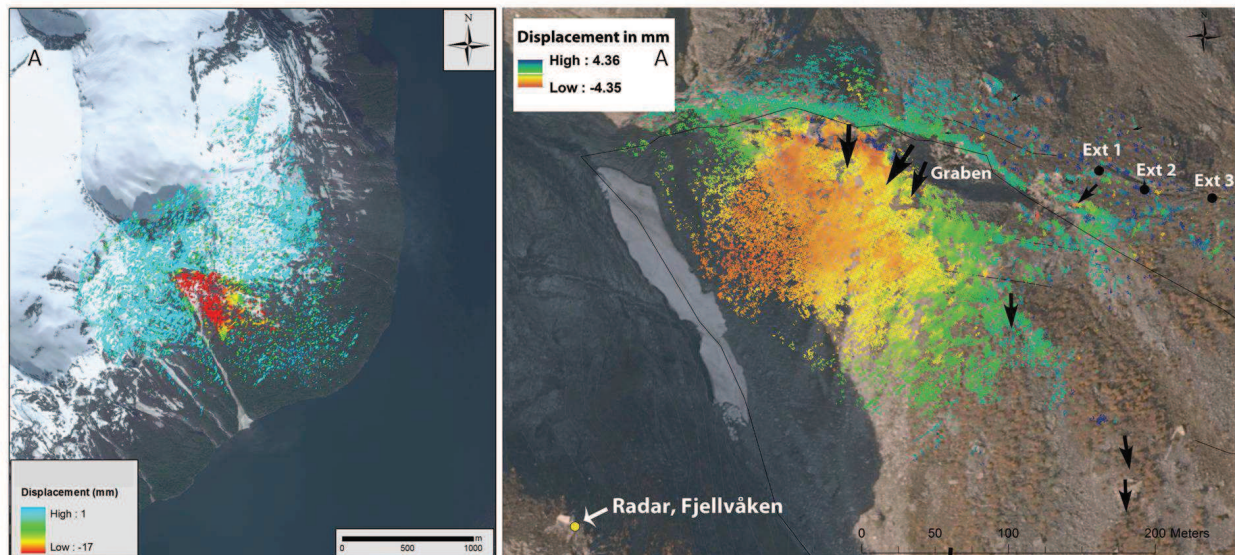


Figure 84. Cumulated displacement map related to the acquisition campaign of July-October 2012 from Oaldsbygda (A). Cumulated displacement map related to the four weeks long acquisition campaign from Fjellvåken (B) (courtesy of Kristensen et al., 2013).

The maps in Figure 83 show a quite consistent displacements, measured from year to year of maximum 15-20 mm in 3-4 months intervals. These values correspond well to other displacement measurements (Kveldsvik et al., 2006, Kristensen et al., 2013). Slight differences exist in the magnitude of displacements, generally explicable by the different lengths of the measurement campaigns. As regards the displacements obtained in the 2012 campaign, it also accords with the others, with maximum displacement values around 17 mm in a period of about 3 months (Figure 84).

The displacement values obtained from Fjellvåken are referred to the most active portion of the landslide and, in comparison with the data observed from Oaldsbygda, they present lightly lower values in relation with the different LOS.

Literature data, especially the ones obtained from the comparison between GPS data and GB-InSAR data (Figure 81), have been used to test the approach proposed in this thesis, to by-pass the problem of the possibility to detect only LOS displacements, by using InSAR techniques.

Assuming as the most probable displacement direction the downslope direction, GB-InSAR data, provided by Åknes/Tafjord Early Warning Centre, have been projected along this chosen direction, following the procedure described in the sub-paragraph 2.3.2 of this thesis. Starting from the LOS data, the objective was to evaluate the percentage of displacement detected by the instrument with respect to the downslope direction and compare these percentages with the ones obtained by GPS campaigns (real displacement values).

The results can be summarized in a map showing the percentage of the “real” displacement values (considering as “real” the displacements that happen in downslope direction) detected in each sector of the landslide (Figure 85).

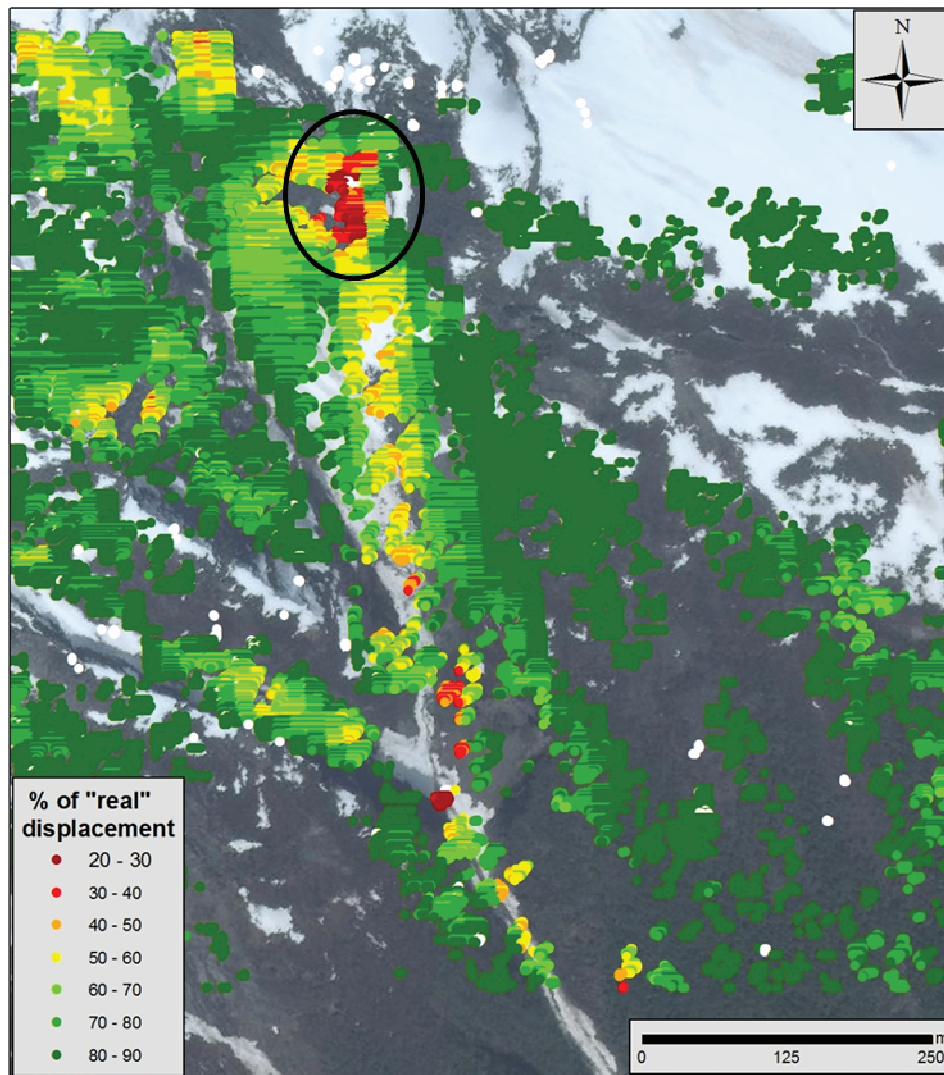


Figure 85. Map related to the % of real displacements detectable along the GB-InSAR LOS, considering as “real” the downslope direction. The sector emphasized by a black dash represents the upper part of the landslide, mainly interested by vertical displacements.

The map in Figure 85 shows the variation of the percentage of real displacement values in a range between 20 and 90%. In the upper part of the landslide, where the major crack develops, the principal displacement direction is vertical, so that in this area displacements registered on the GB-InSAR LOS represent only the 30% of the real ones, according to the results obtained by [Kristensen et al., 2013](#) (Figure 81). Concerning the other portion of the landslide, displacements observable on the radar LOS are in general higher than 50%; the yellow band (% of detected displacements between 50 and 60) in Figure 85 refers to an area where the downslope direction is slightly west-most oriented than the LOS direction, which is oriented more or less SSE-NNW.

Thanks to the Northern Research Institute (NORUT- <http://norut.no/>), that is a Norwegian research and innovation group located in Northern Norway, also satellite InSAR datasets have been made available to the objectives of this thesis.

Also in the case of satellite InSAR acquisitions, the vegetation cover that interests the lower part of the landslide causes loss of coherence in the radar signal. Moreover, the available

satellite InSAR datasets present non optimal LOS for measuring the horizontal component of the movement. In general earth observing satellites, flying in polar orbits, have a direction close to NS; in this plane, the horizontal displacements are near to be not visible, especially if snow or vegetation cover interests the observed area, or if there is high variability in soil moisture. These unfavourable conditions widely interest mountainous Norwegian regions.

In the specific case of Åknes, two datasets are available, acquired by RADARSAT-2 and by a combination of TerraSAR-X and TanDEM-X, both in ascending orbit, which is the best configuration to reduce the distortions in east facing slopes observations. The LOS of both the satellites ranges between 76 and 77° in azimuth and between 25 and 28° in look angle. RADARSAT-2 dataset includes images acquired between October 2008 and August 2013, with a revisiting time of 24 days; while TerraSAR-X/Tandem-X acquisitions are related to a shorter period, between July 2010 and October 2012, with repeating time of 11 days. Only summer-early autumn periods are meaningful, because in other periods the snow cover strongly reduces the satellite visibility.

Raw data have been processed by [NORUT \(2013\)](#), applying SBAS (Small Baseline Subset) and PSI (Persistent Scatterer Interferometry) methods.

In order to better interpret the satellite datasets, NORUT researchers have compared them with data obtained from GPS measurements. Considering the small portion of displacements detectable by space borne platforms, the comparison has been implemented projecting GPS data on the LOS direction of the satellites (Figure 86). Indeed, satellite LOSs have angles of about 62° for RADARSAT-2 and 65° for TerraSAR-X/Tandem-X, with respect to the horizontal direction, and an ENE orientation. This acquisition geometry makes the LOS near to be perpendicular to the downslope direction.

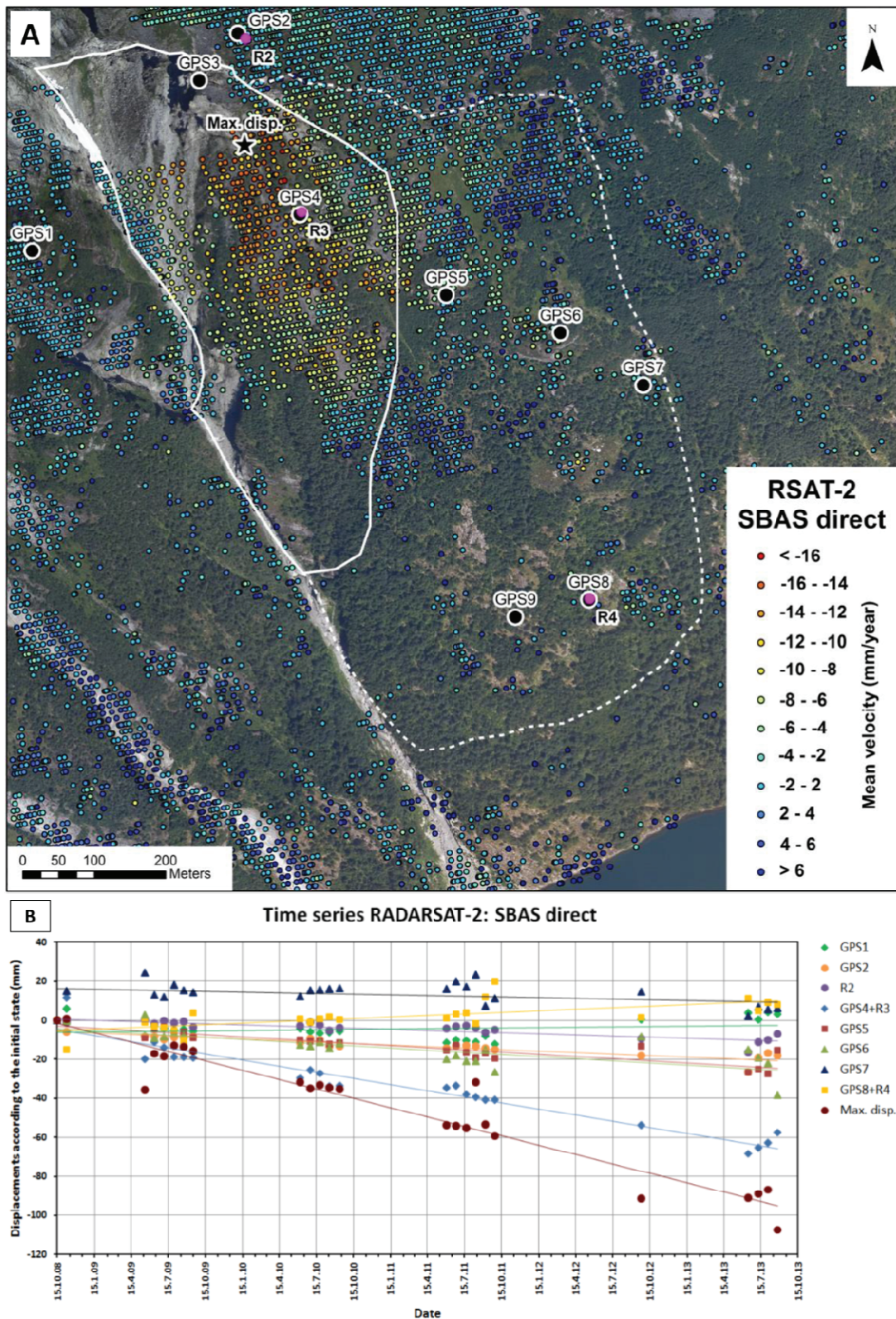


Figure 86. A: Radarsat-2 dataset processed by applying SBAS algorithms; white lines represent main rockslide scenarios; black circles stay for GPS positions, pink circles for corner reflectors location and the black stars represent the locations of the points characterized by maximum displacements. B: Radarsat-2 time series related to maximal displacement points and displacement values registered by GPS/corner reflectors approximately in the same locations of the Radarsat-2 points (courtesy of NORUT, 2013).

Comparison provided a good correspondence between the mean velocity values registered by satellite and the mean velocities registered by GPS, that have been estimated to reach approximately 20 mm/year (Figure 86). The results also show that RADARSAT-2 datasets are more relevant than TerraSAR-X/Tandem-X datasets, which registered maximum velocity values around 15 mm/year (Figure 87). Indeed, X-band sensors suffer more the effects of phase ambiguity, in relation with their shorter wavelength respect to the C-band instruments (such as RADARSAT-2). Despite the improvement of spatial resolution, the use of X-band sensors determines a detriment of detectable displacement, which is limited to the range between $-\lambda/4$ and $\lambda/4$. This problem affects more those landslides whose movement rate reaches high values in the span between two subsequent satellite acquisitions; it is the case of the Åknes rockslide.

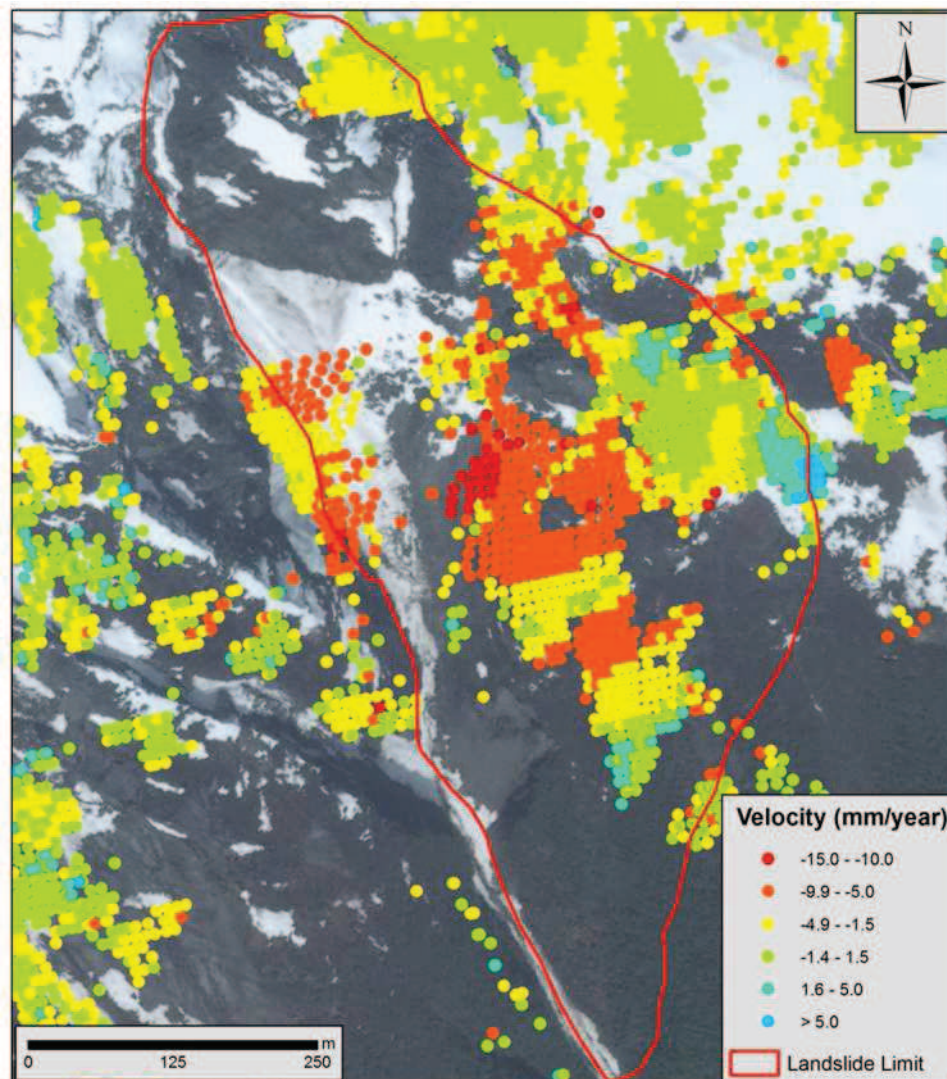


Figure 87. Mean velocities registered by TerraSAR-X/Tandem-X between 2010 and 2012 (values detectable on the satellite's LOS). Red line corresponds to the landslide limit in the most dangerous scenario.

As in the case of GB-InSAR data, satellite InSAR data provided by NORUT have been projected on downslope direction, to further analyse the problems related with the LOS that these data encountered. Except for the upper part of the landslide, where it is known that the displacements mainly follow a vertical direction, in general it is considered acceptable to

assume as direction of real displacement the downslope direction. Also in this case, satellite InSAR data have been projected downslope, following the procedure proposed in the subparagraph 2.3.2 of this thesis.

Because of the LOS directions of the two satellite platforms are more or less similar, the results of the projection are also not so different. For this reason in Figure 88, only the percentage of "real" displacement map related to TerraSARX/TandemX data is shown.

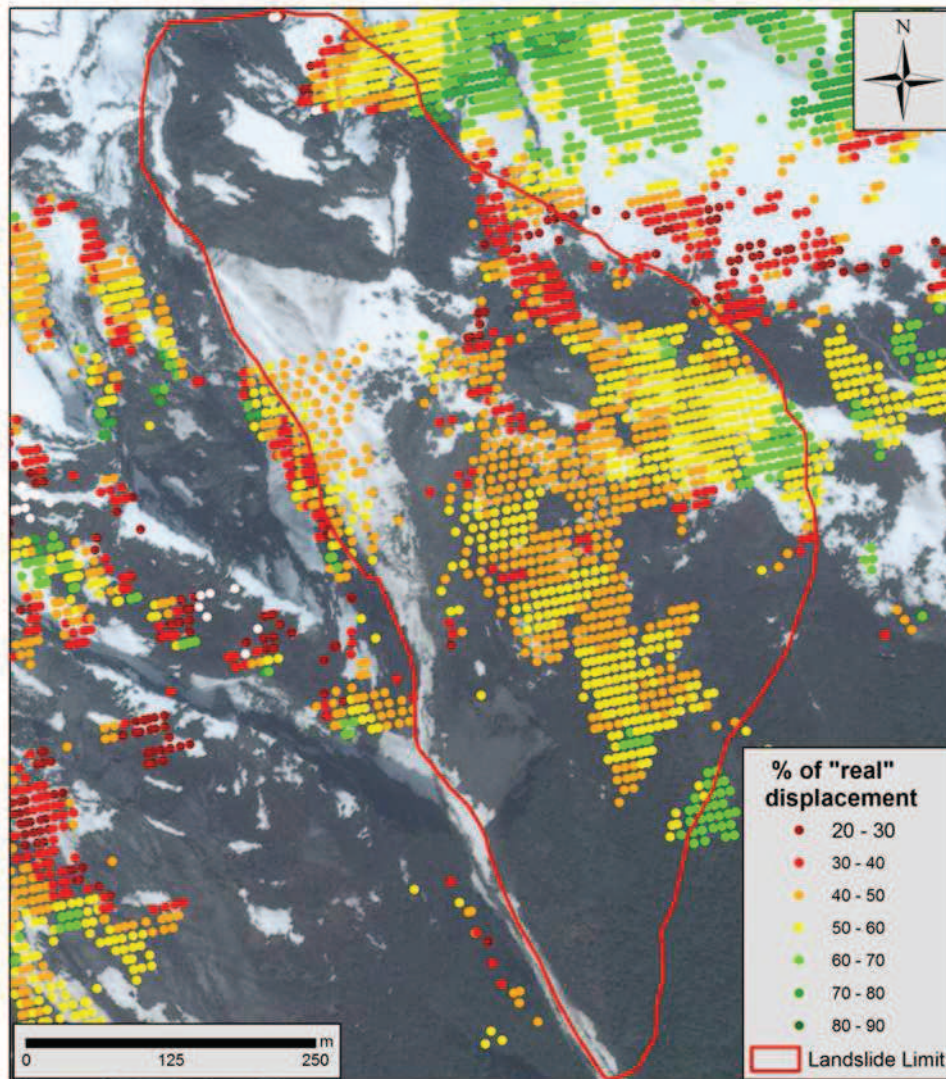


Figure 88. % of "real" displacements detected by TerraSAR-X/Tandem-X satellites. Red line corresponds to the landslide limit in the most dangerous scenario.

Excluding limited areas on the boundaries of the landslide, the downslope displacements detectable by satellite platforms are up to 60% of the real ones. Moreover, on average, satellites are able to measure less than 50-40% of the real displacements. The upper part of the landslide, which corresponds to the upper crack, is completely not visible from space borne platforms.

4.4.3 Satellite- and GB- InSAR data comparison

In the context of the here presented research project, a qualitative comparison between GB-InSAR and satellite-InSAR data of the Åknes rockslide has been produced.

In the previous sub-chapter, the projection of the available datasets on a common direction, defined as the downslope one, has been presented. Downslope direction, especially for the middle part of the landslide, is considered approximately similar to the real displacement direction as the rockslide movement can be considered parallel to the topographic surface. In the upper part of the landslide, on the contrary, the main movement is along a vertical direction.

The data projection on the same direction allows us to make some comparisons. First of all, the detectable area from the different sensors is not the same: GB-InSAR coverage is much less in the middle and lower parts of the slopes than the satellite coverage, which in turn is lacking in the upper part of the landslide, near the major crack. Concerning the displacements, RADARSAT-2 shows very similar patterns to the GB-InSAR ones. To better compare the datasets, a restricted period of about 3 months (from July to October 2010) has been selected in the RADARSAT-2 acquisitions, in order to be comparable with the available data of the 2010 GB-InSAR campaign. Data projection permitted to display the two datasets on the same map (Figure 89).

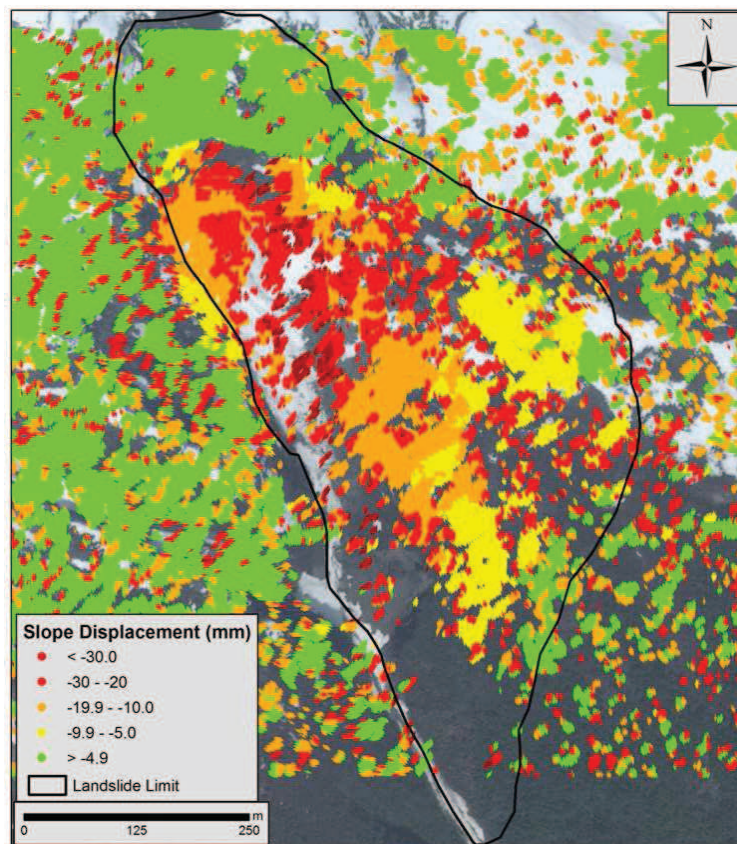


Figure 89. Displacements projected downslope, detected by the GB-InSAR and the satellite RADARSAT-2 in the period between July and October 2010. Black line corresponds to the landslide limit in the most dangerous scenario.

Displacement values detected by RADARSAT-2 and the GB-InSAR agree to define the “middle” part of the landslide (defining as “landslide” only the portion of the rockslide which is included in the limits that define the most dangerous possible scenario – Black line in Figure 89) as interested by the major movement, reaching about 30 mm of displacement in about 3 months. The upper part of the landslide, mainly interested by vertical displacements, show displacement values around 5 mm in downslope direction: it is probably an underestimation related to the differences between real displacement directions and downslope one.

Landslide boundaries can be clearly identified in the map (Figure 89), which also takes the advantage related to the data mixing, which permits to observe more or less all the landslide area, by overlapping the area observed from space borne platforms to the one observed from the ground based instrument.

For the same period (July-October 2010) also TerraSAR-X/TandemX datasets have been projected downslope. The resulting map is shown in Figure 90.

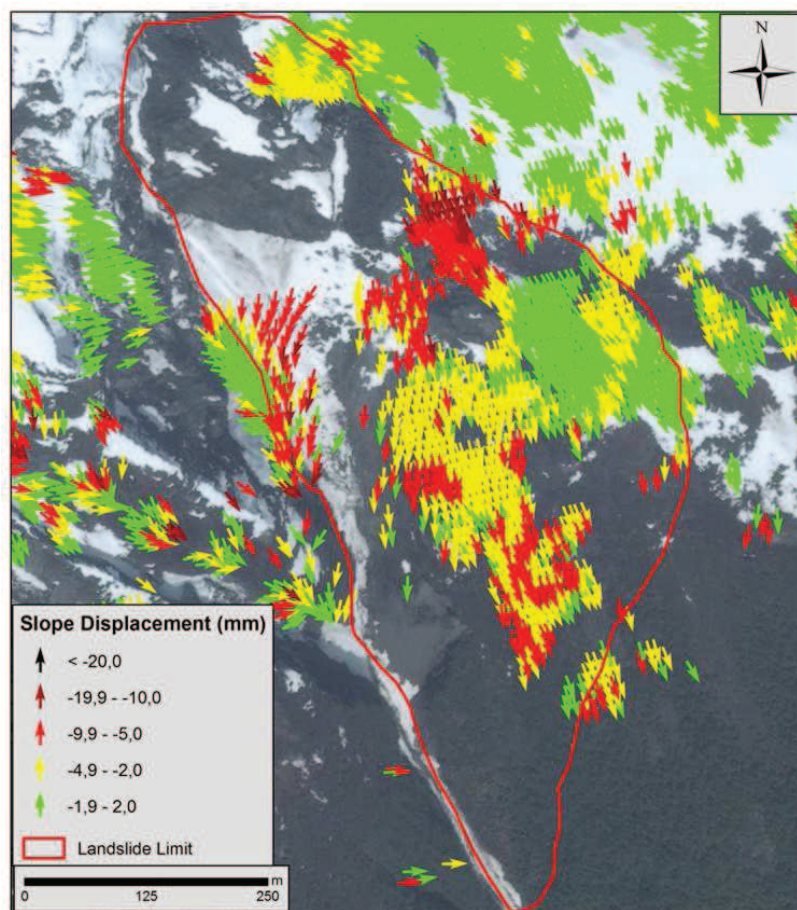


Figure 90. Slope displacements registered by TerraSAR-X/TandemX in 2010. Arrows are oriented along downslope direction. Red line corresponds to the landslide limit in the most dangerous scenario.

On the contrary, TerraSAR-X/Tandem-X datasets show displacement values lower than the obtained from RADARSAT-2 and from the GB-InSAR. This underestimation has been explained in the previous sub-paragraph and it is mainly related to the higher aliasing effect, which interests new-generation X-band satellites.

5. Discussion and results

The main objective of this PhD programme was to give a contribution to the field of landslide risk mitigation, by working on one of the most complete existing mitigation measures: Early Warning Systems.

The concept of early warning is not new, so the objective was to improve the existing EWSs, implementing them through the exploitation of the advantages of the InSAR techniques.

Several EWSs, as defined by UNISDR in 2009 and organized following the guidelines proposed by [SafeLand Project \(2011\)](#), are already operative.

The most complete EWS structure is probably the one implemented in Norway, to reduce the risks related to the possible trigger of the Åknes rockslide ([Blikra, 2008](#)), which takes advantage of a series of “traditional” monitoring instruments. By the word “traditional” we mean every instrument useful in monitoring landslide displacements except the ones based on InSAR technology. Åknes EWS can exploit data obtained from GPS-networks, extensometers, geophones, inclinometers, piezometers and meteorological sensors. InSAR data are also available at Åknes, but they don’t contribute to the EWS, because of some limitations are still present in their application in this field.

The specific objective of this research was to give some contributions to overcome these drawbacks, always taking into account that a well-structured EWS has to be well-organized in all its phases (Design, Monitoring, Forecast, Education- [Intrieri et al., 2013](#)).

Therefore, during this PhD programme, InSAR systems were analysed taking into account their utility throughout all the phases of a well-organized EWS.

Focusing the attention on InSAR systems installed on ground based platforms, the main advantages and limitations of these instrument applications were investigated, trying to improve some of the benefits and overcome the main drawbacks.

Considering the list of advantages and limits proposed in Table 4 and analysing the GB-InSAR prerogatives, it is possible to claim the extreme utility of this system in emergency conditions. Its versatility and transportability, the facility of installation, the possibility to detect spatial movements and the advantages typical of every remote sensing technique (among other things, the possibility to install and monitor the phenomena without accessing the unstable area) make the instrument particularly useful to manage landslide emergencies.

The main goal of this research was to take note of these features, improving them in order to make the instrument application in emergency phases even more efficient. Therefore, the first step of the research project was to optimize GB-InSAR instruments by working on its hardware features.

A prototype of an implemented system was tested: it is characterized by modularization of its main components and reduction in the linear rail length and in its total weight. These first

modifications allowed us to strongly reduce the installation time and the transportation problems. Indeed, a reduction in the amount of occupied space, especially thanks to the reduction of the linear rail length, was obtained, notably increasing the transportability of the instrument also using normal vehicles. The weight reduction also implied the possibility of manual transportation, over short distances, using four operators. However, transportation by vehicles is necessary and a further implementation of transportability is required to make these instruments really "portable" and manoeuvrable in restricted areas far from communication routes, or where the viability is interrupted by the landslide itself. A further reduction in the occupied space could be required as well, in order to install the instrument in those areas where installation space is limited.

In the context of the hardware features, some modifications have been proposed to also increase the flexibility of the instrument. GB-InSAR systems can select the acquisition parameters that better adapt themselves to the investigation of the observed scenario. The selection of these parameters is the competence of the software part of the system, but, also acting on the hardware components, it can also increase the instrument's flexibility. The adopted modification operates on the relation between synthetic aperture length and temporal and spatial resolutions. The implemented system has been structured to be able to interchange the synthetic aperture length, alternating different resolution acquisitions from the same scenario. In particular, fast acquisitions have been obtained, using synthetic aperture lengths that are as short as possible. A reduction in these lengths also implies a reduction in the extension of the visible area, balanced by an increase in the temporal resolution: shorter acquisition times determine the possibility to increase the acquisition frequency and, consequently, to observe higher landslide velocities that do not exceed the threshold values, which determines aliasing problems.

The first test of the instrument was performed in 2013, to monitor the Capriglio landslide, which affected the Tizzano Val Parma municipality (Parma Province, Emilia Romagna Region). The event, a roto-translational earth slide evolved into earth-flow, affected an area of about 1 km²; the landslide partially involved also the villages of Capriglio and Pianestolla, located on the boundaries of the landslide body. A GB-InSAR instrument was installed far away from the villages (about 4.5 km far from Capriglio and about 2.8 km far from Pianestolla). Fast acquisitions were made to observe the landslide body area, whose high values of displacements required, in the beginning phases, very fast acquisitions. A synthetic aperture of 1 meter and an acquisition time of 28 seconds were the input parameters used in the first period of monitoring. These fast acquisitions allowed us to detect velocities up to 7 m/day, overcoming the pre-defined detectable velocity limit by using these instruments. Actually, taking into account the [Cruden & Varnes](#) landslide classification (1996), only displacements classified as "fast" were considered detectable (velocity range entering in class 5) until the introduction of this new acquisition method, which determined the possibility of detecting velocity values, belonging to the 6th class of Cruden & Varnes (very fast movements).

These acquisitions were interchanged with "slow" ones, finalized to the observation of wider areas also including the villages, and able to detect the centimetric displacements, which

characterized Capriglio and Pianestolla, in the early phases of monitoring. The system was installed for long term monitoring, and is in fact still active.

The test allowed us to validate the effective improvement in the transportability and versatility of the system, especially in the installation phase, when two potential installation points were identified. The selection of one of them was submitted to trials on both the sites, in order to better define the solution. It would not have been possible without the application of the implemented instrument, which allowed us to install and obtain acquisitions in very short periods.

Actually, when the instrument was installed, about 1 month after the landslide trigger, the velocity of the earth flow was already decreasing. Fast acquisitions, every 28 seconds, allowed us to observe maximum displacements during that period (*i.e.*, about 7 m/day); but, if the instrument had been installed previously, it would not have been able to observe the landslide displacements even in fast acquisition configuration.

Moreover, the resolution in correspondence with the villages is very low, in relation to the high distances that exist from instruments with these targets. Therefore, related data could not be fully reliable, especially when the atmospheric interactions become particularly strong.

Summarizing, the first test of the implemented hardware features of the GB-InSAR concluded well as regards the installation times, the application in emergency conditions and the detection of fast displacement values. More efforts are still required to further increase the value of the detectable displacement and the spatial resolution, especially in those areas located far away from the sensor and characterized by very low values of azimuth resolution.

As regards the problems related to the atmospheric effect, high attention has been addressed to this topic in the section of this PhD programme, focused on the GB-InSAR software features optimization.

During this step of the research, a new algorithm to determine the atmospheric component of the wave phase was proposed. Its name, REACT, is the acronym of *Region-removal Atmospheric Corrective Transformation* and it is based on the evaluation of the atmospheric contribution over the whole observed area, discarding the areas considered unstable *a priori*. With respect to the most widespread corrective algorithms, REACT is based on the opposite logic: the most used algorithms analyse the atmospheric contribution on specific points, defined stable, and interpolate linearly these obtained values over the whole observed area. REACT, analysing the atmospheric contribution on a wider area, is characterized by more precision in its definition and, moreover, the interpolation in this case is not defined linearly *a priori*, but is defined by adapting it to the specific conditions of the scenario.

The new algorithm has been tested for the first time on the images acquired on the A16 highway, where the implemented GB-InSAR instrument, also used in Tizzano Val Parma, was installed on July 2014.

Here, in addition to the implemented hardware features, the instrument was also equipped with this new algorithm.

As regards the hardware component, the monitoring campaign carried out along the highway, in the field of a NOP project, confirmed the positive results obtained in Tizzano Val Parma, especially regarding the reduced installation times, related to the increase in instrument versatility and transportability.

The application of REACT allowed us to obtain clearer interferograms, if compared with the ones processed by using classical algorithms. Moreover, an *ad hoc* system was implemented with the corrective algorithm already installed to be applied *in situ* to process raw images; indeed, it is light enough in weight to act while occupying a minimum memory space. Therefore, images can be transferred already corrected, also reducing data flow on the internet network.

The case of the A16, with its restricted scenario and its well-known characteristics in terms of stability, lends itself well to the application of REACT.

The necessity to have a complete knowledge of the area, before the algorithm application, represents the main limitation to its use. Moreover, the definition of stable areas could not be easy, especially during emergency conditions when corrected images have to be obtained as soon as possible. Therefore, REACT is useful in well-known areas, where the unstable portion of the slope is clearly definable in the early phases of monitoring.

To be useful in EWS structures, InSAR data must be fast to acquire and perfectly explicative of the observed movement pattern. GB-InSAR optimizations were created in order to implement these aspects, but more information can be obtained integrating these datasets with the ones obtained applying the same technique on data acquired from space borne platforms.

In the context of GB-InSAR optimization, a proposal of a procedure to integrate these datasets has been presented. Actually, these datasets, besides their common technical principle, present some differences. These diversities represent an advantage in the phase of qualitative integration, because the techniques show some kind of complementarities: satellite view is wider (hundreds of square km) if compared with the GB-InSAR instruments which are able to detect only a few square km wide area. Moreover, thanks to the number of past and current spatial missions, more or less in every place of the world a historical archive of satellite InSAR data exists; this allows us to exploit pre-event data, in spite of the case of GB-InSAR acquisitions, which are generally delimited in time to the emergency and post-emergency phases.

Generally, the costs of satellite InSAR data are restrained especially if compared with the price of the GB-InSAR instrument.

Moreover, nowadays, new-generation satellites exist. They work by using X-band microwave, unlike the old generation ones, which generally used the C-band; this wavelength allows us to obtain better resolutions, although they are more affected by the aliasing effect. The new-generation satellites orbiting now are TerraSAR-X, Tandem-X and COSMO-SkyMed. The last one is an Italian satellite and a special mission named "Map Italy" used it to map the stability/instability of the whole Italian territory.

Before the launch of the COSMO-SkyMed mission, the reduced revisit capacity of orbiting satellites (the first generation satellites have a revisiting time in the order of weeks) was the most serious gap for the extensive use of satellite SAR information as an operational monitoring tool. A further critical issue, for the operational employment of remotely sensed data in risk management applications, was generally the limited capability of previous Earth Observation (EO) satellite systems to offer an efficient response to user's specific needs, in terms of image resolution and accuracy, reaction time, latency of data and delivery time. In a few words, in landslide-related emergency situations, dealing with space-borne sensors, the main limiting factor to be overcome is the time to "refresh" a single image. Now, the COSMO-SkyMed (CSK) constellation represents an existing opportunity thanks to its revisiting times, which can determine an increase in the acquisition frequency. The enhanced temporal repetitiveness of the CSK constellation (in the order of hours in emergency mode), the unprecedented speed in terms of response time (quasi-real-time delivery of data within a few hours of acquisition) and the flexibility of mission configuration now offer the opportunity to effectively employ radar imagery as a quasi-real-time monitoring tool, in the emergency and post-emergency phases associated with natural phenomena.

These features have been considered favourable to be included in the EWS development project, proposed in this thesis.

Qualitative integration between the satellite- and GB- InSAR datasets required only an integrated analysis on GIS platforms to produce binary maps, distinguishing stable and unstable areas. This is a preliminary step to proceed to the semi-quantitative integration. This further step requires the data homogenization in terms of spatial and temporal resolution and among others, in terms of Line of Sight (LOS). In the field of this thesis, the attention was widely focused on the LOS problem, which is the only direction along with the InSAR techniques are able to detect displacements. The problem related to the different resolutions has been solved by re-sampling data on the basis of the worst resolution values (generally related to the satellite datasets). In order to overcome the LOS problem, it has been proposed to project the datasets on a similar direction, defined as the downslope direction, as the most probable direction along which a landslide develops. A *MatLab* script was created in order to automatize the projection procedure.

The selection of a common direction for the projection of data allows us to evaluate the effective correlation between the two datasets, determining the possibility to effectively analyse them simultaneously. But, the reduction in resolution, necessary to compare the datasets, determines an information loss; moreover, the real comparison between the datasets is possible only in the time span that corresponds to the simultaneous acquisition of the datasets. In case of emergency conditions, the implemented possibility to obtain satellite acquisitions "*on demand*", with shorter revisiting times, also leads to the increase in temporal resolution of data obtained from space borne platforms and, consequently, it supports the application of integrated data analysis.

Data integration proved to be very useful, for example, in the study of the San Fratello landslide, where a qualitative and then a "semi-quantitative" integration has been created. The

qualitative integration allowed to redefine landslide limits; semi-quantitative integration, especially as regards the integrated study of time series, allowed us to test the integration approach quantitatively comparing every data acquisition.

Integration algorithm was also applied, for a validation, to the Åknes rockslide data. In this case, the existence of literature data regarding a comparison between real displacement values (obtained from GPS measurements) and GB-InSAR values permitted a validation of the procedure, especially regarding the data projection on the downslope direction.

In those cases, like Åknes, where the landslide main movement direction is sub-parallel to the topography, it is acceptable to assume downslope as the real movement direction. Unfortunately, it is not the case everywhere. Therefore only in those cases, projected data could be considered as the "real" values and, in these terms, they could be quantitatively integrated with the satellite ones, projected in the same direction.

In those cases where the movement direction is more or less parallel to the topography (translational landslides), the projection was also produced for GB-InSAR data, in the case of unavailability of InSAR satellite data. It is the case of the monitoring activities carried out along the A16 highway, where the downslope data projection allowed us to define the percentages of real displacements detected by the instrument, in relation to its installation point.

In those cases in which it can be applied, it could be useful to effect the projection in order to define the percentages of real displacements detectable by the instrument, in correspondence with more possible installation points, in order to select the best LOS.

InSAR data, considering both their optimized features and the technique evolution, especially in the field of satellite data, could be exploited in the main phases of the EWS structure.

In recent years, the idea that risk mitigation has to be managed not only in the emergency phases but starting from the politics of prevention has become widespread. In Italy, the law establishing the existence of National Civil Protection (L.225/92) defined, among its roles, the primary importance of the activities of prevention, forecasting, emergency and post-emergency management. In this sense, an EWS has to be conceived also taking into account the phases of prevention and prevision of the risk, not only participating in emergency activities. Actually, this is the attitude by which the risk can be managed in reality and in this sense InSAR data could be widely exploited, especially in the previous phases of early warning, such as monitoring and forecasting.

A sort of pre-EWS was proposed, based only on satellite data, to observe wide areas by exploiting both near-real time acquisitions of new-generation satellites and historical archives. It was proposed in order to identify those areas where an increase in the landslide risk requires an increase in the early warning activities. For localized areas, an effective EWS was proposed, based on the integrated use of GB-InSAR and InSAR satellite techniques. It is useful in those cases in which satellite data are available or can become available scheduling *ad hoc* acquisitions; as regards the budget, a consistent financial commitment is necessary for the employment of GB-InSAR systems.

As regards the design phase of the EWS, it is useful to take into account, at this stage, all the limitations and advantages in the application of InSAR techniques, such as the costs, the possibility of exploiting only a specific range of landslide velocity values, the existence or not of available satellite data, the benefits of remote sensing, etc.

In monitoring activities, these techniques can be very useful, especially from space borne platforms, thanks to the availability of historical archives which allow us to exploit long term monitoring data. In those cases in which it is possible to install a GB-InSAR also during the monitoring phases (as was done on the A16 highway), it can provide high precision data that can be integrated with satellite data, especially as regards the time series. Displacements can be studied with very high precision, also increasing the precision in the definition of early warning switch level, by applying threshold values.

Also in the forecasting phase, the integration between GB- and satellite-InSAR data could be useful to better recognize the eventual time series trends, considering that the soundness of the prevision mainly depends on the sample number and on the precision of the measurements.

All the information derived from InSAR data and useful to the EWS must be transferred to all the involved stakeholders, accomplishing the education phase.

In 2010, Lu suggested: *"...finally but not the least, more attentions are needed to be...focused on those efforts to increase the communication between researchers and decision makers and those attempts to bring the science into society for an extensive public participation."*

In this sense, the education phase of an EWS assumes crucial importance and it allows us to connect science to its final goal, which is to create products easily usable by all the people involved in the risk; the soundness of an EWS is subordinate to the population's ability to take advantage of it, by putting into practice the proposed procedures adopted at every level (generally ordinary, attention and alarm).

6. Conclusions

InSAR techniques have been exploited in order to make them useful in the field of landslide risk mitigation and, specifically, in the production of Early Warning Systems (EWSs).

Among the InSAR techniques, more attention has been given to ground based instruments (GB-InSAR) and some of its features have been implemented to the finality of Early Warning.

Hardware characteristics of GB-InSAR systems have been optimized to increase the applicability of this type of instrument in emergency conditions: an increase in versatility and transportability of the prototypal system represented the main results. The implemented system is in fact characterized by a general weight reduction and by a minimal amount of space of each of its components. Flexibility has also been achieved by allowing a wider range selection of parameters in the acquisition phase.

Also some software features have been achieved with the creation of a new algorithm finalized to the correction of the atmospheric distortions in the radar images, which proved to be very useful in those conditions in which the scenario is wide and far away from the installation point; *a priori* knowledge of the general characteristics of the scenario (in terms of stability and instability) is required.

New generation satellite products have also been investigated in terms of applicability in Early Warning System activities. X-band satellites are in fact characterized by shorter revisiting times and higher spatial resolutions, which make them exploitable also in EWSs. Specifically, these data could be exploited by integrating them with the ones provided by GB-InSAR systems; to this end, a procedure to create a qualitative and a semi-quantitative integration has been proposed. The integration procedure allowed us to partially overcome an important limitation related to InSAR data: their capability to detect only displacements observed along their line of sight. By projecting datasets in a common direction it is possible to evaluate, in specific situations, the percentage of real displacements that the instruments, both installed on space borne and ground based platforms, are able to detect, on their line of sight (LOS).

After a description of the main requirements that an Early Warning System must accomplish, a proposal of an EWS completely based on InSAR data has been suggested, in all its principal phases: design, monitoring, forecasting and education.

The introduced methodologies were tested on four case studies, selected to be as representative as possible of the proposed theoretical approaches.

The Capriglio landslide, located in Tizzano Val Parma municipality (Parma Province, Emilia Romagna Region, Northern Italy), benefitted from long term GB-InSAR monitoring, carried out by installing an implemented instrument. It also represented an opportunity to test the proposed hardware optimizations on the system.

On a section of the A16 highway (Naples-Bari highway, Southern Italy), an optimized GB-InSAR system was installed. Hardware and software implementation was tested and integrated in an Early Warning structure.

The third case study presented regards the San Fratello landslide, which affected the San Fratello village (Messina Province, Southern Italy), in the beginning of 2010. The availability, in this area, of both GB-InSAR and satellite InSAR data allowed us to successfully test the integration procedure.

The last case study regarded a Norwegian rockslide, which affected the Western coast of the country: the Åknes rockslide. The availability of literature data on detectable displacement percentages, along the line of sight of the GB-InSAR system, installed on the site, allowed us to test and validate the proposed method to overcome the LOS problem.

In conclusion, InSAR techniques have been implemented in order to create an EWS that is completely based on their application. The improvements produced in the context of this research project allowed us to overcome some of the InSAR technique limitations and to propose a new EWS, adaptable to those landslides whose range of velocities is detectable by these monitoring systems.

7. References

- AGU, 2010 Blogosphere American Geophysical Union. *Maps of global fatal landslides*. (Available at: <http://blogs.agu.org/landslideblog/2010/02/12/maps-of-global-fatal-landslides/>).
- Antonello G., Casagli N., Farina P., Leva D., Nico G., Sieber A.J., Tarchi D., 2004. *Ground based SAR interferometry for monitoring mass movements*. *Landslide*, 1, 21-28.
- Ardizzone F., Cardinali M., Galli M., Galli M., Guzzetti F., Reichenbach P., et al., 2007. *Identification and mapping of recent rainfall-induced landslides using elevation data collected by airborne Lidar*. *Natural Hazards and Earth System Science*, 7 (6), 637-650.
- Ardizzone F., Basile G., Cardinali M., Casagli N., Del Conte S., Del Ventisette C., Fiorucci F., Gigli G., Garfagnoli F., Guzzetti F., Iovine G., Mondini A.C., Moretti S., Panebianco M., Reichenbach P., Rossi M., Tantaro L., Terranova O., 2012. *Landslide inventory map for the Briga and the Giampilieri catchments, NE Sicily, Italy*. *Journal of Maps*, 8(2), 176-180.
- Atzeni C., Basso M., Canuti P., Casagli N., Leva D., Luzi G., Moretti S., Pieraccini M., Sieber A.J., Tarchi D., 2001. *Ground-based radar interferometry for landslide monitoring and control*. Proc. ISSMGE Field Workshop on Landslides and Natural/Cultural Heritage, Trabzon (Turkey). ISSMGE TC-11, Kyoto, pp. 195-209.
- Azimi C., Biarez J., Desvarreux P., Keime F., 1988. *Forecasting time failure for a rockslide in gypsum*. Proceedings of the 5th International Symposium on Landslides, Lausanne. A. A. Balkema, Rotterdam, 1, 531-536.
- Bardi F., Frodella W., Ciampalini A., Bianchini S., Del Ventisette C., Gigli G., Fanti R., Moretti S., Basile G., Casagli N. *Integration between ground based and satellite SAR data in landslide mapping: The San Fratello case study*. *Geomorphology*, 223, 45-60.
- Basher R., 2006. *Global early warning systems for natural hazards: systematic and people-centred*. *Philosophical Transactions of the Royal Society of London, Series A*, 364 (1845), 2167-2182.
- Baum R.L., Godt J.V., 2009. *Early warning of rainfall-induced shallow landslides and debris flows in the USA*. *Landslides*, 7 (3), 259-272.
- Bell R., Glade T., Danscheid M., 2005. *Risks in defining acceptable risk levels*. In Hungr, O., Couture, R., Eberhardt, E. & Fell, R. (eds.), Proceedings, 2005 International Conference on Landslide Risk Management, Vancouver, 31.05. - 04.06.2005.
- Bell R., Glade T., Thiebes B, Jaeger S., Krummel H., Janik M., Holland R., 2009. *Modelling and web processing of early warning*. In: Malet J.P., Remaître A. & T. Bogaard (eds.): *Landslide*

Processes: from geomorphological mapping to dynamic modelling. Strassbourg, France, pp. 249-252.

Bellotti F., Bianchi M., Colombo D., Ferretti A., Tamburini A., 2014. *Advanced InSAR Techniques to Support Landslide Monitoring*. In *Mathematics of Planet Earth, Lecture Notes in Earth System Sciences 2014*, (ed. Springer Berlin Heidelberg), 287–290.

Bertolini G. and Pellegrini M., 2001. *The landslides of the Emilia Apennines (northern Italy) which resumed activity in the 1994-99 period and required Civil Protection interventions*. *Quaderni di Geologia Applicata*, Pitagora Ed., Bologna, 8, 27-74.

Bertolini G., Guida M., Pizziolo M., 2005. *Landslides in Emilia-Romagna region (Italy): strategies for hazard assessment and risk management*. *Landslides* 2, 302–312.

Bianchini S., Cigna F., Righini G., Proietti C., Casagli N., 2012. *Landslide Hotspot Mapping by means of Persistent Scatterer Interferometry*. *Environ. Earth. Sci.* 67(4), 1155–1172.

Bianchini S., Ciampalini A., Raspini F., Bardi F., Di Traglia F., Moretti S., Casagli N., 2014. *Multi-Temporal Evaluation of Landslide Movements and Impacts on Buildings in San Fratello (Italy) By Means of C-Band and X-Band PSI Data*. *Pure Appl. Geophys*, doi: 10.1007/s00024-014-614 0839-2.

Billi A., Presti D., Faccenna C., Neri G., Orecchio B., 2007. *Seismotectonics of the Nubia plate compressive margin in the South Tyrrhenian Region, Italy: Clues for subduction inception*. *Journal of Geophysical Research* 112, B08302, doi:10.1029/2006JB004837.

Blikra L.H., Longva O., Braathen A., Anda E., Stalsberg K., 2004. *Rock-slope failures in Norwegian fjord areas: Examples, spatial distribution and temporal pattern*. In: *Massive Rock Slope Failure NATO Science Series*, Edited by S.G. Evans, G. Scarascia Mugnozza, A. Strom and R.L. Hermanns, Kluwer Academic Publishers, Dordrecht.

Blikra L.H., Longva O., Harbitz C., Løvholt F., 2005. *Quantification of rock-avalanche and tsunami hazard in Storfjorden, Western Norway*. In: *Senneset, K., Flaate, K., Larsen, J. (Eds.), Landslides and Avalanches: ICFL 2005 Norway*. Taylor and Francis Group, pp. 57–63.

Blikra L. H., 2008. *The Åknes rockslide: Monitoring, threshold values and early-warning*. 10th International Symposium on Landslides and Engineered Slopes, 30th June-4th July, Xian, China, pp. 1089-1094.

Bliss D., Forsythe K., Fawcett G., 2006. *MIMO Radar: Resolution, Performance & Waveforms*. ASAP workshop MIT Lincoln Lab, 6 June 2006.

Borgatti L., Soldati M., 2010. *Landslides as a geomorphological proxy for climate change: A record from the Dolomites (northern Italy)*. *Geomorphology* 120 (1), 56-64.

Braathen A., Blikra L. H., Berg S. S., Karlsen F., 2004. *Rock-slope failures of Norway; type, geometry, deformation mechanisms and stability*. Norwegian Journal of Geology (NGT), 84, 67 – 88.

Brabb, 1991. *The world landslide problem*. Episodes, 14 (1), 52-61. (Available at: <http://www.episodes.co.in/www/backissues/141/Articles--52.pdf>).

Canuti & Casagli, 1996. *Considerazioni sulla valutazione del rischio di frana*. (Available at: <http://www.adbarno.it/rep/biblio/Canuti.pdf>). In Italian.

Canuti P., Casagli N., Ermini L., Fanti R., Farina P., 2004. *Landslide activity as a geoindicator in Italy: significance and new perspectives from remote sensing*. Environmental Geology, 45(7), 907-919.

Casagli N., Colombo D., Ferretti A., Guerri L., Righini G., 2008. *Case Study on Local Landslide Risk Management During Crisis by Means of Remote Sensing Data*. Proceedings of the First World Landslide Forum, Tokyo Japan.

Casagli N., Tibaldi A., Merri A., Del Ventisette C., Apuani C., Guerri L., Fortuny-Guasch J., Tarchi D., 2009. *Deformation of Stromboli Volcano (Italy) during the 2007 crisis revealed by radar interferometry, numerical modeling and field structural data*. Journal of Volcanology and Geothermal Research, 182(3-4), 182-200.

Casagli N., Catani F., Del Ventisette C., Luzi G., 2010. *Monitoring, prediction, and early warning using ground-based radar interferometry*. Landslides, 7(3), 291-301.

Cascini L., Fornaro G., Peduto D., 2010. *Advanced low and full resolution DInSAR map generation for slow moving landslide analysis at different scales*. Eng. Geol., 112, 29–42.

Catalano S., De Guidi G., Lanzafame G., Monaco C., Torrisi S., Tortorici G., Tortorici L., 2006. *Inversione tettonica positiva Tardo-Quaternaria nel Plateau Ibleo (Sicilia SE)*. Rendiconti della Società Geologica Italiana 2, 118-120 (in Italian).

Ciampalini A., Bardi F., Bianchini S., Frodella W., Del Ventisette C., Moretti S., Casagli N., 2014. *Analysis of building deformation in landslide area using multisensor PSInSAR technique*. International Journal of Applied Earth Observation and Geoinformation, 33, 166-180.

Colesanti C., Ferretti A., Prati C., Rocca F., 2003a. *Monitoring landslides and tectonic motion with the Permanent Scatterers technique*. Eng. Geol., 68, 3–14.

Colesanti, C., Ferretti, A., Locatelli, R., Novali, F., Savio, G. (2003b). Permanent Scatterers: Precision Assessment and Multi-platform Analysis. IGARSS, Toulouse, France. 1-3.

Colesanti C. and Wasowsky J., 2006. *Investigating landslides with space-borne Synthetic Aperture Radar (SAR) interferometry*. Engineering Geology, 88, 173-199.

- Columbia University, 2000. *Global landslide total economic loss risk deciles*. Vol.1. (Available at: <http://sedac.ciesin.columbia.edu/data/set/ndh-landslide-total-economic-loss-risk-deciles>).
- Cooper A. H., 2006. *The classification, recording, databasing, and use of information about building damage caused by subsidence and landslides*. Quarterly Journal of Engineering Geology and Hydrogeology 41, 409-424.
- Cornelius R.R. and Scott P. A., 1993. *Materials failure relation of accelerating creep as empirical description of damage accumulation*. Rock Mechanics And Rock Engineering, 26 (3), 233-252.
- Corrado S., Aldega L., Balestrieri M. L., Maniscalco R., Grasso M., 2009. *Structural evolution of the sedimentary accretionary wedge of the alpine system in Eastern Sicily: Thermal and thermochronological constraints*. Geol. Soc. Am.Bull. 121(11–12), 1475–1490.
- Crosetto M., Monserrat O., Luzi G., Cuevas-González M., Devanthéry N., 2014. *Discontinuous GBSAR deformation monitoring*. ISPRS Journal of Photogrammetry and Remote Sensing 93, 136-141.
- Crosta G.B. and Agliardi F., 2002. *How to obtain alert velocity thresholds for large rockslide/rock avalanches*. Physics and chemistry of the earth, 27 (36), 1557-1565.
- Crosta G.B. and Agliardi F., 2003. *A methodology for physically based rockfall hazard assessment*. Natural Hazards and Earth System Sciences, 3(5): 407-422.
- Cruden D. M., 1991. *A simple definition of a landslide*. Bulletin International Association for Engineering Geology, 43: 27–29.
- Cruden D.M. and Varnes D.J., 1996. *Landslide types and processes*. In, Landslides: Investigation and Mitigation: Sp. Rep. 247 eds. Turner, A.K. & Schuster, R.L., Transportation Research Board, National research Council, National Academy Press, Washington, DC, 36–75.
- D.R.P.C. - Dipartimento Regionale Protezione Civile – 2010. *La frana di san Fratello (ME) del 14 febbraio 2010*. Relazione geologica e rapporto di sintesi sulle indagini geognostiche (Palermo, 2010). (In Italian).
- Del Ventisette C., Intrieri E., Luzi G., Casagli N., Fanti R., Leva D., 2011. *Using ground based radar interferometry during emergency: the case of the A3 motorway (Calabria Region, Italy) threatened by a landslide*. Natural Hazard Heart System Sciences, 11, 2483-2011.
- Del Ventisette C., Casagli N., Fortuny-Guasch J., Tarchi D., 2012a. *Ruinon landslide (Valfurva, Italy) activity in relation to rainfall by means of GBInSAR monitoring*. Landslides, 9 (4), 497-509.
- Del Ventisette C., Garfagnoli F., Ciampalini A., Battistini A., Gigli G., Moretti S., Casagli N., 2012b. *An integrated approach to the study of catastrophic debris-flows: geological hazard and human influence*. Natural Hazards and Earth System Science, 12, 2907-2922.

Derron M. H., Blikra L.H., Jaboyedoff M., 2005. *High resolution digital elevation model analysis for landslide hazard assessment (Åkerneset, Norway)*. In: Senneset, K., Flaate, K. & Larsen, J.O. (eds.). *Landslide and Avalanches ICFL 2005 Norway*. Taylor & Francis Group, London.

Di Biagio E. and Kjekstad O., 2007. *Early Warning, Instrumentation and Monitoring Landslides*. 2nd Regional Training Course, RECLAIM II, 29th January-3rd February 2007.

Di Traglia F., Del Ventisette C., Rosi M., Mugnai F., Intrieri E., Moretti S., Casagli N., 2012. *Understanding conduit dynamics and forecasting major strombolian explosions by ground-based radar interferometry*. EGU General Assembly Conference Abstracts, 2012.

Di Traglia F., Del Ventisette C., Mugnai F., Intrieri E., Rosi M., Moretti S., Casagli N., 2013. *Ground Based InSAR reveals conduit pressurization pulses at Stromboli volcano*. *Terra Nova*, 25, 192-198.

Dieterich J.H., 1978. *Time dependent friction and mechanics of stick-slip*. *Pageoph*. 116, no. 4–5, 790–806.

Dieterich J. H., 1979. *Modeling rock friction. Experimental results and constitutive equations*. *J. Geophys. Res.* 84, 2161–2168.

Durville J.-L., Bonnard C., Pothérat P., 2011. *The Séchilienne (France) landslide: a non-typical progressive failure implying major risks*. *Journal of Mountain Science*, 8 (2), 117-123.

Dvigalo V.N. and Melekestsev I.V., 2009. *The geological and geomorphic impact of catastrophic landslides in the Geyser Valley of Kamchatka: Aerial photogrammetry*. *Journal of Volcanology and Seismology*, 3 (5), 314-325.

Eberhardt E., 2008. *Twenty-ninth Canadian Geotechnical Colloquium: The role of advanced numerical methods and geotechnical field measurements in understanding complex deep-seated rock slope failure mechanisms*. *Canadian Geotechnical Journal*, 45(4), 484-510.

Eidsvig U. and Harbitz C., 2005. *Innledende numeriske analyser som følge av mulige skred fra Åkneset (Preliminary numerical analyses of tsunamis generated by a slide at Åknes)*. Tech. Rep. 20031100-2. Norwegian Geotechnical Institute (NGI), Oslo, Norway, 100p. (In Norwegian).

Faranda P., 2010. *Città-giardino: il piano di Acquadolci. Storia e urbanistica di una città fondata in era fascista (1922–1932)*. Qanat, Palermo, Italy. (In Italian).

Farina, P., Colombo, D., Fumagalli, A., Gontier, E., Moretti, S., 2003. *Integration of permanent scatterers analysis and high resolution optical images within landslide risk analysis*. In *FRINGE*, Frascati, Italy, 1–8.

Farina, P., Colombo, D., Fumagalli, A., Marks, F., Moretti, S., 2006. *Permanent Scatterers for landslide investigations: outcomes from the ESA-SLAM project*. *Engineering Geology*. 88:200–217.

- Farina, P., Leoni, L., Babboni, F., Coppi, F., Mayer, L., & Ricci, P., 2011. *IBIS-M, an innovative radar for monitoring slopes in open-pit mines*. In Slope stability 2011: international symposium on rock slope stability in open pit mining and civil engineering, Vancouver (pp. 18-21).
- Fell R., Corominas J., Bonnard C., Cascini L., Leroi E., Savage W., 2008. *Guidelines for landslide susceptibility, hazard and risk zoning for land use planning*. Eng. Geol., 102, 85–98.
- Feltus W. R., 1993. *Victorious East failure at Ora Banda - a case study*. Geotechnical Instrumentation and Monitoring in Open Pit and Underground Mining, 21-23 June 1993, ed. Szwedzicki T., Rotterdam, Balkema, pp. 155-159.
- Ferretti, A., Prati, C., Rocca, F., 2000. *Non linear subsidence rate estimation using Permanent Scatterers in differential SAR interferometry*. IEEE Transactions on Geoscience and Remote Sensing. 38 (5), 2202–2212.
- Ferretti A., Prati C., Rocca F., 2001. *Permanent scatterers in SAR interferometry*. IEEE Trans. Geosci. Remote Sens., 39 (1), 8 –20.
- Ferretti A., Fumagalli A., Novali F., Prati C., Rocca F., Rucci A., 2011. *A new Algorithm for Processing Interferometric Data-Stacks: SqueeSAR*. IEEE Transaction on Geoscience and Remote Sensing, 49(9), 3460-3470.
- Franceschetti G. and Lanari R., 1999. *Synthetic Aperture Radar processing*. CRC Press, 9-17.
- Frei C.H., Loew S., Leuenberger-West F., 2008. *First results of a large-scale multi-tracer test within an unstable rockslide area (Åknes, Norway)*. Geophysical Research Abstracts 10 EGU2008-A-08930, s. Ref-ID: 1607-7962/gra/EGU2008-A-08930.
- Froese C. R., Carter G., Langenberg W., Moreno F., 2006. *Emergency response planning for a second catastrophic rock slide at Turtle Mountain, Alberta*. First Specialty Conference on Disaster Mitigation, Calgary, Alberta, Canada, 23-26 May 2006, pp. 1-10.
- Fukuzono T., 1985a. *A new method for predicting the failure time of a slope failure*. Proceedings of the 4th International Conference and Field Workshop on Landslides, Tokyo (Japan), pp. 145-150.
- Fukuzono T., 1985b. *A method to predict the time of slope failure caused by rainfall using the inverse number of velocity of surface displacement*. Journal of Japanese Landslide Society, n. 22, pp. 8-13.
- Fukuzono T., 1990. *Recent studies on time prediction of slope failure*. Landslide News, n. 4, pp. 9-12.
- Gabriel A.K., Goldstein R.M., Zebker H.A., 1989. *Mapping small elevation changes over large areas*. Differential interferometry Journal of Geophysical Research, 94, pp. 9183–9191.

- Galli M., Ardizzone F., Cardinali M., Guzzetti F., Reichenbach P., 2008. *Comparing landslide inventory maps*. *Geomorphology*, 94(3), 268-289.
- Ganerød G. V., Grøneng G., Rønning J. S., Dalsegg E., Elvebakk H., Tønnesen J. F., Kvelde V., Eiken T., Blikra L. H., Braathen A., 2008. *Geological model of the Åknes rockslide, western Norway*. *Engineering Geology*, 102(1-2), 1-18.
- Geotechnical Engineering Office (1998). *Guide to Slope Maintenance (Geoguide 5)*. Geotechnical Engineering Office, Hong Kong, 91 p. (Second edition).
- Gigli G., Fanti R., Canuti P., Casagli N., 2011. *Integration of advanced monitoring and numerical modeling techniques for the complete risk scenario analysis of rockslides: The case of Mt. Beni (Florence, Italy)*. *Eng. Geol.*, 120, 48-59.
- Giunta G., Nigro F., Renda P., Giorgianni A., 2000. *The Sicilian-Maghrebides Tyrrhenian Margin: a neotectonic evolutionary model*. *Italian Journal of Geosciences* 119, 553-565.
- Goldstein R., Zebker H., Werner C., 1988. *Satellite radar interferometry: Two-dimensional phase unwrapping*. *Radio Science*, 23, pp. 713-720.
- Gorsevski P., Jankowski P., Gessler P., 2006. *An heuristic approach for mapping landslide hazard by integrating fuzzy logic with analytic hierarchy process*. *Control and cybernetics*, 35 (1), 122-144.
- Goswami R., Mitchell N. C., Brocklehurst S. H., 2011. *Distribution and causes of landslides in the eastern Peloritani of NE Sicily and western Aspromonte of SW Calabria, Italy*. *Geomorphology* 132, 111-122.
- Graham L.C., 1974. *Synthetic Interferometer Radar for Topographic Mapping*. *Proceedings of the IEEE*, 62 (6), 763.
- Guzzetti F. and Cardinali M., 1989. *Carta Inventario dei Fenomeni Franosi della Regione dell'Umbria ed aree limitrofe*. CNR Gruppo Nazionale per la Difesa dalle Catastrofi Idrogeologiche Publication n. 204, 2 sheets, scale 1:100,000, (in Italian).
- Guzzetti F., 2000. *Landslide fatalities and evaluation of landslide risk in Italy*. *Engineering Geology*. 58,89-107.
- Guzzetti, 2006. *Dissertation on Landslide Hazard and Risk Assessment*. PhD thesis.
- Guzzetti F., Mondini A. C., Cardinali M., Fiorucci M., Santangelo M., Chang K.T., 2012. *Landslide inventory maps: new tools for an old problem*. *Earth Science Reviews*. 112, 1-25.
- Herrera G., Fernández-Merodo J.A., Mulas J., Pastor M., Luzi G., Monserrat O., 2009. *A landslide forecasting model using ground based SAR data: The Portalet case study*. *Engineering Geology*, 105, 220-230.

- Herrera G., Gutiérrez F., García-Davalillo J. C., Guerrero J., Notti D., Galve J.P., Fernández-Merodo J.A., Cooksley G., 2013. *Multi-sensor advanced DInSAR monitoring of very slow landslides: The Tena Valley case study (Central Spanish Pyrenees)*. *Remote Sensing of Environment*, 128, 31-43.
- Holzner J. and Bamler R., 2002. *Burst-mode and ScanSAR interferometry*. *IEEE Transaction on Geoscience and Remote Sensing*. 40(9), 1917–1934.
- Hooper A., Zebker H.A., Segall P., Kampes B., 2004. *A new method for measuring deformation on volcanoes and other natural terrains using InSAR persistent scatterers*. *Geophysical Research Letters*. 31.
- Hungr O. and Kent A., 1995. *Coal mine waste dump failure in British Columbia, Canada*. *Landslide News*, n. 9, pp. 26-28.
- Iannini L., Guarnieri A.M., 2011. *Atmospheric phase screen in ground-based radar: statistics and compensation*. *IEEE Geosci. Remote Sens. Lett.* 8 (3), 537-541.
- Iglesias R., Fabregas X., Aguasca A., Mallorqui J.J., Lopez-Martinez C., Gili J.A., Corominas J., 2013. *Atmospheric phase screen compensation in ground-based SAR with a multiple-regression model over mountainous regions*. *IEEE Trans. Geosci. Remote Sens.* 99, 1–14.
- IGOS, 2004. *IGOS Geohazards theme report: for the monitoring of our environment from space and from earth*. European Space Agency Publication, p. 55.
- Intrieri E., Gigli G., Mugnai F., Fanti R., Casagli N., 2012. *Design and implementation of a landslide early warning system*. *Engineering Geology* 147-148: 124-136.
- Intrieri E., Gigli G., Casagli N., Nadim F., 2013. *Landslide early warning system: toolbox and general concepts*. *Nat. Hazard Earth Sys.* 13: 85–90.
- IPCC, 2012. *A Special Report of Working Groups I and II of the Intergovernmental Panel on Climate Change (IPCC). Glossary of Terms*. In: *Managing the Risks of Extreme Events and Disasters to Advance Climate Change Adaptation* (eds.), Cambridge University Press, Cambridge, p. 555-564. Used in the IPCC Fourth Assessment Report: Annex 1 Glossary. Intergovernmental Panel on Climate Change. (Available at: http://www.ipcc.ch/pdf/special-reports/srex/SREX-Annex_Glossary.pdf [accessed 18 March 2014]).
- ISSMGE, 2004. *ISSMGE TC32 - Technical Committee on Risk Assessment and Management Glossary of Risk Assessment Terms*. Version 1, July 2004.
- ISO, 2009. International Organization for Standardization - *Guideline 73:2009(E/F) Risk Management – Vocabulary*. Available at: <http://www.iso.org/iso/home/standards/iso31000.htm>
- Jakob M. and Lambert S., 2009. *Climate change effects on landslides along the south-west coast of British Columbia*. *Geomorphology*. 107, 275-284.

Jørstad F., 1968. *Waves generated by landslides in Norwegian fjords and lakes*. Norwegian Geotechnical Institute. Publication No. 79.

Kennedy B. A. and Niermeyer K. E., 1970. *Slope monitoring systems used in the prediction of a major slope failure at Chuquicamata Mine, Chile*. Proceedings of Planning Open Pit Mines, Johannesburg, 29th August-4th September 1970. Ed. Van Rensburg P. W. J., A. A. Balkema, Cape Town, pp. 215-225.

Kristensen L., Rivolta C., Dehls J., Clikra L.H., 2013. *Gb-InSAR measurement at the Åknes rockslide, Norway*. International Conference Vajont 1963-2013. Thoughts and analyses after 50 years since the catastrophic landslide Padua, Italy - 8-10 October 2013.

Kunlong Y., Lixia C., Guirong Z., 2007. *Regional Landslide Hazard Warning and Risk Assessment*. Earth Science Frontiers, 14(6), 85–97.

Kveldsvik V., Eiken T., Ganerød G.V., Grøneng G., Ragvin N., 2006. *Evaluation of movement data and ground conditions for the Åknes rock slide*. Stability of Rock Slopes in Open Pit Mining and Civil Engineering Situations, Cape Town. The SouthAfrican Institute of Mining and Metallurgy, pp. 279 –300.

L.225/92. Legge della Repubblica Italiana, 24 febbraio 1992, n.225. *Istituzione del servizio nazionale della protezione civile*. (In Italian).

Lacasse S. and Nadim F., 2009. *Landslide risk assessment and mitigation strategy*. Eds. Sassa K., Canuti P., Landslides - Disaster Risk Reduction: Springer - Verlag Berlin Heidelberg, pp. 31-61.

Lagomarsino D., Segoni, R. Fanti, F. Catani, 2012. *Updating and tuning a regional-scale landslide early warning system*. Landslides, 10, 91–97. doi: 10.1007/s10346-012-0376-y.

Lavecchia G., Ferrarini F., De Nardis R., Visini F., Barbano M. S., 2007. *Active thrusting as possible seismogenic source in Sicily (Southern Italy): Some insights from integrated structural kinematic and seismological data*. Tectonophysics 445, 145-167.

Lentini F., Catalano S., Carbone S., 2000. *Carta Geologica della provincia di Messina scala 1:50.000*. S.EL.CA., Firenze, (in Italian).

Leonard G., Johnston D., Paton D., Christianson A., Becker J., Keys H., 2008. *Developing effective warning systems: Ongoing research at Ruapehu volcano, New Zealand*. Journal of Volcanology and Geothermal Research, 172 (3-4): 199-215.

Leva D., Nico G., Tarchi D., Fortuny-Guasch J., Sieber A.J., 2003. *Temporal analysis of a landslide by means of a ground-based SAR interferometer*. IEEE Transactions on Geoscience and Remote Sensing, 41 (4), 745-752.

Lillesand T.M. and Kiefer R.W., 1979. *Remote sensing and image interpretation*. Sec. Ed., John Wiley and Sons, Inc.: Toronto.

- LiSALab, 2010. *Guida alla valutazione e all'impiego della tecnologia GB-InSAR LiSALab nel monitoraggio dei dissesti idrogeologici*. Manuale d'uso. Available at: www.lisalab.com (in Italian).
- Longva O., Blikra L.H., Dehls J.F., 2009. *Rock avalanches — distribution and frequencies in the inner part of Storfjorden, Møre og Romsdal County, Norway*. Tech. Rep.2009:002. Geological Survey of Norway (NGU).
- Lu P., 2010. *Remote Sensing: applications for landslide hazard assessment and risk management*. PhD thesis, University of Firenze.
- Luzi G., Pieraccini M., Mecatti D., Noferini L., Guidi G., Moia F., Atzeni C., 2004. *Ground-based radar interferometry for landslides monitoring: Atmospheric and instrumental decorrelation sources on experimental data*. IEEE Transactions on Geoscience and Remote Sensing. 42(11), 2454-2466.
- Luzi G., 2010. *Ground based SAR interferometry: a novel tool for geoscience*. P. Imperatore, D. Riccio (Eds.), Geoscience and Remote Sensing. New Achievements, InTech, pp. 1–26. (Available at: <http://www.intechopen.com/articles/show/title/ground-based-sar-interferometry-a-novel-toolfor-geoscience>).
- Luzi G., Monserrat O., Crosetto M., Copons R., Altimir J., 2010. *Ground-Based SAR interferometry applied to landslide monitoring in mountainous areas*. Proceedings of the Mountain Risks conference, 24-26 November 2010a, Florence, Italy.
- Magliulo P., Di Lisio A., Russo F., Zelano A., 2008. *Geomorphology and landslide susceptibility assessment using GIS and bivariate statistics: a case study in southern Italy*. Earth and Environmental Science, vol. 47, n. 3, pp. 411-435.
- Mantovani F., Soeters R., Van Westen C.J., 1996. *Remote sensing techniques for landslide studies and hazard zonation in Europe*. Geomorphology, 15, 213–225.
- Massonet D. and Rabaute T., 1993. Radar interferometry: limits and potential. IEEE Transaction on Geoscience and Remote Sensing. 31, 455-464.
- Massonnet D. and Feigl K.L., 1995. *Discrimination of geophysical phenomena in satellite radar interferograms*. Geophysical Research Letters, 22.
- Massonnet D. and Feigl K.L., 1998. Radar interferometry and its application to changes in the Earth's surface. Reviews of Geophysics. 36.
- Max Geldens Stichting, 2002. *“Als je leven je lief is!”*. Available online at: http://www.maxgeldens.nl/publicaties/alsjelevenjeliefis_voorwoord.htm. (In Dutch).
- Medina-Cetina Z. and Nadim F., 2008. *Stochastic design of an early warning system*. Georisk: Assessment and Management of Risk for Engineered Systems and Geohazards, 2 (4), 223-236.

Meisina C., Notti D., Zucca F., Ceriani M., Colombo A., Poggi F., Roccati A., Zaccone A., 2013. *The use of PSInSARTM and SqueeSARTM techniques for updating landslide inventories*. In *Landslide Science and Practice, Proc. of The Second World Landslide Forum, Volume 1: Landslide Inventory and Susceptibility and Hazard Zoning* (eds. Margottini C., Canuti C., Sassa K.) (Roma, Italy), pp. 81–88.

Meta A., Mittermayer J., Prats P., Scheiber R., Steinbrecher U., 2010. *TOPS imaging with TerraSAR-X: Mode design and performance analysis*. *IEEE Transaction on Geoscience and Remote Sensing*, 40(2), 759–769.

Metternicht G., Hurni L., Gogu R., 2005. *Remote sensing of landslides: An analysis of the potential contribution to geo-spatial systems for hazard assessment in mountainous environments*. *Remote Sens. Environ.*, 98, 284–303.

Mileti D.S. and Sorensen J.H., 1990. *Communication of Emergency Public Warnings: A social science perspective and state-of-the-art assessment*. Oak Ridge Laboratory ORNL-6609.

Mitchell J.K., Campanella R.G., Singh A., 1968. *Soil creep as a rate process*. *Journal of the Soil Mechanics and Foundations Division, ASCE Journal SMFD* vol. 94, 231–253.

Mondini A. C., Guzzetti F., Reichenbach P., Rossi M., Cardinali M., Ardizzone F., 2011. *Semiautomatic recognition and mapping of rainfall induced shallow landslides using optical satellite images*. *Remote Sensing of Environment* 115, 1743-1757.

Monserrat O., Crosetto M., Luzi G., 2014. *A review of ground-based SAR interferometry for deformation measurement*. *ISPRS Journal of Photogrammetry and Remote Sensing* 93, 40-48.

Monti Guarnieri A. and Prati C., 1996. *ScanSAR focusing and interferometry*. *IEEE Transaction on Geoscience and Remote Sensing*. 34(4), 1029–1038.

Monti Guarnieri A. and Rocca F., 1999. *Combination of low- and high resolution SAR images for differential interferometry*. *IEEE Transaction on Geoscience Remote Sensing*. 37, 2035–2049.

Moreira A., Mittermayer J., Scheiber R., 1996. *Extended chirp scaling algorithm for air- and spaceborne SAR data processing in stripmap and ScanSAR imaging modes*. *IEEE Transaction on Geoscience Remote Sensing*. 34(5) 1123–1136.

Mufundirwa A., Fujii Y., Kodama J., 2010. *A new practical method for prediction of geomechanical failure-time*. *International Journal of Rock Mechanics & Mining Sciences*, 47 (7), 1079-1090.

Nadim F. and Intrieri E., 2011. *Early warning systems for landslides: challenges and new monitoring technologies*. Keynote lecture, 5th Canadian Conference on Geotechnique and Natural Hazards. Kelowna, BC, Canada. 15-17 May 2011, pp. 1-15.

- Nadim F., Kjekstad O., Peduzzi P., Herold C., Jaedicke C., 2006. *Global landslide and avalanche hotspots*. *Landslides*. 3(2),159-173.
- Nitti D.O., Rana F., Bovenga F., Nutricato R., Tragni M., Chiaradia M.T., Ober G., Candela L., 2009. *Analisi del sisma del 6 Aprile 2009 in Abruzzo con le tecniche di interferometria SAR differenziale*. Atti 13^a conferenza nazionale ASITA - Bari 1-4 dicembre 2009, (in Italian).
- NOAA (National Oceanic and Atmospheric Administration Coastal Services Center) 2012. *Lidar 101: An Introduction to Lidar Technology, Data, and Applications*. Revised. Charleston, SC: NOAA Coastal Services Center.
- Noon D. and Harries N., 2007. *Slope stability radar for managing rock fall risks in open cut mines*. In: Proc. Large Open Pit Mining Conference Perth, Australia, 10–11 September 2007.
- Noferini L., Pieraccini M., Mecatti D., Luzi G., Atzeni C., Tamburini, Broccolato M., 2005. *Permanent scatterers analysis for atmospheric correction in ground-based SAR interferometry*. *IEEE Transactions on Geoscience and Remote Sensing*, 43 (7), 1459-1471.
- Noferini L., Takayama T., Mecatti D., Macaluso G., Luzi G., Atzeni C., 2008. *Analysis of ground-based SAR data with diverse temporal baselines*. *IEEE Trans. Geosci. Remote Sens.* 46 (6), 1614-1623.
- Nordvik T. and Nyrnes E., 2009. *Statistical analysis of surface displacements - an example from the Åknes rockslide, western Norway*. *Nat. Hazards Earth Syst. Sci* 9, 713–724.
- NORUT, 2013. *SBAS and PS InSAR Processing of Åknes rockslide using RADARSAT-2 (2008–2013) and TerraSAR-X/TanDEM-X (2010–2012) satellite data*. Authors: Rouyet L., Lauknes T.R., Dehls J., Report 04/2013.
- PAI, Hydrogeological Setting Plan databases, 2010. *PAI - Piano Stralcio di Bacino per l'Assetto Idrogeologico*. AdB Regione Sicilia (Available at: <http://www.sitr.regione.sicilia.it/pai>).
- Pardeshi S.D., Autade S.E., Pardeshi S.S., 2013. *Landslide hazard assessment: recent trends and techniques*. Springer Plus 2, 523.
- Pino P., Cotone S., Quattrocchi S., 2010. *Carta geomorfologica della frana di San Fratello*. Dipartimento Regionale della Protezione Civile Regione Siciliana.
- Raspini, 2012. *Use of radar interferometric techniques for monitoring hydro-geological instability events*. PhD thesis, University of Firenze.
- Raspini F., Moretti S., Casagli N., 2013. *Landslide Mapping Using SqueeSAR Data: Giampilieri (Italy) Case Study*. In *Landslide Science and Practice, Proc. of The Second World Landslide Forum, Volume 1: Landslide Inventory and Susceptibility and Hazard Zoning* (eds. Margottini, C., Canuti, C., Sassa, K.)(Roma, Italy 2013) pp. 147–154.

Raucoules D., Bourguine B., Michele M., Le Gozannet G., Closset L., Bremmer C., Veldkamp H., Tragheim D., Bateson L., Crosetto M., Agudo M., Engdahl M., 2009. *Validation and intercomparison of persistent scatterers interferometry: PSIC4 project results*. Journal of Applied Geophysics, 68 (3), 335–347.

Righini G., Pancioli V., Casagli N., 2012. *Updating landslide inventory maps using Persistent Scatterer Interferometry (PSI)*. International Journal of Remote Sensing, 33, 2068-2096.

Rose N. D. and Hungr O., 2007. *Forecasting potential rock slope failure in open pit mines using the inverse velocity method*. International Journal of Rock Mechanics and Mining Science, 44 (2), 308-320.

Rosen P.A., Hensley S., Joughin I.R., Li F.K., Madsen S.N., Rodriguez E., Goldstein R.M., 2000. *Synthetic aperture radar interferometry*. Proceeding of IEEE. 88 (3).

SafeLand, 2011. *Deliverable 4.8: Guidelines for landslide monitoring and early warning systems in Europe: design and required technology*. December 2011.

Saito M., 1965. *Forecasting the time of occurrence of slope failure*. Proceeding of 6th International Conference on Soil Mechanics and Foundation Engineering, Montreal, vol. 2, pp. 537-541.

Saito M., 1969. *Forecasting time of slope failure by tertiary creep*. Proceedings of the 7th International Conference on Soil Mechanics and Foundation Engineering, Mexico City, vol. 2, pp. 677-683.

Salvati P., Bianchi C., Rossi M., Guzzetti F., 2010. *Societal landslide and flood risk in Italy*. Natural Hazards and Earth System Sciences. 10, 465–483.

Sammartino P.F., Tarchi D., Oliveri F., 2010. *GB-SAR and MIMO radars: alternative ways of forming a synthetic aperture*. Proceeding of the International Conference on Synthetic Aperture Sonar and Synthetic Aperture Radar 2010 - ISBN:9781617389573 vol. 1 p. 174-180. Publisher: Curran Associates, Inc.

Sammartino P.F., Basso M., Broussolle J., Kyovtorov V., Giuliani R., Figueiredo Morgado J., Oliveri F., Tarchi D., Ferraro G., Castiglione G., 2014. *MELISSA, a new class of ground based InSAR system. An example of application in support to the Costa Concordia emergency*. ISPRS Journal of Photogrammetry and Remote Sensing, 91, 50-58.

Sassa K., 1989. *Geotechnical classification of landslides*. Landslides News, Japan Landslide Society 3, 21-24

Schuster R.L. and Fleming R.W., 1986. *Economic losses and fatalities due to landslides*. Bulletin of American Association of Engineering Geology. 23, 11–28.

- Somma R., Messina A., Mazzoli S., 2005. *Syn-orogenic extension in the Peloritani Alpine Thrust Belt (NE Sicily, Italy): Evidence from the Ali unit*. *Comptes Rendues Geoscience* 337, 861-871.
- Sousa J. J., Hooper A. J., Hanssen R. F., Bastos L. C., Ruiz A. M., 2011. *Persistent Scatterer InSAR: a comparison of methodologies based on a model of temporal deformation vs. spatial correlation selection criteria*. *Remote Sensing of Environment*, 115, 2652–2663.
- Sousa J. J., Ruiz A.M., Hanssen R. F., Bastos L., Gil A. J., Galindo-Zaldívar J., Sanz de Galdeano C., 2010. *PS-InSAR processing methodologies in the detection of field surface deformation. Study of the Granada basin (Central Betic Cordilleras, Southern Spain)*. *Journal of Geodynamics*, 49 (3–4), 181–189.
- Strozzi T., Werner C., Wiesmann A., Wegmuller U. *Topography Mapping With a Portable Real-Aperture Radar Interferometer*. *IEEE Geosci. Remote Sens. Lett.*,9(2):277-281, March 2012.
- Suwa H., 1991. *Visually observed failure of a rock slope in Japan*. *Landslide News*, n. 5, pp. 8-10.
- Tapete D., Fanti R., Cecchi R., Petrangeli P., Casagli N., 2012. *Satellite radar interferometry for monitoring and early stage warning of structural instability in archaeological sites*. *J. Geophys. Eng.* 9, S10–S25.
- Tarchi D., Ohlmer E., Sieber A.J., 1997. *Monitoring of structural changes by radar interferometry*. *Res. Nondestruct. Eval.*, 9, 213– 225.
- Tarchi D., Rudolf H., Luzi G., Chiarantini L., Copp P., Sieber A. J., 1999. *SAR interferometry for structural change detection: a demonstration test on a dam*. *Proceedings of Geoscience and Remote Sensing Symposium, IGARSS 1999*, 3, 1525-1527.
- Tarchi D., Casagli N., Canuti P., Moretti S., Leva D., Sieber A.J., 2002. *Monitoring landslide displacements using ground-based differential SAR interferometry: application to the Ruinon landslide in the Italian Alps*. *Journal Geophysical Research (U.O. 2.14)*.
- Tarchi D., Casagli N., Fanti R., Leva D., Luzi G., Pasuto A., Pieraccini M., Silvano S., 2003. *Landslide monitoring by using ground-based SAR interferometry: an example of application to the Tessina landslide in Italy*, *Eng. Geol.*, vol. 1, no. 68, pp. 15-30.
- Tarchi, D., Oliveri, F., Sammartino, P.F., 2012. *MIMO Radar and Ground-Based SAR Imaging Systems: Equivalent Approaches for Remote Sensing*. *IEEE Commun. Mag.* DOI 10.1109/TGRS.2012.2199120.
- Tveten, E., Lutro O., Thorsnes T. , 1988. *Bergrunnskart Alesund*. 1:250000. Geological map. In Norwegian.
- UNISDR (United Nations International Strategy For Disaster Reduction), 2005. *Hyogo Framework for Action 2005-2015: Building the resilience of nations and communities to*

disasters HFA. International Strategy for Disaster Reduction, 28 pp. (Available at: <http://www.unisdr.org/eng/hfa/hfa.htm>).

UNISDR (United Nations International Strategy For Disaster Reduction), 2006a. *Global Survey of Early Warning Systems*. Geneva, Switzerland, 56 pp. (Available at: <http://www.unisdr.org/2006/ppew/info-resources/ewc3/Global-Survey-of-Early-Warning-Systems.pdf>).

UNISDR (United Nations International Strategy For Disaster Reduction), 2006b. *The International Early Warning Programme - The four elements of effective early warning systems - Brochure*. Platform for the Promotion of Early Warning (PPEW), 4 pp. (Available at: <http://www.unisdr.org/2006/ppew/iewp/IEWP-brochure.pdf>).

UNISDR (United Nations International Strategy for Disaster Reduction), 2009. *Terminology on Disaster Risk Reduction*. 13 pp. (Available at: http://unisdr.org/files/7817_UNISDRTerminologyEnglish.pdf).

Varnes D. J., 1978. *Slope movement types and processes*. In R. L. Schuster and R. J. Krizek, editors, *Landslides: Analysis and Control*, pages 11-33. Transportation Research Board, 1978. 1, 81

Villagran de León J.C. and Bogardi J., 2006. *Early Warning Systems in the context of Disaster Risk Management*. In: *Entwicklung & Ländlicher Raum* 2: 23-25.

Voight B., 1988. *A method for prediction of volcanic eruption*. *Nature*, vol. 332, n. 10, March 1988, pp. 125-130.

Voight B., 1989a. *A relation to describe rate-dependent material failure*. *Science*, vol. 243, n. 4888, January 1999, pp. 200-203.

Voight B., 1989b. *Materials science law applies to time forecasts of slope failure*. *Landslide News*, vol. 3, pp. 8-11.

Wang, F. Ghosh, A. Sankaran, C. Fleming, P. Hsieh, F., Benes S. J., 2008. *Mobile WiMAX systems: performance and evolution*. *IEEE Commun. Mag.*, 46, no. 10, pp. 41-49.

Wang W. Q., 2011. *Space-time coding MIMO-OFDM SAR for high-resolution imaging*. *IEEE Trans Geosci Remote Sens*, , 49: 3094-3104.

Werner C., Strozzi T., Wesmann A., Wegmuller U., 2008. *Gamma's portable radar interferometer*. 13th FIG Symposium on Deformation Measurements and analysis, LNEC, Lisbon May 12-16 2008.

Zebker, H. A. and Goldstein, R. M., 1986. *Topographic Mapping From Interferometric Synthetic Aperture Radar Observations*. *Journal of Geophysical Research*. (91), 4993-4999.

Zebker, H.A. and Villasenor, J., 1992. *Decorrelation in interferometric radar echoes*. IEEE Transaction on Geoscience Remote Sensing, 30 (5).

Zebker H.A., Rosen P.A, Hensley S.,1997. *Atmospheric effects in interferometric synthetic aperture radar surface deformation and topographic maps*. Journal of Geophysical Research, 102(B4): 7547–7563.

Zvelebill J., 1984. *Time prediction of a rockfall from a sandstone rock slope*. Proceedings of the 4th International Symposium on Landslides, Toronto. University of Toronto Press, Toronto, Ontario, 16-21 September 1984, vol. 3, pp. 93-95.

Zvelebill J. and Moser M., 2001. *Monitoring based time-prediction of rock falls: Three case-histories*. Physics and Chemistry of the Earth, Part B: Hydrology, Oceans and Atmosphere, 26 (2), 159-167.

<http://eijournal.com>

<http://nhm2.uio.no/norlex/past/download.html>

<http://norut.no/>

<http://rsgb.org/>

<http://treuropa.com/it/technique/insar-evolution/>

<http://www.aknes.no/>

<http://www.cosmo-skymed.it/docs/ASI-CSM-ENG-RS-093-A-CSKSysDescriptionAndUserGuide.pdf>

<http://www.nasa.gov/>

<http://www.nrcan.gc.ca/>

<http://www.ntns.it/>

<http://www.protezionecivile.gov.it/>

<http://www.r-project.org/>

<http://www.unisdr.org/we/inform/terminology>

www.gamma-rs.ch

www.idscorporation.com/

www.lisalab.com

8. Publications

Published:

- **Bardi F.**, Frodella W., Ciampalini A., Bianchini S., Del Ventisette C., Gigli G., Fanti R., Moretti S., Basile G., Casagli N., 2014. *Integration between ground based and satellite SAR data in landslide mapping: The San Fratello case study*. *Geomorphology*, 223, 45-60.
- Bianchini S., Ciampalini A., Raspini F., **Bardi F.**, Di Traglia F., Moretti S., Casagli N., 2014. *Multi-Temporal Evaluation of Landslide Movements and Impacts on Buildings in San Fratello (Italy) By Means of C-Band and X-Band PSI Data*. *Pure Appl. Geophys.*
- Ciampalini A., **Bardi F.**, Bianchini S., Frodella W., Del Ventisette C., Moretti S., Casagli N., 2014. *Analysis of building deformation in landslide area using multisensor PSInSAR technique*. *International Journal of Applied Earth Observation and Geoinformation*, 33, 166-180.
- Di Traglia F., Intrieri E., Nolesini T., **Bardi F.**, Del Ventisette C., Ferrigno F., Frangioni S., Frodella W., Gigli G., Lotti A., Tacconi C., Tanteri L., Leva C., Casagli N., 2014. *The ground based InSAR monitoring system at Stromboli volcano: linking changes in displacement rate and intensity of persistent volcanic activity*. *Bullettin of Volcanology*, 76, 786.

Accepted by Journals:

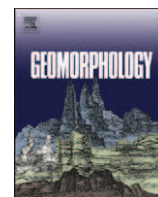
- Ciampalini A., Raspini F., Bianchini S., Frodella W., **Bardi F.**, Lagomarsino D., Di Traglia F., Moretti S., Proietti C., Pagliara O., Corazza A., Duro A., Basile G. *Remote sensing as tool for development of landslide databases: The case of the Messina Province (Italy) geodatabase*. (Accepted for publication by *Geomorphology*).

In preparation:

- Raspini F., Ciampalini A., Bianchini S., **Bardi F.**, Di Traglia F., Moretti S. *Updated landslide inventory map of the area between the Furiano and Rosmarino creeks*. (Submitted to *Journal of Maps*).
- **Bardi F.**, Kristenses C., Blikra L., Kveldsvik V., Casagli N. *Semi-quantitative integration between ground based and satellite SAR data applied on the Åknes rockslide test site*. (In preparation).
- Frodella W., **Bardi F.**, Morelli S., Gigli G., Lombardi L., Nocentini M., Raspini F., Casagli N. *The Tizzano Val Parma landslide: aerial mapping and GB-InSAR monitoring*. (In preparation).
- Versace P., Artese G., Autiero M., **Bardi F.**, Borgia A., Cancelliere A., Capparelli G., Casagli N., Cavallaro L., Di Massa G., Fidolini F., Intrieri E., Muto F., Viggiani G., ... *An integrated System for Landslide Monitoring, Early Warning and Risk Mitigation along Lifelines*. *Proc. Of Mediterranean meeting on Monitoring, modeling, early warning of extreme events triggered by heavy rainfall*. (In preparation).

Annexes

- **Bardi F.**, Frodella W., Ciampalini A., Bianchini S., Del Ventisette C., Gigli G., Fanti R., Moretti S., Basile G., Casagli N., 2014. *Integration between ground based and satellite SAR data in landslide mapping: The San Fratello case study*. *Geomorphology*, 223, 45-60 (Annex 1).
- Bianchini S., Ciampalini A., Raspini F., **Bardi F.**, Di Traglia F., Moretti S., Casagli N., 2014. *Multi-Temporal Evaluation of Landslide Movements and Impacts on Buildings in San Fratello (Italy) By Means of C-Band and X-Band PSI Data*. *Pure Appl. Geophys* (Annex 2).
- Ciampalini A., **Bardi F.**, Bianchini S., Frodella W., Del Ventisette C., Moretti S., Casagli N., 2014. *Analysis of building deformation in landslide area using multisensor PSInSAR technique*. *International Journal of Applied Earth Observation and Geoinformation*, 33, 166-180 (Annex 3).
- Di Traglia F., Intrieri E., Nolesini T., **Bardi F.**, Del Ventisette C., Ferrigno F., Frangioni S., Frodella W., Gigli G., Lotti A., Tacconi C., Tanteri L., Leva C., Casagli N., 2014. *The ground based InSAR monitoring system at Stromboli volcano: linking changes in displacement rate and intensity of persistent volcanic activity*. *Bullettin of Volcanology*, 76, 786 (Annex 4).
- Judgements concerning the PhD thesis manuscript as a requirement for awarding the “Doctor Europaeus” Certificate.



Integration between ground based and satellite SAR data in landslide mapping: The San Fratello case study



Federica Bardi ^{a,*}, William Frodella ^a, Andrea Ciampalini ^a, Silvia Bianchini ^a, Chiara Del Ventisette ^a, Giovanni Gigli ^a, Riccardo Fanti ^a, Sandro Moretti ^a, Giuseppe Basile ^b, Nicola Casagli ^a

^a Earth Science Department, Università di Firenze, via La Pira 4, Firenze 50121, Italy

^b Dipartimento Regionale della Protezione Civile, Regione Siciliana, Servizio Rischi Idrogeologici e Ambientali, via Abela 5, Palermo 90141, Italy

ARTICLE INFO

Article history:

Received 5 February 2014

Received in revised form 12 June 2014

Accepted 13 June 2014

Available online 6 July 2014

Keywords:

Satellite interferometry

Ground-based radar

PSI

Landslide mapping

Ground deformation

SAR data integration

ABSTRACT

The potential use of the integration of PSI (Persistent Scatterer Interferometry) and GB-InSAR (Ground-based Synthetic Aperture Radar Interferometry) for landslide hazard mitigation was evaluated for mapping and monitoring activities of the San Fratello landslide (Sicily, Italy). Intense and exceptional rainfall events are the main factors that triggered several slope movements in the study area, which is susceptible to landslides, because of its steep slopes and silty-clayey sedimentary cover.

In the last three centuries, the town of San Fratello was affected by three large landslides, developed in different periods: the oldest one occurred in 1754, damaging the northeastern sector of the town; in 1922 a large landslide completely destroyed a wide area in the western hillside of the town. In this paper, the attention is focussed on the most recent landslide that occurred on 14 February 2010: in this case, the phenomenon produced the failure of a large sector of the eastern hillside, causing severe damages to buildings and infrastructures. In particular, several slow-moving rotational and translational slides occurred in the area, making it suitable to monitor ground instability through different InSAR techniques.

PS-InSAR™ (permanent scatterers SAR interferometry) techniques, using ERS-1/ERS-2, ENVISAT, RADARSAT-1, and COSMO-SkyMed SAR images, were applied to analyze ground displacements during pre- and post-event phases. Moreover, during the post-event phase in March 2010, a GB-InSAR system, able to acquire data continuously every 14 min, was installed collecting ground displacement maps for a period of about three years, until March 2013. Through the integration of space-borne and ground-based data sets, ground deformation velocity maps were obtained, providing a more accurate delimitation of the February 2010 landslide boundary, with respect to the carried out traditional geomorphological field survey. The integration of GB-InSAR and PSI techniques proved to be very effective in landslide mapping in the San Fratello test site, representing a valid scientific support for local authorities and decision makers during the post-emergency management.

© 2014 The Authors. Published by Elsevier B.V. This is an open access article under the CC BY-NC-ND license (<http://creativecommons.org/licenses/by-nc-nd/3.0/>).

1. Introduction

Landslide mapping in the field is often a quite complex task; this can be owing to (i) the size of the landslide, often too large to be completely observed in the field; (ii) the viewpoint of the investigator, often inadequate to see all parts of a landslide (e.g., the scarp, lateral edges, deposit, toe) with the same detail; or (iii) the fact that old landslides are often partially or totally covered by vegetation or have been partly dismantled by other landslides, erosion processes, and human actions, including agricultural and forest practices (Guzzetti et al., 2012). The reduced visibility of the slope failure makes it difficult to accurately follow a landslide

boundary in the field: this is a consequence of the local perspective of the size of the landslide and of the fact that the landslide boundary is often indistinct.

Thus, the perspective offered by a distant view of the landslide is preferable and can result in more accurate and more complete landslide mapping (Guzzetti et al., 2012).

In this paper, an improvement of the 2010 San Fratello landslide map was performed through the use of radar interferometry, specifically integrating the Persistent Scatterer Interferometry (PSI) with the Ground-based Synthetic Aperture Radar Interferometry (GB-InSAR).

The PSI is a well-known powerful and advanced multitemporal interferometric SAR technique, which allows measuring centimetric and subcentimetric ground displacements occurring during a defined range of time with millimeter accuracy (Ferretti et al., 2001). This work fully exploits both the satellite systems operating in the microwave C-band (i.e., ERS 1/2, ENVISAT, and RADARSAT-1 interferometric archives) and

* Corresponding author at: via La Pira 4, Firenze 50121, Italy. Tel.: +39 055 2757777; fax: +39 055 2757788.

E-mail address: federica.bardi@unifi.it (F. Bardi).

new generation SAR data acquired in X-band by the recent space missions, such as COSMO-SkyMed. The analysis of the benefits introduced by the aforementioned new satellite missions, in terms of technical performances and improvements in applications, was here investigated.

The GB-InSAR is a powerful terrestrial technique, widely used in engineering and in geological applications to detect the target (structure and ground) displacements (Casagli et al., 2002; Tarchi et al., 2003a; Noferini et al., 2007; Casagli et al., 2009; Herrera et al., 2009; Casagli et al., 2010; Del Ventisette et al., 2011). A GB-InSAR is a ground-based system that works with the same principles as space-borne sensors for monitoring ground deformation phenomena.

The interferometric technique is based on a comparison between two SAR images acquired at different times; this permits evidence of eventual displacements occurring during the time span between the two acquisitions. The time necessary to the sensor to realize two subsequent acquisitions is connected to the range of displacement velocities that the instrument can recognize. Therefore, satellite data are useful in monitoring extremely or very slow movements, whereas the GB-InSAR devices allow the assessment of ground deformations of faster landslides, thanks to the possibility of realizing higher frequency measurements (Corsini et al., 2006; Noferini et al., 2008). In addition, the spatial coverage of satellite data is limited by the SAR imaging geometry caused by layover, foreshortening and shadowing effects (Ferretti et al., 2001). A GB-InSAR, on the other hand, also can be placed in front of steep slopes, which are in most cases not visible from space-borne platforms.

The PSI and GB-InSAR work at different spatial and temporal scales. Because of the above-mentioned characteristics and differences, the integration of these techniques enables us to obtain useful information on the ground displacement measurements, with high precision and improved spatial and temporal resolution. In particular, the use of PSI allows performing a preliminary study on ground displacements at a basin scale, providing hotspot mapping (which can be useful prior to planning a GB-InSAR system installation for a monitoring campaign) over a specific area affected by landslides.

Between the end of 2009 and the beginning of 2010, the Nebrodi Mountains (western Sicily, Italy) were highly affected by several landslide events causing intense damages and casualties. Some of these landslides are still active at present day. Intense and exceptional rainfall events (about 900 mm in the period between October 2009 and January 2010) were the main factor that, combined with the strong topographical relief, triggered several slope movements. In this work, the PSI and GB-InSAR techniques were qualitatively integrated in order to improve the 2010 landslide map. The satellite data, measured along the satellite Line Of Sight (LOS), were projected on the slope direction, providing the component of the velocity registered by the sensors on the direction of the slope (V_{slope}). The line of sight of the GB-InSAR system is quite similar to the slope direction, so the displacements registered in this direction are comparable to the projected satellite data.

A list of the used satellite data is shown in Table 1 together with the characteristics of the sensors. The GB-InSAR data were recorded during the monitoring campaign, realized between March 2010 and March 2013: in this period the instrument generated interferograms continuously, every 14 min.

The integration was based on a binary approach to divide the areas characterized by displacements from the ones without displacements. The method was validated comparing the results with the evidence of the damage assessment map produced by the Department of Civil Protection (Fig. 5) and on the basis of the results of field trips, which allowed us to detect soil fractures and landslide scarps (Figs. 4C and 5). The integration was used to update the map of the San Fratello landslide.

2. Geomorphological and geological framework

The town of San Fratello is located in northeastern Sicily, Italy (Messina Province, Fig. 1B), on the northwestern hillside of the Nebrodi Mountains (Fig. 1A), a 70-km-long ridge with an ENE–WSW direction, within the southern Apennine chain.

The geomorphology of the study area shows the typical features of the Sicilian Tyrrhenian coastline: steep slopes rise abruptly from the coastal plain and are deeply cut by N–NW-directed creek valleys (called *fiumare*). In this context, the town of San Fratello is located about 5 km south of the seaside, on a divide separating the Furiano Creek valley to the west from the Inganno Creek valley to the east (Fig. 1C).

From a geological point of view, the study area is part of the north-eastern sector of the Apennine–Maghrebic orogenic belt, and it is characterized by the tectonic overriding of the uppermost Kabilian–Calabrid units, consisting of dolomitic limestones and sandstones (Fig. 2A, B), formed in this area mainly by marlstone and claystone formations (Ogniben, 1960; Atzori and Vezzani, 1974; Lentini and Vezzani, 1975; Atzori et al., 1978; Lentini et al., 1990, 1994, 1995; Finetti et al., 1996; Lentini et al., 2000). This geological framework determines the overlapping of geological formations with marked differences in geotechnical properties, deeply influencing the study area landscape and slope instability phenomena: hilltops, made of hard-brittle lithologies, are undermined by the weathering and erosional processes taking place in the underlying soft clayey formations. In the San Fratello area, on the top of the bedrock, a silty–clayey cover lies with an average thickness of about 10 m; the 2010 landslide affected this layer, involving all the thickness or the biggest part of it, with a surface rupture 8–10 m deep (Pino et al., 2010). The low quality of the geotechnical properties of this layer probably played an important role in the landslide trigger, together with the steep slope angle (more than 30°) and the intense precipitation events of the period. In particular, the period between October 2009 and January 2010 recorded more than 900 mm of precipitation (Fig. 3). The area was impacted by other similar phenomena in the past; in 1754, a large landslide damaged the northeastern sector of

Table 1
Characteristics of the satellites used for the PS-InSAR monitoring of the San Fratello landslide.

Satellite	ERS 1/2	ERS 1/2	ENVISAT	ENVISAT	RADARSAT-1	RADARSAT-1	COSMO-SkyMed
Band	C	C	C	C	C	C	X
Geometry	Ascending	Descending	Ascending	Descending	Ascending	Descending	Descending
Repeat time (days)	35	35	35	35	24	24	4
Temporal range	11/09/92–05/06/00	01/05/92–08/01/01	22/01/03–22/09/10	07/07/03–13/09/10	30/12/05–04/09/09	31/01/06–06/10/09	16/05/11–02/05/12
N° scenes	34	70	65	49	46	47	32
PS/km ²	6.55	2.25	64.74	20.41	112.73	86.86	400.62
Spatial accuracy (m)	±4–±10	±4–±10	±4–±10	±4–±10	±4–±8	±4–±8	±3
0 ± dev. stand. (mm/y) (0 ± σ)	0 ± 2.5	0 ± 1.7	0 ± 2.1	0 ± 1.5	0 ± 2.5	0 ± 2.1	0 ± 3.7
LOS vel. range (min, max) (mm/y)	–9.5, +7.2	–26.8, +8.6	–39.3, +10.1	–22.5, +5.9	–46.8, +19.8	–26.3, +20.5	–56.4, +31.8
Mean LOS vel. (mm/y)	–0.5	–0.4	0.0	–0.6	–0.4	0.0	–1.0

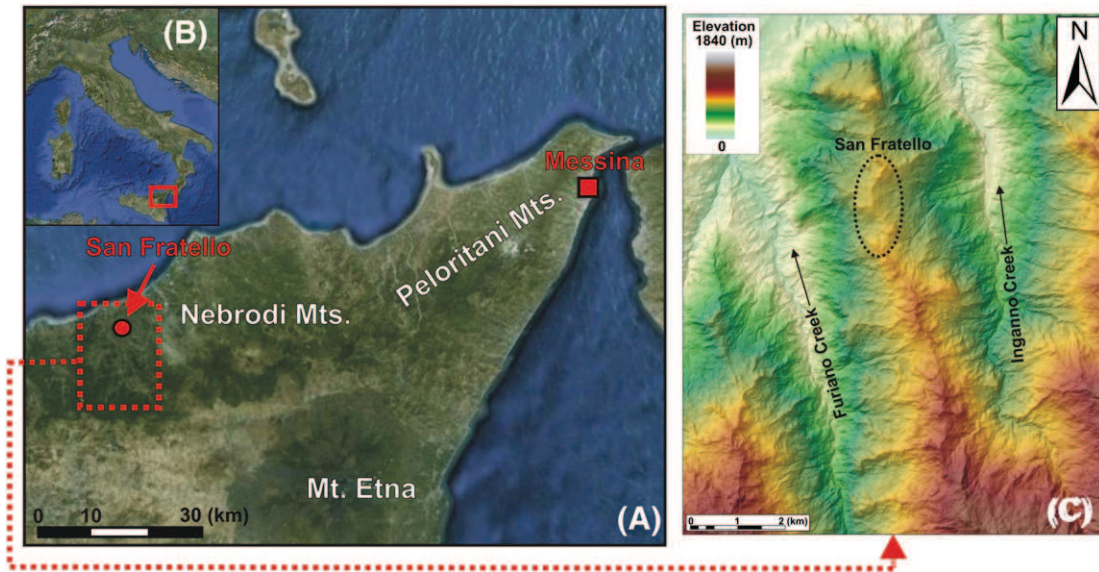


Fig. 1. Geographic framework (A–B) and digital elevation model (C) of the San Fratello area.

the town; in 1922 a wide area in the western hillside of the town was completely destroyed by another landslide (Fig. 4A). In Fig. 4B, the landslide inventory map (PAI, Hydrogeological Setting Plan databases) of the area is shown; it was performed before the 2010 collapse and confirmed the existence of a large, dormant, complex, landslide phenomena as well as several other smaller, active, and shallow-seated mass movements.

The 14 February 2010 landslide (Fig. 4) represents the most recent event, causing the failure of a large sector of the eastern hillside, inducing severe damages to buildings and infrastructures, in particular in the quarters of Stazzone, Riana, Porcaro, and San Benedetto (Bianchini et al., 2014) (Fig. 4C).

In detail, the 2010 landslide, affecting an area of about 1 km², developed from the eastern sector of the town area toward the Inganno Creek valley for a length of about 1.8 km (Fig. 4C). This landslide, mainly involving the silty–clayey overlay, is a complex rotational mass movement that intensively modified the topographic slope surface, producing multiple failures, traction cracks, and counterslopes (Fig. 4C). On this geomorphological map, some kinematic indicators are represented, emphasizing the direction of the flow toward the valley of Inganno Creek (Fig. 4C); the areas characterized by ground and building lacerations were also pointed out, together with the damaged drain pipelines and the hydrographic network that was intensely modified, producing concentrated runoff and several small landslide lakes. The landslide, in its lower sector, evolved in an earth flow, channelizing into a stream bed corresponding to a tributary of the Inganno Creek.

An overview of the building damages and of the fracture pattern is represented in Fig. 5.

In particular, the landslide main scarps, characterized by heights between 5 and 10 m, are located in the middle and upper part of the slope about 500 m east of the town center (Fig. 5D, correspondent to sector 1, Porcaro quarter, in Fig. 4C). In this latter sector, where the ground surface planar translation reached 50 m, severe damages to some isolated buildings and local roads occurred. In the eastern town sector, characterized by a high building density, translational sliding phenomena determined subparallel fracture systems and scarps in the Riana quarter (sector 3 in Fig. 4C), while in correspondence with the Stazzone quarter (sector 2 in Fig. 4C), rotational phenomena induced several extensional and compressive fractures (Fig. 5). In both quarters, several buildings were intensively damaged (e.g., the church and the primary school in the Stazzone quarter in particular, Fig. 5A) or completely destroyed together with the sewer system. The southern town sector (San Benedetto

quarter, sector 4 in Fig. 4C) was affected by translational and rotational phenomena, which induced intense ground laceration and formed scarps up to 5 m high, destroying several buildings (Fig. 5C), water pipes, and roads. The upper part of the town, in correspondence with the divide (sector 5 in Fig. 4C), was also affected by intense ground deformation phenomena (Fig. 5B).

3. Methodology

The InSAR techniques, applied from space-borne and ground-based platforms, have proven to be a powerful tool in the field of ground displacement analysis, thanks to their high spatial and temporal resolution as well as all-weather capability (Massonnet and Feigl, 1998; Singhroy et al., 1998; Crosetto et al., 2011).

Radar techniques are an example of active remote sensing: radar sensors emit a microwave radiation in order to scan objects and areas, recording the reflecting or backscattering radiation of the target. The SAR interferometry techniques are based on the evaluation of the phase difference (interferometric phase) between two or more acquisitions of SAR images, enabling us to detect movements along the Line Of Sight (LOS) (Tarchi et al., 1997; Antonello et al., 2004; Crosetto et al., 2005). In the absence of errors caused by the propagation of the radar signal in the atmosphere, to the pixel scattering, and to the instrumental and geometrical decorrelation, the lag owing to the propagation is proportional only to the distance between the sensor and the target. When a displacement occurs in the elapsing time between two acquisitions, the interferometric phase will vary accordingly. The SAR interferometry uses this effect in order to measure ground deformation (Ferretti et al., 2000). Because of the ambiguous nature of the 2π interferometric phase-wrapping, a quarter of the wavelength represents the maximum displacement that can be recorded between two successive acquisitions; this effect is called *aliasing* and it represents one of the main limitations of the technique applications (e.g., Hanssen, 2005; Crosetto et al., 2010).

3.1. PSI technique

Space-borne InSAR is an effective technique for ground deformation measurements over large areas, ideal for monitoring subvertical displacements of the ground surface characterized by low velocity. The principal limitations of the classical DInSAR (Differential Interferometric SAR) techniques are caused by temporal and geometrical decorrelation

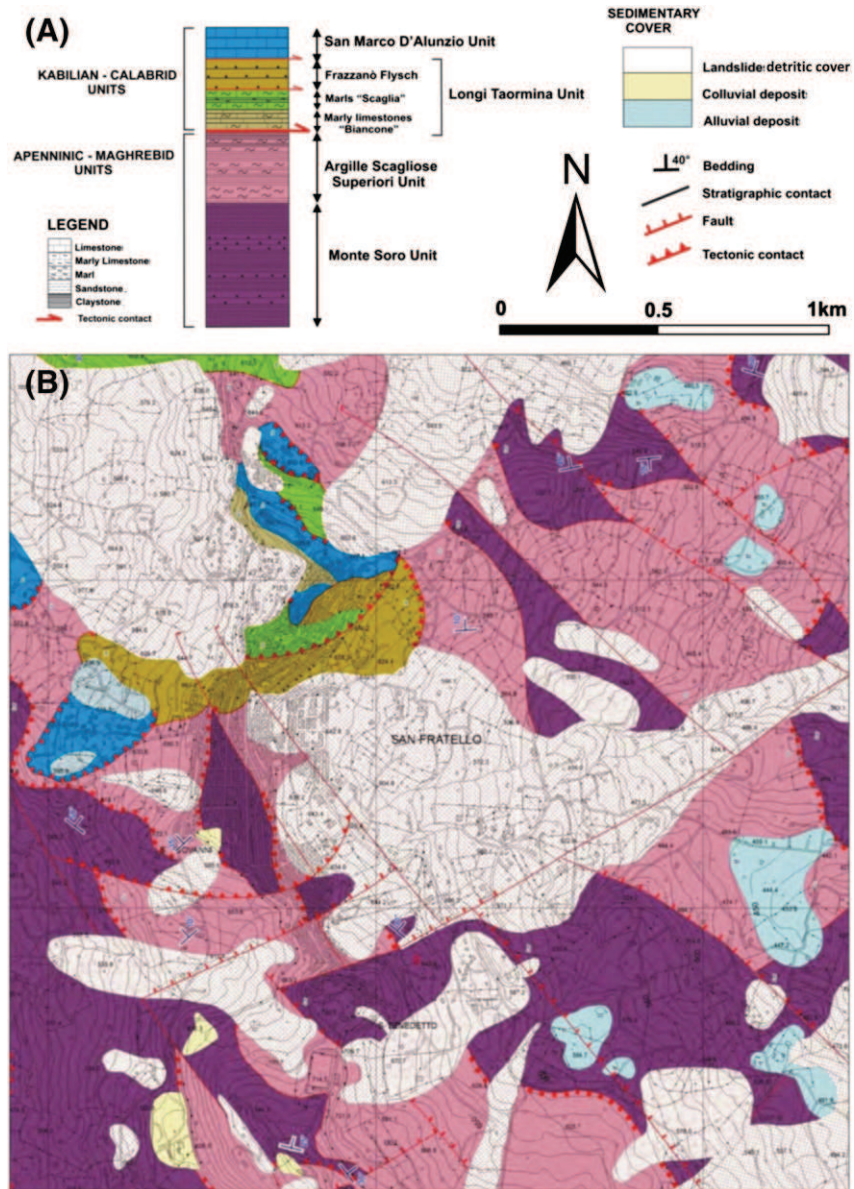


Fig. 2. Tectono-stratigraphic section (A) and geological map (B) of the San Fratello area (modified after Pino et al., 2010).

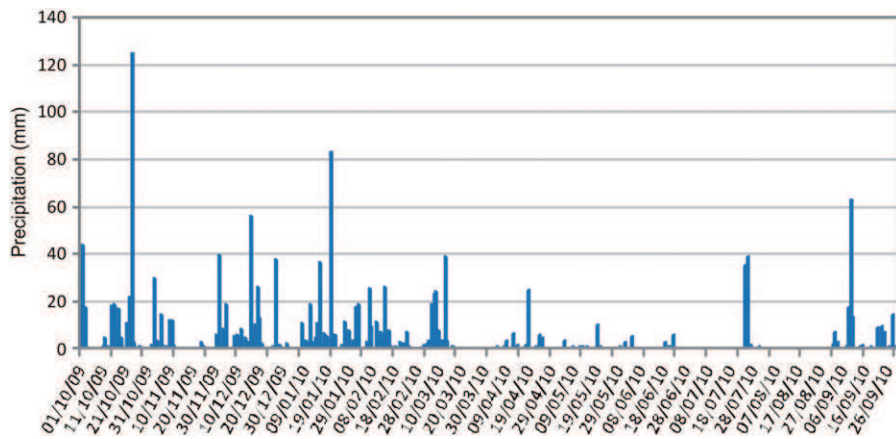


Fig. 3. Daily precipitation value (mm) registered in the San Fratello area between October 2009 and October 2010.

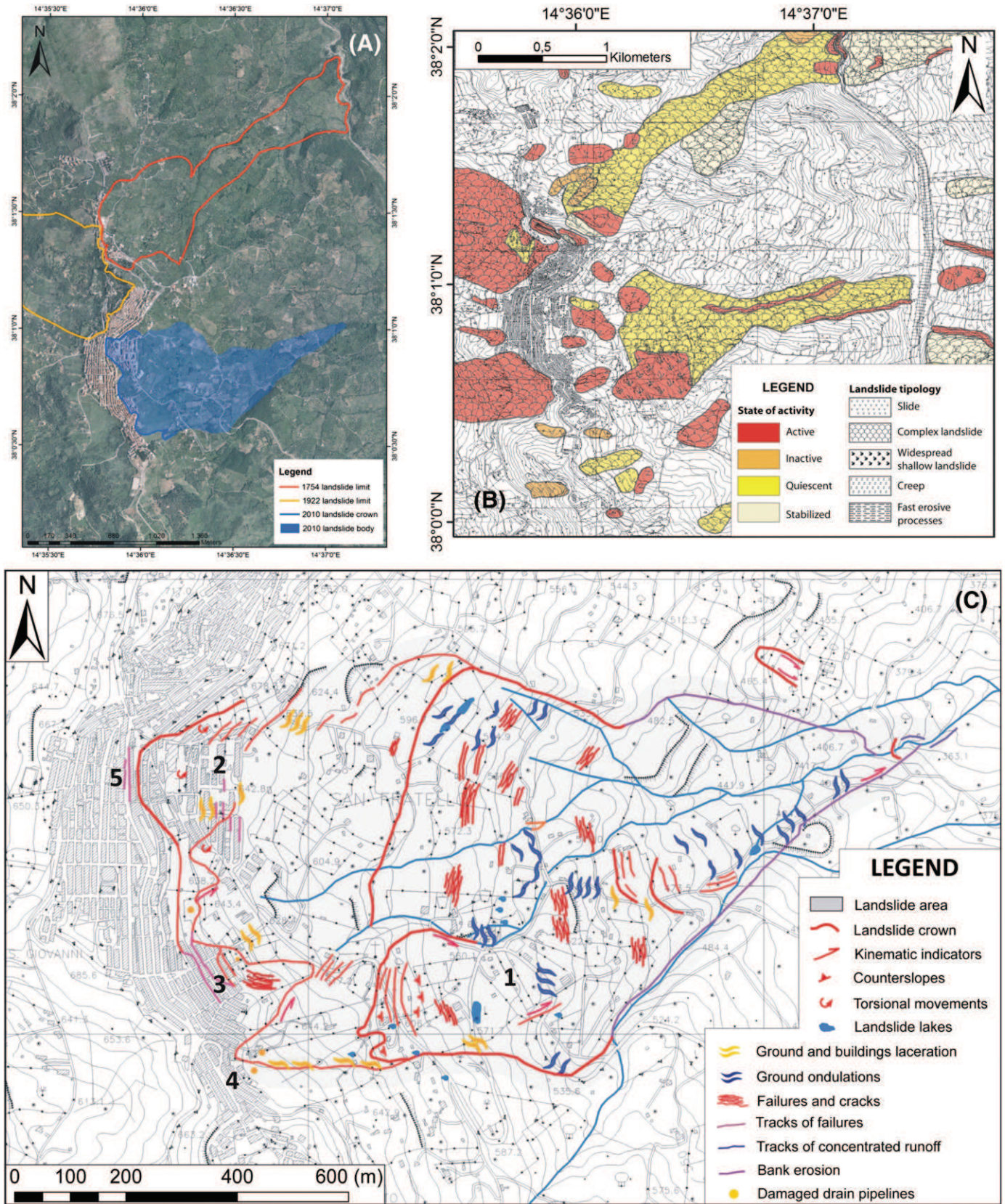


Fig. 4. (A) The three landslides affecting San Fratello: the 1754 landslide in red, the 1922 landslide in yellow and the 2010 landslide in blue. (B) Inventory landslide map of the San Fratello area (PAI, 2010). (C) Geomorphological map of the 2010 landslide (Pino et al., 2010). San Fratello quarters: 1, Porcaro; 2, Stazzone; 3, Riana; 4, S. Benedetto; and 5, Letteri Street.

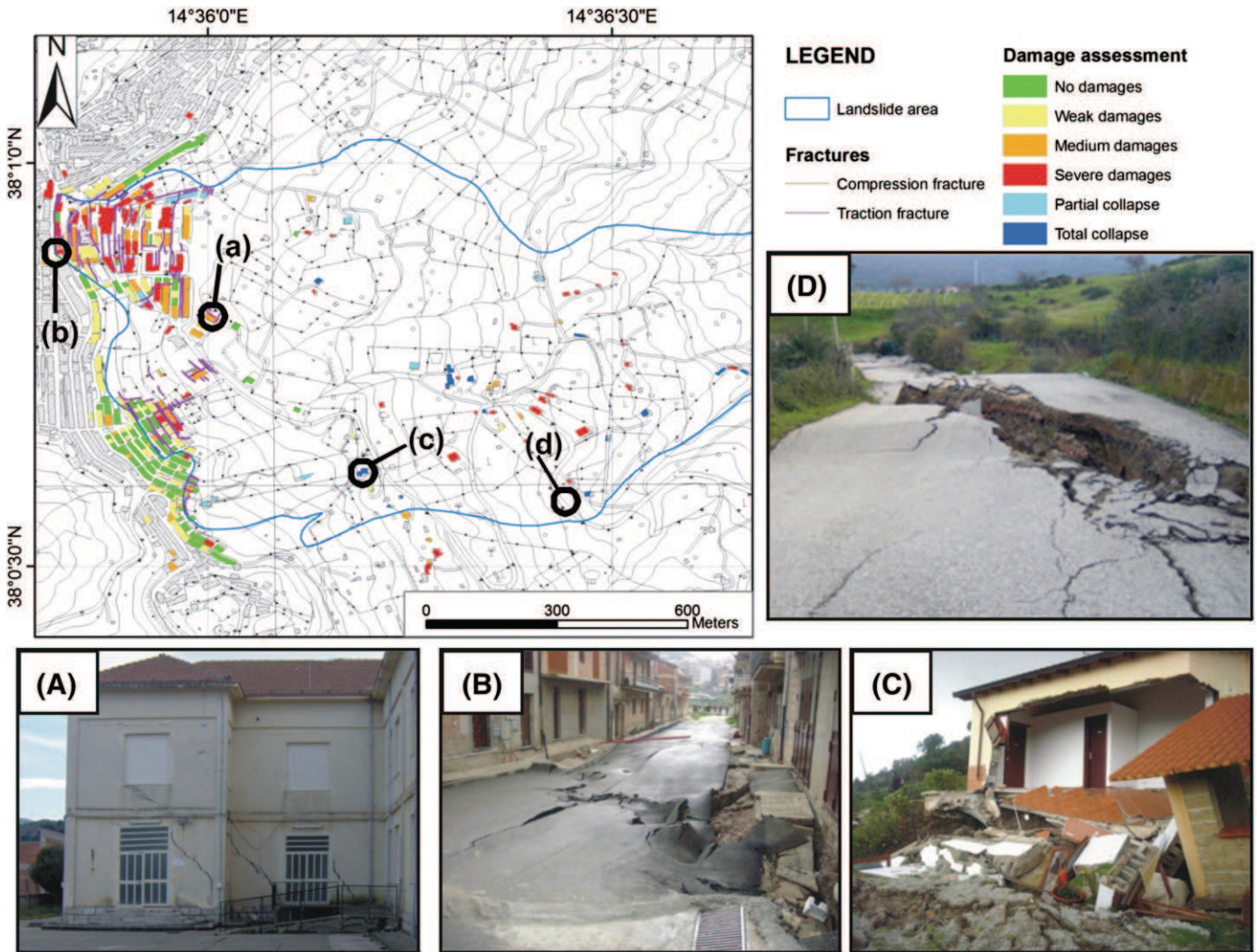


Fig. 5. Building damage and fracture pattern maps (courtesy of the Regional Civil Protection Department, Sicily) and example of ground deformations and damages to buildings and structures in the 2010 landslide area (A, structural damages to the primary school building, Stazzone Quarter; B, damages to the pavement of Latteri Street; C, building failure in San Benedetto quarter; D damages to local road in Porcaro Quarter).

and atmospheric noises (Colesanti et al., 2003). On the contrary, the multi-interferogram approach, such as the PS-InSAR™ technique (Ferretti et al., 2001), obtains a precise ground deformation map on a sparse grid of phase-stable radar targets (the so-called permanent scatterer, PS). The PS targets correspond mainly to man-made (monuments, metallic structures) or natural objects (such as rock outcrops) that are stable and coherent scatterers (Ferretti et al., 2000). Therefore, urbanized zones and cities are characterized by a high PS density; whereas, within vegetated, rural, and forested areas, benchmarks are very few and PSI tends to occasionally fail. Satellites follow near-polar orbits and are rightward side-looking. Thus, in ascending orbit, the LOS of the satellite is oriented toward the east, and it is more useful to detect the displacements that occur in this direction. On the contrary, the descending orbit satellites are more suitable for the observation of west-facing slopes.

The PS-InSAR™ technique is able to identify the PS displacement as the only contribution to the signal phase shift, until the aliasing effect is negligible; this technique permits us to have a long temporal series of SAR data. Multiple differential interferograms obtained from a set of radar scenes, acquired on the same track, provide displacement measurements with high precision. Specifically, the precision on the average LOS deformation rate is about 0.1–1 mm/y; while on the displacement time series a single measure is 1.5 mm/y (Ferretti et al., 2000, 2001,

2005; Hanssen, 2005; Raucoules et al., 2008; Crosetto et al., 2010). Accordingly, this technique has been successfully applied in the field of geology (e.g., subsidence, earthquakes, volcanic activities) for scientific studies and for hazard and risk assessment strategies (Farina et al., 2004; Meisina et al., 2008; Cigna et al., 2011; Pulvirenti et al., 2011; Bianchini et al., 2012; Ciampalini et al., 2012; Cigna et al., 2012; Raspini et al., 2012; Zhao et al., 2012; Del Ventisette et al., 2013; Ciampalini et al., 2014). Within the study area, in order to produce ground deformation velocity maps, the following satellite SAR data were employed: ERS 1/2, ENVISAT (European Space Agency), and RADARSAT-1 (Canadian Space Agency) data, provided by the Italian Civil Protection Department (DPC), and COSMO-SkyMed (Italian Space Agency) data. Satellite SAR frames cover areas up to 100 km², with resolutions of a few meters. The revisiting time of the present satellites over the same area ranges between 4 and 35 days. In Table 1, more information about the revisiting time, the temporal range and the number of available satellite scenes, the PS density, and the spatial accuracy of the SAR data are recorded; statistical data about the records of the satellites are also included in Table 1.

The ERS 1/2, ENVISAT, and RADARSAT-1 data stack in descending and ascending orbits and the COSMO-SkyMed in descending orbit has been processed by Tele-Rilevamento Europa (TRE) using SqueeSAR™, which represents the evolution of the PS-InSAR™ technique (Ferretti

et al., 2001, 2011). For measuring ground displacements, this new advanced multitemporal interferometric technique uses permanent scatterers and the so-called distributed scatterers (DS), which correspond to homogeneous areas spread over a group of pixels in a SAR image (rangeland, pasture, shrubs, and bare soils). The SqueeSAR™ technique increases the density of the point targets that register ground motion with respect to the traditional PS-InSAR™ technique, and it is very useful in the case of sparse vegetation landscapes (Meisina et al., 2013; Raspini et al., 2013; Bellotti et al., 2014). As recorded in Table 1, the ERS 1/2, ENVISAT, and RADARSAT 1 satellites acquired in C-band (COSMO-SkyMed uses the X-band data) that improves the level of detail of the investigation and the PSI capability for landslide mapping and monitoring. Indeed, the X-band satellites produce a new generation of SAR data, characterized by shorter revisiting time and higher spatial and temporal resolution with respect to C-band satellites, that can represent an effective tool for rapid updating of landslide inventory maps and for hazard and risk studies (Crosetto et al., 2010; Bovenga et al., 2012; Frattini et al., 2013). Regarding the aliasing effect, velocities compromising the PSI processing depend on the employed SAR microwave length and on the satellite repeat cycle: they are about 15 cm/y for ERS/ENVISAT data (C band), 21 cm/y for RADARSAT (C-band), and about 70 cm/y for COSMO-SkyMed (X-band).

As the 2010 landslide affected the east-facing slope, the best information about displacement was obtained from data stacks in ascending orbit. On the other hand, the descending orbit acquisition was more useful to identify recent displacements of the historical 1922 landslide, which took place on the west-facing slope. Considering the limitation related to the vegetation cover and in correspondence with the central and lower parts of the 2010 landslide, the highest number of PS was located in correspondence with the San Fratello town area, where the crown of both landslides was located.

3.2. GB-InSAR technique

In recent years, the GB-InSAR has proven to be a reliable and consistent technique for landslide monitoring applications (Luzi et al., 2004; Casagli et al., 2010; Gigli et al., 2011). A GB-InSAR system consists in a computer-controlled microwave transceiver, characterized by a transmitting and receiving antenna that, by moving along a mechanical linear rail, is able to synthesize a linear aperture along the azimuth direction. The transmitting antenna produces step-by-step continuous waves at discrete frequency values, sweeping a specific bandwidth generally in Ku band. A SAR image contains amplitude and phase information of the observed objects backscattered echo within the investigated scenario, and it is obtained by combining the spatial resolution along the direction perpendicular to the rail (range resolution, ΔR_r) and the one parallel to the synthetic aperture (azimuth or cross-range resolution, ΔR_{az}) (Luzi et al., 2010). The working principle of the GB-InSAR

technique is the evaluation of the phase difference, pixel by pixel, between two pairs of averaged sequential SAR complex images, which constitutes an interferogram (Bamler and Hartl, 1998). The latter does not contain topographic information, given the antennas fixed position during different scans (zero baseline condition); therefore, in the time elapsed between the acquisition of two or more subsequent coherent SAR images, it is possible to derive from the obtained interferogram a map of the displacements that occurred along the sensor LOS with a millimeter accuracy in the Ku band (Tarchi et al., 1997, 2000; Pieraccini et al., 2000a,b, 2003). Specifically, using ground-based platforms it is also possible to obtain centimetric spatial resolution with an accuracy of <0.5 mm. According to the specific acquisition geometry, only this component of the real displacement vector can be estimated, whereas the displacements that occurred along a direction perpendicular to the LOS are missed. This is one of the limitations of the GB-InSAR technique. The radar system must be placed in order to make the sensor LOS as parallel as possible to the expected direction of the landslide motion. Nevertheless, the GB-InSAR represents a versatile and flexible technology, allowing rapid changes in the type of data acquisition, such as geometry and temporal sampling, based on the characteristics of the monitored slope failure.

In the post-event phase, in order to monitor the San Fratello 2010 landslide and to assess its residual risk, a GB-InSAR system was set up on the left flank of the Inganno Creek valley in the Sanguinera village area opposite the San Fratello town (Fig. 6). The instrument was installed on 8 March 2010 and it started to acquire data two days later. The employed system is a ground-based SAR, designed and implemented by the Joint Research Centre (JRC) of the European Commission and its spin-off company Ellegi-LiSALab (Tarchi et al., 2003a,b; Antonello et al., 2004; Casagli et al., 2009, 2010; Gigli et al., 2011; Del Ventisette et al., 2012a,b; Tapete et al., 2012; Di Traglia et al., 2013; Intrieri et al., 2013). The radar system was installed at an average distance of 2100 m with respect to the landslide (Fig. 6). The area covered by a GB-InSAR system depends on this distance, which is usually limited to a few hundreds of meters up to a few kilometers, corresponding to a patch-landscape scale. In the specific case of San Fratello, the covered area is about 1 km², like the landslide extension. The accurate displacement maps can be produced only for the upper part of the landslide because the vegetated part is not visible by the GB-InSAR.

The radar parameters used during the measurement campaign are summarized in Table 2. Regarding the aliasing effect, it reduces to 4.4 mm the maximum displacement that can be recognized without ambiguity using the system installed on the test site. Contrary to the satellite systems, the *repeat cycle* of the GB-InSAR instruments is characterized by higher frequency; in the case of San Fratello, the measures were acquired every 14 min: during the monitoring period the displacements never exceeded the threshold of 4.4 mm in 14 min, so the aliasing effect was avoided.

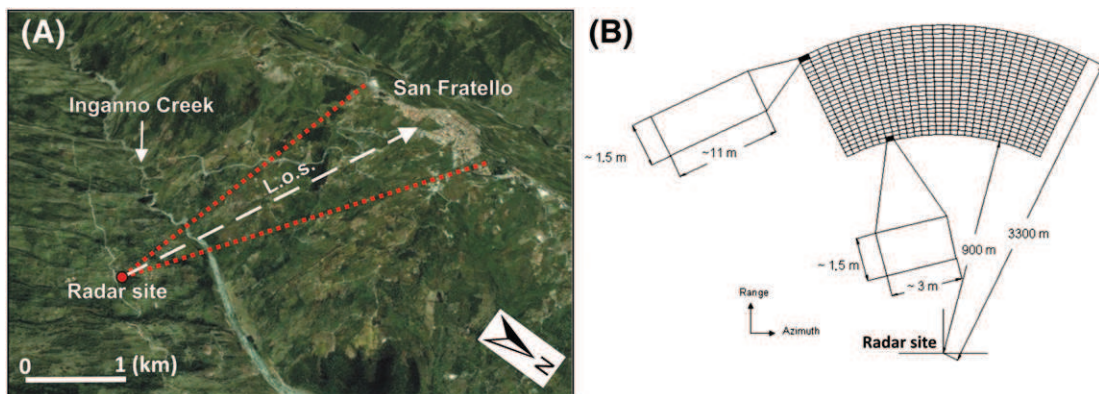


Fig. 6. Location of the San Fratello GB-InSAR system installation (A) and resolution grid size and parameters used during the monitoring campaign (B).

Table 2
GB-InSAR system parameters used to monitor the San Fratello landslide.

Central frequency	Band width	Synthetic aperture	Min. distance	Max. distance	ΔR_r	ΔR_{az} (at 900-m distance)	ΔR_{az} (at 3300-m distance)	Scanning time
17.1 GHz	200 MHz	3.00 m	900 m	3300 m	1.5 m	3 m	11 m	14 min

3.3. Data integration

Regarding the San Fratello 14th February 2010 landslide, the displacements were studied during the pre- and post-event by the integration between space-borne and ground based InSAR techniques. The integration methodology is schematically described in Fig. 7 and consisted of three principal steps: the data collection, the SAR data post-processing, and the pre- and post-event data integration. During the data collection phase, geological and geomorphological field surveys were realized together with the acquisition of ancillary data (i.e., an orthophoto of the study area, landslide inventory map PAI databases, 2010, damage assessment map). Then satellite and ground-based SAR data were collected, covering a period of pre- (ERS 1/2, ENVISAT, RADARSAT-1) and post-event (COSMO-SkyMed and GB-InSAR). During the second step, the SAR data post-processing was performed: in order to increase the comparability of the different data sets, the satellite data were projected along the slope direction, which is quite similar to the GB-InSAR LOS; the procedure used for the projection is the same described in Colesanti and Wasowski (2006) and later in Bianchini et al. (2013) and in Herrera et al. (2013). The downslope projected velocity is called V_{slope} . Ground deformation velocity (V_{slope}) maps were obtained and superimposed on the orthophoto (characterized by a 1-m geometric resolution) and compared with the available landslide delimitation, performed a few days after the event, on the basis of the field evidences (geomorphological surveys and building damage assessment; Figs. 4C and 5).

To classify the PSI data, a stability V_{los} threshold at ± 2 mm/y for C-band data was considered. This threshold is based on several published PSI analyses on landslide studies (e.g., Righini et al., 2012; Herrera et al., 2013).

In the study area, the velocity ranges of PSI data measured by the different satellite systems are comparable for all the PS populations: all the maximum (positive) and minimum (negative) velocity values range within a few tens of millimeters per year. The C-band data show a standard deviation of the velocity of about 2.0. The X-band PSI data have a slightly higher standard deviation (3.7) than C-band. This feature mainly depends on the number and distribution of SAR scenes used for the processing over the temporal acquisition period. Nevertheless, in our case, X-band COSMO-SkyMed data set includes a sufficient number of images (i.e., 32 images) homogeneously distributed over one year acquisition. Considering this characteristic, the same stability threshold value (± 2 mm/y) has been used for C-band and for X-band data in order to make all the used PSI data acquired by different satellite sensors as comparable as possible. Moreover, this value is acceptable as it does not exceed the precision of the PSI technique.

To classify V_{slope} data, the same statistical considerations were taken into account, considering the negative skewness of the V_{slope} PS population. So the V_{slope} positive data that represent outliers in the distribution are negligible, and therefore the V_{slope} stability value is chosen between 0 and -2 mm/y. Statistical data of the PSI data sets are displayed in Table 1.

At the same time, GB-InSAR data were analyzed to obtain displacement maps and time series of 10 stable points, chosen in areas where the radar signal is characterized by high stability, high signal/noise ratio, and high power and coherence parameters.

The third step is defined *data integration* and consisted of the qualitative integration between space-borne V_{slope} maps and ground-based displacement maps; the integration was based on a binary approach to identify the areas characterized by displacements to the ones without evidence of movement, during the pre- and post-event period. The

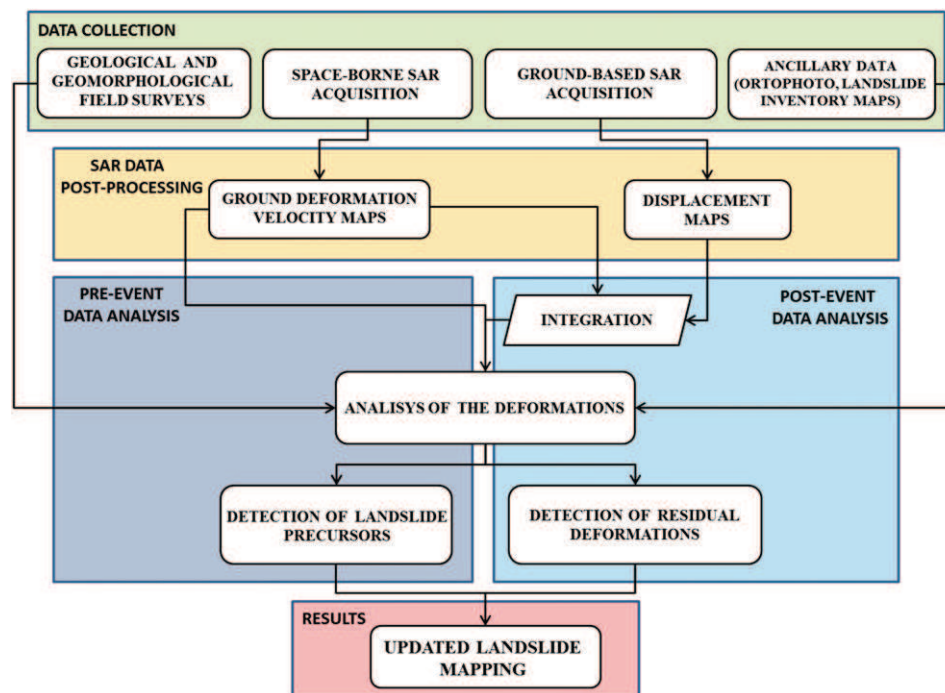


Fig. 7. Flowchart showing the used methodology.

target was to update the landslide limit, to perform a more precise landslide map. The combined use of the space-borne and the ground-based SAR data provided ground displacement measurements with high spatial and temporal accuracy, allowing us to better and more accurately trace the delimitation of the 2010 landslide. Furthermore, the integration of PS- and GB-InSAR approaches allows overcoming their physical limitations. Therefore, in order to compare the results of both techniques, it is possible to study the same area from different points of view and in different temporal intervals.

In order to validate the integration results, the new landslide map resulting from the SAR data integration was qualitatively compared with the field survey results, i.e., the geomorphological map (Fig. 4C), the building damage assessment and the fracture pattern map (Fig. 5).

4. Results

4.1. PSI data

The ground deformation velocity maps were characterized by different PS density and acquisition periods. The ERS 1/2, ENVISAT, and RADARSAT-1 data were acquired during the pre-event phase (1992–2010) with respect to the 2010 landslide and COSMO-SkyMed data were collected during the post-event phase (2011–2012). The PS distribution within the 2010 landslide is not homogeneous; most of the PS are located in correspondence with the buildings of San Fratello, allowing the observation of the ground deformation phenomena along the landslide crown, whereas within the landslide body, the presence of PS is strongly reduced from the absence of reflectors. Each PS is characterized by a V_{los} that can be positive or negative. The first case occurs

when the target approaches the sensor along the LOS; on the contrary, negative values characterize PS moving away from the sensor. Projecting PSI data on the downslope direction, only the negative portion of the displacements is emphasized and -2 mm/y is considered the stability threshold value.

4.1.1. ERS 1/2

In Fig. 8, the ground deformation velocity maps, obtained using ERS 1/2 V_{slope} data (1992–2001), are shown in both acquisition orbits. The PS average density is low (Table 1), but it is sufficient to make some observations about the stability of the town of San Fratello. In Fig. 8, it is possible to note that the crown of the 2010 landslide is basically stable, except an area characterized by displacements between -2 and -5 mm/y , emphasized with a red dashed line in the figure; nevertheless very little information can be retrieved about the landslide body. The areas involved in the crowns of the historical landslides of 1754 and 1922 show a residual activity, with average velocities between -2 and more than -20 mm/y (Fig. 8), as highlighted by the V_{slope} maps acquired in ascending and descending orbits (Fig. 8A and B).

4.1.2. ENVISAT and RADARSAT-1

The ground deformation velocity (V_{slope}) maps obtained through the processing of ENVISAT (2003–2010) and RADARSAT-1 (2005–2009) images, acquired in ascending and descending orbits, are shown in Fig. 9. The data obtained by these two satellites were superimposed on the same map because the temporal range of acquisition of RADARSAT-1 data partially overlaps to that of ENVISAT, therefore their results have proven to be useful for a comparison of the measured ground deformations. These maps proved to be more useful with

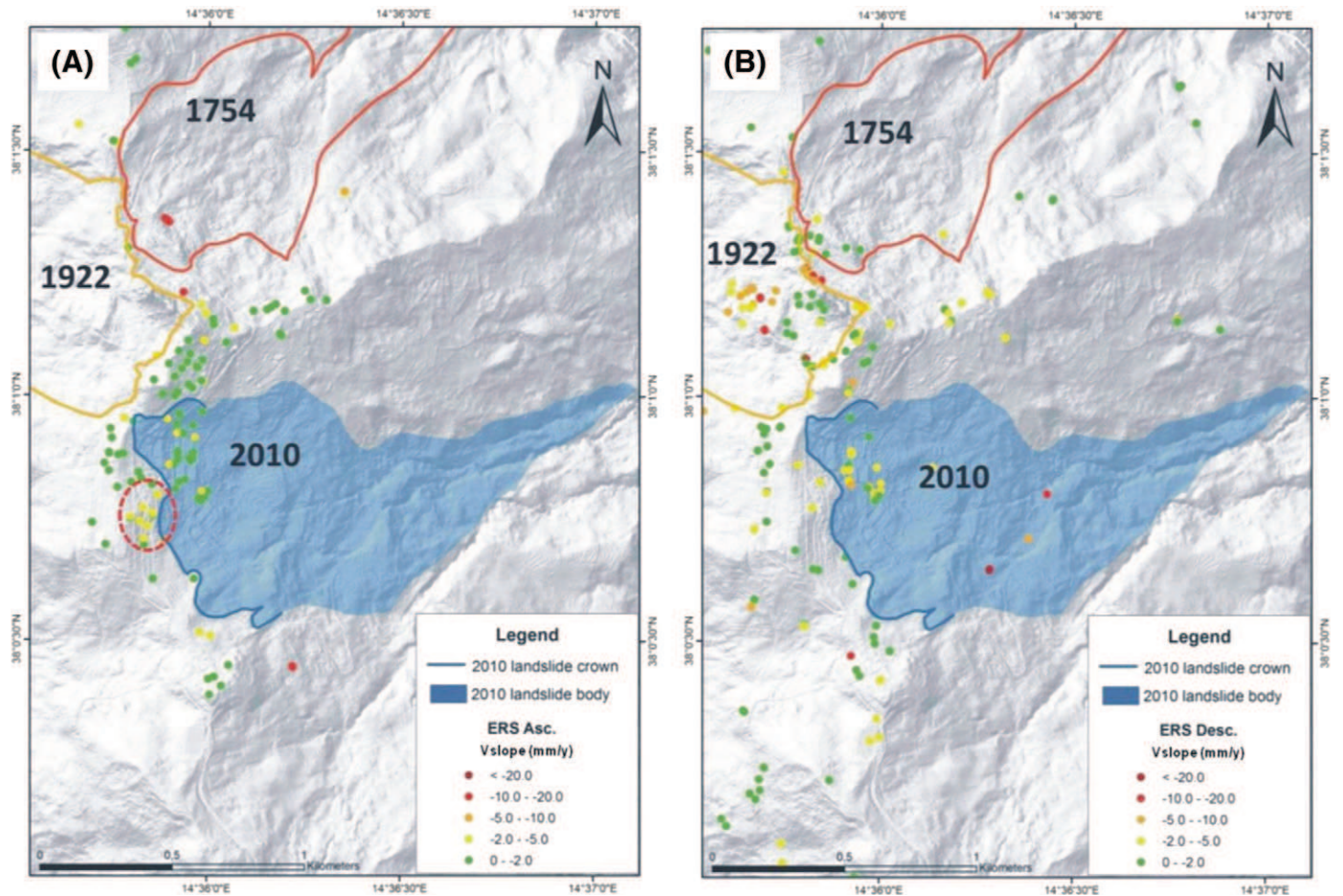


Fig. 8. PS ground deformation velocity maps (V_{slope}), using ERS 1/2, obtained through data acquired in ascending (A) and descending (B) orbits. The areas characterized by higher displacements are emphasized with a red dashed line.

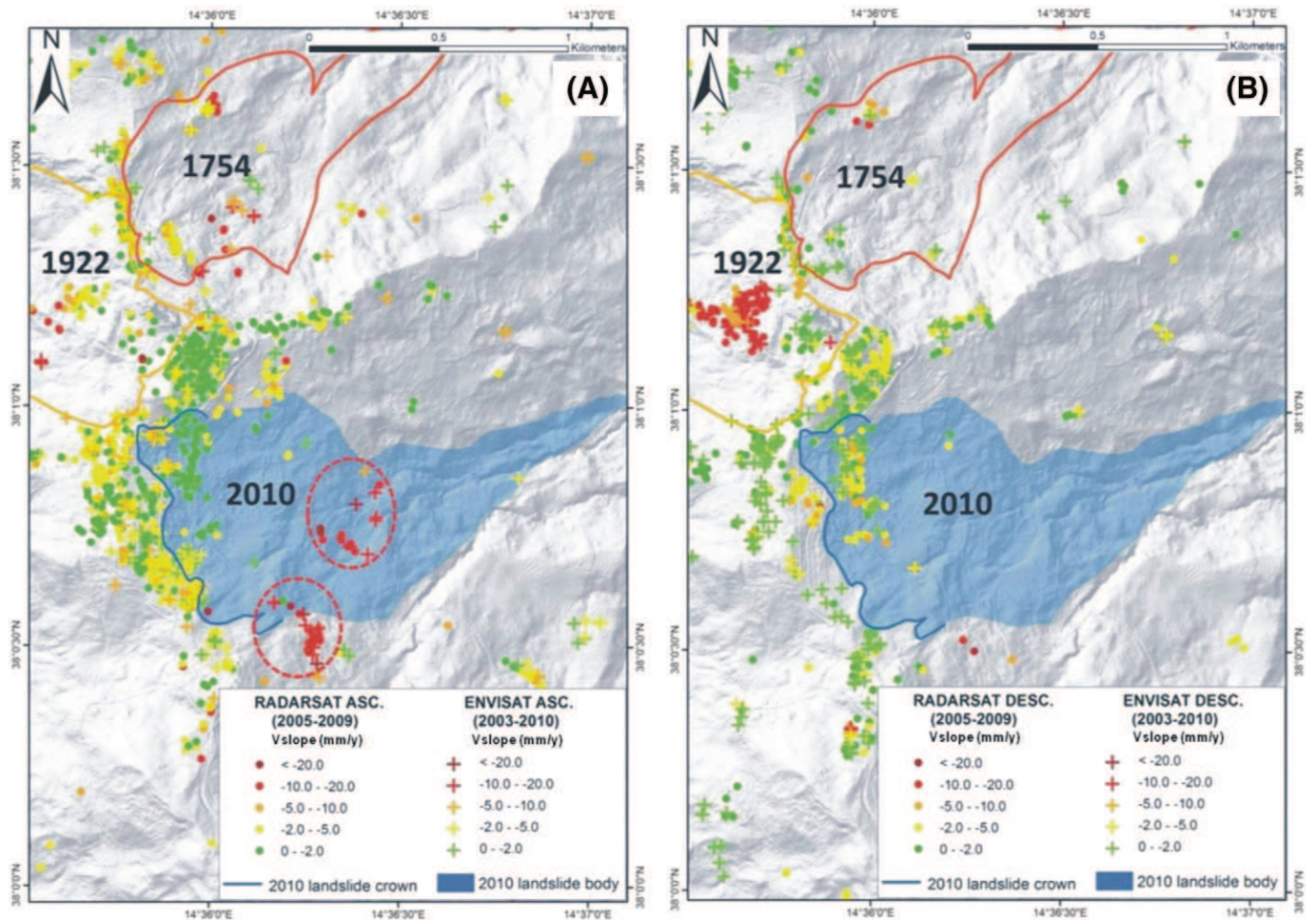


Fig. 9. PS ground deformation velocity maps (V_{slope}), using ENVISAT and RADARSAT-1, obtained through data acquired in ascending (A) and descending (B) orbits. The ENVISAT PSs are shown as crosses, and the RADARSAT are shown as circles. The areas characterized by higher displacements are emphasized with red dashed lines.

respect to those obtained by ERS 1/2 because of their higher PS density (Table 1). In particular, the map obtained using the ascending orbit (Fig. 9A) is characterized by a good density of targets, also within the 2010 landslide body, allowing a better understanding of the pre-event ground deformations affecting the east-facing slope.

The ENVISAT data, indicated with crosses in Fig. 9, show the presence of relevant displacements on the east-facing slope since 2003, more evident in ascending orbit (Fig. 9A) data stacks, where they are characterized by velocities between -5 and more than -20 mm/y (Fig. 9A). Considering the 2010 landslide body, most of the unstable PSs are placed outside the landslide boundary. Data acquired in descending orbit clearly show displacements located on the west-facing slope in the area affected by the 1922 landslide crown (Fig. 9B). Furthermore, several PSs show displacements in correspondence with the 1754 landslide crown (Fig. 9A).

As regards RADARSAT-1 data among the C-band sensors, they are characterized by the highest PS density (Table 1).

According to ENVISAT data, the ascending RADARSAT-1 ones (indicated with circles in Fig. 9A) clearly show within the 2010 landslide body two areas affected by ground deformation that reach velocities ranging from -5 to more than -20 mm/y and that are marked with red dashed lines in Fig. 9A. These data sets are very interesting because the acquisition interval ends a few months before the 2010 landslide. In addition, these maps clearly show deformations in correspondence with the area affected by the 1754 landslide crown (Fig. 9A). The descending data set highlights ground deformation in the 1922 landslide area (Fig. 9B) with velocities between -5 and more than -20 mm/y.

4.1.3. COSMO-SkyMed

The COSMO-SkyMed data were available only in descending orbit; the related ground deformation velocity map (V_{slope}) is shown in Fig. 10. The COSMO-SkyMed data are representative of the 2010 landslide post-event period and are related to a shorter acquisition period (2011–2012) with respect to the other employed satellites. The acquired COSMO-SkyMed ground deformation V_{slope} map is characterized by a higher PS density with respect to those obtained using the C-band sensors, but the PS population is affected by higher velocity standard deviations because of the short acquisition period (1 year).

In particular, Fig. 10 shows the presence of relevant displacements located in the northern part of the 2010 landslide (Stazzone quarter, sector 2 in Fig. 4C). The southern part of the San Fratello town (San Benedetto quarter, sector 4 in Fig. 4C) is also affected by deformation, highlighted by the presence of a cluster of PS showing velocities between -5 and more than -20 mm/y. The qualitative ground validation, based on the damages of buildings and structures, and on the scarps and fractures observed during the field surveys confirms displacement trends according to those registered by the satellite data. The COSMO-SkyMed ground deformation velocity (V_{slope}) map, if compared to those acquired during the pre-event phase, clearly shows that most of the deformation phenomena are located along the 2010 landslide crown; nevertheless evidence of ground displacement is also present in the landslide body. These more recent satellite data continue to show the presence of deformation phenomena located in correspondence with the 1754 landslide crown, according to the C-band satellite data. Information about the 1922 landslide displacements is spatially

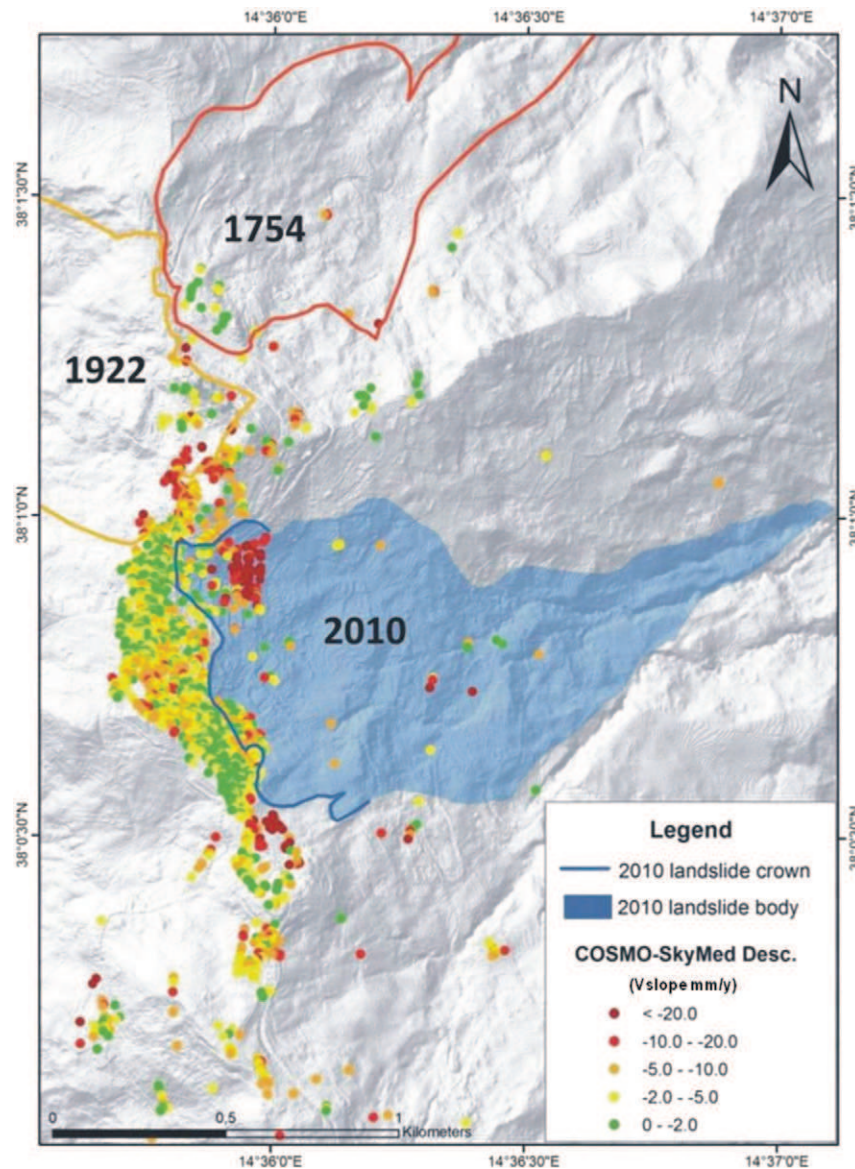


Fig. 10. PS ground deformation velocity map (V_{slope}), using COSMO-SkyMed, obtained by data acquired in descending orbit.

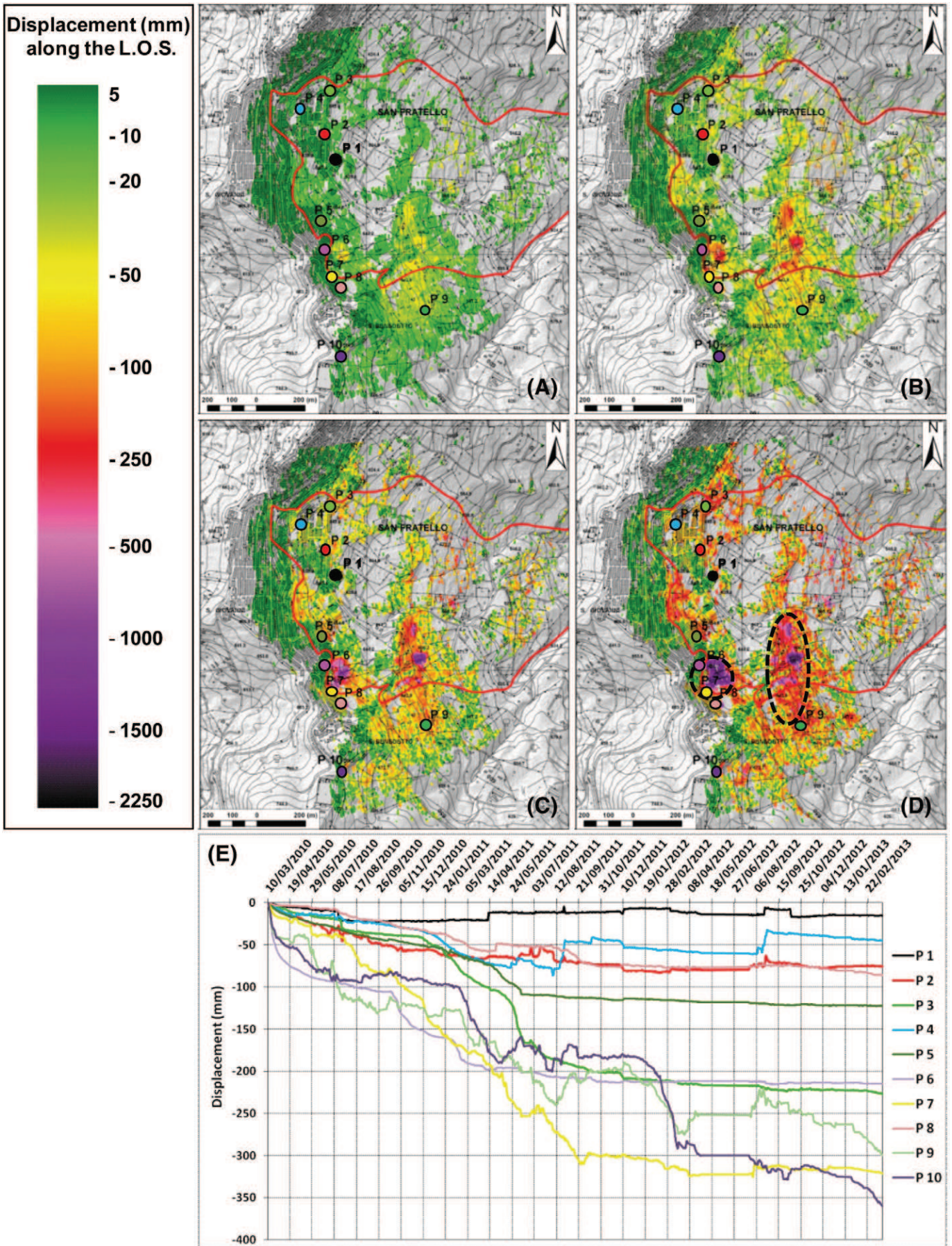
reduced because the town of San Fratello is located along the western boundary of the used COSMO-SkyMed SAR scenes. Nevertheless, in this area deformation velocities, >-20 mm/y, were detected between 2011 and 2012 along the crown of the 1922 landslide (Fig. 10). However, correspondence is good between the damages to buildings and structures and the evidence of movements observed during the field surveys and the ground deformation recorded by the COSMO-SkyMed data (Figs. 4C and 5).

4.2. GB-InSAR data

During the monitoring campaign (10 March 2010–14 March 2013), GB-InSAR data such as cumulative displacement maps were produced as well as displacement time series of some representative points selected prevalently on the town area for civil protection purposes. The collected displacement maps are shown in Fig. 11 with a color scale visualizing (i) stable areas in green; (ii) sectors characterized by light displacements (between about 50 and 300 mm) with colors ranging from yellow to red; and (iii) sectors characterized by the highest monitored displacement in purple (from light to dark tones). The logistic of the GB-InSAR system installation favored a good spatial coverage of

the data on the monitored area, especially with regard to the Stazzone, Riana, San Benedetto, and Porcaro quarters (located as shown in Fig. 4C). Nevertheless, shadowing effects caused by the radar divide, hide part of the western town area from the radar scene; counterslope surfaces cause the same effect in correspondence with some eastern slope sectors, so that in these areas no GB-InSAR data are available, as it is possible to observe in Fig. 11. According to the collected cumulative displacement maps, the peak deformations within the monitored area (dashed ovals in Fig. 11D) are located in correspondence with the San Benedetto (2294 mm) and Porcaro quarters (2178 mm); whereas in correspondence with the Stazzone and Riana quarters, ground deformations reached 604 and 545 mm, respectively.

Displacement time series were also extracted on the displacement maps of 10 control points, selected in correspondence with areas where the radar signal is characterized by high stability, high signal/noise ratio, and high power and coherence parameters to accurately monitor the deformations of structures and buildings (Fig. 11E). The control points selected in correspondence with the Stazzone quarter (P1, P2, P3, P4) record cumulative displacements between 15 (P1) and 226 mm (P3); whereas in the Riana quarter (P5, P6, P7, P8), they range from 86 (P5) to 321 mm (P7). The peak displacements are



recorded in the Porcaro (P9 = 299 mm) and San Benedetto quarters (P10 = 360 mm). The displacements recorded in correspondence with the control points are related to their specific location, thus they do not necessarily reflect the maximum displacement of the whole investigated area (Fig. 11).

5. Discussion

On 14 February 2010, a complex landslide occurred along the eastern slope of the San Fratello town. In this paper, space-borne and ground-based InSAR data were analyzed and integrated to perform a more accurate delimitation of the landslide.

Space-borne InSAR techniques are useful to monitor unstable areas only under specific conditions: the main limitations related to its applicability regard the revisiting time, the slope exposure with respect to the satellite LOS, and the velocity of the investigated movements. Nevertheless, the space-borne InSAR technique ability of measuring very slow and gradual ground displacements (up to few millimeters per year) represents a valuable support to landslide hazard prevention activities, giving the opportunity to detect extremely slow movements that usually occur several weeks or months before the catastrophic failure, preceding major landslide disasters as highlighted by ENVISAT and RADARSAT-1 data.

On the other hand, GB-InSAR allows a continuous monitoring of the displacements from few millimeters per day up to 1 or more meters per day over unstable areas. Furthermore, the instrument versatility enables the investigation of very steep unstable slope not visible from the satellite, and it permits us to choose the best LOS. These characteristics make this technique particularly useful for emergency phases.

Information about ground deformation, obtained using the GB-InSAR technique, can be refined when combined with space-borne InSAR data.

As regard the San Fratello landslide, the GB-InSAR instrument was installed on the facing slope of the landslide: this location represents the best solution considering the geomorphology of the area. The distance is quite high, and this can determine noise, especially where the cross range resolution is lower. The presence of wide vegetation cover, on the interested slope, limits the possibility to investigate the whole landslide area. Only the portion of the landslide that involves the village can be analyzed because the housing and infrastructure represent good reflectors for radar monitoring. This problem can be solved using the space-borne SAR data, which allow the observation of the higher part of the study area nonvisible to the GB-InSAR.

The combined space-borne and ground-based InSAR analysis was performed in order to monitor the evolution of the 2010 landslide and to manage the post-emergency phase. With respect to the 2010 landslide geomorphological map (Fig. 4C), the analysis of the available SAR data enhanced areas affected by ground deformations also outside the surveyed landslide perimeter, showing that the latter was slightly underestimated.

The PSI data projected along the downslope direction, which is quite similar to the GB-InSAR LOS, that confirm the presence of widespread slope instability in the area, not only in correspondence with the 2010 landslide: ground deformations within two large areas, but also in correspondence with the two historical landslide crowns (1754 and 1922) are also detected (Figs. 8, 9, and 10).

As regards the 2010 landslide, ground deformation velocity maps obtained through PSI projected data (V_{slope}), acquired since 1992, allowed highlighting the occurrence of ground displacements during the pre-event phase and identifying eventual displacements in the post-emergency phase related to the landslide.

In particular, between the 1992 and 2001 (ERS 1/2 acquisition period), no important deformations were detected; whereas ENVISAT and RADARSAT-1 ground deformation velocity maps (V_{slope}) highlight the occurrence of displacements between the 2003 and the beginning of the 2010. During this period, the landslide crown area was characterized by stability, and an area characterized by ground deformation velocities higher than -20 mm/y is located on the landslide body, partially outside the DRPC boundary, performed by Pino et al., 2010 (Fig. 4C). This latter area was intensely damaged on 14 February 2010. Unfortunately, no evidence of displacements can be retrieved in correspondence with the landslide toe because of the lack of PS, owing to the intense vegetation cover. These results are in agreement with the landslide evolution trend, which was characterized by a retrogressive behavior: indeed, the pre-event data (ERS 1/2, ENVISAT, and RADARSAT) show the major displacements in the body area and the minor in the crown area. Observing in sequence ERS 1/2, ENVISAT, and RADARSAT data, an increase of ground deformation velocities in the crown area that became more marked in the post-event data, was observed. This is in agreement with the cumulated GB-InSAR displacements.

The PSI data acquired between 2003 and 2010 were useful to highlight the potential risk of the area, but their distribution could not be used to forecast the possible 14 February 2010 landslide spatial extent.

Considering the post-event available PSI data, COSMO-SkyMed ones were very useful to refine the 2010 landslide crown boundary. The higher PS density allowed us to detect a high number of targets in correspondence with the town area; several buildings located outside the DRPC landslide boundary (Pino et al., 2010) showed deformations. The presence of areas affected by ground deformation along the crown can be related to the higher X-band sensibility in the detection of displacements and/or to the retrogression of the landslide, which continued after 14 February 2010, affecting part of the town not severely involved in the event. The most interesting results were obtained in the western sector of the San Benedetto quarter, which was not initially damaged by the landslide. Here field-surveyed fractures and building damages started to develop from 2011, as confirmed by COSMO-SkyMed data. However, other buildings affected by deformation are also located outside the DRPC boundary, also in the Riana quarter and north of the Stazzone quarter, confirming the need to refine the landslide boundary crown.

The GB-InSAR monitoring, carried out during the post-2010 landslide event phase, provided the monitoring of the related displacement pattern evolution. The GB-InSAR data also proved to be very useful to confirm the results obtained through COSMO-SkyMed ground deformation velocity map (V_{slope}), given its temporal coverage with the latter PSI data. In Fig. 12, the GB-InSAR cumulative displacement map (from March 2010 to March 2013) is shown together with the COSMO-SkyMed V_{slope} , whose acquisition period partially corresponds to the GB-InSAR period (May 2011–May 2012). On the map (Fig. 12), it is also possible to observe the proposed new landslide boundary. The cumulative displacement map highlights that the higher ground deformations (up to 2.3 m) took place in correspondence with the San Benedetto-Riana quarters (Fig. 12). Furthermore, a widespread area affected by ground deformation is detected in correspondence with the Porcaro quarter and north of the Stazzone quarter. The above-mentioned areas are partially located outside the DRPC landslide boundary (Pino et al., 2010).

The use of the GB-InSAR cumulative displacement maps proved their usefulness also to recognize the areas affected by the most important residual risk, which are placed in correspondence with the Porcaro and San Benedetto quarters. Considerable deformation can be assessed also in the Stazzone and Riana quarters confirming the instability of the

Fig. 11. San Fratello landslide cumulative displacement maps: (A) 2010; (B) 2010; (C) 2011; and (D) 2012. Dashed ovals represent the areas affected by the peak displacements; P1–10 stand for the location of the control points. (E) Time series of the selected control points.

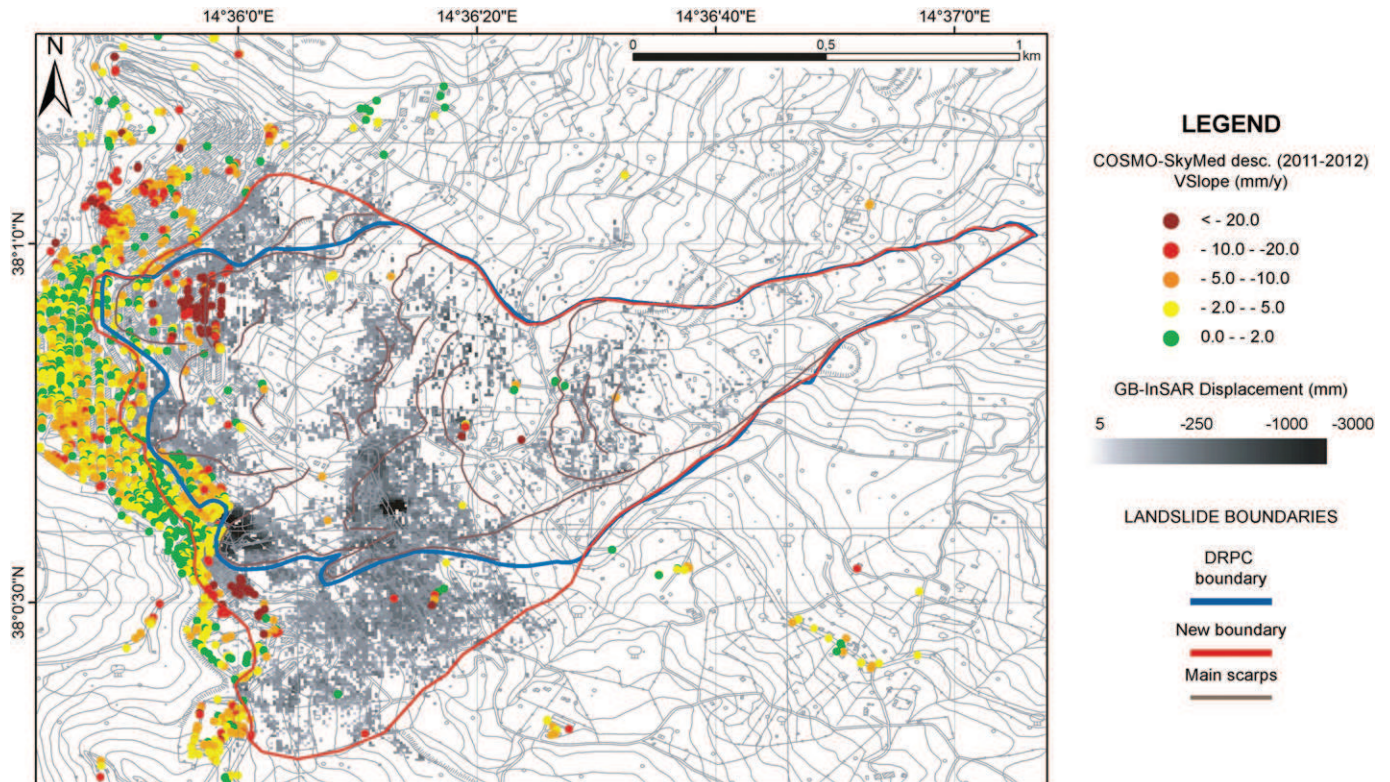


Fig. 12. Comparison between the DRPC (Pino et al., 2010) and the new boundary inferred by the integration between PSI and GB-InSAR data. On the background: the GB-InSAR cumulative displacement map (from March 2010 to March 2013) and the COSMO SkyMed V_{slope} data, together with the main scarp pattern.

crown area during the post-event phase and the retrogressive behavior of the mass movement.

The extension of the landslide boundaries is confirmed by the spatial distribution of the damages of buildings and infrastructures. In particular, in Fig. 12 it is possible to observe how the main scarps delineate areas affected by major displacements, also recognized by the SAR data (Fig. 12). The new boundary determines a new estimation of the landslide area, from 1 to 1.2 km².

Considering the historical landslides, the space-borne multisensor approach allowed the detection of deformation phenomena located along the crown of the 1922 landslide. This instability was observed since the beginning of the ERS 1/2 acquisition (1992–2001) and continues today passing from -9 mm/y to more than -20 mm/y recorded by COSMO-SkyMed.

6. Conclusions

The integration between PS and GB-InSAR data, applied to the 2010 landslide in San Fratello test site, allowed us to analyze the landslide displacements in different time intervals and with different LOS and ground resolutions for a period spanning between 1992 and 2013.

This multisensor approach was employed in order to improve the 2010 landslide boundary obtained through geomorphological mapping and performed immediately after the event. The new boundary considers the areas affected by ground deformation, detected by the C-band sensors (ERS1/2, ENVISAT, and RADARSAT-1), and the areas characterized by slope instability, highlighted during the post-event phase by the X-band COSMO-SkyMed satellite and by the GB-InSAR system located inside and outside the previous limits.

In order to better compare space-borne data with the GB-InSAR data, satellite data were projected in the downslope direction that is quite similar to the GB-InSAR LOS direction.

In this work, the combined use of GB-InSAR and PSI techniques was applied to improve the capacity of the monitoring system of slow-

moving landslides. Results prove the usefulness of this methodology to accurately map and monitor the area affected by ground deformation. The GB-InSAR, coupled with traditional and innovative space-borne SAR, allowed for the production of maps benefitting from the different spatial and temporal resolutions of the radar sensors. The PSI data were used primarily to perform regional scale investigations for the detection of unstable areas and for the assessment of the long-term behavior of the considered landslide. The GB-InSAR system was used in a specific area of interest, improving the spatial resolution of the measurement and reducing the revisiting time.

The obtained accuracy in mapping and in monitoring an area subjected to mass movement is fundamental in risk management and in preparation of emergency plans.

Acknowledgments

The research leading to these results received funding from the European Union Seventh Framework Program (FP7/2007–2013) under grant agreement No. 242212 (Project DORIS). This study was funded by the Seventh Framework Program of European Commission: Landslide Modelling and Tools for vulnerability assessment preparedness and recovery management (LAMPRE).

We thank five anonymous reviewers and the editor Richard A. Marston for their suggestions which greatly improved this work.

References

- Antonello, G., Casagli, N., Farina, P., Leva, D., Nico, G., Sieber, A.J., Tarchi, D., 2004. Ground-based SAR interferometry for monitoring mass movements. *Landslide* 1, 21–28.
- Atzori, P., Vezzani, L., 1974. Lineamenti petrografico-strutturali della catena peloritana. *Geol. Romana* 13, 21–27.
- Atzori, P., Ghisetti, F., Pezzino, A., Vezzani, L., 1978. Strutture ed evoluzione geodinamica recente dell'area peloritana (Sicilia nord-orientale). *Boll. Soc. Geol. Ital.* 97, 31–56.
- Bamler, R., Hartl, P., 1998. Synthetic aperture radar interferometry. *Inverse Probl.* 14, 1–54.

- Bellotti, F., Bianchi, M., Colombo, D., Ferretti, A., Tamburini, A., 2014. Advanced InSAR techniques to support landslide monitoring. In: Pardo-Igúzquiza, E., Guardiola-Albert, C., Heredia, J., Moreno-Merino, L., Durán, J.J., Vargas-Guzmán, J.A. (Eds.), *Mathematics of Planet Earth, Lecture Notes in Earth System Sciences*. Springer, Berlin Heidelberg, pp. 287–290.
- Bianchini, S., Cigna, F., Righini, G., Proietti, C., Casagli, N., 2012. Landslide hotspot mapping by means of persistent scatterer interferometry. *Environ. Earth Sci.* 67 (4), 1155–1172.
- Bianchini, S., Herrera, G., Mateos, R.M., Davide Notti, D., Garcia, I., Mora, O., Moretti, S., 2013. Landslide activity maps generation by means of persistent scatterer interferometry. *Remote Sens.* 5 (12), 6198–6222. <http://dx.doi.org/10.3390/rs5126198>.
- Bianchini, S., Ciampalini, A., Raspini, F., Bardi, F., Di Traglia, F., Moretti, S., Casagli, N., 2014. Multi-temporal evaluation of landslide movements and impacts on buildings in San Fratello (Italy) by means of C-band and X-band PSI data. *Pure Appl. Geophys.* <http://dx.doi.org/10.1007/s00024-014-0839-2>.
- Bovenga, F., Wasowski, J., Nitti, D.O., Nutricato, R., Chiaradia, M.T., 2012. Using COSMO-SkyMed X-band and ENVISAT C-band SAR interferometry for landslides analysis. *Remote Sens. Environ.* 119, 272–285.
- Casagli, N., Farina, P., Leva, D., Nico, G., Tarchi, D., 2002. Monitoring the Tessina landslide by a ground-based interferometer and assessment of the system accuracy. *Proceedings of the International Geoscience and Remote Sensing Symposium (IGARSS)*, Toronto, Canada, pp. 2915–2917.
- Casagli, N., Tibaldi, A., Merri, A., Del Ventisette, C., Apuani, T., Guerri, L., Fortuny-Guasch, J., Tarchi, D., 2009. Deformation of Stromboli Volcano (Italy) during the 2007 eruption revealed by radar interferometry, numerical modelling and structural geological field data. *J. Volcanol. Geotherm. Res.* 182, 182–200.
- Casagli, N., Catani, F., Del Ventisette, C., Luzi, G., 2010. Monitoring, prediction, and early warning using ground-based radar interferometry. *Landslides* 7, 291–301.
- Ciampalini, A., Cigna, F., Del Ventisette, C., Moretti, S., Liguori, V., Casagli, N., 2012. Integrated geomorphological mapping in the north-western sector of Agrigento (Italy). *J. Maps* 8 (2), 136–145.
- Ciampalini, A., Bardi, F., Bianchini, S., Frodella, W., Del Ventisette, C., Moretti, S., Casagli, N., 2014. Analysis of building deformation in landslide area using multisensor PSInSAR™ technique. *Int. J. Appl. Earth Obs. Geoinform.* 33, 166–180.
- Cigna, F., Del Ventisette, C., Liguori, V., Casagli, N., 2011. Advanced radar-interpretation of InSAR time series for mapping and characterization of geological processes. *Nat. Hazards Earth Syst. Sci.* 11, 865–881.
- Cigna, F., Del Ventisette, C., Gigli, G., Menna, F., Agili, F., Liguori, V., Casagli, N., 2012. Ground instability in the old town of Agrigento (Italy) depicted by on-site investigations and Persistent Scatterers data. *Nat. Hazards Earth Syst. Sci.* 12, 3589–3603.
- Colesanti, C., Wasowski, J., 2006. Investigating landslides with space-borne Synthetic Aperture Radar (SAR) interferometry. *Eng. Geol.* 88, 173–199.
- Colesanti, C., Ferretti, A., Prati, C., Rocca, F., 2003. Monitoring landslides and tectonic motion with the Permanent Scatterers technique. *Eng. Geol.* 68, 3–14.
- Corsini, A., Farina, P., Antonello, G., Barbieri, M., Casagli, N., Coren, F., Guerri, L., Ronchetti, F., Sterzai, P., Tarchi, D., 2006. Space-borne and ground-based SAR interferometry as tools for landslide hazard management in civil protection. *Int. J. Remote Sens.* 27 (12), 2351–2369.
- Crosetto, M., Crippa, B., Biescas, E., 2005. Early detection and in-depth analysis of deformation phenomena by radar interferometry. *Eng. Geol.* 79 (1–2), 81–91.
- Crosetto, M., Monserrat, O., Iglesias, R., Crippa, B., 2010. Persistent scatterer interferometry: potential, limits and initial C- and X-band comparison. *Photogramm. Eng. Remote Sens.* 76 (9), 1061–1069.
- Crosetto, M., Monserrat, O., Cuevas, M., Crippa, B., 2011. Spaceborne differential SAR interferometry: data analysis tools for deformation measurement. *Remote Sens.* 3, 305–318.
- Del Ventisette, C., Intrieri, E., Luzi, G., Casagli, N., Fanti, R., Leva, D., 2011. Using ground based radar interferometry during emergency: the case of the A3 motorway (Calabria Region, Italy) threatened by a landslide. *Nat. Hazard Earth Syst. Sci.* 11, 2483–2495.
- Del Ventisette, C., Casagli, N., Fortuny-Guasch, J., Tarchi, D., 2012a. Ruinon landslide (Valfurva, Italy) activity in relation to rainfall by means of GBInSAR monitoring. *Landslides* 9 (4), 497–509.
- Del Ventisette, C., Garfagnoli, F., Ciampalini, A., Battistini, A., Gigli, G., Moretti, S., Casagli, N., 2012b. An integrated approach to the study of catastrophic debris-flows: geological hazard and human influence. *Nat. Hazards Earth Syst. Sci.* 12, 2907–2922.
- Del Ventisette, C., Ciampalini, A., Manunta, M., Calò, F., Paglia, L., Ardizzone, F., Mondini, A.C., Reichembach, P., Mateos, R.M., Bianchini, S., Garcia, I., Füsü, B., Deak, Z.V., Radi, K., Graniczny, M., Kowalski, Z., Piatkowska, A., Przulucka, M., Retzo, H., Strozzi, T., Colombo, D., Mora, O., Sanches, F., Herrera, G., Moretti, S., Casagli, S., Guzzetti, F., 2013. Exploitation of large archives of ERS and ENVISAT C-band SAR data to characterize ground deformations. *Remote Sens.* 5 (8), 3896–3917.
- Di Traglia, F., Del Ventisette, C., Mugnai, F., Intrieri, E., Rosi, M., Moretti, S., Casagli, N., 2013. Ground based InSAR reveals conduit pressurization pulses at Stromboli volcano. *Terra Nova* 25, 192–198.
- Farina, P., Moretti, S., Colombo, D., Fumagalli, A., Manunta, P., 2004. Landslide risk analysis by means of remote sensing techniques: results from the ESA SLAM project. *Int. Geosci. Remote Sens. Symp. (IGARSS)* 1, 62–65.
- Ferretti, A., Prati, C., Rocca, F., 2000. Non-linear subsidence rate estimation using permanent scatterers in differential SAR interferometry. *IEEE Trans. Geosci. Remote Sens.* 38 (5), 2202–2212.
- Ferretti, A., Prati, C., Rocca, F., 2001. Permanent scatterers in SAR interferometry. *IEEE Trans. Geosci. Remote Sens.* 39 (1), 8–20.
- Ferretti, A., Bianchi, M., Prati, C., Rocca, F., 2005. Higher-order permanent scatterers analysis. *Eurasip J. Appl. Signal Process.* 20, 3231–3242.
- Ferretti, A., Fumagalli, A., Novali, F., Prati, C., Rocca, F., Rucci, A., 2011. A new algorithm for processing interferometric data-stacks: SqueeSAR. *IEEE Trans. Geosci. Remote Sens.* 49 (9), 3460–3470.
- Finetti, I., Lentini, F., Carbone, S., Catalano, S., Del Ben, A., 1996. Il sistema Appennino meridionale-Arco Calabro-Sicilia nel Mediterraneo centrale: studio geologico-geofisico. *Boll. Soc. Geol. Ital.* 115, 529–559.
- Fratini, P., Crosta, G.B., Allievi, J., 2013. Damage to buildings in large slope rock instabilities monitored with the PSInSAR™ technique. *Remote sensing, special issue: remote sensing for landslides investigation: from research into practice.* 5 (10), 4753–4773.
- Gigli, G., Fanti, R., Canuti, P., Casagli, N., 2011. Integration of advanced monitoring and numerical modeling techniques for the complete risk scenario analysis of rockslides: the case of Mt. Beni (Florence, Italy). *Eng. Geol.* 120, 48–59.
- Guzzetti, F., Mondini, A.C., Cardinali, M., Fiorucci, F., Santangelo, M., Chang, K.T., 2012. Landslide inventory maps: new tools for an old problem. *Earth Sci. Rev.* 112, 42–66.
- Hanssen, R.S., 2005. Satellite radar interferometry for deformation monitoring: a priori assessment of feasibility and accuracy. *Int. J. Appl. Earth Obs. Geoinform.* 6, 253–260.
- Herrera, G., Fernández-Merodo, J.A., Mulas, J., Pastor, M., Luzi, G., Monserrat, O., 2009. A landslide forecasting model using ground based SAR data: the Portalet case study. *Eng. Geol.* 105, 220–230.
- Herrera, G., Gutiérrez, F., García-Davallillo, J.C., Guerrero, J., Notti, D., Galve, J.P., Fernández-Merodo, J.A., Cooksley, G., 2013. Multi-sensor advanced DInSAR monitoring of very slow landslides: the Tena Valley case study (Central Spanish Pyrenees). *Remote Sens. Environ.* 128, 31–43.
- Intrieri, E., Di Traglia, F., Del Ventisette, C., Gigli, G., Mugnai, F., Luzi, G., Casagli, N., 2013. Flank instability of Stromboli volcano (Aeolian Islands, Southern Italy): integration of GB-InSAR and geomorphological observations. *Geomorphology* 201, 60–69.
- Lentini, F., Vezzani, L., 1975. Le Unità mesozoiche della copertura sedimentaria del basamento cristallino peloritano (Sicilia nord-orientale). *Boll. Soc. Geol. Ital.* 94, 537–554.
- Lentini, F., Carbone, S., Catalano, S., Grasso, M., Monaco, C., 1990. Principali elementi strutturali del thrust belt appenninico-maghrebide in Sicilia centro-orientale. *Mem. Soc. Geol. Ital.* 45, 495–502.
- Lentini, F., Carbone, S., Catalano, S., 1994. Main structural domains of the central Mediterranean region and their tectonic evolution. *Boll. Geofis. Teor. Appl.* 36 (141–144), 103–125.
- Lentini, F., Carbone, S., Catalano, S., Grasso, M., 1995. Principali lineamenti strutturali della Sicilia nord-orientale. *Studi Geol. Camerti Vol. Spec.* 1995/2, 319–329.
- Lentini, F., Catalano, S., Carbone, S., 2000. Carta Geologica della provincia di Messina scala 1:50.000. S.EL.CA., Firenze.
- Luzi, G., Pieraccini, M., Mecatti, D., Noferini, L., Guidi, G., Moia, F., Atzeni, C., 2004. Ground-based radar interferometry for landslides monitoring: atmospheric and instrumental decorrelation sources on experimental data. *IEEE Trans. Geosci. Remote Sens.* 42 (11), 2454–2466.
- Luzi, G., Monserrat, O., Crosetto, M., Copons, R., Altirir, J., 2010. Ground-based SAR interferometry applied to landslide monitoring in mountainous areas. *Mountain Risks Conference: Bringing Science to Society*, Firenze, Italy, pp. 24–26.
- Massonnet, D., Feigl, K.L., 1998. Radar interferometry and its application to changes in the Earth's surface. *Rev. Geophys.* 36, 441–500.
- Meisina, C., Zucca, F., Notti, D., Colombo, A., Cucchi, A., Savio, G., Giannico, C., Bianchi, M., 2008. Geological interpretation of PSInSAR data at regional scale. *Sensors* 8, 7469–7492 (ISSN 1424-8220).
- Meisina, C., Notti, D., Zucca, F., Ceriani, M., Colombo, A., Poggi, F., Roccati, A., Zaccone, A., 2013. The use of PSInSAR™ and SqueeSAR™ techniques for updating landslide inventories. In: Margottini, C., Canuti, P., Sassa, K. (Eds.), *Landslide Science and Practice*. Springer, Berlin Heidelberg, pp. 81–87.
- Noferini, L., Pieraccini, M., Mecatti, D., Macaluso, G., Atzeni, C., Mantovani, M., Marcato, G., Pasuto, A., Silvano, S., Tagliavini, F., 2007. Using GB-SAR technique to monitor slow moving landslide. *Eng. Geol.* 95, 88–98.
- Noferini, L., Takayama, T., Student Member, I.E.E.E., Pieraccini, M., Mecatti, D., Macaluso, G., Luzi, G., Atzeni, C., 2008. Analysis of ground-based SAR data with diverse temporal baselines. *IEEE Trans. Geosci. Remote Sens.* 46, 6.
- Ogniben, L., 1960. Nota illustrativa dello schema geologico della Sicilia nord-orientale. *Riv. Min. Sicil.* 11 (64–65), 183–212.
- PAI—Piano Stralcio di Bacino per l'Assetto Idrogeologico, 2010. AdB Regione Sicilia. <http://www.sitr.regione.sicilia.it/pai>.
- Pieraccini, M., Tarchi, D., Rudolf, H., Leva, D., Luzi, G., Atzeni, C., 2000a. Interferometric radar for remote monitoring of building deformations. *Electron. Lett.* 36 (6), 569–570.
- Pieraccini, M., Tarchi, D., Rudolf, H., Leva, D., Luzi, G., Bartoli, G., Atzeni, C., 2000b. Structural static testing by interferometric synthetic radar. *NDTandE Intl.* 33 (8), 565–570.
- Pieraccini, M., Casagli, N., Luzi, G., Tarchi, D., Mecatti, D., Noferini, L., Atzeni, C., 2003. Landslide monitoring by ground-based radar interferometry: a field test in Valdarno (Italy). *Int. J. Remote Sens.* 24 (6), 1385–1391.
- Pino, P., Cotone, S., Quattrocchi, S., 2010. Carta geomorfologica della frana di San Fratello. Dipartimento Regionale della Protezione Civile Regione Siciliana.
- Pulvirenti, L., Chini, M., Pierdicca, N., Guerriero, L., Ferrazzoli, P., 2011. Flood monitoring using multi-temporal COSMO-SkyMed data: image segmentation and signature interpretation. *Remote Sens. Environ.* 115, 990–1002.
- Raspini, F., Cigna, F., Moretti, S., 2012. Multi-temporal mapping of land subsidence at basin scale exploiting persistent scatterer interferometry: case study of Gioia Tauro plain (Italy). *J. Maps* 8, 514–524.
- Raspini, F., Moretti, S., Casagli, N., 2013. Landslide mapping using SqueeSAR data: Giampileri (Italy) case study. In: Margottini, C., Canuti, P., Sassa, K. (Eds.), *Landslide Science and Practice*. Springer, Berlin Heidelberg, pp. 147–154.
- Raucoles, D., Parcharidis, I., Feurer, D., Novali, F., Ferretti, A., Carnec, C., Lagios, E., Sakkas, V., Le Mouelic, S., Cooksley, G., Hosford, S., 2008. Ground deformation detection of the greater area of Thessaloniki (Northern Greece) using radar interferometry techniques. *Nat. Hazards Earth Syst. Sci.* 8 (4), 779–788.
- Righini, G., Pancioli, V., Casagli, N., 2012. Updating landslide inventory maps using Persistent Scatterer Interferometry (PSI). *Int. J. Remote Sens.* 33, 2068–2096.

- Singhroy, V., Mattar, K., Gray, L., 1998. Landslide characterization in Canada using interferometric SAR and combined SAR and TM images. *Adv. Space Res.* 2 (3), 465–476.
- Tapete, D., Fanti, R., Cecchi, R., Petrangeli, P., Casagli, N., 2012. Satellite radar interferometry for monitoring and early-stage warning of structural instability in archaeological sites. *J. Geophys. Eng.* 9, S10–S25.
- Tarchi, D., Ohlmer, E., Sieber, A.J., 1997. Monitoring of structural changes by radar interferometry. *Res. Nondestruct. Eval.* 9, 213–225.
- Tarchi, D., Rudolf, H., Pieraccini, M., Atzeni, C., 2000. Remote monitoring of buildings using a ground-based SAR: application to cultural heritage survey. *Int. J. Remote Sens.* 21 (18), 3545–3551.
- Tarchi, D., Casagli, N., Moretti, S., Leva, D., Sieber, A.J., 2003a. Monitoring landslide displacements by using ground-based radar interferometry: application to the Ruinon landslide in the Italian Alps. *J. Geophys. Res.* 108 (B8–2387), 101–114.
- Tarchi, D., Casagli, N., Fanti, R., Leva, D., Luzi, G., Pasuto, A., Pieraccini, M., Silvano, S., 2003b. Landslide monitoring by using ground-based SAR interferometry: an example of application to the Tessina landslide in Italy. *Eng. Geol.* 68, 15–30.
- Zhao, C., Lu, Z., Zhang, Q., De La Fuente, J., 2012. Large-area detection and monitoring with ALOS/PALSAR imagery data over Northern California and Southern Oregon, USA. *Remote Sens. Environ.* 124, 348–359.

Multi-Temporal Evaluation of Landslide Movements and Impacts on Buildings in San Fratello (Italy) By Means of C-Band and X-Band PSI Data

SILVIA BIANCHINI,¹ ANDREA CIAMPALINI,¹ FEDERICO RASPINI,¹ FEDERICA BARDI,¹ FEDERICO DI TRAGLIA,^{1,2}
SANDRO MORETTI,¹ and NICOLA CASAGLI¹

Abstract—This work provides a multi-temporal and spatial investigation of landslide effects in the San Fratello area (Messina province within the Sicily region, Italy), by means of C-band and X-band Persistent Scatterer Interferometry (PSI) data, integrated with in situ field checks and a crack pattern survey. The Sicily region is extensively affected by hydrogeological hazards since several landslides regularly involved local areas across time. In particular, intense and catastrophic landslide phenomena have recently occurred in the San Fratello area; the last event took place in February 2010, causing large economic damage. Thus, the need for an accurate ground motions and impacts mapping and monitoring turns out to be significantly effective, in order to better identify active unstable areas and to help proper risk-mitigation measures planning. The combined use of historical and recent C-band satellites and current X-band Synthetic Aperture Radar sensors of a new generation permits spatially and temporally detection of landslide-induced motions on a local scale and to properly provide a complete multi-temporal evaluation of their effects on the area of interest. PSI ground motion rates are cross-compared with local failures and damage of involved buildings, recently recognized by in situ observations. As a result, the analysis of landslide-induced movements over almost 20 years and the validation of radar data with manufactured crack patterns, permits one to finally achieve a complete and reliable assessment in the San Fratello test site.

Key words: Synthetic Aperture Radar, Persistent Scatterer Interferometry, field survey, landslides, San Fratello.

1. Introduction

The occurrence of landslides in populated areas can pose a serious threat to human lives, property and structures. Moreover, where significant cultural

heritage is present, the socio-economic losses and damages are stronger because of the higher value of the elements at risk.

The detection of active ground movements on unstable slopes and landslide-prone areas can greatly benefit from advanced remote sensing techniques, i.e., Persistent Scatterer Interferometry (PSI), thanks to their non-invasiveness, availability and high precision (FERRETTI *et al.* 2001). Furthermore, radar satellite data analysis and traditional geomorphological tools, like field surveys and in situ observations are complementary for the mapping and monitoring of the impacts of such natural phenomena on buildings and manufactures of affected areas.

Persistent Scatterer Interferometry throughout the use of medium resolution Synthetic Aperture Radar (SAR) data in C-band (e.g., from ERS/ENVISAT satellites) has been demonstrated to be a valuable tool for back-monitoring slow-moving landslides, with good accuracy (up to 1 mm/year) and maximum detectable movement of about 15–20 cm/year (HANSSEN 2005; FERRETTI *et al.* 2005; ADAM *et al.* 2008; CASCINI *et al.* 2010; CIGNA *et al.* 2013).

The launch of new SAR sensors that operate at 3 cm wavelength in X-band, i.e., TerraSAR-X and COSMO-SkyMed, with higher spatial resolution and reduced revisiting time (4–16 days) compared to the previous C-band satellites, has enhanced PSI capability for landslides detection and monitoring, allowing the identification of more recent and faster ground movements affecting small areas with improved precision. X-band SAR images make the number of retrieved PS targets higher by a factor of approximately 100–200, compared to medium resolution data (CUEVAS *et al.* 2011). Most of the PS

¹ Department of Earth Sciences, University of Firenze, Via G. La Pira 4, 50121 Florence, Italy. E-mail: silvia.bianchini@unifi.it

² Department of Earth Sciences, University of Pisa, Via Santa Maria 53, 50126 Pisa, Italy.

targets show up on housetops and especially on facades and roofs of buildings, enabling a site-specific investigation. Therefore, the use of X-band data significantly improves the level of detail of the analysis, since small structures now act as stable scatterers and PS from different surfaces can be separated due to the very high resolution of up to 1 m in azimuth and range direction (ROTH *et al.* 2003; GE *et al.* 2010; GERNHARDT *et al.* 2010; NOTTI *et al.* 2010).

C-band satellites provide the availability of long historical archives of motion rates and time series, covering wide areas at a relatively low cost and medium spatial resolution. On the other hand, X-band data, with higher spatial and temporal resolution, allow for a more detailed investigation even at the scale of a single building movement, in a recent and shorter span of time (e.g., some months) (CROSETTO *et al.* 2010; TOMÁS 2010; BOVENGA *et al.* 2012; BRU *et al.* 2013).

Radar data can provide an initial and non-invasive evaluation of most critical unstable areas, to be performed “at desk”, prior to in situ survey. Thus, PSI data give a preliminary and rapid discrimination of the most unstable slopes over wide areas and, consequently, need to be integrated with additional geoinformation and auxiliary data to obtain a more robust interpretation at a local scale. A detailed structural damage analysis of several buildings is required for cross-comparing crack pattern survey with PSI motion rates, for achieving a complete investigation (HERRERA *et al.* 2010).

The Sicily region of Italy is extensively affected by hydrogeological hazards, and several landslides occurred at localized areas across time, causing casualties and large economic damage (ARDIZZONE *et al.* 2012; CIAMPALINI *et al.* 2012; CIGNA *et al.* 2012). In particular, intense and catastrophic landslides have recently occurred in the San Fratello area. The recent activity coupled with the historical significance of many of the affected structures, field observations of damage, and the availability of SAR data make this an ideal field site.

In this paper the impacts of landslides in San Fratello are investigated from 1992 to 2012 by combining the available C-band and X-band SAR data along with a field survey of structural damages.

Multi-temporal estimation of radar velocities and related impacts on cultural and social heritage lead to an assessment of ground movements and landslide damage occurring within San Fratello over 20 years.

2. Study Area

2.1. Geographical and Geological Setting

San Fratello village is located in the NE sector of the Sicily Region (Southern Italy), within Messina province, at 640 m a.s.l. on the Nebrodi Mountains, which, together with the Peloritani Mountains, represent part of the Apenninic-Maghrebian orogenic chain (CUBITO *et al.* 2005) (Fig. 1).

This area is made up of imbricate sheets of Mesozoic–Tertiary rocks, made of the lowermost autochthonous African foreland units, overlapped by the Apenninic-Maghrebian sequences (CORRADO *et al.* 2009). These Apenninic units are tectonically overthrust by allochthonous Kabilo-Calabrian Units, which represent different tectonic assemblages derived from the European continental margin (according to OGNIBEN 1969; KNOTT 1987; DIETRICH 1988) or, according to an opposite interpretation, to an Eo-Alpine chain (Austroalpine sector) piled up toward the European foreland (AMODIO-MORELLI *et al.* 1976). Overall, the tectonic nappes are E–SE verging and show a total thickness of about 15 km.

The rocks outcropping in the area consist of a sequence of terrigenous to calcareous sedimentary sequences belonging to the different already mentioned paleogeographic domains (Fig. 1). The western and southern part of the study area are mostly characterized by terrigenous terrains, since the lower Cretaceous clayey sequences—called the Argille Scagliose Unit—extensively crop out (Apenninic-Maghrebid Units). In the northern portion of the area, the top units (Kabilo-Calabride Units) made of predominantly carbonate complexes outcrop, represented by Liassic limestone platform sequences, overlapped by a terrigenous Late Eocene–Oligocene Flysch (Frazzanò Flysch). The uppermost Cretaceous pelagic dolostones and limestones close the tectonic sequence (San Marco D’Alunzio Unit), outcropping towards N–NW San Fratello village (NIGRO and SULLI 1995; LAVECCHIA *et al.* 2007).

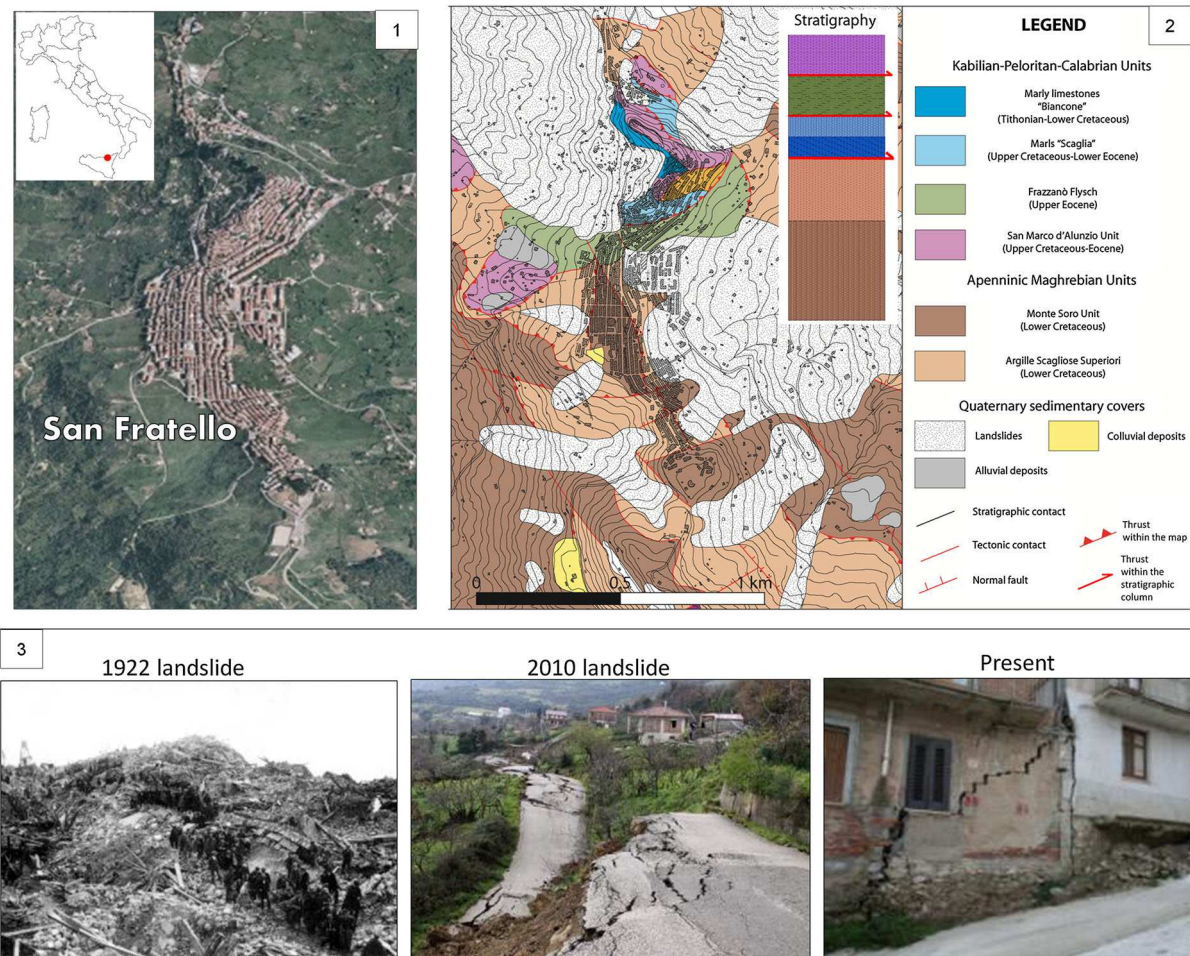


Figure 1

Study area: 1 Geographical location of San Fratello village (Messina province) in South Italy; 2 geological map and stratigraphic sequence; 3 photos referred to the most recent recorded landslides and present scenario

Throughout the inhabited area, an aquifer is also present, at a depth of between 0.5 and 2.5 m from the surface ground level (D.R.P.C. 2010).

From a geomorphological point of view, the test site is strongly influenced by the geo-structural conditions and the recent tectonic activity. The landscape is typical of recently uplifted areas: steep slopes, narrow valleys, high topographical gradient and remarkable relief energy are the most impressive geomorphological features of the study area. Moreover, all the geological units are highly tectonized, being these clays highly fissured and the stone-like lithotypes extensively fractured.

3. Landslides Occurrence

Messina province is prone to landslide hazard, mainly due to the steep topography, the nature of the lithotypes, mainly consisting of flysch units with tectonized silt-clay levels, and the occurrence of intense and seasonally high rainfall events (MONDINI *et al.* 2011; DEL VENTISETTE *et al.* 2012; RASPINI *et al.* 2013).

The main landslide types can be prevalently classified as debris flows, complex slides (VARNES 1978) and shallow and deep-seated landslides.

San Fratello has been chronically affected by landslides (Fig. 1). A severe landslide event dates

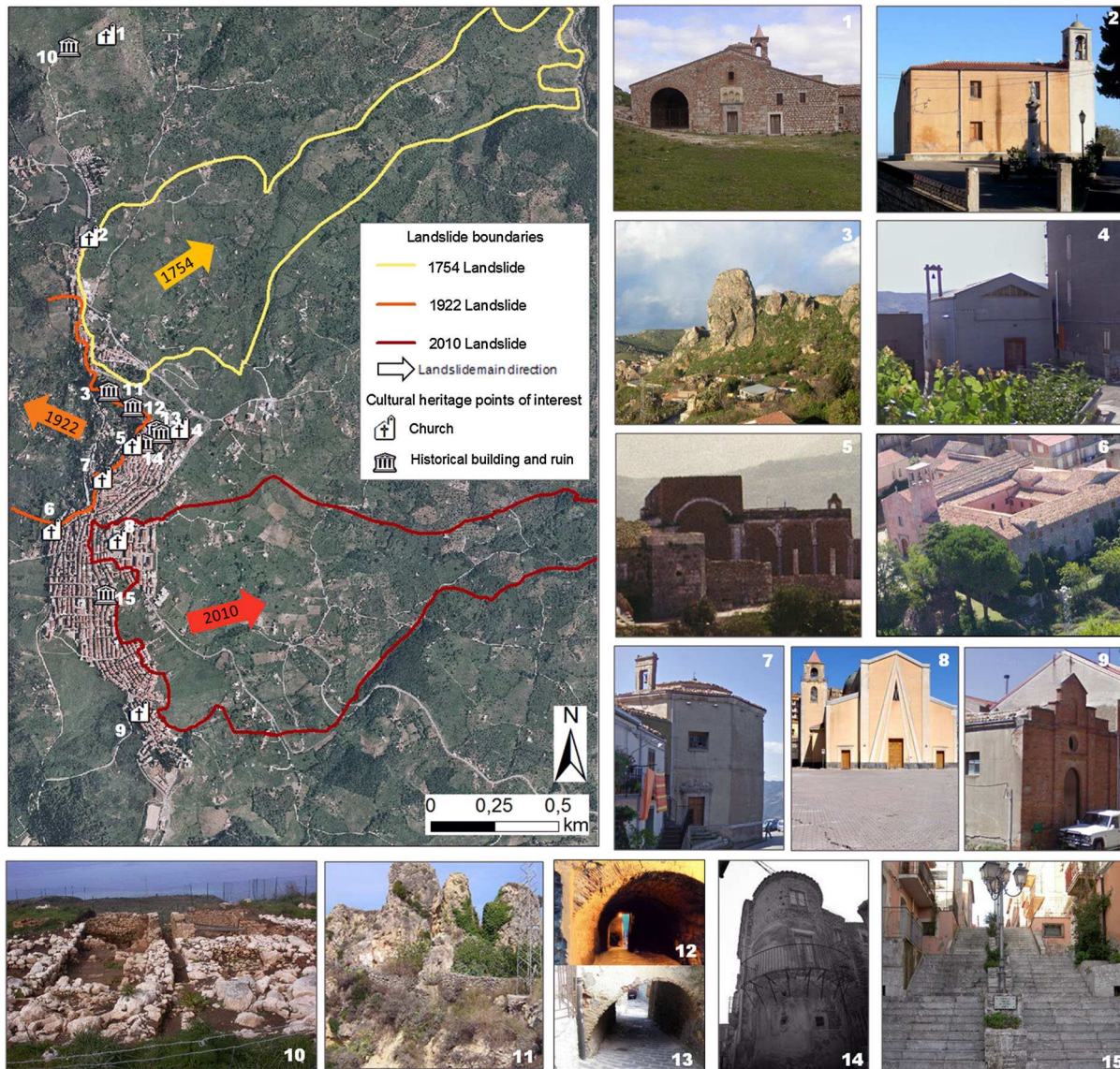


Figure 2

Boundaries and main directions of the three most important and recorded landslides in San Fratello, occurring in 1754, 1922, 2010. Location and photos of the main cultural sites of interest: 1 sanctuary of the three Saints Alfio, Filadelfio and Cirino on the Old Mountain; 2 Maria St. delle Grazie Church; 3 rocky massif Roccaforte; 4 St. Antonio Abate Church; 5 St. Nicolò Old Cathedral; 6 complex of St. Maria Assunta, former convent of S.S. Maria di Gesù and library; 7 St. Crocifisso Church; 8 St. Nicolò New Cathedral (now demolished); 9 St. Benedetto Il Moro Church; 10 Apollonia Archeological site; 11 ruins of St. Filadelfio Castle; 12 St. Nicolò Arcway 13 Stesicorea Arcway; 14 Historical Mammana palace; 15 Historical Stairway of Vittorio Veneto knights

back to 1754 and almost completely destroyed the village. The most recent phenomena are recorded in 1922 and 2010 (Fig. 2). On 8 January 1922, a landslide occurred in the northwestern sector of San Fratello, causing hundreds of deaths; about ten thousand people were evacuated and another village (called Acquedolci) was built along the coast, as

ordered by a Royal Decree (FARANDA 2010). However, San Fratello was re-populated again across time and, more recently, on 14 February 2010, another wide landslide, triggered by intense rainfall and extended up about 1 km², developed on the opposite southern–eastern slope, causing huge damages to the roads and structures (Fig. 2). This landslide affected

the eastern urban districts (i.e., the Stazzone and Riana districts) and the first boundary of damaged area was released on 22 February 2010 (Fig. 2). About 2,000 inhabitants were initially evacuated, approximately 300 houses were slightly damaged and 50 needed to be demolished (D.R.P.C. 2010).

This latest landslide affected the whole E-facing slope, consisting of roto-translational slide and flow, and involving the surface debris cover, which is about 10 m thick and mainly made of wet and fissured clayey lithotypes. As a result, the phenomenon has been caused by predisposing variables that deal with soil and rock geo-mechanical properties, and with the geostructural and hydrogeological setting of the area. The triggering factors may have been the intense rainfall that has increased the static water table within the shallow aquifer, determining soil saturation processes in the clays and causing mass movements.

Ground movements kept on being active up to nowadays, and, thus, the instability scenario is still very critical in San Fratello area.

4. Cultural Heritage

San Fratello is an old village, characterized by several sites of cultural-artistic interest that have been affected by the long-lasting catastrophic natural phenomena (Fig. 2). The remains of the very first inhabited territory of San Fratello, dating back to the III century B.C., are located uphill on the Old Mountain (718 m a.s.l.), northward of the present town (Fig. 2, point 1), where the ancient Norman Sanctuary of the three Saints, built up in the XII century, is also located (Fig. 2, point 1). Since the Norman age, San Fratello village expanded near the rocky massif called Roccaforte (Fig. 2, points 3 and 11) and developed until the Middle Age, when many churches and religious sites were built across time. Thus, on the one hand, San Fratello was a rural village, mainly inhabited by farmers and artisans, but on the other hand, about a hundred households were among the richest and most powerful of Sicily region and undertook a struggle for possessions and interests even in building and embellishing the churches of the town: some examples are the St. Crocifisso Church characterized by an octagonal medieval shape plant

(Fig. 2, point 7), the St. Maria delle Grazie Church dating back to the XVIII century (Fig. 2, point 2), the St. Benedetto il Moro Church (Fig. 2, point 9) and the St. Antonio Abate Church (Fig. 2, point 4).

Many cultural sites of San Fratello have been destroyed by landslides and re-built again across time. The landslide that occurred on 8th January 1922 destroyed most of the town (about two-thirds of San Fratello village). The Maria St. Assunta mother-church, built in the XIII century in the western portion of San Fratello, was completely destroyed by the phenomenon. The newly built Maria St. Assunta church, together with the former convent of Santissima Maria di Gesù and the library (Fig. 2, point 6), can be regarded today as the center of religion, culture and art of San Fratello.

The Old St. Nicolò Cathedral (Fig. 2, point 5), dating back to the XVI century, has been severely damaged by the 1922 landslide and nowadays the only remaining portions are the right sector and the lower part of the bell tower. In the 50s a new St. Nicolò Cathedral was built in the modern Stazzone district (Fig. 2, point 8). Unfortunately also this church has been affected by the 14 February 2010 landslide and has recently been demolished, in February 2013, due to the irreversible and non-repairable damages.

The majority of the historical old houses of San Fratello, the oldest ones dating back to the Norman settlement, have remained uninjured after the natural disasters up to nowadays (Fig. 2, points 12–15). Hence, the damage assessment and conservation strategies for the cultural heritage are strongly recommended and can be addressed to the most important sites of interest of the village.

5. Methodology

The approach of this work consists in a multi-temporal and spatial investigation of landslide effects by means of PSI technique and field survey (Fig. 3). Firstly, we analyzed the available PSI data that highlighted ground motions in historical, recent and current time intervals. A down slope projection of Line-of-Sight (LOS) velocities was performed, following the procedure of COLESANTI and WASOWSKI

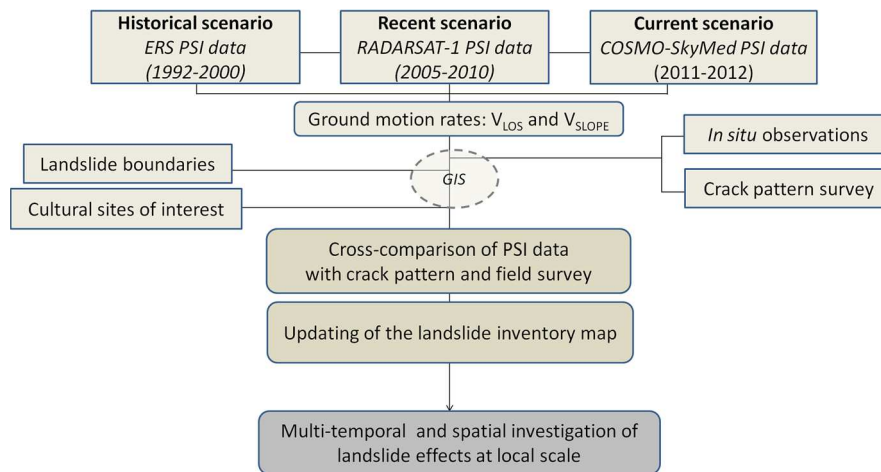


Figure 3
Methodology flow chart

(2006), in order to homogenize all the PSs in the same direction of the maximum local slope, and to obtain vectors of displacement that account more specifically for topographic features of landslides phenomena.

Then, radar movement rates were cross-validated and compared with local failures and with the in-situ observations on historical buildings carried out in the spring of 2010 and in the winter of 2012–2013. The radar mapping and subsequent zoning of the unstable urban sectors of San Fratello were performed by focusing on individual targets, i.e., buildings within the built-up area. In particular, PSI data, local cadastre, the distribution of churches and sites of cultural interest, and pre-existing landslide boundaries were compared and over-layered in a Geographical Information System environment (Fig. 3).

Radar-interpretation and photo-interpretation procedures (e.g., FARINA *et al.* 2006; BIANCHINI *et al.* 2012; CIGNA *et al.* 2013; RIGHINI *et al.* 2012) combined with a field survey allowed the mapping and characterization of landslides. In particular, on the one hand, the recognition of features related to topographic surface movements and the typology classification were mainly based on visual interpretation of orthophotos; on the other hand, the evaluation of the velocity and state of activity of phenomena took advantage from multi-interferometry-based information. For newly detecting

and enlarging phenomena, the two most recent available datasets (i.e., RADARSAT-1 and COSMO-SkyMed data) were employed when improving the landslide inventory map of the study area.

Only “very slow” and “extremely slow” phenomena (velocity <16 mm/year and 16 mm/year ≤ velocity <1.6 m/year, respectively, according to CRUDEN and VARNES 1996) can be detected by PSI data due to the satellite technical acquisition parameters (i.e., signal wavelength and revisiting time; CANUTI *et al.* 2004). Moreover, N–S oriented ground movements are not or only partially illuminated by InSAR sensors, due to the intrinsic acquisition parameters of the satellites that move along N–S orbits with a right-side looking system.

Overall, the outcomes of the work leads to an accurate mapping and monitoring of ground motions and impacts at a local scale, permitting proposing new boundaries of the landslide-affected areas in San Fratello village, and to update the landslide inventory map of the site (Fig. 3).

6. InSAR Processing and Data

Available radar data used in this work consist of SAR images acquired in historical (1992–2001), recent (2005–2010) and current (2011–2012) time intervals. In particular, in C-band (5.6 cm wavelength), 104 SAR images were acquired by ERS 1/2

Table 1

Main acquisition characteristics of the used SAR datasets and PSI velocity values before and after downslope projection of LOS values

Satellite	ERS 1/2	RADARSAT-1	COSMO-SKYMED
Microwave band	C	C	X
Acquisition mode	Ascending and descending	Ascending and descending	Descending
Incidence angle (°)	23	34	26
Track angle (°)	348	349	185
	192	191	
Repeat cycle (days)	35	24	4
Cell resolution in azimuth (m) and range (m)	4 × 20	4 × 10	3 × 3
Critical baseline (m)	1,286	1,825	5,728
Number of SAR images	34 Ascending 70 Descending	46 Ascending 47 Descending	32
Temporal span	1992–2001	2005–2010	2011–2012
Acquisition dates interval	Ascending 11/09/1992–05/06/2001 Descending 01/05/1992–08/01/200	Ascending 30/12/2005–26/01/2010 Descending 31/01/2005–03/02/2010	16/05/2011–02/05/2012
Processing technique	SqueeSAR TM	SqueeSAR TM	SqueeSAR TM
PS density (PS/km ²)	16	112	400
V _{LOS} PSI data velocity range (mm/yr)	Ascending (−9.5, +7.2) Descending (−26.8, +8.6)	Ascending (−46.8, +19.8) Descending (−26.3, +20.5)	(−56.4, +31.8)
Correction factor (C)	Ascending (−0.33, +0.96) Descending (−0.41, +0.96)	Ascending (−0.54, +0.99) Descending (−0.52, +1.00)	(−0.45, +1.00)
Maximum V _{SLOPE} values (V _{LOS} /C)	Ascending (−33.4, +6.8) Descending (−84.5, +50.0)	Ascending (−142.1, +146.6) Descending (−71.5, +21.0)	(−119.8, +111.3)
V _{SLOPE} PSI data velocity range (mm/yr)	Ascending (−33.4, +0.0) Descending (−84.5, +0.0)	Ascending (−142.1, +0.0) Descending (−71.5, +0.0)	(−119.8, +0.0)

satellites in the period 1992–2001 in ascending (34 scenes) and descending orbit (70 scenes), and 93 SAR images were acquired by RADARSAT-1 satellite, in ascending (46 images) and descending (47 images) modes, in the spanning time 2005–2010. Moreover, 32 SAR scenes were collected by COSMO-SkyMed satellite in X-band (3.1 cm wavelength) in descending geometry, in a 1 year-long period from May 16th, 2011 to May 2, 2012 (Table 1).

All the SAR images were processed through the SqueeSARTM algorithm (FERRETTI *et al.* 2011) to obtain PSI data. The SqueeSARTM is a new multi-temporal interferometric processing technique, being an advance on the PSInSARTM algorithm (FERRETTI *et al.* 2011), which permits measurement of ground displacements by means of traditional Permanent Scatterers (PS) like buildings, rock and debris, as well as from Distributed Scatterers (DS). DS are homogeneous areas spread over a group of pixels in a SAR image such as rangeland, pasture, shrubs and bare soil. These targets do not produce the same high

signal-to-noise ratios of PS, but are, nonetheless, distinguishable from the background noise and their reflected radar signals are less strong, but statistically consistent. The SqueeSARTM algorithm was developed to process the signals reflected from these low-reflectivity homogeneous areas, but it also incorporates PSInSARTM; hence, no information is lost and movement measurement accuracy is improved (FERRETTI *et al.* 2011). As a result, the SqueeSARTM algorithm extracts geophysical parameters not only from point-wise deterministic objects (i.e., PS), but also from DS. PS and DS are jointly processed taking into account their different statistical behavior. The coherence matrix associated with each DS is properly “squeezed” to provide a vector of optimum (wrapped) phase values (FERRETTI *et al.* 2011). The SqueeSARTM technique allows an increase of density of the point targets that register ground motion, especially in non-urban areas, as sparse vegetation landscapes (MEISINA *et al.* 2013; RASPINI *et al.* 2013; BELLOTTI *et al.* 2014).

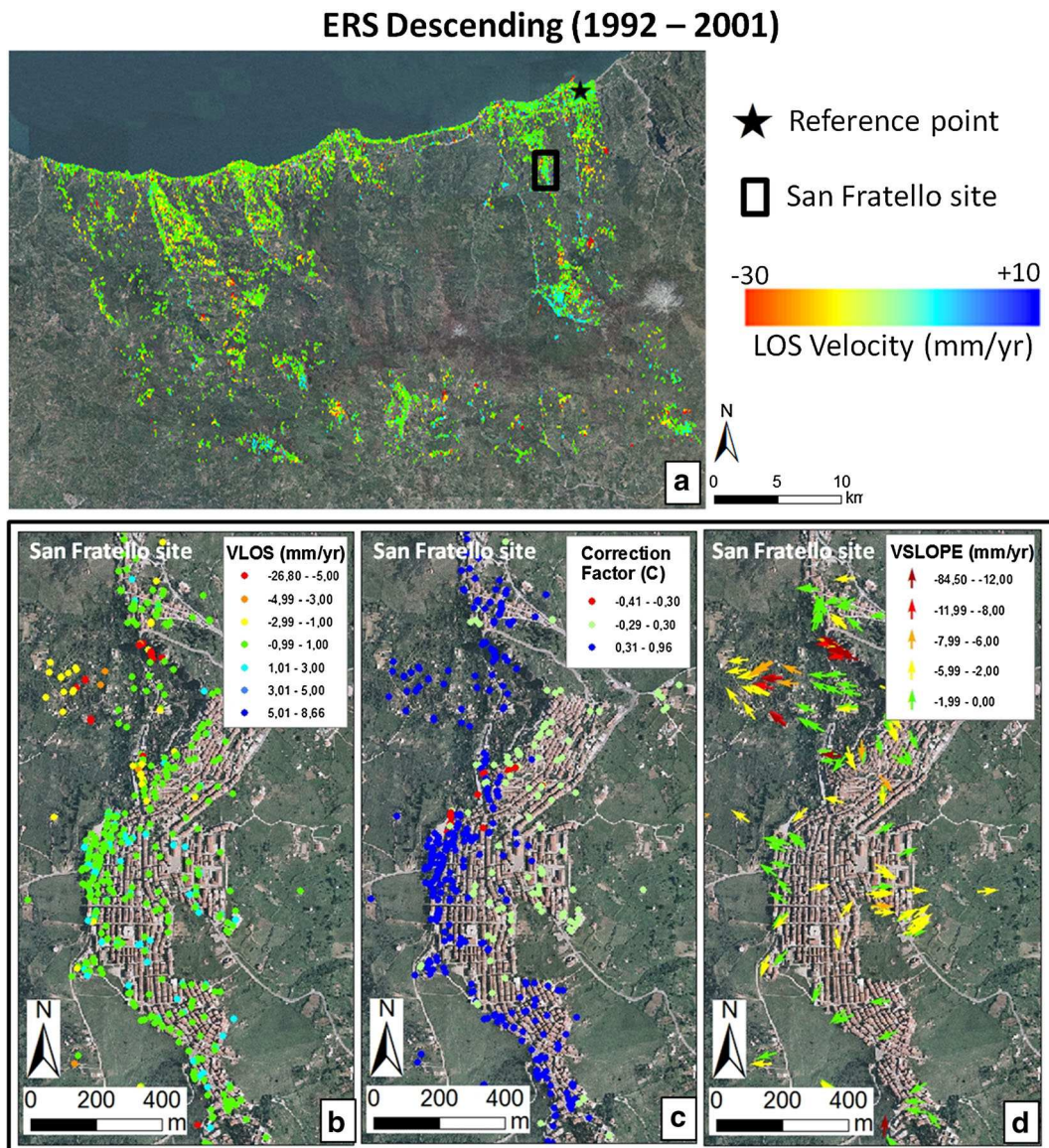


Figure 4

ERS PSI dataset in descending geometry within the study area: **a** PS LOS data distribution and reference point location; **b** V_{LOS} values on the San Fratello village; **c** correction factor (C) distribution values; **d** V_{SLOPE} values on the San Fratello village

Persistent Scatterer Interferometry datasets for each satellite used on the San Fratello village in descending geometry are shown in Figs. 4, 5 and 6

Since satellite systems measure velocities just along their LOS, only the component of motion that is parallel to the LOS direction is measured. A projection of the LOS displacement measures along the most probable direction of movement can be performed. Thus, assuming a simple translational

movement parallel to the slope, in this work LOS velocity of each available PS point (V_{LOS}) was projected along the direction of the maximum slope (V_{SLOPE}), in order to account more specifically for topographic and geomorphological slope conditions within a local-scale landslides analysis. Moreover, this conversion permits comparing landslide velocities with different slope orientations, resolving the satellite acquisition orbit differences and allowing a more feasible interpretation.

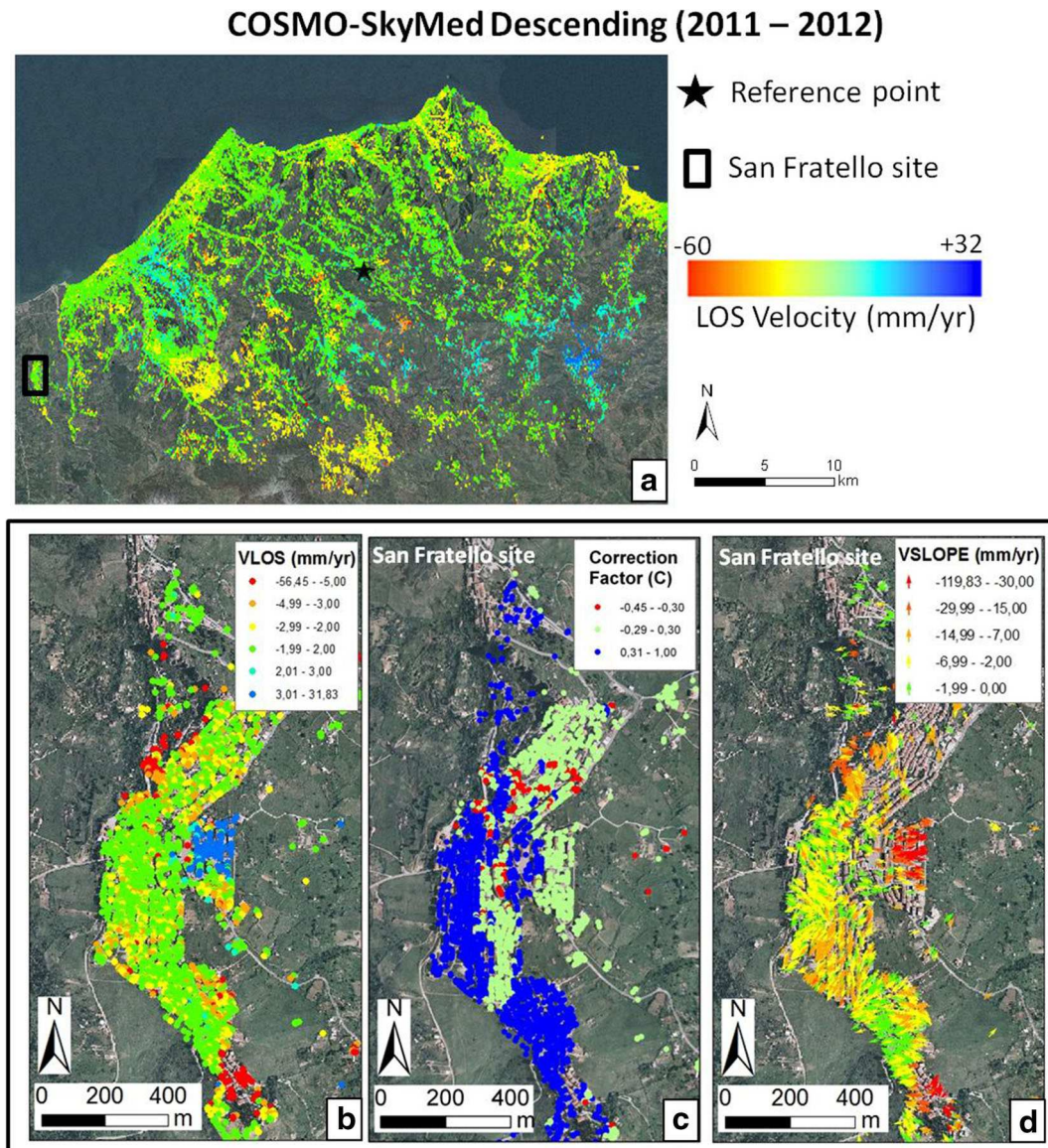


Figure 6

COSMO-SkyMed PSI dataset in descending geometry within the study area: **a** PS LOS data distribution and reference point location; **b** V_{LOS} values on the San Fratello village; **c** correction factor (C) distribution values; **d** V_{SLOPE} values on the San Fratello village

direction, being close to 0 when this angle is almost 90° . The factor C shows negative values when the movement is registered with reverse direction. The V_{SLOPE} values are obtained through the V_{LOS}/C ratio (BIANCHINI *et al.* 2013) (Figs. 4, 5, 6). When the C value is close to 0, then the V_{SLOPE} rate tends to infinity. In order to reduce any exaggeration of the downslope projection when C tends towards 0, we set $C = -0.3$ when $-0.3 < C < 0$ and $C = 0.3$ when $0 < C < 0.3$, according to previously tested

procedures (BIANCHINI *et al.* 2013; HERRERA *et al.* 2013). The maximum V_{SLOPE} values obtained after the downslope projection calculations, as well as the PS velocity distribution features are included in Table 1.

It is worthwhile to highlight that PS rates on flat areas (slope gradient lower than 5°) were not projected downslope and that positive V_{SLOPE} values, which would represent uphill movement, were discarded, following the approach of BIANCHINI *et al.*

(2013) and HERRERA *et al.* (2013). This is because landslide occurrence on almost flat areas is very rare and positive V_{SLOPE} values indicate that a landslide is going up the slope. Although positive movements may be present at the toe of landslides where vertical displacements can occur, the horizontal vector of the movement should remain oriented downhill (HERRERA *et al.* 2013).

V_{LOS} and V_{SLOPE} measurements of each satellite employed within the analysis on San Fratello village, as well as the C factor values, are shown in Figs. 4, 5 and 6. As the coefficient C represents the percentage of real motion measured by the satellite, the projectability map showing C distribution reveals the amount of velocity along the local slope seen for each PS and can be considered as a quantitative evaluation of the projection procedure of V_{LOS} along the local slope.

The pre-existing available inventory map of the study area is the Piano Assetto Idrogeologico (PAI, Hydrogeological Setting Plan), which is dated up to 2012 and includes landslide phenomena classified according to the type and the state of activity. The most representative typologies are slow-moving complex, translational slides, and earth slips. Landslides are classified as active, dormant, inactive (including relict and abandoned phenomena) and stabilized, according to a simplified version of CRUDEN and VARNES (1996) classification.

In situ observations and crack pattern survey were performed in two different time periods: just after the 2010 landslide, and during the period November 2012–January 2013.

Field surveys focused on both ground surface cracks and building cracks. Fractures on buildings were qualitatively classified with respect to orientation (vertical, oriented or horizontal) and typology, according to ALEXANDER (1989) (Fig. 7a, b). Although building cracks differently develop according to building material and foundation typology, from the features and distribution of the crack system observed on the facades, the main cause and movement direction can be supposed (HARP 1998). Some examples are shown in Fig. 7c. Many extension cracks with a unique dip direction on a facade reveal a failure due to a differential foundation settlement induced by a translational movement

(Fig. 7c1). Cracks showing up as an arc on a facade can be induced by a sinking motion of the foundation (Fig. 7c2). Vertical extensional cracks are usually caused by a translational mass movement and show up orthogonally to the main tensile stress direction (Fig. 7c3) (DI ROMOLO 2008).

7. Cross-Validation Between PSI Data and the Field Survey

Radar-interpretation combined with photo-interpretation analysis (FARINA *et al.* 2006) permitted one to successfully update the pre-existing inventory map of the whole area around San Fratello village, extended up about 25 km² (ADB 2012). In particular, this procedure allowed detecting some new potentially hazardous areas and enlarging the boundaries of most of the already mapped phenomena (BIANCHINI *et al.* 2014) (Fig. 8).

At a more detailed and local scale, PSI analysis compared with the in situ survey was exploited over the urban fabric of San Fratello village. Historical, recent and current PS V_{LOS} and V_{SLOPE} ground motion rates were analyzed for instability detection over the most significant areas of San Fratello, primarily considering the distribution of the sites of cultural interest of the village and the boundaries of the two most recent catastrophic landslides occurring in 1922 and 2010.

The soil crack pattern mapping within San Fratello built-up area was performed just after the 2010 landslide. Moreover, further and more recent site-specific field checks and building cracks surveys were carried out in November 2012 and January 2013, in order to validate PSI-based impact assessment performed at a desk, prior to in situ investigations.

At the northern entrance of San Fratello, where the Church of St. Maria delle Grazie is located on a raised position close to the road running along the slope crest (Fig. 9), the spatial distribution of V_{LOS} and V_{SLOPE} displacements in the historical time period (ERS descending data in 1992–2000) seems to show a quite relative stability over the buildings and infrastructure (i.e., yearly motion rate not exceeding ± 2.0 mm/year), with no PS identified over the east-facing slope. Nevertheless, PS RADARSAT-1

data acquired in the recent period (2005–2010) reveal a significant ground instability of the area, with velocity rates up to -15 mm/year along the slope. Field checks also allowed the recognition of indicators of landslide movements and soil creep over the upper part of the slope, such as the loss of verticality of the lights poles and vineyards (Fig. 9). Furthermore, a severe crack pattern affects the concrete structures and retaining walls located along the scarp. The presence of extension fractures, with wide aperture up to 2 cm (Fig. 9), confirms the slow-moving slide displacement downslope, permitting one to locally update the pre-existing landslide inventory accordingly (Fig. 9).

High motion rates were detected in historical, recent and current time periods, in and close to the two main landslides occurring on opposite slopes in

Figure 8

Updating of the landslide inventory map within the whole study area around San Fratello village: **a** Pre-existing landslide inventory map from PAI (Piano di Assetto Idrogeologico–Hydrogeological Setting Plan) referred to 2012 (ADB 2012). Phenomena are classified according to typology and state of activity; **b** Improved landslide inventory map updated to 2012 by means of photo-interpretation and radar-interpretation. Phenomena are classified according to typology and comparison with a pre-existing inventory map

1922 and 2010, affecting several urban sectors of San Fratello.

In particular, in the north-eastern portion of the village, both historical and recent PS data allow detecting the persistence of a suspicious W-directed displacement pattern over an enclosed sector within the area of the 1922 landslide, north-westward of the old districts of the village (Fig. 10). The yearly

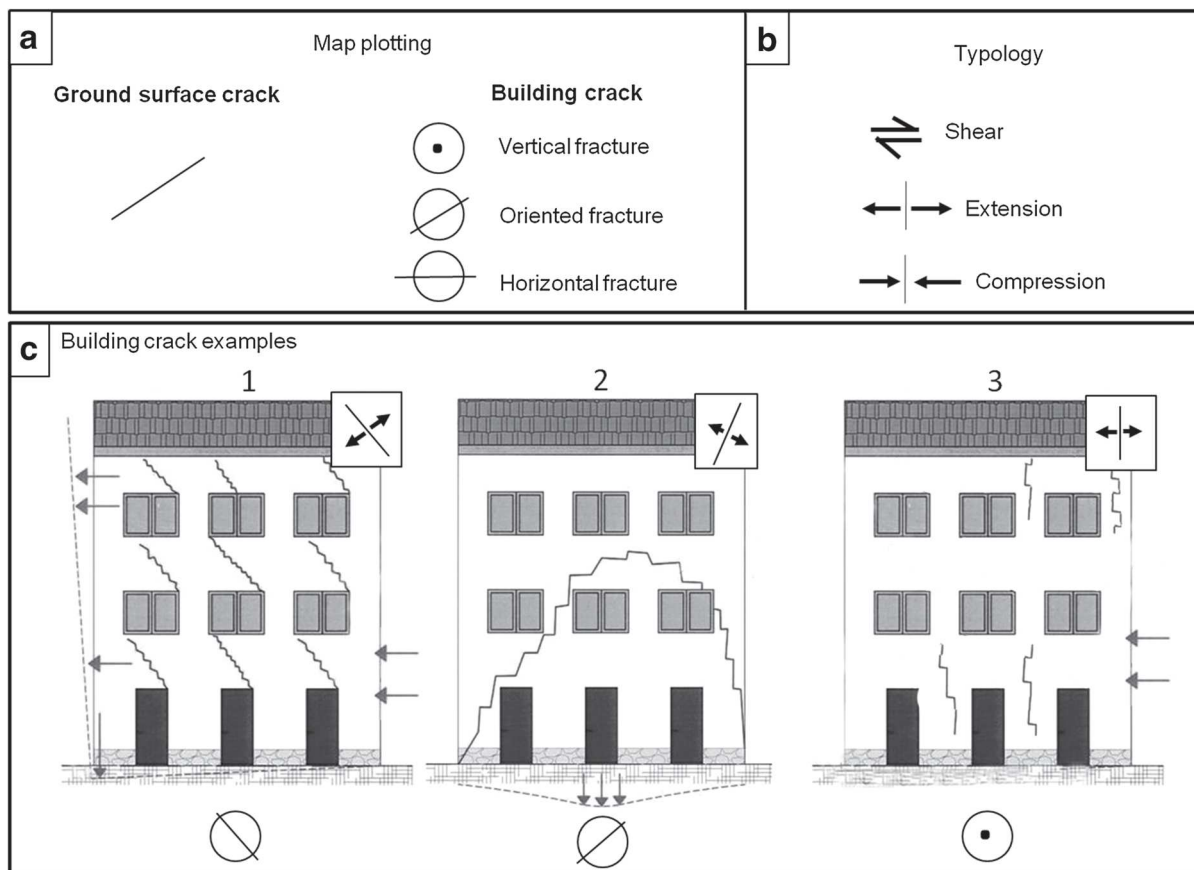
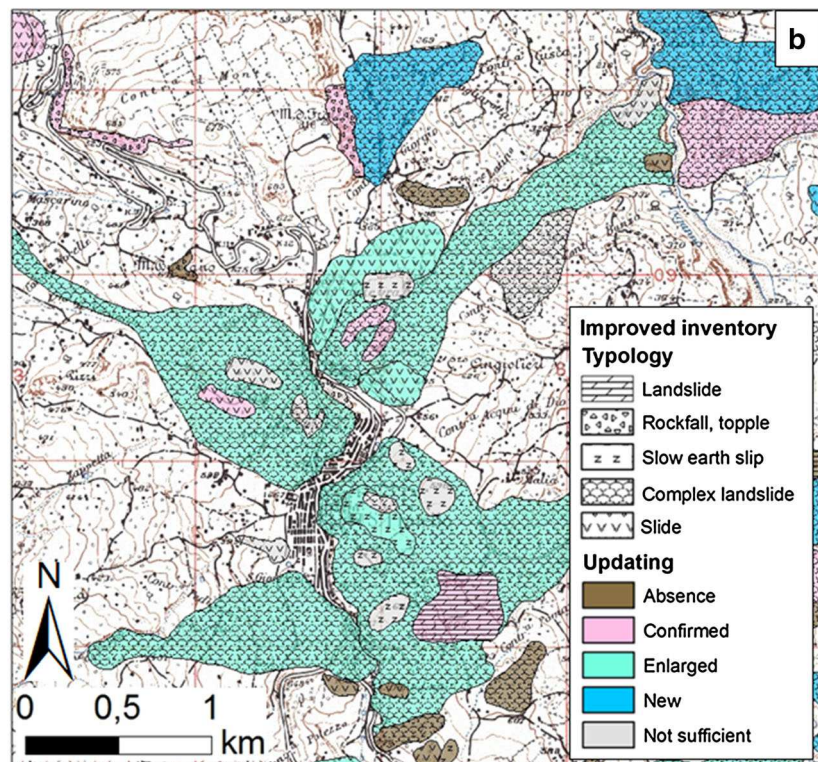
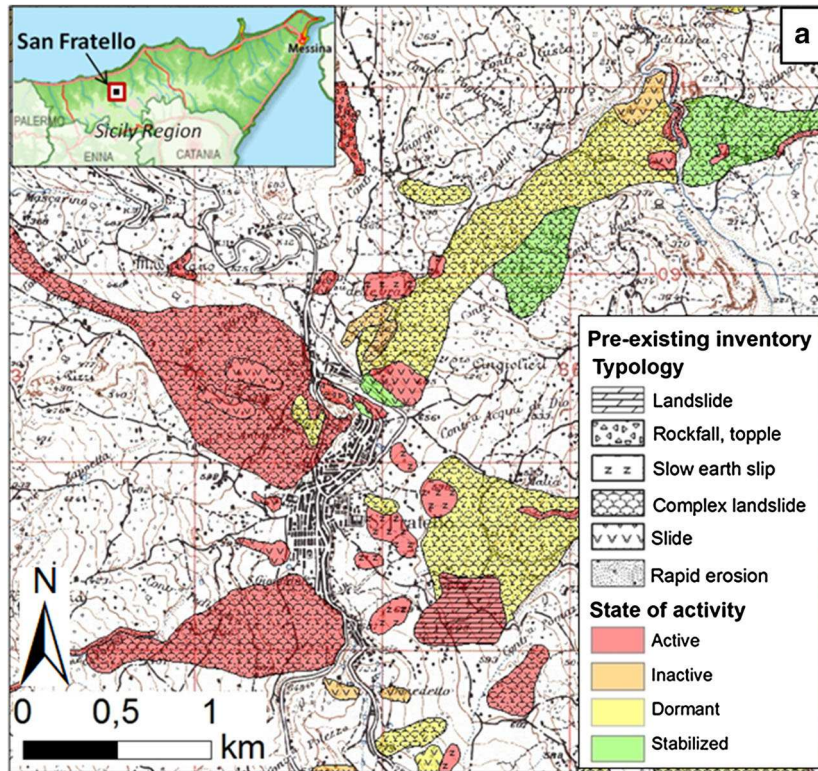


Figure 7

Symbology for ground surface and buildings cracks: **a** symbology for plotting cracks on the map; **b** typology of cracks (from ALEXANDER 1989); **c** building crack examples (modified from: <http://www.controllofessure-mg.it/>): 1 oriented extensional cracks showing a unique orientation and dip direction; 2 extensional cracks distributed as “an arc” on the building façade; 3 vertical tension cracks

Multi-Temporal Evaluation of Landslide Movements



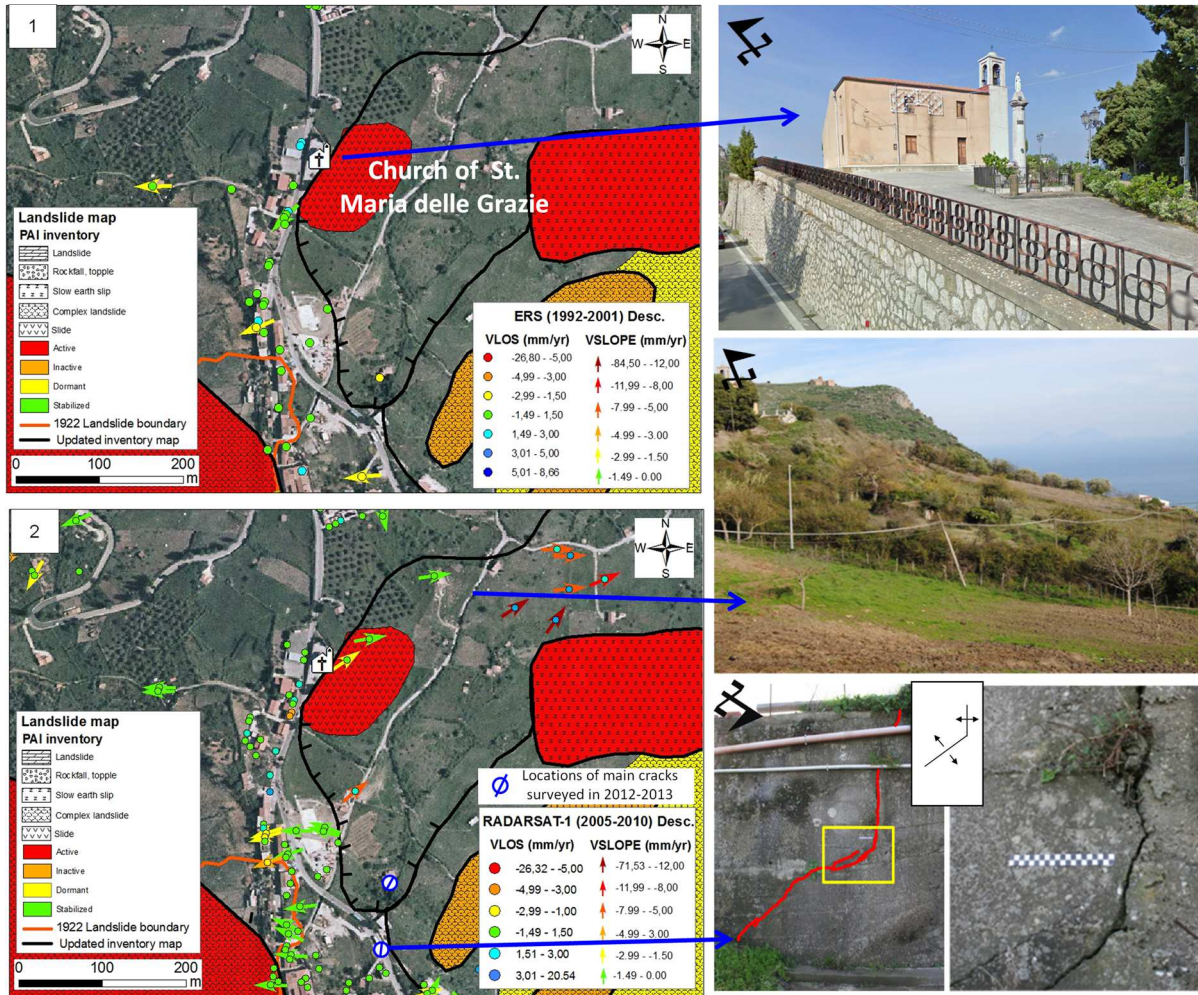


Figure 9

Northern portion of San Fratello village: 1 PSI ERS (V_{LOS} and V_{SLOPE}) displacement map in the historical time interval, 1992–2001 2 PSI RADARSAT-1 (V_{LOS} and V_{SLOPE}) displacement map in the recent time interval, 2005–2010. Photos are explained within the text

motion rates reach values of -6 mm/year measured along the LOS (V_{LOS}) and -11 mm/year along the local slope (V_{SLOPE}) in the historical period (ERS data), and values ranging from -5 to -14 mm/year and from -8 to -19 mm/year, respectively, in the LOS and local slope directions, during the recent acquisition time (RADARSAT-1 data). These rates indicate that the area has been continuously unstable in the last 20 years, and allow confirming the boundary and state of activity of this landslide-affected sector of the slope. Persistent and comparable high ground motion rates from 1992 up to 2012 are also observable along the mapped 1922 landslide boundary, and needed to be taken into account, due to

the near presence of some cultural sites of interest (the Roccaforte and the St. Filadelfio Castle ruins) (Fig. 10).

Close to the eastern boundary of the 1922 landslide, unexpected high displacement rates were detected (Fig. 11), especially by COSMO-SkyMed data, around the Old Cathedral of St. Nicolò, which was severely damaged by the 1922 landslide. Ground surface cracks and building fractures near the Old Cathedral of St. Nicolò were surveyed in November 2013. Radar-detected movements retrieved by COSMO-SkyMed show good correlation with the distribution and the opening of the cracks along the pavement, which are located orthogonally to the

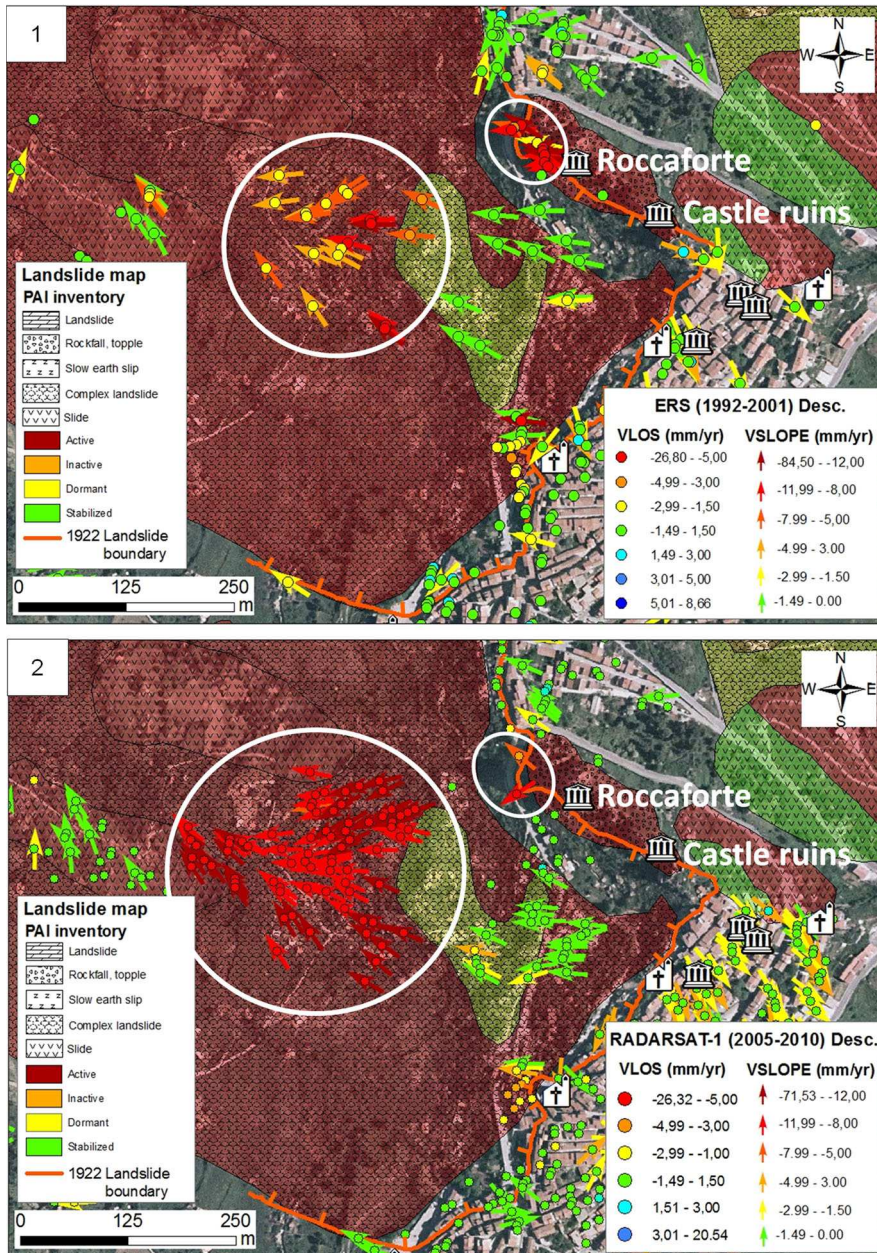


Figure 10

Area within the 1922 landslide on the W-facing slope in San Fratello village: 1 PSI ERS displacement map (V_{LOS} and V_{SLOPE}) in the historical time interval, 1992–2001; 2 PSI RADARSAT-1 (V_{LOS} and V_{SLOPE}) displacement map in the recent time interval, 2005–2010

ground motion direction, and along wall surfaces of the old districts. The vertical extension cracks observed on the walls reveal the subhorizontal vector of displacement. Overall, the instability affects the Old Cathedral of St. Nicolò and most of the surrounding civil buildings along the scarp, as well as the apparently stable Church of St. Crocifisso, with

V_{SLOPE} displacement up to -30 mm/year estimated in the most recent time interval, 2011–2012.

It is worth noting that for the Church of St. Crocifisso, the field checks completed the PS-based mapping of ground deformation. Although the radar processing did not provide a sufficiently dense set of PS over the monument neither in X-band, the in situ

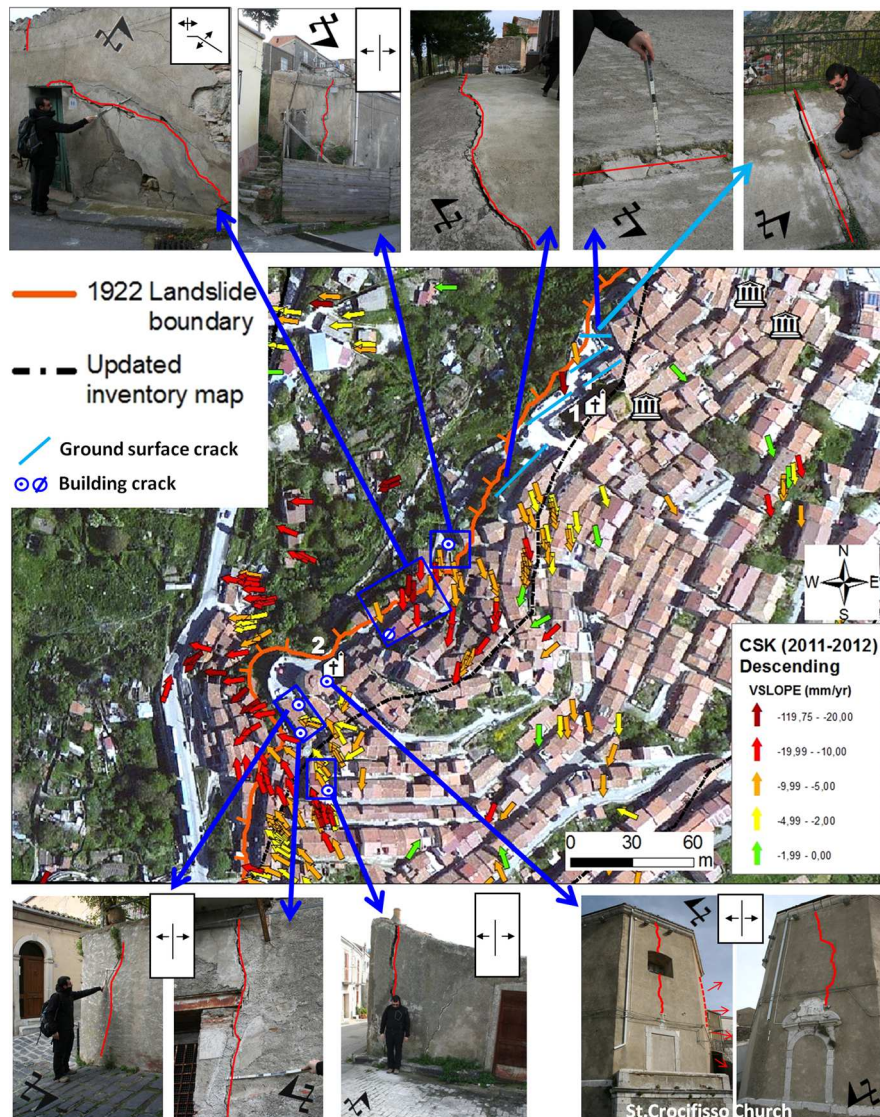


Figure 11

Displacement map of the area in and close to the crown of the 1922 landslide, representing the oldest remaining part of San Fratello village: V_{SLOPE} COSMO-SkyMed PSI data acquired in 2011–2012 overlapped on a recent (2011) orthophoto. *Above and below* the map: photos showing some of the pavement and building cracks surveyed in November 2012–January 2013

inspections permitted one to discover and survey not only surface cracks, but also a sort of bulging of the external walls (Fig. 11), as a further indicator of the structural instability currently affecting the church, due to the general instability of the terrace on which it is built.

As a result, radar data validated with in situ data led us to assign a high level of criticality to the entire sector of the old districts along the scarp, and to update the boundary of the damaged area of the 1922

phenomenon, including further buildings and monuments within the crown of the ancient landslide. The proposed newly mapped boundary is shown in Fig. 11. Moreover, this area will need careful monitoring, since it is the oldest remaining part of San Fratello village.

Regarding the opposite slope and the area in and close to the 2010 landslide, PS data and field validation survey allowed the landslide boundary to be updated, thereby including further urban districts

Multi-Temporal Evaluation of Landslide Movements

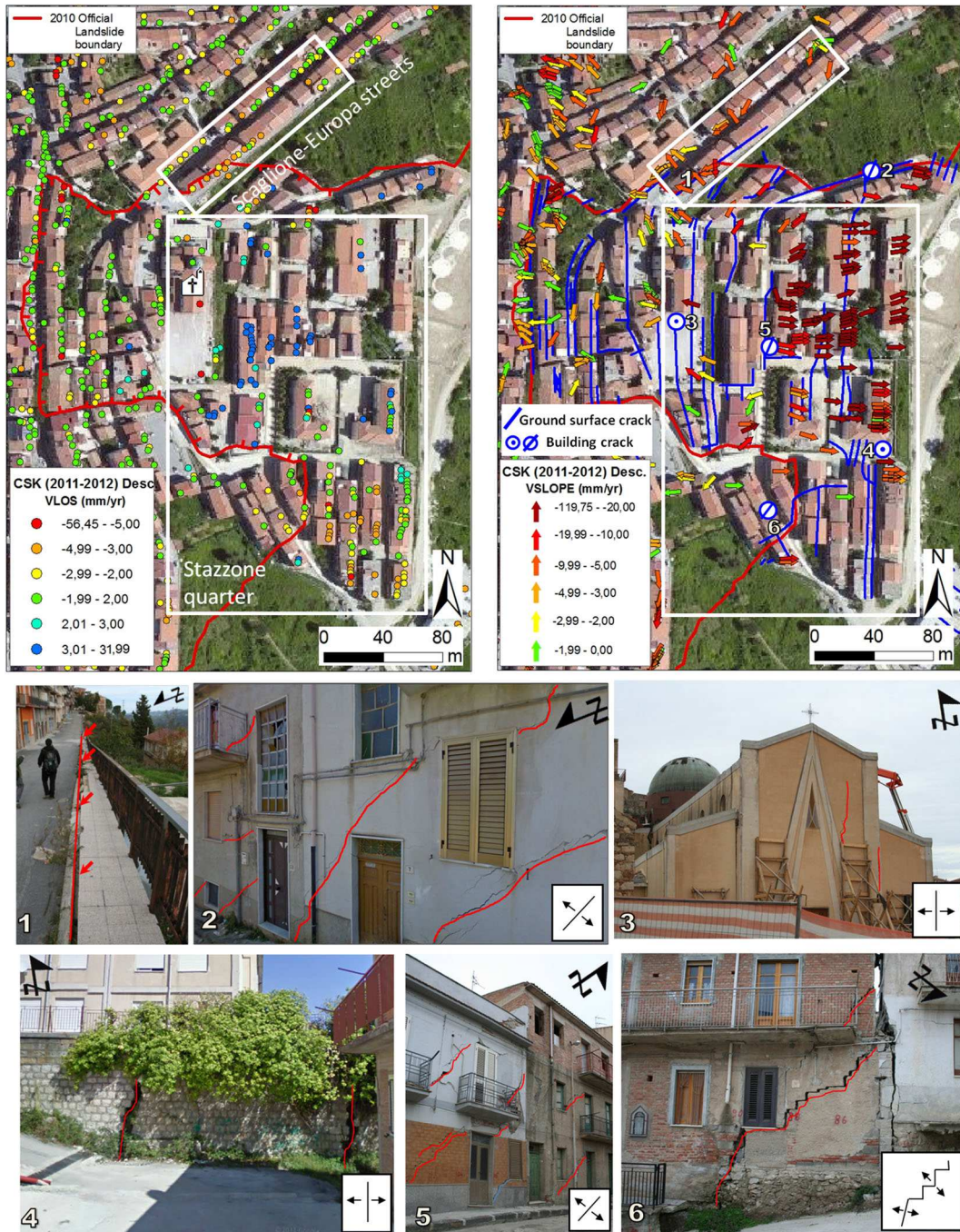


Figure 12

Displacement map of the area in and close to 2010 landslide, focusing on Scaglione-Europa streets area and Stazzone quarter: **a** V_{LOS} COSMO-SkyMed PSI data; **b** V_{SLOPE} COSMO-SkyMed PSI data and cracks plotting: pavement cracks mapped in March 2010 and location of the main building cracks surveyed in November 2012–January 2013. Below the map: 1 pavement crack in Scaglione street (November 2012); 2 oriented extensional cracks on buildings in Fontana Nuova street (November 2012); 3 St. Nicolò New Cathedral (photo taken in November 2012), now demolished; 4 severely damaged wall in Generale Artale street (March 2010); 5 oriented extensional cracks on buildings in Pirandello street; 6 extensional cracks in Stazzone street (November 2012)

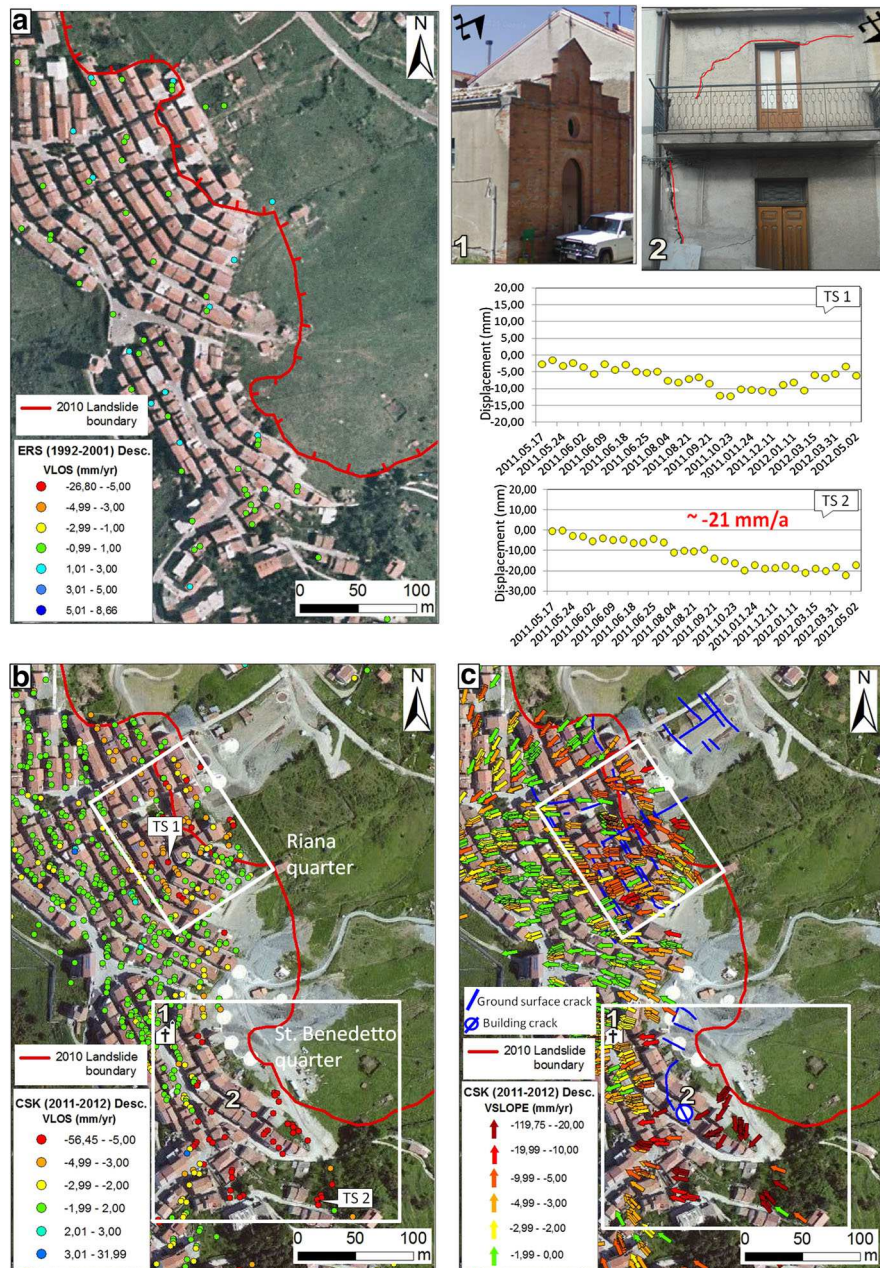


Figure 13

Displacement map of the area in and close to 2010 landslide, focusing on Riana and St. Benedetto districts: **a** V_{LOS} ERS PSI data overlapped on a historical (2000) orthophoto (Volo Italia 2000) and time series of two selected PS targets; **b** V_{LOS} COSMO-SkyMed PSI data overlapped on a recent (2011) orthophoto; **c** V_{LOS} COSMO-SkyMed PSI data and cracks plotting, overlapped on a recent (2011) orthophoto. Photos: 1 St. Benedetto Il Moro Church; 2 Example of damages on a building in Roma street

previously not considered as being critical (Figs. 12, 13). COSMO-SkyMed (2011–2012) PS data in descending geometry show up on housetops and facades of buildings, enabling a highly detailed investigation and precisely detecting the buildings

affected by ground deformation. In particular, four main areas located close to the official zoning of the 2010 landslide were definitely recognized as affected by ground motions instability in the last years of monitoring (Figs. 12, 13). A strong spatial correlation

between the identified COSMO-SkyMed PS targets and the surveyed cracks and damages was found.

Northward of the 2010 landslide boundary, some PS show high motion rates, confirmed by the damages observed in situ along Scaglione and Europa streets. In particular, the presence of tension cracks along the pavement may indicate the occurrence of a surface ground deformation (D.R.P.C. 2010) (Fig. 12).

Another unstable area is the Stazzone district, located on the upper part of the 2010 landslide. The N–S-oriented cracks on the ground, mapped after the 2010 landslide, derive from tensile stresses within the translational landslide characterized by a main planar motion component (D.R.P.C. 2010). Severe crack patterns were found on the buildings of the whole quarter during the recent field survey, revealing that soil moved away from foundations. The New Cathedral of St. Nicolò was demolished in February 2013 due to non-repairable damages (Fig. 12).

PS data and field checks in the Riana district, located just out of the mapped landslide boundary, also reveal high motion rates up to -12 mm/year along the satellite LOS and up to -15 mm/year along the steepest slope, during the acquisition period 2011–2012 (Fig. 13).

In the southern St. Benedetto district, ground deformations are the highest (up to -21 mm/year in 2011–2012) and visible only through the current data measured by the satellite COSMO-SkyMed, while, in the previous periods, ERS and RADARSAT data do not reveal any movements (Fig. 13). Therefore, buildings in this part of the village started being affected by instability since 2011, as confirmed by the inhabitants and from the in situ survey carried out in November 2012.

In conclusion, thanks to the cross-comparison of local failures and displacement features of single edifices observed in situ with radar data, an updating of the pre-existing landslide inventory map of the whole study area was performed. In particular, within the San Fratello urban area, radar data validated by localized field checks allowed a new zoning of the western boundary of the 2010 landslide with respect to the official mapping released on 22 February 2010, enlarging it to include urban areas previously not considered as being unstable.

If the above result was reasonably expected in light of the state of activity and actual extent of the recent 2010 landslide, the satellite data evidenced critical conditions retrieved also for the historical districts of San Fratello along the scarp of the old 1922 landslide, proposing a new mapping also for the eastern boundary of this mapped phenomenon.

8. Discussion

The multi-temporal comparison of PS motion velocities of all the available datasets (i.e., ERS-1/2 1992–2001; RADARSAT-1 2005–2010; COSMO-SkyMed 2011–2012) highlighted persistent ground deformation in San Fratello village, especially over the old districts around the crown of the 1922 landslide and along the western boundary of the 2010 landslide. In particular, COSMO-SkyMed data definitely proved the current critical condition of this sector of San Fratello, thereby increasing the alert level for an area otherwise classified as stable.

Ground motion within the area is assumed to be characterized by a steady-state nature, given the linear deformation model assumption made in the PSI processing approach (CROSETTO *et al.* 2010; HOOPER 2006). A linear regression model is fitted to the data within the processing technique, and, thus, PSI time series show a linear deformation trend in time (Fig. 13). As a result, the non-linear nature of the deformation cannot be analyzed by the PSInSARTM and SqueeSARTM (HOOPER 2006). However, in this case, the non-steady and episodic motion within the landslide is assumed to be actually small in magnitude, just determined by intense rainfall that cause acceleration and groundwater level change, because plastic deformations were recognized along the whole slope, being independent from the recently occurred catastrophic movements (D.R.P.C. 2010).

The affordability of X-band data rely on their potential for accurate deformation measurements that benefits from high spatial and temporal resolution. Overall, the use of X-band SAR sensors, i.e., COSMO-SkyMed, with high spatial resolution up to 1 meter (ROTH *et al.* 2003; GERNHARDT *et al.* 2010) and short revisiting time improves PSI capability for

ground motions detection (BIANCHINI *et al.* 2013; HERRERA *et al.* 2010; NOTTI *et al.* 2010).

X-band radar data turn out to be particularly suited for local detection of landslide processes at small scales, especially in urbanized areas, since the great density of PS point targets in X-band permits to better understand and accurately describe deformation phenomena, entering at the level of the site-specific ground motions investigation. In the San Fratello test site, COSMO-SkyMed data show a PS density 40 times higher than the one of the medium resolution satellite (i.e., ERS) (Table 1). These advantages improve the level of detail of the analysis and allow studying highly localized surface displacements and their dynamic evolution patterns. Although temporal decorrelation is more problematic at X-band compared to longer wavelengths like C-band, the high-bandwidth data acquired by COSMO-SkyMed sensor permit more PSI targets to be identified, and so higher deformation gradients can be detected compared to C-band satellites (GE *et al.* 2010). This is due to the shorter monitoring period of only 12 months (05/16/2011–02/05/2012) as well as to the shorter temporal sampling (up to 4 days), allowing the retrieving of more coherent pixels that show displacements. Some of the PS targets identified by X-band sensors would not be detected over a longer monitoring period or with a worst temporal resolution because the coherence would be lost.

The use of the new SqueeSARTM algorithm (FERRETTI *et al.* 2011), exploiting both ‘point-wise’ PS and ‘spatially distributed scatterers’ (DS), increases the PS targets retrieval also in not-densely urbanized areas and produces improvements in the quality of the displacement time series (MEISINA *et al.* 2013; RASPINI *et al.* 2013). PSI technique is not a stand-alone technique, and it must be considered as a complementary support to the analyses of the areas affected by slope instability. Ground movement evidence obtained from radar data need always to be validated and compared as much as possible with other kinds of techniques and auxiliary information, in order to achieve a reliable investigation (FARINA *et al.* 2006; RIGHINI *et al.* 2012). Thus, the combined use of radar data with traditional geomorphological tools like photo-interpretation, field surveys and in situ campaigns give useful effort for the mapping

and monitoring of the impacts of landslide phenomena on buildings and manufactures of the investigated sites (HERRERA *et al.* 2010; PARCHARIDIS *et al.* 2010; CIGNA *et al.* 2011; TAPETE *et al.* 2012; FRATTINI *et al.* 2013).

In this work, PSI radar-interpreted data were successfully cross-compared with a field survey, which includes observations on landslide-induced damages and crack pattern survey of urban structures. A good agreement between the satellite ground motion evidences and the ground truth was found in the San Fratello village.

In order to compare more specifically InSAR results with local failures and building damages, PSI data measured along the satellite LOS were projected downslope along the maximum steepest slope, following the approach presented and applied in previous works by the scientific community (COLESAANTI and WASOWSKI 2006; CASCINI *et al.* 2009; CIGNA *et al.* 2012, 2013; GRIEF and VLCKO, 2012; BIANCHINI *et al.* 2013; HERRERA *et al.* 2013).

The so-called V_{SLOPE} values obtained through the projection of LOS displacement values (V_{LOS}) allow a more intelligible interpretation of radar data with respect to the local morphology (CIGNA *et al.* 2013; BIANCHINI *et al.* 2013). Several limitations need to be accounted for when projecting the velocity along the slope. The V_{LOS} projection is only valid when the landslide movement is parallel to the slope, thus, this requirement typically holds for planar slides with slow flow but not for rotational landslides, which generally possess a vertical movement at the crown and horizontal movement at the toe. The landslide movements in San Fratello are mainly ascribed as translational slides associated with localized flows (D.R.P.C. 2010; ADB 2012), so they are compatible with the assumed limitations of the projection procedure. Moreover, V_{LOS} values may vary due to vertical displacements, i.e., soil consolidation, which should not be projected, and, if the V_{LOS} data are noisy, the projection will amplify any errors. In the San Fratello test site, in order to reduce these problems within the PSI analysis, the V_{SLOPE} positive values were discarded as indicating uphill motion and only PS velocities over 5° slope were projected since movement on flat areas (slope <5°) would be related to other causes. As shown in Figs. 4, 5 and 6, for the same area of interest

and the same satellite, the value of the correction factor C can vary strongly with the irregularity of the slope. The real direction of motion is most likely more uniform. For this reason, when calculating the C factor for performing the downslope projection, it is better to use a DEM with a lower resolution or resample a detailed DEM to smooth out these variations. In the San Fratello test site, a DEM with 20 m resolution was used to perform the analysis.

The outcomes of this work are a valuable proof of the capability of PSI-based approach to selectively detect areas actually unstable especially if combined with in situ data, useful for cultural heritage applications. As a result, the implementation of PSI data in this work expands the current applications of PSI to landslides monitoring, by suggesting review of the pre-existing landslide inventory and consequently by demonstrating it to be potentially for supporting strategies of land planning and activities of built heritage management.

9. Conclusions

In this paper a multi-temporal landslide effects investigation was performed in San Fratello (Italy) chronically affected by landslide phenomena, in order to evaluate the ground motion impacts on the village, especially on the cultural heritage of the site. The analysis combines InSAR data, which maps the active slide movements over 20 years, with a reconnaissance of damage observed in built structures.

The most recent landslide phenomena in the San Fratello site occurred in 1922 and in February 2010, on the two opposite slopes on which the village is built.

The combined use of historical C-band from 1992 and new generation X-band SAR data up to 2012 permitted one to spatially and temporally detect and monitor ground deformations at a local scale, achieving a comprehensive detailed multi-temporal and spatial investigation of the village.

The InSAR results come from a dual persistent and distributed scatterer approach by means of SqueeSARTM processing technique.

Persistent Scatterer Interferometry data were analyzed and combined with other available

information on the test site, such as orthophotos and field survey observations carried out in March 2010 just after the 2010 phenomenon, and more recently in November 2012 and January 2013.

The obtained results allow improving the landslide inventory map of the area, properly providing an updated assessment of the instability on the study area. In particular, the outcomes of the work lead to proposed new boundaries of the landslide-affected areas in San Fratello village, not only for the 2010 landslide, where PSI data revealed four main unstable areas otherwise classified as stable, but also for the 1922 landslide, where a suspicious ground motion pattern was recognized by means of historical and recent PSI datasets up to 2010.

The cross-comparison of PSI data with local failures and damage of single edifices observed in situ allowed a validation of radar data, to finally achieve a complete analysis that can be particularly useful for strategies of cultural heritage and building management.

Acknowledgments

This work has been carried out in the framework of the DORIS project funded by the EC-GMES-FP7 initiative (Grant Agreement No. 242212). Persistent Scatterer Interferometry data were processed by Tele-Rilevamento Europa and were available within the DORIS project. Federico Di Traglia is supported by a post-doc fellowship founded by the Regione Toscana (UNIFI-FSE) under the project RADSAFE (UNIFI-4) in the framework of the research agreement between DST-UNIFI, DST-UNIFI and Ellegi s.r.l.—LiSALab. The authors would like to thank the Italian Civil Protection for field survey data collected after the 2010 landslide. Information on the cultural and historical heritage of San Fratello mostly derive from the websites of San Fratello village: <http://sottolapietra.blogspot.it/> and <http://www.san-fratello.com/>.

Open Access This article is distributed under the terms of the Creative Commons Attribution License which permits any use, distribution, and reproduction in any medium, provided the original author(s) and the source are credited.

REFERENCES

- ADAM, N., EINEDER, M., YAGUE-MARTINEZ, N., BAMLER, R., High resolution interferometric stacking with TerraSAR-X, In *Proc. of the Geoscience and Remote Sensing Symposium, IGARSS* (Boston, MA, Jul. 7–11, 2008) pp. II-117–II-120.
- AdB Regione Sicilia (2012), *PAI – Piano Stralcio di Bacino per l’Assetto Idrogeologico*, <http://www.sitr.regione.sicilia.it/pai>.
- ALEXANDER, D. (1989), *Urban landslides. An International review of geographical work in the natural and environmental sciences*, *Progress in Phys Geography* 13, 157–191.
- AMODIO-MORELLI, L., BONARDI, G., COLONNA, V., DIETRICH, D., GIUNTA, G., IPPOLITO, F., LIGUORI, V., LORENZONI, F., PAGLIONICO, A., PERRONE, V., PICCARRETA, G., RUSSO, M., SCANDONE, P., ZANETTIN-LORENZONI, E., ZUPPETTA, A. (1976), *L’Arco Calabro-Peloritano nell’orogene appenninico-maghrebide*, *Mem Soc Geol It* 17, 1–60.
- ARDIZZONE, F., BASILE, G., CARDINALI, M., CASAGLI, N., DEL CONTE, S., DEL VENTISETTE, C., FIORUCCI, F., GARFAGNOLI, F., GIGLI, G., GUZZETTI, F., IOVINE, G., MONDINI, A. C., MORETTI, S., PANEBIANCO, M., RASPINI, F., REICHENBACH, P., ROSSI, M., TANTERI, L., TERRANOVA, O. (2012), *Landslide inventory map for the Briga and the Giampileri catchments, NE Sicily, Italy*, *J Maps*, doi:10.1080/17445647.2012.694271.
- BELLOTTI, F., BIANCHI, M., COLOMBO, D., FERRETTI, A., TAMBURINI, A. (2014), *Advanced InSAR Techniques to Support Landslide Monitoring*. In *Mathematics of Planet Earth, Lecture Notes in Earth System Sciences 2014*, (ed. Springer Berlin Heidelberg), 287–290. doi:10.1007/978-3-642-32408-6_64.
- BIANCHINI, S., CIGNA, F., RIGHINI, G., PROIETTI, C., CASAGLI, N. (2012), *Landslide HotSpot Mapping by means of Persistent Scatterer Interferometry*, *Environ Earth Sci* 67(4), 1155–1172.
- BIANCHINI, S., HERRERA, G., NOTTI, D., MATEOS, R.M., GARCIA, I., MORA, O., MORETTI, S. (2013), *Landslide activity maps generation by means of Persistent Scatterer Interferometry*, *Remote Sens* 5(12), 6198–6222.
- BIANCHINI, S., TAPETE, D., CIAMPALINI, A., DI TRAGLIA, F., DEL VENTISETTE, C., MORETTI, S., CASAGLI, N. (2014), *Multi-Temporal Evaluation of Landslide-Induced Movements and Damage Assessment in San Fratello (Italy) by Means of C- and X-Band PSI Data*. In *Mathematics of Planet Earth, Lecture Notes in Earth System Sciences*, (ed. Springer Berlin Heidelberg), 257–261.
- BOVENGA, F., WASOWSKI, J., NITTI, D.O., NUTRICATO, R., CHIARADIA, M.T. (2012), *Using COSMO-SkyMed X-band and ENVISAT C-band SAR interferometry for landslides analysis*, *Remote Sens Environ*, 119, 272–285.
- BRU, G., HERRERA, G., TOMÁS, R., DURO, J., DE LA VEGA, R., MULAS, J. (2013), *Control of deformation of buildings affected by subsidence using persistent scatterer interferometry*, *Struct Infrastruct Eng* 9, 188–200.
- CANUTI, P., CASAGLI, N., ERMINI, L., FANTI, R., FARINA, P. (2004), *Landslide activity as a geoinicator in Italy: significance and new perspectives from remote sensing*, *Environ Geol* 45(7), 907–919.
- CASCINI, L., FORNARO, G., PEDUTO, D. (2009), *Analysis at medium scale of low-resolution DInSAR data in slow-moving landslide affected areas*, *J Photogramm Remote Sens* 64(6), 598–611.
- CASCINI, L., FORNARO, G., PEDUTO, D. (2010), *Advanced low and full resolution DInSAR map generation for slow moving landslide analysis at different scales*, *Eng Geol* 112, 29–42.
- CIAMPALINI, A., CIGNA, F., DEL VENTISETTE, C., MORETTI, S., LIGUORI, V., CASAGLI, N. (2012), *Integrated geomorphological mapping in the north-western sector of Agrigento (Italy)*, *J Maps* 8(2), 136–145.
- CIGNA, F., DEL VENTISETTE, C., LIGUORI, V., CASAGLI, N. (2011), *Advanced radar-interpretation of InSAR time series for mapping and characterization of geological processes*, *Nat Haz Earth Sys Sci* 11, 865–881.
- CIGNA, F., DEL VENTISETTE, C., GIGLI, G., MENNA, F., AGILI, F., LIGUORI, V., CASAGLI, N. (2012), *Ground instability in the old town of Agrigento (Italy) depicted by on-site investigations and Persistent Scatterers data*, *Nat Haz Earth Sys Sci* 12, 3589–3603.
- CIGNA, F., BIANCHINI, S., CASAGLI, N. (2013), *How to assess landslide activity and intensity with Persistent Scatterer Interferometry (PSI): the PSI-based matrix approach*, *Landslides* 10(3), 267–283.
- COLESANTI, C. and WASOWSKI, J. (2006), *Investigating landslides with space-borne Synthetic Aperture Radar (SAR) Interferometry*, *Eng Geol* 88, 173–199.
- CORRADO, S., ALDEGA, L., BALESTRIERI, M. L., MANISCALCO, R., GRASSO, M. (2009), *Structural evolution of the sedimentary accretionary wedge of the alpine system in Eastern Sicily: Thermal and thermochronological constraints*, *Geol Soc Am Bull* 121(11–12), 1475–1490.
- CROSETTO, M., MONSERRAT, O., IGLESIAS, R., & CRIPPA, B. (2010), *Persistent Scatterer Interferometry: potential, limits and initial C- and X-band comparison*, *Photogramm Eng Remote Sens* 76(9), 1061–1069.
- CRUDEN, D.M., VARNES, D.J. (1996), *Landslide types and processes*. In *Landslides: Investigation and Mitigation: Sp. Rep.* 247 eds. Turner, A.K. & Schuster, R.L.), Transportation Research Board, National research Council, National Academy Press, Washington, DC, 36–75.
- CUBITO, A., FERRARA, V., PAPPALARDO, G. (2005), *Landslide hazard in the Nebrodi Mountains (Northeastern Sicily)*, *Geomorphology* 66, (1–4), 359–372.
- CUEVAS, M., CROSETTO, M., MONSERRAT, O., *Monitoring urban deformation phenomena using satellite images*, In *9th International Geomatic Week* (Barcelona, Spain, 15–17 March 2011).
- DEL VENTISETTE, C., GARFAGNOLI, F., CIAMPALINI, A., BATTISTINI, A., GIGLI, G., MORETTI, S., CASAGLI, N. (2012), *An integrated approach to the study of catastrophic debris-flows: geological hazard and human influence*, *Nat Haz Earth Sys Sci* 12, 2907–2922.
- DIETRICH, D. (1988), *Sense of overthrust shear in the Alpine nappes of Calabria (Southern Italy)*, *J Struct Geol* 10(4), 373–381.
- DI ROMOLO, F., *Lesioni degli edifici. Applicazioni di geotecnica e geofisica nell’analisi dei cedimenti delle fondazioni* (Hoepli ed., Italy 2008).
- D.R.P.C. - Dipartimento Regionale Protezione Civile - (2010), *La frana di san Fratello (ME) del 14 febbraio 2010 - Relazione geologica e rapporto di sintesi sulle indagini geognostiche* (Palermo, 2010).
- FARANDA, P., *Città - giardino: il piano di Acquadolci. Storia e urbanistica di una città fondata in era fascista (1922–1932)* (Qanat, Palermo, Italy 2010).
- FARINA, P., COLOMBO, D., FUMAGALLI, A., MARKS, F., & MORETTI, S. (2006), *Permanent Scatterers for landslide investigations: outcomes from the ESA-SLAM project*, *Eng. Geol.* 88, 200–217.
- FERRETTI, A., PRATI, C., ROCCA, F. (2001), *Permanent Scatterers in SAR Interferometry*, *IEEE Trans Geosci Remote Sens* 39, 1, 8–20.

- FERRETTI, A., PRATI, C., ROCCA, F., CASAGLI, N., FARINA, P., YOUNG, B., Permanent Scatterers technology: a powerful state of the art tool for historic and future monitoring of landslides and other terrain instability phenomena, In *Proc. of 2005 International Conference on Landslide Risk Management*, (Vancouver, Canada, 2005).
- FERRETTI, A., FUMAGALLI, A., NOVALI, F., PRATI, C., ROCCA, F., RUCCI, A. (2011), *A new Algorithm for Processing Interferometric Data-Stacks: SqueeSAR*, IEEE Transaction on Geo Sci Remote Sens 49(9), 3460–3470.
- FRATTINI, P., CROSTA, G.B., ALLIEVI, J. (2013), *Damage to Buildings in Large Slope Rock Instabilities Monitored with the PSInSAR™ Technique*, Remote Sens, Special issue: Remote Sensing for Landslides Investigation: From Research into Practice 5(10), 4753–4773.
- GE D., WANG Y., ZHANG L., GUO X., and XIA Y., Mapping urban subsidence with TerraSAR-X data by PSI analysis, In *Proc. of Geoscience and Remote Sensing Symposium (IGARSS), 2010 IEEE International*, (Honolulu, Hawaii, USA, 2010) pp. 3323–3326.
- GERNHARDT, S., ADAM, N., EINEDER, M., BAMLER, R. (2010), *Potential of very high resolution SAR for Persistent Scatterer Interferometry in urban areas*, Ann. GIS 16(2), pp. 103–111.
- GRIEF, V., VLCKO, J. (2012), *Monitoring of post-failure landslide deformation by the PS-InSAR technique at Lubietova in Central Slovakia*. Environ Earth Sci 66(6), 1585–1595.
- HARP E.L. (1998), Origin of fractures triggered by the earthquake in the Summit Ridge and Skyland Ridge areas and their relation to landslides, In *The Loma Prieta, California, Earthquake of October 17, 1989–Landslides*, (ed. Keefer D.K.), U.S. Geological survey professional paper, pp. 1551–C.
- HANSEN, R.F. (2005), *Satellite radar interferometry for deformation monitoring: a priori assessment of feasibility and accuracy*, Int J Appl Earth Obs 6, 253–260.
- HERRERA, G., TOMÁS, R., MONELLS, D., CENTOLANZA G., MALLORQUI J. J., VICENTE, F., NAVARRO, V. D., LOPEZ-SANCHEZ, J. M., CANO, M., MULAS, J., SANABRIA, M. (2010), *Analysis of subsidence using TerraSAR-X data: Murcia case study*, Eng. Geol 116, 284–295.
- HERRERA, G., GUTIÉRREZ, F., GARCÍA-DAVALILLO, J.C., GUERRERO, J., GALVE, J.P., FERNÁNDEZ-MORODO, J.A., and COOKSLEY, G. (2013), *Multi-sensor advanced DInSAR monitoring of very slow landslides: the Tena valley case study (central Spanish Pyrenees)*, Remote Sens Environ 128, 31–43.
- HOOPER, A. (2006), *Persistent scatterer radar interferometry for crustal deformation studies and modeling of volcanic deformation*, Ph.D. thesis, Stanford University.
- KNOTT, S.D. (1987), *The Liguride Complex of Southern Italy—a Cretaceous to Paleogene accretionary wedge*, Tectonophysics 142, 217–226.
- LAVECCHIA, G., FERRARINI, F., DE NARDIS, R., VISINI, F., BARBANO, M.S. (2007), *Active thrusting as possible seismogenic source in Sicily (Southern Italy): Some insights from integrated structural-kinematic and seismological data*, Tectonophysics 445, 145–167.
- MEISINA, C., NOTTI, D., ZUCCA, F., CERIANI, M., COLOMBO, A., POGGI, F., ROCCATI, A., ZACCONE, A., The use of PSInSAR™ and SqueeSAR™ techniques for updating landslide inventories, In *Landslide Science and Practice, In Proc. of The Second World Landslide Forum, Volume 1: Landslide Inventory and Susceptibility and Hazard Zoning* (eds. Margottini, C., Canuti, C., Sassa, K.) (Roma, Italy, 2013) pp. 81–88.
- MONDINI, A.C., GUZZETTI, F., REICHENBACH, P., ROSSI, M., CARDINALI, M., ARDIZZONE, F. (2011), *Semi-automatic recognition and mapping of rainfall induced shallow landslides using optical satellite images*, Remote Sens Environ 115(7), 1743–1757.
- NIGRO, F. AND SULLI, A. (1995), *Plio-Pleistocene extensional tectonics in the Western Peloritani area and its offshore (northeastern Sicily)*, Tectonophysics 252, 295–305.
- NOTTI, D., DAVALILLO, J.C., HERRERA, G., MORA, O., (2010), *Assessment of the performance of X-band satellite radar data for landslide mapping and monitoring: Upper Tena Valley case study*, Nat Haz Earth Sys Sci 10, 1865–1875.
- OGNIBEN, L., (1969), *Nota illustrativa dello schema geologico della Sicilia nord-orientale*, Riv Min Sicil 11, n. 64–65, 183–212.
- PARCHARIDIS, I., FOUMELIS, M., PAVLOPOULOS, K., KOURKOULI, P., Ground deformation monitoring in cultural heritage areas by time series SAR interferometry: the case of ancient Olympia site (Western Greece), In *European Space Agency publications, Fringe Conference, ESA* (Noordwijk, Holland, 2010).
- RASPINI, F., MORETTI, S., CASAGLI, N., Landslide Mapping Using SqueeSAR Data: Giampileri (Italy) Case Study, In *Landslide Science and Practice, Proc. of The Second World Landslide Forum, Volume 1: Landslide Inventory and Susceptibility and Hazard Zoning* (eds. Margottini, C., Canuti, C., Sassa, K.) (Roma, Italy 2013) pp. 147–154.
- RIGHINI, G., PANCIOLI, V., CASAGLI, N., (2012), *Updating landslide inventory maps using Persistent Scatterer Interferometry(PSI)*, Int J Remote Sens 33(7), 2068–2096.
- ROTH, A., TerraSAR-X: A new perspective for scientific use of high resolution spaceborne SAR data, In *Proc. of the 2nd GRSS/ISPRS Joint workshop on remote sensing and data fusion on urban areas*, (Berlin, Germany, 2003), pp. 4–7.
- TAPETE, D., FANTI, R., CECCHI, R., PETRANGELI, P., CASAGLI, N. (2012), *Satellite radar interferometry for monitoring and early-stage warning of structural instability in archaeological sites*, J Geophys Eng 9, S10–S25.
- TOMÁS, R., HERRERA, G., LOPEZ-SANCHEZ, J.M., VICENTE, F., CUENCA, A., MALLORQUÍ J.J. (2010), *Study of the land subsidence in the Orihuela city (SE Spain) using PSI data: distribution, evolution and correlation with conditioning and triggering factors*, Eng Geol 115, 105–121.
- VARNES, D. J., Slope movements, type and processes, In *Landslide analysis and control. Transportation Research Board, National Academy of Sciences*, (eds Schuster, R. L., Krizek, R. J.) (Washington, D.C., 1978), Special report 176, pp. 11–33.



Contents lists available at ScienceDirect

International Journal of Applied Earth Observation and Geoinformation

journal homepage: www.elsevier.com/locate/jag

Analysis of building deformation in landslide area using multisensor PSInSARTM technique



Andrea Ciampalini*, Federica Bardi, Silvia Bianchini, William Frodella, Chiara Del Ventisette, Sandro Moretti, Nicola Casagli

Department of Earth Sciences, University of Firenze, Via La Pira 4, 50121 Firenze, Italy

ARTICLE INFO

Article history:

Received 25 March 2014

Accepted 23 May 2014

Available online 12 June 2014

Keywords:

Landslide

Radar

PSInSAR

Buildings

Damages

ABSTRACT

Buildings are sensitive to movements caused by ground deformation. The mapping both of spatial and temporal distribution, and of the degree of building damages represents a useful tool in order to understand the landslide evolution, magnitude and stress distribution. The high spatial resolution of space-borne SAR interferometry can be used to monitor displacements related to building deformations. In particular, PSInSAR technique is used to map and monitor ground deformation with millimeter accuracy. The usefulness of the above mentioned methods was evaluated in San Fratello municipality (Sicily, Italy), which was historically affected by landslides: the most recent one occurred on 14th February 2010. PSInSAR data collected by ERS 1/2, ENVISAT, RADARSAT-1 were used to study the building deformation velocities before the 2010 landslide. The X-band sensors COSMO-SkyMed and TerraSAR-X were used in order to monitor the building deformation after this event. During 2013, after accurate field inspection on buildings and structures, damage assessment map of San Fratello were created and then compared to the building deformation velocity maps. The most interesting results were obtained by the comparison between the building deformation velocity map obtained through COSMO-SkyMed and the damage assessment map. This approach can be profitably used by local and Civil Protection Authorities to manage the post-event phase and evaluate the residual risks.

© 2014 The Authors. Published by Elsevier B.V. This is an open access article under the CC BY-NC-ND license (<http://creativecommons.org/licenses/by-nc-nd/3.0/>).

Introduction

Landslides are globally widespread phenomena, causing a significant number of human loss of life and injury, as well as extensive economic damages to private and public properties. In Europe and in Italy in particular, where half a million active landslides exist, mass movements represent the primary cause of death caused by natural hazards (Guzzetti et al., 1999, 2012). Recently, significant results in the study of ground deformation were obtained using spaceborne Synthetic Aperture Radar (SAR) sensors, locally integrated with ground observations (Ferretti et al., 2001; Guzzetti et al., 2009; Lauknes et al., 2010; Herrera et al., 2010, 2013; Tomás et al., 2012). This approach allows delivering innovative and accurate information relevant to the Civil Defense Authorities covering the pre-event, event and post-event management phases. Nowadays slow ground deformations can be easily detected and monitored using satellite radar techniques at a relatively low

cost. C-band satellites acquire SAR images since 1992, providing a very wide archive of the ground displacements historical evolution of a selected area. These sensors are characterized by a medium spatial resolution (20 m × 4 m) and a 35 days revisiting time. The new X-band COSMO-SkyMed (CSK) and TerraSAR-X (TSX) missions reduced the revisiting time to 4 (CSK) and 11 (TSX) days, enhancing the spatial resolution to 1 m × 1 m. Classical Differential Interferometry (DInSAR) is used to measure the relative motion between two image acquisitions (Costantini et al., 2000; Crosetto et al., 2011). A phase difference image or interferogram, which is directly connected to ground motion, can be obtained. PSInSAR is a non-invasive surveying technique used to calculate motions of individual ground and structure point-like target over wide-areas (Ferretti et al., 2000). The PSI technique takes conventional DInSAR a step further by correcting the atmospheric, orbital and DEM errors in order to derive relatively precise displacement and velocity measurements at specific points on the ground. This well-established technique is particularly useful in landslides mapping and monitoring (Liu et al., 2013; Bianchini et al., 2014a). San Fratello is a town located in the Messina Province (Sicily, Italy), which was affected in the last three centuries by at least three important landslides: the first two, occurred in 1754 and 1922 respectively,

* Corresponding author. Tel.: +39 0552757785.

E-mail addresses: andrea.ciampalini@unifi.it, andrea.ciampalini76@gmail.com (A. Ciampalini).

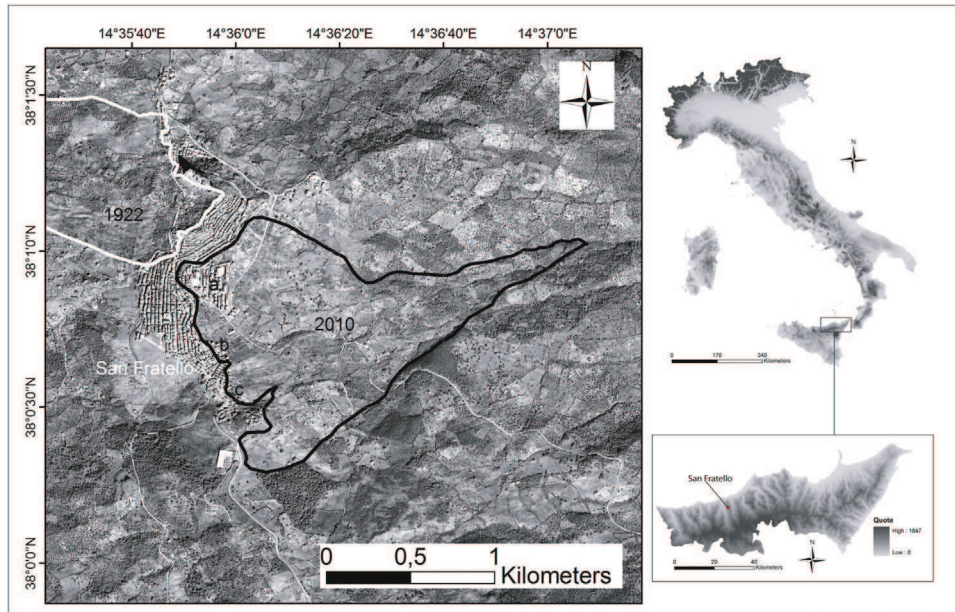


Fig. 1. Location of the study area and 1922 and 2010 landslides boundaries. (a) Stazzone quarter; (b) Riana quarter; (c) San Benedetto quarter.

destroyed the northern sector of the town, while the most recent one took place on the 14th February 2010, affecting the mid-eastern quarters of the town. This latter landslide, which is still active, caused severe damages to buildings and infrastructures with an estimated cost of 300 million Euros for the disaster mitigation and reconstruction program. This work presents an analysis of the San Fratello town building deformation velocities, obtained by the combined of PSI data and buildings map, with the aim of understanding the deformation evolution of the involved structures. In particular, C-band data collected before the 2010 event, were used to evaluate the presence of precursory symptoms of instability, whereas the X-band data, collected after the event, were analyzed in order to detect the residual risks in the post-event phase. Finally, the obtained post-event building deformation velocity map was

compared with the damage assessment map. This application, based on the PSInSAR technique, can be suitable to evaluate how the abundance of the elements at risk in a landslide affected area may change with time, contributing to the risk assessment, which is very important for decision making by Civil Protection Authorities, especially during the landslide post-event phase.

Geological setting

The town of San Fratello is located in the northeastern sector of Sicily (Italy), along the Tyrrhenian coastline (Fig. 1), close to the boundary between the Nebrodi and Peloritani mountain chains. The study area was historically affected by landslides (Goswami et al., 2011; Mondini et al., 2011; Del Ventisette et al., 2012;

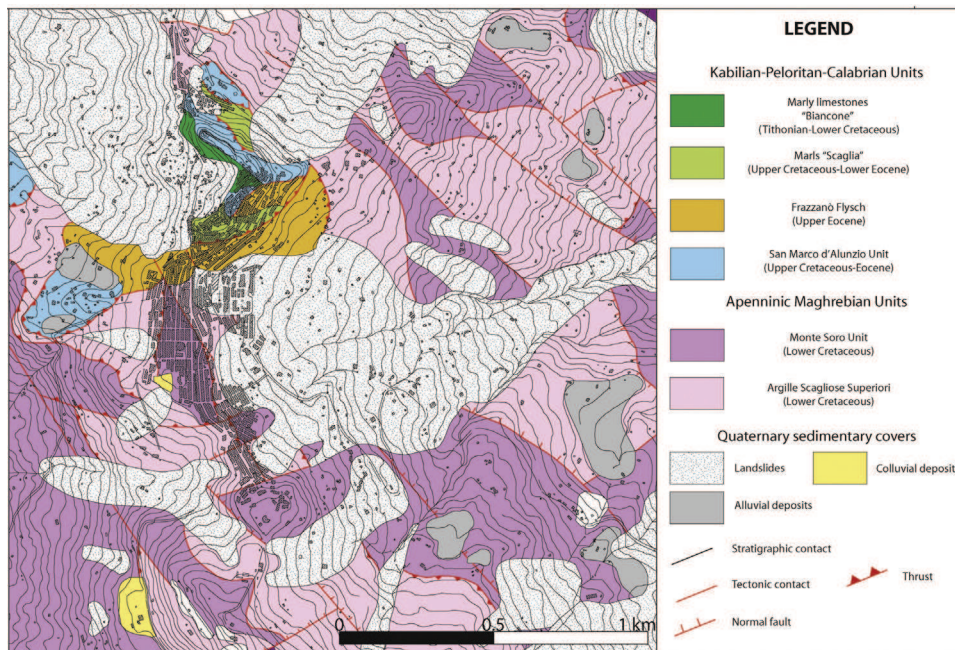


Fig. 2. Schematic geological map of the town of San Fratello (courtesy of DRPC).

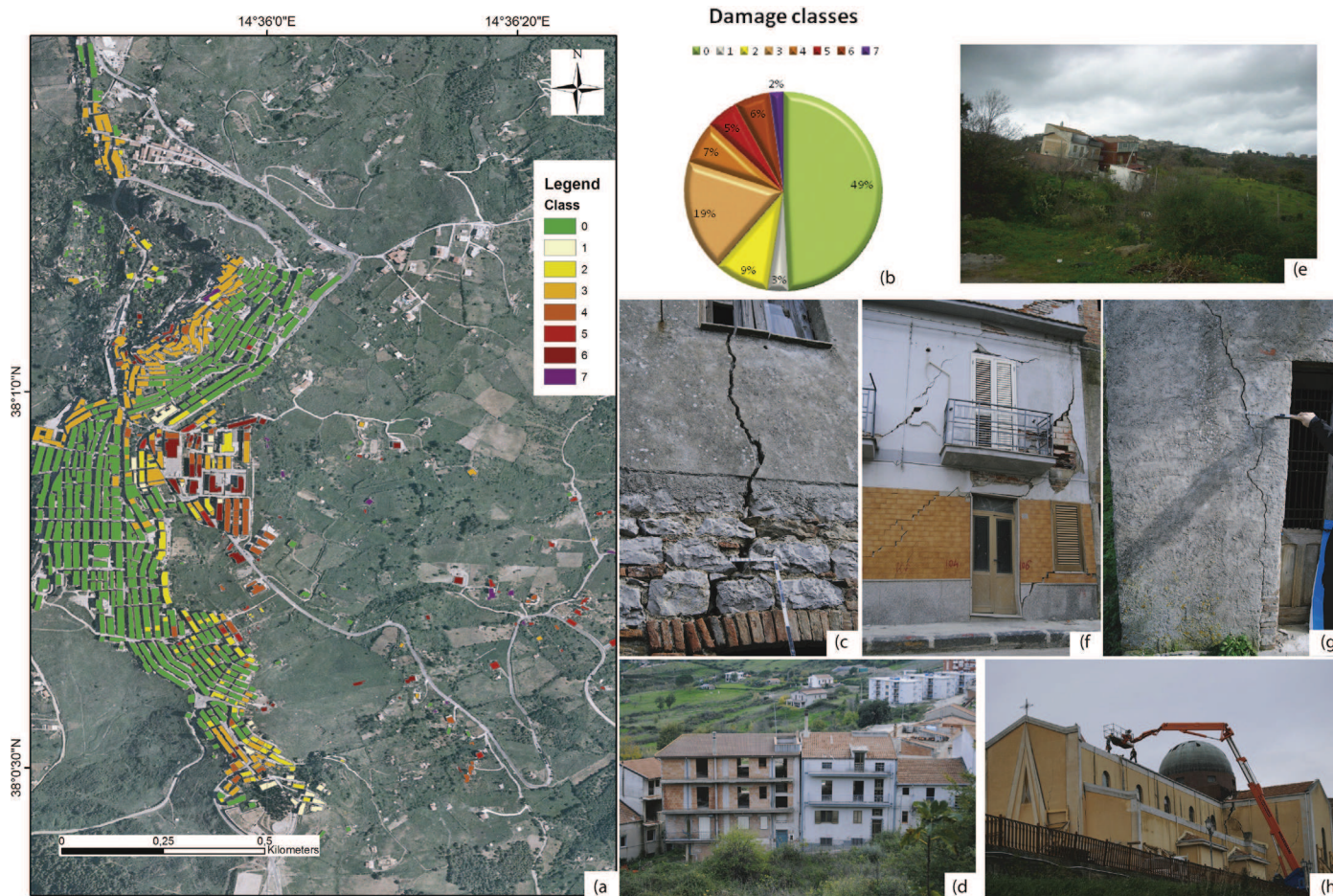


Fig. 3. Damage assessment map of San Fratello according to the degree of damages of Table 1 (a); and the related frequency of buildings considering the degree of damages (b). Some examples of the damages of San Fratello (c) class 3; (d) class 6; (e) class 7; (f) class 5; (g) class 2; (h) class 5.

Table 1
Ranking scheme of building damage categories (modified after Cooper, 2006).

Class	Description
0	No damages.
1	Hairline cracking not visible from outside. Fine cracks, generally restricted to internal wall finishes: rarely visible in external brickwork. Typical crack widths up to 1 mm. Generally not visible from outside.
2	Cracks not necessarily visible externally, some external repointing may be required. Doors and windows may stick slightly. Typical crack widths up to 5 mm. Difficult to record from outside.
3	Cracks that can be patched by a builder. Repointing of external brickwork and possibly a small amount of brickwork to be replaced. Doors and windows sticking, slight tilt to walls, service pipes may fracture. Typical crack widths are 5–15 mm, or several of say 3 mm. Visible from outside.
4	Extensive damage that requires breaking-out and replacing sections of walls, especially over doors and windows. Windows and door frames distorted, floors sloping noticeably; some loss of bearing in beams, distortion of structure. Service pipes disrupted. Typical crack widths are 15–25 mm, but also depends on number of cracks. Noticeable from outside.
5	Structural damage, which requires a major repair job, involving partial or complete rebuilding. Beams lose bearing capacity, walls lean badly and require shoring. Windows broken with distortion. Danger of instability. Typical crack widths are >25 mm, but depend on the number of cracks. Very obvious from outside.
6	Partial collapse. Very obvious from outside.
7	Total collapse. Very obvious from outside.

Table 2
used PS InSAR datasets.

Sensor	Geometry	Time interval	No. of scenes	Density (PS/km ²)
ERS 1/2	Ascending	11/09/92–05/06/00	34	6.55
ERS 1/2	Descending	01/05/92–08/01/01	70	46.45
ENVISAT	Ascending	22/01/03–22/09/10	65	64.74
ENVISAT	Descending	07/07/03–13/09/10	49	20.41
RADARSAT	Ascending	30/012/05–26/01/10	47	85.86
RADARSAT	Descending	31/01/06–03/02/10	47	85.86
COSMOSky-Med	Descending	16/05/11–02/05/12	32	400.62
TERRASar-X	Descending	28/10/11–22/09/12	30	813

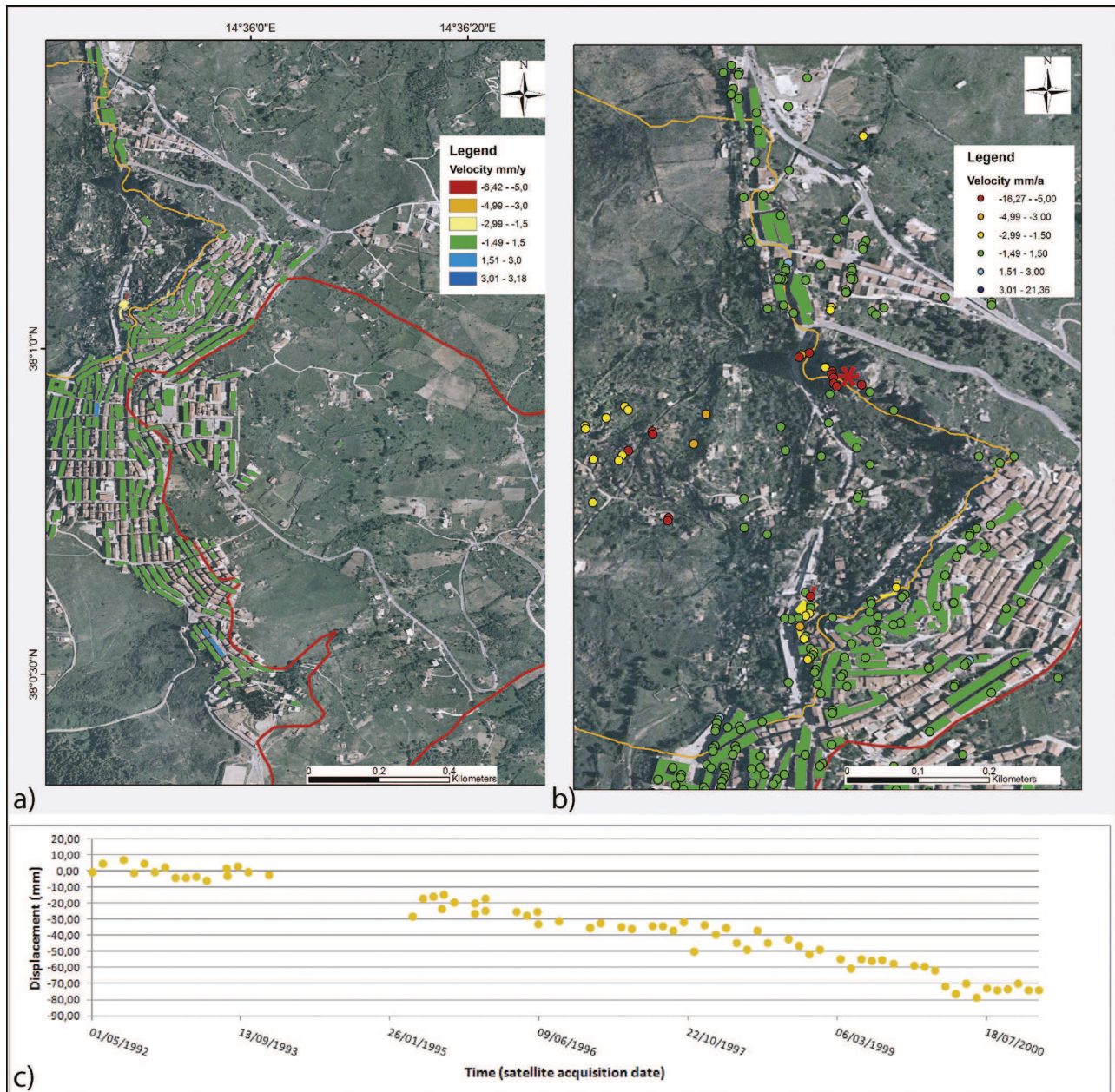


Fig. 4. (a) Buildings deformation velocity map obtained using ERS 1/2 descending data. (b) Details of the 1922 landslide with the PS dataset. The red asterisk stands for the PS time series of (c). The red line corresponds to the 2010 landslide boundary; the orange line corresponds to the 1922 landslide boundary.

Bianchini et al., 2014b). The oldest documented one occurred in 1754, destroying the north-eastern part of the town, medieval in age. The 8th of January 1922 another large landslide seriously damaged the north-western quarters, causing the town delocalization. The most recent landslide occurred on February 14th 2010 causing several damages to buildings and infrastructures. This landslide affected the eastern sector of the town, determining the evacuation of more than 2000 people. From a geomorphological point of view San Fratello is located at about 650 m a.s.l. along a N–S oriented divide on which both the west and east facing slopes are characterized by a steep gradient and creek erosion at their toe.

From a geological point of view, the study area is part of the collisional system, developed since the Late Cretaceous, as the result of the convergence between the European and African-Adriatic plates (Corrado et al., 2009). The study area is characterized by the presence of two main structural domains: the

Kabalian-Peloritan-Calabrian units at northeast, overthrust on the Apenninic-Maghrebian domain to the southwest (Lentini et al., 2000; Lavecchia et al., 2007). The Kabalian-Peloritan-Calabrian units are made of imbricate sheets of Paleozoic metamorphic and igneous rocks and the related Mesozoic sedimentary cover (Somma et al., 2005). These units, cropping out within the Peloritani mountains, are covered by Upper Oligocene-Lower Burdigalian deposits (Lentini et al., 2000). The Apenninic-Maghrebian domain crops out in the Nebrodi Mountains and is made of imbricate sheets of Mesozoic-Tertiary sedimentary rocks. The boundary between these two domains, corresponds to the limit between the Peloritani and Nebrodi mountain chains; this boundary is represented by an active frontal thrust marked by the Longi-Taormina lineament (Catalano et al., 2006; Billi et al., 2007). San Fratello is located in proximity to this fault (Fig. 2). The rocks outcropping within the San Fratello area consist of a Cretaceous-Oligocene terrigenous-flyschoid to

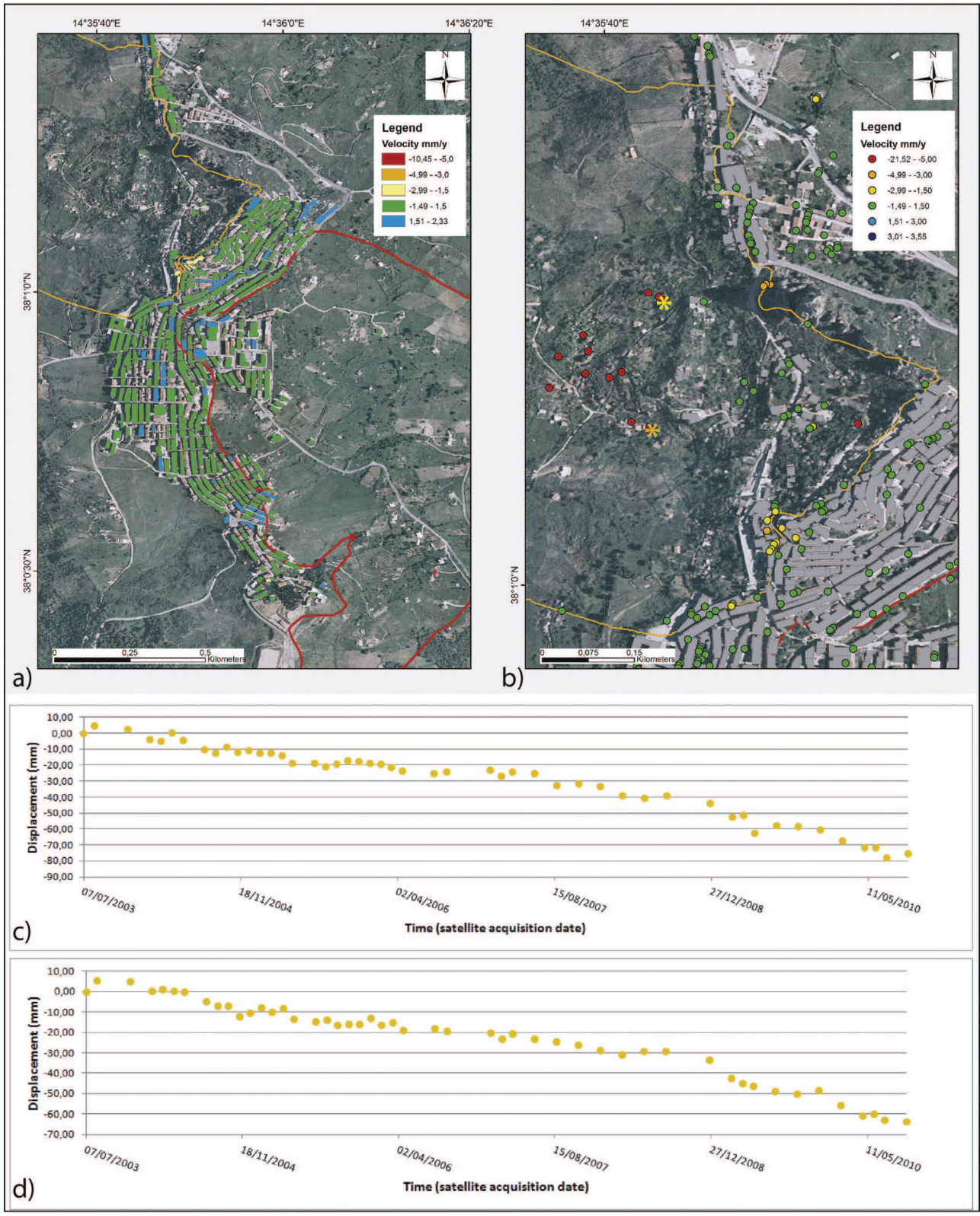


Fig. 5. (a) Building deformation velocity map using both ascending and descending ENVISAT datasets. (b) ENVISAT PS dataset related to the 1922 landslide with two selected time series (c and d). (c) Corresponds to the yellow asterisk; (d) corresponds to the orange asterisk.

calcareous sedimentary sequence. In particular, the western and southern part of the study area is mostly characterized by terrigenous terrains, represented by the Appeninic-Maghrebid Units (clays alternating with sandstones and clayey-marly formations).

In the northern portion of the area, the uppermost units (Kabilo-Calabride Units) crop out, occurring as Liassic carbonate platform sequences overlapped by a terrigenous Late Eocene-Oligocene Flysch. Cretaceous pelagic dolostones and limestones (San Marco

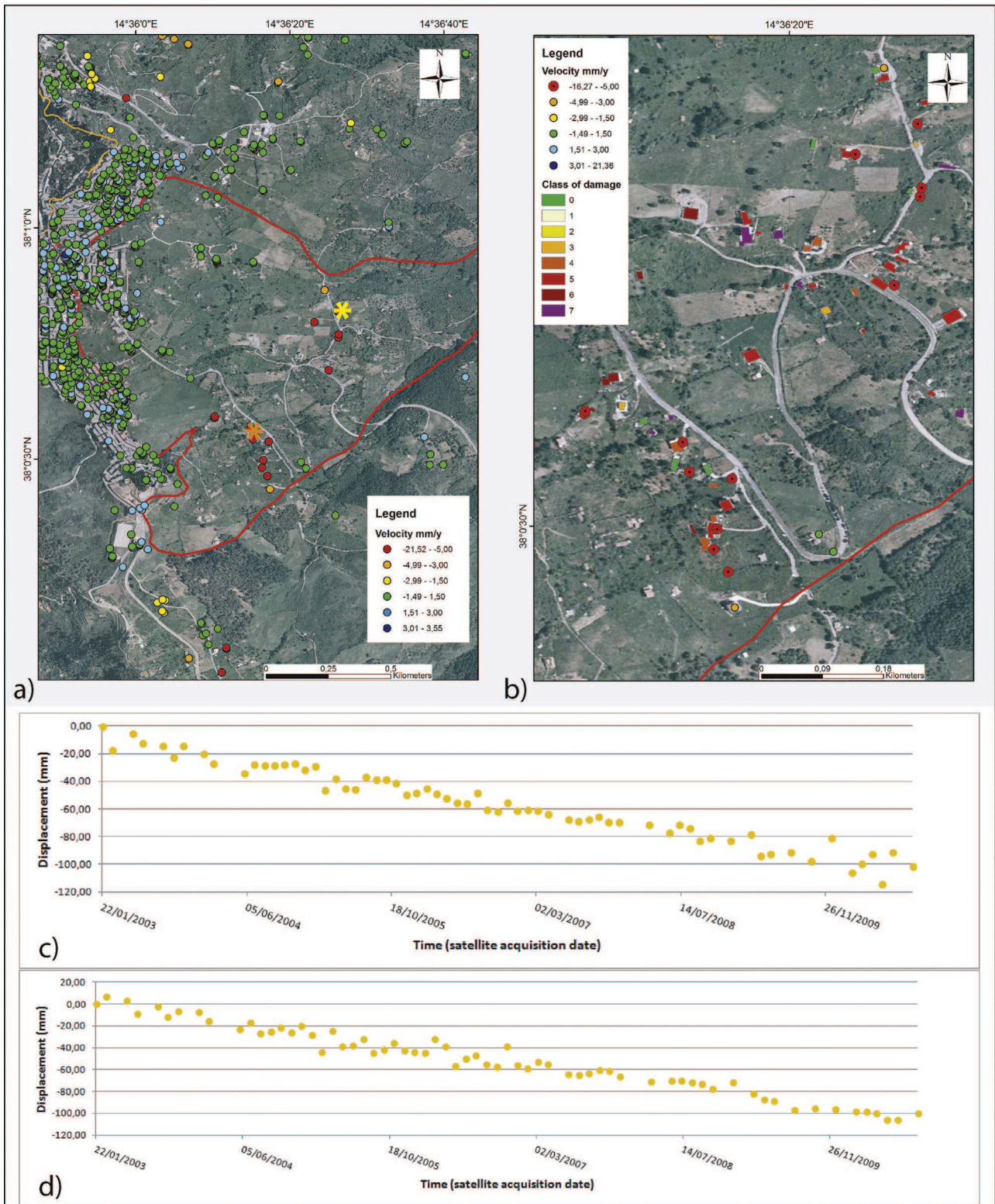


Fig. 6. (a) ENVISAT ascending PS dataset; (b) comparison between the ground deformation velocity map and the damage assessment map; (c) time series correspondent to the yellow asterisk; (d) time series correspondent to the orange asterisk.

D'Alunzio Unit) crop out in the N-NE sector of San Fratello (Giunta et al., 2000; Lavecchia et al., 2007). The poor geotechnical properties of the clay-silt and flyschoid lithotypes are one of the triggering factors of the landsliding phenomena, combined with the steep topography and the occurrence of intense rainfall events.

Methodology

Damage assessment map

The damage assessment map was performed after an accurate field survey, covering the whole town area of San Fratello. A total

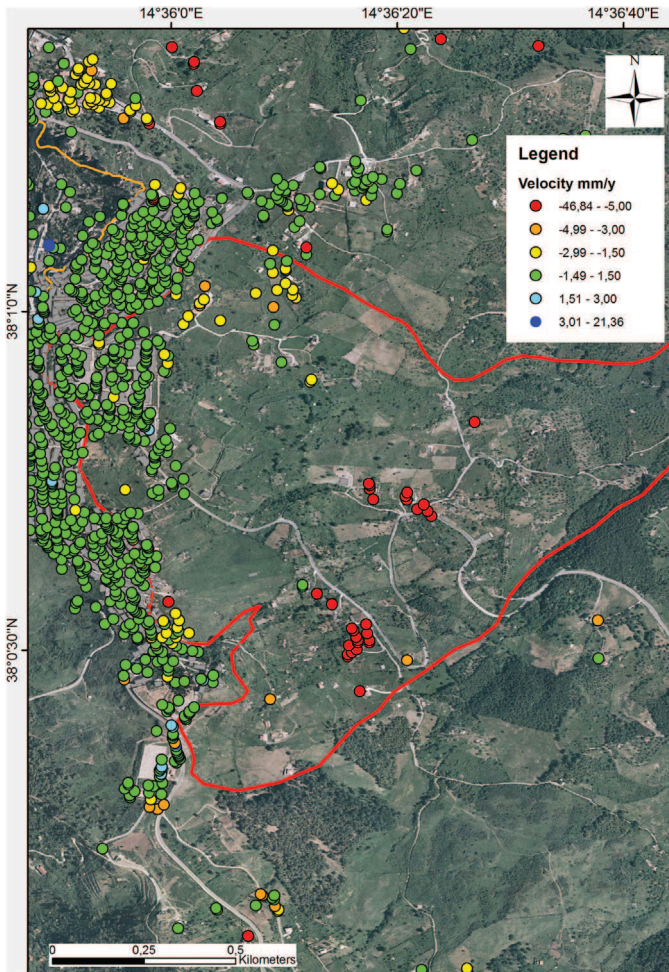


Fig. 7. Building deformation velocity map using both ascending and descending RADARSAT-1 datasets.

amount of 738 buildings were mapped on the basis of the damages observable on their walls and facades. Buildings interior damages were evaluated by interviewing the local inhabitants. The degree of damages for each building was evaluated using a modified version of ranking scheme of building damage categories of Cooper (2006) (Table 1).

Radar interferometry

Spaceborne Interferometric radar approach represents a powerful tool to detect movements on the Earth's surface. Mapping geomorphologic processes and monitoring slope instability can greatly benefit from satellite data analysis due to the great cost–benefits ratio, non-invasiveness, wide area coverage and high precision. Spaceborne InSAR can offer a useful support in the detection and characterization of slow surface displacements, providing rapid and easily updatable ground velocity measurements, along the satellite line of sight (LOS). Multi-interferometric InSAR technique has turned out to be a valuable and successful tool to detect and measure surface displacements with millimeter accuracy, and also to reconstruct the deformation history of the investigated areas (Bovenga et al., 2006; Colesanti and Wasowski, 2006; Cascini et al., 2009; Cigna et al., 2011; Hung et al., 2011; Bianchini et al., 2012; Ciampalini et al., 2012; Raspini et al., 2012; Del Ventisette et al., 2014; Bianchini et al., 2014b). In the last 20 years, several different radar satellite missions were launched, providing different

types of SAR images to be used for ground movement detection and monitoring. Consequently, today many satellite interferometric data are available, including both historical archives, acquired since the early 1990s (e.g. ERS 1/2, ENVISAT), and images from currently operating satellites (e.g. TerraSAR-X, COSMO-SkyMed), spanning a time interval of more than 20 years, which can allow the analysis of both past and recent ground displacements of the observed scenes (Bianchini et al., 2012). PSInSAR can be used to analyze archival SAR data, providing annual velocities and deformation time series on grids of stable reflective point-wise targets, called Persistent Scatterers (PS), characterized by a coherent electromagnetic behavior in all the radar images (Ferretti et al., 2001). Several of these PS correspond to hand-made artifacts, such as buildings, railways or highways, making this method suitable for the monitoring of urbanized areas where the density of the PS is higher. This can provide exclusive information for an improved understanding of the long term behavior of slow and very-slow ground deformation phenomena (Del Ventisette et al., 2013). PSI analysis, properly integrated with auxiliary data, has been mainly used for mapping and monitoring slow-moving landslides, and for evaluating their state of activity and intensity (Ferretti et al., 2000; Meisina et al., 2008; Herrera et al., 2009, 2010; Guzzetti et al., 2009; Notti et al., 2010; Righini et al., 2012; Bianchini et al., 2014b). The recorded displacements are measured considering a ground point of known coordinates, called reference point, considered stable on the basis of the geological knowledge of the area. Satellite sensors are side-looking and acquire images in two different geometries, following an approximately N–S direction and a perpendicular line of sight (LOS). For this reason, sensors moving from south to north acquire in ascending geometry and are more suitable to detect movements located on west facing slopes. On the contrary, sensors moving from north to south acquire in descending geometry making them suitable for the observation of east-facing slopes. Five different sensors were used to monitor the buildings of San Fratello: ERS 1/2, ENVISAT, RADARSAT-1, COSMO-SkyMed (CSK) and TerraSAR-X (TSX) (Table 2) covering a very long interval of time, spanning from 1992 up to 2012. Satellite SAR data were processed by T.R.E. (Tele Rilevamento Europa). The ground deformation velocity of each building was calculated considering the average velocity of all the PS included in the polygon corresponding to the building. The calculation was performed for each C- and X-band dataset. To avoid problems related to a possible shift between the buildings and the PSI layers, due to a non-extremely accurate georeferencing process, PS located in a range of 2 m outside the buildings were included in the calculation of the average velocity. Furthermore, the use of these 2 m wide buffer improved the number of usable PS. Considering the ground deformation velocity, a stability threshold was chosen between ± 1.5 mm/y for the C-band data and ± 2 mm/y for the X-band data. These thresholds were decided on the basis of both the investigated phenomena (slow moving) and the standard deviation of the PS population.

Results

Damage assessment map

The damage assessment map (Fig. 3) reports the degree of damages of a total of 738 buildings classified following the scheme reported in Table 1. The map shows that more than half of San Fratello buildings are affected by damages caused by slope instability; amongst them 20% of buildings are strongly damaged (more than class 4). The most affected areas are located on the town eastern slope, within the Stazzone quarter and East of the city center (Fig. 3a). In these areas, also some of the most recent buildings collapsed or were damaged to the point that they required to be

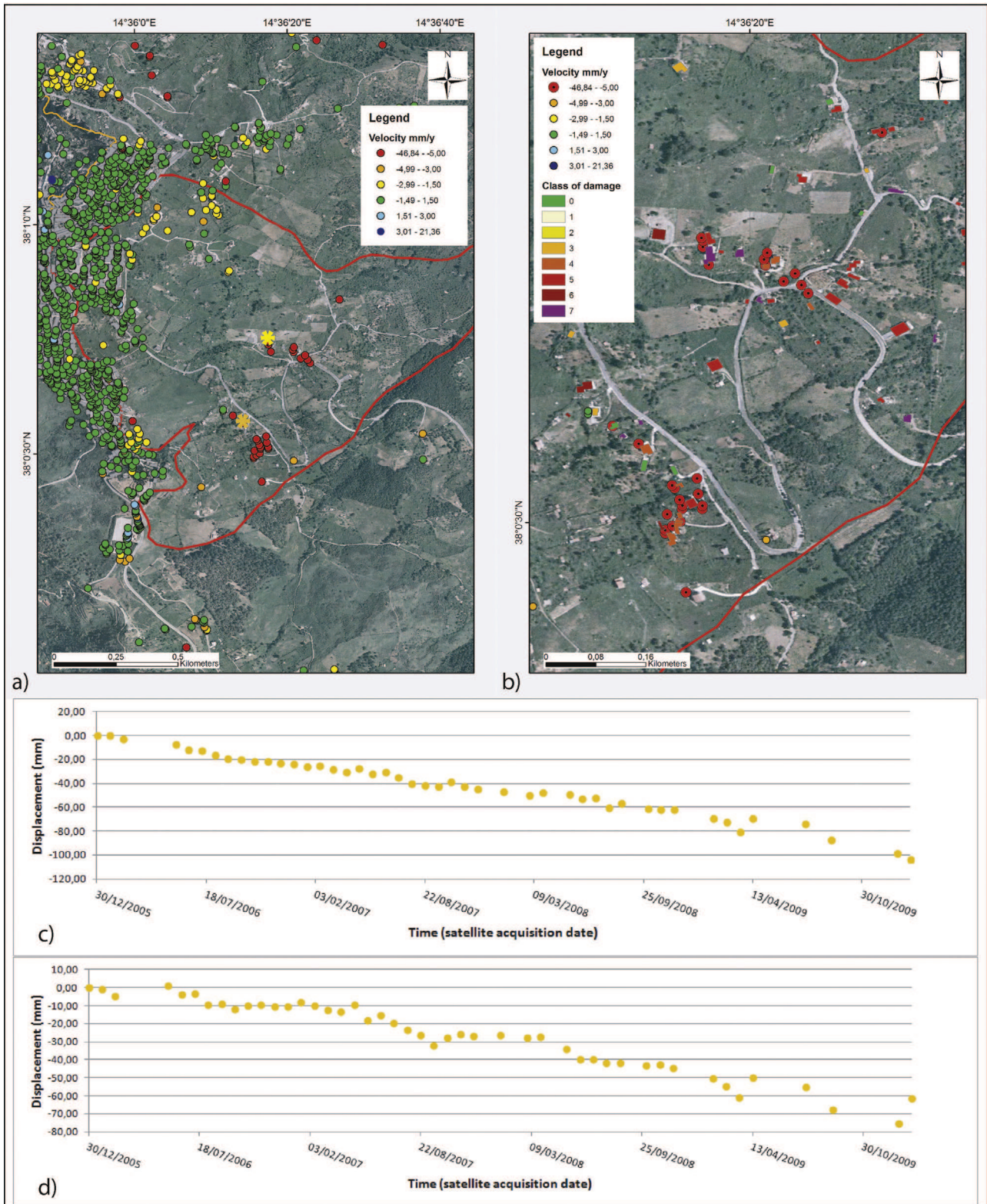


Fig. 8. (a) RADARSAT-1 ascending PS dataset; (b) comparison between the ground deformation velocity map and the damage assessment map; (c) time series correspondent to the yellow asterisk; (d) time series correspondent to the orange asterisk.

demolished. Intense damages can be observed also in the Riana and San Benedetto quarters along the 2010 landslide crown (Fig. 3e). The field surveys revealed also the presence of several damaged buildings located in the northwestern part of town, corresponding to the 1922 landslide crown area.

Radar interferometry

ERS 1/2 (1992–2001)

The buildings deformation velocity maps using the ERS 1/2 datasets highlight that no buildings located in the area of the 2010

landslide are affected by deformation, however a maximum of 178 (24.12%) buildings were mapped using the descending dataset (Fig. 4a). Along the 1922 landslide crown, some buildings show a deformation velocity, which is consistent with the damages observed on their walls and facades. In this case, the extent of the area affected by deformation is underestimated. A better result can be obtained by the observation of the whole PS dataset (Fig. 4b). PS targets clearly show the presence of at least two other areas characterized by ground deformation, one located along the 1922 landslide crown (Fig. 4a), where the mean deformation velocity is up to -9 mm/y (Fig. 4b and c), and another one within the landslide body (Fig. 4b).

ENVISAT (2003–2010)

The use of the ENVISAT datasets allowed the mapping of up to 279 (37.80%) of the town buildings. The related building deformation velocity map (Fig. 5a) is very similar to those obtained with ERS 1/2 datasets. Results highlight a substantial stability of the town. A very small amount of buildings is characterized by deformation velocities outside the stability range. Along the eastern slope, only one edifice shows an average velocity of -10 mm/y. On the western slope, along the 1922 landslide crown, the buildings affected by deformation are almost the same of those highlighted by the map obtained with ERS 1/2. The use of ENVISAT sensor increased the number of monitored buildings; however, these PS data were still not suitable to detect possible ground displacements to be considered as landslide precursors. Also in this case using the whole PS datasets it was possible to retrieve more information about slope instability (Fig. 5b). Along the western town sector the area affected by ground deformation could be better recognized using PS which highlighted the presence of a wide area affected by deformation, located along in the eastern sector of the 1922 landslide (Fig. 5b). The most interesting information obtained using the ENVISAT data concerns the ground deformation of the eastern slope (Fig. 6a). Here two areas, showing clusters of PS characterized by high ground deformation velocities, can be recognized. Even though both these areas are located inside the 2010 landslide body, including a very low number of buildings, the number of PS is sufficient to highlight ground deformation. The comparison between the PS and the damage assessment map shows a good agreement between the distribution of the PS having the highest velocities and the most damaged buildings by the 2010 landslide (Fig. 6b).

RADARSAT-1 (2005–2010)

RADARSAT-1 data can be used to confirm the results obtained by ENVISAT data due to the partial overlapping of their temporal coverage. The main advantage of the use of RADARSAT-1 is represented by the higher density of PS that allows mapping the deformation velocity of almost the half (48.37%) of the monitored buildings. Results clearly highlight three areas where buildings are affected by deformation (Fig. 7). The first area is located within the eastern slope, confirming the results of ENVISAT data. In addition, the deformation of the edifices located along the 1922 landslide crown is confirmed. The third area corresponds to the San Benedetto quarter, where four buildings show velocities slightly higher than the stability range. Considering the whole PS RADARSAT-1 ascending dataset (Fig. 8a), the area affected by ground deformation located within the eastern slope is clearly recognizable. Also, in this case, the agreement between the ground deformation velocities and the damage assessment map is good (Fig. 8b), confirming the usefulness of the C-band sensors relatively to this area, where the buildings affected by severe damages are surrounded by PS showing the highest velocities. Also along the western slope, RADARSAT-1 confirms the results obtained by ENVISAT highlighting the presence of ground deformation within the body and along the 1922 landslide crown.

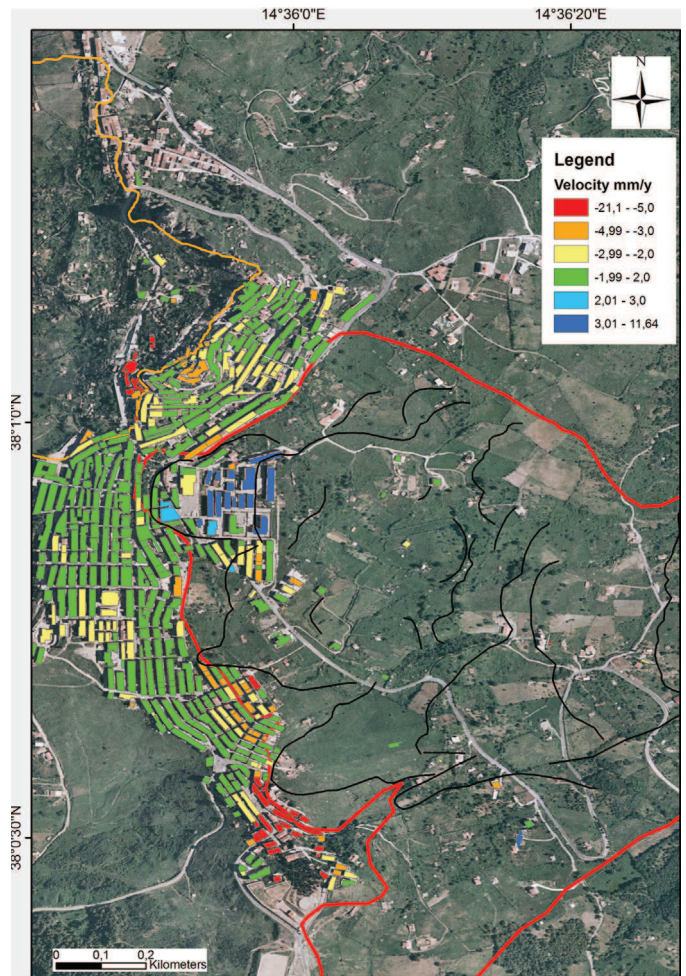


Fig. 9. Building deformation velocity map using both ascending and descending COSMO-SkyMed datasets. The black lines correspond to the secondary scarps developed during the 2010 landslide.

COSMO-SkyMed (2011–2012)

CSK images were acquired after the 2010 landslide, thus they can be useful to evaluate possible post-event ground deformation phenomena. The available data were acquired only in descending orbit, making them suitable especially to study the deformation of the western slope. Anyway, the high density of the PS allowed to retrieve also interesting information about the eastern slope deformation. The stability range for CSK data was increased to ± 2 mm/y because of the higher average standard deviation of PS velocity, if compared to those of the C-band data. The increase of the standard deviation is related to the short acquisition period (only one year) and to the location of San Fratello, which turns out to be far from the reference point and at the boundary of the used SAR images. In this case, the building deformation velocity map permits to recognize three different areas (Fig. 9), along the 2010 landslide crown, where several buildings are affected by a considerable deformation. These areas correspond, from north to south, to the Stazzone, Riana and San Benedetto quarters, which were intensely damaged during the event. The difference in colors between the Stazzone and San Benedetto quarters, that represent different displacement direction, is related to the different position of the areas within the 2010 landslide. Buildings that are moving toward the satellite characterize Stazzone quarter, whereas in San Benedetto the edifices are moving away with respect to the sensor. The first ones are located inside the landslide body, whereas the second ones are placed along the landslide crown.

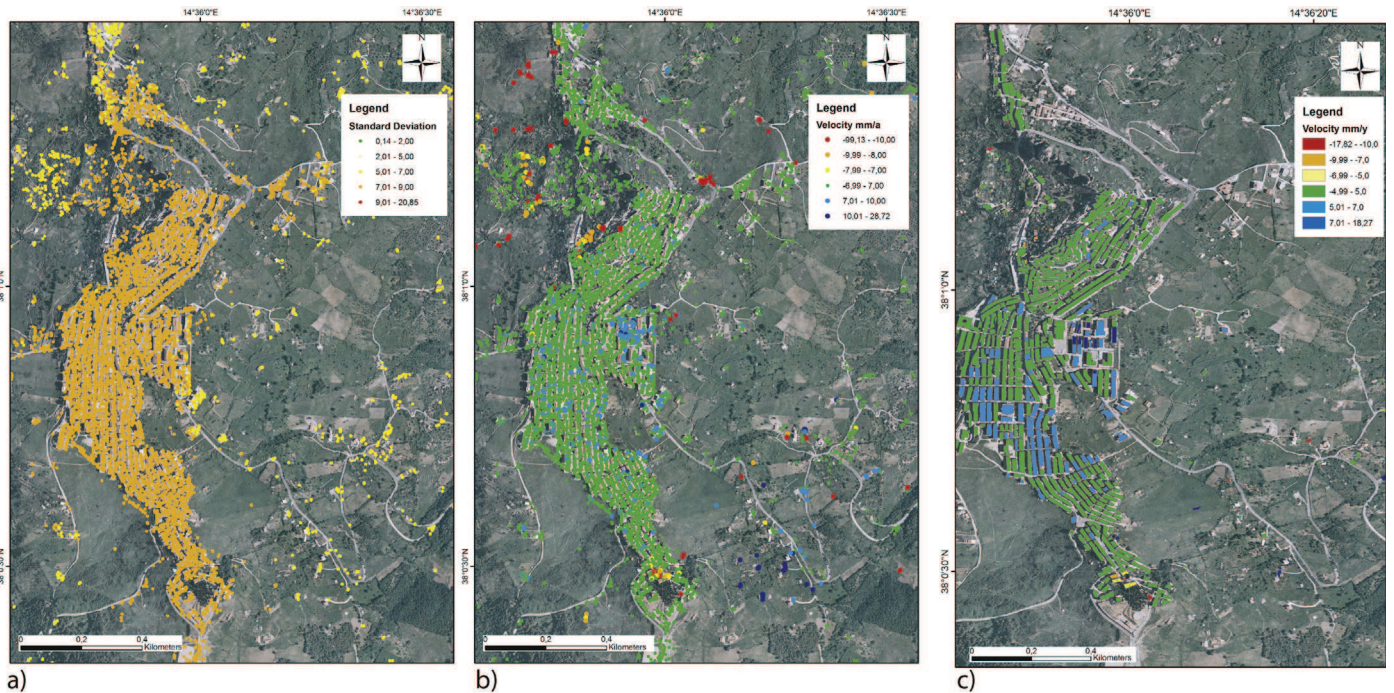


Fig. 10. Standard deviation (a), ground deformation velocity map with ± 7 mm/y stability range (b) and building deformation velocity map with ± 5 mm/y stability range (c) using the descending TerraSAR-X dataset.

The fractures patterns developed on the building facades suggest that Stazzone is moving downhill, on the contrary part of the building located within the San Benedetto is characterized by mainly vertical movement. This is consistent with the geometry of the landslide, which is rotational in the upper part and translational downward. Another interesting result is represented by the presence of a strip, located along the crown of the 1922 landslide, characterized by several buildings showing high deformation velocities. These edifices present well developed fractures on their facades, confirming that this area is interested by slow but continuous ground deformation. The comparison between the building deformation velocity map, obtained using CSK data, and the damage assessment map shows a very good agreement, confirming that the most intensely damaged area during the 2010 landslide are, today, characterized by residual movements, which compromise their stability. Several of these buildings were recently evacuated and some of them completely demolished. The measurement of the velocities related to residual movements must be used with caution because of the high standard deviation.

TerraSAR-X (2011–2012)

The available TSX data were acquired between October 2011 and December 2012. Part of the acquisition period is overlapped with that of the CSK data. This dataset is affected by a very high standard deviation, especially in correspondence of San Fratello town area, where the average standard deviation is 7.6 (Fig. 10a and b). These high values depend on several factors (e.g. the choice of the reference point, the short acquisition period, the topographic factor and the position of the area, located close to the boundary of the SAR images). For these reasons, TSX data could not be used to calculate the building deformation velocities. However, some consideration about the ground deformation can be made considering as not moving the areas resulting stable from CSK. A differential analysis can be useful to highlight areas affected by ground deformation. In this case, the applied stability threshold was selected between ± 7 mm/y, considering the standard deviation. Results suggest that almost three areas of the town are affected by ground deformation:

the northern one is located along the crown of the 1922 landslide, the second one is represented by part of the Stazzone quarter and the southern one corresponds to the San Benedetto quarter (Fig. 10c). Ground displacements highlighted by TSX confirm the results obtained using CSK but, considering the standard deviation, the evaluation of the ground deformation velocities can be made only with the last one.

Reprocessed X-band data

Considering the interesting results highlighted by X-band sensors, the TSX and CSK datasets were reprocessed, choosing a different reference point, in order to minimize the standard deviations. The new reference points were located inside San Fratello, in correspondence of buildings considered stable. This procedure allowed a more accurate measurement of building deformations velocities. During the reprocessing of the CSK data, several PS, located in the western part of the town were lost, but the building deformation velocity map clearly shows that Stazzone and San Benedetto quarters are affected by important deformations (Fig. 11). In addition the reprocessed TSX data (Fig. 12) confirmed that these two areas are subjected to ground deformations, especially San Benedetto where the extent, the geometry of the deformations and the average velocities are comparable to the CSK data. TSX data can be useful also to observe the deformations located along the western slope, where several buildings show high velocities.

Discussion

Landslides may affect different kind of buildings in different ways. Construction methods, with regard to depth of foundations and used material, can counteract the development of the damages caused by ground displacement. This fact is fundamental to be taken into account in a town such as San Fratello, where very different kinds of buildings are present. San Fratello town is composed by historical buildings made of bricks, having very shallow foundations, as well as recent buildings with deeper foundations and

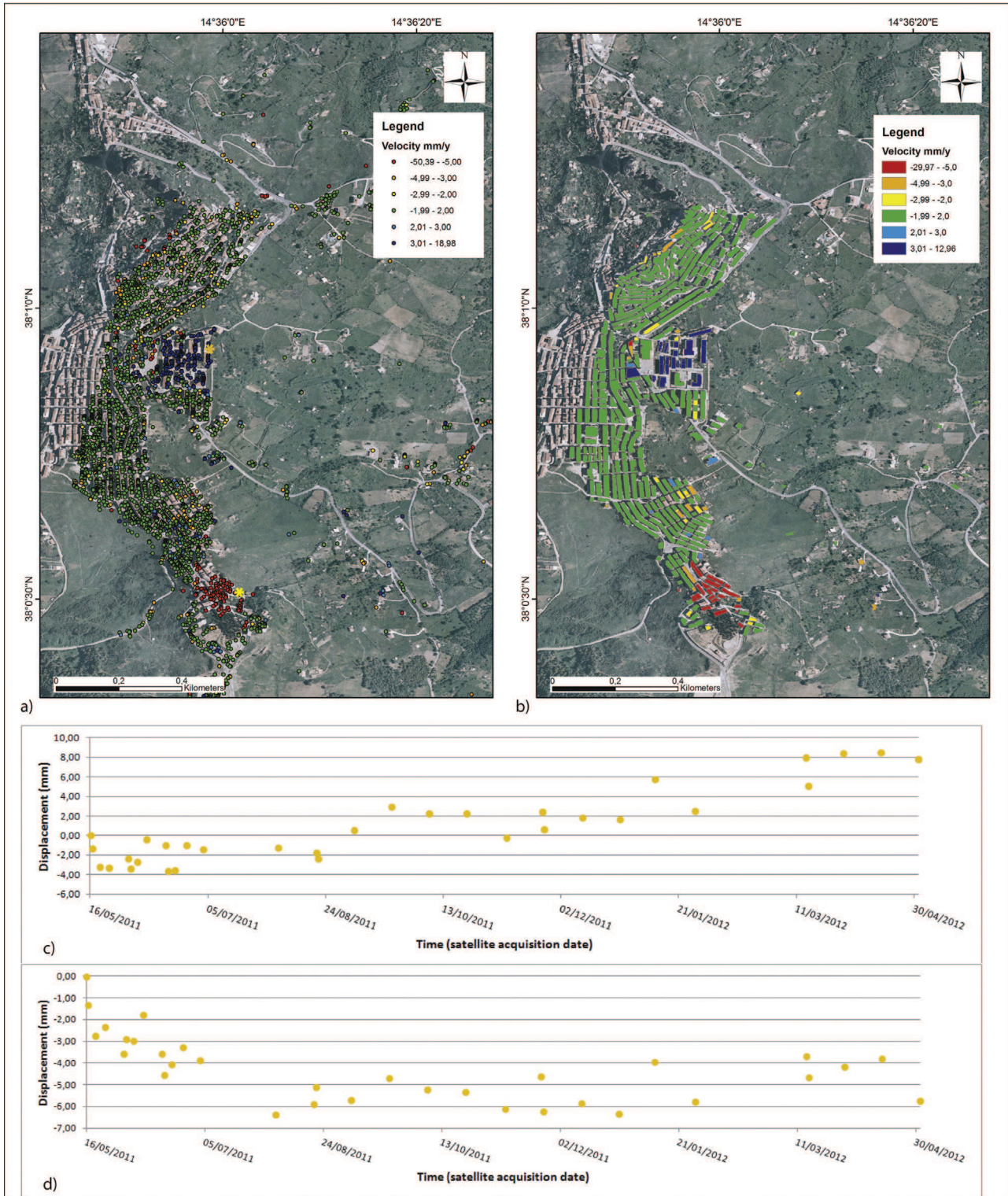


Fig. 11. (a) CSK ground deformation velocity map; (b) building deformation velocity map obtained by using CSK data; (c) time series correspondent to the orange asterisk and (d) time series correspondent to the yellow asterisk.

a reinforced concrete structure. After the 2010 landslide the first ones show various degrees of damages, going from well-developed fractures on their walls and facades, distortion of windows and door frames, up to the structural partial or total collapse (Fig. 3). The more recent buildings stood up well to the landslide induced deformations, but in some cases, they show a rotation of the whole structure. The combined use of the buildings map and the PS radar

datasets (Table 3) highlighted that the PS density is a fundamental parameter in order to evaluate the feasibility of this application for building monitoring activities. Only the X-band datasets, bearing a high target density ($\gg 200$ PS/km²), resulted useful to understand the displacement velocities of at least more than the half of the buildings of the San Fratello town. Anyway, some information were also retrieved by RADARSAT-1 datasets. The number of

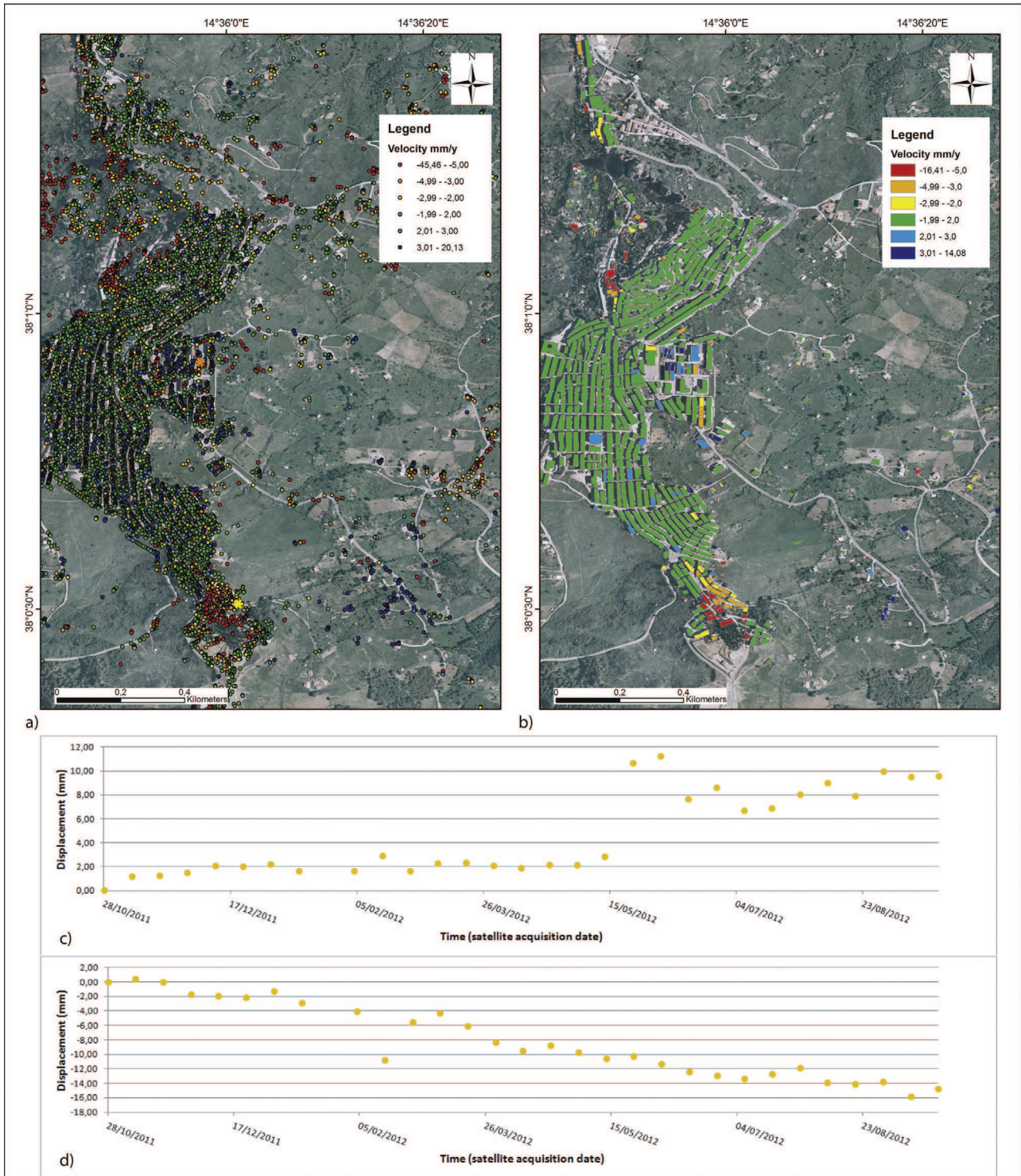


Fig. 12. (a) TSX ground deformation velocity map; (b) building deformation velocity map obtained by using TSX data; (c) time series correspondent to the orange asterisk and (d) time series correspondent to the yellow asterisk.

monitored buildings was sensibly improved considering a buffer of 2 m for each building. The size of the buffer was decided considering the proximity among the buildings. A wider buffer can lead to consider PS belonging to another building, especially in the city center, where several streets are very narrow. The use of a 2 m wide buffer allowed a considerable PS number improvement, which were used to calculate the buildings deformation velocity (Table 4). This improvement was observed for all the dataset even if

the C-band sensors (ERS 1/2 and ENVISAT) were still characterized by a low percentage of monitored buildings. Only RADARSAT-1, among the C-band sensors, permitted the monitoring of a sufficient amount of buildings. When the percentages of monitored buildings were less than 40%, the use of the whole PS dataset was considered more appropriate in order to avoid the loss of information. The comparison between the building deformation velocity maps, highlights that before the 2010 event, all the C-band satellites

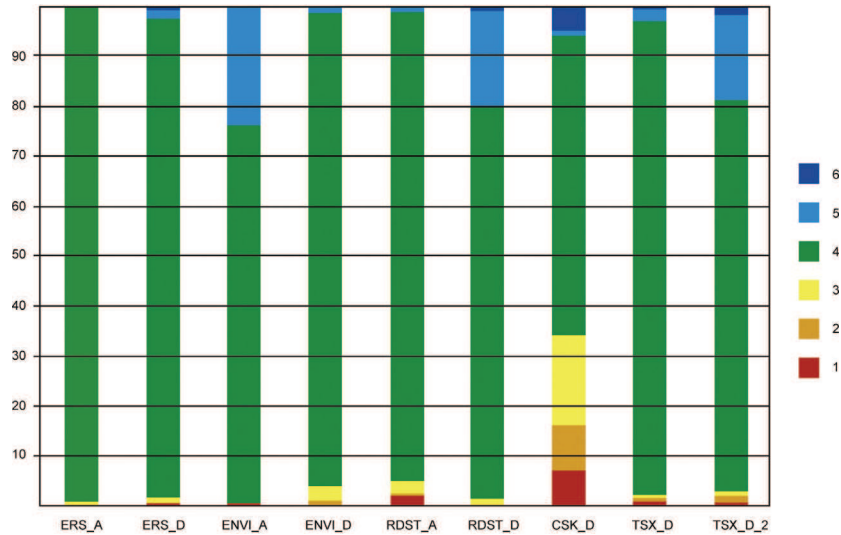


Fig. 13. Percentages of buildings monitored with the available sensors considering the used velocity (in mm/y) classification described in the previous paragraphs. For C-band sensors: class 1: <-5; class 2: -4.99 to -3.00; class 3: -2.99 to -1.5; class 4: -1.49 to 1.5; class 5: 1.51-3.00; class 6: >3. For CSK: class 1: <-5; class 2: -4.99 to -3.00; class 3: -2.99 to -2.0; class 4: -1.99 to 2.0; class 5: 2.01-3.00; class 6: >3. For TSX.D: class 1: <-10; class 2: -9.99 to -8.00; class 3: -7.99 to -7.0; class 4: -6.99 to 7.0; class 5: 7.01-9.00; class 6: >9; for TSX.D.2: class 1: <-10; class 2: -9.99 to -7.00; class 3: -6.99 to -5.0; class 4: -4.99-5.0; class 5: 5.01-7.00; class 6: >7.

Table 3
Results of the interpolation between the considered PS datasets and the buildings map using a simple intersection.

Dataset	No. of PS	PS/km ²	No. of buildings	%
ERS 1/2.asc	63	35	45	6.10
ERS 1/2.desc	247	137.2	128	17.34
ENVISAT.asc	418	232.2	199	26.97
ENVISAT.desc	115	63.89	75	10.16
RADARSAT-1.asc	298	165.56	203	27.51
RADARSAT-1.desc	480	266.67	259	35.10
COSMO-SkyMed.desc	1447	803.89	405	54.95
TerraSAR-X	1567	870.56	442	59.98

Table 4
Results of the interpolation between the considered PS datasets and the buildings map using an intersection with a 2 m tolerance.

Dataset	No. of PS	PS/km ²	No. of buildings	%
ERS 1/2.asc	149	82.22	101	13.69
ERS 1/2.desc	359	199.44	178	24.12
ENVISAT.asc	634	352.22	279	37.80
ENVISAT.desc	310	172.22	170	23.04
RADARSAT-1.asc	653	362.78	357	48.37
RADARSAT-1.desc	757	420.56	348	47.15
COSMO-SkyMed.desc	3036	1686.67	506	68.56
TerraSAR-X	4718	2621.11	608	82.38

indicate a substantial stability of the town (Fig. 13). In particular, up to the 96% of the monitored buildings with ERS 1/2 are characterized by velocities included within the stability range. Despite of the low number of monitored edifices, the ground deformation velocity maps for the eastern slope also confirm these results: no significant deformations were observed. The number of buildings affected by higher deformation velocities increases considering ENVISAT and RADARSAT-1. This increase can be related to the higher PS density. The ground deformation velocity maps obtained using ENVISAT and RADARSAT-1 suggest that the area corresponding to the 2010 landslide body was affected by ground deformation. Thanks to the higher PS density of RADARSAT-1, the instability can be also appreciated in the related building deformation velocity map. The number of buildings affected by deformation increases sensibly considering the X-band sensors, especially with regards to CSK, which highlights that only 60% of the monitored buildings are

characterized by velocities within the stability range. These results are confirmed by the comparison between the building deformation velocity map and the damage assessment map. Buildings characterized by the highest residual velocities are located in the area affected by the 2010 landslide. A direct correlation between the deformation velocity and the degree of the damage was not observed because of the type of building affects their response to the deformation. For example, modern buildings having reinforced concrete foundations better resist to the stress with respect to the historical buildings. The X-band data highlighted the presence of considerably residual movements along the eastern slope even two years after the event. TSX data can be used with caution because of their high standard deviation, which makes PS velocities not reliable. Only a differential analysis can be performed to highlight moving areas with respect to stable areas. The TSX building deformation velocity map confirmed the same areas affected by ground deformation detected by CSK. An improvement in the measured velocities accuracy was obtained thanks to the reprocessing of the X-band datasets. Using these datasets, it was possible to reduce the standard deviation and to evaluate the deformation velocities more accurately. Interesting results were obtained also along the 1922 landslide crown. In this area, slow but continuous deformation was detected since 1992. In this sector, the correlation between the damaged buildings and the building deformation velocity map is very high. Some evidences of deformations of the edifices can be observed also using C-band sensors, but the lower PS density suggests that the use of the ground deformation velocity map is more suitable.

Conclusions

PSInSAR technique, using five different sensors, was successfully used to evaluate the building deformation velocities of the San Fratello municipality, which was affected by two landslides occurred in 1922 and 2010 respectively. The C-band data were acquired before the 2010 event, in order to observe the presence of landslide precursory symptoms, whereas X-band satellite radar data were acquired during the post event phase, with the aim of detecting the landslide residual risk.

The advantages of the X-band data are represented by the high PS density, which allowed to measure the deformation velocity of

a large number of the surveyed buildings (more than 80%). On the contrary, the C-band satellites were characterized by a low percentage of mapped edifices. Only RADARSAT-1 data seemed to be effective in order to understand possible presence of deformation areas within the San Fratello town. The low density of the C-band sensors suggests that the use of the ground deformation velocity map is more suitable with respect to the building deformation velocity map. Using the latter, several information about ground deformation can be lost, in case of several PS do not correspond to buildings. Usually X-band SAR images are most expensive but, at the local scale, the advantages of the higher PS density is much greater in terms of obtained results.

This work proves the effectiveness of the combined use of ground and building deformation velocity maps to understand the behavior of landslide phenomena during the pre- and post-event management phase. In particular X-band data, applied to the monitoring of building deformation, combined with the damage assessment map, can be profitably used by the Civil Protection and local Authorities during the post event, in order to evaluate the residual risk and to plan evacuation procedures and mitigation measures regarding the most damaged and unstable buildings. This work also highlights the importance of the continuous monitoring of urbanized areas affected by slope instability phenomena. In this case, the long term monitoring was performed using five different sensors, but this approach can be relevant to the design of future products based on data routinely acquired by the new ESA Sentinel mission.

Acknowledgements

The research leading to these results received funding from the European Union Seventh Framework Program (FP7/2007–2013) under grant agreement No. 242212 (Project DORIS) and Project LAMPRE. We also thank two anonymous reviewers for the helpful suggestions.

References

- Bianchini, S., Cigna, F., Righini, G., Proietti, C., Casagli, N., 2012. *Landslide hotspot mapping by means of persistent scatterer interferometry*. *Environ. Earth Sci.* 67 (4), 1155–1172.
- Bianchini, S., Tapete, D., Ciampalini, A., Di Traglia, F., Del Ventisette, C., Moretti, S., Casagli, N., 2014a. *Multi-temporal evaluation of landslide-induced movements and damage assessment in San Fratello (Italy) by means of C- and X-band PSI data*. In: Pardo-Igúzquiza, E., Guardiola-Albert, C., Heredia, J., Moreno-Merino, L., Durán, J.J., Vargas-Guzmán, J.A. (Eds.), *Mathematics of Planet Earth*. Springer, Berlin/Heidelberg, pp. 257–261.
- Bianchini, S., Ciampalini, A., Raspini, F., Bardi, F., Di Traglia, F., Moretti, S., Casagli, N., 2014b. *Multi-temporal evaluation of landslide movements and impacts on buildings in San Fratello (Italy) by means of C-band and X-band PSI data*. *Pure Appl. Geophys.* <http://dx.doi.org/10.1007/s00024-014-0839-2>.
- Billi, A., Presti, D., Faccenna, C., Neri, G., Orecchio, B., 2007. *Seismotectonics of the Nubia plate compressive margin in the South Tyrrhenian Region, Italy: clues for subduction inception*. *J. Geophys. Res.* 112 (B08302), <http://dx.doi.org/10.1029/2006JB004837>.
- Bovenga, F., Nutricato, R., Refice, A., Wasowski, J., 2006. *Application of multi-temporal differential interferometry to slope instability detection in urban/peri-urban areas*. *Eng. Geol.* 88, 219–240.
- Cascini, L., Fornaro, G., Peduto, D., 2009. *Analysis at medium scale of low-resolution DInSAR data in slow-moving landslide-affected areas*. *ISPRS J. Photogram. Rem. Sens.* 64 (6), 598–611.
- Catalano, S., De Guidi, G., Lanzafame, G., Monaco, C., Torrisi, S., Tortorici, G., Tortorici, L., 2006. *Inversione tettonica positiva Tardo-Quaternaria nel Plateau Ibleo (Sicilia SE)*. *Rendiconti Della Soc. Geol. Ital.* 2, 118–120.
- Cigna, F., Del Ventisette, C., Liguori, V., Casagli, N., 2011. *Radar-interpretation of InSAR time series and 'back monitoring' of ground deformation for mapping, characterization and mitigation of geological risk in urban area*. *Nat. Haz. Earth Syst. Sci.* 11, 865–881.
- Ciampalini, A., Cigna, F., Del Ventisette, C., Moretti, S., Liguori, V., Casagli, N., 2012. *Integrated geomorphological mapping in the north-western sector of Agrigento (Italy)*. *J. Maps* 8 (2), 136–145.
- Colesanti, C., Wasowski, J., 2006. *Investigating landslides with space-borne Synthetic Aperture Radar (SAR) Interferometry*. *Eng. Geol.* 88, 173–199.
- Cooper, A.H., 2006. *The classification, recording, databasing, and use of information about building damage caused by subsidence and landslides*. *Q. J. Eng. Geol. Hydrogeol.* 41, 409–424.
- Corrado, S., Aldega, L., Balestrieri, M.L., Maniscalco, R., Grasso, M., 2009. *Structural evolution of the sedimentary accretionary wedge of the alpine system in Eastern Sicily: Thermal and thermochronological constraints*. *Geol. Soc. Am. Bull.* 11–12, 1475–1490.
- Costantini, M., Iodice, A., Magnapane, L., Pietranera, L., 2000. *Monitoring terrain movements by means of sparse SAR differential interferometric measurements*. In: *Proc. IGAARSS, Honolulu, USA*, pp. 3225–3227.
- Crosetto, M., Monserrat, O., Cuevas, M., Crippa, B., 2011. *Spaceborne Differential SAR interferometry: data analysis tools for deformation measurement*. *Rem. Sens.* 3, 305–318.
- Del Ventisette, C., Garfagnoli, F., Ciampalini, A., Battistini, A., Gigli, G., Moretti, S., Casagli, N., 2012. *An integrated approach to the study of catastrophic debris-flows: geological hazard and human influence*. *Nat. Haz. Earth Syst. Sci.* 12 (9), 2907–2922.
- Del Ventisette, C., Ciampalini, A., Manunta, M., Calò, F., Paglia, L., Ardizzone, F., Mondini, A.C., Reichenbach, P., Mateos, R.M., Bianchini, S., Garcia, I., Füsü, B., Villó Deak, Z., Radi, K., Graniczny, M., Kowalski, Z., Piatkowska, A., Przylucka, M., Retzo, H., Strozzi, T., Colombo, D., Mora, O., Sanchez, F., Herrera, G., Moretti, S., Casagli, N., Guzzetti, F., 2013. *Exploitation of large archives of ERS and ENVISAT C-band SAR data to characterize ground deformation*. *Rem. Sens.* 5, 3896–3917.
- Ferretti, A., Prati, C., Rocca, F., 2000. *Nonlinear subsidence rate estimation using permanent scatterers in differential SAR interferometry*. *IEEE Trans. Geosci. Rem. Sens.* 38, 2202–2212.
- Ferretti, A., Prati, C., Rocca, F., 2001. *Permanent scatterers InSAR interferometry*. *IEEE Trans. Geosci. Rem. Sens.* 39 (1), 8–20.
- Del Ventisette, C., Righini, G., Moretti, S., 2014. *Multitemporal landslide inventory map updating using spaceborne SAR analysis*. *Int. J. Appl. Earth Obs. Geoinf.* 30, 238–246.
- Giunta, G., Nigro, F., Renda, P., Giorgianni, A., 2000. *The Sicilian-Maghrebides Tyrrhenian Margin: a neotectonic evolutionary model*. *Ital. J. Geosci.* 119, 553–565.
- Goswami, R., Mitchell, N.C., Brocklehurst, S.H., 2011. *Distribution and causes of landslides in the eastern Peloritani of NE Sicily and western Aspromonte of SW Calabria, Italy*. *Geomorphology* 132, 111–122.
- Guzzetti, F., Carrara, A., Cardinali, M., Reichenbach, P., 1999. *Landslide hazard evaluation: a review of current techniques and their application in a multi-scale study, Central Italy*. *Geomorphology* 31, 181–216.
- Guzzetti, F., Manunta, M., Ardizzone, F., Pepe, A., Cardinali, M., Zeni, G., Reichenbach, P., Lanari, R., 2009. *Analysis of ground deformation detected using the SBAS-DInSAR technique in Umbria*. *Pure Appl. Geophys.* 166 (8–9), 1425–1459.
- Guzzetti, F., Mondini, A.C., Cardinali, M., Fiorucci, F., Santangelo, M., Chang, K.T., 2012. *Landslide inventory maps: new tools for an old problem*. *Earth-Sci. Rev.* 112 (1–2), 42–66.
- Herrera, G., Davalillo, J.C., Cooksley, G., Monserrat, O., Pancioli, V., 2009. *Mapping and monitoring geomorphological processes in mountainous areas using PSI data: Central Pyrenees case study*. *Nat. Haz. Earth Syst. Sci.* 9, 1587–1598.
- Herrera, G., Tomás, R., Monells, D., Centolanza, G., Mallorqui, J.J., Vicente, F., Navarro, V.D., Lopez-Sanchez, J.M., Sanabria, M., Cano, M., Mulas, J., 2010. *Analysis of subsidence using TerraSAR-X data: Murcia case study*. *Eng. Geol.* 116, 284–295.
- Herrera, G., Gutierrez, F., Garcia-Davalillo, J.C., Guerrero, J., Notti, D., Galve, J.P., Fernandez-Merodo, J.A., Cooksley, G., 2013. *Multi-sensor advanced DInSAR monitoring of very slow landslides: the Tena Valley case study (Central Spanish Pyrenees)*. *Remote Sens. Environ.* 128, 31–43.
- Hung, W.C., Hwang, C., Chen, Y.A., Chang, C.P., Yen, J.Y., Hooper, A., Yang, C.Y., 2011. *Surface deformation from persistent scatterers SAR interferometry and fusion with leveling data: a case study over the Choushui River alluvial fan, Taiwan*. *Remote Sens. Environ.* 115, 957–967.
- Lauknes, T.R., Piyush Shanker, A., Dehls, J.F., Henderson, I.H.C., Larsen, Y., 2010. *Detailed rockslide mapping in northern Norway with small baseline and persistent scatterer interferometric SAR time series methods*. *Rem. Sens. Environ.* 114, 2097–2109.
- Lavecchia, G., Ferrarini, F., De Nardis, R., Visini, F., Barbano, M.S., 2007. *Active thrusting as possible seismogenic source in Sicily (Southern Italy): some insights from integrated structural-kinematic and seismological data*. *Tectonophysics* 445, 145–167.
- Lentini D F., Catalano D S., Carbone D S., 2000. *Carta geologica della Provincia di Messina: Servizio Geologico, S.E.L.C.A., Provincia Regionale di Messina, Assessorato Territorio, scale 1:50,000*.
- Liu, P., Li, Z., Hoey, T., Kincal, C., Zhang, J., Zeng, Q.M.J.P., 2013. *Using advanced InSAR time series techniques to monitor landslides movements in Badong of the Three Gorges region, China*. *Int. J. Appl. Earth Obs. Geoinf.* 21, 253–264.
- Meisina, C., Zucca, F., Notti, D., Colombo, A., Cucchi, G., Giannico, C., Bianchi, M., 2008. *Geological interpretation of PSInSAR data at regional scale*. *Sensors* 8 (11), 7469–7492.
- Mondini, A.C., Guzzetti, F., Reichenbach, P., Rossi, M., Cardinali, M., Ardizzone, F., 2011. *Semi-automatic recognition and mapping of rainfall induced shallow landslides using optical satellite images*. *Remote Sens. Environ.* 115, 1743–1757.
- Notti, D., García-Davalillo, J.C., Herrera, G., Cooksley, G., 2010. *Assessment of the performance of X-band satellite radar data for landslide mapping and monitoring: Upper Tena Valley case study*. *Nat. Haz. Earth Syst. Sci.* 10, 1865–1875.

- Raspini, F., Cigna, F., Moretti, S., 2012. [Multi-temporal mapping of land subsidence at basin scale exploiting persistent scatterer interferometry: case study of Gioia Tauro plain \(Italy\)](#). *J. Maps* 8 (4), 514–524.
- Righini, G., Pancioli, V., Casagli, N., 2012. [Updating landslide inventory maps using Persistent Scatterer Interferometry \(PSI\)](#). *Int. J. Remote Sens.* 33 (7), 2068–2096.
- Somma, R., Messina, A., Mazzoli, S., 2005. [Syn-orogenic extension in the Peloritani Alpine Thrust Belt \(NE Sicily, Italy\): evidence from the Ali unit](#). *Compt. Rend. Geosci.* 337, 861–871.
- Tomás, R., García-Barba, J., Cano, M., Sanabria, M.P., Ivorra, S., Duro, J., Herrera, G., 2012. [Subsidence damage assessment of a gothic church using Differential Interferometry and field data](#). *Struct. Health Monit.* 11, 751–762.

The ground-based InSAR monitoring system at Stromboli volcano: linking changes in displacement rate and intensity of persistent volcanic activity

Federico Di Traglia · Emanuele Intrieri · Teresa Nolesini · Federica Bardi · Chiara Del Ventisette · Federica Ferrigno · Sara Frangioni · William Frodella · Giovanni Gigli · Alessia Lotti · Carlo Tacconi Stefanelli · Luca Tanteri · Davide Leva · Nicola Casagli

Received: 21 June 2013 / Accepted: 17 November 2013
© Springer-Verlag Berlin Heidelberg 2014

Abstract Stromboli volcano (Aeolian Archipelago, Southern Italy) experienced an increase in its volcanic activity from late December 2012 to March 2013, when it produced several lava overflows, major Strombolian explosions, crater-wall collapses pyroclastic density currents and intense spatter activity. An analysis of the displacement of the NE portion of the summit crater terrace and the unstable NW flank of the volcano (Sciara del Fuoco depression) has been performed with a *ground-based interferometric synthetic aperture radar* (GBInSAR) by dividing the monitored part of the volcano into five sectors, three in the summit vents region and two in the Sciara del Fuoco. Changes in the displacement rate were observed in sectors 2 and 3. Field and thermal surveys revealed the presence of an alignment of fumaroles confirming the existence of an area of structural discontinuity between sectors 2 and 3. High displacement rates in sector 2 are interpreted to indicate the increase in the magmatic pressure

within the shallow plumbing systems, related to the rise of the magma level within the conduits, while increased displacement rates in sector 3 are connected to the lateral expansion of the shallow plumbing system. The increases and decreases in the displacement rate registered by the GBInSAR system in the upper part of the volcano have been used as a proxy for changes in the pressure conditions in the shallow plumbing system of Stromboli volcano and hence to forecast the occurrence of phases of higher-intensity volcanic activity.

Keywords Aeolian Archipelago · GBInSAR · Strombolian activity · Volcano monitoring · Stromboli

Introduction and rationale for the study

Hazard at Stromboli Island (Aeolian Archipelago, Southern Italy; Fig. 1) is associated with tsunamis generated by sub-aerial and/or submarine landslides of unstable portions of its NW flank (Sciara del Fuoco (SdF)) frequently caused by the opening of effusive fractures, as in the crisis of 1930 and 2002–2003 (Barberi et al. 2009; Rosi et al. 2013). Hazards are also associated with “major” strombolian explosions, whose ejecta may affect the summit area where visitors usually have access, and especially with the more violent “explosive paroxysms”, that often affect the surrounding villages of Stromboli and, especially, Ginostra with ash and bombs (Barberi et al. 1993; Bertagnini et al. 2011). The “ordinary” activity consists of frequent, small-scale, impulsive explosions of gas and particles, producing 100–200 m high scoria-rich jets, associated with persistent, quiescent magma outgassing and discrete gas explosions (Rosi et al. 2013).

Editorial responsibility: J. Taddeucci

F. Di Traglia (✉) · E. Intrieri · T. Nolesini · F. Bardi · C. Del Ventisette · F. Ferrigno · S. Frangioni · W. Frodella · G. Gigli · A. Lotti · C. T. Stefanelli · L. Tanteri · N. Casagli
Department of Earth Sciences, University of Firenze, Via La Pira 4, Firenze, Italy
e-mail: federico.ditraglia@unifi.it

F. Traglia
e-mail: ditraglia@dst.unipi.it

F. Di Traglia
Department of Earth Sciences, University of Pisa, Via Santa Maria 53, Pisa, Italy

D. Leva
Ellegi s.r.l. LisaLab, via Petrarca 55, Rovello Porro, Como, Italy

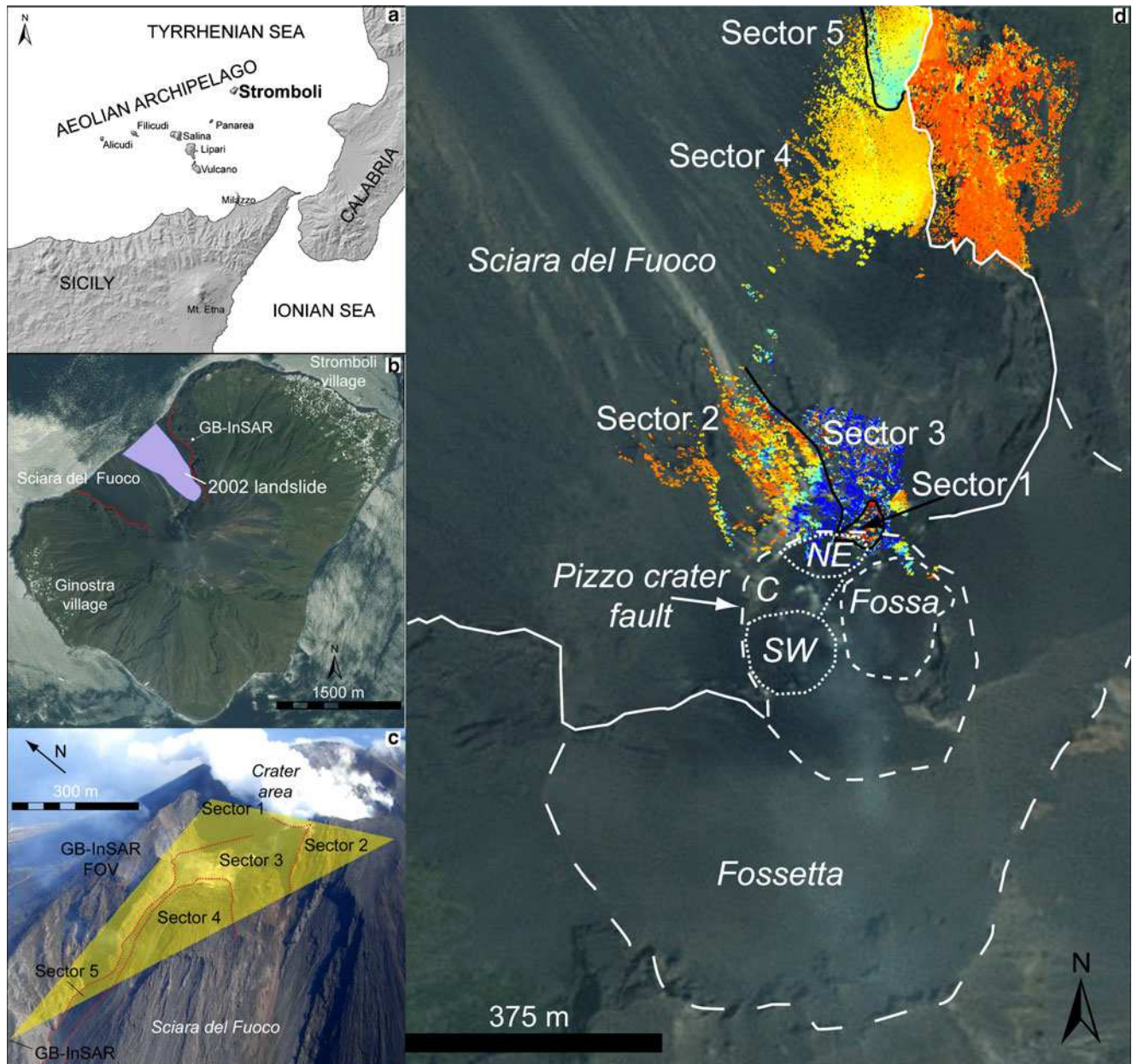


Fig. 1 **a** Geographical setting of Stromboli island; **b** SPOT (2009) image with the main geomorphological features (from Intrieri et al. 2013a); **c** field of view of the GBInSAR which shows the sectors described in the text (modified after Intrieri et al. 2013a); sector 1, a new sector with respect to Di Traglia et al. (2013); sector 2, corresponding to sectors 1 and 2 of Di Traglia et al. (2013); sector 3, as in Di Traglia et al. (2013); sector

4, corresponding to SdF1 in Intrieri et al. (2013a) and Nolesini et al. (2013); and sector 5, corresponding to SdF2 in Intrieri et al. (2013a) and Nolesini et al. (2013); **d** SPOT (2009) image and GBInSAR cumulated (2010–2013) displacement map (max displacement, 150 mm in sector 2) with the main structural features of the summit area of Stromboli volcano (from Finizola et al. 2003)

Volcanic crises at Stromboli were not preceded by evident accelerations of phenomena that are typical of quiescent close-conduit volcanoes. However, variations of some parameters, such as CO_2 soil and SO_2 plume flux (Inguaggiato et al. 2011), CO_2/SO_2 within the volcanic plume (Aiuppa et al. 2009; Aiuppa et al. 2010), deformation (recorded by the ground-based interferometric synthetic aperture radar (GBInSAR); Casagli et al. 2009) and the number and intensity of Strombolian explosions (Andronico et al. 2008; Taddeucci

et al. 2013) provide evidence regarding of the state of the volcano and abnormal variations demand the attention of Civil Protection and monitoring institutions. When Stromboli experiences a high level of activity, one of the primary questions is whether the “crisis” will lead to a paroxysmal explosion and/or to a flank effusion, during which tsunamis are more likely.

Given the highly developed monitoring system installed at Stromboli, which provides increased knowledge of volcano's

behaviour, indicators of change in volcanic activity have become sufficiently apparent to prompt scientists to issue public statements, to engage with media, local land managers, public officials and to start other activities in preparation for an emergency. However, de-escalation from a crisis, without occurrence of paroxysmal explosion or flank effusion, can threaten the credibility of the scientific community and the civil protection authorities responsible for evacuations and/or access restrictions, and announcement of a crisis can also bring unwanted economic and social disruption (Moran et al. 2011; Garcia and Fearnley 2012; Intrieri et al. 2013b). To avoid these consequences, it is necessary to analyse in detail different crises, to identify any different trends in geophysical and geochemical parameters which distinguish crisis that does not evolved into flank effusion and/or paroxysmal explosions from those that did, as the well-studied 2007 crises (Aiuppa et al. 2009; Casagli et al. 2009; Inguaggiato et al. 2011).

To contribute toward this aim, the study presented here examinee the displacement data recorded by the GBInSAR monitoring system of Stromboli during the last crisis, which lasted 4 months (December 2012 to March 2013) and during which lava overflows from the summit vents, crater-wall collapses and major explosions occurred.

Stromboli volcano

Geological background

The 916-m high Stromboli Island is the emerged portion of a ~3,000-m high stratovolcano located in the north-eastern tip of the Aeolian Archipelago in the southern Tyrrhenian sea (Fig. 1a) and it persistently erupts a potassium-rich, basaltic magma at multiple vents residing in an area located at ~750 m above sea level (Tibaldi 2001; Corazzato et al. 2008). Together with Vulcano and Lipari, Stromboli is one of the active volcanic islands of the Aeolian Archipelago (Rosi et al. 2013; Di Traglia et al. 2013). The rock composition at Stromboli varies and includes basaltic andesite, shoshonite and latite-trachyte (e.g. Hornig-Kjarsgaard et al. 1993), with the oldest exposed products dated approximately 100 ka (Gillot and Keller 1993).

Stromboli has been affected by three caldera collapses and five sector collapse events, each followed by reorganisation of the eruptive centres (Tibaldi 2001; Tibaldi et al. 2009). From 13 ka, lateral collapses formed a nested horseshoe-shaped scar (Fig. 1b) opening to the northwest, called the SdF depression (Tibaldi 2001; Di Roberto et al. 2010). Small-scale flank instability and related tsunamis are also frequent and occurred during many recent flank effusions (1879, 1916, 1919, 1930, 1944, 1954 and 2002; Barberi et al.

1993; Tinti et al. 2006). During the last flank effusion (February–April 2007) a paroxysmal explosion occurred (15th March 2007; Pistolesi et al. 2011; Andronico et al. 2013), and the opening of effusive vents at the base of the NE vents and in the SdF area produced small landslides, but tsunamis were not detected (Barberi et al. 2009).

Volcanic activity

Strombolian activity is characterised by mild to moderate energy explosions that occur once a gas slug—a discrete volume of gas rising in the conduit system at a relatively high velocity with respect to the surrounding basaltic magma—reaches the cooled upper surface of a magma column and causes it to raise, up-dome and ultimately explosively release of gas that is accompanied by ejected magma clots (Blackburn et al. 1976; Parfitt 2004; Del Bello et al. 2012). This type of activity is fed by a mostly degassed, high-porphyricity (HP) basaltic magma that is thought to reside in the shallower, cooler portion of the conduit system (Bertagnini et al. 2003).

Strombolian paroxysms and major explosions are characterised by more efficient fragmentation, higher mass discharge rates and total erupted mass, compared with the “ordinary” Strombolian events (Rosi et al. 2006; Houghton and Gonnermann 2008; Andronico and Pistolesi 2010; Pistolesi et al. 2011; Lautze et al. 2012; Houghton et al. 2013). Major explosions are clustered in a relatively short time period (1 to 2 months), during which the activity is characterised by frequent explosions (>5 events/h, Andronico et al. 2008), high CO₂ plume flux (>1,000 t/day, Aiuppa et al. 2011), and they may be associated with lava overflows from the summit vents (Rosi et al. 2013). These periods are characterised by high displacement rates registered by the GBInSAR monitoring system without flank instability, corresponding to conduit overpressure in the order of 10⁻¹ MPa (Di Traglia et al. 2013; Nolesini et al. 2013). Paroxysmal and major explosions commonly involve a deep-derived, volatile-rich, low-porphyricity (LP) basalt, together with the HP-type one (Bertagnini et al. 2003; Pistolesi et al. 2008; La Felice and Landi 2011; Bertagnini et al. 2011).

Flank effusions and paroxysmal explosions are generally correlated with substantial changes in the state of volcanic activity state changes prior and after the main event (Rosi et al. 2006; Pistolesi et al. 2011), and with variations in the structural activity (intense fracturing, inflation and deflation of the vents area, sliding of the SdF; Casagli et al. 2009; Giordano and Porreca 2009) and degassing pattern (Aiuppa et al. 2009; Aiuppa et al. 2010; Inguaggiato et al. 2011).

Materials and methods: the GBInSAR monitoring system and the handheld thermal survey at Stromboli volcano

The northernmost part of the SdF depression has been continuously monitored since the 2002 collapse event by a GBInSAR system (Antonello et al. 2004; Casagli et al. 2010), that is able to detect instability phenomena such as summit area collapse, pit crater formation, lateral vent opening and explosion-related ground deformation (Tarchi et al. 2008; Casagli et al. 2009; Di Traglia et al. 2013; Intrieri et al. 2013a; Nolesini et al. 2013). This monitoring system is the only reported example in literature of such technology used in surveillance of an active volcano. The system consists of a ground-based interferometer producing, on average, 130 images/day of the NE flank of the vents area and the upper part of the SdF. Radar images (produced every 11 min) are obtained through sampling techniques, so frequency and spatial steps have to be selected to avoid ambiguity in range and cross-range (Antonello et al. 2004).

The GBInSAR measures line-of-sight (LoS) ground displacement in the time interval between two acquisitions. The displacement is calculated from the phase difference between the back-scattered signals received at different times, through the cross-correlation between two SAR images. Interferometric analysis of sequences of consecutive images allows one to derive the displacement field of the observed portion of the SdF and of the vents area in the elapsed time. Negative and positive values of displacement indicate, respectively, a movement towards or away from the sensor. As the GBInSAR is located in a stable area north of the SdF, and its LoS allows us to detect the N-S components of the movements in all direction, negative and positive displacement may represent inflation and deflation of the volcano (Casagli et al. 2009; Di Traglia et al. 2013).

Range and cross-range resolution (i.e. the minimum separation of two targets or equal cross section that can be resolved as separate targets) are on average 2×2 m, with a measurement precision referred to the displacement (and not to the displacement rate) of less than 1 mm (Casagli et al. 2009). The displacement rate is the result of the mathematical division between the displacement measured in an interferogram (referred to the difference between two SAR images) and the elapsed time between the two images. The precision in the displacement measurement is 0.1 mm for punctual (few pixels) automatic extraction (see Intrieri et al. 2013a) or 0.5 mm for areal (entire sector) visual-based assignment (made by the operator). The key concept of the GBInSAR analysis is the elapsed time between the two SAR images used to create interferograms (Antonello et al. 2004; Casagli et al. 2009; Di Traglia et al. 2013). This procedure allowed Nolesini et al. (2013) and Intrieri et al. (2013a) to identify the displacement rate (0.01–0.001 mm/h) related to the creep of the northern sector of the SdF.

The ability of InSAR to measure volcano deformations depends on the persistence of phase coherence over appropriate time intervals on various types of volcanic deposits (Lu et al. 2002). Loss in coherence mainly depends on chaotic ground movements (Antonello et al. 2004), e.g. grain avalanches. A coherence mask is set to avoid the noisy areas of the interferogram; the pixels with coherence lower than a threshold (set to 0.8) are filtered out and in the interferogram these pixels are black. For the selection of coherent reflectors, that is regions characterised by a stable phase, Ferretti et al. (2001) introduce the dispersion index (DA), defined as the ratio between the standard deviation and the mean of the amplitude.

Deformation maps are derived by accumulating the displacements from consecutive interferograms. The phase values can be affected by ambiguity (unwrapped phase) but, due to the short elapsed time (11 min) between two subsequent measurements on Stromboli volcano, the interferometric displacements are usually smaller than half wavelength and unwrapping procedures (as described by Ghiglia and Romero 1994) are not necessary. Detailed description of the GBInSAR system of Stromboli can be found in Antonello et al. (2004), Bonforte et al. (2008), Casagli et al. (2010) and Luzi et al. (2010).

In addition to the GBInSAR monitoring system, on the 9th January 2013, during the December-March 2013 crisis, thermograms of the SdF and the NE vents area were collected for rapid detection of newly formed fractures connected to the latest eruptive activity. Thermal imaging systems have been increasingly adopted for volcano surveillance during the last decade (Spampinato et al. 2011 and references therein). The use of thermal imagery at Stromboli (obtained from handheld or helicopter-based thermal infrared cameras) increased since 2001 (Bonaccorso et al. 2003; Calvari et al. 2005; Rosi et al. 2006; Lodato et al. 2007; Harris et al. 2008; Spampinato et al. 2008; Andronico and Pistolessi 2010; Pistolessi et al. 2011); it is a powerful tool for the study of effusive and explosive eruptions, opening of fractures and eruptive vents, slope failures and flank collapses.

Thermographic data were acquired by means of a handheld thermal camera from the GBInSAR system location (Fig. 1c), for a period of about 1 h between 13:00 and 14:00 local time. A FLIR SC 620 thermal camera was used with a $24^\circ \times 18^\circ$ field of view and a 0.65-mrad angular resolution, leading to a 640-by-480 pixel image. The camera sensor is a Focal Plane Array micro-bolometer sensor, capable of measuring electromagnetic radiation across the 7.5 and 13 μm spectral band, with a thermal resolution of ± 2 °C. The camera software permits internal calibration and atmospheric correction using the proper input data: path length, air temperature, relative humidity (collected by means of a pocket thermohygrometer) and emissivity. A value of 0.95 emissivity was used, according to the typical values adopted for basalt at

Stromboli in the 8 to 14 μm wave band (Calvari et al. 2005). A built-in 3.2-Mp optical camera, acquiring images simultaneously with respect to thermal data, allowed us to compare the latter with the optical images to improve interpretation of the detected thermal anomalies.

The 2012–2013 effusive–explosive crisis

Early signs of renewed activity were observed, from the Calabrian coasts 50–60 km opposite of the Island of Stromboli, on 22nd November 2012, with a series of strong strombolian explosions from the central vents (INGV Report 2012) associated with the rise of an ash-free plume. Afterwards (10th December 2012), an increase in spatter activity was observed. The crisis comprised five discrete phases, characterised by lava overflows and major explosions.

The crisis started on 24th December 2012 with collapse of the external rim of the NE vents followed by the emission of a lava flow. The lava emission was unsteady and produced frequent and isolated overflows during the following days until 27th December 2012 (phase 1). Effusive activity stopped for 10 days before renewing on 7th January 2013 and a third overflow occurred on 10th January 2013 (phase 2). During the period of no lava emission, intense spattering was produced by the NE vents (INGV Report 2013).

On 12th January 2013, a second crater-wall collapse occurred, producing a small pyroclastic flow, similar to the one observed by Cole et al. (2005) at Arenal Volcano. The flow travelled down the SdF depression and entered the sea, followed by a large co-pyroclastic flow ash column that rose from the sea (phase 3). The ash-column was drifted by the western wind and produced ash fallout in the eastern sector of the island (Fig. 2). During the 12th and 13th January, bomb and lapilli-sized products were launched and landed largely beyond the vents area

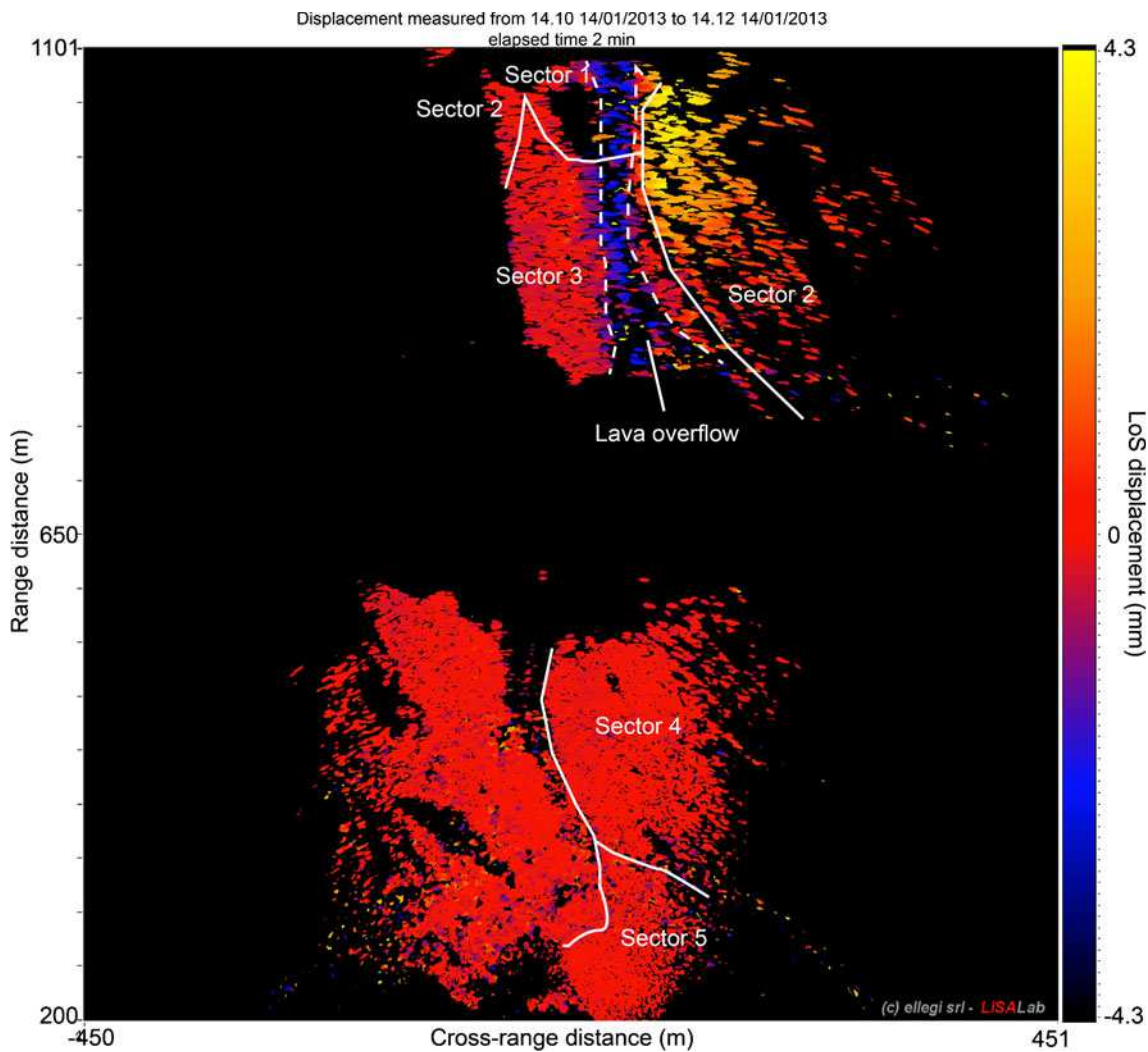


Fig. 2 Volcanic activity during the 2012–2013 eruption. **a** Ash plume formed after the 12th January 2013 pyroclastic density current induced by crater-wall collapse of the NE vents; **b** strombolian explosion (13th

January 2013); **c** ash-laden plume from the pit crater formed in the SW vents area (20th January); **d** lava overflow from the breached NE vents (15th January) taken from a helicopter

(beyond maximum dispersal area for ordinary Strombolian activity; Fig. 2). Samples collected soon after the explosions showed the presence of mingled HP and LP magmas (detected by hand specimen observations; Mauro Rosi, personal communications). During the afternoon of 13th January a pit-crater formed in the south-western part of the vents area (Fig. 2). On 14th January, two lava overflows occurred from the NE vents (Fig. 2). During 16th–18th January, the activity was characterised by higher-intensity Strombolian activity from the NE vents and ash-rich explosions from the SW vents. Bomb and lapilli-sized pyroclasts, rich in LP

component (detected by hand specimen observations; Marco Pistolesi, personal communication), were recognised beyond the vents area during a survey carried on 20th January, with the lapilli dispersed in the eastern sector of the Pizzo area by the western wind. During the following days, the activity decreased, albeit with fluctuations in the intensity of the Strombolian bursts from the NE vents and the continuous emission of ash-rich plumes from the SW vents. Effusive activity recurred 11th–27th February (phase 4) and on 1st of March (phase 5) with overflows from the NE vents and intense spattering activity.



Fig. 3 Interferogram between 14:10 UT and 14:12 UT of 14th March 2013 (time interval of 2 min). The different sectors have been *highlighted*

Data analysis

The analysis of displacement has been performed by dividing the part of the volcano monitored by the GBInSAR into five regions (Fig. 1): (1) the external rim of the NE vents; (2) the flanks of the vents area; (3) the slope at the base of the NE vents; (4) the portion of the SdF within the 2002 tsunamigenic landslide; and (5) a small portion of the SdF outside the 2002 tsunamigenic landslide. The shadow zone (i.e. a topographically obscured area) between sectors 3 and 4 (Fig. 1) corresponds to a flat zone in the upper portion of the SdF, called Pianoro, which resulted from the seaward motion of the northern part of the SdF occurred during the 2002–2003 and 2007 flank effusions (Casagli et al. 2009; Giordano and Porreca 2009).

During routine operations, the SAR antennas are moved at regular intervals every few millimetres along a track that serves as a means to realise the synthetic aperture, a technique used to achieve a higher spatial resolution. During the

emergency phases, the antennas can be moved continuously on the rail without the usual stop-and-go procedure. This procedure allows us to produce interferograms with a delay between the two following SAR images of 2 min (Fig. 3).

In order to account for the geomorphological changes occurred at Stromboli in the study period, an analysis of the evolution of the debris cone (sector 3) has been carried out from the power images, containing the reflectivity information of the scenario to microwaves.

Sector 1

Detectable displacements in sector 1 are related to the slow movement of pyroclastic materials (mainly spatter bombs and agglutinate) deposited on the external rim of the NE vents area. During the 2012–2013 crisis, displacement in this area was rarely detected because of the low coherence (<0.8) of the SAR signal caused by the fast remobilisation of ejecta from the NE vents. Sector 1 has had large morphological



Fig. 4 a NE vents before the 12th January 2013 crater-wall collapse (10th January 2013). The sectors recognized from the GBInSAR data are highlighted. b Detail of the rim of the NE vents are before the 12th

January 2013 crater-wall collapse. c Rim of the NE vents area after the 12th January 2013 crater-wall collapse (13th January 2013). d Refill of the breached rim of the NE vents area (20th January 2013)

modifications resulting from frequent collapses before the onset of lava overflows from the NE crater (Fig. 4).

Sector 2

The displacements in sector 2 were of two types: (1) long-lived movements (from October to December 2012) which have maximum displacement at the slip zone that accommodated the collapse of the vents area during the 2007 crisis

(Fig. 5); (2) short-lived (minutes) movements, localised in the upper part of the external flank of the vents area and already interpreted as syn-explosive deformations linked to major explosions (Di Traglia et al. 2013). A rise in displacement rate in sector 2 was observed starting from 16th October 2012. The displacement involved the entire external flank of the vents area (Fig. 5). The geometry of the displacement was very similar to the one detected before the 2007 flank effusion (Casagli et al. 2009). A strong increase in the displacement

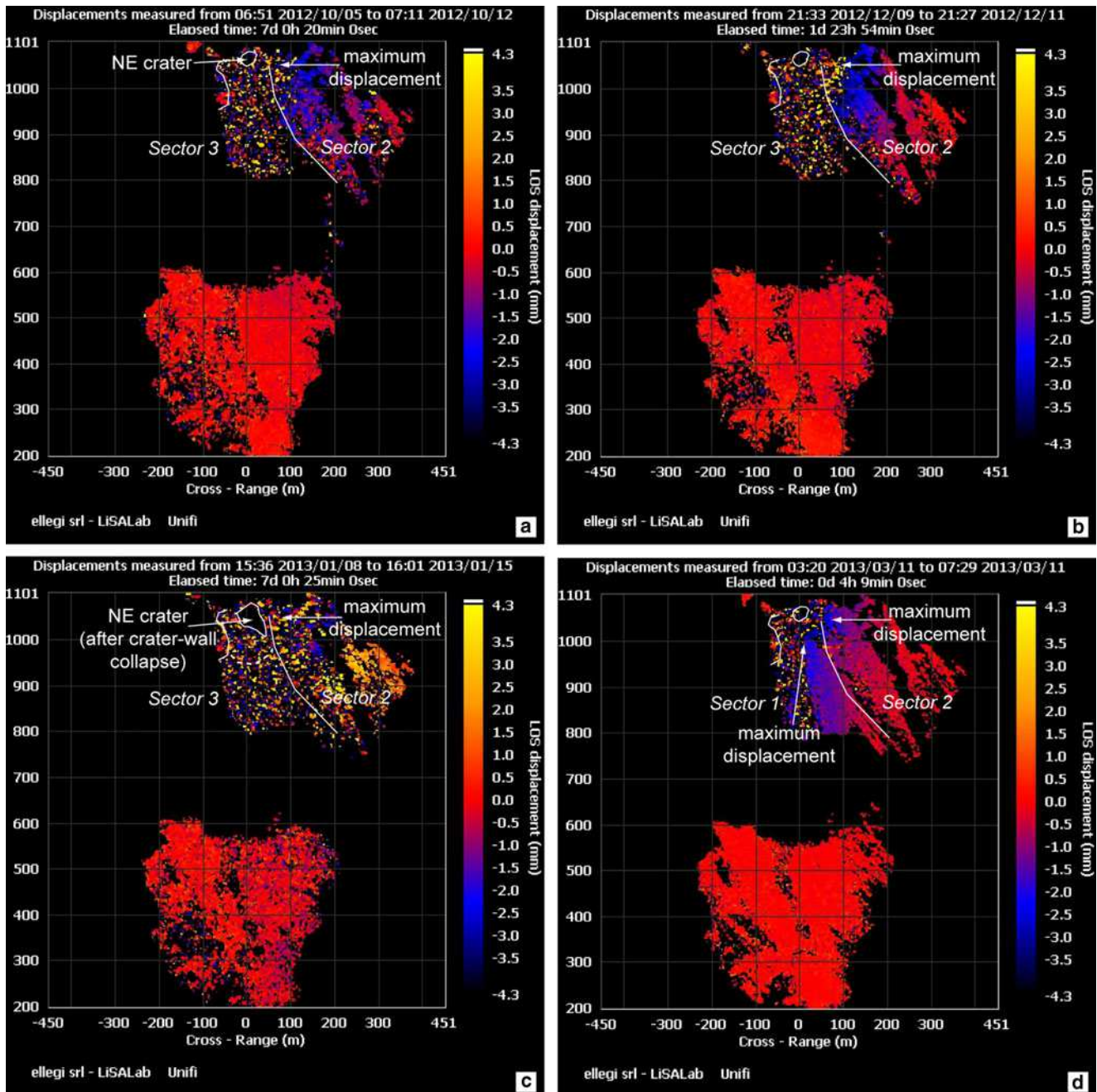


Fig. 5 SAR interferograms showing typical displacement signals in sector 2. **a** Temporal baseline of 7 days during October 2012 (inflation); **b** temporal baseline of 2 days during December 2012 (inflation); **c**

temporal baseline of 7 days during January 2013 (deflation); **d** temporal baseline of 4-h during February 2013 (inflation)

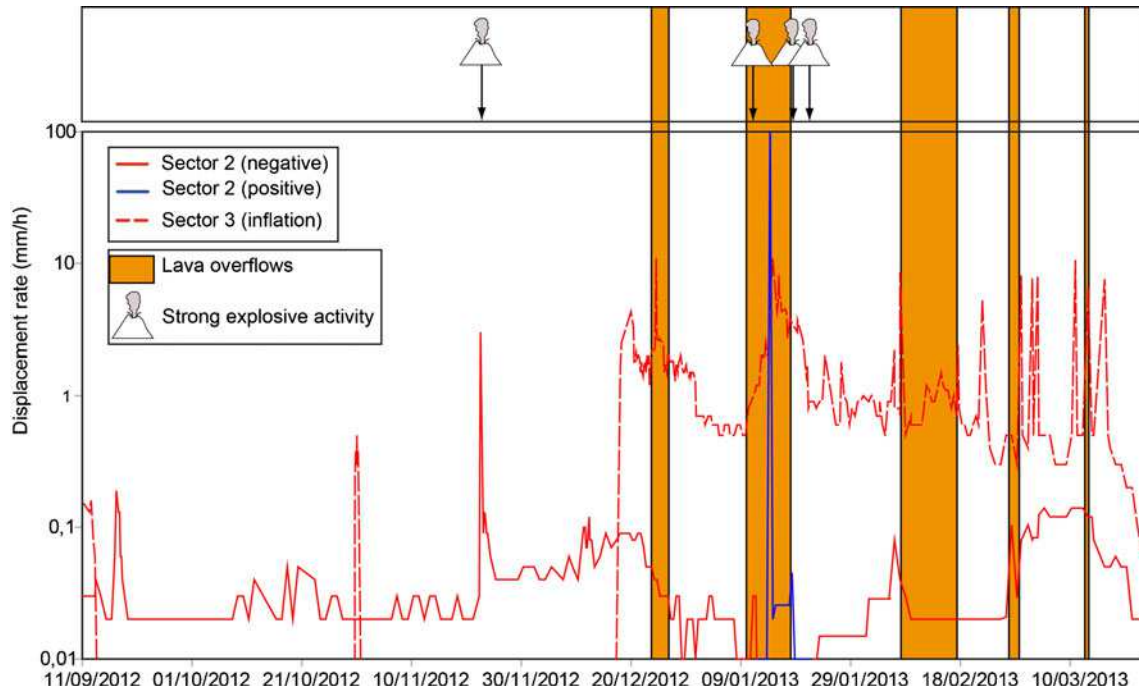


Fig. 6 GBInSAR data during the September 2012–March 2013 period. The velocities of sectors 2 and 3 have been plotted against time. The red line represents a displacement toward the SAR sensor (negative radar displacement); the blue line represents the deformation away from the

SAR sensor (positive radar displacement). The main events (overflows and higher-intensity explosive activity) that occurred in the 2012–2013 crisis are reported

rate was observed during the period 11th–22nd December 2012 (0.09–0.12 mm/h) and then it decreased until 12th January 2013 (red solid line in Fig. 6). In the following days (14th–21st January), the GBInSAR system recorded displacement away from the sensor (blue solid line in Fig. 6). This displacement rate inversion peaked on the 14th January, during a large lava overflow from the NE vents. Afterwards, displacement was again toward the sensor, with rates increasing from 1st February to 6th February (0.08 mm/h), the again successively from 27th February until 13th March (0.18 mm/h).

Short duration, elastic, displacements were observed only on 22nd November 2012, coincidentally with strong explosions recorded by the INGV network (INGV Report 2012). The displacement rate reached 3 mm/h (Fig. 6).

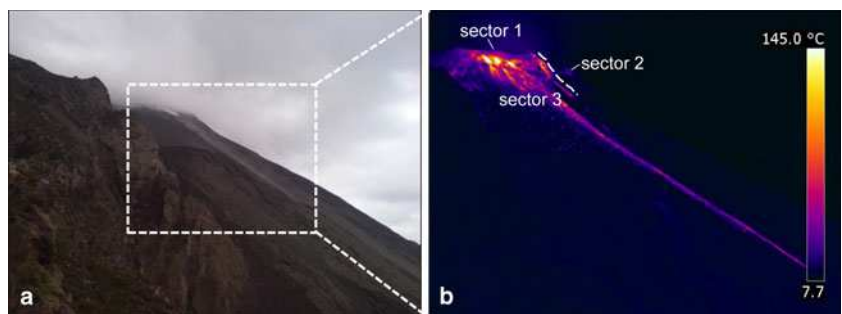
Thermograms of the NE vents area (collected at 850 m mean distance, determining an approximately 361×271 m

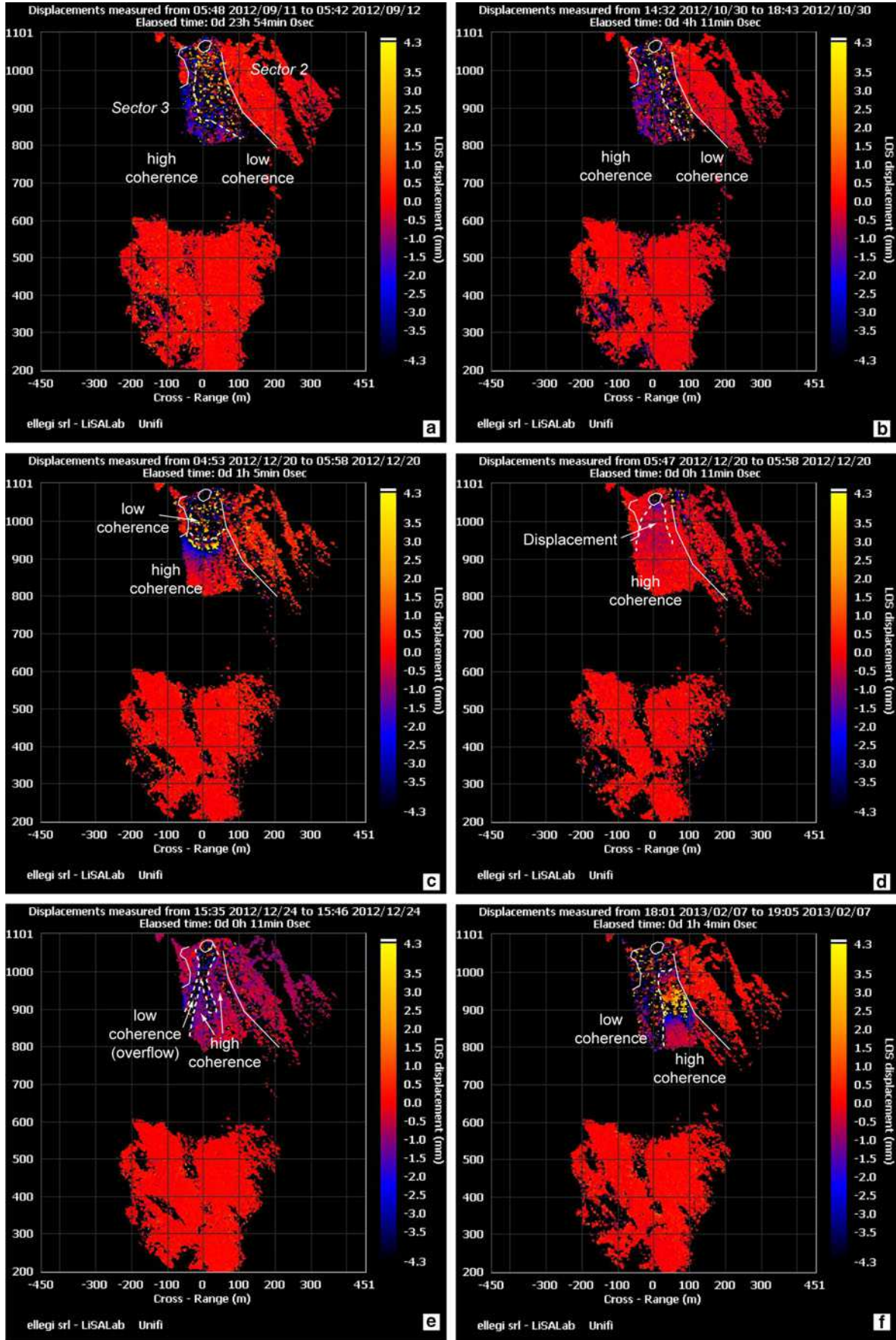
field of view with 56.5 cm pixel dimension) revealed thermal anomalies (Fig. 7b), corresponding to a persistent alignment of fumaroles lying exactly at the boundary between sectors 2 and 3 and possibly related to a structural discontinuity separating the two sectors (Fig. 7a).

Sector 3

Sector 3 is generally decorrelated in interferograms spanning more than 12 h because of the fast accumulation and remobilisation of ejecta. During the analysed periods, sector 3 was characterised by higher coherence, because of a consistent movement of the entire sector (Di Traglia et al. 2013), and allowing measurements of the increased displacement rate (1–12 h interferograms, e.g. Fig. 8a–c, f). Short-term interferograms (2–11 min) were used during periods of very high displacement (23rd December 2012–21st February 2013)

Fig. 7 Optical (a) and corresponding thermal image of the investigated crater area (b) acquired on 9th January 2013 at 13:01. The thermal anomalies in sector 3 are related to hot materials ejected from the NE crater, while the anomalies at the border between sectors 2 and 3 correspond to fumaroles





◀ **Fig. 8** SAR interferograms showing typical inflation signals in sector 3. **a** Temporal baseline of 24 h during September 2012; **b** temporal baseline of 4 h during October 2012; **c** temporal baseline of 1 h during December 2012; **d** temporal baseline of 11 min during December 2012 (same inflation of c); **e** temporal baseline of 11 min during the 25th December 2012 lava overflow; **f** temporal baseline of 1 h during February 2013. Displacements moved from the lower to the upper part of sector 2 after the 12th January 2013 crater-wall collapse

and also allowed us to pinpoint fast lava flows in sector 3, which were easily visible because of the great loss of coherence in longer-term interferograms for the lavas compared with the surrounding area (Fig. 8d, e).

The two main increases in displacement rate have also been observed on 12th September and 30th–31st October (dashed line in Fig. 6). A strong increase in displacement rate in sector 3 has been recorded since 18th December 2012 (1.7 mm/h) to the time of writing, with an increase in the coherence of the SAR signal compatible with a deep-rooted movement of the entire sector (Di Traglia et al. 2013). This contrasts with the less coherent signal of the typical surface processes (rolling and minor sliding of erupted material) that characterised the previous days. During the December 2012–early January 2013 period, sector 3 showed increases and decreases in displacement rate, with two peaks respectively on the 24th December 2012 (10.9 mm/h) and on the 14th January 2013 (10.9 mm/h). During late January, February and early March the displacement rate trend has been more fluctuating, with 12 peaks respectively on the 24th January (2 mm/h), 27th January (1.8 mm/h), 6th February (2.2 mm/h), 7th February (8.6 mm/h), 17th February (2.4 mm/h), 22nd February 2013 (5.3 mm/h), 1st March (8.1 mm/h), 3rd March (7.6 mm/h) and

4th March (8.1 mm/h), 10th March (10.6 mm/h), 13th March (6.6 mm/h) and 16th March (7.6 mm/h).

This sector experienced a considerable geomorphological evolution assessable also through visual inspection. A quantification of how much the debris cone grew in length can be obtained by analysing daily power images over the period 15th November 2012–31st March 2013. In particular, this analysis measures how much the central visible part of the debris cone's bottom has reduced its range distance from the sensor (i.e. its distance along the radar line of sight). By comparing the first and last power images of this time interval (Fig. 9) it is evident how the cone approached the GBInSAR, moving from a distance of 804 m to a distance of 784 m (around 20 m in 136 days), while on the right-hand side, a whole new portion was set in-place from 800 to 751 m (white circle in Fig. 9b). Even though a mean progradation value of 0.15 m/day can be extracted (that is a shortening between target area and the GBInSAR in the power images), an average would not be representative of this evolution. In fact, as shown in Fig. 10, the progradation increased during the period 15th November 2012–31st March 2013, occurred in pulses rather than in a linear trend of the sort seen in the period 15th November to 3rd December 2012 (around 7 m in 18 days). It is also possible to identify three time intervals, during which the debris cone was more or less stable, separated by two abrupt “growth steps”, respectively between 24th and 25th December 2012 (around 10 m in 1 day) and between 12th and 13th February 2013 (6 m in 1 day).

The dispersion of the measurements related to the temporal variations in the reflectivity of the target area, has been assessed using the dispersion index D_A (Ferretti et al. 2001) calculated on a region covering the central zone of the debris

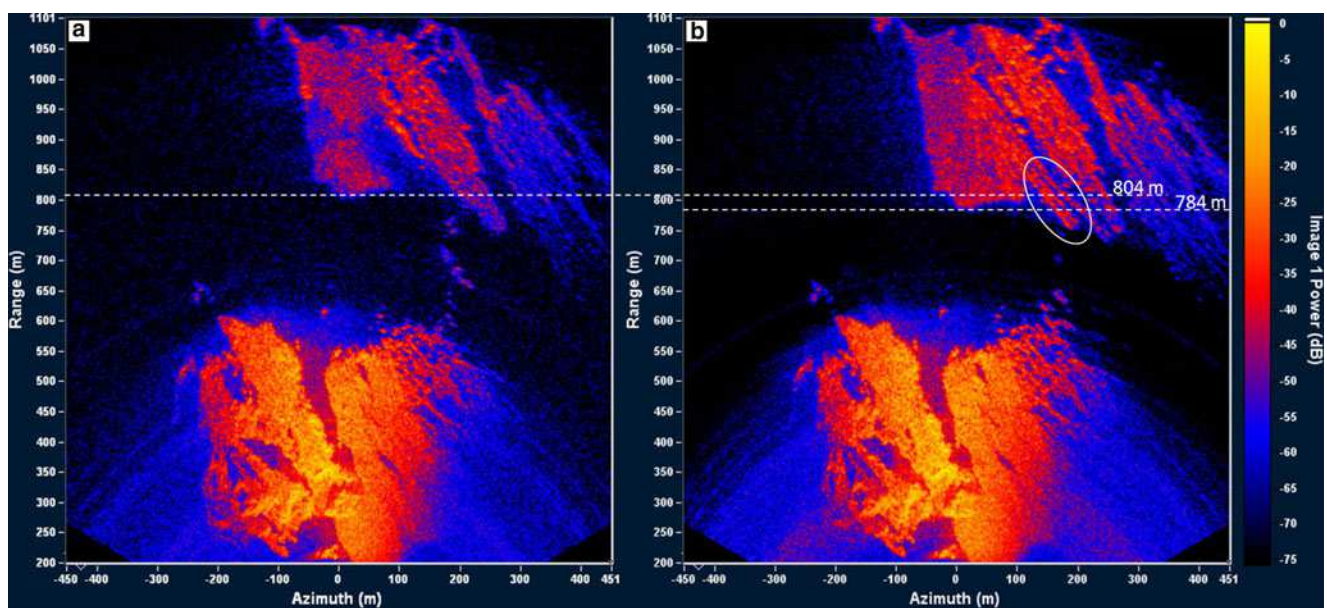


Fig. 9 Comparison between two power images from 15th November 2012 (left) and 31st March (right), respectively. Dashed lines indicate the minimum range distance reached by the debris cone. The circled area highlights the portion most affected by lava flows during this period

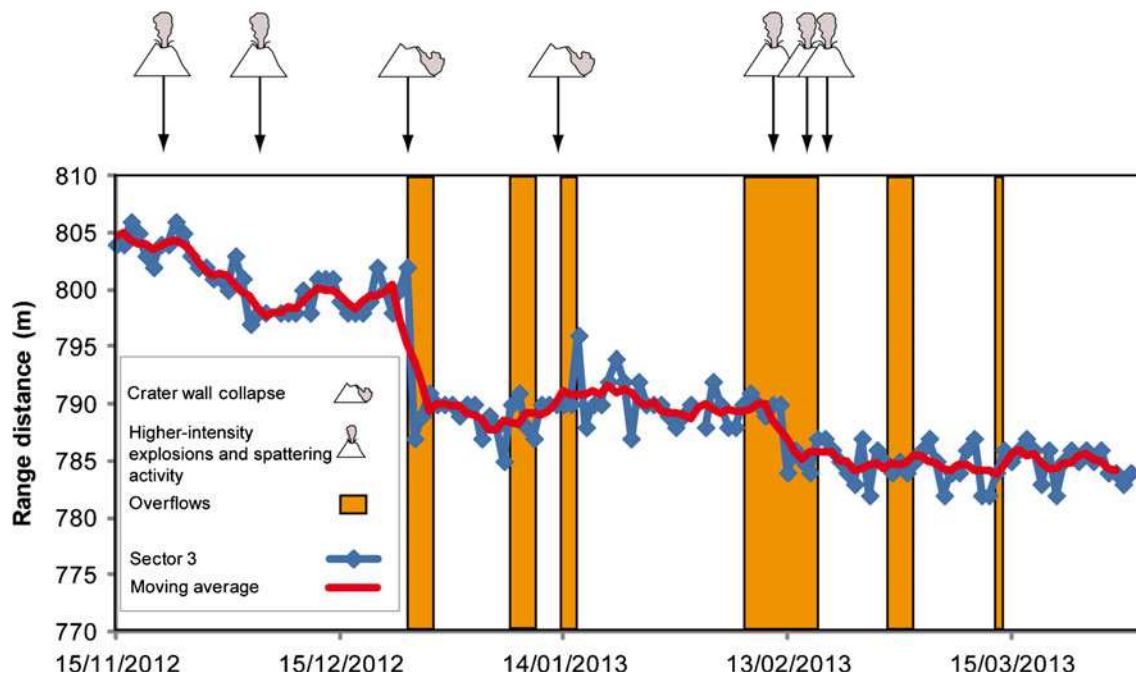


Fig. 10 Variation through time of the range distance (i.e. along sensor's line of sight) between the GBInSAR and the central visible part of the bottom of the debris cone. The occurrence of lava overflows, crater wall collapses and higher-intensity explosive and spattering activity is also indicated

cone. Over the period spanning 15th November 2012 to 31st March 2013, for this region the D_A has a value of 0.22, just below the threshold of 0.25 suggested by Ferretti et al. (2001). It is important to emphasise that, in this case, the index is not used to define stable reflectors usable as persistent scatterers, but to explain the variability in amplitude visible in Fig. 10. We estimate a measurement precision of ± 2.5 m and hence we consider the abrupt changes described above (10 m between the 24th and 25th December and 6 m between the 12th and 13th of February) outside of the error range, as evident from Fig. 9.

If we compare the time of occurrence of some important events that characterised this period with the variation with time of the range distance of the central part of the cone from the GBInSAR, it is possible to note that both “steps” occur during strong lava overflow phases and, in the first case, also concurrently with a crater-wall collapse. Lava overflows are also responsible for the growth of the right portion of the debris cone which reaches a range distance of 751 m (indicated in Fig. 9); this has been the preferred path for lava flows from NE vents since 13th February 2013 (Figs. 2d and 7).

Sectors 4 and 5

During the entire investigated period, the GBInSAR detected very slow displacement rates (0.001–0.003 mm/h) in these sectors. The maximum values were recorded in sector 5 during January 2013. The analysis of displacement was

conducted using long (monthly) to very long (annual) temporal baseline interferograms, with the aim of distinguishing superficial erosive processes from gravitational deep-rooted movements (Intrieri et al. 2013a; Nolesini et al. 2013). Monthly and annually based interferograms show that sector 5 is clearly distinguishable for its nail-shaped geometry with maximum displacement at its upper part, while sector 4 is characterised by two different movements, clearly visible in the annually based interferograms. One movement is related to erosion in the central portion of sector 4 and interpreted to indicate erosion of the most superficial portion of the SdF because of accumulation of material on the upper part, while the other movement involves the entire sector and is interpreted as the creep of a portion of the 2002 landslide (Intrieri et al. 2013a; Nolesini et al. 2013).

Thermograms of the SdF, collected on 9th January 2013 at a 250-m mean distance leading to an approximately 106×80 m field of view with a 16.6-cm pixel dimension, were focused on sector 5, where field inspections and optical images had detected a fracture developed in the lava and the volcaniclastic cover (Fig. 11). The corresponding thermogram did not highlight the presence of surface thermal anomalies connected to magma intrusion, confirming the stability of the investigated SdF sectors (Fig. 11). This is in good agreement with evidences that many minor movements affected the lower portion of the northern-part of SdF, both during the 2002–2003 and 2007 flank effusions (Puglisi et al. 2005; Bonforte et al. 2008).

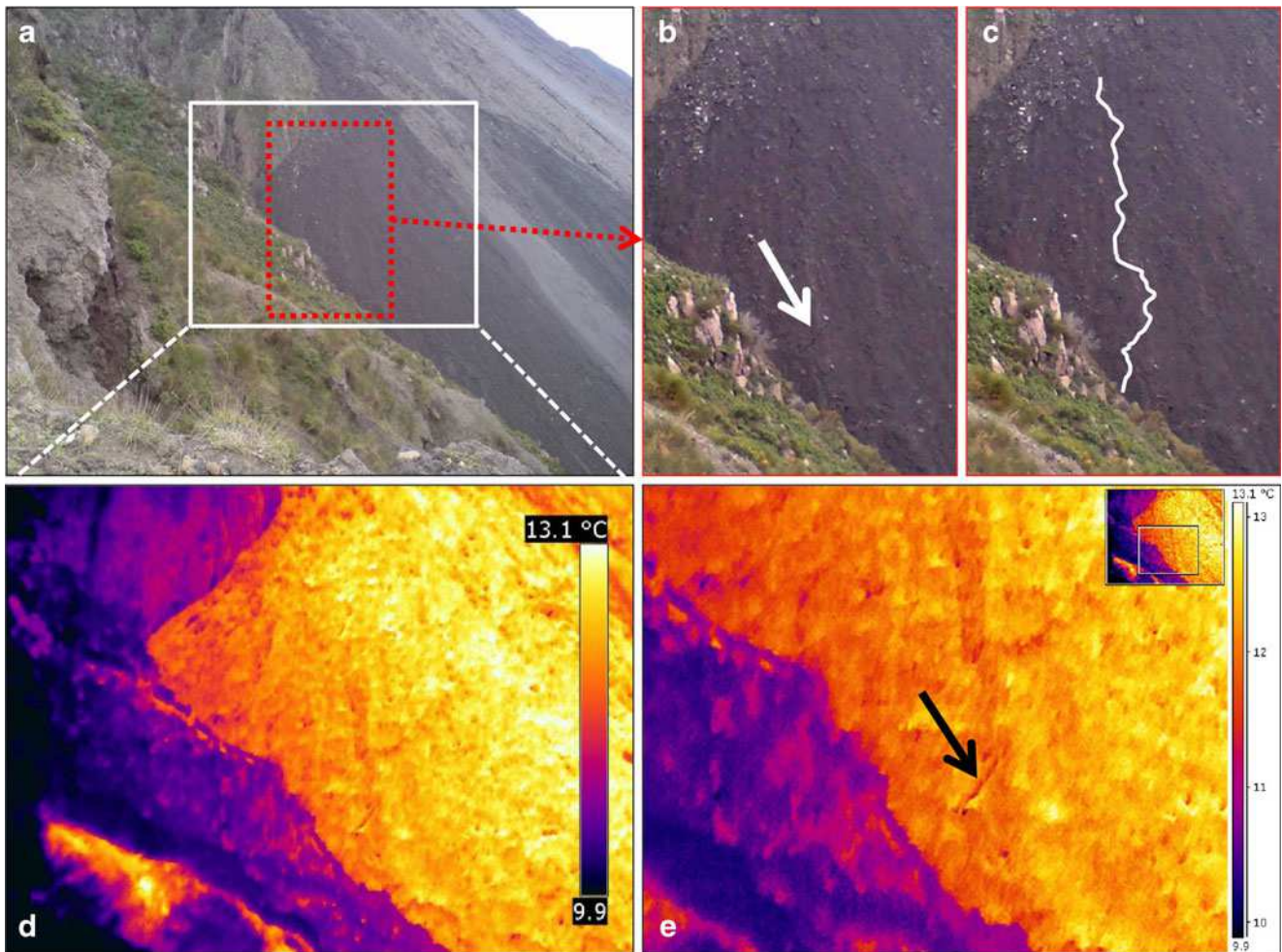


Fig. 11 Optical image (a) and related zooms (b–c) of the SdF (sector 5) where the fracture was detected (acquired January 9th 2013 at 13:17 by the digital camera built-in the FLIR SC 620). **d** Corresponding thermal image and **e** related zoom

Discussion

Structural setting of the summit vents area

The chronology and nature of the 2012–2013 crisis, together with data from previous ones, could be used to constrain the structural setting of the summit vents area of Stromboli volcano. The 2007 and 2012–2013 events were preceded by a strong increase in the displacement rate on the summit vents area (sector 2) respectively 2 months and 15 days before the onset of the 2007 and the 2012–2013 crises, respectively.

The structural framework of the vents area at Stromboli comprises the large Pizzo circular crater, about 350 m in diameter, several nested craters (i.e. La Fossa) within the Pizzo crater and the complex of presently active vents (Fig. 1d). The presence of several slip zones regulating collapse of the summit vents area in recent years has already been recognised by Finizola et al. (2003) by means of geophysical surveys. During the 2007 crisis, the collapse of part of the

upper SdF allowed observation of the inner structure of the northern part of the summit area. This is affected by a series of slip planes dipping towards the NW (i.e. towards the sea) at angles of 60–80°. Field observations indicate the presence of normal offsets and down-throw of the seaward blocks (Casagli et al. 2009). The Pizzo slip zones are invoked to explain the geometry of the summit collapses (large pit crater formation) at Stromboli, while our GBInSAR data show that the same structural features are also involved during the inflation–deflation fluctuations of the volcano. By integrating GBInSAR, numerical modelling and structural field data, Casagli et al. (2009) interpreted the onset of the 2007 crisis. Pressurisation of the shallow conduit system has been invoked to explain the observed variations in the displacement rate (Casagli et al. 2009). Increase in displacement rate in sector 2 has been related to the increases in the magmatic pressure within the conduit, as a consequence of the rise of the magma level, while increases in displacement rate in sector 3 have been considered as the evidence for lateral expansion of the shallow conduit system of Stromboli volcano (Di Traglia et al.

2013). Sector 3 corresponds to the opening area of the eccentric vent for 2002–03 and 2007 effusive eruptions (Neri et al. 2008) and vent opening in sector 3 occurred when the magma overpressure exceeded the rock stiffness (Casagli et al. 2009; Nolesini et al. 2013).

In sector 3, the two main events that preceded the 2012–2013 crisis occurred on 12th September and on 30th–31st October, and each case is considered a pressurisation pulse of the shallow conduit system, as proposed by Di Traglia et al. (2013) for the same phenomenon observed at Stromboli during the 2009–2011 period. In sector 2, the GBInSAR system registered an increase in the displacement rate after the 25th of November 2012, and, while in sector 3 since the 18th of December 2012. Since 24th December 2012, when the first lava overflow occurred after a small crater rim collapse, fluctuation in inflation have been registered in both sector 2 and sector 3 (Fig. 6). Fluctuations in sector 2 were of longer period than to the ones registered in sector 3. It is worth remarking that the GBInSAR system at Stromboli is able to detect only northward displacements and hence can constrain only the N–S component of the NW-ward movement of sector 2, because the E–W direction is orthogonal to the LoS. The external flank of the summit vent, however, involves movements of the whole area with a radial deformation, coherent with the inflation of the entire upper sector of the volcanic system (Ferretti et al. 2008). The different behaviour of the two sectors suggests a mechanical decoupling between sector 2 and 3, bounded by the slip zone of the 2007 crater collapse. The decoupling occurred during the onset of the crisis (24th December 2012). While sector 2 registered a decrease in the inflation, related to a decrease in the isotropic magma overpressure on the entire summit area, deformation in sector 3 testified that the magma overpressure was mainly directed to the NE portion of the crater area, as a consequence of the NE-ward expansion of the very shallow feeder conduit (Casagli et al. 2009). As shown before, major morphological changes in sector 3 are related to the accumulation of lava overflows on the external slope of the NE vents. This implies that the displacements recorded by GBInSAR recorded before the occurrence of lava overflows in sector 3 were mainly related to the conditions within the shallow conduit of Stromboli rather than to morphological phenomena.

At Stromboli, the upward flow is channelled toward the central conduit, but it was also outward through intrusions that extended mostly toward the marginal vents (NE or SW) buttressed from the conduit, as also observed in other scoria cones (Petronis et al. 2013). During lateral intrusion propagation in the summit vents area, the energy available to drive fracture propagation could change, depending on the type of boundary conditions applied and on the sheet geometry (Gudmundsson 2012). When the boundaries of the summit vents area cannot move during an unrest period (constant displacement; Gudmundsson 2012), the source of potential

energy for intrusive sheet development is the strain energy stored in the volcano (Gudmundsson 2009, 2011, 2012). The constant-displacement boundary conditions result in stable lateral propagation, i.e. as the conduit propagates the energy available to drive the fracture gradually decreases (Gudmundsson 2012). Otherwise, if the boundaries of the summit vents area can move (constant-load boundary conditions; Gudmundsson 2012), the lateral propagation of Stromboli conduit is stable. Loading is inferred to be primarily related to inflation of the summit vents area. Thus, constant-displacement boundary conditions favour lava overflows from the NE or SW vents, while constant-load boundary conditions result in unstable fracture propagation and, therefore, comparatively large effusions would be favoured by such boundary conditions.

The chronology of the onset of the 2012–2013 effusive-explosive crisis, in terms of inflation and NE-ward expansion of the summit area vs. deflation, resembles the sequence of events that occurred at the beginning of the 2007 flank effusion (inflation; eccentric effusion at the base of the NE vents; collapse of the summit area). At Stromboli, the GBInSAR recorded displacement rates in sector 2 of 0.1–0.3 mm/h for both the 2007 and the 2012–2013 crisis. The peak in displacement rate in the 2007 crisis has been reached only during the eccentric vent opening (>300 mm/h; 27th February 2007), i.e. when the magma overpressure was high enough to drive lateral propagation of the conduit system, forming a NE–SW trending dike (Casagli et al. 2009; Nolesini et al. 2013). During the (magma) pressure built up of both crises, resulting from the rise of the magma level in the conduit, the existence of an upper limit to the displacement rate (0.1–0.3 mm/h) suggests that the initial phases of Stromboli crises are characterised by a constant load (the boundary of the summit area can move during the pressure build-up). When the displacement rate threshold is exceeded, the boundary conditions change and the sheet propagation occurs at fixed boundary (constant displacement) condition. Horizontally propagating intrusions can only emplace themselves if edifice load prevents eruption through the central area and if magma is negatively buoyant at shallow depth (Pinel and Jaupart 2004; Di Traglia et al. 2013). In a volcanic edifice, at small distances from the axis, confining stresses act to prevent vertical propagation and a bulge develops at some distance from the focal area; this also gives rise to eccentric eruptive vents (Pinel and Jaupart 2004; Di Traglia et al. 2013). This implies that, if there is no magma overpressure (due to pressurisation of the HP-filled conduit that we interpret as resulting from degassing of the LP magma; Di Traglia et al. 2013) or weakening of the country rocks, the fracture stops to propagate, preventing the development of an eccentric eruption. Shallow intrusive events are common during the construction of mafic volcanoes that commonly appear to be dominated by eruptions producing pyroclastic deposits (e.g. Németh and Cronin 2008, 2011).

Contribution to the understanding the conduit dynamics at Stromboli volcano

Each phase of lava overflows observed during the 2012–2013 crisis was preceded by a repose period (characterised by a slight increase in the displacement rate in sectors 2 and 3 and by minor explosive activity at the vents) and was accompanied by a rapid decrease in the displacement rate of both sectors 2 and 3. The fluctuating displacement rate (Fig. 6) can be related to variations in the flow rate through the shallow conduit system and thus to increased rise speed of the magma beneath the vent (Parfitt 2004). These variations in the flow rate can be related to magma convection within the plumbing system of Stromboli, which results from density difference

between ascending low-density magma and descending high-density magma (Burton et al. 2007; Witham 2011). Magmas with different vesicularity may reside in the upper part (<1 km) of Stromboli's conduit system and their relative abundances reflect on-going vesiculation and mixing/mingling of different magmas (Lautze and Houghton 2005, 2007). Displacement rates in sector 2 decreased as the degassed magma column was pushed out from the conduit due to the rise of volatile-rich magma forming a lava overflow (Fig. 12). After the crisis, the displacement rate decreased to a low level again. Higher-intensity activity at mafic volcanoes is generally followed by a reduction in the magma density (Di Traglia et al. 2009; Cimarelli et al. 2010). Hence, the low deformation rates observed in the summit vents area of

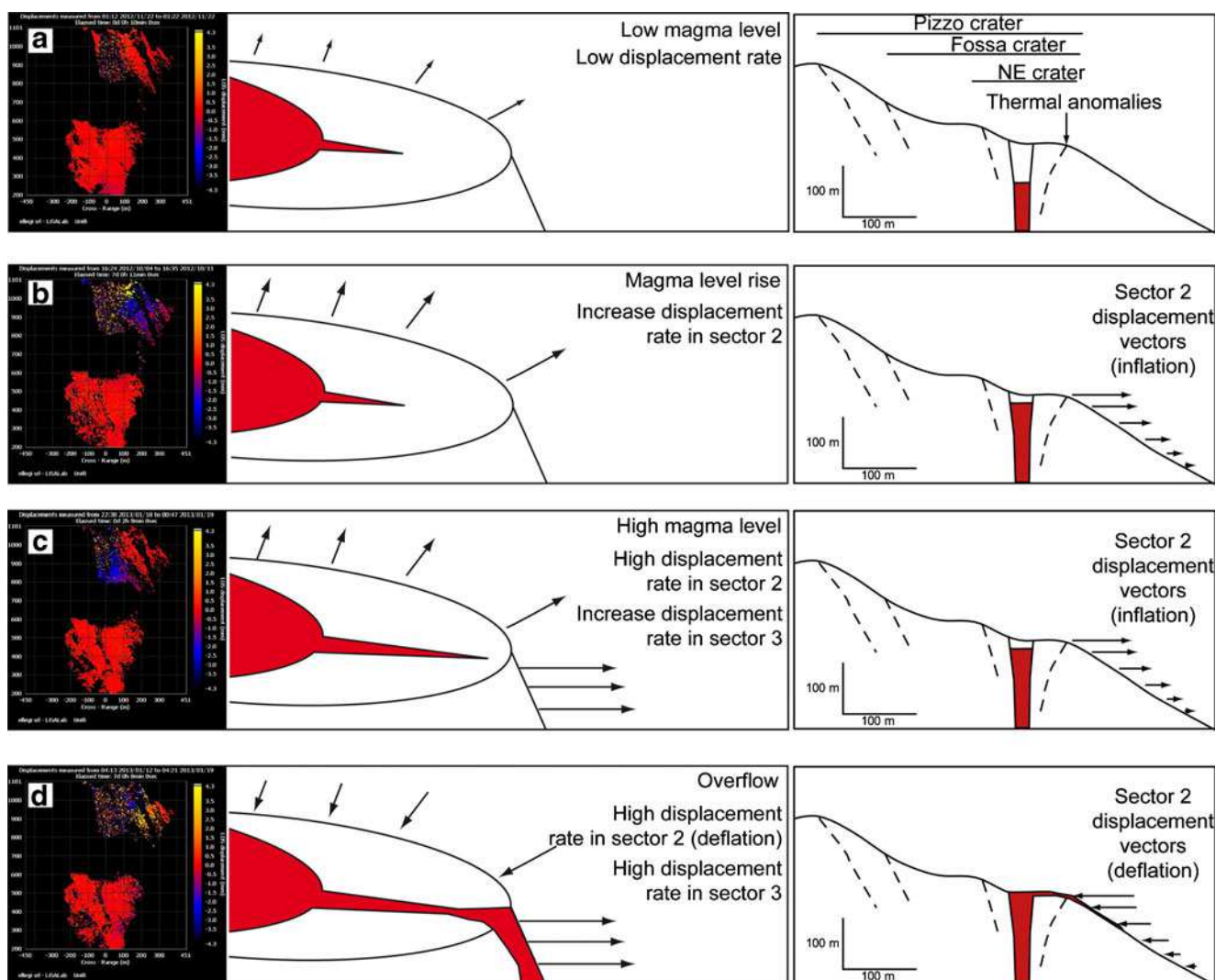


Fig. 12 Schematic representation of the SAR displacement fields in sectors 2 and 3. **a** Low magma level during ordinary strombolian activity. The structural features of the NE crater area derived from field survey during the 2007 eruption (after Casagli et al. 2009) and geophysical survey (Finizola et al. 2003) when a series of steep slip planes was exposed; **b** increase in displacement rate in sector 2 as a consequence

of the isotropic expansion due to the rise of the magma level within the Stromboli shallow storage system; **c** constant-displacement boundary conditions (high displacement rate in sector 2) favour the lateral expansion of the shallow storage system, as testified by the increase in displacement rate in sector 3; **d** deflation of sector 2 as the degassed magma column is pushed out from the conduit forming a lava overflow

Stromboli volcano during normal activity can be related to a conduit system filled with a smaller volume (lower gas fraction) of HP magma (Di Traglia et al. 2013).

Implications for volcano monitoring

Displacement detected in the different sectors monitored by the GBInSAR system could be used as a precursor of the shift to more intense eruptive activity. In particular, the increase in displacement rate in sector 3 (12th September) was followed by the increase in the displacement rate in sector 2 since the 16th October 2012. Both phenomena are related to the conduit pressurisation (increase in the magmatic pressure and increase in the overpressure component) due to the increase in the volatile volume fraction in the magma.

Therefore, considering changes in the displacement rate of both sectors, it may be possible to forecast not only the shift in more intense period of activity, but also the pressure conditions in the NE vents' conduit of Stromboli volcano.

Conclusions

During early December 2012, Stromboli volcano (Aeolian Islands, Southern Italy) experienced an increase in its volcanic activity that peaked with several lava overflows, major Strombolian explosions, crater-wall collapses and intense spatter activity from late December 2012 to March 2013. Analysis of the displacement of the NE vents area and of the SdF has been performed with the GBInSAR system by dividing the monitored part of the volcano into five regions, corresponding to the external rim of the NE vents (sector 1), the flank of the summit vents area (sector 2), the slope of the NE vents (sector 3), and two portions of the SdF within and outside of the 2002 tsunamigenic landslide (sectors 4 and 5).

Major changes in displacement rate have been observed in sectors 2 and 3. Rise and fall of displacement rate in sector 2 are related to changes in magmatic pressure of the shallow plumbing systems, while increases in the displacement rate in sector 3 are interpreted as overpressure-related lateral expansion of the shallow plumbing system.

The field and thermal survey revealed the presence of thermal anomalies caused by an alignment of fumaroles in the zone of maximum displacement in sector 2, confirming the existence of a structural discontinuity between sectors 2 and 3.

This different behaviour, coupled with structural data from published studies, suggests a decoupling between the two sectors, localised along the slip zone of the 2007 crater collapse (Pizzo fault; Finizola et al. 2003).

The use of power images permitted us to assess geomorphological variations of the debris cone and to link them to major phases of lava effusion; this allowed us to discriminate

between the effects of geomorphological processes and overpressure-induced deformations.

The GBInSAR installed at Stromboli volcano has been used as a remarkable early warning tool for mass gravitational movements on the SdF. Increases in the displacement rate in sector 3 are related to anomalous degassing and could be used as early warning signals for civil protection purposes before the occurrence of major explosions and lava emission. Here, changes in the displacement rate registered by the GBInSAR system on the upper part of the volcano, corresponding to the external flank of the summit vents (sector 2) and at the base of the NE vents area (sector 3), can be used to monitor the change in the pressure conditions in the shallow plumbing system of Stromboli volcano.

Acknowledgements This work has been sponsored in part by the National Civil Protection Department (DPC) within the framework of the SAR.net2 and InGrID projects. The DPC is acknowledged for supporting the project and permitting this publication. The authors are grateful to I. Binda Rossetti and C. Rivolta (Ellegi-Lisalab) for technical support during the 2012–2013 eruptive crisis, to D. Mangione (DPC) for the crisis management, and to A. Di Roberto (INGV-Pisa) and P. Papale (INGV-Pisa) for helpful suggestions and discussions. M. Rosi (Università di Pisa) is sincerely thanked for his precious discussions and for his “faith” in the GBInSAR system. The authors are grateful to J. Taddeucci (INGV-Roma, associate editor), J.D.L. White (University of Otago, editor in chief), G. Wadge (University of Reading) and A. Bonforte (INGV-Catania-Osservatorio Etno) for their valuable corrections and suggestions that allowed us to significantly improve the manuscript. This work is dedicated in the memory of Stefano Scibilia.

References

- Aiuppa A, Federico C, Giudice G, Giuffrida G, Guida R, Gurrieri S, Liuzzo M, Moretti R, Papale P (2009) The 2007 eruption of Stromboli volcano: Insights from real-time measurement of the volcanic gas plume CO₂/SO₂ ratio. *J Volcanol Geoth Res* 182: 221–230
- Aiuppa A, Bertagnini A, Métrich N, Moretti R, Di Muro A, Liuzzo M, Tamburello G (2010) A model of degassing for Stromboli volcano. *Earth Planet Sc Lett* 295:195–204
- Aiuppa A, Burton M, Allard P, Caltabiano T, Giudice G, Gurrieri S, Liuzzo M, Salerno G (2011) First observational evidence for the CO₂-driven origin of Stromboli's major explosions. *Solid Earth* 2: 135–142
- Andronico D, Corsaro RA, Cristaldi A, Polacci M (2008) Characterizing high energy explosive eruptions at Stromboli volcano using multi-disciplinary data: an example from the 9 January 2005 explosion. *J Volcanol Geoth Res* 176:541–550
- Andronico D, Pistolesi M (2010) The November 2009 paroxysmal explosion at Stromboli. *J Volcanol Geoth Res* 196:120–125
- Andronico D, Taddeucci J, Cristaldi A, Miraglia L, Scarlato P, Gaeta M (2013) The 15 March 2007 paroxysm of Stromboli: video-image analysis, and textural and compositional features of the erupted deposit. *Bull Volcanol* 75(7):1–19
- Antonello G, Casagli N, Farina P, Leva D, Nico G, Sieber AJ, Tarchi D (2004) Ground-based SAR interferometry for monitoring mass movements. *Landslides* 1:21–28

- Barberi F, Rosi M, Sodi A (1993) Volcanic hazard assessment at Stromboli based on review of historical data. *Acta Vulcanol* 3:173–187
- Barberi F, Civetta L, Rosi M, Scandone R (2009) Chronology of the 2007 eruption of Stromboli and the activity of the Scientific Synthesis Group. *J Volcanol Geoth Res* 182:123–130
- Bertagnini L, Metrich N, Landi P, Rosi M (2003) Stromboli volcano (Aeolian Archipelago, Italy): an open window on the deep-feeding system of a steady state basaltic volcano. *J Geophys Res* 108(B7):2336
- Bertagnini A, Di Roberto A, Pompilio M (2011) Paroxysmal activity at Stromboli: lessons from the past. *B Volcanol* 73:1229–1243
- Blackburn EA, Wilson L, Sparks RSJ (1976) Mechanisms and dynamics of strombolian activity. *J Geol Soc London* 132:429–440
- Bonaccorso A, Calvari S, Garfi G, Lodato L, Patané D (2003) December 2002 flank failure and tsunamis at Stromboli volcano inferred by volcanological and geophysical observations. *Geophys Res Lett* 30:1941
- Bonforte A, Aloisi M, Antonello G, Casagli N, Fortuny-Guash J, Guerri L, Nunnari G, Puglisi G, Spata A, Tarchi D (2008) Movements of the Sciarra del Fuoco. In: *The Stromboli Volcano: An Integrated Study of the 2002–2003 Eruption* (Calvari S, Inguaggiato S, Puglisi G, Ripepe M, Rosi M, eds). American Geophysical Union Monograph Series 182:183–199
- Burton MR, Mader HM, Polacci M (2007) The role of gas percolation in quiescent degassing of persistently active basaltic volcanoes. *Earth Planet Sc Lett* 264:46–60
- Calvari S, Spampinato L, Lodato L, Harris AJL, Patrick MR, Dehn J, Burton MR, Andronico D (2005) Chronology and complex volcanic processes during the 2002–2003 flank eruption at Stromboli volcano (Italy) reconstructed from direct observations and surveys with a handheld thermal camera. *J Geophys Res* 110
- Casagli N, Tibaldi A, Merri A, Del Ventisette C, Apuani T, Guerri L, Fortuny-Guasch J, Tarchi D (2009) Deformation of Stromboli Volcano (Italy) during the 2007 crisis by radar interferometry, numerical modeling and field structural data. *J Volcanol Geoth Res* 182:182–200
- Casagli N, Catani F, Del Ventisette C, Luzi G (2010) Monitoring, prediction and early warning using ground-based radar interferometry. *Landslides* 7:291–301
- Cimarelli C, Di Traglia F, Taddeucci J (2010) Basaltic scoria texture from zone conduit as precursor to violent Strombolian activity. *Geology* 38:439–442
- Cole PD, Fernandez E, Duarte E, Duncan AM (2005) Explosive activity and generation mechanisms of pyroclastic flows at Arenal volcano, Costa Rica between 1987 and 2001. *Bull Volcanol* 67:695–716
- Corazzato C, Francalanci L, Menna M, Petrone CM, Renzulli A, Tibaldi A, Vezzoli L (2008) What controls sheet intrusions in volcanoes? Structure and Petrology of the Stromboli sheet complex. *Italy. J Volcanol Geoth Res* 173:26–54
- Del Bello E, Llewellyn EW, Taddeucci J, Scarlato P, Lane SJ (2012) An analytical model for gas overpressure in slug-driven explosions: Insights into Strombolian volcanic eruptions. *J Geophys Res* 117, B02206
- Di Roberto A, Rosi M, Bertagnini A, Marani MP, Gamberi F (2010) Distal turbidites and tsunamigenic landslides of Stromboli Volcano (Aeolian Islands, Italy). Submarine mass movements and their consequences. *Adv Nat Technol Haz* 28:719–731
- Di Traglia F, Cimarelli C, de Rita D, Gimeno Torrente D (2009) Changing in eruptive style in explosive basaltic volcanism: examples from Crosat complex scoria cone, Garrotxa Volcanic Field (NE Iberian Peninsula). *J Volcanol Geoth Res* 180:89–100
- Di Traglia F, Del Ventisette C, Mugnai F, Intrieri E, Rosi M, Moretti S, Casagli N (2013) Ground Based InSAR reveals conduit pressurization pulses at Stromboli volcano. *Terra Nova* 25:192–198
- Ferretti A, Prati C, Rocca F (2001) Permanent scatterers in SAR interferometry. *IEEE T Geosci Remote* 39:8–20
- Ferretti A, Bianchi M, Novali F, Tamburini A, Rucci A (2008) Volcanic Deformation Mapping using PSInSARTM: Piton de la Fournaise, Stromboli and Vulcano test sites for the Globvolcano project. In: *Use of Remote Sensing Techniques for Monitoring Volcanoes and Seismogenic Areas, 2008. USEReST 2008*. doi: [10.1109/USEREST.2008.4740340](https://doi.org/10.1109/USEREST.2008.4740340)
- Finizola A, Sortino S, Lénat J-F, Aubert M, Ripepe M, Valenza M (2003) The summit hydrothermal system of Stromboli: new insights from self-potential, temperature, CO₂ and fumarolic fluid measurements—structural and monitoring implications. *B Volcanol* 65:486–504
- Garcia C, Fearnley CJ (2012) Evaluating critical links in early warning systems for natural hazards. *Environ Hazards* 11:123–137
- Ghiglia DC, Romero LA (1994) Robust two-dimensional weighted and un-weighted phase unwrapping that uses fast transforms and iterative methods. *J Opt Soc Am* 11:107–117
- Gillot PY, Keller J (1993) Radiochronological dating of Stromboli. *Acta Vulcanol* 3:69–77
- Giordano G, Porreca M (2009) Field observations on the initial lava flow and the fracture system developed during the early days of the Stromboli 2007 eruption. *J Volcanol Geoth Res* 182:145–154
- Gudmundsson A (2009) Toughness and failure of volcanic edifices. *Tectonophysics* 471:27–35
- Gudmundsson A (2011) *Rock fractures in geological processes*. Cambridge University Press, Cambridge
- Gudmundsson A (2012) Strengths and strain energies of volcanic edifices: implications for eruptions, collapse calderas, and landslides. *Nat Hazard Earth Sys* 12:2241–2258
- Harris AJL, Ripepe M, Calvari S, Lodato L, Spampinato L (2008) The 5 April 2003 Explosion of Stromboli: Timing of Eruption Dynamics Using Thermal Data. In: *Calvari S, Inguaggiato S, Puglisi G, Ripepe M, Rosi M (Eds.), Learning from Stromboli and its 2002–03 Eruptive Crisis: Am Geophys Union Geophys Monogr* 182:305–316
- Hornig-Kjarsgaard I, Keller J, Koberski U, Stadlbauer E, Francalanci L, Lenhart R (1993) Geology, stratigraphy and volcanological evolution of the island of Stromboli, Aeolian arc, Italy. *Acta Vulcanol* 3:21–68
- Houghton BF, Gonnemann HM (2008) Basaltic explosive volcanism: constraints from deposits and models. *Chem Erde-Geochem* 68:117–140
- Houghton BF, Swanson DA, Rausch J, Carey RJ, Fagents SA, Orr TR (2013) Pushing the volcanic explosivity index to its limit and beyond: constraints from exceptionally weak explosive eruptions at Kilauaea in 2008. *Geology* 41:627–630
- Inguaggiato S, Vita F, Rouwet D, Bobrowski N, Morici S, Sollami A (2011) Geochemical evidence of the renewal of volcanic activity inferred from CO₂ soil and SO₂ plume fluxes: the 2007 Stromboli eruption (Italy). *B Volcanol* 73:443–456
- INGV Report (2012) Istituto Nazionale di Geofisica e Vulcanologia, Bollettino settimanale sul monitoraggio vulcanico, geochimico, delle deformazioni del suolo e sismico del vulcano Stromboli del 27/11/2012, Rep. N° 48/2012. Available at: http://193.206.213.9/intranet/gest_news/uploads/488BollettinoStromboli20121127.pdf
- INGV Report (2013) Istituto Nazionale di Geofisica e Vulcanologia, Bollettino settimanale sul monitoraggio vulcanico, geochimico, delle deformazioni del suolo e sismico del vulcano Stromboli del 27/11/2012, Rep. No. 2/2013. Available at: http://193.206.213.9/intranet/gest_news/uploads/1794BollettinoStromboli20130108.pdf
- Intrieri E, Di Traglia F, Del Ventisette C, Gigli G, Mugnai F, Luzi G, Casagli N (2013a) Flank instability of Stromboli volcano (Aeolian Islands, Southern Italy): integration of GB-InSAR and geomorphological observations. *Geomorphology* 201:60–69
- Intrieri E, Gigli G, Casagli N, Nadim F (2013b) Landslide early warning system: toolbox and general concepts. *Nat Hazard Earth Sys* 13:85–90
- La Felice S, Landi P (2011) The 2009 paroxysmal explosions at Stromboli (Italy): magma mixing and eruption dynamics. *B Volcanol* 73:1147–1154

- Lautze NC, Houghton BF (2005) Physical mingling of magma and complex eruption dynamics in the shallow conduit at Stromboli volcano, Italy. *Geology* 33(5):425–428
- Lautze NC, Houghton BF (2007) Linking variable explosion style and magma textures during 2002 at Stromboli volcano, Italy. *Bull Volcanol* 69(4):445–460
- Lautze NC, Taddeucci J, Andronico D, Cannata C, Tornetta L, Scarlato P, Houghton B, Lo Castro MD (2012) SEM-based methods for the analysis of basaltic ash from weak explosive activity at Etna in 2006 and the 2007 eruptive crisis at Stromboli. *Phys Chem Earth* 45–46: 113–127, Parts A/B/C
- Lodato L, Spampinato L, Harris AJL, Calvari S, Dehn J, Patrick M (2007) The morphology and evolution of the Stromboli 2002–2003 Lava flow field: An example of Basaltic flow field emplaced on a steep slope. *B Volcanol* 69:661–679
- Lu Z, Power JA, McConnell VS, Wicks C Jr, Dzurisin D (2002) Preruptive inflation and surface interferometric coherence characteristics revealed by satellite radar interferometry at Makushin Volcano, Alaska: 1993–2000. *J Geophys Res* 107(B11):2266
- Moran SC, Newhall C, Roman DC (2011) Failed magmatic eruptions: late-stage cessation of magma ascent. *B Volcanol* 73:115–122
- Németh K, Cronin SJ (2008) Volcanic craters, pit craters and high level magma-feeding systems of a mafic island-arc volcano: Ambrym, Vanuatu, South Pacific. In: Thomson K, Petford N (eds.) *Structure and emplacement of high-level magmatic systems*. Geological Society, London, special publication, Geological Society, London, 302:87–102
- Németh K, Cronin SJ (2011) Drivers of explosivity and elevated hazard in basaltic fissure eruptions: the 1913 eruption of Ambrym Volcano, Vanuatu (SW-Pacific). *J Volcanol Geoth Res* 201:194–209
- Neri M, Lanzafame G, Acocella V (2008) Dyke emplacement and related hazard in volcanoes with sector collapse: the 2007 Stromboli (Italy) eruption. *J Geol Soc London* 165:883–886
- Nolesini T, Di Traglia F, Del Ventisette C, Moretti S, Casagli N (2013) Deformations and slope instability on Stromboli volcano: Integration of GBInSAR data and analogue modeling. *Geomorphology* 180–181: 242–254
- Parfitt EA (2004) A discussion of the mechanisms of explosive basaltic eruptions. *J Volcanol Geoth Res* 134:77–107
- Petronis MS, Delcamp A, Van Wyk De Vries B (2013) Magma emplacement into the Lemptégy scoria cone (Chaîne Des Puys, France) explored with structural, anisotropy of magnetic susceptibility, and Paleomagnetic data. *B Volcanol* 75:753
- Pinel V, Jaupart C (2004) Magma storage and horizontal dyke injection beneath a volcanic edifice. *Earth Planet Sc Lett* 221:245–262
- Pistolesi M, Rosi M, Pioli L, Renzulli A, Bertagnini A, Andronico D (2008) The paroxysmal explosion and its deposits. *American Geophysical Union Monograph Series n. 182*, in: Calvari S, Inguaggiato S, Puglisi G, Ripepe M, Rosi M (eds.). *The Stromboli volcano: an integrated study of the 2002–2003 eruption*. pp. 317–329
- Pistolesi M, Delle Donne D, Pioli L, Rosi M, Ripepe M (2011) The 15 March 2007 explosive crisis at Stromboli volcano, Italy: assessing physical parameters through a multidisciplinary approach. *J Geophys Res* 116, B12206
- Puglisi G, Bonaccorso A, Mattia M, Aloisi M, Bonforte A, Campisi O, Cantarero M, Falzone G, Puglisi B, Rossi M (2005) New integrated geodetic monitoring system at Stromboli volcano (Italy). *Eng Geol* 79:13–31
- Rosi M, Bertagnini A, Harris AJL, Pioli L, Pistolesi M, Ripepe M (2006) A case history of paroxysmal explosion at Stromboli: timing and dynamics of the April 5, 2003 event. *Earth Planet Sc Lett* 243:594–606
- Rosi M, Pistolesi M, Bertagnini A, Landi P, Pompilio M, Di Roberto A (2013) Stromboli Volcano, Aeolian Islands (Italy): present eruptive activity and hazard. In: Lucchi F, Peccerillo A, Keller J, Tranne CA, Rossi PL (eds.) *J Geol Soc London Mem. Geology of the Aeolian Islands (Italy)*
- Spampinato L, Calvari S, Harris AJL, Dehn J (2008) Evolution of the lava flow field, *American Geophysical Union monograph series n. 182*, in: Calvari S, Inguaggiato S, Puglisi G, Ripepe M, Rosi M (eds.). *The Stromboli volcano: an integrated study of the 2002–2003 eruption*. pp. 201–212
- Spampinato L, Calvari S, Oppenheimer C, Boschi E (2011) Volcano surveillance using infrared cameras. *Earth Sci Rev* 106:63–91
- Tarchi D, Casagli N, Fortuny-Guassch J, Guerri L, Antonello G, Leva D (2008) Ground deformation from ground-based SAR interferometry. *American Geophysical Union Monograph Series n. 182*. In: Calvari S, Inguaggiato S, Puglisi G, Ripepe M, Rosi M (eds.). *The Stromboli volcano: an integrated study of the 2002–2003 eruption*. pp. 359–372
- Taddeucci J, Palladino DM, Sottili G, Bernini D, Andronico D, Cristaldi A (2013) Linked frequency and intensity of persistent volcanic activity at Stromboli (Italy). *Geophys Res Lett* 40:3384–3388
- Tibaldi A (2001) Multiple sector collapses at Stromboli volcano, Italy: how they work. *B Volcanol* 63:112–125
- Tibaldi A, Corazzato C, Marani M, Gamberi F (2009) Subaerial–submarine evidence of structures feeding magma to Stromboli Volcano, Italy, and relations with edifice flank failure and creep. *Tectonophysics* 469:112–136
- Tinti S, Pagnoni G, Zaniboni F (2006) The landslides and tsunamis of the 30th of December, 2002 in Stromboli analysed through numerical simulations. *B Volcanol* 68:462–479
- Witham F (2011) Conduit convection, magma mixing, and melt inclusion trends at persistently degassing volcanoes. *Earth Planet Sc Lett* 301: 345–352

Barcelona, 26th January 2015

**JUDGEMENT CONCERNING THE PHD THESIS MANUSCRIPT AS A REQUIREMENT FOR AWARDING THE
"DOCTOR EUROPAEUS" CERTIFICATE**

External Referee Approval

Referee General Information

Dr. Guido Luzi, Senior Researcher

Laurea degree in applied Physics and PhD degree in electronic systems engineering from the University of Florence, Florence, Italy, in 1986 and 2003 respectively.

Affiliation

Remote Sensing Department of the Centre Tecnològic de Telecomunicacions de Catalunya (CTTC) Division of Geomatics, Av. Gauss, 7 E-08860 Castelldefels (Barcelona) Spain

E-mail: gluzi@cttc.cat

Research areas/interests

Microwave remote sensing, active and passive. Design and experimentation of radar-based sensing sensors for Cultural Heritage and Environmental monitoring. GB-SAR interferometry. Innovative applications of microwave techniques, for geophysical and civil applications.

Evaluation of Doctoral Thesis Proposal

PhD student: **Federica Bardi**

PhD University: **Department of Earth Sciences, University of Florence (ITALY)**

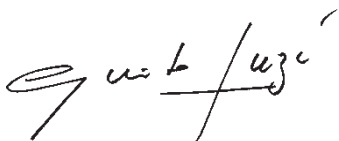
PhD thesis title: **Optimization of ground based radar techniques for early warning systems**

General comments and remarks about thesis evaluation:

The PhD thesis of Federica Bardi focuses on the use Ground Based SAR interferometry to improve early Warning Systems aimed at reducing landslide risk. The goal is attained analysing and trying to optimize both hardware and software aspects. Generally the state of the art is exhaustive, except for the atmospheric effect which deserved a wider literature analysis. Anyway, the spatial and temporal performances of the presently available systems are well analyzed, identifying the relevance of these issues for the improvement of the early warning. This gives a consistent originality to the work and an important impact to the knowledge from an operational point of view. The work is well presented and the methodology well explained. The publications issued during the thesis period are of main concern to the topic. Some of the main positive aspects are: the evidence of the operational nature of the work, the wide set of the analyzed experimental data, and the strong link to the community responsible for the landslide risk reduction and monitoring.

In conclusion I believe that the goals of the PhD thesis can be considered more than satisfactory achieved, the description of the results is clear and the work, originally developed, is of scientific relevance.

Faithfully



Barcelona (Spain) January 26th, 2015



Universita Degli Studi Firenze
Attn.: Nicola Casagli
Florence

DATE
2015-01-21

OUR REF
bgk/rf
YOUR REF
Your reference

ITALY

NGI review of PhD thesis of Federica Bardi

NGI has been contacted by Prof Nicola Casagli at Universita Degli Studi Firenze for making a short review of the PhD thesis of Federica Bardi as Ms Bardi spent parts of her time of the PhD work at NGI, Norway. This letter summarises the main points in the review made by Mr. Bjørn Kalsnes (NGI contact person for Ms Bardi during her stay in Norway) and Dr Regula Frauenfelder (NGI remote sensing expert). The review is based on the version of the thesis sent by Ms Bardi to NGI on 9th January 2015. Our main comments are:

- General comments:
 - The thesis needs a thorough English review. The spelling seems to be ok, but the linguistic rhythm and sentence build-up are in many occasions awkward which makes it difficult for the reader to understand what is really meant.
 - In some occasions it was unclear what has been achieved by the work of Ms Bardi and what has been achieved outside the thesis work (e.g. optimization of hardware characteristics and implementation of software features, p. 156 and elsewhere). Please also be aware that the Åknes landslide has NOT taken place yet (p. 157).
 - Here and there, statements, equations and figures are lacking proper reference (e.g., Figure 3, Figure 5?, equations on p. 8-12). Figure 17 contains two times the same image pair. For some figures (e.g., Figure 19), image quality is an issue.
- Introduction: The landslide statistics (some without reference, though, which needs to be amended) and major challenges are well presented. We do however miss a discussion of how monitoring techniques in general may improve the situation, and a presentation of how monitoring techniques and early warning systems historically have been developed and used positively for landslide mitigation causes.
- Chapter 1 explains the principle of radar and InSAR and gives a nice overview over the state of the art of space-borne and ground-based InSAR and its possible application to landslide monitoring. Ms Bardi shows a thorough analysis of the advantages and challenges related to both methods (space-borne versus ground-based). There are some inconsistencies concerning nomenclature, however. The Gamma instrument, for example, is not an InSAR, but an InRAR (real-aperture radar). This should be amended.
- Chapter 2 reports on new improvements of hard- and software of the LiSALab instrument, leading to the prototype LiSA-Mobile. The new prototype is very promising. As mentioned above, it is not always easy to see which part of the reported work was contributed by the PhD candidate Ms Bardi. This needs to be stated clearer, either in each chapter or by adding an extra chapter or section where Ms Bardi states for each chapter what her contribution was.
- Chapter 3 presents procedures for use of early warning systems for mitigating landslide risk. In recent risk literature uncertainty is a key element (ISO 31000 definition of risk being: "effect of uncertainty on objectives"). The concept of uncertainty, and it's effect on early warning, could therefore with luck be introduced in this chapter.

NORWEGIAN GEOTECHNICAL INSTITUTE
NGI.NO

Main office
PO Box 3930 Ullevaal St.
NO-0806 Oslo
Norway

Trondheim office
PO Box 5687 Sluppen
NO-7485 Trondheim
Norway

T (+47)22 02 30 00
F (+47)22 23 04 48
NGI@ngi.no

BIC NO. DNBANOKK
IBAN NO26 5096 0501 281
COMPANY NO
958 254 318MVA

ISO 9001/14001
CERTIFIED BY BSI
FS 32989/EMS 612006

- Chapter 4 highlights four test cases and shows the high potential of the new prototype instrument design and the new algorithm and its applicability for the combination of ground-based and space-borne InSAR measurements.
- In Chapter 5 the obtained results are discussed with respect to their applicability of a well-functioning EWS.
- Chapter 6 concludes the thesis. Among the noteworthy statements is the finding that the new, improved system proved to be very useful in those conditions in which the hazard area is wide and far away from the installation point. Ms Bardi also correctly points out that when applying InSAR or InRAR, *a priori* knowledge of the general characteristics of the scenario (in terms of stability and instability) is always required in order to correctly interpret the results.

Overall, the thesis gives a thorough comparison of existing InSAR/InRAR techniques and how they can be integrated into an EW system. We believe that it will be a valuable contribution to the scientific community, once the above mentioned points are amended.

And last, but certainly not least: It was a pleasure to host Ms Bardi during her stay in Norway and we wish her all the best for her future.

Sincerely yours
for NORWEGIAN GEOTECHNICAL INSTITUTE



Bjørn Kalsnes

*Technical Lead Georisk and Climate change impact
Soil Slides and Georisk, Natural Hazards division*



Regula Frauenfelder

*Technical Lead remote sensing
techniques
Geomapping, Natural Hazards
division*